THEORETICAL SOIL MECHANICS

THEORETICAL SOIL MECHANICS

By
KARL TERZAGHI

EIGHTH PRINTING

London: CHAPMAN AND HALL, Limited
JOHN WILEY AND SONS, INC.
NEW YORK

EIGHTH PRINTING, AUGUST, 1956

PRINTED IN THE UNITED STATES OF AMERICA

To HARVARD UNIVERSITY

in appreciation of its liberal encouragement of the pursuit of knowledge, this book is gratefully dedicated

PREFACE

In the fifteen years since the author published his first book on soil mechanics interest in this subject has spread over the whole globe and both our theoretical and our practical knowledge of the subject have expanded rapidly. The *Proceedings of the First International Conference on Soil Mechanics* (Cambridge 1936) alone contains a greater amount of quantitative information regarding soils and foundations than the entire engineering literature prior to 1910. Yet, as in every other field of engineering, the first presentation of the theoretical principles has been followed by a period of transition characterized by a tendency toward indiscriminate application of theory and by unwarranted generalizations. Hence, when the author began work on a new textbook on soil mechanics he considered it advisable to separate theory completely from practical application. This volume deals exclusively with the theoretical principles.

Theoretical soil mechanics is one of the many divisions of applied mechanics. In every field of applied mechanics the investigator operates with ideal materials only. The theories of reinforced concrete, for instance, do not deal with real reinforced concrete. They operate with an ideal material, whose assumed properties have been derived from those of the real reinforced concrete by a process of radical simplification. This statement also applies to every theory of soil behavior. The magnitude of the difference between the performance of real soils under field conditions and the performance predicted on the basis of theory can only be ascertained by field experience. The contents of this volume has been limited to theories which have stood the test of experience and which are applicable, under certain conditions and restrictions, to the approximate solution of practical problems.

Besides providing the reader with a working knowledge of useful methods of analysis, theoretical soil mechanics also serves an important educational purpose. The radical separation between theory and application makes it easy to impress upon the reader the conditions for the validity of the different mental operations known as theories. Once the reader has grasped, on the basis of the results of the analysis, the manifold factors which determine the behavior of simple, ideal materials under the influence of internal and external forces he will be less likely to succumb to the omnipresent danger of unwarranted generalizations based on inadequate data.

In order to be useful, the knowledge of theory must be combined with a thorough knowledge of the physical properties of real soils and the difference between the behavior of soils in the laboratory and in the field. Otherwise the engineer is unable to judge the margin of error associated with his numerical results. The properties of real soils and the performance of soils under field conditions will be discussed in a companion volume.

For the author, theoretical soil mechanics never was an end in itself. Most of his efforts have been devoted to the digest of field experiences and to the development of the technique of the application of our knowledge of the physical properties of soils to practical problems. Even his theoretical investigations have been made exclusively for the purpose of clarifying some practical issues. Therefore this book conspicuously lacks the qualities which the author admires in the works of competent specialists in the general field of applied mechanics. Nevertheless he could not evade the task of writing the book himself, because it required his own practical background to assign to each theory its proper place in the entire system.

The sources from which the subject matter has been collected are listed in the bibliography. The approximate methods of computing the bearing capacity of footings in Articles 46 to 49, the earth pressure of sand on the walls of shafts in Article 74, the critical head of piping in Articles 94 to 96, the gas pressure in bubbles and voids in Article 112, and the approximate solutions of the drainage problems given in Articles 118, 119, and 122 have not previously been published.

The first draft for the manuscript was thoroughly studied and commented upon by Mr. Albert E. Cummings and Dr. Ralph B. Peck. Their comments were so helpful and constructive that they induced the complete revision of several chapters and the partial revision of several others. The author is also indebted to his wife, Dr. Ruth D. Terzaghi, for careful scrutiny of the manuscript in its various stages and to Dr. Phil M. Ferguson for valuable suggestions.

KARL TERZAGHI

GRADUATE SCHOOL OF ENGINEERING
HARVARD UNIVERSITY
CAMBRIDGE, MASS.
December 1942.

SYMBOLS

In 1941 the American Society of Civil Engineers issued a manual containing a list of symbols to be used in soil mechanics (*Soil Mechanics Nomenclature.* Manual of Engineering Practice No. 22). The author used these symbols except those for loads and resistances and those for some of the linear dimensions. In the manual an attempt was made to trace a sharp boundary between load (p and P) and resistance (q and Q). Since these two quantities are sometimes equal and opposite, the discrimination is neither necessary nor useful. Therefore the author retained the conventional symbols q and Q for external loads and p and P or f and F for pressures and forces on inner surfaces such as the surface of contact between a retaining wall and a backfill. The symbols for some of those quantities which appear conspicuously in the diagrams, such as length or width, have been omitted from the list because rigid standardization of the symbols for such quantities is unnecessary.

In the following list the dimensions of the quantities expressed by the symbols are given in cm-gm-sec. They could as well be expressed in any other units, for instance in ft-lb-hr, without changing the exponents. The terms *gram* and *pound* indicate a weight which is a force. If a quantity is given in one unit system, for instance

$$E = 120{,}000 \text{ (gm cm}^{-2}\text{)}$$

and we want to express it in another one, for instance in pounds and feet, we must introduce into the preceding equation

$$1 \text{ gm} = \frac{1}{454} \text{ lb} \quad \text{and} \quad 1 \text{ cm} = \frac{1}{30.5} \text{ ft}$$

whereupon we obtain

$$E = 120{,}000 \left(\frac{1}{454} \text{ lb} \times \frac{30.5^2}{\text{ft}^2} \right) = 120{,}000 \text{ (2.05 lb ft}^{-2}\text{)}$$
$$= 245{,}000 \text{ lb ft}^{-2}$$

If no dimension is added to a symbol, the symbol indicates a pure number.

When selecting the names for the values expressed by the symbols the author applied the term *coefficient* to those values which are the

same for every point in a given space, as the coefficient of permeability, or on a plane, as the coefficient of earth pressure. For values which refer to an average (bearing capacity factor) or a total (stability factor) the word *factor* was chosen. The term "hydrostatic pressure ratio" has been avoided, because its use became customary in connection with both the total and the unit earth pressures. This can be misleading.

A (cm^2) = area.
A_A = earth pressure factor (ratio between normal component of total earth pressure on a given, plane surface and total pressure of equivalent liquid on the same surface in those instances in which the distribution of these two pressures is not identical).
a (cm) = amplitude (vibrations).
a_v ($gm^{-1} cm^2$) = coefficient of compressibility (a_{vc}) or coefficient of swelling. (a_{vs}) refers to the unit of volume of solid matter. The second subscript may be omitted.
C (gm or gm cm^{-1}) = resultant cohesion.
C (any dimension) = constant of integration.
c (gm cm^{-2}) = cohesion in Coulomb's equation.
c_a (gm cm^{-2}) = adhesion (retaining walls); corrected cohesion (stability of slopes).
c_c (gm cm^{-2}) = critical cohesion (theory of stability of slopes).
c_v ($cm^2 sec^{-1}$) = coefficient of consolidation (c_{vc} in compression and c_{vs} in expansion).
c_d (gm cm^{-1} sec) = coefficient of viscous damping (vibrations).
c_r (gm cm^{-2}) = required cohesion (theory of slopes).
c_s (gm cm^{-1}) = spring constant (vibrations).
d_s (gm cm^{-3}) = coefficient of dynamic subgrade reaction (vibrations).
E (gm cm^{-2}) = modulus of elasticity. (If E refers to a definite state or range of stress, subscripts are used.)
E_l (gm cm) = energy loss (pile driving).
e = void ratio = volume of voids per unit of volume of solid soil constituents.
F (gm or gm cm^{-1}) = total internal force.
f (gm cm^{-2}) = force per unit of area (f_n = normal and f_t = tangential component).
f (sec^{-1}) = frequency (vibrations).
f_0 (sec^{-1}) = natural frequency (vibrations).
G (gm cm^{-2}) = modulusof shear (vibrations).
G_a = air space ratio (drainage).
G_s = factor of safety.
g (cm sec^{-2}) = acceleration of gravity.
H_c (cm) = critical height of slope.
h (cm) = hydraulic head.
h_c (cm) = height of capillary rise.
h_p (cm) = critical head with respect to piping.
h_w (cm) = piezometric head.
I (cm^4) = moment of inertia of a beam.
I_σ = influence values pertaining to pressure distribution.
I_ρ = influence values pertaining to settlement.
i = hydraulic gradient.
K_0 = coefficient of earth pressure at rest (ratio between normal stress on a vertical and a horizontal section at a given point of a mass of soil in the initial state of elastic equilibrium of the mass).

K_A = coefficient of active earth pressure (ratio between normal component of earth pressure of a cohesionless mass on a plane surface and the corresponding liquid pressure, if pressure distribution is hydrostatic).

K_P = coefficient of passive earth pressure of cohesionless soil.

K_{Pm} = coefficient of mobilized part of passive earth pressure of cohesionless soil = K_P divided by factor of safety (theory of bulkheads).

k (cm sec^{-1}) = coefficient of permeability (Darcy's coefficient).

k_I and k_{II} (cm sec^{-1}) = coefficient of permeability parallel and at right angles to the planes of stratification.

k_h (gm cm^{-3}) = coefficient of horizontal pile or soil reaction.

k_p (gm cm^{-1}) = coefficient of vertical pile reaction.

k_s (gm cm^{-3}) = coefficient of subgrade reaction.

M (gm cm or gm) = total moment or moment per unit of length.

m (gm cm^{-1} sec^2) = mass = weight ÷ acceleration of gravity (vibrations).

m_v (gm^{-1} cm^2) = coefficient of volume change (m_{vc} in compression, m_{vs} in swelling), refers to unit of total volume.

N = ratio, factor or coefficient which is a pure number (N_c, N_q, and N_γ = bearing capacity factors, N_s = stability factor in the theory of stability of slopes, N = magnification factor in theory of forced vibrations).

$N_\phi = \tan^2 (45° + \phi/2)$ = flow value.

n = porosity = ratio between total volume of voids and total volume of soil.

n_a = ratio between elevation of point of application of earth pressure and total height of lateral support.

n_D = depth factor (stability of slopes).

n_e = coefficient of elastic restitution (pile driving).

n_g = ratio between acceleration produced by an earthquake shock and acceleration of gravity.

P_A (gm cm^{-1}) = active earth pressure if arching effect is absent (retaining walls) or disregarded (anchored bulkheads).

P_{An} (gm cm^{-1}) = normal component of P_A.

P_{At} (gm cm^{-1}) = tangential component of P_A.

P_P (gm cm^{-1}) = passive earth pressure without adhesion component.

P_{Pc} (gm cm^{-1}) = resultant of P_P and the adhesion between soil and contact face.

P_a (gm cm^{-1}) = active earth pressure on supports which induce arching (timbering in cuts).

p (gm cm^{-2}) = total normal pressure per unit of area.

$\bar{p}$ (gm cm^{-2}) = effective normal pressure per unit of area (bar may be omitted).

p_a (gm cm^{-2}) = atmospheric pressure.

p_g (cm cm^{-2}) = gas pressure, as for instance in air bubbles.

Q (cm^3 sec^{-1} or cm^2 sec^{-1}) = total discharge or discharge per unit of length, per unit of time; also used for total load (gm) or load per unit of length (gm cm^{-1}).

Q_D (gm cm^{-1}) = ultimate bearing capacity of continuous footings at depth D below the surface, per unit of length. It consists of three parts, whose values depend on the cohesion (Q_c), on the depth of foundation (Q_q), and on the unit weight of the soil (Q_γ).

Q_d (gm) = dynamic pile driving resistance.

q (gm cm^{-2}) = load per unit of area.

q' (gm cm^{-1}) = line load per unit of length.

q_D (gm cm^{-2}) = Q_D divided by width of footing. It consists of three parts. q_c, q_q, and q_γ, corresponding to Q_c, Q_q, and Q_γ.

S (gm or gm cm^{-1}) = total shearing force.

$S\%$ = degree of saturation.
s (gm cm^{-2}) = shearing resistance per unit of area.
T (degrees Centigrade) = temperature.
T_s (gm cm^{-1}) = surface tension of water.
T_v = time factor (theory of consolidation).
t (sec) = time.
U (gm or gm cm^{-1}) = total excess hydrostatic pressure.
$U\%$ = degree of consolidation.
U_w (gm or gm cm^{-1}) = total neutral force.
u (gm cm^{-2}) = excess hydrostatic pressure.
u_w (gm cm^{-2}) = neutral stress.
V (cm^3) = total volume.
v (cm sec^{-1}) = discharge velocity.
v_s (cm sec^{-1}) = seepage velocity.
W (gm or gm cm^{-1}) = total weight, or weight per unit of length.
$\overline{W}$ (gm or gm cm^{-1}) = effective weight.
W' (gm or gm cm^{-1}) = submerged weight.
W_H (gm) = weight of hammer.
W_P (gm) = weight of pile.
α,β (degrees) = angles.
γ (gm cm^{-3}) = unit weight.
γ' (gm cm^{-3}) = submerged unit weight.
γ_w (gm cm^{-3}) = unit weight of water = 1 gm cm^{-3} = 62.4 lb ft^{-3}.
Δ = increment.
δ (degrees) = angle of wall friction.
ϵ = base of Napierian logarithms; unit strain.
η (gm cm^{-2} sec) = coefficient of viscosity.
θ (degrees) = central angle.
λ (sec^{-1}) = damping factor.
μ = Poisson's ratio.
ν = concentration factor (theory of bearing capacity).
ρ (cm) = settlement; vertical displacement.
σ (gm cm^{-2}) = total normal stress.
$\bar{\sigma}$ (gm cm^{-2}) = effective normal stress (bar may be omitted).
σ_I, σ_{II}, and σ_{III} (gm cm^{-2}) = major, intermediate, and minor principal stress.
τ (sec) = period (vibrations).
τ (gm cm^{-2}) = shearing stress.
ϕ (degrees) = angle of internal friction or of shearing resistance.
ψ (degrees) = angle.
ω (sec^{-1}) = angular velocity.
ζ and ξ (cm) = components of total displacement in two different directions.
$\log a$ = Napierian (natural) logarithm of a.
$\log_{10} a$ = logarithm of a to the base 10.
$\overline{ab}$ = distance ab measured along a straight line.
$\widehat{ab}$ = distance ab measured along an arc.
$\approx$ means approximately equal.
(15)3 indicates equation 3 in Article 15. The article number appears at the top of each page.
Names followed by dates, for instance (Darcy 1858), indicate references which are given in the bibliography in alphabetic order.

CONTENTS

CHAPTER VI

CHAPTER VII

CHAPTER VIII

CHAPTER IX

CHAPTER X

CHAPTER XV

SECTION D. ELASTICITY PROBLEMS OF SOIL MECHANICS

CHAPTER XVI

CHAPTER XVII

CHAPTER XVIII

Section A

GENERAL PRINCIPLES INVOLVED IN THE THEORIES OF SOIL MECHANICS

Chapter I

INTRODUCTION

1. Scope and aim of the subject. Soil mechanics is the application of the laws of mechanics and hydraulics to engineering problems dealing with sediments and other unconsolidated accumulations of solid particles produced by the mechanical and chemical disintegration of rocks, regardless of whether or not they contain an admixture of organic constituents. In geology such accumulations are called *mantle* or *regolith.* The term *soil* is reserved for the decomposed upper layer which supports plants. On the other hand, in civil engineering the material which the geologist calls mantle is commonly known as soil or earth. The soil of the geologist and agronomist does not receive any consideration in this book, because it can be used neither as a basis for structures nor as a construction material. Since this book deals with a branch of civil engineering it is unfortunately necessary to retain the ambiguous terms soil and earth for material which should appropriately be called mantle.

Soil mechanics includes (1) theories of behavior of soils under stress, based on radically simplifying assumptions, (2) the investigation of the physical properties of real soils, and (3) the application of our theoretical and empirical knowledge of the subject to practical problems.

The development of some of the theories pertaining to soils was practically completed half a century ago, but our knowledge of the physical properties of real soils has been accumulated almost exclusively during the last 25 years. Prior to this period the inadequate knowledge of the properties of real soils very often led to a misapplication of theoretical reasoning to engineering problems dealing with soils, and as a result the theories were discredited.

The rapid advancement of our knowledge of the physical properties of soils and of the details of the structure of natural soil strata has led us to realize that the prospects of computing accurately the effect of a change in the conditions of loading or of drainage on the soil in advance

of construction are usually very slight. This statement applies particularly to all those instances in which the action of water is involved, because this action often depends on minor details of stratification which cannot be detected by test borings. For these reasons the role of theoretical soil mechanics in earthwork engineering is very different from the application of theory to structural design. When used in connection with the design of a steel or a reinforced concrete structure, applied mechanics provides us at the very start with conclusive information, because the data on which the computations are based are relatively reliable. On the other hand, the theories of soil mechanics provide us only with working hypotheses, because our knowledge of the average physical properties of the subsoil and of the orientation of the boundaries between the individual strata is always incomplete and often utterly inadequate. Nevertheless, from a practical point of view, the working hypothesis furnished by soil mechanics is as useful as the theory of structures in other branches of civil engineering. If the engineer is fully aware of the uncertainties involved in the fundamental assumptions of his computations he is able to anticipate the nature and the importance of the differences which may exist between reality and his original concept of the situation. On the basis of his knowledge of these possible differences he can plan in advance all the observations which should be made during construction in order to adapt the design to the real conditions before it is too late. Thus he fills the gaps in his knowledge while construction proceeds and he will never be taken by surprise.

By means of this " learn as we go " method we are often in a position to proceed in our earthwork operations without any risk on the basis of a lower factor of safety than the factor which is customarily required in other fields of civil engineering, for instance in the design of reinforced concrete structures. Therefore the practical value of a thorough grounding in the theories of soil mechanics cannot possibly be overemphasized. Although these theories deal only with ideal materials and with ideal geological conditions, they represent the key to an intelligent solution of the complex problems to be encountered in the field.

Every empirical rule based on past experience is valid only statistically. In other words it expresses a probability and not a certainty. Otherwise it could be replaced by a mathematical equation. In this respect the empirical rule does not differ from the working hypothesis furnished by soil mechanics. However, if we start our operations with such a working hypothesis we are fully aware of the uncertainties involved. Hence the element of surprise is eliminated. On the other hand, if we trust in empirical rules, as has been done in the past, we are

at the mercy of the laws of statistics. The working of these laws is disclosed by the fact that no year has passed without several major accidents in the field of earthwork engineering. It is more than a mere coincidence that most of these failures are due to the unanticipated action of water. The action of water depends much more on minor geological details than does the behavior of the soil. As a consequence the departure from the average expressed by empirical rules such as those which are used in the design of dams on permeable strata is exceptionally important. For the same reason the results of theoretical computations concerning the action of water on structures should only be used as a basis for planning the layout of pressure gages, which serve to inform us on the real flow conditions while construction proceeds. If accepted at face value, the results of the computation are no better and sometimes worse than empirical rules. This is the spirit in which soil mechanics should be studied and practiced.

2. Theory and reality. With the exception of steel subject to stresses within the elastic range there is no construction material whose real mechanical properties are simple enough to be acceptable as a basis for theoretical analysis. Hence practically every theory in applied mechanics is based on a set of assumptions concerning the mechanical properties of the materials involved. These assumptions are always to a certain extent at variance with reality. In spite of this procedure, rigorous mathematical solutions are commonly too complicated for general use in connection with the design of structures. In such cases we are obliged to make additional simplifying assumptions in order to facilitate the mathematical part of the investigation.

The nature and the implications of the aforementioned approximations are illustrated by the accepted method of computing the extreme fiber stresses in a reinforced concrete beam with free end supports which is acted upon by a system of loads. The first step is to determine the maximum bending moment by an analytical or a graphical procedure. The result of this operation is absolutely reliable, because the computation is based exclusively on the laws of mathematics and pure mechanics. The next step consists in computing the stresses in the section by means of one of the customary equations. This second operation involves no less than four supplementary assumptions. These assumptions are (*a*) every plane section oriented at right angles to the neutral axis of the beam remains plane during the process of bending, (*b*) the tensile strength of the concrete is equal to zero, (*c*) under compression the concrete obeys Hooke's law, and (*d*) the ratio between the modulus of elasticity of steel and concrete is equal to some definite value such as 15. The first of these assumptions is slightly inconsistent with the theory of elasticity, the importance of the error depending on the ratio between the height of the beam and the distance between the supports. The three others are conspicuously at variance with the properties of real concrete. For this reason the term "theory of reinforced concrete" assigned to the method of computation is not accurate. It is not a theory

of reinforced concrete. It is the theory of an ideal substitute for reinforced concrete, and the mechanical properties assigned to this substitute represent a radical simplification of the properties of the real material. However, in general, the procedure is perfectly acceptable, because when applied to the design of normal reinforced concrete structures, the errors involved are known to be well within the margin provided by the safety factor. In concrete design the factor is usually equal to 3.5 or 4.

Since the assumptions regarding the mechanical properties of the material subject to investigation determine the range of validity of the conclusions, no theory should be presented without a complete and concise statement of the assumptions on which the theory is based. Otherwise the results are likely to be applied to cases which are beyond the range of their validity.

The alleged incompatibility between practical experience and Coulomb's theory of the active earth pressure is an instructive example of a misjudgment due to inadequate knowledge of the limits of the validity of a theory. In one of the following articles it will be shown that Coulomb's theory is valid only under the condition that the upper edge of the lateral support of the soil yields in a horizontal direction to or beyond a certain critical distance. Until a few years ago this important limiting condition was not known. As a consequence it was general practice to apply the theory to the computation of the lateral earth pressure on the timbering of cuts in sand. Owing to the stiffness of the top row of struts the upper rim of the lateral support in a cut cannot yield in the manner just described and Coulomb's theory is therefore not valid in this special case. The few engineers who had learned from experience that the computed pressure distribution in cuts is radically different from the observed pressure distribution were led to the erroneous conclusion that the theory as such was worthless and should be discarded. Other engineers continued to use the theory in connection with the timbering in cuts, to the detriment of economy and safety, and no reasonable compromise could be made until the real cause of the apparent inconsistency became known.

In a similar fashion almost every one of the alleged contradictions between theory and practice can be traced back to some misconception regarding the conditions for the validity of the theory. For this reason, special attention will be paid to these vital and fundamental conditions.

3. Cohesionless and cohesive soils. The mechanical properties of soils range between those of plastic clay and those of clean perfectly dry or completely immersed sand. If we dig into a bed of dry or of completely immersed sand, the material at the sides of the excavation slides towards the bottom. This behavior of the material indicates the complete absence of a bond between the individual sand particles. The sliding material does not come to rest until the angle of inclination of the slopes becomes equal to a certain angle known as the *angle of repose*. The angle of repose of dry sand as well as that of completely immersed sand is independent of the height of the slope. On the other hand a trench 20 to 30 feet deep with unsupported vertical sides can be excavated in stiff plastic clay. This fact indicates the existence of a

firm bond between the clay particles. However, as soon as the depth of the trench exceeds a certain critical value, dependent upon the intensity of the bond between the clay particles, the sides of the cut fail and the slope of the mass of debris which covers the bottom of the cut after failure is far from vertical. The bond between the soil particles is called *cohesion*. No definite angle of repose can be assigned to a soil with cohesion, because the steepest slope at which such a soil can stand decreases with increasing height of the slope. Even sand, if it is moist, has some cohesion. As a consequence, the steepest slope at which it will stand decreases with the height of the slope.

In spite of the apparent simplicity of their general characteristics the mechanical properties of real sands and clays are so complex that a rigorous mathematical analysis of their behavior is impossible. Hence theoretical soil mechanics deals exclusively with imaginary materials referred to as *ideal sands* and *ideal clays* whose mechanical properties represent a simplification of those of real sands and clays. The following example may illustrate the difference between the real and the ideal soils. Most real soils are capable of sustaining considerable deformation without appreciable loss of shearing resistance. In order to simplify our theories we assume that the shearing resistance of the ideal soils is entirely independent of the degree of deformation. On account of this assumption all the theories involving the shearing resistance of soils are more or less at variance with reality. Rigorous mathematical solution of the problems does not eliminate the error associated with the fundamental assumption. In many cases this error is much more important than the error due to a radical simplification of the mathematical treatment of the problem. However, the difference between the assumed and the real mechanical properties is very different for different soils. The investigation of this difference and of its influence on the degree of reliability of the theoretical results belongs in the realms of soil physics and applied soil mechanics, which are beyond the scope of this volume.

In applied mechanics, materials whose shearing resistance is independent of the degree of deformation are called *plastic materials*. In accordance with our assumption an ideal sand is a plastic material without cohesion. Plastic materials fail by shear followed by plastic flow. The term *plastic flow* indicates continuous deformation at a constant state of stress.

4. Stability and elasticity problems. The problems of soil mechanics may be divided into two principal groups — the stability problems and the elasticity problems. The stability problems deal with the conditions for the equilibrium of ideal soils immediately pre-

ceding ultimate failure by plastic flow. The most important problems in this category are the computation of the minimum pressure exerted by a mass of soil on a lateral support (earth pressure problems), the computation of the *ultimate* resistance of the soil against external forces, such as the vertical pressure exerted on the soil by a loaded footing (bearing capacity problems), and the investigation of the conditions for the stability of slopes. In order to solve these problems it is sufficient to know the stress conditions for the failure of the soil. No consideration need be given to the corresponding state of strain unless there are certain limitations imposed upon the deformation of the soil, such as the limitation due to the incapacity of one part of a lateral support to change its position. Even if such limitations exist, it is sufficient to consider them in a general way without attempting a quantitative analysis of the corresponding strain effects.

Elasticity problems deal with the deformation of the soil due to its own weight or due to external forces such as the weight of buildings. All settlement problems belong in this category. In order to solve these problems we must know the relationship between stress and strain for the soil, but the stress conditions for failure do not enter into the analysis.

Intermediate between these two groups is the problem of determining the conditions of loading and of support required to establish the plastic state at one point of a mass of soil. In connection with problems of this type, both the elastic properties and the stress conditions for failure must be taken into consideration. The transition from the initial state to the ultimate failure of the soil by plastic flow is known as *progressive failure.*

In nature the voids of every soil are partly or completely filled with water. The water may be in a state of rest or in a state of flow. If it is in a state of rest, the methods for solving stability and deformation problems are essentially identical with those for solving similar problems in the mechanics of solids in general. On the other hand, if the water percolates through the voids of the soil, the problems cannot be solved without previously determining the state of stress in the water contained in the voids of the soil. In this case we are obliged to combine the mechanics of solids with applied hydraulics. (Chapters XII to XV.)

Chapter II

STRESS CONDITIONS FOR FAILURE IN SOILS

5. Relation between normal stress and shearing resistance. In this book the term *stress* is exclusively used for a force per unit of area of a section through a mass. It is generally assumed that the relation between the normal stress σ on every section through a mass of cohesive soil and the corresponding shearing resistance s per unit of area can be represented by an empirical equation

$$s = c + \sigma \tan \phi \qquad [1]$$

provided σ is a compressive stress. The symbol c represents the cohesion, which is equal to the shearing resistance per unit of area if $\sigma = 0$. The equation is known as *Coulomb's equation*. For cohesionless soils ($c = 0$) the corresponding equation is

$$s = \sigma \tan \phi \qquad [2]$$

The values c and ϕ contained in the preceding equations can be determined by means of laboratory tests, by measuring the shearing resistance on plane sections through the soil at different values of the normal stress σ. In practice we are chiefly interested in the shearing resistance of saturated or almost saturated soils. A change of stress in a saturated soil is always associated with some change of its water content. The rate of the change of the water content produced by a given change of the state of stress depends on several factors, including the degree of permeability of the soil. If the stresses which ultimately lead to failure of the test specimen are applied more rapidly than the corresponding changes in the water content of the specimen can occur, part of the applied normal stress σ will be carried, at the instant of failure, by the excess hydrostatic pressure which is required to maintain the flow of the excess water out of the voids of the soil. At a given value of σ, the part of σ which is carried by the water depends on the test conditions. Hence in this case both the values c and ϕ depend not only on the nature of the soil and its initial state but also on the rate of stress application, on the permeability of the material, and on the size of the specimen. The value ϕ obtained from such tests is called the *angle of shearing resistance*. For clays this angle can have any value up to 20° (exceptionally more) and for loose, saturated sands any value

up to 35°. In other words, no definite value can be assigned to the angle ϕ for any soil, because it depends on conditions other than the nature and the initial state of the soil.

On the other hand, if the stresses on the test specimen are applied slowly enough, the normal stress σ which acts on the surface of sliding at the instant of failure is almost entirely transmitted from grain to grain. Tests of this kind are known as *slow shear tests.* The rate at which such tests must be made depends on the permeability of the soil.

If shear tests on sand with a given initial density are made in such a manner that the stresses are entirely transmitted from grain to grain, we find that the shearing resistance $s = \sigma \tan \phi$ is practically independent of the character of the changes of the stress which preceded the failure. For instance, it makes practically no difference whether we increase the unit load on the sample continuously from 0 to 1 ton per square foot or whether we first increase the load from 0 to 5 tons per square foot and then reduce it to 1 ton per square foot. If the load on the sample at the instant of failure is equal to 1 ton per square foot, the shearing resistance s is the same in both cases. In other words, the shearing resistance s depends solely on the normal stress on the potential surface of sliding. A shearing resistance of this type is called a *frictional resistance* and the corresponding value of ϕ represents an *angle of internal friction.* Within the range of pressure involved in engineering problems the angle of internal friction of sand can usually be considered constant for practical purposes. Its value depends on the nature and initial density of the sand. It varies between the extreme limits of about 30° and 50°. The difference between the angle of internal friction of a given sand in the densest and in the loosest state may be as high as 15°.

Early investigators of soil problems generally assumed that the angle of internal friction of sand is identical with the angle of repose described in Article 3. However, as stated above, laboratory experiments have shown that the angle of internal friction of sand depends to a large extent on the initial density. In contrast to the angle of internal friction, the angle of repose of dry sand has a fairly constant value. It is always approximately equal to the angle of internal friction of the sand in the loosest state. Some textbooks even contain a list of values for the angle of repose of cohesive soils, although, as shown in Article 4, the angle of repose of such soils depends on the height of the slope.

When equation 2 is used in connection with stability computations the value ϕ always represents the angle of internal friction of the sand. In this book there will be no exception to this rule.

The results of slow shear tests on cohesive materials can usually be

expressed with sufficient accuracy by equation 1,

$$s = c + \sigma \tan \phi$$

In order to find out whether the term $\sigma \tan \phi$ satisfies the requirements for a frictional resistance, i.e., whether the resistance $\sigma \tan \phi$ depends solely on the normal stress σ, we submit our material with a given initial water content to two different tests. In one test we increase σ from zero to σ_1 and determine the corresponding shearing resistance s_1. In the second test, we first consolidate our material under a pressure σ_2 which is very much higher than σ_1; then we reduce it to σ_1 and finally we determine, by means of a slow shear test, the corresponding shearing resistance s_1'. The process of temporarily keeping a sample under pressure which is higher than the ultimate pressure is known as *preconsolidation*. Experiments show that the shearing resistance s_1' of the preconsolidated material may be equal to or greater than s_1. If the two values are equal, $\sigma \tan \phi$ in equation 1 represents a frictional resistance and we are justified in considering ϕ an angle of internal friction. On the other hand, if s_1' is greater than s_1, we know that the resistance $\sigma \tan \phi$ represents the sum of a frictional resistance and some other resistance which is independent of σ. The most conspicuous permanent change produced by preconsolidation consists in an increase of the density of the material and a corresponding reduction of its water content. If s_1' is appreciably greater than s_1 we always find that the water content corresponding to s_1' is lower than that corresponding to s_1. We know from experience that the value c in equation 1 increases for a given clay with decreasing initial water content. Therefore in most cases we are justified in drawing the following conclusion. If s_1' is appreciably greater than s_1, the resistance $\sigma \tan \phi$ in equation 1 consists of two parts with different physical causes. The first part is the friction produced by the normal stress σ and the second part is the increase of the cohesion due to the reduction of the water content which occurred while the pressure on the specimen was increased from zero to σ.

This statement can be expressed by an equation

$$s = c + \sigma \tan \phi = c + \frac{\sigma_I + \sigma_{III}}{2} N + \sigma \tan \phi_f \qquad [3]$$

wherein σ_I and σ_{III} represent the extreme principal stresses at failure after a slow test, and N is an empirical factor. The fraction $\sigma \tan \phi_f$ of the shearing resistance changes with the orientation of a section through a given point, while the fractions c and $\frac{\sigma_I + \sigma_{III}}{2} N$ are independent of the orientation. The customary methods for experimentally investigating the shearing resistance of cohesive soils merely furnish

the values c and ϕ on the left-hand side of the equation. The determination of the values ϕ_f and N requires elaborate supplementary investigations which belong in the realm of soil physics.

For cemented sand the value s_1' is usually very close to that of s_1. For such materials the value $\sigma \tan \phi$ in equation 1 represents only a frictional resistance. On the other hand, when experimenting with clay we find that the shearing resistance s_1' of the preconsolidated sample is always appreciably greater than s_1 at the same load. Hence in connection with clays the angle ϕ in equation 1 represents neither an angle of internal friction nor a constant for the clay, even when its value has been determined by means of slow shearing tests. If one makes a series of slow tests on a clay with a given initial water content after increasing the pressure on the samples from zero to different values σ_1, σ_2, etc., one gets an equation

$$s = c + \sigma \tan \phi$$

If one makes another series of tests on specimens of the same material after preceding consolidation of the samples under a pressure which is higher than the test pressures one gets another equation

$$s = c' + \sigma \tan \phi'$$

wherein c' is considerably higher than c and ϕ' considerably smaller than ϕ. Hence when using Coulomb's equation 1 in connection with clays, the reader should remember that the values c and ϕ contained in this equation represent merely two empirical coefficients in the equation of a straight line. The term cohesion is retained only for historical reasons. It is used as an abbreviation of the term *apparent cohesion.* In contrast to the apparent cohesion, the *true cohesion* represents that part of the shearing resistance of a soil which is a function only of the water content. It includes not only c in Coulomb's equation but also an appreciable part of $\sigma \tan \phi$. There is no relation between apparent and true cohesion other than the name.

In order to visualize the difference between apparent and real cohesion we consider again a material whose cohesion increases with increasing compaction. By making a series of shear tests with the material we obtain

$$s = c + \sigma \tan \phi$$

However, when investigating which part of the shearing resistance of the material is due to cohesion we obtain equation 3,

$$s = c + \frac{\sigma_I + \sigma_{III}}{2} N + \sigma \tan \phi_f$$

Comparing the two preceding equations we find that the true cohesion of the material is equal not to c but to

$$c_e = c + \frac{\sigma_I + \sigma_{III}}{2} N$$

If the entire pressure on a clay is transmitted from grain to grain the true cohesion is never smaller than the apparent cohesion.

If $\sigma \tan \phi$ in equation 1 is equal to zero we obtain

$$s = c \qquad [4]$$

For liquids the values c and ϕ are zero which means that

$$s = 0 \qquad [5]$$

6. Effective and neutral stresses. In the field, the voids of every fine-grained soil are partly or wholly filled with water. If we take a section through a saturated soil, part of it passes through the solid particles and part of it through the water. In order to ascertain the mechanical implications of this fact, consider the test arrangement illustrated by Figure 1. This figure represents a section through a layer of a cohesionless soil which occupies the bottom of a vessel. At the outset of the test the free water level is supposed to be located immediately above the surface of the soil and the layer is assumed to be so thin that we may neglect the stress due to the weight of the soil and the water which are located above the horizontal section ab. If we raise the water level to an elevation h_w above its original position the normal stress on the section ab increases from almost zero to

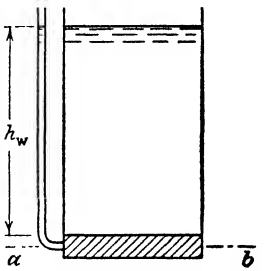

FIG. 1. Apparatus used to demonstrate difference between effective and neutral stress.

$$\sigma = h_w \gamma_w$$

wherein γ_w is the unit weight of the water. Yet, this increase of the compressive stress from practically zero to σ on every horizontal section within the soil does not produce a measurable compression of the layer of soil. On the other hand, if we increase the intensity of the pressure on the layer by the same amount, $h_w \gamma_w$, by loading the surface of the layer with lead shot, the resulting compression of the layer is very appreciable. By an appropriate modification of the test arrangement it can also be demonstrated that the position of the water level in the vessel has no influence on the shearing resistance s of the soil, whereas an equivalent solid surcharge increases the shearing resistance very

considerably. These and similar experiments lead to the conclusion that the compressive stress in a saturated soil consists of two parts with very different mechanical effects. One part which is equal to the pressure in the water produces neither a measurable compression nor a measurable increase of the shearing resistance. This part is is called the *neutral stress* u_w.[1] It is equal to the product of the unit weight of the water γ_w and the height h_w to which the water rises in a piezometric tube at the point under consideration. The corresponding equation is

$$u_w = h_w \gamma_w \qquad [1]$$

The height represents h_w the *piezometric head* at the point of observation. It can be positive or negative. Hence u_w can also be positive or negative. If u_w is positive it is usually called the *pore-water pressure.*

The second part $\bar{\sigma}$ of the total stress σ is equal to the difference between the total stress and the neutral stress u_w. This second part

$$\bar{\sigma} = \sigma - u_w \qquad [2]$$

is called the *effective stress,* because it represents that part of the total stress which produces measurable effects such as compaction or an increase of the shearing resistance. The total normal stress is

$$\sigma = \bar{\sigma} + u_w \qquad [3]$$

The influence of the pore-water pressure on the relation between stress, strain, and shearing resistance in cohesive soils can be investigated most accurately by means of *triaxial compression tests* on cylindrical specimens, because the test arrangement permits simultaneous measurement of the total and of the neutral stress.

The principle of the triaxial compression test is illustrated by Figure 2. This figure represents a section through a vertical cylindrical specimen of a saturated clay. The top surface of the specimen is covered with a metal disk and its base rests on a porous stone whose voids communicate with an outlet valve V. The outer surface of the specimen and of the porous stone is covered with an impermeable membrane as indicated in the figure. The specimen is immersed in oil or water which can be maintained under pressure, by means of a pump or an accumulator. The external, hydrostatic pressure σ exerted by the liquid on the water-

[1] From this definition it is evident that the neutral stress does not represent the real pressure in the water, because it does not include the pressure exerted by the weight of the atmosphere. Whenever we are interested in the real pressure in the water, as for instance in the theory of capillarity in Chapter XIV, the atmospheric pressure must be added to the neutral stress.

tight skin of the specimen can be combined with a supplementary, axial pressure $\Delta\sigma$ per unit of area of the top surface of the specimen. The external hydrostatic pressure combined with the supplementary axial pressure produces a state of stress which is symmetrical about the vertical axis of the specimen. Hence, during the test every horizontal section through the specimen is acted upon by a vertical stress $\sigma_I = \sigma + \Delta\sigma$ and every vertical section by a horizontal stress $\sigma_{II} = \sigma_{III} = \sigma$, which is equal to the external hydrostatic pressure.

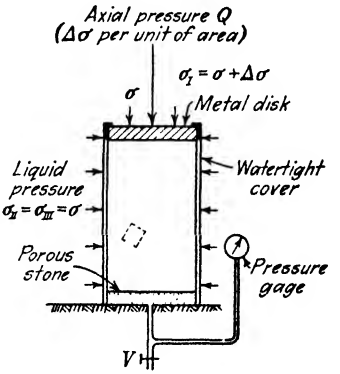

FIG. 2. Apparatus for triaxial compression test.

The tests can be made in two ways, with the outlet valve V (Fig. 2) closed or with it open. In a first series of tests we keep the valve closed, in order to keep the water content of the clay constant throughout the test. By connecting the column of water located above the closed outlet valve with a sensitive pressure gage we can experimentally demonstrate that every change in the total state of stress in the specimen is associated with some change in the pore-water pressure; and we can measure the pore-water pressure immediately preceding a failure of the specimen by shear. Thus we obtain one set of data informing us on the relationship between stress, strain, shearing resistance, and pore-water pressure.

In a second series of tests we keep the outlet valve open and at every stage of the tests we postpone our strain readings until the water content of the specimen becomes constant, when the pore-water pressure is approximately equal to zero. Hence, the data thus obtained inform us on the relationship between stress, strain, and shearing resistance at a pore-water pressure of zero.

Both series of tests, those with a closed and those with an open outlet valve, have been repeatedly made. By combining the data obtained from two such series, performed on a silty clay, Rendulic (1937) arrived at the following conclusions. The stress conditions for failure, as well as the volume change, depend solely on the intensity of the effective stresses; i.e., the mechanical effects of establishing a given state of total stress depends only on the difference between the total stress and the pore-water pressure. The same results are obtained if similar tests are carried out with sand or any other soil in a saturated state. The presence of gas bubbles in the voids of a soil influences merely the rate of deformation but not the final result of the tests. Therefore we

are compelled to assume that both the strain in soils and the stress conditions for failure depend exclusively on the effective stresses

$$\bar{\sigma}_I = \sigma_I - u_w$$

$$\bar{\sigma}_{II} = \sigma_{II} - u_w \qquad [4]$$

$$\bar{\sigma}_{III} = \sigma_{III} - u_w$$

On account of the decisive influence of the pore-water pressure u_w on the stress conditions for failure, this pressure must also be considered in connection with the failure conditions expressed by equations 5(1) and 5(2).

The shearing resistance of cohesionless materials such as sand is determined by equation 5(2). When discussing this equation in Article 5 it was emphasized that the normal stress σ in this equation represents a grain-to-grain stress which is synonymous with an effective normal stress. Therefore we can write this equation

$$s = \bar{\sigma} \tan \phi$$

wherein ϕ is the angle of internal friction. The resistance $\bar{\sigma} \tan \phi$ is a pure frictional resistance. A frictional resistance depends only on the effective normal stress on the surface of sliding. Hence if the total normal stress is σ and the pore-water pressure is u_w, the shearing resistance of the sand is determined by the equation

$$s = (\sigma - u_w) \tan \phi \qquad [5]$$

From slow shear tests on cohesive materials we obtain Coulomb's equation

$$s = c + \bar{\sigma} \tan \phi \qquad [6]$$

For cemented sands and similar materials the item $\bar{\sigma} \tan \phi$ represents a pure frictional resistance, which justifies the substitution

$$\bar{\sigma} = \sigma - u_w$$

Thus we obtain

$$s = c + (\sigma - u_w) \tan \phi \qquad [7]$$

On the other hand, in connection with clays, the item $\bar{\sigma} \tan \phi$ includes both a frictional resistance and another resistance which depends on the water content of the clay. (See Art. 5.) Since this second resistance is not a simple function of the normal stress on the surface of sliding, the substitution which led to equation 7 is not justified, except under very limited conditions such as those which exist in a clay during a triaxial compression test. Furthermore, when dealing with

clays, we are seldom in a position to compute the pressure which develops in the pore water while the point of failure is approached. For these reasons, the data required for making a stability computation pertaining to clays can at present be obtained only by means of the following, purely empirical procedure. We test the clay in the laboratory under conditions of pressure and drainage similar to those under which the shear failure is likely to occur in the field and we introduce the values c and ϕ thus obtained into our equations. It is obvious that the success of this procedure depends chiefly on the degree to which the experimenter has succeeded in imitating the field conditions. The influence of the test conditions on the numerical values c and ϕ in equation 5(1) will be discussed in a volume on applied soil mechanics.

In the following articles the symbol $\bar{\sigma}$ for the effective stress will be used only if it is necessary for preventing misunderstandings. Otherwise the effective normal stress will be represented by the symbol σ, which also indicates mixed normal stresses.

7. Mohr's diagram and the conditions for plastic equilibrium in ideal soils. The triaxial compression test illustrated by Figure 2 informs us on the intensity of the vertical pressure, σ_I per unit of area, which is required to produce a failure of the specimen at a given horizontal pressure $\sigma_{II} = \sigma_{III}$. Since the failure occurs along an inclined surface of sliding we are interested in the state of stress along inclined sections through the specimen. Figure 3*a* represents the specimen. Every horizontal section *I I* through the specimen is acted upon by a normal stress σ_I and the corresponding shearing stress is equal to zero. According to the accepted nomenclature in applied mechanics the normal stress on any section which is not acted upon by a shearing stress is called a *principal stress*. The section itself represents a *principal plane*. The normal stress on every vertical section of our specimen is $\sigma_{II} = \sigma_{III}$. The corresponding shearing stress must also be equal to zero. Otherwise the conditions for the equilibrium of the specimen would not be satisfied. Hence the stress $\sigma_{II} = \sigma_{III}$ also represents a principal stress.

If σ_{II} and σ_{III} are different, the conditions for equilibrium require that the directions of σ_I, σ_{II}, and σ_{III} intersect at right angles. Whatever the state of stress may be it is always possible to make through every point of the body three principal sections which are acted upon only by principal stresses. Wherever it may be necessary to distinguish between principal and ordinary normal stresses the former will be indicated by the symbol σ with a roman numeral as a subscript. σ_I is the major principal stress, and the symbol σ_{II} will be reserved for the principal stress whose intensity is intermediate between that of σ_I and σ_{III}.

In soil mechanics we deal chiefly with continuous masses of earth with a constant cross section whose outer boundaries are perpendicular to a single vertical plane. Every slice of earth oriented parallel to this plane is acted upon by the same external and internal forces. The thickness of the slice is not changed by a change in a state of stress in the slice.

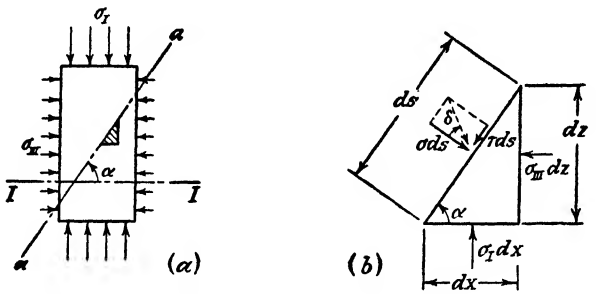

FIG. 3. Stress conditions in soil during triaxial compression test.

In applied mechanics such a type of deformation is known as *plane deformation*. When dealing with problems of plane deformation it is sufficient to investigate the stresses which act parallel to the sides of one slice.

In order to determine the stresses on an arbitrary inclined section *aa* through the specimen shown in Figure 3*a* we investigate the conditions for the equilibrium of a small prism (shown shaded), one side of which is located on the inclined section. The other two sides are parallel to the direction of the principal stresses, σ_I and σ_{III}. The slope of the inclined surface is determined by the angle α. The angle α is measured in a counterclockwise sense from the principal section *II*, which is acted upon by the larger principal stress σ_I. We also specify arbitrarily that the compressive stresses are positive. Figure 3*b* represents the prism on a larger scale. The equilibrium of the prism requires that

$$\sum \text{horizontal forces} = \sigma_{III} \sin \alpha \, ds - \sigma \sin \alpha \, ds + \tau \cos \alpha \, ds = 0,$$

and

$$\sum \text{vertical forces} = \sigma_I \cos \alpha \, ds - \sigma \cos \alpha \, ds - \tau \sin \alpha \, ds = 0$$

Solving these equations for σ and τ we obtain

$$\sigma = \tfrac{1}{2} (\sigma_I + \sigma_{III}) + \tfrac{1}{2} (\sigma_I - \sigma_{III}) \cos 2\alpha \qquad [1]$$

and

$$\tau = \tfrac{1}{2} (\sigma_I - \sigma_{III}) \sin 2\alpha \qquad [2]$$

In Figure 3 the angle α is smaller than 90°. For such a value we

obtain from equation 2 a positive value for the shearing stress τ. The corresponding resultant stress deviates in a clockwise direction from the normal stress σ. Since the shearing stress τ is positive we assign a positive value to the corresponding angle δ between the normal stress and the resultant stress.

The values of the stresses σ and τ can be computed by introducing the numerical values for σ_I, σ_{III}, and α into equations 1 and 2. However, we can also determine these values by means of the graphical procedure illustrated by Figure 4. In this diagram the compressive stresses (positive) are plotted on a horizontal axis from the origin O to the right and the positive shearing stresses on a vertical axis from point O in an upward direction. Hence positive values of the angle δ appear above the horizontal axis. The horizontal axis is reserved for the principal stresses because the corresponding shearing stress is equal to zero. In order to determine the values σ (eq. 1) and τ (eq. 2) for any plane forming an arbitrary angle α with the principal plane $I\ I$ in Figure 3*a*, we make $O\ III = \sigma_{III}$, $O\ I = \sigma_I$ (Fig. 4), trace a circle with a diameter $I\ III = \sigma_I - \sigma_{III}$, whose center A is located halfway between I and III and trace through A a line Aa which makes an angle 2α with AI. For geometrical reasons the abscissa of the point a thus obtained is equal to the normal stress σ (eq. 1), and its ordinate is equal to the shearing stress τ (eq. 2). The distance Oa represents the resultant stress on the inclined section through the specimen shown in Figure 3.

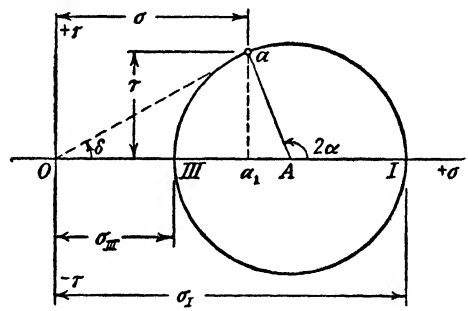

FIG. 4. Graphic determination of stresses by means of circle of stress.

In the diagram (Fig. 4) the co-ordinates of a point on the upper part of the circle represent the two stress components for a definite section which forms an arbitrary angle $\alpha < 90°$ with the principal direction $I\ I$ (Fig. 3*a*). In a similar manner the co-ordinates of a point on the lower part of the circle represent the two stress components for a section which forms an angle $\alpha > 90°$ with this direction. Hence the circle of which $I\ III$ (Fig. 4) is a diameter represents the locus of all the points which are defined by equations 1 and 2. For this reason the circle is commonly called the *circle of stress*.

The procedure illustrated by Figure 4 can also be used to compute the state of stress on any arbitrary section aa through a point B (Fig.

5a) of a large body of soil, provided the intensity and the direction of the principal stresses σ_I and σ_{III} are known. If the section aa intersects the principal plane $I\,I$ (Fig. 5a) at an angle α, the state of stress on the section is determined by the co-ordinates of the point a on the circle of stress shown in Figure 5b. Point a is obtained by plotting the angle

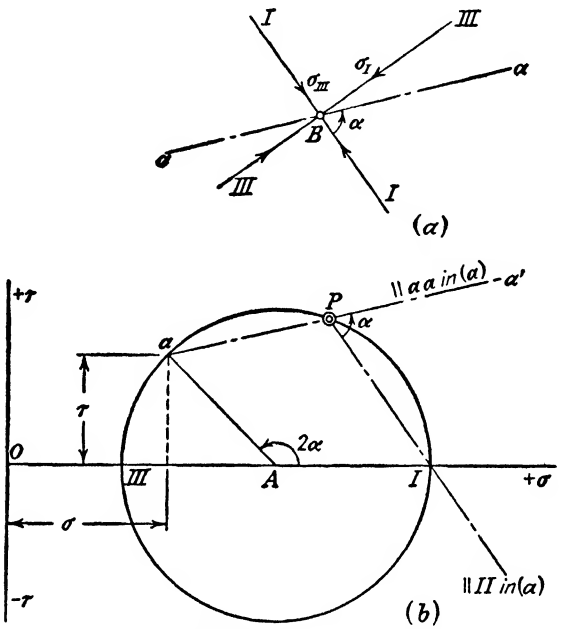

FIG. 5. Graphic determination of stresses by means of pole method.

2α from AI in Figure 5b in a counterclockwise sense. However, the position of point a can also be determined without laying off either α or 2α by means of the following procedure. We trace through I (Fig. 5b) a line parallel to the principal section $I\,I$ in Figure 5a. This line intersects the circle at point P. Then we trace through point P a line parallel to aa in Figure 5a. It intersects the line PI at an angle α. By geometry this angle is equal to one half of the angle aAI. Hence the line must intersect the circle of stress at the point a whose co-ordinates represent the state of stress on the inclined section aa in Figure 5a. This simple relation makes it possible to ascertain in the diagram (Fig. 5b) the position of the point whose co-ordinates represent the stresses on any arbitrary section by tracing a straight line through the point P parallel to the section under consideration. The point P is called the *pole* of the diagram and is indicated by a double circle.

The principle of the procedure can be condensed into the following

statement: Every point a on the circle of stress in Figure 5*b* represents the state of stress on one particular section through point B in Figure 5*a*. Thus for instance point a represents the state of stress on section aa. If we select several such points on the circle of stress and trace through each one of these points a line parallel to the corresponding section in Figure 5*a*, all the lines thus obtained intersect the circle of stress at the same point, the pole P. Hence if we know the orientation of the section corresponding to a single point on the circle of stress we obtain the pole by tracing through this point a line parallel to the section.

The graphic procedures illustrated by Figures 4 and 5 are valid for any material and regardless of whether or not the stresses σ_I and σ_{III} include a pore-water pressure u_w, because no assumption has been made regarding the physical properties of the material under investigation.

In soil mechanics the most important application of the stress circle method illustrated by Figures 4 and 5 consists in solving the following problem: We know the direction of the extreme principal stresses and the intensity of one of them. We also know, for instance from the results of shear tests, that the earth fails by shear as soon as the shearing stresses on any section satisfy Coulomb's equation

$$s = c + \sigma \tan \phi \qquad 5(1)$$

We want to determine the intensity of the second extreme principal stress.

With equation 5(1) we introduce for the first time an empirical element into our analysis, whereupon it becomes necessary to examine very carefully the assumptions which are associated with the equation. First of all, we assume, in sufficiently close agreement with experience, that the equation is valid for any value of the intermediate principal stress σ_{II} which acts at right angles to the plane of the drawing (Fig. 6*a*). We are also obliged to assume, in the following investigation, that the values c and ϕ in equation 5(1) are the same for every section through point B. Regarding this important assumption, we must distinguish between cohesionless materials such as sand and cohesive materials such as clay. The shearing resistance of a sand is determined by the equation

$$s = \sigma \tan \phi \qquad 5(2)$$

wherein σ represents an effective normal stress and ϕ the angle of internal friction. From experience we know that the validity of this equation invariably justifies aforementioned assumption. Hence the results of

theoretical investigations based on equation 5(2) are always accurate enough for any practical purpose.

The shearing resistance of clay is determined by the equation

$$s = c + \sigma \tan \phi \qquad 5(1)$$

wherein σ is either an effective or a total normal stress and ϕ is the angle of shearing resistance. In Article 5 it has been shown that the item $\sigma \tan \phi$ consists of two parts. One part is a frictional resistance whose intensity depends only on the value of the normal stress σ. This value is different for different sections through a given point. The second part of $\sigma \tan \phi$ depends on the water content, which is the same along every section through the point. Hence for clays the assumption that the value $\tan \phi$ in equation 5(1) is independent of the orientation of a section through a given point is not even approximately justified. However, for the sake of simplicity, we cannot avoid it. The nature and the importance of the errors due to this assumption will briefly be discussed at the end of this article.

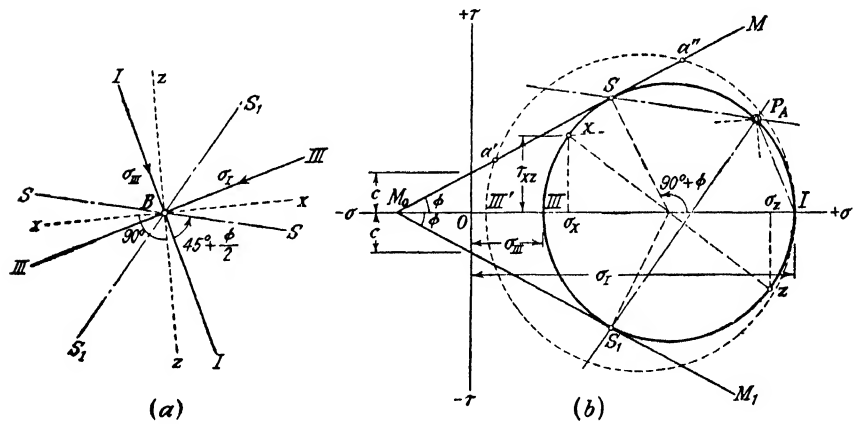

FIG. 6. Graphic presentation of Mohr's theory of rupture for ideal plastic materials (Mohr's diagram).

At the outset of this investigation it was assumed that the direction of the extreme principal stresses σ_I and σ_{III} and the intensity of one of these stresses are known. Our problem consists in determining the value which must be assigned to the second principal stress in order to satisfy the conditions for a shear failure at the selected point (B in Fig. 6a) and the orientation of the surfaces of sliding at point B. In Figure 6a the principal planes are shown by the lines $I\ I$ and $III\ III$ which always intersect at right angles. In the stress diagram (Fig. 6b)

equation 5(1) is represented by the straight lines M_0M and M_0M_1. These two lines are commonly called the *lines of rupture.* They intersect the horizontal axis at an angle ϕ and the vertical axis at a distance c from the origin O.

In order to solve our problem it is sufficient to remember that for a given value of σ_I, the stresses on any section through point B in Figure 6*a* are represented by the co-ordinates of the corresponding point on some circle of stress which passes through point I in the stress diagram (Fig. 6*b*) provided that $OI = \sigma_I$. Since the unknown stress σ_{III} is assumed to be the smaller principal stress the corresponding circle of stress must be located on the left side of point I. If the circle of stress representing the state of stress at point B does not intersect the lines of rupture M_0M and M_0M_1 (Fig. 6*b*) there is no section through point B in Figure 6*a* which satisfies the stress conditions for failure, represented by the lines of rupture. On the other hand, if the circle of stress, such as that over $I\,III'$ in Figure 6*b*, intersects the lines of rupture, equilibrium could not exist on any one of the sections corresponding to the points located on the arc $a'a''$. Hence the only circle of stress which satisfies the condition that it represents the state of stress in existence at point B at the instant of failure by shear is the circle which is tangent to the lines of rupture. It passes through point III on the horizontal axis, at a distance σ_{III} from the origin. It is called the *circle of rupture* and the diagram is called *Mohr's diagram* (Mohr 1871). In order to determine the orientation of the planes of failure with reference to the principal planes in Figure 6*a* we trace IP_A (Fig. 6*b*) $\parallel I\,I$ (Fig. 6*a*), thus obtaining the pole P_A of the diagram. The failure occurs simultaneously along two planes, SS (Fig. 6*a*) $\parallel P_AS$ (Fig. 6*b*) and S_1S_1 (Fig. 6*a*) $\parallel P_AS_1$ (Fig. 6*b*). The planes intersect the principal section $I\,I$ in Fig. 6*a* at an angle of $45° + \phi/2$. Hence the orientation of the planes of shear is independent of the value c (eq. 5(1)). The shearing stress on the planes of shear is equal to the ordinate of point S (or S_1) in Figure 6*b*.

If we determine by means of the diagram (Fig. 6*b*) the orientation of the resultant stresses on the shear planes we find that the direction of the resultant stress on each one of these planes is parallel to the other plane, provided $c = 0$ (cohesionless material). Thus for instance if $c = 0$ the resultant stress on SS in Figure 6*a* is parallel to S_1S_1 and that on S_1S_1 is parallel to SS. In applied mechanics any two sections which satisfy this condition are called *conjugate sections.* Hence in cohesionless materials the shearing planes represent conjugate sections.

The geometrical relations shown in Mohr's diagram demonstrate that

failure occurs as soon as the principal stresses satisfy the equation

$$\sigma_I = 2c \tan\left(45° + \frac{\phi}{2}\right) + \sigma_{III} \tan^2\left(45° + \frac{\phi}{2}\right) = 2c\sqrt{N_\phi} + \sigma_{III} N_\phi \quad [3]$$

The value

$$N_\phi = \tan^2\left(45° + \frac{\phi}{2}\right) \quad [4]$$

appears in many equations concerning the plastic equilibrium of earth. It will briefly be called the *flow value.*

When dealing with sand ($c = 0$) we operate only with effective normal stresses. Introducing into equation 3 the value $c = 0$, we obtain

$$\sigma_I = \sigma_{III} \tan^2\left(45° + \frac{\phi}{2}\right) = N_\phi \sigma_{III} \quad [5]$$

wherein ϕ is the angle of internal friction. Hence, if a mass of cohesionless soil is in a state of plastic equilibrium, the ratio between the major and the minor effective principal stresses in every point of this mass must be equal to the flow value N_ϕ. This value depends only on the angle of internal friction of the material.

Equation 3 can also be written in the form

$$\frac{\sigma_I + \sigma_{III}}{2} \sin \phi = \frac{\sigma_I - \sigma_{III}}{2} - c \cos \phi \quad [6]$$

For the normal stresses σ_x and σ_z on an arbitrary pair of planes intersecting each other at 90°, such as those represented by the lines xx and zz in Figure 6*a* and by the points x and z in Figure 6*b*, we obtain from Mohr's diagram for the state of incipient failure

$$\sqrt{\left(\frac{\sigma_z - \sigma_x}{2}\right)^2 + \tau_{xz}^2} - \frac{\sigma_z + \sigma_x}{2} \sin \phi = c \cos \phi \quad [7]$$

For ideal sands the cohesion c is equal to zero. In every equation pertaining to ideal sands the angle ϕ represents the angle of internal friction and the normal stresses are effective stresses. Substituting $c = 0$ in the preceding equations we get

$$\frac{\sigma_I - \sigma_{III}}{\sigma_I + \sigma_{III}} = \sin \phi \quad [8]$$

and

$$\frac{\sqrt{(\sigma_z - \sigma_x)^2 + 4\tau_{xz}^2}}{\sigma_z + \sigma_x} = \sin \phi \quad [9]$$

If the stresses in every point of a mass of soil satisfy any one of the equations 3, 6, or 7 the earth is said to be in a *state of plastic equilibrium.* This state may be preceded either by a state of *plastic flow* or by a state of *elastic equilibrium* involving the existence of stresses which are everywhere below the point of failure. The theory on which the computation of the stresses in a state of plastic equilibrium is based is called the *theory of plasticity.* There are several theories of plasticity, based on different assumptions regarding the conditions for plastic flow (Nadai 1931). These assumptions have been obtained by simplifying the real stress conditions for the plastic flow of the materials subject to investigation. The theory of plasticity pertaining to soils is based on Mohr's theory of rupture because we have not yet a substitute which describes the plastic properties of the soils in a more satisfactory manner. On the basis of Mohr's concept we obtained equations 3, 6, and 7, which represent three different forms of the fundamental equations of the theory of plastic equilibrium in ideal soils with which the following chapters deal. The equations have been derived on the assumption, stated at the outset, that equation 5(1) is valid not only for the shear plane but for any other section through a given point of a mass in a state of plastic equilibrium.

Mohr's diagram is nothing but a device for solving graphically some of our problems in plasticity on the assumption that Mohr's concept of the stress conditions for failure is justified. This assumption also implies that the cohesion c of the material subject to investigation is a constant of the material.

If c in equation 5(1) is equal to zero (cohesionless materials) and if, in addition, σ represents an effective normal stress, this assumption is approximately correct. The discrepancies which exist between the assumption and the mechanical properties of real clays will be described in a volume on applied soil mechanics. An analysis of their influence on the validity of Mohr's diagram and the corresponding equations for clays has led to the following conclusions. In spite of the discrepancies, equations 3 to 7 are always tolerably reliable. On the other hand, the difference between the real and the computed orientation of the surfaces of sliding with reference to the principal planes is always important. In general, if the stresses in the equations or in the diagrams represent effective stresses, the error is likely to be less important than the error associated with similar computations involving mixed stresses.

The preceding investigations were also based on the tacit assumption that plastic flow, involving a continuous deformation under constant stress, has no influence on the values c and ϕ contained in equation 5(1). Thus both the ideal sand and the ideal clay are assumed to be capable

of flowing indefinitely at unaltered values of c and ϕ. Therefore we are justified in calling them plastic materials. Yet there are no real soils whose physical properties strictly justify such an assumption. The departure of the behavior of real soils from the ideal plastic behavior varies notably not only with the nature of the soil particles but also with the porosity. These deviations and their bearing on the importance of the errors involved in the theoretical analysis will also be discussed in a volume on applied soil mechanics.

8. Buoyancy or hydrostatic uplift. In practice we deal chiefly with soils whose voids are filled with water. In order to determine the effective stresses in such soils the neutral stresses must be known. The methods for computing the pore-water pressure in percolating water will be presented in Chapter XII. However, if the water is in a state of static equilibrium, the computation is so simple that the stress problems can be solved without considering the details of the hydraulics of soils. As an example we investigate the state of stress in a sedimentary deposit which is completely submerged. Figure 7 is a vertical section through this deposit. The total pressure on a horizontal section through the soil at a depth z below the surface of the water is equal to the sum of the weight of the solid soil particles and of the water located above this section. Let

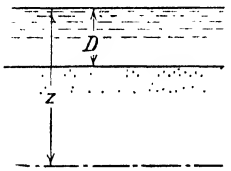

FIG. 7. Section through submerged stratum of sand.

n = the porosity of the deposit (ratio between the volume of the voids and the total volume of the soil)
γ_s = the unit weight of the solid particles
γ_w = the unit weight of the water
D = the depth of the water above the surface of the deposit

The weight of the solid soil particles per unit of area of the horizontal section is $\gamma_s(1 - n)(z - D)$ and the corresponding weight of the water is $n\gamma_w(z - D) + \gamma_w D$. Hence the total normal stress on the horizontal section is

$$\sigma = \gamma_s(1 - n)(z - D) + n\gamma_w(z - D) + \gamma_w D$$

According to equation 6(1) the neutral stress at depth $h_w = z$ below the free water surface is equal to $u_w = \gamma_w z$ and the corresponding effective stress per unit of area is

$$\bar{\sigma} = \sigma - \gamma_w z = (\gamma_s - \gamma_w)(1 - n)(z - D) \qquad [1]$$

In this equation the product $(\gamma_s - \gamma_w)(1 - n)$ represents the weight of the solid particles per unit of volume reduced by the weight of the water displaced by the solid particles. This weight is called the *submerged unit weight* of the soil mass and it is designated by the symbol γ'. From the preceding equation we obtain

$$\gamma' = (\gamma_s - \gamma_w)(1 - n) \qquad [2]$$

Hence the effective normal stress on a horizontal section is

$$\bar{\sigma} = \gamma'(z - D) \qquad [3]$$

It should be emphasized once more that the preceding equations are not valid unless the water contained in the voids of the soil is in a state of perfect equilibrium.

Since the surface of the soil is horizontal the shearing stress on horizontal sections is equal to zero, which shows that the normal stress $\bar{\sigma}$ (eq. 3) represents either the major or the minor principal stress. Hence, if the deposit is in a state of plastic equilibrium, the other extreme principal stress can be computed by means of equation 7(5).

Chapter III

PLASTIC EQUILIBRIUM IN A SEMI-INFINITE MASS WITH A PLANE SURFACE

9. Definitions. A *semi-infinite mass* is a homogeneous mass bounded by a horizontal plane and extending to infinity downward and in every horizontal direction. The unit weight of the material is equal to γ. The state of stress in every point of the deposit can be represented by a circle of stress in Mohr's diagram, an example of which is shown in Figure 6*b*. If none of these circles of stress touches the lines of rupture, M_0M and M_0M_1, the deposit is in a state of elastic equilibrium or in a state of rest. The term "elastic equilibrium" does not imply any definite relation between stress and strain. It merely implies that an infinitely small increase of the stress difference produces no more than an infinitely small increase of the strain. On the other hand, if the circles of stress touch the lines of rupture, an infinitely small increase of the stress differences produces a steady increase of the corresponding strain. This phenomenon constitutes plastic flow. The flow is preceded by a state of plastic equilibrium. (See Art. 7.)

In Mohr's diagram every circle which does not touch or intersect the lines of rupture represents a state of elastic equilibrium. Through any point on the horizontal axis of such a diagram, for instance through point Z in Figure 8*b*, an infinite number of different circles can be traced which satisfy the condition for elastic equilibrium provided one of the principal stresses is equal to the abscissa OZ of the point. The circle C is one of them. Yet, there are only two circles through point Z which satisfy the conditions for plastic equilibrium. One of these circles is located on the right-hand side and the other one on the left-hand side of point Z. Therefore, in contrast to the two states of plastic equilibrium, represented by these two circles, the state of elastic equilibrium or of rest is statically indeterminate. The corresponding ratio σ_{h0}/σ_{v0} between the vertical and the horizontal principal stresses for a mass of soil in a state of rest depends on the type of soil, on the geological origin of the soil, and on the temporary loads which have acted on the surface of the soil. Its value may or may not be independent of depth. If the nature of a mass of soil and its geological history justify the assumption that the ratio σ_{h0}/σ_{v0} is approximately the

same for every point of the mass, it will be called the *coefficient of earth pressure at rest* and designated by the symbol K_0.

In order to define the subject of the following investigations let us assume a homogeneous mass with a horizontal surface. The unit weight of the mass is γ. We propose to establish in every point of the mass a state of incipient plastic failure by subjecting it to a process of deforma-

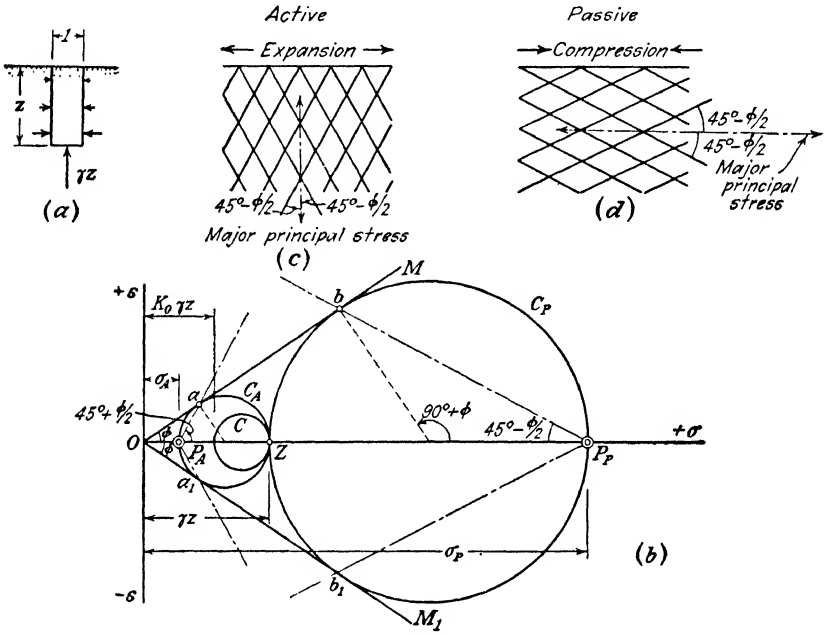

FIG. 8. Semi-infinite cohesionless mass with horizontal surface. (*a*) Stresses at boundaries of prismatic element; (*b*) graphic representation of state of stress at failure; (*c*) shear pattern for active state; (*d*) shear pattern for passive state.

tion parallel to a plane at right angles to the surface of the mass. Such deformation is known as *plane deformation.* Every vertical section through the mass represents a plane of symmetry for the entire mass. Therefore the shearing stresses on vertical and on horizontal sections are equal to zero. Figure 8*a* represents a prismatic block from this mass, with a width equal to unity. The deformation of the mass occurs parallel to the plane of the drawing. Since the shearing stresses on the vertical sides of the prism are equal to zero, the normal stress, σ_v, on the base of the prism is a principal stress. It is equal to the weight of the prism,

$$\sigma_v = \gamma z$$

The initial state of elastic equilibrium of the mass of which the prism

is an element can be changed into a state of plastic equilibrium by two different operations. Either we stretch the entire mass uniformly in a horizontal direction or we compress it uniformly in the same direction. If we stretch it, the pressure on the vertical sides of the prism decreases until the conditions for plastic equilibrium are satisfied while the pressure on the base remains unchanged. Any further stretching merely causes a plastic flow without changing the state of stress. The transition from the state of plastic equilibrium to that of plastic flow represents the *failure* of the mass. On account of the physical properties which we ascribe to the ideal soils it makes no difference whether or not the state of plastic equilibrium is reached simultaneously in every point of the soil. Since the weight of the soil assists in producing an expansion in a horizontal direction the subsequent failure is called *active failure.*

On the other hand, if we compress the soil in a horizontal direction the pressure on the vertical sides of the prism increases while the pressure on its base remains unchanged. Since the lateral compression of the soil is resisted by the weight of the soil the subsequent failure by plastic flow is called a *passive failure.* Since the stresses which start the plastic flow are assumed to be identical with those required to maintain the state of flow, any further compression of the soil has no influence on the state of stress.

Thus the transition of the soil from a state of elastic equilibrium to a state of plastic equilibrium can be accomplished by two different operations, lateral stretching or lateral compression. In either case the transition involves incipient shear failure along two sets of surfaces of sliding (see Figs. 8*c* and 8*d*). The intersection between a surface of sliding and the plane of the drawing is known as a *shear line* or, if curved, as a *curve of sliding.* The shear lines or the curves of sliding which represent the two sets of surfaces of sliding constitute the *shear pattern.*

Our problem consists in determining the stresses associated with the states of plastic equilibrium in the semi-infinite mass and the orientation of the surfaces of sliding. This problem was solved for the first time by Rankine (1857). Therefore the plastic states which are produced by stretching or by compressing a semi-infinite mass of soil parallel to its surface will be called the *active* and the *passive Rankine states,* respectively. In the following article it will be shown that the shear pattern for semi-infinite masses with a horizontal surface consists of two sets of parallel lines which are arranged symmetrically with reference to the vertical direction. For the active Rankine state the surfaces of sliding descend from the surface at an angle $45° + \phi/2$ to the horizontal (see Fig. 8*c*). For the passive Rankine state the sur-

faces of sliding descend at an angle $45° - \phi/2$ to the horizontal (see Fig. 8*d*).

If the active or the passive Rankine state exists only in one part of a semi-infinite mass with a horizontal surface, this part will be called a *Rankine zone.* Within a Rankine zone the shear pattern is identical with one of the two patterns indicated in Figures 8*c* or 8*d*. Thus for instance Figure 15*a* shows an active Rankine zone on the right-hand side and a passive zone on the left-hand side of point *a*.

It is obvious that the operation of stretching or compressing every part of a semi-infinite mass to the point of failure can be performed only in our imagination. There is no process in engineering practice which has any resemblance to such an operation. Nevertheless, by means of a series of mental operations described in Chapter IV it is possible to adapt the results of the following investigations to the solution of several engineering problems of considerable practical importance, such as the computation of the earth pressure on retaining walls or of the ultimate bearing capacity of continuous footings.

10. Active and passive Rankine state in a semi-infinite cohesionless mass. Figure 8*a* shows a prismatic element of a semi-infinite, cohesionless mass with a horizontal surface. The unit weight of the material is equal to γ and the stress conditions for failure are determined by the line of rupture *OM* in Figure 8*b*, with the equation

$$s = \sigma \tan \phi \qquad 5(2)$$

The normal stress on the base of the element is equal to the weight γz of the element. Since the shearing stress on horizontal sections is equal to zero, the normal stress γz on the base of the element is a principal stress. In Mohr's diagram (Fig. 8*b*) this principal stress is represented by the distance *OZ*.

While the mass is in its original state of elastic equilibrium, intermediate between the active and the passive Rankine state, the ratio between the horizontal and the vertical principal stresses is equal to the coefficient of earth pressure at rest, K_0 (see Art. 9), and the horizontal principal stress is

$$\sigma_{h0} = K_0 \gamma z \qquad [1]$$

In order to produce the active Rankine state in the soil, we must stretch it in a horizontal direction until the stress conditions for plastic equilibrium are satisfied. Since the transition to the active Rankine state involves a decrease of the horizontal principal stress at a constant value of the vertical one, the circle of rupture which represents the active Rankine state at depth z is located on the left-hand side of

point Z. It touches the line of rupture OM at point a. The corresponding pole will be called the *active pole*, P_A. According to Article 7 and Figure 5 the pole is located at the intersection of the circle and a line drawn through Z parallel to the plane on which the stress γz acts. Since this plane is horizontal and since, in addition, point Z is located on the horizontal axis, the active pole P_A is located at the point of intersection between the circle and the horizontal axis of Mohr's diagram. The planes of shear failure in Figure 8*c* are parallel to the lines $P_A a$ and $P_A a_1$ in Figure 8*b*. Both sets of planes rise at an angle of $45° + \phi/2$ to the horizontal. From the angles and dimensions indicated in Figure 8*b* we obtain for the normal stress σ_A (active pressure) on a vertical section at depth z below the surface the value

$$\sigma_A = \gamma z \tan^2 \left(45° - \frac{\phi}{2}\right) = \gamma z \frac{1}{N_\phi} \qquad [2]$$

wherein N_ϕ is the flow value (eq. 7(4)).

The pressure per unit of area of a horizontal section at the same depth is γz. The ratio

$$\frac{\sigma_A}{\gamma z} = \tan^2 \left(45° - \frac{\phi}{2}\right) = \frac{1}{N_\phi} \qquad [3]$$

is independent of depth. Hence, the normal stress on a vertical section increases like a hydrostatic pressure in simple proportion to depth. For inclined sections the value σ_A can be determined rapidly by means of Mohr's diagram. The method has been explained in Article 7. It also increases like a hydrostatic pressure in simple proportion to depth.

If the failure of the soil is preceded by lateral compression, involving an increase of the horizontal principal stress, the state of stress at the instant of failure must be represented in Figure 8*b* by the circle through Z which is tangent to the rupture line OM at point b. The corresponding planes of shear (Fig. 8*d*) are parallel to $P_P b$ and $P_P b_1$ (Fig. 8*b*). They form an angle of $45° + \phi/2$ with the vertical. From the angles and stresses indicated in Figure 8*b* we find

$$\sigma_P = \gamma z \tan^2 \left(45° + \frac{\phi}{2}\right) = \gamma z N_\phi \qquad [4]$$

and the ratio between the horizontal and the vertical pressure is

$$\frac{\sigma_P}{\gamma z} = \tan^2 \left(45° + \frac{\phi}{2}\right) = N_\phi \qquad [5]$$

The stresses on inclined sections can be determined by means of Mohr's diagram. Since the ratio $\sigma_P/\gamma z$ is independent of depth, the passive

earth pressure on plane sections increases like the active earth pressure in simple proportion to depth. From equations 3 and 5 we obtain

$$\sqrt{\sigma_A \sigma_P} = \gamma z \qquad [6]$$

In order to investigate the Rankine states in a semi-infinite mass with a plane surface at an angle $\beta < \phi$ to the horizontal, we examine the conditions for equilibrium of the prismatic element shown in Figure 9*a* with vertical sides and a base parallel to the surface of the mass.

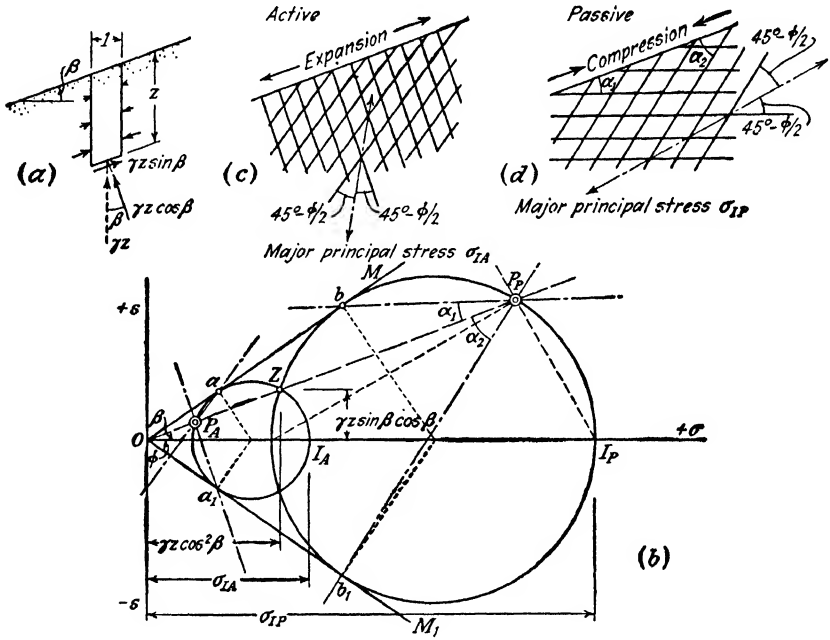

FIG. 9. Semi-infinite cohesionless mass with inclined surface. (*a*) Stresses at boundaries of prismatic element; (*b*) graphic representation of state of stress at failure; (*c*) shear pattern for active state; (*d*) shear pattern for passive state.

Since the state of stress along a vertical section is independent of the location of the section, the stresses on the two vertical sides of the element must be equal and opposite. Hence, the force which acts on the base of the element must be equal and opposite to the weight γz of the element. If we resolve this force into a normal and a tangential component and if we consider the fact that the width of the base of the element is equal to $1/\cos\beta$ we obtain for the normal stress on the base the value

$$\sigma = \gamma z \cos^2 \beta \qquad [7]$$

and for the shearing stress the value

$$\tau = \gamma z \sin \beta \cos \beta \qquad [8]$$

In Mohr's diagram (Fig. 9*b*) the stress conditions for failure are determined by the lines of rupture OM and OM_1. The state of stress on the base of the element at a depth z below the surface is represented by the point Z with an abscissa σ (eq. 7) and an ordinate τ (eq. 8). Since the resultant stress on the base of the prism acts at an angle β to the normal on the base, point Z in Figure 9*b* must be located on a straight line through O, which rises at an angle β to the horizontal. The circle which represents the state of stress at the instant of active failure passes through Z and is tangent to the rupture line OM at point a.

To find the pole P_A we draw through Z a line parallel to the plane on which the stress represented by Z acts, i.e., parallel to the base of the element (see Art. 7 and Fig. 5). This plane rises at an angle β to the horizontal and the line OZ also rises at an angle β to the horizontal. Therefore the pole P_A is located at the point of intersection between the circle and the line OZ. One set of the surfaces of shear in Figure 9*c* is parallel to $P_A a$ and the other set to $P_A a_1$ (Fig. 9*b*). They are oriented at an angle $45° - \phi/2$ to the direction of the major principal stress. The intensity of the major principal stress is determined by the distance OI_A (Fig. 9*b*). In a similar manner we find that the circle of stress for passive failure passes through point Z and touches the line of rupture OM at point b. One of the two sets of surfaces of shear in Figure 9*d* is parallel to $P_P b$ and the other set is parallel to $P_P b_1$ (Fig. 9*b*). The intensity of the major principal stress is determined by the distance OI_P (Fig. 9*b*) and its direction is perpendicular to $P_P I_P$.

Rankine solved the problems illustrated by Figures 8 and 9 analytically. However, by means of the graphical procedures described above the same results may be obtained in a small fraction of the time required for an analytical solution.

11. Plastic equilibrium in surcharged or stratified or partially immersed cohesionless masses with horizontal surfaces. If the surface of the mass shown in Figure 8 carries a uniform surcharge, q per unit of area, the stress on the base of the prism represented in Figure 8*a* becomes equal to

$$\sigma_v = q + \gamma z = \gamma \left(\frac{q}{\gamma} + z \right) \qquad [1]$$

σ_v is a principal stress. For the corresponding normal stress on a

vertical section we obtain by means of equation 7(5) for the active state

$$\sigma_A = \gamma \left(\frac{q}{\gamma} + z\right) \frac{1}{N_\phi} \qquad [2]$$

and for the passive state

$$\sigma_P = \gamma \left(\frac{q}{\gamma} + z\right) N_\phi \qquad [3]$$

wherein

$$N_\phi = \tan^2 \left(45° + \frac{\phi}{2}\right)$$

is the flow value.

The values of σ_A and σ_P of the earth pressure on inclined sections can be determined rapidly by means of Mohr's diagram (Fig. 9*b*).

Figure 10*a* represents a section through a cohesionless deposit with a horizontal surface, which consists of a series of horizontal layers with thicknesses d_1, $d_2 \cdots$, unit weights γ_1, $\gamma_2 \cdots$ and angles of internal friction ϕ_1, $\phi_2 \cdots$. Since the shearing stresses along horizontal sections are equal to zero, the normal stresses on horizontal and vertical sections are principal stresses and their values can be computed by means of equation 7(5). If the mass is in an active state, the normal stress σ_v on horizontal sections corresponds to the major principal stress σ_I in equation 7(5). At any depth $z < d_1$ the vertical principal stress σ_{v1} is $\gamma_1 z$ and the corresponding horizontal principal stress is

$$\sigma_{A1} = \gamma_1 z \frac{1}{N_{\phi 1}} \qquad [4]$$

wherein $N_{\phi 1} = \tan^2 (45° + \phi_1/2)$.

In Figure 10*a* this equation is represented by the straight line ab_1. At any depth $z > d_1$ the vertical principal stress is

$$\sigma_{v2} = \gamma_1 d_1 + \gamma_2 (z - d_1)$$

and the horizontal principal stress at the same depth is

$$\sigma_{A2} = \left[\gamma_1 d_1 + \gamma_2 (z - d_1)\right] \frac{1}{N_{\phi 2}} = \frac{\gamma_2}{N_{\phi 2}} \left[z + d_1 \left(\frac{\gamma_1}{\gamma_2} - 1\right)\right] \qquad [5]$$

wherein $N_{\phi 2} = \tan^2 (45° + \phi_2/2)$.

The corresponding pressure distribution is shown in Figure 10*a* by the straight line $b_2 c_2$, which intersects the reference line ca at point a_1 at an elevation $d_1 (\gamma_1/\gamma_2 - 1)$ above the surface. The value $d_1 (\gamma_1/\gamma_2)$ represents the thickness of a stratum with a unit weight γ_2 which exerts on the surface of the second stratum the same pressure as the stratum which actually rests on this surface.

In Figure 8c the surfaces of sliding rise at an angle of $45° + \phi/2$ to the horizontal. Since each of the layers shown in Figure 10*a* is entirely independent of the others, the orientation of the surfaces of sliding is as indicated in Figure 10*b*.

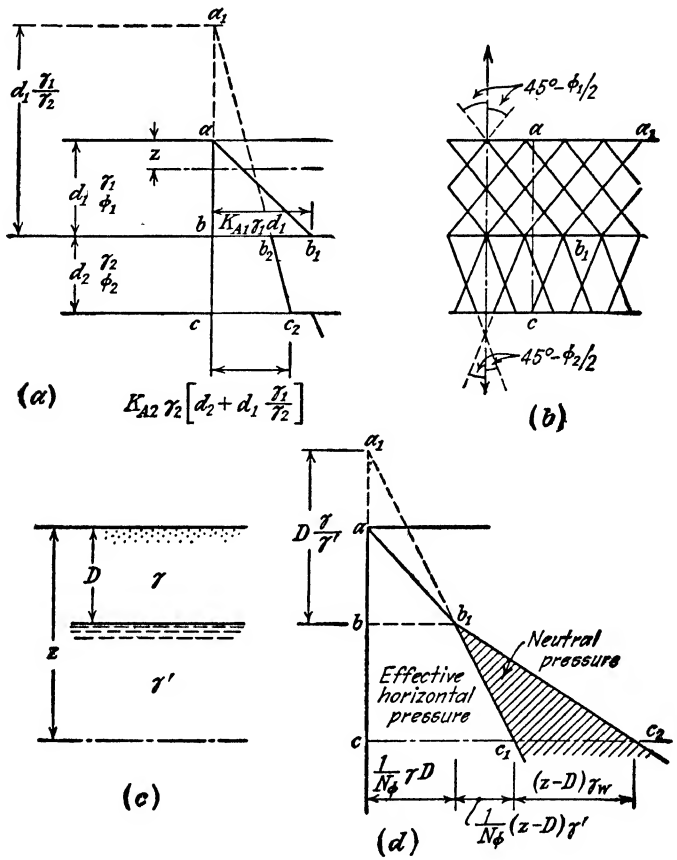

FIG. 10. (*a*) Horizontal pressure acting on vertical section through semi-infinite, cohesionless, stratified mass in active Rankine state; (*b*) corresponding shear pattern; (*c*) vertical section through semi-infinite cohesionless partly submerged mass in active Rankine state; (*d*) horizontal pressure on vertical section through this mass.

Figure 10*c* is a section through a cohesionless deposit whose horizontal surface is located at an elevation D above the water table. When dealing with cohesionless materials such as sand we always operate with effective stresses. That means the shearing resistance of the material is determined by the equation

$$s = \sigma \tan \phi$$

wherein σ represents the effective normal stress and ϕ the angle of internal friction. In accordance with experience we assume that the presence of the water in the voids of the sand has no influence on the angle of internal friction ϕ. The unit weight of the sand above the water table is γ and the neutral stress is equal to zero. The immersed unit weight of the sand as defined by equation 8(2) is γ'. The stresses computed by means of γ' represent effective stresses. Since there are no shearing stresses on horizontal sections, both horizontal and vertical sections are acted upon by principal stresses. The relation between these stresses is determined by equation 7(5)

$$\sigma_{III} = \sigma_I \frac{1}{N_\phi}$$

wherein σ_I is the major and σ_{III} the minor principal stress, and $N_\phi = \tan^2(45° + \phi/2)$. If the deposit is in an active state the vertical principal stress corresponds to the major principal stress σ_I.

Between the surface and the water table the neutral stress is equal to zero, the vertical principal stress is γz, and the horizontal principal stress is

$$\sigma_A = \gamma z \frac{1}{N_\phi} \qquad [6]$$

Below the water table the neutral stress is

$$u_w = (z - D)\gamma_w \qquad [7]$$

wherein γ_w is the unit weight of the water, the effective vertical principal stress is

$$\gamma D + \gamma' (z - D)$$

and the effective horizontal principal stress is

$$\sigma_A = [\gamma D + \gamma'(z - D)]\frac{1}{N_\phi} = \frac{\gamma'}{N_\phi}\left[z + \left(\frac{\gamma}{\gamma'} - 1\right)D\right] \qquad [8]$$

In Figure 10*d* the effective horizontal unit pressure σ_A is represented by the abscissas of the broken line ab_1c_1. At any depth z the neutral pressure u_w (eq. 7) is equal to the horizontal distance between the lines b_1c_1 and b_1c_2 at that depth. The total magnitude and the distribution of the horizontal pressure on the vertical section ac are given by the pressure area acc_2b_1.

12. Active and passive Rankine state in semi-infinite cohesive masses. Figure 11*a* is a vertical section through a prismatic element of a semi-infinite mass of cohesive soil with a horizontal surface. The unit weight of the soil is γ and the stress conditions for failure are determined

by the line of rupture M_0M (Fig. 11*b*) whose equation is

$$s = c + \sigma \tan \phi \qquad 5(1)$$

Since every vertical section through a homogeneous, semi-infinite mass with a horizontal surface represents a plane of symmetry, the

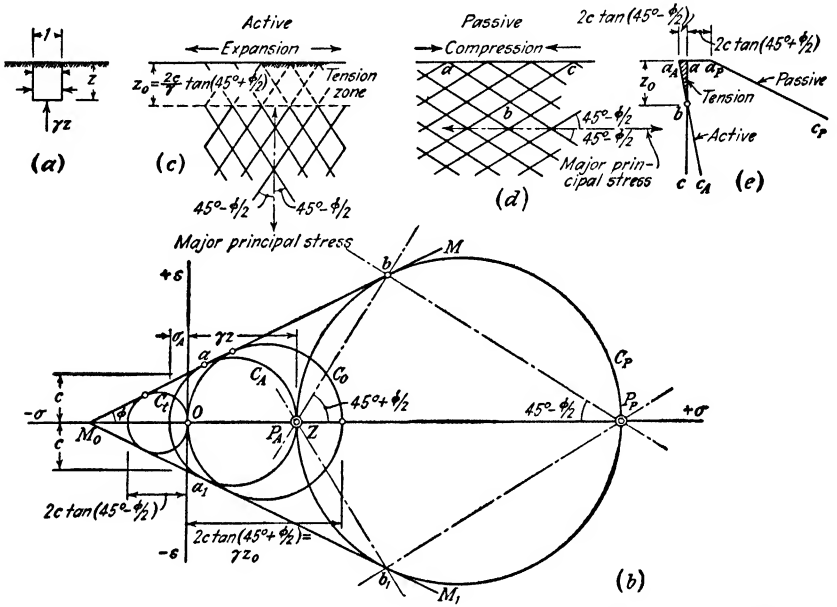

FIG. 11. Semi-infinite cohesive mass with horizontal surface. (*a*) Stresses at boundaries of prismatic element; (*b*) graphic representation of state of stress at failure; (*c*) shear pattern for active state; (*d*) shear pattern for passive state; (*e*) stresses on vertical section through the mass.

shearing stresses on these sections are equal to zero and the normal stresses on both the vertical sides and on the base of the element are principal stresses. The normal stress σ_v on the base of the element is equal to the weight of the prism

$$\sigma_v = \gamma z$$

In Mohr's diagram (Fig. 11*b*) the stress σ_v is represented by the distance OZ. The lines of rupture M_0M and M_0M_1 intersect the vertical axis of the diagram at a distance c from the origin O. The corresponding active Rankine state is represented by a circle C_A located on the left-hand side of point Z, tangent to the lines of rupture. If this circle intersects the horizontal axis on the left-hand side of the origin O, as shown in Figure 11*b*, the horizontal principal stress at depth z is a

tensile stress. For $z = 0$ we obtain the circle C_t, whose diameter represents the simple tensile strength of the soil. As z increases, the corresponding tensile stress decreases, and at a certain depth z_0 the tensile stress becomes equal to zero. The state of stress at which the soil starts to flow at a depth z_0 is represented by a circle C_0 which passes through the origin and touches the lines of rupture. From the geometrical relations indicated in Figure 11*b* it may be shown by trigonometry that

$$z_0 = \frac{2c}{\gamma} \tan\left(45° + \frac{\phi}{2}\right) = \frac{2c}{\gamma}\sqrt{N_\phi} \qquad [1]$$

Between the surface and depth z_0 the active Rankine state involves a state of tension in a horizontal direction. For the ideal plastic material subject to investigation it is assumed that a state of tension can exist permanently and that a plastic flow can take place in the tension zone without causing a decrease in the tensile strength of the soil. However, in a real soil tensile stresses always lead sooner or later to the formation of open tension cracks. The investigation of the influence of such cracks on the state of stress in the deposit is beyond the scope of the present theory. The practical consequences of the formation of the fissures will be discussed in Articles 57 and 62.

If z is greater than z_0 the entire corresponding circle of rupture is located on the right-hand side of the origin O. For any depth z the pole P_A coincides with the left-hand point of intersection between the circle and the horizontal axis. Figure 11*c* shows the two sets of planes of shear for $z > z_0$. They are parallel to the lines $P_A b$ and $P_A b_1$ in Figure 11*b*, which connect the pole with the points of contact between the circle of stress and the lines of rupture. They form an angle of $45° - \phi/2$ with the vertical.

For the passive Rankine state, produced by a lateral compression of the soil, all the circles of stress which represent a state of incipient failure are located entirely on the right-hand side of point O, because in this state the gravity stress γz is the smallest principal stress. As a consequence the soil fails at every depth by shear. The circle C_P represents the state of stress at failure for an arbitrary depth z. The lines of rupture are tangent to it at b and b_1 and the two sets of shear planes (Fig. 11*d*) are parallel to the lines $P_P b$ and $P_P b_1$ (Fig. 11*b*). They intersect the horizontal direction at an angle $45° - \phi/2$.

The earth pressure on inclined sections can be determined by means of Mohr's diagram. The normal stresses on vertical sections are principal stresses. Hence, they can be computed by means of equation 7(3). Substituting σ_A for the minor principal stress σ_{III} in equation

7(3) and γz for σ_I we obtain for the active earth pressure per unit of area of a vertical section at a depth z below the surface

$$\sigma_A = -2c\frac{1}{\sqrt{N_\phi}} + \gamma z\frac{1}{N_\phi} \qquad [2]$$

wherein $N_\phi = \tan^2(45° + \phi/2)$ represents the flow value. The passive earth pressure is obtained by substituting σ_P for the major principal stress σ_I in equation 7(3) and γz for the minor principal stress σ_{III}. Thus we get

$$\sigma_P = 2c\sqrt{N_\phi} + \gamma z N_\phi \qquad [3]$$

According to these equations both the active and the passive earth pressure can be resolved into one part which is independent of depth and a second part which increases like a hydrostatic pressure in simple proportion to depth. The second part, $\gamma z/N_\phi$ of σ_A (eq. 2), is identical with the active earth pressure on vertical sections through a cohesionless mass whose unit weight is γ and whose angle of shearing resistance is ϕ. The second part, $\gamma z N_\phi$, of the passive earth pressure σ_P (eq. 3) is identical with the passive earth pressure in the cohesionless mass described above. In Figure 11*e* the horizontal unit pressure for the active state σ_A is represented by the abscissas of the straight line $a_A c_A$ and the horizontal unit pressure for the passive state by those of the line $a_P c_P$.

If the surface of the deposit carries a uniform surcharge q per unit of area, we obtain from equation 7(3) for vertical sections through the deposit

$$\sigma_A = -2c\frac{1}{\sqrt{N_\phi}} + \gamma\left(z + \frac{q}{\gamma}\right)\frac{1}{N_\phi} \qquad [4]$$

and

$$\sigma_P = 2c\sqrt{N_\phi} + \gamma\left(z + \frac{q}{\gamma}\right)N_\phi \qquad [5]$$

Figure 12 illustrates the graphical method of determining the state of stress in a cohesive deposit on the verge of passive failure, of which the plane surface rises at an angle β, smaller than ϕ, to the horizontal. In Mohr's diagram (Fig. 12*b*) all the points which represent the stress on sections parallel to the surface are located on a line through O, which rises at an angle β to the horizontal axis. The reason has been explained in the text to Figure 9*b*. (See Art. 10.) The circle C_0 which touches both the vertical axis and the lines of rupture represents the state of stress at a depth z_0 below the surface. The active pole P_A ($z = z_0$) coincides with the origin O. Hence, at depth z_0 the major principal stress is vertical and the minor principal stress is equal to zero. From the geometrical relationship shown in Figure 12*b* we obtain

$$z_0 = \frac{2c}{\gamma}\tan\left(45° + \frac{\phi}{2}\right) = \frac{2c}{\gamma}\sqrt{N_\phi}$$

which is identical with equation 1. Between the surface and depth z_0 the active Rankine state involves a state of tension. Beyond depth z_0 both principal stresses are compressive stresses. With increasing values of z the active pole P_A moves along the line which rises through O at an angle β to the horizontal. Hence, with increasing depth the orientation of the surfaces of sliding with respect to the vertical

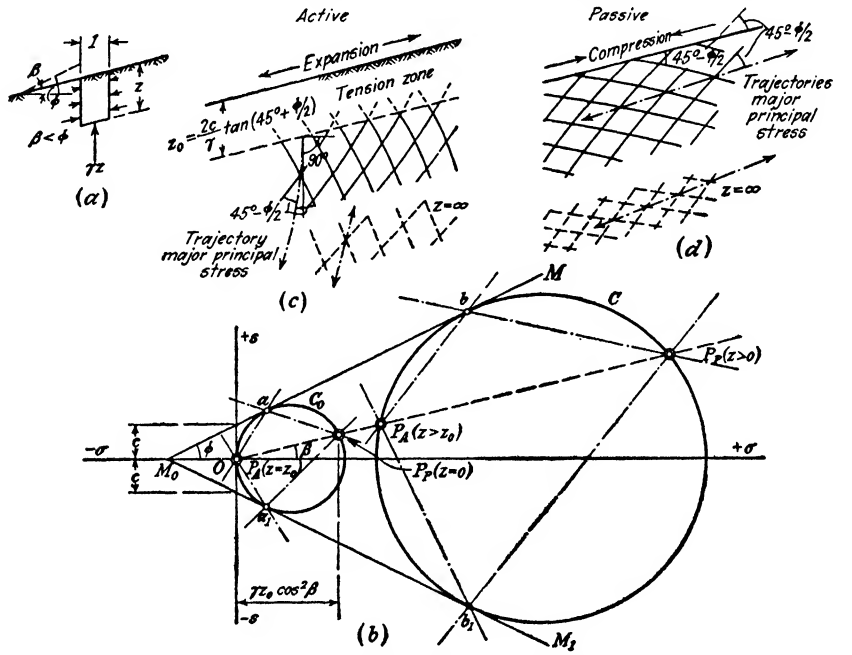

FIG. 12. Semi-infinite cohesive mass whose surface rises at an angle $\beta < \phi$. (*a*) Stresses at boundaries of prismatic element; (*b*) graphic representation of state of stress at failure; (*c*) shear pattern for active state; (*d*) shear pattern for passive state.

direction changes. For $z = \infty$ it becomes identical with the orientation of the surfaces of sliding in a cohesionless mass with an angle of internal friction ϕ whose surface rises at an angle β to the horizontal, because at infinite depth the cohesion is negligible compared to the shearing resistance due to internal friction. As a consequence the surfaces of sliding are slightly curved, as shown in Figure 12*c*. The dotted lines at the lower rim of the figure represent the orientation of the surfaces of sliding at infinite depth. In the passive Rankine state the surfaces of sliding are also curved, but they intersect the surface of the deposit at an angle of $45° - \phi/2$. With increasing depth the surfaces of sliding approach the position which they occupy in an equivalent cohesionless deposit.

If the surface of the cohesive mass rises at an angle $\beta > \phi$ the investigation leads to the diagram shown in Figure 13. All the points which represent the state o stress on a section parallel to the surface of the soil are located on a line ON through point O, which rises at an angle β to the horizontal axis. This line intersects the line of rupture M_0M at a point b. On the basis of the geometrical relationships represented in Figure 13*b* it may be shown that the normal stress represented by

the abscissa of point b is equal to

$$\sigma = \frac{c}{\tan\beta - \tan\phi} \qquad [6]$$

and that the corresponding depth is equal to

$$z_1 = \frac{c}{\gamma} \frac{1}{(\tan\beta - \tan\phi)\cos^2\beta} \qquad [7]$$

The circle of rupture C_1 through point b intersects the line ON at the point P_1. According to the theory illustrated by Figure 5 this point represents the pole of the circle C_1. If we connect this pole with the points of contact b and b_1 we obtain

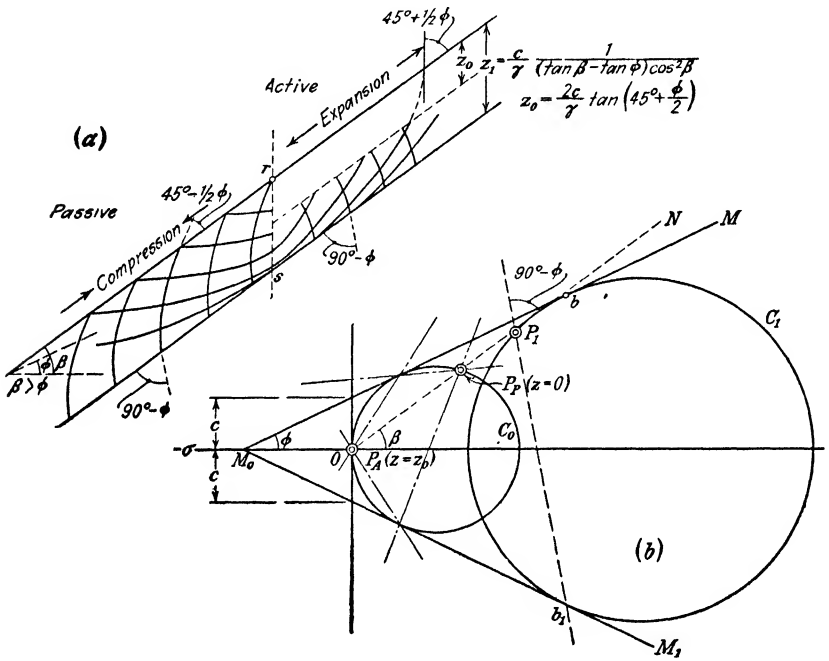

FIG. 13. Semi-infinite cohesive mass whose surface rises at an angle $\beta > \phi$. (a) Right-hand section shows shear pattern for active and left-hand section for passive state of failure; below depth z_1 the mass is not in a state of equilibrium; (b) graphic representation of state of stress at failure.

the direction of the corresponding surfaces of sliding. One of these surfaces is very steep and the other one is parallel to the surface of the soil. On the right-hand side of point b the line ON is located above the line of rupture OM. Hence, below depth z_1 the soil must be in a state of plastic flow, because on the right-hand side of b the state of stress represented by the line ON becomes inconsistent with the conditions for equilibrium.

In the active Rankine state, the soil located between the surface and a depth

z_0 fails by tension. From the geometrical relationships shown in Figure 13*b* we obtain

$$z_0 = \frac{2c}{\gamma} \tan\left(45° + \frac{\phi}{2}\right) = \frac{2c}{\gamma} \sqrt{N_\phi}$$

This equation is identical with equation 1. Below depth z_0 there is no tension and the soil fails by shear. The state of stress at depth z_0 is represented by the circle C_0. The corresponding surfaces of sliding are shown on the right-hand side of Figure 13*a*. In the passive Rankine state the entire mass is under compression. The corresponding surfaces of sliding are shown on the left-hand side of Figure 13*a*. At a depth z_1 the surfaces of sliding for active and for passive failure are identical. This is indicated by the fact that there is only one circle of rupture to which the line of rupture is tangent at point *b* in Figure 13*b*. The same figure shows that at the depth z_1 the states of stress corresponding to these two types of failure are identical.

The analytical solution of the problems illustrated by Figures 11 to 13 has been worked out by J. Résal (1910). Frontard (1922) derived the equations of the surfaces of sliding shown in Figure 13*a*. He attempted to utilize his solution for the purpose of ascertaining the critical height of slopes of cohesive earth. However, his results are open to serious objections (Terzaghi 1936*a*).

Chapter IV

APPLICATION OF GENERAL THEORIES TO PRACTICAL PROBLEMS

13. Stress and deformation conditions. If the solution of a problem satisfies the fundamental equations of a general theory, such as the theory of elasticity or of a theory of plasticity, it also satisfies the condition that the computed state of stress and strain in the interior of the body subject to investigation is compatible with the assumptions regarding the mechanical properties of the material on which the theory is based. However, in connection with a specific problem the computed state of stress and strain must also be compatible with the conditions which are known in advance to exist along the boundaries of the body subject to investigation. These boundary conditions can be divided into two groups, the *boundary stress conditions* and the *boundary deformation conditions.* They will briefly be called the *stress conditions* and the *deformation conditions.*

In connection with elasticity problems there is seldom any doubt regarding the nature of stress conditions, nor can there be any doubt regarding the deformation conditions. As an example we consider the problem of computing the state of stress produced by a surcharge q per unit of area on a small portion of the upper surface of an elastic layer whose lower surface rests on a rigid base. There is no doubt that the solution must satisfy the condition that the vertical displacement of the base of the elastic layer must everywhere be equal to zero.

On the other hand, in connection with plasticity problems of soil mechanics, the deformation conditions have seldom received the attention which they deserve. As an example of the influence of the deformation conditions on the state of stress in a mass of soil on the verge of sliding, let us consider the practical applications of the theory of plastic equilibrium in semi-infinite cohesionless masses, described in Article 10. It has been emphasized that the transition of semi-infinite masses from a state of elastic into a state of plastic equilibrium can only be accomplished by an imaginary process of stretching or compressing the soil which is without any parallel in the physical world. The states of plastic equilibrium produced in soils by engineering operations never extend beyond the boundaries of very narrow zones. In order to apply the

theory of plastic equilibrium in semi-infinite masses to engineering practice, we investigate the conditions for the equilibrium of a wedge-shaped section *abc* (Fig. 14*a*) of a semi-infinite mass in an active Rankine state. This section is assumed to be located between a surface of sliding *bc* and a vertical section *ab*. During the transition of the mass from its original state into the active Rankine state, the soil contained within the section undergoes elongation in a horizontal direction. The amount of stretching is represented by the width of the shaded area aa_1b (Fig. 14*a*). At any depth z below the surface the width Δx of the shaded area is equal to the width x of the wedge at that depth times the horizontal stretching ϵ per unit of length which is required to transfer the soil at depth z from its original state of elastic equilibrium to that of plastic equilibrium. Hence at depth z the width of the shaded area is equal to $\epsilon \cdot x$. The value ϵ depends not only on the type of soil, on its density, and on the depth z but also on the initial state of stress. Hence the only general statement which can be made concerning the shaded area is that its width must increase from zero at point *b* to a maximum at point *a*. For a sand with a uniform density one can assume with crude approximation that ϵ is independent of depth z. On this assumption the shaded area is triangular as shown in the figure. For a given initial state of stress in the sand the value ϵ decreases with increasing density of the sand. As soon as the active state is reached, the resultant F of the stresses on the surface *bc* acts at an angle ϕ to the normal on *bc* (Fig. 14*a*). The stress on *ab* is horizontal and increases directly with depth, giving a resultant P_A which acts at the top of the lower third of *ab*. The weight of the soil in the wedge is W. The three forces F, W, and P_A constitute a set of concurrent forces in equilibrium.

If we replace the overstressed soil below and to the right of *bc* by a mass of soil in an elastic state of stress, without changing the state of stress and deformation within the zone *abc*, the force F retains both its direction and magnitude. The weight of the soil in the zone *abc* remains unchanged. Hence, if we replace the soil on the left side of *ab* by an artificial support without changing the state of stress and deformation within the zone *abc*, the equilibrium of the system requires that the support furnish the horizontal reaction P_A described above. In other words, if the substitutions which we have made do not change the state of stress and deformation within the zone *abc* the forces F, W, and P_A are identical with those described above.

If the soil has been deposited behind an artificial support *ab* the preceding conclusion retains its validity provided the following conditions are satisfied. First, the presence of the artificial support should not produce any shearing stresses along *ab*. This is the boundary stress

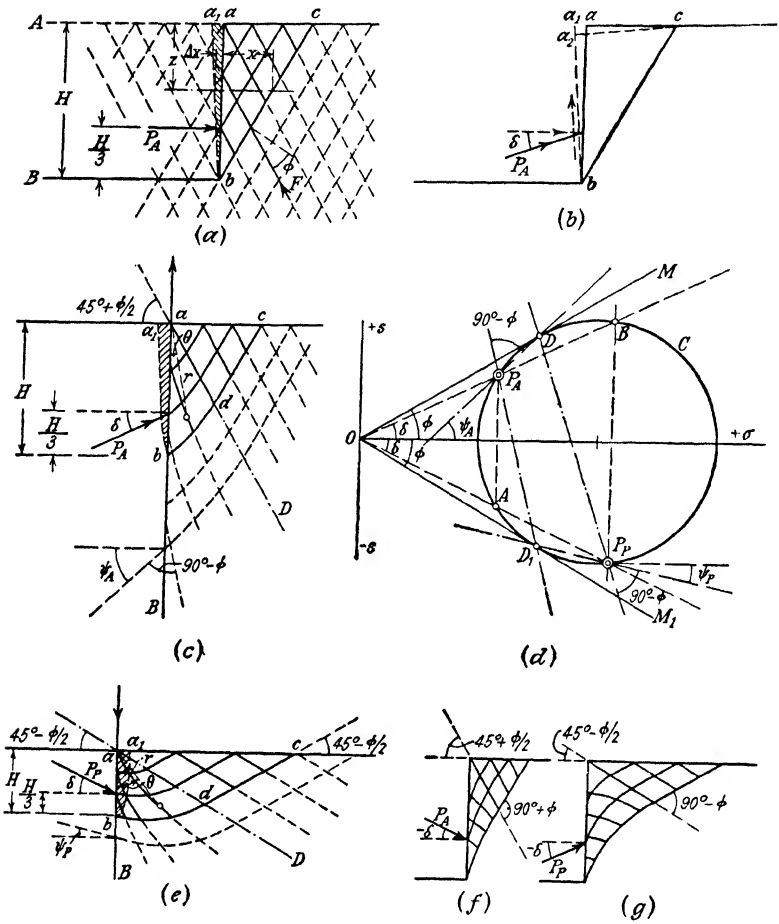

FIG. 14. Diagrams pertaining to local state of plastic equilibrium in ideal sand. Shaded areas in (*a*), (*c*), and (*e*) represent minimum displacement or deformation of an originally vertical plane required to produce such a state. The type of plastic equilibrium is indicated by corresponding shear pattern. (*a*) Shear pattern corresponding to active state along frictionless vertical surface; (*b*) diagram showing that a yield of rough surface by tilting produces positive wall friction; (*c*) shear pattern corresponding to active state along rough surface if wall friction is positive; (*d*) graphic method for determining slope of surfaces of sliding at points of intersection with rough surface; (*e*) shear pattern corresponding to passive state along rough surface if wall friction is positive; (*f*) shear pattern for active and (*g*) for passive state along rough surface, if wall friction is negative.

condition. Second, the support must yield during or after the process of backfilling from its original position *ab* into a position at or beyond the line a_1b in Figure 14*a*. This conclusion is based on the following reasoning. It has been observed that the lateral earth pressure on the back of a perfectly rigid, fixed wall is very much greater than the active earth pressure. In order to pass into the active Rankine state the soil adjoining the wall must undergo a lateral expansion at least as great as that required to produce the same change in the state of stress in the triangular section *abc* of the semi-infinite mass shown in Figure 14*a*. This expansion requires the lateral yield of the wall mentioned above. This is the boundary deformation condition. If either one of these two conditions is not satisfied, the identification of the backfill of an artificial support with the section *abc* in Figure 14*a* is not justified. It is, for instance, conceivable that a lateral support is retained at point *a* in Figure 14*a* while the lower end is capable of yielding far beyond point *b*. On this condition, the upper part of the bank cannot expand in a horizontal direction, which prevents this part of the bank from passing into an active Rankine state. Yet, if the lower part of the support yields far enough another type of plastic equilibrium will develop. In Chapter V it will be shown that the lateral confinement of the upper part of the supported soil induces arching which increases the lateral pressure on the upper part of the support and relieves the pressure on the lower part. The surface of sliding through the foot of the lateral support is strongly curved and it intersects the surface of the soil at right angles. Hence, if the upper edge of the lateral support cannot advance into the position indicated by a_1 in Figure 14*a*, neither the shape of the sliding wedge nor the orientation of the forces which act on the wedge have any resemblance to what is shown in Figure 14*a*, though all the other conditions for the validity of the preceding reasoning, including the absence of shearing stresses on *ab* (Fig. 14*a*) may be satisfied.

Finally, if the wall can yield only to a position intermediate between *ab* and a_1b (Fig. 14*a*) the conditions for a failure of the earth will nowhere be satisfied, and the unit pressure on *ab* will have some value intermediate between the unit earth pressure at rest, determined by the equation

$$\sigma_{h0} = K_0 \gamma z \qquad 10(1)$$

and the unit active earth pressure

$$\sigma_A = \gamma z \tan^2\left(45° - \frac{\phi}{2}\right) = \gamma z \frac{1}{N_\phi} \qquad 10(2)$$

A state of plastic equilibrium will nowhere exist.

The preceding analysis demonstrates that the practical importance of the boundary deformation conditions cannot possibly be overemphasized. If the practical implications of these conditions had been recognized, engineers would never have been tempted to apply Rankine's or Coulomb's theory of earth pressure on retaining walls to the computation of the earth pressure on the timbering of cuts or on tunnel tubes. Neither the conditions which determine the distribution of the earth pressure on the timbering of cuts nor those which determine the intensity and the distribution of the earth pressure on tunnel tubes have any resemblance to the fundamental conditions for the validity of Rankine's theory and its generalizations. In order to prevent the flagrant misapplication of theories of this or a similar type, each of the following theoretical investigations will be preceded by a complete statement of the conditions and assumptions. Every one of the theories contained in the following chapters of this volume can be relied upon to give sufficiently accurate results when applied to practical cases provided the field conditions correspond at least approximately to the stated conditions and assumptions. Otherwise the theory is inapplicable regardless of how sound it may be within the range of its validity.

14. Rankine's theory of earth pressure on retaining walls. The best known application of the principles explained in the preceding article is Rankine's theory of the earth pressure on retaining walls. If a retaining wall yields, the backfill of the wall expands in a horizontal direction, whereupon the lateral pressure exerted by the soil on the back of the wall gradually decreases and approaches a lower limiting value, which is called the *active earth pressure.* On the other hand, if we force the wall in a horizontal direction towards the backfill, thus compressing the soil in a horizontal direction, the resistance of the soil increases until it assumes an upper limiting value, the *passive earth pressure.* When the movement of the wall brings about either of these two limiting values, the soil fails by plastic flow. To illustrate the essential characteristics and defects of Rankine's theory we compute the earth pressure exerted by a cohesionless backfill with a horizontal surface on the vertical back of an artificial support with a height H. The shearing resistance of the soil is determined by the equation

$$s = \sigma \tan \phi \qquad 5(2)$$

and the unit weight is γ. According to Rankine's theory the lateral pressure on ab (Fig. 14a) is identical with the stresses on a vertical section through a semi-infinite mass with a horizontal surface, for an active Rankine state. The shearing stresses on such a section are

always equal to zero. Hence the vertical section is acted upon only by normal stresses.

In the case of active failure the normal stress on a vertical section is

$$\sigma_A = \gamma z \tan^2\left(45° - \frac{\phi}{2}\right) = \gamma z \frac{1}{N_\phi} \qquad 10(2)$$

wherein $N_\phi = \tan^2 (45° + \phi/2)$ represents the flow value and the total pressure on the section with a height H is per unit length of the wall

$$P_A = \int_0^H \sigma_A \, dz = \tfrac{1}{2}\gamma H^2 \frac{1}{N_\phi} \qquad [1]$$

If the failure is due to lateral thrust (passive failure) we obtain

$$\sigma_P = \gamma z N_\phi \qquad 10(4)$$

and

$$P_P = \int_0^H \sigma_P \, dz = \tfrac{1}{2}\gamma H^2 N_\phi \qquad [2]$$

In both cases the distribution of the vertical pressure over the face ab is hydrostatic and the point of application of the pressure is at a height $H/3$ above the base of the section.

If the backfill material is cohesive, its shearing resistance is

$$s = c + \sigma \tan \phi$$

At the instant of active failure the normal stresses on a vertical section are

$$\sigma_A = -2c \frac{1}{\sqrt{N_\phi}} + \gamma z \frac{1}{N_\phi} \qquad 12(2)$$

and

$$P_A = \int_0^H \sigma_A \, dz = -2cH \frac{1}{\sqrt{N_\phi}} + \tfrac{1}{2}\gamma H^2 \frac{1}{N_\phi} \qquad [3]$$

The distribution of the active pressure on the vertical face ab is represented by the pressure line $a_A c_A$ in Figure 11*e*. The point of application of the pressure is located at a distance less than $H/3$ above the base of the section. If

$$H = H_c = \frac{4c}{\gamma}\sqrt{N_\phi}$$

the total lateral pressure on the face ab is equal to zero. According to Article 12 the soil is in a state of tension to a depth

$$z_0 = \frac{2c}{\gamma}\sqrt{N_\phi} \qquad 12(1)$$

Combining this equation with the preceding one, we obtain

$$H_c = \frac{4c}{\gamma}\sqrt{N_\phi} = 2z_0 \qquad [4]$$

If the earth fails by lateral compression (passive failure) the stress on a vertical section at depth z is

$$\sigma_P = 2c\sqrt{N_\phi} + \gamma z N_\phi \qquad 12(3)$$

and

$$P_P = \int_0^H \sigma_P \, dz = 2cH\sqrt{N_\phi} + \tfrac{1}{2}\gamma H^2 N_\phi$$

The distribution of the passive earth pressure over the vertical face ab is shown by the pressure line $a_P c_P$ in Figure 11*e*. The point of application of the pressure is located within the middle third of the height H, because the pressure area $aa_P c_P c$ shown in Figure 11*e* is trapezoidal.

If the soil carries a uniformly distributed surcharge q per unit of area, the horizontal pressure per unit of area at depth z is

$$\sigma_P = 2c\sqrt{N_\phi} + \gamma\left(z + \frac{q}{\gamma}\right)N_\phi \qquad 12(5)$$

and the total passive earth pressure is

$$P_P = 2cH\sqrt{N_\phi} + \tfrac{1}{2}\gamma H^2\left(\frac{2q}{\gamma H} + 1\right)N_\phi \qquad [6]$$

Rankine has also derived equations for computing the earth pressure of backfills with an inclined surface on walls with an inclined back. Since these equations are rather complicated it is decidedly preferable to determine the corresponding Rankine pressure and the direction of this pressure graphically, by means of Mohr's diagram, as explained in Chapter III.

15. Influence of wall friction on the shape of the surface of sliding. In connection with retaining walls, one of the boundary conditions for the validity of equations 14(1) and 14(2) is never satisfied because there are no retaining walls with a perfectly smooth back. The effect of the roughness of the back of the wall on the active earth pressure is illustrated by Figure 14*b*. It represents a section through a cohesionless fill, supported along a vertical face ab. The lateral yield of the wall causes a subsidence of the top surface of the wedge abc, as indicated by the slope of the line ca_2 (Fig. 14*b*). The downward movement of the soil along the rough face ab changes the direction of the earth pressure on ab from its original horizontal position into a position at an angle δ

to the normal on ab as indicated in the figure. The angle δ is called the *angle of wall friction*. For active pressure, δ is considered positive when it is measured downward from the normal as in the figure.

This stipulation has no relation to the convention regarding the sign of the shearing stresses in Mohr's diagram. In Mohr's diagram a shearing stress is positive if the corresponding resultant stress deviates from its normal component in a clockwise sense. In connection with the active earth pressure on retaining walls, the wall friction is positive if it acts in an upward direction. As shown in Figure 14*b* the positive wall friction corresponds in Mohr's diagram to a negative shearing stress. On the other hand, if we assume that the soil is located on the left-hand side of the wall, it would appear in Mohr's diagram as a positive shearing stress. The angle of wall friction can also be negative. Negative wall friction develops if the wall, owing to a heavy surcharge established on its crest or to some other cause, settles more than the fill. In any case the existence of wall friction invalidates Rankine's equation 14(1) because this equation is based on the assumption that $\delta = 0$.

If δ is not equal to zero, the determination of the real shape of the surface of sliding is very difficult. The problem has been solved rigorously only on the assumption that the cohesion of the soil is equal to zero. Nevertheless, the equations are far too complicated for practical application. The following paragraphs contain a summary of the results of the investigations of Reissner and of other workers in this field. On account of the elementary treatment of the subject, some of the statements must be accepted without rigorous proof.

Figure 14*c* is a vertical section through a semi-infinite mass of ideal sand. When this mass is deformed by stretching it uniformly in a horizontal direction the material passes through the active Rankine state and fails along two sets of plane surfaces of sliding such as those on the right-hand side of the line aD. If we introduce into this mass a diaphragm aB with rough faces and pull the diaphragm, the state of stress in the sand changes only in the wedge-shaped space DaB between the diaphragm and the Rankine surface of sliding aD through the upper edge a of the diaphragm.

In order to visualize the mechanical causes of this important feature of the state of plastic equilibrium, let us assume that we increase gradually the angle of wall friction from zero to its ultimate value δ, while the mass of sand remains in a state of plastic equilibrium. During this process the shearing stresses on every plane section through a located between the diaphragm and aD will increase. However, on the surface of sliding aD the shearing stresses remain unchanged, because the mass of sand located above aD was from the very outset on the verge of sliding along aD in a downward direction.

The resultant P_A of the lateral pressure on any part of the diaphragm slopes at an angle δ to the horizontal, as indicated in the figure.

The angle at which the surfaces of sliding join the face of the diaphragm can be determined rapidly by means of Mohr's diagram (Fig. 14*d*). In this diagram the circle C represents the state of stress for some point next to the right-hand face of the diaphragm. Since the resultant stress on the surface *ab* in Figure 14*c* deviates from the normal on *ab* in a counterclockwise sense, the corresponding shearing stress must be introduced into Mohr's diagram (Fig. 14*d*) with a negative sign (see Art. 7). Point A, which represents the state of stress on this face of the diaphragm, is located on a straight line which passes through point O and descends toward the right at an angle δ to the horizontal. This line intersects the circle at two points. Point A is the left-hand point of intersection because the diaphragm is acted upon by the active earth pressure. The pole P_A for active earth pressure is located on the line AP_A (Fig. 14*d*) parallel to aB (Fig. 14*c*). If we connect the pole P_A with the points of contact D and D_1 between the circle C and the lines of rupture OM and OM_1, we obtain the lines P_AD and P_AD_1. These two lines determine the orientation of the surfaces of sliding immediately adjacent to the right-hand face of the diaphragm.

Reissner (1924) has shown that the members of both sets of surfaces of sliding located within the wedge-shaped zone *abD* must be curved. The pressure of the sand on the rough diaphragm has been investigated in succession by Kármán (1926), Jáky (1938), and Ohde (1938). The equations which have been obtained for the earth pressure are too complicated for practical use. However, the following general results are of practical interest. If the plastic equilibrium exists in every point of a semi-infinite mass of sand which is acted upon by a rough diaphragm, the shape of the members of each one of the two sets of surfaces of sliding located within the zone *BaD* can be expressed by an equation $r = r_0 f(\theta)$, wherein r is the distance of a point of the surface from a (Fig. 14*c*), and θ is the corresponding center angle; r_0 represents the value of r for $\theta = 0$. This characteristic property of the surfaces of sliding involves an increase of the earth pressure in simple proportion to depth. Hence the normal component p_{An} of the active earth pressure per unit of area of the diaphragm can be expressed by an equation

$$p_{An} = \gamma z K_A \qquad [1]$$

wherein γ is the unit weight of the soil, z the depth below the surface, and K_A a dimensionless coefficient, called the *coefficient of active earth pressure*, whose value depends only on the angles ϕ and δ. If the angle of wall friction δ is equal to zero, the earth pressure becomes identical with the active Rankine pressure σ_A (eq. 10(2)) and

$$K_A = \frac{1}{N_\phi} = \tan^2\left(45° - \frac{\phi}{2}\right) \qquad [2]$$

wherein N_ϕ is the flow value, equal to $\tan^2 (45° + \phi/2)$.

The shape of the surfaces of sliding is similar to that shown in Figure 14*c*. With decreasing values of δ the curved part of the surfaces becomes

flatter and for $\delta = 0$ the surfaces are perfectly plane, as shown in Figure 14*a*.

By repeating the reasoning which has led to Rankine's earth pressure theory (see Art. 13) we are justified in drawing the following conclusion from Figure 14*c*. If a wall with a rough back yields in such a manner that the deformation of the wedge-shaped mass of sand adjoining the wall is identical with that of the sand located within the zone *abc* in Figure 14*c*, the sand fails along a surface of sliding similar to *bc* (Fig. 14*c*) and the distribution of the earth pressure on the back of the wall will be hydrostatic. The transition of the semi-infinite mass from its initial state into a state of active plastic equilibrium requires that the horizontal stretching of the mass exceed in every point of the mass a certain lower limiting value per unit of length which depends on the elastic properties of the sand and on the initial state of stress. The corresponding horizontal deformation of the sand located within the zone *abc* (Fig. 14*c*) is indicated by the shaded area. Any deformation in excess of that represented by the shaded area has no influence on the state of stress in the sand. Hence, if the wall yields into any position beyond a_1b, the sand fails by sliding along the surface *bc* (Fig. 14*c*) and the distribution of the earth pressure on *ab* will be hydrostatic. On the other hand, if the wall yields, for instance, by tilting around the upper edge *a*, the shape of the surface of sliding must be different from *bc* and the distribution of the earth pressure depends on the type of yield.

The preceding reasoning can be applied without any modification to a backfill acted upon by negative wall friction and to the passive earth pressure. Figure 14*f* shows the shear pattern for active plastic equilibrium and negative wall friction.

If a semi-infinite mass of sand, located on both sides of a rough stationary diaphragm, is transferred by horizontal compression into a state of passive plastic equilibrium, the shear pattern shown in Figure 14*e* is obtained. Since the lateral compression causes the sand to rise in a vertical direction while the diaphragm remains stationary, the resultant passive earth pressure deviates from its normal component in an upward direction. The corresponding angle of wall friction δ is called positive. The influence of the wall friction on the state of stress in the sand does not extend beyond the Rankine surface *aD* through the upper rim of the diaphragm, because at any value of δ the sand located above *aD* is on the verge of sliding along *aD* in an upward direction. Within the wedge-shaped zone *aBD* both surfaces of sliding are curved. Their shape has been investigated by Jáky (1938) and Ohde (1938). The equation for each set can be written in the form $r = r_0 f(\theta)$, wherein r is the distance of a point from *a* and θ the corresponding center angle.

At any depth z below the surface the normal component p_{Pn} of the passive earth pressure per unit of area of the diaphragm is equal to

$$p_{Pn} = \gamma z K_P \qquad [3]$$

wherein K_P, called the *coefficient of passive earth pressure,* depends only on ϕ and δ. If the diaphragm is pulled out of the sand, the angle of wall friction is negative and the shear pattern shown in Figure 14*g* is obtained. The angle at which the surfaces of sliding intersect the diaphragm can be determined by means of Mohr's diagram (Fig. 14*d*). If $\delta = 0$ we get

$$K_P = N_\phi = \tan^2\left(45° + \frac{\phi}{2}\right) \qquad [4]$$

Point B (Fig. 14*d*), whose ordinate represents the shearing stress on ab (Fig. 14*e*), is located on a line OB which rises at an angle δ. The corresponding pole P_P is located on a line BP_P, which is parallel to aB in Figure 14*e*. Along the right-hand side of the diaphragm one set of surfaces of sliding is parallel to P_PD in Figure 14*d* and the other set is parallel to P_PD_1.

In Figure 14*e* the minimum lateral displacement of ab required to produce the state of plastic equilibrium associated with the shear pattern shown in the figure is represented by the shaded area aa_1b. If the section ab is advanced toward the soil into any position beyond a_1b, the surface of sliding will be similar to bc and the distribution of the passive earth pressure over ab will be hydrostatic, as indicated by equation 3. On the other hand, if the face ab is advanced, for instance by tilting around a, into a position which intersects a_1b, the shape of the surface of sliding will be different from that of bc and the distribution of the passive earth pressure over ab will depend on the type of yield.

The preceding statements apply only to cohesionless masses. The rigorous theory of the plastic equilibrium of heavy, cohesive, semi-infinite masses has not yet matured beyond the initial stages. From a practical point of view we are chiefly interested in obtaining information on the passive earth pressure of such masses. In this connection it should be remembered that the shear pattern for the passive Rankine state in semi-infinite masses with a horizontal surface is independent of cohesion (see Art. 12 and Fig. 11*d*). If the surface of the soil carries a uniformly distributed surcharge, q per unit of area, the passive Rankine pressure per unit of area of a vertical section at a depth z below the surface is

$$\sigma_P = 2c\sqrt{N_\phi} + qN_\phi + \gamma z N_\phi \qquad 12(5)$$

wherein $N_\phi = \tan^2(45° + \phi/2)$ is the flow value. The first two terms on the right-hand side of this equation, $2c\sqrt{N_\phi}$ and qN_ϕ, are independent

of the depth and of the unit weight of the soil. The third term, $\gamma z N_\phi$, contains the unit weight γ as a factor, and it increases like a hydrostatic pressure in simple proportion to the depth.

If a semi-infinite mass of cohesive soil in a state of passive plastic equilibrium is acted upon by adhesion and friction along the rough sides of a plane diaphragm, the influence of the shearing stresses along the faces of the diaphragm on the state of stress in the soil does not extend beyond the Rankine shear planes *aD*, Figure 14*e*, through the upper edge of the diaphragm. Above these shear planes the shear pattern is identical with that shown in Figure 14*e* for a cohesionless mass. The state of stress which exists within the wedge-shaped zone *aBD* has not yet been rigorously analyzed. However, by analogy with the relation expressed by equation 12(5) the following assumption appears to be acceptable. If a state of plastic equilibrium exists in every point of a semi-infinite mass of cohesive soil which is acted upon by friction and adhesion along a rough, plane contact face, the normal component of the passive earth pressure per unit of area of this section can be represented approximately by a linear equation

$$p_{Pn} = cK_{Pc} + qK_{Pq} + \gamma z K_{P\gamma} \qquad [5]$$

wherein K_{Pc}, K_{Pq}, and $K_{P\gamma}$ are pure numbers whose values are independent of z. From the results of estimates we know that the shape of the surface of sliding for positive and negative values of the angle of wall friction δ is similar to that shown in Figures 14*e* and 14*g* respectively.

The deformation conditions for the validity of equation 5 are similar to those for the validity of equation 3. If these conditions are not satisfied, the shape of the surface of sliding will be different from that of *bc* and the distribution of the passive earth pressure over the contact face *ab* will depend on the type of movement of this face.

16. Plastic equilibrium produced by loading part of the surface of semi-infinite masses. In the mass represented by Figures 14*c* and 14*e* the transition from the state of elastic to the state of plastic equilibrium was accomplished by an imaginary operation which consisted in elongating or compressing the mass in a horizontal direction. However, the transition can also be accomplished by means of a continuous surcharge which covers the surface of the mass on one side of a straight line. The equations which determine the plastic equilibrium of semi-infinite masses due to local surcharges are difficult to solve. A complete solution has been worked out only on the assumption that the soil has a unit weight equal to zero (Prandtl 1920). The investigations regarding the influence of the weight of the mass on the characteristics of the state of plastic equilibrium produced by a surcharge have not passed beyond the

stage of establishing the differential equations (Reissner 1924). Yet, even in this preliminary stage, the results furnish valuable information of a general nature. The following paragraphs contain a summary of those findings which are of immediate practical interest, without attempting a rigorous proof of the statements.

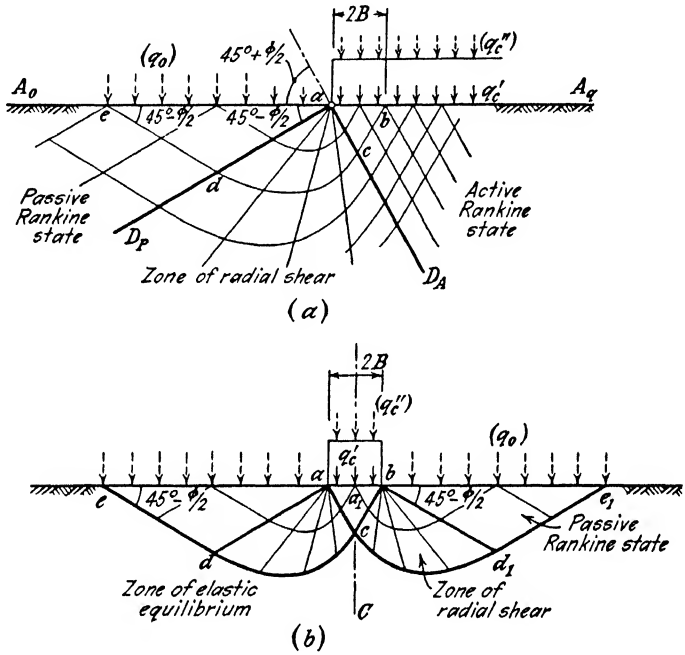

FIG. 15. Plastic flow in semi-infinite cohesive weightless solid due to uniformly distributed surcharge which covers (*a*) one half of the entire surface, and (*b*) a strip with infinite length. (*After Prandtl 1920.*)

The surcharge q_c' per unit of area required to establish a state of plastic equilibrium in every point of a weightless semi-infinite mass of a cohesive material with an angle of internal friction ϕ is uniformly distributed over the surface on one side of a straight line, indicated by a in Figure 15*a*. The entire mass can be divided by two planes through a into three sections with different shear patterns. One of these planes, aD_P, descends toward the left through a at an angle of $45° - \phi/2$ to the horizontal, and the other one, aD_A, toward the right at an angle of $45° + \phi/2$. Above the plane aD_A the shear pattern is identical with that corresponding to an active Rankine state (Fig. 11*c*) and above the plane aD_P with that corresponding to a passive Rankine state (Fig. 11*d*). Hence, above aD_P the major principal stress is everywhere hori-

zontal and above aD_A it is everywhere vertical. These two Rankine zones are separated from each other by a *zone of radial shear*, D_AaD_P. Within this zone one set of surfaces of sliding appears in Figure 15*a* as a set of straight lines through point *a* and the other one as a set of logarithmic spirals which intersect the straight lines at angles of $90° - \phi$ (Prandtl 1920). If the surface of the semi-infinite mass on the left-hand side of *a* is loaded with q_0 per unit of area, the load required to establish a state of plastic equilibrium increases from q_c' to $q_c' + q_c''$ per unit of area, wherein q_c'' is a function only of ϕ and q_0. The shear pattern remains unaltered. If $c = 0$ and $q_0 = 0$ the weightless mass cannot carry any one-sided surcharge, regardless of what the value of the angle of internal friction ϕ may be, because there is no resistance against the lateral yield of the loaded mass toward the left of the loaded area. Hence in this case the critical load q_c' is equal to zero. This conclusion is also valid for the immediate vicinity of the boundary of a loaded area on the horizontal surface of a cohesionless mass with weight. This can easily be recognized when considering the conditions for the equilibrium of the surcharge. The surfaces of sliding resemble those shown in Figure 15*a*, although this figure refers to cohesive materials. In order to sink into the ground, a surcharge located within a distance $2B$ from the loaded area must displace the soil located above the surface of sliding *bcde*. If the soil has no cohesion the displacement is resisted only by the friction due to the weight of the body of soil *bcde*. Since the weight of this body increases with the square of $2B$, the greatest surcharge Q which can be carried by the strip per unit of its length is determined by an equation

$$Q = NB^2$$

wherein N is a factor whose value is independent of B. The maximum surcharge per unit of area which the strip can carry is

$$q = \frac{dQ}{dB} = 2NB$$

This surcharge increases in simple proportion to the distance from the boundary *a* of the loaded area. At the boundary it is equal to zero.

The conditions for the plastic equilibrium of the semi-infinite mass shown in Figure 15*a* are also valid for any limited section of this mass, provided the states of stress along the boundaries of this section are maintained. For instance, if we remove the surcharge on the right-hand side of point *b* (Fig. 15*a*) the material located beneath the surface of sliding *bcde* passes from the state of plastic equilibrium into that of elastic equilibrium. Yet the material located above this surface re-

mains in a state of plastic equilibrium. This method of reasoning is similar to that which led to Rankine's earth pressure theory. It informs us on the conditions for the plastic equilibrium beneath loaded strips with a finite width, such as the strip shown in Figure 15*b*. In this figure the line *bcde* corresponds to the line *bcde* in Figure 15*a*. A slight increase of the surcharge in excess of $q_c' + q_c''$ causes the material located above the surface represented by the line *bcde* to flow. However, it should be noted that the system of internal and external forces which act on the loaded material is perfectly symmetrical with reference to the vertical plane a_1C. Therefore the zone of plastic equilibrium must also be symmetrical with reference to this plane. Hence the lower boundary of the zone of plastic equilibrium will be as shown in the figure by the line $edcd_1e_1$.

The preceding investigation was based on the assumption that the unit weight of the loaded material is equal to zero. In reality there is no weightless material. The weight of the material complicates the situation very considerably. At given values of c and ϕ it increases the critical load and it changes the shape of the surfaces of sliding within both the active Rankine zone and the zone of radial shear. Thus for instance in the zone of radial shear the radial lines of shear are not straight as shown in Figure 15*a*, but curved (Reissner 1924).

The problem of computing the critical load on the assumption that $\gamma > 0$ has been solved only by approximate methods. However, for practical purposes these methods are sufficiently accurate. They will be presented in Chapter VIII.

17. Rigorous and simplified methods of solving practical problems. The solution of a problem is rigorous if the computed stresses are strictly compatible with the conditions for equilibrium, with the boundary conditions, and with the assumed mechanical properties of the materials subject to investigation.

The stress conditions in the interior of a body are illustrated by Figure 16*a*. This figure represents a prismatic element of a body which is acted upon by no body force other than its own weight $\gamma dx\, dz$. One pair of sides is parallel to the direction of the force of gravity. The sides are acted upon by the stresses indicated in the figure. The conditions for the equilibrium of the element can be expressed by the equations

$$\frac{\partial \sigma_z}{\partial z} + \frac{\partial \tau_{zx}}{\partial x} = \gamma \qquad [1]$$

and

$$\frac{\partial \sigma_x}{\partial x} + \frac{\partial \tau_{xz}}{\partial z} = 0 \qquad [2]$$

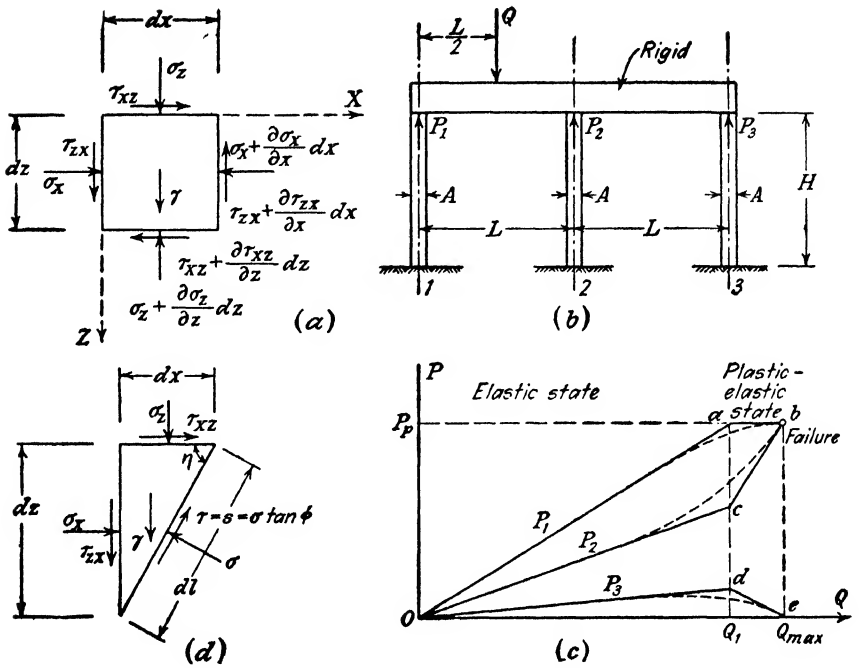

FIG. 16. Diagrams illustrating equilibrium and compatibility conditions.

These equations are satisfied if

$$\sigma_x = \frac{\partial^2 F}{\partial z^2} \qquad [3a]$$

$$\sigma_z = \frac{\partial^2 F}{\partial x^2} \qquad [3b]$$

and

$$\tau_{xz} = -\frac{\partial^2 F}{\partial x\,\partial z} + \gamma x + C \qquad [3c]$$

wherein F is an arbitrary function of x and z and C is the constant of integration. Equations 3 demonstrate that there is an infinite variety of states of stress which satisfy equations 1 and 2. Yet only one of them corresponds to reality. Hence, to solve our problem, equations 1 and 2 must be supplemented by others. One set of supplementary equations is obtained by establishing the boundary conditions. Thus for instance, if the body has a free surface which is not acted upon by external forces, both the normal stress and the shearing stress on this surface must be equal to zero.

A second set of equations is obtained by expressing the condition that the state of stress should be compatible with the mechanical properties of the material. If the material is perfectly elastic, the relations between stress and strain are determined by Hooke's law. If Hooke's law is valid, the stresses must satisfy not only equations 1 and 2 but also the equation

$$\left(\frac{\partial^2}{\partial x^2} + \frac{\partial^2}{\partial z^2}\right)(\sigma_x + \sigma_z) = 0 \qquad [4]$$

provided the body is acted upon by no body force except its own weight (see, for instance, Timoshenko 1934). It should be noticed that this equation does not contain any one of the elastic constants of the material. Combining this equation with equations 3 we obtain the standard differential equation for the two-dimensional state of stress in elastic bodies, when weight is the only body force. The equation is

$$\frac{\partial^4 F}{\partial x^4} + 2\frac{\partial^4 F}{\partial x^2\,\partial z^2} + \frac{\partial^4 F}{\partial z^4} = 0 \qquad [5]$$

The function F is known as *Airy's stress function* (Airy 1862). The mathematical part of the problem consists in finding a function F which satisfies both equation 5 and the boundary conditions of the problem. In some textbooks equation 5 is written in the form

$$\nabla^4 F = \nabla^2 \nabla^2 F = 0$$

The symbol ∇^2 represents Laplace's operator,

$$\nabla^2 = \left(\frac{\partial^2}{\partial x^2} + \frac{\partial^2}{\partial z^2}\right)$$

A solution obtained by means of equation 5 is valid only if the deformation of the body is purely elastic. On the other hand, if the stresses exceed the yield point in one part of the body, three different zones should be distinguished. In one zone the stresses must satisfy equation 5, which is only valid for perfectly elastic materials. In a second zone the state of stress must satisfy the conditions for plastic equilibrium, and a third zone represents a zone of transition from the elastic into the plastic state. The existence of this zone of transition makes the problem of computing the stresses extremely complicated. In order to simplify the analysis the existence of a zone of transition is always disregarded. For the elastic zone the stresses are computed by means of equation 5 and for the plastic zone they are computed in such a way as to satisfy the stress conditions for plastic equilibrium in every point of the plastic zone. For soils these conditions are deter-

mined sufficiently accurately by equation 7(7), which represents Mohr's rupture hypothesis,

$$\sqrt{\left(\frac{\sigma_x - \sigma_z}{2}\right)^2 + \tau_{xz}^2} - \frac{\sigma_x + \sigma_z}{2} \sin \phi = c \cos \phi \qquad 7(7)$$

In accordance with the simplified assumptions on which the analysis is based, the boundary between the two zones is a surface of discontinuity with respect to the rate of the change of stress in every direction except in a direction tangential to the boundary.

Finally, if the problem deals with a body which is entirely in a state of plastic equilibrium the solution needs only to satisfy the general equilibrium condition represented by equations 3, the condition for plastic equilibrium, expressed by equation 7(7), and the boundary conditions. The Rankine state of stress in a semi-infinite mass of soil can be computed in this manner.

In order to visualize the physical meaning of the preceding general equations, we can compare them to the equations which determine the pressure exerted by a perfectly rigid, continuous beam on nonrigid supports. Figure 16*b* shows such a beam. It rests on three columns, 1 to 3, with equal height H. The cross sections, A, of the columns are all equal, and all the columns have the same elastic properties. The beam is acted upon by a load Q at a distance $\frac{1}{2}L$ from support 1 and it exerts the pressures P_1, P_2, and P_3 on the columns 1, 2, and 3 respectively. Therefore the columns 1 to 3 can be replaced by reactions which are equal and opposite to these pressures. The equilibrium of the system requires that the sum of all the forces and the sum of all the moments acting on the beam must be equal to zero. The moments can be taken around any point, for instance, the top of the support 1. These two conditions are expressed by the following equations:

$$-Q + P_1 + P_2 + P_3 = 0 \qquad [6a]$$

and

$$\tfrac{1}{2}QL - P_2L - 2P_3L = 0 \qquad [6b]$$

These two equations contain three unknown quantities, P_1 to P_3. Hence the conditions for equilibrium are satisfied, if we assign to one of these quantities, for instance, to the reaction P_1, an arbitrary value. This quantity is called the statically indeterminate reaction. In a similar manner, there is an infinite number of different functions which satisfy the general equations 3 indicating that the problem is indeterminate. Yet there can be only one value of P_1 or one function F which will give the correct solution of our problem. This solution depends

on the mechanical properties of the supports. In order to compute that one value or that one function we must establish a supplementary equation which expresses these properties.

In accordance with the customary assumptions regarding the mechanical properties of construction materials capable of plastic flow we establish the supplementary equation on the basis of the following assumptions. For any pressure P smaller than a critical value P_p the columns strictly obey Hooke's law. After the pressure on a column has become equal to P_p a further increase of the applied load Q produces in the column a state of plastic flow at constant pressure. If this flow does not relieve the pressure on the column the system fails. Hence if the load Q on the beam is increased, the system passes in succession through three stages. In the first stage the pressure on each one of the three columns is smaller than P_p. In this stage an increase of the load merely produces an elastic shortening of the columns and the system is in a state of elastic equilibrium. The second stage begins as soon as the load on one of the columns becomes equal to P_p. Any further increase of the load Q must be carried by the elastic action of the two other columns while the load on the third column remains equal to load P_p. This is the state of plastic-elastic equilibrium. It continues to exist until the load on a second column becomes equal to P_p. A further increase of the load Q causes a continuous plastic shortening of both of the columns at constant load. This condition constitutes failure. Hence the load Q_{max} required to increase the load on two columns to P_p is the greatest load the system can carry. For $Q = Q_{max}$ the system is in a state of plastic equilibrium.

In the elastic stage the ratio p/ϵ of the unit load $p = P/A$ on a column to the corresponding unit shortening ϵ of the column is called *Young's modulus* E. Hence in this stage the total shortening of the columns produced by a given load Q is

$$\zeta_1 = \frac{P_1 H}{AE}, \quad \zeta_2 = \frac{P_2 H}{AE}, \quad \text{and} \quad \zeta_3 = \frac{P_3 H}{AE}$$

Since the beam is perfectly rigid the heads of the columns must be located on a straight line, which requires

$$\zeta_3 = \zeta_1 - 2(\zeta_1 - \zeta_2) = 2\zeta_2 - \zeta_1$$

or

$$P_3 = 2P_2 - P_1$$

Combining this equation with equations 6 we obtain as a solution of our problem

$$P_1 = \tfrac{7}{12}Q, \quad P_2 = \tfrac{4}{12}Q, \quad \text{and} \quad P_3 = \tfrac{1}{12}Q \qquad [7]$$

This solution satisfies the conditions for the equilibrium of the system, the boundary conditions, and Hooke's law. Therefore it represents an analogue to a solution of the general equation 5.

The relation between Q and the reactions P_1, P_2, and P_3, determined by equations 7, is represented in the diagram (Fig. 16*c*) by three straight lines through the origin O. The load Q_1 required to increase the reaction P_1 to P_p determines the beginning of the plastic-elastic stage. For this stage the supplementary equation required for the solution of our problem is

$$P_1 = P_p \qquad [8]$$

Combining this equation with equations 6 we obtain

$$P_2 = \tfrac{3}{2}Q - 2P_p \quad \text{and} \quad P_3 = P_p - \tfrac{1}{2}Q \qquad [9]$$

valid for any load Q greater than Q_1 and smaller than $Q_{\max}$. In Figure 16*c* this relation is represented by three straight lines, *ab*, *cb*, and *de*, none of which passes through the origin of the system.

The condition for the plastic equilibrium of the system shown in Figure 16*b* is

$$P_1 = P_2 = P_p \quad \text{and} \quad Q = Q_{\max}$$

The corresponding solution is

$$Q_{\max} = 2P_p, \quad P_1 = P_2 = P_p \quad \text{and} \quad P_3 = 0$$

The computation of $Q_{\max}$ in this problem corresponds to computing the force, the load, or the system of forces required to produce the failure of a mass of soil by separation along a surface of sliding. Immediately before the slide occurs the mass of soil located above the surface of sliding may be in a plastic-elastic or entirely in a plastic state of equilibrium. Along the surface of sliding the state of stress must satisfy in every point Coulomb's equation

$$s = c + \sigma \tan \phi$$

wherein σ is the normal stress on the surface of sliding and s the shearing resistance per unit of area. It must also satisfy the conditions for equilibrium expressed by equations 1 and 2. Figure 16*d* represents an element *dl* of a surface of sliding together with a prismatic element of the adjoining soil. By combining Coulomb's equation for cohesionless sand,

$$s = \sigma \tan \phi$$

with equations 1 and 2 Kötter (1888) obtained the equation

$$\frac{d\sigma}{dl} - 2\sigma \tan \phi \frac{d\eta}{dl} = \gamma \sin (\eta - \phi) \cos \phi \qquad [10]$$

wherein η is the angle between the element dl of the surface of sliding and the horizontal as shown in Figure 16*d*. Equation 10 is known as *Kötter's equation*. If the shape of a surface of sliding in a mass of sand and the angle of internal friction of the sand are known, it is possible to determine by means of this equation the distribution of the normal stresses on this surface and the line of action of the resultant pressure, provided that the neutral stresses are equal to zero. Jáky (1936) showed that equation 10 is also valid for cohesive soils. If the stresses in a sand include both effective and neutral stresses, Kötter's equation must be replaced by an equation which takes into consideration the effect of neutral stresses on the stress conditions for failure (Carrillo 1942*a*).

Kötter's equation has been used by Ohde (1938) for the determination of the distribution of the horizontal pressure of sand on a vertical support which yields by tilting around the upper edge. (See Art. 20.) The error of the results of such investigations depends on the degree to which the assumed surface of sliding deviates from the real one. A summary of Kötter's important contributions to earth pressure theory has been published by Reissner (1909).

The equations given in the preceding paragraphs represent the fundamental equations for the rigorous solution of two-dimensional stress problems in terms of Cartesian co-ordinates. Under certain conditions it is more convenient to operate with polar or bipolar co-ordinates, whereupon the fundamental equations must be transformed accordingly.

In no case can the rigorous solutions based on the aforementioned fundamental equations be closer to reality than the assumptions upon which these equations are based. There are no real construction materials with the exception of steel and there are no soils whose mechanical properties are more than approximately the same as the assumed ones.

In order to visualize the practical consequences of the discrepancies between the assumptions and reality we return to the example illustrated by Figure 16*b*. In accordance with the fundamental assumptions of the theories of elasticity and plasticity we assumed that there is an abrupt transition of the elastic to the plastic behavior of the columns. As a consequence the lines which represent the relation between the load Q and the pressure on the columns show a sharp break with the abscissa $Q = Q_1$. In reality there is a gradual transition from elastic to plastic behavior, involving a decrease of the pressure-compression ratio P/ζ as the yield point is approached. As a consequence the real relation between Q and the reactions P_1 to P_3 is similar to that indicated by the dotted lines (Fig. 16*c*). Nevertheless the relation represented by the unbroken lines is commonly called the rigorous solution of the problem. The difference between the ordinates of the solid and the corresponding dotted lines represents the error associated with the rigorous solution of the problem as indicated by the solid lines.

In spite of the radically simplifying assumptions on which the rigorous

solutions are based, the prospects for rigorous solutions for many problems of outstanding practical importance are rather remote. The final equations obtained by rigorously solving other problems are so cumbersome that they are unfit for practical use. Therefore, in practice, we depend to a great extent on simplified solutions.

In connection with elasticity problems, the efforts to obtain simplified solutions have led to such theories as those involving a coefficient of subgrade reaction (Chapter XVI). According to the concept of subgrade reaction the soil under load behaves like a bed of uniformly spaced springs with uniform stiffness. The error associated with such an assumption can be very important. Far more accurate are the simplified theories dealing with the conditions for equilibrium of a mass of soil located above a potential surface of sliding. They are commonly referred to as earth-pressure theories and theories of the stability of slopes.

The rigorous solutions of most of the problems in these categories are very complicated. Hence there is an urgent need for simplified procedures. These procedures consist in replacing the real surface of sliding by an imaginary one with a simple equation. The position of the surface of sliding within the soil must be such that the force required to prevent a slip along the surface should be a maximum. Comparison of the results thus obtained with rigorous solutions has shown that the error due to simplifying the shape of the surface of sliding is often insignificant. The best-known method of this type is Coulomb's theory of the active earth pressure on retaining walls, based on a substitution of a plane surface of sliding for the curved one shown in Figure 14*c*. The theoretical error due to this substitution is not in excess of 5 per cent. (See Art. 23.) A difference of several per cent between the results of a rigorous and a simplified computation is usually very small compared with the difference between either of them and reality. It appears insignificant in comparison with the advantages associated with simple equations.

Most of the older approximate theories share the defect that the importance of the theoretical error remains unknown until a rigorous solution has been secured. Coulomb's theory of the passive earth pressure is an example. This theory has been used for more than a century without anybody suspecting that the computed passive earth pressure may be as much as 30 per cent higher than the real one. In other fields of applied mechanics such risk has been eliminated by new methods which are known under the collective title *Relaxation Methods*. They could also be called Methods of Successive Approximation (Southwell 1940). One of the earliest and best-known applications of this

method to an engineering problem is Hardy Cross' Moment Distribution Method for the analysis of continuous frames (Cross 1932). The method is based on the principle that every state of equilibrium of a given system is identical with the state in which the potential energy of the system is a minimum.

Since the relaxation methods provide us with relatively simple solutions with a known range of error, they seem to be ideally adapted to dealing with the problems of soil mechanics, whose very nature excludes both the possibility and the necessity of accurate solutions. The methods have the further advantage that the investigator is compelled by the procedure to have at every stage of his computations a clear mental picture of what he is doing. Since most of the misapplications of the theories of soil mechanics were due to erroneous conceptions concerning the physical meaning of the mathematical operations, this advantage has considerable weight.

So far no direct application of the methods of relaxation to the problems of soil mechanics has been attempted. Yet the prospects are encouraging.

In connection with the practical application of soil mechanics the importance of simplicity cannot be overemphasized, provided the simplicity is not achieved at the price of ignoring the influence of vital factors. The necessity for simplicity is due to the nature of the soils. Since there are no perfectly homogeneous soils and since the mechanical properties of real soils are complicated, all the theories of soil mechanics combined represent no more than a small step toward grasping the complex phenomena subject to investigation. As a consequence, in every field of applied soil mechanics the most important operation consists not in obtaining a rigorous solution but in ascertaining the influence of various possible deviations of the real conditions from the assumed ones. This can be done only on the basis of simple equations which inform us at a glance of the relative weight of the different factors which enter into the problem. Most rigorous solutions are by far too complicated to serve this vital purpose. The principal value of these solutions is their ability to show the importance of the theoretical errors involved in the results of simplified analysis. In this connection the rigorous solutions are of inestimable value. However, after a complicated rigorous solution has rendered this service it is not likely to be of further use unless the results are presented in the form of tables or graphs. The ability to obtain rigorous solutions is not a prerequisite for successful work in the field of soil mechanics. For both the research man and the practicing engineer it is sufficient to know the general procedure by means of which the rigorous solutions are obtained. The rigorous solution of the problems should be left to professional mathematicians. For the same reason only the simplified methods will be discussed in this book. Wherever it is necessary or advisable to refer to rigorous solutions, only the results will be presented.

In many advanced papers on soil mechanics the mathematical refinement is out of proportion to the importance of the errors due to simplify-

ing assumptions. If these assumptions are clearly and completely stated, such papers have at least the merit of honest mental experiments and the reader may be in a position to judge for himself to what extent the experiment can be considered successful. However, statements covering all the vital assumptions are rather exceptional. Since few readers know the subject well enough to recognize a gap in the set of assumptions, a theoretical paper with an incomplete set may do more harm than good.

Occasionally investigators make assumptions of grave import without suspecting it themselves. On closer scrutiny of their papers one may even find that their attempts to solve old problems by apparently more rigorous methods have increased the error owing to the fact that a set of conspicuous but tolerable assumptions was replaced by less conspicuous but far more detrimental ones. The most instructive examples of such misdirected efforts can be found among the advanced theories dealing with the stability of slopes and with the bearing capacity of piles and pile groups.

The existence of many papers with one or more of the aforementioned shortcomings makes it difficult for the beginner to orient himself in the field of soil mechanics without guidance. If a paper of this category is mentioned in the following chapters at all, its defects will be indicated.

Section B

CONDITIONS FOR SHEAR FAILURE IN IDEAL SOILS

Chapter V

ARCHING IN IDEAL SOILS

18. Definitions. If one part of the support of a mass of soil yield while the remainder stays in place the soil adjoining the yielding part moves out of its original position between adjacent stationary masses of soil. The relative movement within the soil is opposed by a shearing resistance within the zone of contact between the yielding and the stationary masses. Since the shearing resistance tends to keep the yielding mass in its original position, it reduces the pressure on the yielding part of the support and increases the pressure on the adjoining stationary part. This transfer of pressure from a yielding mass of soil onto adjoining stationary parts is commonly called the *arching effect*, and the soil is said to *arch* over the yielding part of the support. Arching also takes place if one part of a yielding support moves out more than the adjoining parts.

Arching is one of the most universal phenomena encountered in soils both in the field and in the laboratory. Since arching is maintained solely by shearing stresses in the soil, it is no less permanent than any other state of stress in the soil which depends on the existence of shearing stresses, such as the state of stress beneath the footing of a column. For instance, if no permanent shearing stresses were possible in a sand, footings on sand would settle indefinitely. On the other hand, every external influence which causes a supplementary settlement of a footing or an additional outward movement of a retaining wall under unchanged static forces must also be expected to reduce the intensity of existing arching effects. Vibrations are the most important influence of this sort.

In the following article two typical cases will be investigated, viz., arching in an ideal sand due to the local yield of a horizontal support and arching in the sand adjoining a vertical support whose lower part yields in an outward direction.

19. State of stress in the zone of arching. The local yield of the horizontal support of a bed of sand shown in Figure 17*a* can be produced by gradually lowering a strip-shaped section *ab* of the support. Before the strip starts to yield, the vertical pressure per unit of area on the horizontal support is everywhere equal to the depth of the layer of sand

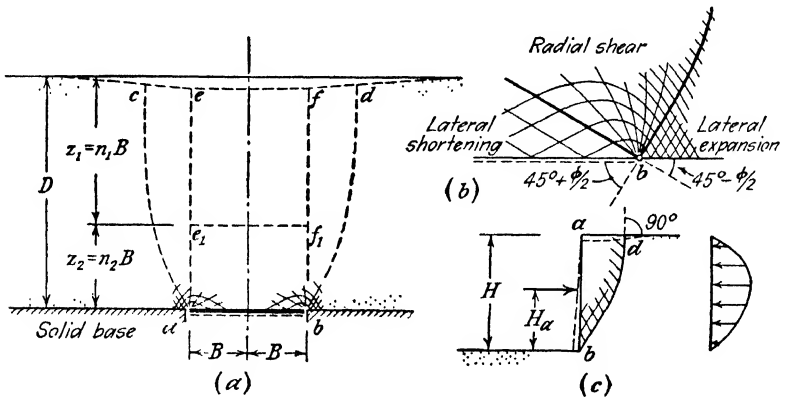

FIG. 17. Failure in cohesionless sand preceded by arching. (*a*) Failure caused by downward movement of a long narrow section of the base of a layer of sand; (*b*) enlarged detail of diagram (*a*); (*c*) shear failure in sand due to yield of lateral support by tilting about its upper edge.

times its unit weight. However, a lowering of the strip causes the sand located above the strip to follow. This movement is opposed by frictional resistance along the boundaries between the moving and the stationary mass of sand. As a consequence the total pressure on the yielding strip decreases by an amount equal to the vertical component of the shearing resistance which acts on the boundaries, and the total pressure on the adjoining stationary parts of the support increases by the same amount. In every point located immediately above the yielding strip the vertical principal stress decreases to a small fraction of what it was before the yield commenced. The total vertical pressure on the base of the layer of sand remains unchanged, because it is always equal to the weight of the sand. Therefore the decrease of the vertical pressure on the yielding strip must be associated with an increase of the vertical pressure on the adjoining parts of the rigid base, involving an abrupt increase of the intensity of the vertical pressure along the edges of the strip. This discontinuity requires the existence of a zone of radial shear comparable to that shown in Figure 15*a*. The radial shear is associated with a lateral expansion of the sand located within the high-pressure zone, on both sides of the yielding strip towards the low-

pressure zone located above the strip. If the base of the layer of sand were perfectly smooth, the corresponding shear pattern should be similar to that indicated in Figure 17*a* and, on a larger scale, in Figure 17*b*.

As soon as the strip has yielded sufficiently in a downward direction, a shear failure occurs along two surfaces of sliding which rise from the outer boundaries of the strip to the surface of the sand. In the vicinity of the surface all the sand grains move vertically downward. This has been demonstrated repeatedly by time-exposure photographs. Such a movement is conceivable only if the surfaces of sliding intersect the horizontal surface of the sand at right angles. When the failure occurs a troughlike depression appears on the surface of the sand as indicated in Figure 17*a*. The slope of each side of the depression is greatest where it intersects the surface of sliding. The distance between these steepest parts of the trough can be measured. It has been found that it is always greater than the width of the yielding strip. Hence, the surfaces of sliding must have a shape similar to that indicated in Figure 17*a* by the lines *ac* and *bd*. The problem of deriving the equations of the surfaces of sliding *ac* and *bd* has not yet been solved. However, experiments (Völlmy 1937) suggest that the average slope angle of these surfaces decreases from almost 90° for low values of $D/2B$ to values approaching $45° + \phi/2$ for very high values of $D/2B$.

The vertical pressure on the lower part of the mass of sand located between the two surfaces of sliding, *ac* and *bd* in Figure 17*a*, is equal to the weight of the upper part reduced by the vertical component of the frictional resistance which acts on the adjoining surfaces of sliding. This transfer of part of the weight of the sand located above the yielding strip onto the adjoining masses of sand constitutes the arching effect.

The preceding reasoning can also be applied to the analysis of the arching effect produced in a mass of sand by the lateral yield of the lower part of a vertical support. In Figure 17*c* the lateral support is represented by *ab*. The surface of the sand is horizontal and the support yields by tilting around its upper edge. After the support has yielded sufficiently, a shear failure occurs in the sand along a surface of sliding *bd* which extends from the foot *b* of the support to the surface of the sand. The stationary position of the upper edge, *a*, of the lateral support prevents a lateral expansion of the upper part of the sliding wedge. Therefore the sand grains located in the upper part of the wedge can move only in a downward direction. Hence the surface of sliding intersects the horizontal surface of the sand at *d* at right angles. The corresponding subsidence of the surface of the sliding wedge is indicated in the figure by a dashed line.

The lateral expansion of the lower part of the sliding wedge is associated with a shortening in a vertical direction. The corresponding subsidence of the upper part of the wedge is opposed by the frictional resistance along the adjoining steep part of the surface of sliding. As a consequence the vertical pressure on the lower part of the wedge is smaller than the weight of the sand located above it. This phenomenon constitutes the arching effect in the sand behind yielding lateral supports whose upper part is stationary.

20. Theories of arching. Most of the existing theories of arching deal with the pressure of dry sand on yielding horizontal strips. They can be divided into three groups. The authors of the theories of the first group merely considered the conditions for the equilibrium of the sand which is located immediately above the loaded strip without attempting to investigate whether or not the results of the computations were compatible with the conditions for the equilibrium of the sand at a greater distance from the strip. The theories of the second group are based on the unjustified assumption that the entire mass of sand located above the yielding strip is in a state of plastic equilibrium.

In the theories of a third group it is assumed that the vertical sections *ae* and *bf* (Fig. 17*a*) through the outer edges of the yielding strip represent surfaces of sliding and that the pressure on the yielding strip is equal to the difference between the weight of the sand located above the strip and the full frictional resistance along the vertical sections (Cain 1916 and others). The real surfaces of sliding, *ac* and *bd* (Fig. 17*a*), are curved and at the surface of the sand their spacing is considerably greater than the width of the yielding strip. Hence the friction along the vertical sections *ae* and *bf* cannot be fully active. The error due to ignoring this fact is on the unsafe side.

The following comments are intended to inform the reader in a general way on the fundamental assumptions of the theories of the first two groups. Engesser (1882) replaced the sand located immediately above the yielding strip by an imaginary arch and computed the pressure on the strip on the basis of the conditions for the equilibrium of the arch. Bierbaumer (1913) compared the sand located immediately above the strip to the keystone in an arch. He assumed that the base of the keystone coincides with the surface of the strip, and that the sides of the keystone are plane and rise from the outer boundaries of the strip towards the center. The pressure on the strip is equal and opposite to the force required to maintain the keystone in its position. Caquot (1934) replaced the entire mass of sand located above the yielding strip by a system of arches. He assumed that the horizontal normal stress in the arches above the center line of the strip is equal to the corresponding vertical normal stress times the flow value N_ϕ, equation 7(4), and he computed the pressure on the strip on the basis of the conditions for the equilibrium of the arches. Völlmy (1937) replaced the curved surfaces of sliding *ac* and *bd* (Fig. 17*a*) by inclined plane surfaces and assumed that the normal stresses on these

surfaces are identical with the normal stresses on similarly oriented sections through a semi-infinite mass of sand in an active Rankine state. The slope of the surfaces of sliding is chosen such that the corresponding pressure on the yielding strip is a maximum. According to the results of some of his investigations an increase of the angle of internal friction of the sand should cause an increase of the pressure on the yielding strip. According to all the other theories and to the existing test results an increase of the angle of internal friction has the opposite effect. Völlmy (1937) also investigated the pressure of the earth on rigid and on flexible culverts and compared the results of his analysis with those obtained by earlier investigators. However, under field conditions the pressure on yielding horizontal supports such as the roofs of culverts or of tunnels depends on many conditions other than those which have been considered so far in theoretical investigations.

All the theories cited above are in accordance with experience in that the pressure on a yielding, horizontal strip with a given width increases less rapidly than the weight of the mass of sand located above the strip and approaches asymptotically a finite value. However, the values furnished by different theories for the pressure on the strip are quite different. In order to find which of the theories deserves preference it would be necessary to investigate experimentally the state of stress above yielding strips and to compare the results with the basic assumptions of the theories. Up to this time no complete investigation of this type has been made, and the relative merit of the several theories is still unknown. The simplest theories are those in the third category which are based on the assumption that the surfaces of sliding are vertical. Fortunately the sources of error associated with this assumption are clearly visible. In spite of the errors the final results are fairly compatible with the existing experimental data. Therefore the following analysis will be based exclusively on the fundamental assumptions of the theories in this category. In connection with a scientific study of the subject Völlmy's publication should be consulted (Völlmy 1937).

If we assume that the surfaces of sliding are vertical as indicated by the lines *ae* and *bf* (Fig. 17*a*) the problem of computing the vertical pressure on the yielding strip becomes identical with the problem of computing the vertical pressure on the yielding bottom of prismatic bins.

For cohesionless materials this problem has been solved rigorously by Kötter (1899). It has also been solved with different degrees of approximation by other investigators. The simplest of the solutions is based on the assumption that the vertical pressure on any horizontal section through the fill is uniformly distributed (Janssen 1895, Koenen 1896). This assumption is incompatible with the state of stress on vertical sections through the soil, but the error due to this assumption is not so important that the assumption cannot be used as a basis for a rough estimate.

Figure 18*a* is a section through the space between two vertical sur-

faces of sliding. The shearing resistance of the earth is determined by the equation

$$s = c + \sigma \tan \phi$$

The unit weight of the soil is γ and the surface of the soil carries a uniform surcharge q per unit of area. The ratio between the horizontal

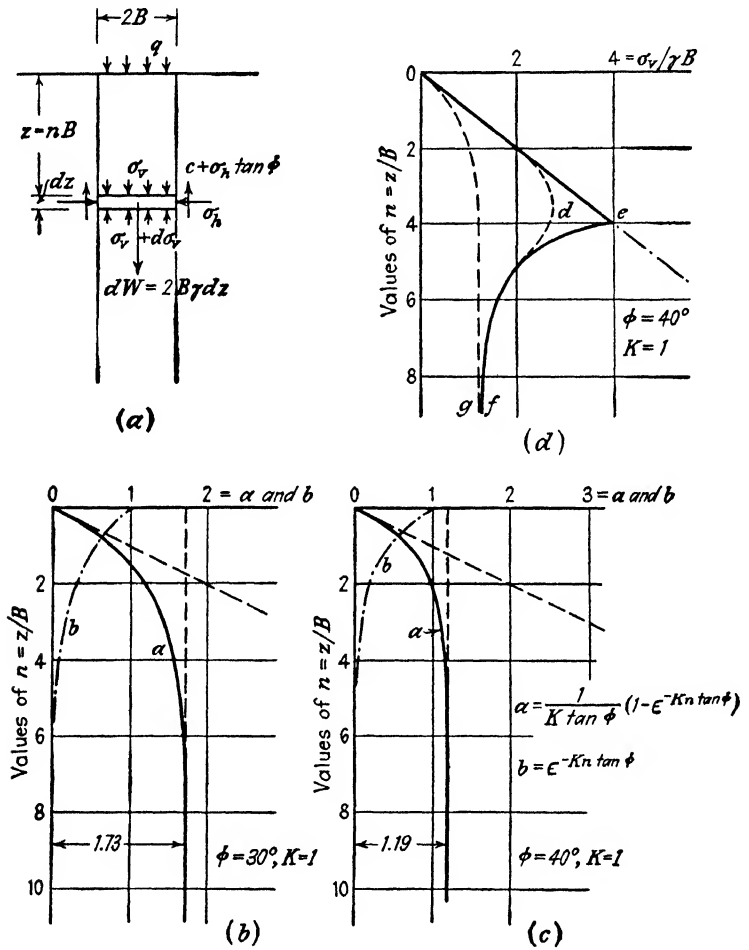

FIG. 18. (*a*) Diagram illustrating assumptions on which computation of pressure in sand between two vertical surfaces of sliding is based; (*c* and *d*) representations of the results of the computations.

and the vertical pressure is assumed to be equal to an empirical constant K at every point of the fill. The vertical stress on a horizontal section at any depth z below the surface is σ_v, and the corresponding normal

stress on the vertical surface of sliding is

$$\sigma_h = K\sigma_v \qquad [1]$$

The weight of the slice with a thickness dz at a depth z below the surface is $2B\gamma\, dz$ per unit of length perpendicular to the plane of the drawing. The slice is acted upon by the forces indicated in the figure. The condition that the sum of the vertical components which act on the slice must be equal to zero can be expressed by the equation

$$2B\gamma\, dz = 2B(\sigma_v + d\sigma_v) - 2B\sigma_v + 2c\, dz + 2K\sigma_v\, dz \tan\phi$$

or

$$\frac{d\sigma_v}{dz} = \gamma - \frac{c}{B} - K\sigma_v \frac{\tan\phi}{B}$$

and

$$\sigma_v = q \quad \text{for} \quad z = 0$$

Solving these equations we obtain

$$\sigma_v = \frac{B(\gamma - c/B)}{K\tan\phi}(1 - \epsilon^{-K\tan\phi\ z/B}) + q\epsilon^{-K\tan\phi\ z/B} \qquad [2]$$

By substituting in this equation in succession the values $c = 0$ and $q = 0$, we obtain

$$c > 0 \quad q = 0 \quad \sigma_v = \frac{B(\gamma - c/B)}{K\tan\phi}(1 - \epsilon^{-K\tan\phi\ z/B}) \qquad [3]$$

$$c = 0 \quad q > 0 \quad \sigma_v = \frac{B\gamma}{K\tan\phi}(1 - \epsilon^{-K\tan\phi\ z/B}) + q\epsilon^{-K\tan\phi\ z/B} \qquad [4]$$

$$c = 0 \quad q = 0 \quad \sigma_v = \frac{B\gamma}{K\tan\phi}(1 - \epsilon^{-K\tan\phi\ z/B}) \qquad [5]$$

If the shearing resistance in a bed of sand is fully active on the vertical sections ae and bf (Fig. 17a), the vertical pressure σ_v per unit of area of the yielding strip ab is determined by equation 5. Substituting in this equation

$$z = nB$$

we obtain

$$\sigma_v = \gamma a B \qquad [6a]$$

wherein

$$a = \frac{1}{K\tan\phi}(1 - \epsilon^{-K\tan\phi\ z/B}) = \frac{1}{K\tan\phi}(1 - \epsilon^{-Kn\tan\phi}) \qquad [6b]$$

For $z = \infty$ we obtain $a = 1/K \tan \phi$ and

$$\sigma_v = \sigma_{v\infty} = \frac{\gamma B}{K \tan \phi} \qquad [7]$$

In Figure 18*b* the ordinates of the curve marked *a* represent the values of $n = z/B$ and the abscissas the corresponding values of a for $\phi = 30°$ and $K = 1$, or for $K \tan \phi = 0.58$. Figure 18*c* contains the same data for $\phi = 40°$ and $K = 1$ or for $K \tan \phi = 0.84$.

Experimental investigations regarding the state of stress in the sand located above a yielding strip (Terzaghi 1936*e*) have shown that the value K increases from about unity immediately above the center line of the yielding strip to a maximum of about 1.5 at an elevation of approximately $2B$ above the center line. At elevations of more than about $5B$ above the center line the lowering of the strip seems to have no effect at all on the state of stress in the sand. Hence we are obliged to assume that the shearing resistance of the sand is active only on the lower part of the vertical boundaries *ae* and *bf* of the prism of sand located above the yielding strip *ab* in Figure 17*a*. On this assumption the upper part of the prism acts like a surcharge q on the lower part and the pressure on the yielding strip is determined by equation 4. If $z_1 = n_1 B$ is the depth to which there are no shearing stresses on the vertical boundaries of the prism *abfe* in Figure 17*a* the vertical pressure per unit of area of a horizontal section $e_1 f_1$ through the prism at a depth z_1 below the surface is $q = \gamma z_1 = \gamma n_1 B$. Introducing this value and the value $z = z_2 = n_2 B$ into equation 4 we obtain

$$\sigma_v = \gamma B a_2 + \gamma B n_1 b_2 = \gamma B (a_2 + n_1 b_2) \qquad [8a]$$

wherein

$$a_2 = \frac{1}{K \tan \phi} (1 - \epsilon^{-K n_2 \tan \phi}) \quad \text{and} \quad b_2 = \epsilon^{-K n_2 \tan \phi} \qquad [8b]$$

For $n_2 = \infty$ the value a_2 becomes equal to

$$a_\infty = \frac{1}{K \tan \phi}$$

and the value b_2 equal to zero. The corresponding value of σ_v is

$$= \sigma_{v\infty} \gamma B a_\infty = \frac{\gamma B}{K \tan \phi}$$

which is equal to the value given by equation 7. In other words, the value $\sigma_{v\infty}$ is independent of the depth z_1 in Figure 17*a*.

The relation between n_2 and a_2 is identical with the relation between

n and a, represented by equation 6*b* and by the plain curves in Figures 18*b* and 18*c*. The relation between the values n and the corresponding values of

$$b = \epsilon^{-Kn \tan \phi}$$

is represented in Figures 18*b* and 18*c* by the dash-dotted curves marked *b*.

In order to illustrate by means of a numerical example the influence of the absence of shearing stresses on the upper part of the vertical sections *ae* and *bf* in Figure 17*a* we assume $\phi = 40°$, $K = 1$, and $n_1 = 4$. Between the surface and a depth $z_1 = n_1 B = 4B$ the vertical pressure on horizontal sections increases like a hydrostatic pressure in simple proportion to depth, as indicated in Figure 18*d* by the straight line *oe*. Below a depth z_1 the vertical pressure is determined by equations 8. It decreases with increasing depth, as shown by the curve *ef* and it approaches asymptotically the value $\sigma_{v\infty}$ (eq. 7).

The dashed line *og* in Figure 18*d* has been plotted on the assumption $n_1 = 0$. The abscissas of this curve are determined by equations 6. With increasing depth they also approach the value $\sigma_{v\infty}$ (eq. 7). The figure shows that the influence of the absence of arching in the upper layers of the bed of sand on the pressure σ_v on a yielding strip practically ceases to exist at a depth of more than about $8B$. Similar investigations for different values of ϕ and of n_1 led to the conclusion that the pressure on a yielding strip is almost independent of the state of stress which exists in the sand at an elevation of more than about $4B$ to $6B$ above the strip (two or three times the width of the strip).

If there is a gradual transition from full mobilization of the shearing resistance of the sand on the lower part of the vertical sections *ae* and *bf* in Figure 17*a* to a state of zero shearing stress on the upper part, the change of the vertical normal stress with depth should be such as indicated in Figure 18*d* by the line *odf*. This line is similar to the pressure curve obtained by measuring the stresses in the sand above the center line of a yielding strip (Terzaghi 1936*e*).

Less simple is the investigation of the effect of arching on the pressure of sand on a vertical support such as that shown in Figure 17*c*. The first attempt to investigate this effect was made on the simplifying assumption that the surface of sliding is plane (Terzaghi 1936*c*). According to the results of the investigation the arching in the sand behind a lateral support with a height H eliminates the hydrostatic pressure distribution and it increases the vertical distance H_a between the point of application of the lateral pressure and the lower edge of the support. The intensity of the arching effect and its influence on the value of the ratio H_a/H depends on the type of yield of the support. If

the support yields by tilting around its lower edge no arching occurs. The distribution of the earth pressure is hydrostatic and the ratio H_a/H is equal to one third. A yield by tilting around the upper edge is associated with a roughly parabolic pressure distribution and the point of application of the lateral pressure is located near midheight. Finally, if the support yields parallel to its original position, the point of application of the lateral pressure may be expected to descend gradually from an initial position close to midheight to a final position at the lower third point. The investigation gave a satisfactory general conception of the influence of the different factors involved, but, owing to the assumption that the surface of sliding is plane, failed to give information regarding the effect of arching on the intensity of the lateral pressure.

In order to obtain the missing information it was necessary to take the real shape of the surface of sliding into consideration. Since the upper edge of the lateral support does not yield, the surface of sliding must intersect the top surface of the backfill at right angles (see Art. 19).

Ohde investigated the influence of this condition on the intensity of the earth pressure on the assumption that the trace of the surface of sliding on a vertical plane is an arc of a circle which intersects the surface of the backfill at right angles (Ohde 1938). The corresponding lateral pressure and the location of the point of application of the lateral pressure have been computed for an ideal sand, with an angle of internal friction $\phi = 31°$, by three different methods.

In one of these, the location of the centroid of the pressure has been determined in such a manner that the stresses along the surface of sliding satisfy Kötter's equation, 17(10). In a second one it has been assumed that the normal stresses on both the wall and the surface of sliding are a function of the second power of the distance from the surface of the backfill, measured along the back of the lateral support and the surface of sliding respectively. The values of the constants contained in the functions have been determined in such a way that the conditions for the equilibrium of the sliding wedge are satisfied. In a third investigation another function has been selected, approximately expressing the distribution of the normal stresses over the boundaries of the sliding wedge. In spite of the differences between the fundamental assumptions, the values obtained by these methods for the ratio between the elevation of the centroid of the earth pressure and the height of the bank range between the narrow limits 0.48 and 0.56. They correspond to an angle of wall friction $\delta = 0$. However, the wall friction was found to have little influence on the location of the centroid of the pressure. Hence we are entitled to assume that the centroid is

located approximately at midheight of the support and the corresponding pressure distribution is roughly parabolic, as shown on the right-hand side of Figure 17*c*. The investigation has also shown that an increase of the ratio H_a/H due to arching is associated with an increase of the horizontal pressure on the lateral support. A simple method of computing the intensity of the lateral pressure is described in Article 67. It is based on the assumption that the curve of sliding is a logarithmic spiral, which intersects the surface at right angles.

A general mathematical discussion of the influence of the wall movement on the earth pressure has been published by Jáky (1938).

Chapter VI

RETAINING WALL PROBLEMS

21. Definitions. Retaining walls are used to provide lateral support for masses of soil. The supported material is called the *backfill.* Figures 19 and 27 represent sections through the two principal types of retaining walls. The wall shown in Figure 19 is called a *gravity wall* because the wall depends on its own weight for stability against the horizontal thrust produced by the lateral earth pressure. On the other hand, the *cantilever retaining wall,* shown in Figure 27, derives part of its stability from the weight of the soil located above the footing at the back of the wall. The side of a retaining wall against which the fill is placed is called the *back of the wall.* The back may be plane or broken, and a plane back may be vertical or inclined (*battered*). The failure of a retaining wall can occur by tilting (*tilting failure*) or by sliding along its base parallel to its original position (*sliding failure*). Either type of failure of the wall is associated with the downward movement of a wedge-shaped body of soil (*abc* in Fig. 19) located immediately back of the wall. This body is called the *sliding wedge.*

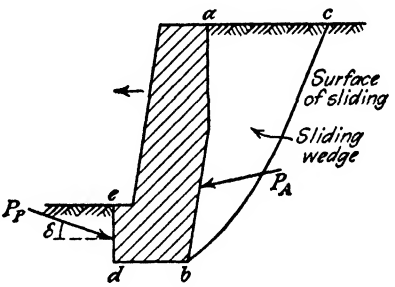

FIG. 19. Earth pressures acting on retaining wall at instant of failure.

22. Assumptions and conditions. Most of the theories of earth pressure are based on the following assumptions: The backfill of the wall is isotropic and homogeneous; the deformation of the backfill occurs exclusively parallel to a vertical plane at right angles to the back of the wall, and the neutral stresses in the backfill material are negligible. Any departure from these fundamental assumptions will be mentioned specifically. In this chapter it will be further assumed that the wall moves to a position which is located entirely beyond the boundary a_1b of the shaded area in Figure 14*c*. This is the deformation condition.

The width of the shaded area aa_1b in Figure 14*c* represents the amount by which the horizontal dimensions of the body of sand *abc* increase while the sand passes from its initial state of stress into that of plastic equilibrium. If a lateral support

yields by tilting about its lower edge every part of the back of the wall crosses almost simultaneously the boundary a_1b of the shaded area, whereupon the sand starts to fail in every point of the sliding wedge. Therefore the deformation condition specified above is satisfied as soon as the sand starts to fail.

If a lateral support yields by tilting about its upper edge a, the upper part of the back of the support remains within the shaded area. This type of yield is incompatible with the deformation conditions specified above regardless of the distance through which the lower edge of the support yields. The mechanical implications of this type of yield will be discussed in Article 67.

Finally, if a lateral support yields parallel to its original position the sand contained within the sliding wedge passes in succession through two stages. During the first stage the upper part of the back of the wall is located within the shaded area aa_1b in Figure 14c while the lower part has already passed beyond it. The slip occurs in this stage, although that part of the sliding wedge which is located next to the upper part of the lateral support is still in a state of elastic equilibrium (first stage). As the outward movement of the support continues the state of plastic equilibrium spreads within the wedge. As soon as the uppermost part of the support leaves the shaded area, the entire wedge is in a state of plastic equilibrium, whereupon the deformation conditions for the validity of the following investigations become satisfied (second stage). Both stages have been investigated experimentally (Terzaghi 1934). The results showed very clearly the two successive stages. During the first stage, when the slip occurred, the point of application of the earth pressure was located at almost half the height of the lateral support. According to the following investigations it should be located at one third of the height. However, as the advance of the wall continued, the point of application moved down and finally it became stationary at one third of the height (second stage). The yield required to establish the second stage is very small. Hence when dealing with retaining walls the first stage can and will be disregarded. (Terzaghi 1936*b*.)

23. Coulomb's theory of the active earth pressure of ideal sand. The unit weight of the sand is γ and the shearing resistance of the sand is determined by the equation

$$s = \sigma \tan \phi \qquad 5(2)$$

wherein σ is the effective normal stress on the surface of sliding and ϕ is the angle of internal friction of the sand. The shearing force which acts on the back of the wall is

$$P_{At} = P_{An} \tan \delta$$

wherein P_{An} is the normal component of the total earth pressure P_A on the back of the wall and δ is the angle of wall friction. The angle δ can either be positive or negative (see Art. 15). In Figure 20 and in all the following figures δ is shown as positive, because in practice the conditions for the occurrence of negative wall friction are seldom realized. However, the results of the following analysis are valid for both positive and negative values of δ. In no case can δ be greater than the angle of internal friction ϕ.

If the deformation condition specified in the preceding article is satisfied, and the back of the wall and the surface of the backfill are plane, the upper part of the inclined boundary of the sliding wedge is plane and the lower part is slightly curved, as shown in Figure 14*c* for a positive value and in Figure 14*f* for a negative value of the angle δ of wall friction. The active earth pressure P_A can be determined rigorously by means of one of the methods which have been worked out by Kármán (1926),

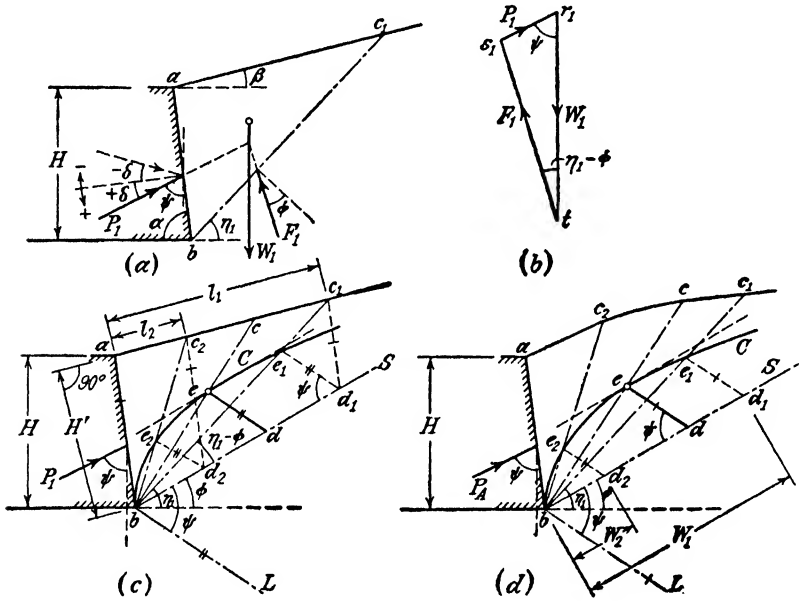

FIG. 20. (*a* and *b*) Diagrams illustrating assumptions on which Coulomb's theory of earth pressure is based; (*c* and *d*) Culmann's graphical method of determining earth pressure of sand.

Jáky (1938), and Ohde (1938). However, the final equations are too complicated for practical use. Sufficiently accurate results can be obtained by means of the simplifying assumption that the inclined boundary of the sliding wedge is plane. This assumption has been introduced into earth pressure theory by Coulomb (1776). The theory which is based on this assumption is called *Coulomb's theory*. It is illustrated by Figure 20*a*. In this figure bc_1 represents an arbitrary plane section through the lower edge of the back of the wall. The wedge-shaped section abc_1 of the backfill with a weight W_1 is acted upon by the following forces: The reaction F_1 along the face bc_1, at an angle ϕ to the normal on bc_1, and the reaction P_1 along the back of the wall

at an angle δ to the normal on the back. Let

α = the angle between the back of the wall and the horizontal surface of the ground in front of the wall,

β = the angle at which the surface of the backfill rises above the horizontal,

η_1 = the angle at which the right-hand side bc_1 of the wedge abc_1 rises above the horizontal, and

ϕ = the angle of internal friction in equation 5(2).

Since the wedge is in a state of equilibrium the polygon of forces shown in Figure 20*b* must be closed. The intensity of the reaction P_1 depends on the slope angle η_1 of the surface bc_1. For $\eta_1 = 180° - \alpha$, P_1 is equal to zero. With decreasing values of η_1, P_1 increases and passes through a maximum. Then it decreases and for $\eta_1 = \phi$ it again becomes equal to zero. The wall must be heavy enough to withstand the greatest lateral pressure, $P_{max} = P_A$ = active earth pressure. Hence the problem is to determine the maximum value of P. Coulomb solved this problem analytically. He obtained

$$P_A = \tfrac{1}{2}\gamma H^2 \frac{K_A}{\sin \alpha \cos \delta} \qquad [1a]$$

wherein

$$K_A = \frac{\sin^2 (\alpha + \phi) \cos \delta}{\sin \alpha \sin (\alpha - \delta) \left[1 + \sqrt{\dfrac{\sin (\phi + \delta) \sin (\phi - \beta)}{\sin (\alpha - \delta) \sin (\alpha + \beta)}}\right]^2} \qquad [1b]$$

The total normal component P_{An} of the earth pressure on the back of the wall is

$$P_{An} = P_A \cos \delta = \tfrac{1}{2}\gamma H^2 \frac{K_A}{\sin \alpha} \qquad [2]$$

The value K_A depends solely on the values of the angles ϕ, δ, α, and β. For $\alpha = 90°$, $\beta = 0$, and $\phi = \delta = 30°$, the difference between the exact value of the earth pressure corresponding to Figure 14*c* and Coulomb's value is smaller than 5 per cent. In connection with practical problems this error is insignificant. With decreasing values of δ the error decreases further and for $\delta = 0$ the Coulomb value of the earth pressure becomes identical with the Rankine value

$$P_A = \tfrac{1}{2}\gamma H^2 \tan^2 \left(45° - \frac{\phi}{2}\right) = \tfrac{1}{2}\gamma H^2 \frac{1}{N_\phi} \qquad 14(1)$$

Although the case illustrated by Figure 20 is a very simple one, equations 1 which represent the result of the computation are rather cumbersome. If the back of the wall or the surface of the backfill

consists of several plane sections, the amount of time required for an analytical solution is practically prohibitive. Hence it is advisable to solve the problem by one of several graphical procedures which have been worked out during the last century (Poncelet 1840, Rebhann 1871, Culmann 1866, Engesser 1880). Although Poncelet's method is better known than any of the others, the methods of Culmann and Engesser are preferable for practical purposes because they do not make it necessary to burden the memory with special rules.

24. Culmann's graphical solution. In Figure 20*c* the line *ab* represents a section through the back of the wall. We tentatively assume a surface of sliding bc_1. Then we trace the *slope line* bS at an angle ϕ (angle of internal friction) to the horizontal, and the *earth pressure line* bL at an angle ψ (angle between the pressure P_1 and the vertical) to the slope line bS. We also trace $c_1d_1 \parallel ab$ and $d_1e_1 \parallel bL$. Thus we obtain the triangle bd_1e_1 (Fig. 20*c*). Since the angles at the vertices b and d_1 of this triangle are equal to the angles at t and r_1 in the polygon of forces (Fig. 20*b*), the triangle bd_1e_1 in Figure 20*c* is similar to the polygon of forces shown in Figure 20*b*. The weight of the wedge abc_1 in Figure 20*c* is

$$W_1 = \tfrac{1}{2}\gamma H' l_1$$

Since the triangle bd_1e_1 in Figure 20*c* is similar to the polygon of forces r_1s_1t we can establish the equation

$$P_1 = W_1 \frac{\overline{e_1d_1}}{\overline{bd_1}} = \tfrac{1}{2}\gamma H' l_1 \frac{\overline{e_1d_1}}{\overline{bd_1}} \qquad [1]$$

In a similar manner we can determine the intensity of the forces P_2, etc., required to maintain the equilibrium on other arbitrarily selected surfaces of sliding bc_2, etc. Since $c_1d_1 \parallel c_2d_2 \parallel$, etc., the ratio n between the true length of the distances $l_1 = ac_1$, $l_2 = ac_2$, etc., and the corresponding distances bd_1, bd_2, etc., is the same for each of these surfaces, or

$$n = \frac{l_1}{\overline{bd_1}} = \frac{l_2}{\overline{bd_2}} = \cdots \qquad [2]$$

Introducing the value n into equation 1 we obtain

$$P_1 = \tfrac{1}{2}\gamma n H' \overline{e_1d_1} = C_n \times \overline{e_1d_1} \qquad [3]$$

wherein $C_n = \gamma n H'/2$ is independent of the slope of the assumed surface of sliding.

By using the same procedure we get

$$P_2 = C_n \times \overline{e_2d_2}$$

and so on. In Figure 20*c* the forces P_1, P_2, etc., are represented by distances e_1d_1, e_2d_2, etc. Thus we obtain in Figure 20*c* several points, e_1, e_2, etc. All these points are located on a curve C which is called the *Culmann line.* In order to determine the maximum value P_A of the lateral pressure we draw a tangent to the curve C, parallel to the slope line bS. The point of contact of this tangent is e. If we trace ed parallel to the earth pressure line bL, the distance ed represents the active earth pressure P_A on the back of the wall in the scale of the drawing. The corresponding surface of sliding bc passes through the point of contact e. Substituting $\overline{ed}$ for $\overline{e_1d_1}$ in equation 3 we obtain for the intensity of the active earth pressure the value

$$P_A = \tfrac{1}{2}\gamma n H' \overline{ed} \qquad [4]$$

The same method can be used if the surface of the fill is broken or curved as shown in Figure 20*d*. However, in this case we cannot avoid computing the weight of the wedges W_1, W_2, etc., which correspond to the different sections bc_1, bc_2, etc. The weights thus obtained are plotted on a convenient scale on the slope line from b toward S.

25. Engesser's graphical solution. Figure 21*a* is a duplicate of the section through the backfill shown in Figure 20*a*. In order to determine the active earth pressure of this backfill by means of Engesser's method we trace the earth pressure line LL_1 through b at an angle ψ (angle between the direction of the earth pressure P_1 and the vertical direction) to the slope line bS. Then we plot the weight of each of the wedges abc_1, abc_2, etc., from point b in Figure 21*a* on the line bS_1 toward the left on a scale $W_1 = \overline{ac_1}$, $W_2 = \overline{ac_2}$, etc. Thus we obtain the points d_1, d_2, etc. Then we trace through each of these points a line parallel to the corresponding section bc_1, bc_2, etc. These lines intersect the earth pressure line LL_1 at the points e_1, e_2, etc. Figure 21*b* represents the polygon of forces for the wedge abc_1. It can readily be seen that this polygon is similar to the triangle bd_1e_1 in Figure 21*a*. For the same reason the triangles bd_2e_2, etc., are similar to the polygons of forces which represent the condition for the equilibrium of the wedges abc_2, etc. The sides d_1e_1, d_2e_2, etc., in Figure 21*a* are tangent to a curve E. If three or four sides have been determined, the curve E can be traced easily and accurately. It intersects the earth pressure line LL_1 at point e. Since the distances be_1, be_2, etc., represent the lateral resistance P_1, P_2, etc., required to prevent a slip along the surfaces bc_1, bc_2, etc., the distance be corresponds to the maximum lateral resistance required to prevent a slip along any plane section through b. Hence it represents the active earth pressure P_A on the scale of the drawing. The surface

of sliding *bc* is parallel to the tangent *ed* to the curve *E* at point *e*. From the geometrical relations represented in Figures 21*a* and 21*b* we obtain for the intensity of the active earth pressure the equation

$$P_A = \tfrac{1}{2}\gamma H' \overline{be} \qquad [1]$$

wherein $\overline{be}$ is the true length of the distance represented by *be*. The curve *E* is called the *Engesser line*.

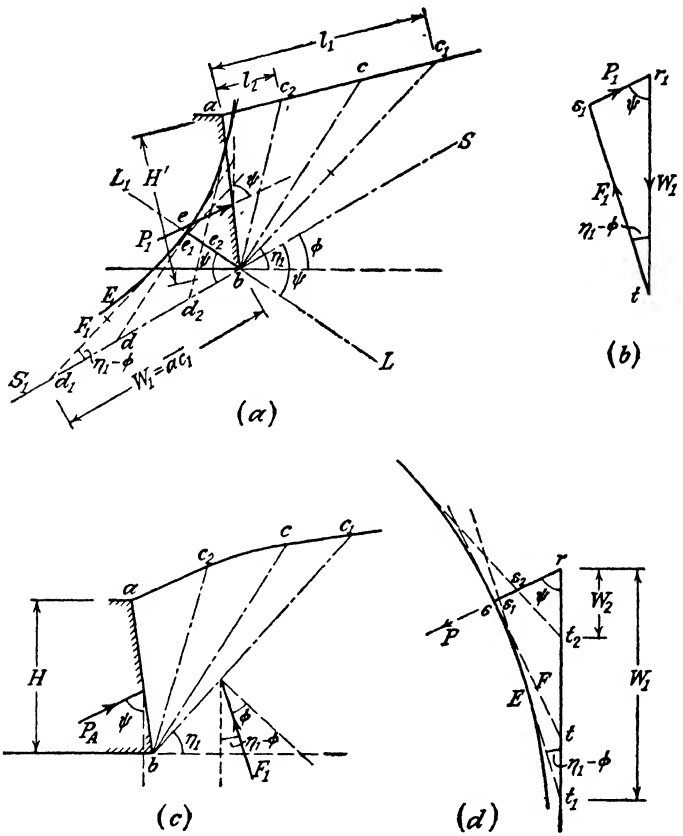

FIG. 21. Engesser's graphical method of determining earth pressure of sand.

If the surface of the backfill is curved, as shown in Figure 21*c*, the weight of the wedges W_1, W_2, etc., must be computed. In this case it is preferable to plot these weights in the polygon of forces (Fig. 21*d*) from point *r* in a downward direction and to construct the Engesser line in this side figure. The rest of the procedure is identical with that described above.

26. Location of the point of application of the active earth pressure. Figure 22*a* is a section through the sliding wedge adjoining a retaining wall with a rough, vertical back. The surface of the fill is horizontal. If the retaining wall yields through a distance sufficient to establish a state of plastic equilibrium in every point of the sliding wedge the shear pattern is like that shown in the figure. Any point b_1 at an arbitrary

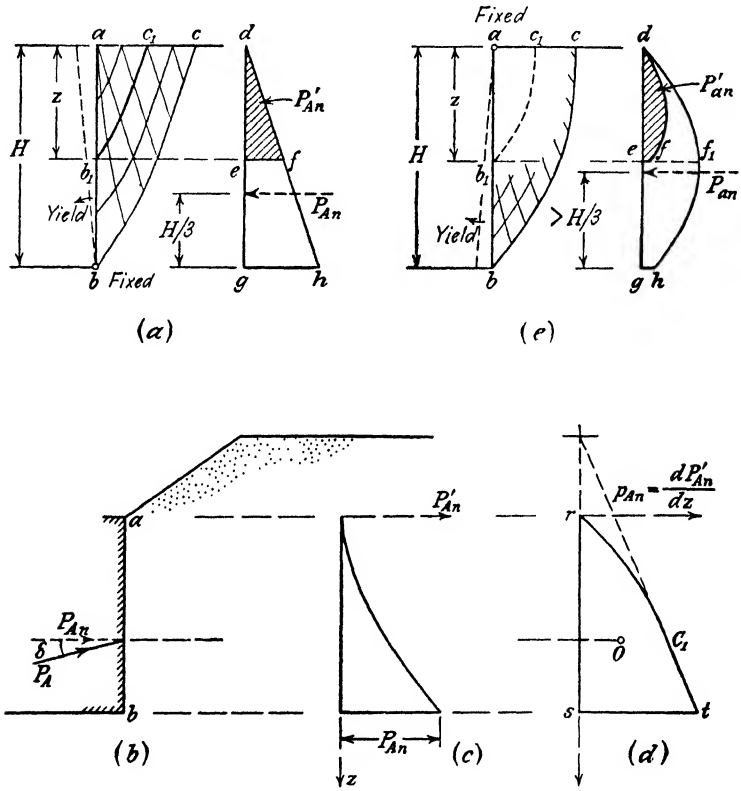

FIG. 22. Position of point of application of resultant earth pressure of sand under different conditions of lateral support.

depth z below point a represents the lower edge of a surface of sliding b_1c_1 which is similar to the surface of sliding bc. As a consequence the lateral pressure on the section ab_1 of the wall is equal to the lateral pressure on the back of a retaining wall with a height z. Substituting $\alpha = 90°$ in equation 23 (2) and replacing H by z we obtain for the normal component of the earth pressure on ab_1 the value

$$P'_{An} = \tfrac{1}{2}\gamma z^2 K_A$$

and the unit normal pressure on the wall at depth z is

$$p_{An} = \frac{dP'_{An}}{dz} = \gamma z K_A \qquad [1]$$

This equation is identical with equation 15(1). It demonstrates that the distribution of the earth pressure on the back of the wall increases like a hydrostatic pressure in simple proportion to depth, as shown on the right-hand side of Figure 22*a*. The point of application of the earth pressure is located at a height $H/3$ above the base of the wall, and the shaded area *def* represents the normal component of the earth pressure on ab_1.

If the surface of the backfill and the back of the wall are not plane, the distribution of the earth pressure on the back of the wall is not hydrostatic. Yet, if the wall yields by tilting about its lower edge or by advancing sufficiently far parallel to its original position, the entire mass of sand located within the sliding wedge passes into a state of plastic equilibrium. In this state every horizontal line on the back of the wall represents the lower edge of a potential surface of sliding. This fact suffices to establish the validity of the equation

$$p_{An} = \frac{dP'_{An}}{dz} \sin \alpha \qquad [2]$$

wherein α is the slope angle of the back of the wall at depth z. On the basis of this equation it is possible to locate the position of the point of application of the earth pressure by using the graphic procedure illustrated by Figure 22*b* to *d*. Figure 22*b* is a section through the vertical back of a wall supporting a backfill with a broken surface. On account of the break in the surface the distribution of the earth pressure on the back of the wall is nonhydrostatic. We determine by means of the method described in the following article the total earth pressure which acts on the back of the wall between its crest and different depths z_1, z_2, etc. By plotting the values P'_{An} thus obtained against depth, we can trace the curve shown in Figure 22*c*. This curve represents the relation between P_{An} and the depth z. From this curve we can get the values p_{An}, equation 2, by means of a simple graphical procedure. After plotting the values of p_{An} against depth we can trace the curve C_1 in Figure 22*d*. The area *rst* located between the curve C_1 and the vertical axis represents the total normal component of the lateral pressure. The point of application of the lateral pressure is located at the elevation of the center of gravity O of the pressure area *rst*. Similar procedures, based on equation 2, have been worked out for determining

the point of application of the earth pressure on a retaining wall whose back is not plane. (See for instance Krey 1936.) Since all these methods are based on the simplifying assumption that the surfaces of sliding are plane, they are far from being rigorous. Nevertheless they are rather cumbersome. For practical purposes simpler methods have been devised which give approximately the same results. Considering the nature of the basic assumptions, it appears doubtful whether the elaborate procedures are more reliable than the simple ones.

The validity of equation 2 is limited by the condition that every part of the mass of soil located within the sliding wedge must be in a state of plastic equilibrium. If the deformation conditions are such that the slip occurs while part of the sliding wedge is still in a state of elastic equilibrium, equation 2 loses its validity and neither of the procedures described before can be used for determining the position of the point of application of the earth pressure. This is illustrated by Figure 22*e*, which shows a vertical bank whose lateral support yields by tilting about its upper edge *a*. The fixed position of *a* prevents the upper part of the sliding wedge from passing into a state of plastic equilibrium. As explained in Article 20, failure occurs along a curved surface of sliding *bc* which intersects the surface of the backfill at right angles and the earth pressure on the support shown in Figure 22*e* is not identical with that on the back of the retaining wall shown in Figure 22*a*. Therefore it will be designated by another symbol, P_{an} instead of P_{An}. In Article 67 it will be shown that the earth pressure P_{an} can be expressed by an equation

$$P_{an} = \tfrac{1}{2}\gamma H^2 A_A$$

wherein A_A is a coefficient whose value is independent of H. Hence the earth pressure on a lateral support of the type shown in Figure 22*e* with a height z is

$$P'_{an} = \tfrac{1}{2}\gamma z^2 A_A$$

If P'_{an} were identical with the earth pressure P''_{an} on the upper part of the lateral support shown in Figure 22*e* we could write

$$P''_{an} = P'_{an} = \frac{z^2}{H^2} P_{an} \qquad [3]$$

and the distribution of the earth pressure would be strictly hydrostatic. Yet we know from experience that the value P''_{an} is always very much greater than the value determined by this equation. This is due to the following facts. If b_1 in Figure 22*e* represented the lower edge of the lateral support the slide would occur along the surface b_1c_1 which

is similar to the surface bc and the earth pressure on ab_1 would be equal to P'_{an}. The shearing stresses along b_1c_1 would be equal to the shearing resistance of the sand. In reality the lower edge of the lateral support is located at b and not at b_1. The line b_1c_1 does not represent a surface of sliding because it is located within a zone of elastic equilibrium. The shearing stresses along any surface passing through this zone, such as b_1c_1 are smaller than the shearing resistance of the sand. Therefore the earth pressure on ab_1 must be greater than P'_{an}. On account of these facts equation 3 is not valid. The distribution of the earth pressure is not hydrostatic. It is roughly parabolic as indicated on the right-hand side of Figure 22*e*. The location of the point of application of the earth pressure depends on the type of movement of the support which precedes the slip in the sand and cannot be ascertained without taking this factor into consideration. The shaded area $def = P'_{an}$ represents the earth pressure on a lateral support with a height z. This pressure is much smaller than the pressure $def_1 = P''_{an}$ on the section ab_1 of the lateral support with the height H.

On account of the decisive influence of the deformation conditions on the distribution of the earth pressure, all but the simplest earth pressure computations should be preceded by a careful investigation of these conditions.

This chapter deals only with retaining walls. Retaining walls yield always in such a manner that the entire mass of soil located within the sliding wedge passes into a state of plastic equilibrium. As a consequence equation 2 can be used as a basis for determining the position of the point of application of the earth pressure.

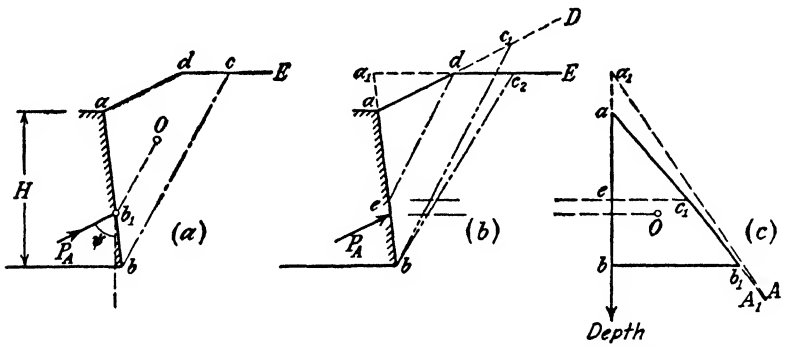

FIG. 23. Earth pressure of backfill with broken surface.

27. Backfill with broken surface. Figure 23*a* shows a section through a backfill with a broken surface. The intensity of the total lateral pressure P_A and the corresponding position of the surface of

sliding bc can be determined by any one of the graphic methods described above, because these methods are applicable regardless of the shape of the surface of the backfill. The point of application of the lateral pressure is located approximately at the point of intersection between the back of the wall and a line Ob_1 which passes through the center of gravity O of the sliding wedge $abcd$ parallel to the surface of sliding bc. This procedure is based merely on the experience that the results are approximately the same as those obtained by the relatively rigorous method for solving the problem, illustrated by Figures 22*b* to *d*.

A third method is illustrated by Figure 23*b*. We first assume that the sloping section ad of the surface of the backfill extends to infinity as shown by the line aD. The position of the corresponding surface of sliding bc_1 can be determined by means of the standard procedure. The line $ed \parallel bc_1$ represents the surface of sliding through point d, because in a backfill with a plane surface aD supported by a wall with a plane back ab all the surfaces of sliding are parallel. Over the section ae of the back of the wall the distribution of the lateral pressure is hydrostatic, as shown by the line ac_1 (Fig. 23*c*), because the top surface of the sliding wedge ade (Fig. 23*b*) is plane. A second computation is made on the assumption that the section dE of the surface of the backfill extends as far as a_1 located on the upward continuation of the back ab of the wall. The distribution of the lateral pressure of a backfill with a plane surface a_1E on a wall with a plane back a_1b is also hydrostatic, as shown by the line a_1A in Figure 23*c*. The error due to the assumption that the weight of the sliding wedge is increased by the weight of the added wedge aa_1d decreases rapidly with depth. Therefore the line a_1A (Fig. 23*c*) represents the asymptote of the real pressure line c_1A_1. At c_1 the real pressure line is almost tangent to ac_1 and with increasing depth it approaches the asymptote a_1A. Therefore it can be traced with sufficient accuracy by hand. The point of application of the pressure is located at the elevation of the center of gravity O of the pressure area abb_1c_1 (Fig. 23*c*).

28. Wall with broken back. Figure 24*a* represents a section through a wall with a broken back, acted upon by a backfill with a plane surface. We determine, first of all, the earth pressure P_{A1} on the upper section ad of the wall. The corresponding pressure distribution is hydrostatic, and the centroid of the pressure is located at the top of the lower third of this section. We know only the direction of the force P_{A2} which acts on the lower section bd. Its intensity and point of application must be determined.

In order to solve our problem by means of one of the standard methods of earth pressure computation, we assume an arbitrary surface of sliding bc_1 and trace the corresponding polygon of forces rus_1t_1 shown in Figure 24*b*. In this polygon we resolve the known force P_{A1} into two components ΔW and P'_{A1}. Thus we reduce the problem to the determination of the maximum value of the total lateral pressure of the earth on the wall in the direction of P_{A2}. Figure 24*b* represents the solution obtained by means of Engesser's method. The weights

of the different sliding wedges W_1, W_2, etc. (see Art. 25) have been plotted from point r in a downward direction. The slip occurs along the surface bc in Figure 24*a*.

The intensity and the direction of the total earth pressure P_A on the broken back of the wall are determined by the line rs in Figure 24*b*.

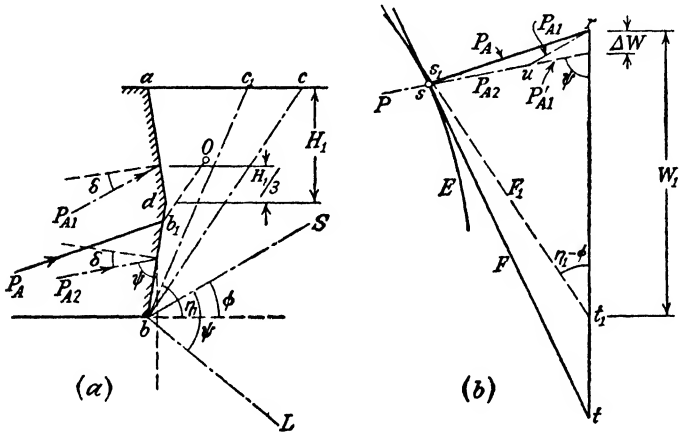

FIG. 24. Earth pressure of sand on wall with broken back.

This line represents the geometric sum of the two earth pressure components $P_{A1} = \overline{ru}$ and $P_{A2} = \overline{us}$. The point of application of P_A is located approximately at the point of intersection b_1 (Fig. 24*a*) between the back of the wall and the line Ob_1, which passes through the center of gravity O of the sliding wedge, $abcd$, parallel to the surface of sliding bc. A better approximation can be obtained by means of the procedure described in Article 26.

29. Lateral pressure due to uniform surcharges. Figure 25*a* is a section through a backfill whose inclined surface carries a uniformly distributed surcharge, q per unit of area. The line d_1c_2 is an arbitrary plane section through a point d_1 on the back of the wall at a depth z below its upper edge. The weight of the corresponding wedge ad_1c_2 without the surcharge is

$$W_1 = \tfrac{1}{2}\gamma z\, l_z \frac{\sin(\alpha+\beta)}{\sin\alpha}$$

The surcharge increases this weight by $q\, l_z$. The weight W_1' of the wedge with surcharge is the same as the weight of a wedge with the section ac_2d_1 and with a unit weight $\gamma_q > \gamma$. From the equation

$$W_1' = \tfrac{1}{2}\gamma z\, l_z \frac{\sin(\alpha+\beta)}{\sin\alpha} + q\, l_z = \tfrac{1}{2}\gamma_q z\, l_z \frac{\sin(\alpha+\beta)}{\sin\alpha}$$

we obtain for the unit weight γ_q the value

$$\gamma_q = \gamma + \frac{2q}{z}\frac{\sin\alpha}{\sin(\alpha+\beta)} = \gamma + N\frac{2q}{z} \qquad [1a]$$

wherein

$$N = \frac{\sin\alpha}{\sin(\alpha+\beta)} \qquad [1b]$$

If we substitute $H = z$, $\gamma = \gamma_q$, and $P_A = P'_A$ in equation 23(1a) we obtain for the active earth pressure on the section ad_1 of the wall shown in Figure 25 the value

$$P'_A = \tfrac{1}{2}\gamma_q z^2 \frac{K_A}{\sin\alpha\cos\delta} = \tfrac{1}{2}\left(\gamma + N\frac{2q}{z}\right)z^2\frac{K_A}{\sin\alpha\cos\delta} \qquad [2]$$

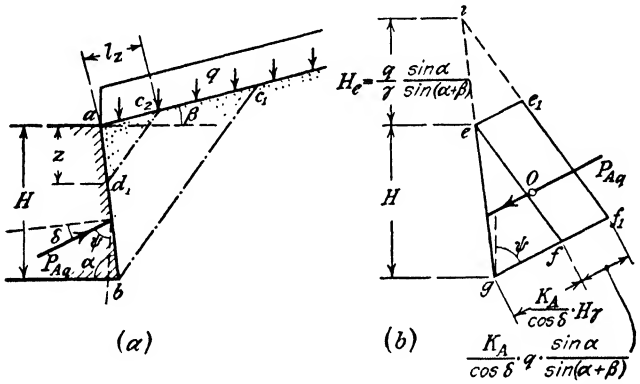

FIG. 25. Effect of uniformly distributed surcharge on earth pressure of sand.

wherein the factor $K_A/\sin\alpha\cos\delta$ is a constant for given values of ϕ, α, δ, and β. The corresponding unit lateral pressure p_A at depth z is

$$p_A = \frac{dP'_A}{dz}\sin\alpha = \frac{K_A}{\cos\delta}\gamma z + \frac{K_A}{\cos\delta}Nq \qquad [3]$$

On the right-hand side of this equation the first term represents the unit earth pressure at depth z due to the weight of the earth. The corresponding distribution of this pressure is hydrostatic, as shown by the triangle efg in Figure 25b. The second term represents the unit earth pressure due to the weight of the surcharge. It is independent of depth. Hence in Figure 25b this part of the earth pressure is represented by a parallelogram ee_1f_1f. The continuation of the side e_1f_1 of this parallelogram intersects the reference line eg at point i at an elevation

$$H_e = N\frac{q}{\gamma} = \frac{q}{\gamma}\frac{\sin\alpha}{\sin(\alpha+\beta)} \qquad [4]$$

above the upper edge of the back of the wall. According to Figure 25*b* the earth pressure on the back of the wall is identical with the earth pressure on the section *ab* of an imaginary wall with the height $H + H_e$ whose backfill does not carry any surcharge. The height H_e (eq. 4) is called the *equivalent height of the surcharge.* From Figure 25*b* we obtain the simple geometrical relation

$$P_{Aq} = P_A \left(\frac{H_e + H}{H}\right)^2 - P_A \left(\frac{H_e}{H}\right)^2 = P_A\left(1 + 2\frac{H_e}{H}\right) \qquad [5]$$

wherein P_A is the earth pressure exerted by the backfill without surcharge, represented by the triangle *efg*. Hence in order to solve our problem it suffices to determine the earth pressure P_A of the backfill without surcharge, to compute the equivalent height H_e by means of equation 4, and to introduce the value H_e into equation 5. The line of action of the earth pressure P_{Aq} passes through the center of gravity *O* of the pressure area gf_1e_1e in Figure 25*b*.

30. Line load parallel to the crest of the wall. If a line load, q' per unit of length of a line parallel to the crest of the wall, acts on the surface of a backfill, the active earth pressure P_A of the backfill increases by ΔP_A. The value of ΔP_A depends not only on the intensity of the load but also on the distance between the load and the crest *a* of the lateral support shown in Figure 26*a*. In order to investigate the influence of the distance on the supplementary earth pressure ΔP_A, we apply the load at an arbitrary distance ac' from the crest as shown in the figure and determine the corresponding value of ΔP_A. This can for instance be done by means of a slight modification of Culmann's procedure (see Art. 24). If the surface of the backfill carries no surcharge, we obtain the Culmann line *C* and the slip occurs along the surface of sliding *bc*. The lateral resistance required to prevent a slip along the arbitrarily selected surface bc' is determined by the distance $d'e'$, and the distance bd' represents the weight of the wedge abc' in the scale of the diagram. If we apply at c' a line load, q' per unit of length, we increase the weight of every wedge whose right-hand boundary is located on the right-hand side of c' by $q' = d'd_1'$. Hence there will be a sharp break in the Culmann line at the point of intersection between this line and the line bc'. This break is represented by the straight section $e'e_1'$. On the right-hand side of point e_1' the Culmann line continues as shown by the curve C'. The lateral resistance required to prevent a slip along the section bc' is determined by the distance $d_1'e_1'$. If this distance is smaller than $\overline{de}$ which represents the earth pressure P_A exerted by the backfill without surcharge, the surcharge has no influence on the lateral

earth pressure and the slip occurs along bc. On the other hand, if $\overline{d_1'e_1'}$ is greater than $\overline{ed}$, the slip occurs along the section bc', because for any section located on either side of bc' the lateral resistance required to prevent a slip is smaller than $\overline{d_1'e_1'}$. The lateral pressure ΔP_A produced by the line load q' is represented by the difference $\overline{d_1'e_1'} - \overline{de}$.

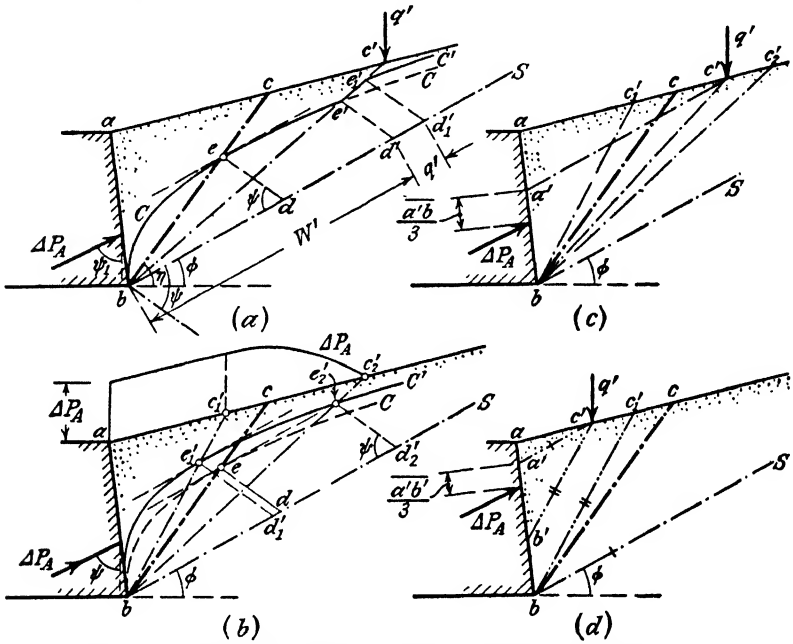

FIG. 26. Earth pressure exerted by backfill which carries a line load.

The graphic determination of ΔP_A, illustrated by Figure 26*a* can be repeated for line loads acting at different distances from the crest a. By plotting the values of ΔP_A as ordinates above the points of application of the line loads, we obtain the influence line ΔP_A in Figure 26*b*. The corresponding Culmann line is marked C'. A tangent parallel to the slope line bS touches the curve C' at point e_1' and the distance $d_1'e_1'$ determines the greatest value which the lateral pressure of the backfill acted upon by a line load q' can possibly assume. If the line load is located between the points a and c_1' the slip occurs along bc_1' and the position of the line load has no influence on the lateral pressure. If the line load moves from point c_1' toward the right the influence of the line load on the lateral pressure decreases and the slip occurs along a plane which passes through b and the line which is occupied by the load. In order to determine the location at which the influence of the line load

on the lateral pressure becomes equal to zero, we trace a tangent to the Culmann curve C (backfill without line load) parallel to the slope line bS. This tangent intersects the curve C' at point e_2'. The straight line be_2' intersects the surface of the fill at point c_2'. If the load acts at the point c_2' the lateral resistance required to prevent a slip along the section bc_2' through the backfill with a line load becomes equal to the lateral resistance required to maintain the equilibrium of the backfill without line load. This resistance is represented by the distance $\overline{ed}$. Hence, if the line load is located on the right-hand side of point c_2' it has no influence on the earth pressure and the slip occurs along bc.

Some engineers believe that a line load has no influence on the lateral pressure unless it is located within the distance ac (Fig. 26*b*), which represents the upper surface of the sliding wedge in a fill without line load. The preceding analysis demonstrates that this opinion is not justified.

Figures 26*c* and 26*d* illustrate a simple method of estimating the location of the point of application of the excess pressure ΔP_A due to a line load q' per unit of length of a line parallel to the crest of the wall. In both figures the points c_1', c, and c_2' are identical with the points indicated by the same letters in Figure 26*b*. If the line load is applied at c' between c_1' and c_2' (Fig. 26*c*) we trace $a'c' \parallel bS$. The point of application of the lateral pressure due to the line load is located on $a'b$ at a distance of approximately $\overline{a'b}/3$ from a'. If the line load is applied at c' between a and c_1' as shown in Figure 26*d* we trace $a'c' \parallel bS$ and $b'c' \parallel bc_1'$. The point of application of the excess pressure is located on $a'b'$ at a distance of approximately $\overline{a'b'}/3$ from a'. In both cases the error is on the safe side.

A more accurate result can be obtained by determining the total pressure on each of several sections of the wall at different depths below the upper edge. This investigation furnishes the data required to ascertain the distribution of the lateral pressure over the back of the wall by graphic differentiation. However, in reality the presence of a line load always increases the curvature of the surface of sliding which in turn increases the error due to the assumption of a plane surface of sliding. Hence the elaborate procedure for ascertaining the point of application of the supplementary pressure due to the line load is out of proportion to the general degree of accuracy of the method of computation.

31. Earth pressure on reinforced concrete walls. Reinforced concrete walls are always constructed on a heavy footing which extends beneath the backfill, as shown in Figure 27*a*. If such a wall yields by tilting or sliding until the backfill starts to fail, one part of the backfill adjoining the wall, represented by the triangle bb_1d, remains practically

undisturbed and acts as if it were a part of the wall. If the stability of the wall were inadequate the backfill would fail by shear along a surface of sliding b_2c. In accordance with our assumptions the wall yields in such a manner that every part of the sliding wedge passes into a state of plastic equilibrium. Hence every point of the left-hand boundary $adbb_2$ of the sliding wedge represents the lower edge of a potential surface of sliding. The line bc_1 indicates the surface of sliding through b.

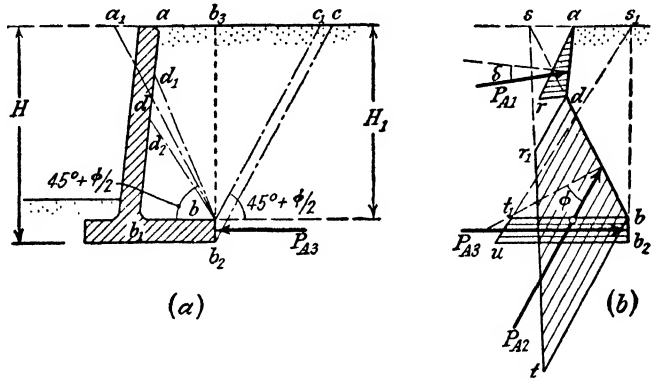

FIG. 27. Earth pressure of sand on cantilever retaining wall.

If the surface bd extended to a point a_1 at the elevation of the crest of the wall, both the boundary stress conditions and the deformation conditions for the wedge bc_1a_1 would be identical with those for a wedge-shaped section located between two intersecting surfaces of sliding in the semi-infinite mass shown in Figure 8c. Hence, as a first approximation, the results of the analysis contained in Article 10 can be applied to the problem under discussion. According to these results the surfaces of sliding bc_1 and bd in Figure 27a rise at angles of $45° + \phi/2$ to the horizontal. The earth pressure P_{A2} on the surface bd acts at an angle ϕ to the direction of its normal component, and its intensity can be determined rapidly by means of Mohr's diagram (Fig. 8b). The lateral pressure P_{A1} on the section ad of the wall can be ascertained by means of Coulomb's equation 23(1) or by one of its graphical substitutes. The pressure P_{A3} on the vertical face bb_2 can be computed with sufficient accuracy on the assumption that it acts in a horizontal direction as indicated in the figure. On this assumption we obtain by means of equations 15(1) and 15(2)

$$P_{A3} = \tfrac{1}{2}\gamma(H^2 - H_1^2)\tan^2\left(45° - \frac{\phi}{2}\right)$$

The distribution of the earth pressure over the section *ad* of the back of the wall is hydrostatic, as shown by the straight line *ar* in Figure 27*b*. The point of application of the pressure is located at a distance of $\overline{ad}/3$ from *d*. The distribution of the earth pressure over a plane section a_1b through a semi-infinite deposit with a horizontal surface ca_1 (Fig. 27*a*) is also hydrostatic. In Figure 27*b* this pressure distribution is shown by the straight line *st*. Therefore we can assume with sufficient accuracy that the pressure on the surface of sliding *bd* in Figure 27*a* is determined by the trapezoid btr_1d in Figure 27*b*. The earth pressure P_{A3} is represented by the area b_2ut_1b.

A more accurate solution of the problem can be obtained by computing the lateral earth pressure on different broken surfaces ad_1b, ad_2b, etc. (Fig. 27*a*), by means of the method described in Article 28. The slip will occur along the section which corresponds to the maximum value of the lateral pressure. The distribution of the earth pressure over the surface of sliding which rises from point *b* toward the back of the wall can be determined point for point by means of the method explained at the end of Article 27.

32. Earth pressure exerted by stratified backfills. Figure 28*a* represents a section through a backfill consisting of two strata with different unit weights γ_1 and γ_2, but with the same angle of internal friction ϕ and the same angle of wall friction, δ. The earth pressure exerted by this system can be directly determined by means of Culmann's method

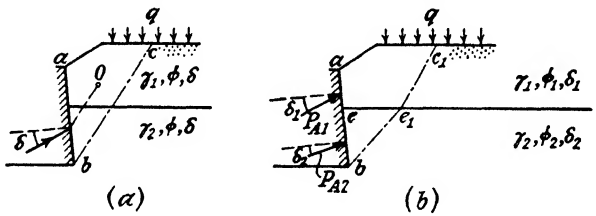

FIG. 28. Earth pressure exerted by stratified, cohesionless backfills.

(Art. 24), because this method involves no assumptions regarding the distribution of the weight within the wedges. In order to find the point of application of the earth pressure we determine the center of gravity *O* of the sliding wedge *abc* and of the surcharge which rests on top of the wedge. The point of application is approximately located at the point of intersection between the back of the wall and a line through *O* parallel to *bc*.

On the other hand, if the angles of internal friction and of wall friction for the two strata are different, as shown in Figure 28*b*, we are obliged to solve our problem in two steps. The first step consists in determining the lateral pressure P_{A1} on the upper section, *ae*, of the wall. This

can be done by means of the procedures described in Articles 27 and 29. In order to determine the lateral pressure P_{A2} on the lower part, *eb*, of the wall, we disregard all the shearing stresses which act along the boundary between the two strata as well as the shearing stresses along any vertical section above this boundary. On this assumption the entire upper stratum can be considered as a simple surcharge and the vertical pressure on any section of the surface of the lower stratum is equal to the weight of the earth and the surcharge q which is located above it. Owing to this simplification of our problem the lateral earth pressure P_{A2} on the section *be* of the wall can be determined by means of Culmann's method. The corresponding surface of sliding is represented by the line be_1. The error involved in this method of computation is on the unsafe side because the neglected shearing stresses tend to increase the lateral pressure on the section *be* of the wall.

33. Earth pressure of cohesive backfills. Figure 29*a* is a section through a cohesive backfill supported by a retaining wall with a rough vertical back. The shearing resistance of the backfill is determined by the equation

$$s = c + \sigma \tan \phi \qquad 5(1)$$

The shearing stresses along the surface of contact between the soil and the back of the wall are assumed to be equal to

$$p_{At} = c_a + p_{An} \tan \delta$$

wherein c_a is the adhesion between the soil and the wall, p_{An} is the normal pressure per unit of area of the back of the wall, and $\tan \delta$ is the coefficient of wall friction. It is assumed that the yield of the wall is sufficient to transfer the entire sliding wedge to a state of plastic equilibrium. If the backfill consists of clay the yield required to satisfy this condition may be greater than 5 per cent of the height of the wall.

The following method of computing the active earth pressure is analogous to that used to compute the active Rankine pressure in cohesive masses. In Article 12 it has been shown that the uppermost layer of a semi-infinite cohesive mass in an active Rankine state is in a state of tension to a depth

$$z_0 = \frac{2c}{\gamma} \tan \left(45° + \frac{\phi}{2}\right) \qquad 12(1)$$

Below depth z_0 the horizontal pressure on a vertical section increases from zero at depth z_0 in simple proportion to depth, as shown by the pressure area bcc_A in Figure 11*e*. If one replaces the soil located above a horizontal section at any depth z below the surface by a surcharge

γz per unit of area the intensity and the distribution of the stresses below this section remain unchanged. The total horizontal pressure on a vertical section between the surface and a depth $2z_0$ is equal to zero. Hence, theoretically, a vertical bank with a height $H_c = 2z_0$ should be able to stand without any lateral support. (See Art. 57.) However, in reality, the state of tension in the top layer sooner or later produces tension cracks which reduce the height H_c to a smaller value H_c'. This value determines the depth to which the soil may detach itself from the back of the wall as indicated in Figure 29*a*. To simplify the following computations we assume that the tension cracks in the soil itself extend to the same depth. This assumption involves an error on the safe side.

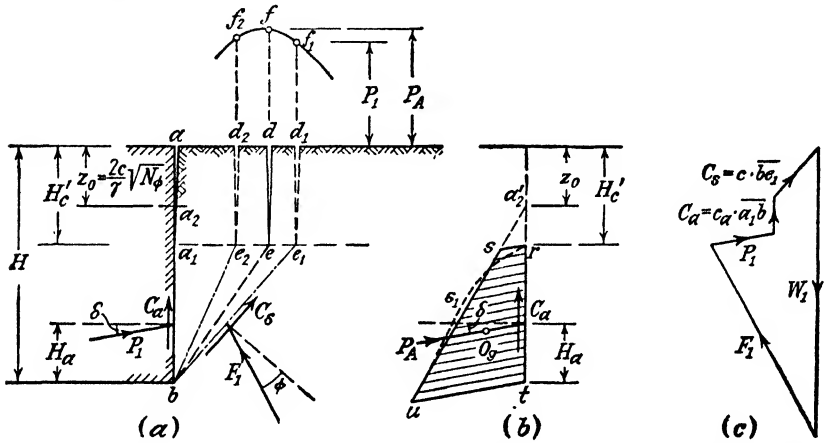

FIG. 29. Active earth pressure on retaining wall backfilled with cohesive soil.

The factors which determine the height H_c' will be discussed in Article 57. In the following analysis H_c' is assumed to be known. It is further assumed that the soil located between the surface and depth H_c' acts like a surcharge $\gamma H_c'$ per unit of area. This condition is satisfied if the surface of sliding *be* (Fig. 29*a*) starts at the bottom *e* of a tension crack with a depth H_c'. Finally it is assumed, as a first approximation and by analogy to the active Rankine state described before, that the pressure on the wall increases with depth below point a_1 (Fig. 29*a*), as indicated by the line *su* in Figure 29*b*. On this assumption, the pressure P_A on the back of the wall can be represented by a trapezoidal pressure area *rsut* in Figure 29*b*. In reality the distribution of the pressure most likely will be such as indicated by the area rs_1ut, whose center of gravity is located a short distance below that of *rsut*.

In order to determine the pressure P_A (resultant of the normal

component P_{An} and the friction component $P_{An} \tan \delta$ of the active earth pressure P_{Ac}) we assume an arbitrary plane surface of sliding be_1 through the foot b of the wall. The force P_1 required to prevent a slip along this surface can be scaled off the polygon of forces shown in

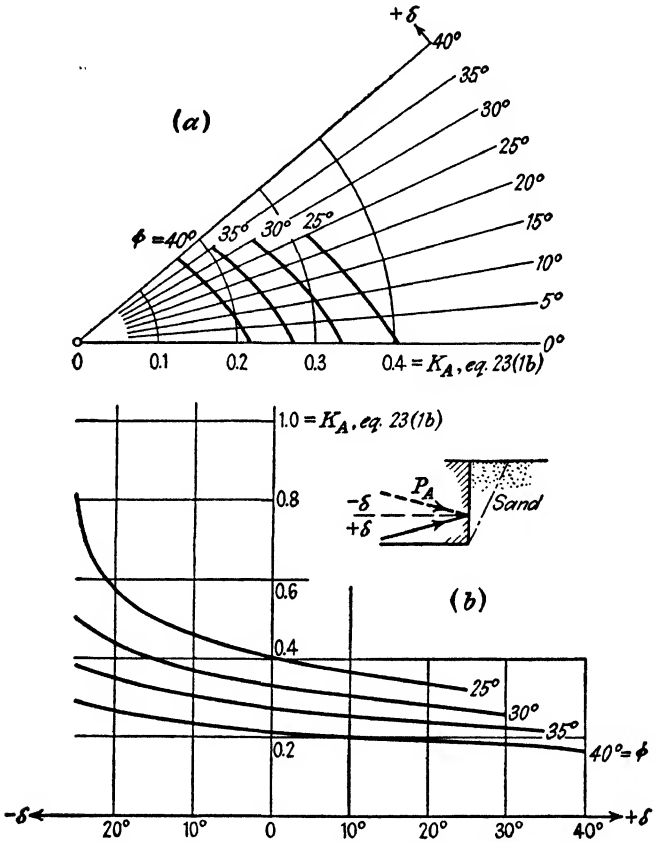

FIG. 30. Two different types of earth pressure graphs, which furnish the value of the coefficient of active earth pressure K_A for different values of ϕ and δ. (*Diagram a after Syffert 1929.*)

Figure 29c. In this polygon the weight W_1 represents the weight of the body of soil abe_1d_1. The forces $C_a = c_a \overline{a_1 b}$ and $C_s = c \overline{be_1}$ represent the cohesion forces which act along the surface of contact a_1b between wall and earth and along the surface be_1 respectively.

In order to find the intensity of the force P_A we repeat the construction for plane sections rising at different angles through b to the elevation of point e_1. The corresponding values P_1, P_2, etc., are plotted as ordinates above the surface of the fill as shown in Figure 29a. The force P_A

is equal to the greatest ordinate of the curve thus obtained. The distribution of the pressure P_A over the back of the wall is represented by the pressure area *rsut* in Figure 29*b*. The active earth pressure P_{Ac} is equal to the resultant of P_A and the adhesion component $C_a = c_a \overline{a_1 b}$ of the earth pressure. The point of application of the active earth pressure P_{Ac} is identical with that of P_A, which in turn is determined by the position of the center of gravity O_g of the pressure area *rsut*, as shown in the figure.

During rainstorms the empty space aa_1 (Fig. 29*a*) between the wall and the upper part of the backfill is invaded by surface waters. In this state the lateral pressure on the back of the wall is equal to the sum of the earth pressure and the pressure exerted by a column of water with a height H_c', unless the space between the wall and the backfill is adequately drained.

34. Earth pressure tables and graphs. In engineering practice the backs of most walls and the surfaces of most backfills encountered are at least approximately plane, and on account of the uncertainties involved in the estimate of the values of ϕ and δ a rough estimate of the earth pressure serves its purpose. In order to reduce the time required to solve problems of that type, earth pressure tables or graphs can be used which contain the values of the hydrostatic pressure ratio K_A (eq. 23(1*b*)) for different values of ϕ and δ and for different values of the slope angle β. Elaborate earth pressure tables have been published by Krey (1936). Figure 30 shows convenient methods of representing graphically the relation between the hydrostatic pressure ratio and the values of ϕ and δ. In Figure 30*a* the values of K_A are plotted on rays through a zero point. The angle between the rays and the horizontal axis is equal to the angle of wall friction δ, and the values of ϕ are inscribed on the curves which represent the relation between K_A and δ (Syffert, 1929). In Figure 30*b* the hydrostatic pressure ratio K_A has been plotted against the angle of wall friction δ. Both diagrams reveal at a glance the importance of the influence of the angle of wall friction on the intensity of the earth pressure.

Chapter VII

PASSIVE EARTH PRESSURE

35. Passive earth pressure in engineering practice. In the broadest sense the term passive earth pressure indicates the resistance of the soil against forces which tend to displace it. In engineering practice the passive earth pressure is frequently utilized to provide a support for structures such as retaining walls or bulkheads which are acted upon by horizontal or inclined forces. The retaining wall shown in Figure 19 depends partly on the passive pressure of the soil located on the left side of the face *de* to prevent failure by sliding along its base *bd*. The equilibrium of the bulkhead shown in Figure 63 is maintained solely by the lateral resistance of the soil on the left side of the face *bd*. The body which tends to displace the soil is called the *seat of the thrust* and the surface of contact between this body and the earth represents the *contact face*.

The passive earth pressure of the soil is also utilized when a building is supported on footings. If the load on a footing exceeds the ultimate bearing capacity of the soil, a wedge-shaped body of soil such as the body *abc* in Figure 15*b* moves together with the footing in a downward direction. It may be in a state of plastic or of elastic equilibrium. In either state the body *abc* is deformed without being displaced. On the other hand the soil adjoining the inclined lower boundaries of this body, *ac* and *bc* in Figure 15*b*, is shoved out of the ground. This event cannot occur unless the pressure which acts on the soil along *ac* and *bc* is greater than the passive earth pressure. In this case the seat of the thrust is represented by the wedge-shaped body of soil *abc* and the contact faces are represented by two surfaces of sliding which are located entirely within the soil.

36. Assumptions and conditions. The following computations are based on the assumption that the soil is isotropic and homogeneous and that the deformation of the soil occurs only parallel to a vertical section at right angles to the contact face. It is further assumed that the contact face advances under the influence of the thrust into a position which is located entirely beyond the boundary a_1b of the shaded area in Figure 14*e*. This area represents the minimum lateral compression which is required to transfer the soil adjoining the contact face from its

original state of elastic equilibrium to the state of plastic equilibrium associated with the shear pattern shown in Figure 14*e*.

The unit weight of the earth is γ and the shearing resistance of the soil is determined by the equation

$$s = c + \sigma \tan \phi \qquad 5(1)$$

wherein c is the cohesion, σ the total normal stress on the surface of sliding, and ϕ the angle of shearing resistance. The shearing stress on the contact face is

$$p_{Pt} = c_a + p_{Pn} \tan \delta \qquad [1]$$

wherein c_a is the adhesion between the soil and the seat of the thrust, p_{Pn} is the normal component of the passive earth pressure per unit of area, and δ is an angle whose value depends on the character of the contact face. If the contact face represents the contact between masonry and soil, the values of c_a and δ may be equal to or smaller than the values c and ϕ, respectively, and δ represents the angle of wall friction. On the other hand, if the contact face cuts across a mass of soil, c_a is equal to c and δ equal to ϕ. In either case the angle δ may be positive or negative (see Art. 15). In all the figures in this chapter δ is shown positive, because in practice the conditions required to produce passive earth pressure combined with negative wall friction are seldom satisfied. The adhesion c_a acts in the direction of the wall friction. Hence if δ is negative, c_a is also negative.

For cohesionless materials the values c and c_a are equal to zero. The shearing resistance is equal to

$$s = \sigma \tan \phi$$

wherein σ is the effective normal stress on the surface of sliding and ϕ is the angle of internal friction. The shearing stresses on the contact face are

$$p_{Pt} = p_{Pn} \tan \delta$$

In the following investigations it will be assumed that the surface of the soil is horizontal and that the angle of wall friction δ is positive. However, the methods described in the following articles can also be used without essential modification if δ is negative or if the surface of the soil is inclined.

If the conditions stated at the outset of this article are satisfied the soil fails as shown in Figure 14*e* for positive values of δ and in Figure 14*g* for negative values. In either case the zone of plastic equilibrium includes a passive Rankine zone whose inclined boundaries rise at an angle of $45° - \phi/2$ to the horizontal. The lower boundary of the

wedge-shaped zone located between the Rankine zone and the contact face is curved. Therefore the lower boundary of the sliding wedge, for instance the wedge *abde* in Figure 31*a*, consists of a curved lower part *bd* and a straight upper part *de* which rises at an angle of $45° - \phi/2$ to the horizontal. The boundary *d* between these two sections is located on a straight line *aD* which descends through the upper edge *a* of the

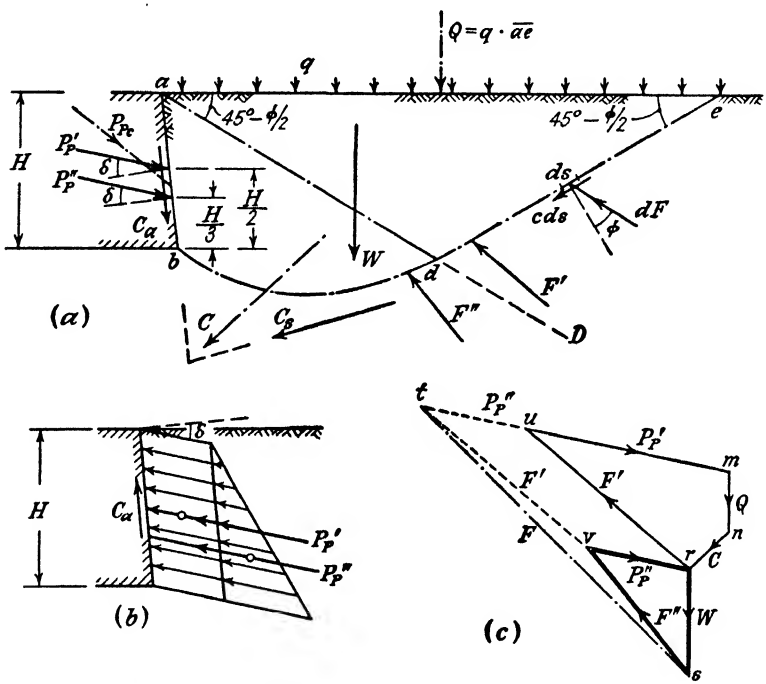

FIG. 31. Approximate determination of position of point of application of resultant passive earth pressure of cohesive soil.

contact face at an angle of $45° - \phi/2$ to the horizontal. This statement is valid for both cohesive and cohesionless materials. The shape of the curved part of the surface of sliding can be determined with sufficient accuracy on the basis of the assumption that it consists either of a logarithmic spiral or of an arc of a circle. For cohesionless materials one can even assume, without excessive error, that the entire lower boundary of the sliding wedge is plane, provided the angle of wall friction δ is small (see Art. 38).

37. Point of application of the passive earth pressure. If the deformation condition stated at the outset of the preceding article is satisfied the normal component p_{Pn} of the passive earth pressure per unit of area of a plane contact face (*ab*, Fig. 31*a*) at depth *z* below *a* can be

expressed approximately by the linear equation

$$p_{Pn} = cK_{Pc} + qK_{Pq} + \gamma zK_{P\gamma} \qquad 15(5)$$

wherein q is the surcharge per unit of area and K_{Pc}, K_{Pq}, and $K_{P\gamma}$ are pure numbers whose values are independent of z and γ. The pressure p_{Pn} can be resolved into two parts. One part,

$$p'_{Pn} = cK_{Pc} + qK_{Pq}$$

is independent of z. The corresponding part of the normal component P_{Pn} of the passive earth pressure is

$$P'_{Pn} = \frac{1}{\sin \alpha} \int_0^H p'_{Pn}\, dz = \frac{H}{\sin \alpha}(cK_{Pc} + qK_{Pq}) \qquad [1]$$

Since this pressure is uniformly distributed, its point of application is located at the midpoint of the contact face. The pressure P'_{Pn} produces a frictional resistance $P'_{Pn} \tan \delta$ on the contact face. By combining P'_{Pn} with the friction component $P'_{Pn} \tan \delta$ we obtain a force P'_P which acts at an angle δ to the normal on the contact face ab.

The second part of the unit pressure p_{Pn}

$$p''_{Pn} = \gamma zK_{P\gamma}$$

increases like a hydrostatic pressure in simple proportion to depth. Therefore the point of application of the resultant pressure

$$P''_{Pn} = \frac{1}{\sin \alpha} \int_0^H p''_{Pn}\, dz = \tfrac{1}{2}\gamma H^2 \frac{K_{P\gamma}}{\sin \alpha} \qquad [2]$$

is located at a height $H/3$ above the base of the contact face. Combining P''_{Pn} with the frictional resistance $P''_{Pn} \tan \delta$ produced by this force we obtain the force P''_P which acts at an angle δ to the normal on the contact face ab.

The total passive earth pressure P_{Pc} is equal to the resultant of the forces P'_p, P''_p, and of the adhesion force

$$C_a = \frac{H}{\sin \alpha} c_a \qquad [3]$$

Hence we can resolve the total passive earth pressure into three components with known direction and known position with reference to the contact face. These components are P'_P, P''_P, and C_a. Their distribution over the contact face ab is shown in Figure 31a. For a cohesionless soil without surcharge P'_p and C_a are equal to zero and P''_P is identical with the passive earth pressure P_P.

The intensity of the forces P'_P and C_a in Figure 31b increases in simple

proportion to the height H of the contact face, and P''_P increases with the square of H. The soil fails by shear along a surface of sliding through the lower edge of the contact face. Since P'_P (eq. 1) does not contain the unit weight γ of the soil, this force represents that part of the total passive earth pressure which is required to overcome the cohesion and the frictional resistance due to the weight of the surcharge. Hence if the unit weight of the soil is reduced to zero the force P_P required to produce a slip on a given surface of sliding is reduced from P_P to P'_P. On the other hand, if we retain the unit weight γ while eliminating the cohesion and the surcharge we reduce this force from P_P to P''_P.

The normal component of the total passive earth pressure is

$$P_{Pn} = P'_{Pn} + P''_{Pn} = \frac{H}{\sin \alpha} (cK_{Pc} + qK_{Pq}) + \tfrac{1}{2}\gamma H^2 \frac{K_{P\gamma}}{\sin \alpha} \qquad [4]$$

In Figure 31*a* the line *bde* represents the surface of sliding. The top surface *ae* of the sliding wedge is acted upon by the uniformly distributed surcharge $Q = \overline{ae}\, q$. In order to resolve the total passive earth pressure P_{Pc} into its constituents, P'_P, P''_P, and C_a, we examine the conditions for the equilibrium of the wedge *abde*. This wedge, with a weight W, is acted upon by the following forces: the surcharge Q, the resultant C of the cohesion C_s along *bde* and of the adhesion force C_a, the resultant F of the elementary reactions dF which act at every point of the surface of sliding *bde* at an angle ϕ to the normal on this surface as shown in the figure, and the forces P'_P and P''_P, which act at an angle δ to the normal on the contact face. Equilibrium requires that the polygon of forces (Fig. 31*c*) constituted by these forces be closed. Among the forces shown in the polygon, the forces Q and C (single lines) increase in simple proportion to the height H of the contact face and the force W (double line) increases with the square of the height. The sum of the forces $P'_P + P''_P$ is represented by the distance *mt*. One part, P'_P, is concurrent with the forces Q and C and increases in simple proportion to H. The second part, P''_P, is concurrent with W. In order to determine the first part, we construct the polygon of forces on the assumption that the unit weight γ of the earth is equal to zero, which means $W = 0$. The direction of the corresponding reaction F' is determined by the condition that the elementary reactions dF act at every point at an angle ϕ to the normal on the surface of sliding. Tracing through *r* a line parallel to the direction of F' we get the polygon of forces *mnru*. The distance *mu* is equal to the force P'_P and the point of application of

this force is at the midpoint of the contact face ab. The force P_P'' is represented by the distance ut. In order to determine this force independently we could construct a second polygon of forces on the assumption that c, c_a and q are equal to zero. The direction of the corresponding reaction F'' is determined by the same condition as that of F'. By tracing sv parallel to this direction and rv parallel to mt we obtain the polygon rsv. The force P_P'' is equal to the distance rv which in turn is equal to ut as shown in the figure. The geometric sum of the two forces F' and F'' is equal to the total reaction F.

The preceding analysis leads to the following conclusion. If either c or q is greater than zero the passive earth pressure can be determined by two successive operations. The first one is based on the assumption that the unit weight γ of the soil is equal to zero. Thus we obtain the component P_P' of the earth pressure. The point of application of this component is at the midpoint of the contact face. The second operation is based on the assumption that c, c_a, and q are equal to zero and the point of application of the component P_P'' thus obtained is located at a height $H/3$ above the lower edge of the contact face.

A more accurate determination of the location of the point of application of the passive earth pressure could be made on the basis of equation 26(2) because this equation is valid for both active and passive earth pressure regardless of cohesion, provided the deformation conditions permit the entire sliding wedge to pass into a state of plastic equilibrium. However, the error associated with the approximate method illustrated by Figure 31 is not important enough to justify the amount of labor required to obtain a more accurate solution.

The following articles 38 to 40 deal with the passive earth pressure of ideal cohesionless materials without surcharge. They are intended to acquaint the reader with the technique of computing the passive earth pressure. The general case, involving the passive earth pressure of cohesive soil with surcharge, will be presented in Article 41.

38. Coulomb's theory of the passive earth pressure of ideal sand. Figure 32*a* is a vertical section through a plane face ab in contact with a mass of sand with a plane surface. If the conditions stated in Article 36 are satisfied, the normal component of the passive earth pressure per unit of area of ab at a depth z below point a is determined by the equation

$$p_{Pn} = \gamma z K_P \qquad 15(3)$$

wherein K_P is the coefficient of the passive earth pressure. Since the earth pressure acts at an angle δ to the normal on the contact face we obtain from equation 15(3) the following expression for the total passive

earth pressure P_P:

$$P_P = \frac{P_{Pn}}{\cos\delta} = \frac{1}{\cos\delta}\int_0^H \frac{p_{Pn}}{\sin\alpha}dz = \tfrac{1}{2}\gamma H^2 \frac{K_P}{\sin\alpha\cos\delta} \qquad [1]$$

Coulomb (1776) computed the passive earth pressure of ideal sand on the simplifying assumption that the entire surface of sliding consists of a plane through the lower edge b of the contact face ab in Figure 32a. The line bc_1 represents an arbitrary plane section through this lower edge. The wedge abc_1 with a weight W_1 is acted upon by the reaction

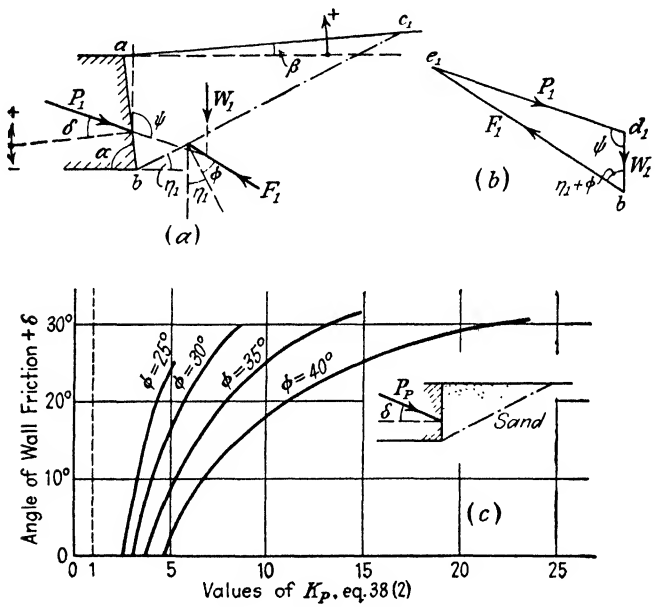

FIG. 32. (a and b) Diagrams illustrating assumptions on which Coulomb's theory of passive earth pressure of sand is based; (c) relation between ϕ, δ, and Coulomb value of coefficient of passive earth pressure K_p.

F_1 at an angle ϕ to the normal on the section bc_1 and by the lateral force P_1 at an angle δ to the normal on the contact face ab. The corresponding polygon of forces, shown in Figure 32b, must be closed. This condition determines the intensity of the force P_1. The slip occurs along the section bc (not shown in the figure), for which the lateral force P_1 is a minimum, P_P. Coulomb determined the value P_P by an analytical method. Replacing P_P in equation 1 by Coulomb's equation for the passive earth pressure and solving for the coefficient of passive

earth pressure K_P one obtains

$$K_P = \frac{\sin^2(\alpha - \phi)\cos\delta}{\sin\alpha\sin(\alpha+\delta)\left[1 - \sqrt{\frac{\sin(\phi+\delta)\sin(\phi+\beta)}{\sin(\alpha+\delta)\sin(\alpha+\beta)}}\right]^2} \qquad [2]$$

This equation is valid for both positive and negative values of β and δ.

In Figure 32*c* the ordinates represent the angle of wall friction and the abscissas the values of K_P for the passive earth pressure of a mass of sand with a horizontal surface, acted upon by a body with a vertical contact face. The curves show the variation of K_P with respect to $+\delta$ for different values of ϕ. They indicate that for a given value of ϕ the value K_P increases rapidly with increasing values of δ.

If the graphical methods of Culmann (Art. 24) and of Engesser (Art. 25) are applied to the determination of the passive earth pressure of cohesionless soil, the slope line *bS* (Figs. 20*c*, 20*d*, and 21*a*) is inclined at an angle of ϕ away from *ab* and not toward it. Everything else remains unchanged. The validity of this procedure can be established on the basis of purely geometrical considerations.

For values $\phi = \delta = 30°$, $\beta = 0°$ (backfill with a horizontal surface), and $\alpha = 90°$ (vertical wall) it has been found that the value of the passive earth pressure determined by means of the exact theory (Art. 15 and Fig. 14*e*) is more than 30 per cent smaller than the corresponding Coulomb value computed by means of equation 2. This error is on the unsafe side and too large even for estimates. However, with decreasing values of δ the error decreases rapidly and for $\delta = 0$ the Coulomb value becomes identical with the exact value

$$P_P = \tfrac{1}{2}\gamma H^2 N_\phi = \tfrac{1}{2}\gamma H^2 \tan^2\left(45° + \frac{\phi}{2}\right) \qquad 14(2)$$

The excessive error associated with Coulomb's method when δ is large is due to the fact that the surface along which the slip occurs, such as the surface *bc* in Figure 14*e*, is not even approximately plane. However, with decreasing values of δ (Fig. 14*e*) the curvature of *bc* decreases rapidly and when $\delta = 0$, the surface *bc* is perfectly plane. If δ is smaller than $\phi/3$, the difference between the real surface of sliding and Coulomb's plane surface is very small and we can compute the corresponding passive earth pressure by means of Coulomb's equation. On the other hand, if δ is greater than $\phi/3$, we are obliged to determine the earth pressure of ideal sand by means of some simplified method which takes the curvature of the surface of sliding into consideration. These methods are the logarithmic spiral method (Ohde 1938) and the friction

circle method (Krey 1936). Either one of these methods can also be used for cohesive earth.

39. **Logarithmic spiral method.** Figure 33*a* is a section through the plane contact face *ab* of a block of masonry which is pressed against a mass of cohesionless soil with a horizontal surface. According to

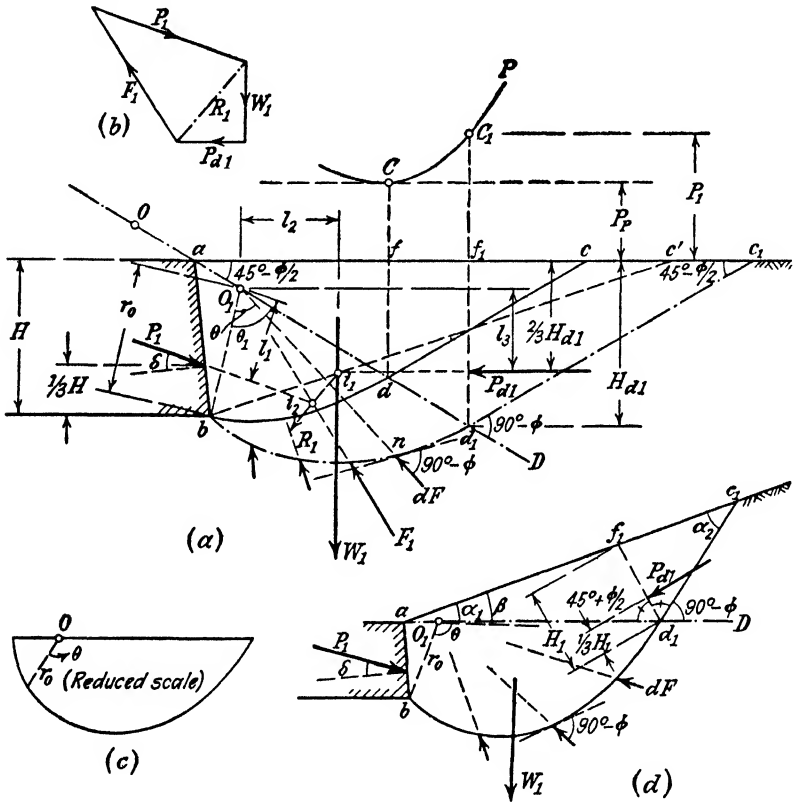

FIG. 33. Logarithmic spiral method of determining passive earth pressure of sand.

Article 36 the surface of sliding *bc* consists of a curved part *bd* and a plane part *dc* which rises at an angle of $45° - \phi/2$ to the horizontal. The point *d* is located on a straight line *aD* which descends at an angle of $45° - \phi/2$ to the horizontal. Since the position of *d* is not yet known, we assume a tentative surface of sliding which passes through an arbitrarily selected point d_1 on the line *aD*. Within the mass of soil represented by the triangle ad_1c_1 the state of stress is the same as that in a semi-infinite deposit in a passive Rankine state. This state of stress has already been described (see Art. 10). The shearing stresses along vertical sections are equal to zero. Therefore the passive earth

pressure P_{d1} on the vertical section d_1f_1 is horizontal. It acts at a depth $2H_{d1}/3$ and it is equal to

$$P_{d1} = \tfrac{1}{2}\gamma H_{d1}^2 \tan^2\left(45° + \frac{\phi}{2}\right) = \tfrac{1}{2}\gamma H_{d1}^2 N_\phi \qquad [1]$$

We assume that the curved part bd_1 of the section through the surface of sliding (Fig. 33*a*) consists of a logarithmic spiral with the equation

$$r = r_0\, \epsilon^{\theta \tan \phi} \qquad [2]$$

whose center O_1 is located on the line ad_1. In this equation r represents the length of any vector O_1n making an angle θ (expressed in radians) with the vector O_1b, and $r_0 = O_1b$ is the length of the vector for $\theta = 0$. Every vector through the center O_1 of the logarithmic spiral of equation 2 intersects the corresponding tangent to the spiral at an angle of $90° - \phi$, as shown in Figure 33*a*. Since the center O_1 of the spiral is located on the line aD the spiral corresponding to equation 2 passes without any break into the straight section d_1c_1. Furthermore, at any point n of the curved section of the surface of sliding the reaction dF acts at an angle ϕ to the normal or at an angle $90° - \phi$ to the tangent to the spiral. This direction is identical with that of the vector O_1n. Hence the resultant reaction F_1 along the curved section bd_1 also passes through the center O_1.

Since the surface of the mass does not carry a surcharge and the cohesion is assumed equal to zero, the point of application of the passive earth pressure on the face ab is located at a height $H/3$ above b (see Art. 37).

The body of soil abd_1f_1 (Fig. 33*a*) with the weight W_1 is acted upon by the horizontal force P_{d1}, by the force P_1 exerted by the body of masonry, and by the reaction F_1 which passes through the center O_1 of the spiral. The equilibrium of the system requires that the moment of all the forces about the center O_1 of the spiral must be equal to zero. These moments are

P_1l_1 = the moment of P_1 about O_1 and

$M_1, M_2, \cdots M_n$ = the moments of all the other forces about O_1.

Since F_1 passes through O_1

$$P_1l_1 + \sum_1^n M_n = P_1l_1 + W_1l_2 + P_{d1}l_3 = 0$$

and we obtain

$$P_1 = -\frac{1}{l_1}\sum_1^n M_n = -\frac{1}{l_1}(W_1l_2 + P_{d1}l_3) \qquad [3]$$

The problem can also be solved graphically, by means of the polygon of forces shown in Figure 33*b*. In order to determine the direction of the force F_1 which appears in the polygon we combine the weight W_1 and the force P_{d1} in Figure 33*b* into a resultant force R_1. In Figure 33*a* this resultant must pass through the point of intersection i_1 of P_{d1} and W_1. It intersects the force P_1 at some point i_2. Equilibrium requires that the force F_1 pass through the same point. As stated above, it must also pass through the center O_1 of the spiral. Hence we know the direction of F_1 and we can close the polygon of forces shown in Figure 33*b* by tracing $P_1 \parallel P_1$ Figure 33*a* and $F_1 \parallel F_1$ Figure 33*a*. Thus we obtain the intensity of the force P_1 required to produce a slip along the surface bd_1c_1.

The next step consists in repeating the investigation for other spirals through b which intersect the plane aD at different points d_2, d_3, etc. The corresponding values P_1, P_2, P_3, etc., are plotted as ordinates f_1C_1, etc., above the points f_1, etc. Thus we obtain the curve P shown in Figure 33*a*. The slip occurs along the surface of sliding corresponding to the minimum value P_P. In the diagram (Fig. 33*a*) this minimum value P_P is represented by the distance fC. The point of intersection d between the surface of sliding and the line aD is located on a vertical line through point f. The plane section of the surface of sliding rises at an angle of $45° - \phi/2$ toward the horizontal surface of the earth.

The greatest error associated with the procedure described above is about 3 per cent, which is negligible. The dashed line bc' indicates the corresponding surface of sliding determined by Coulomb's theory. The width $\overline{ac'}$ of the top of Coulomb's wedge abc' is somewhat greater than the distance $\overline{ac}$.

In order to solve such problems without waste of time, we trace a logarithmic spiral corresponding to equation 2 on a piece of cardboard as shown in Figure 33*c*, selecting a suitable arbitrary value for r_0. The spiral is then cut out and used as a pattern. On account of the geometrical properties of the spiral any vector, such as r_0 (Fig. 33*c*), can be considered as the zero vector provided the angle θ is measured from this vector. In order to trace a spiral through point b in Figure 33*a*, we place the center point O of the pattern on some point O_1 of the line aD (Fig. 33*a*) and rotate the pattern around O_1 until the curved rim of the pattern passes through point b. By following the rim of the disk with a pencil from b to the line aD we obtain point d_1. The line d_1c_1 is tangent to the spiral at point d_1 and rises at an angle of $45° - \phi/2$ to the horizontal. In a similar manner we trace several spirals whose centers O_1, O_2, etc., are located at different points on the line aD. The weight of the soil located above the curved part bd_1 of the assumed surface of sliding bd_1c_1 is represented by the area abd_1f_1. This area consists of two triangles, ad_1f_1 and O_1ab, and the spiral sector O_1bd_1. The area of the sector is determined by the equation

$$A = \int_0^{\theta_1} \tfrac{1}{2} r^2 d\theta = \frac{r_0^2}{4 \tan \phi} (e^{2\theta_1 \tan \phi} - 1) \qquad [4]$$

If the surface of the soil subject to lateral pressure rises at an angle β as shown in Figure 33*d*, the orientation of the line aD and of the plane section d_1c_1 of the surface

of sliding with reference to the surface of the soil is identical with the corresponding orientation of the surfaces of sliding in a semi-infinite mass of soil whose surface rises at an angle β. The method of determining this orientation has been described in Article 10, and the orientation is shown in Figure 9*d*. Within the triangular area ad_1c_1 the state of stress is the same as if the area represented a section of the semi-infinite deposit shown in Figure 9*d*. According to the laws of mechanics, the shearing stresses along any section d_1f_1 which bisects the angle between the planes of shear are equal to zero. Hence the earth pressure P_{d1}, (Fig. 33*d*) acts at right angles to the surface d_1f_1 which bisects the angle ad_1c_1 and its intensity can be determined by means of Mohr's diagram as shown in Article 10 and Figure 9*b*. The rest of the procedure is identical with the one just described.

40. Friction circle method. When using this method we assume that the curved part of the surface of sliding *bc* in Figure 34*a* consists of an arc of a circle bd_1 with a radius r_1 which passes without break into the plane section d_1c. The center of this circle is located on a line drawn through d_1 at an angle ϕ to ad_1 in Figure 34*a*, at a distance $O_1d_1 = O_1b$ from point d_1. At any point n of the curved section the elementary reaction dF is tangent to a circle C_f which is concentric with the circle of which bd_1 is an arc. The radius of the circle C_f is $r_f = r_1 \sin \phi$. This circle is called the *friction circle*. As an approximation, with method of correction to be discussed later, we can assume that the resultant reaction F_1 is also tangent to this circle. In order to determine the force P_1 we combine the forces W_1 and P_{d1} into a resultant R_1 as shown in the polygon of forces (Fig. 34*b*). In Figure 34*a* this resultant must pass through the point of intersection i_1 between P_{d1} and W_1. It intersects the force P_1 at point i_2. To maintain equilibrium, the reaction F_1 must pass through the point of intersection i_2. Since F_1 has been assumed tangent to the friction circle C_f, it must be located as shown in Figure 34*a*. Since the direction of F_1 is known, the force P_1 can be determined from the polygon of forces shown in Figure 34*b*. The minimum value P_P of the lateral force required to produce a slip can be ascertained by plotting a curve similar to *CP* in Figure 33*a*. It requires a repetition of the computation for several circles, each of which passes through *b*. The values of P_1, P_2, P_3, etc., thus obtained are plotted as ordinates above the line representing the horizontal surface of the ground.

The most important error associated with the friction circle method is due to the assumption that the reaction F_1 in Figure 34*a* is tangent to the friction circle C_f with a radius r_f. In reality the resultant reaction F_1 is tangent to a circle whose radius r_f' is greater than r_f. If the force F_1 is tangent to a circle with a radius $r_f' > r_f$ the angle of inclination of F_1 in the polygon of forces (Fig. 34*b*) becomes smaller and the value of P_1 becomes greater. Hence the error due to the assumption that r_f' equals r_f is on the safe side.

The value of the ratio $(r_f' - r_f)/r_f$ depends on the value of the central angle θ_1

and on the distribution of the normal pressure over the curved part of the surface of sliding, bd_1 in Figure 34*a*. In general this distribution is intermediate between a uniform distribution and a sinusoidal distribution, which involves zero pressure at

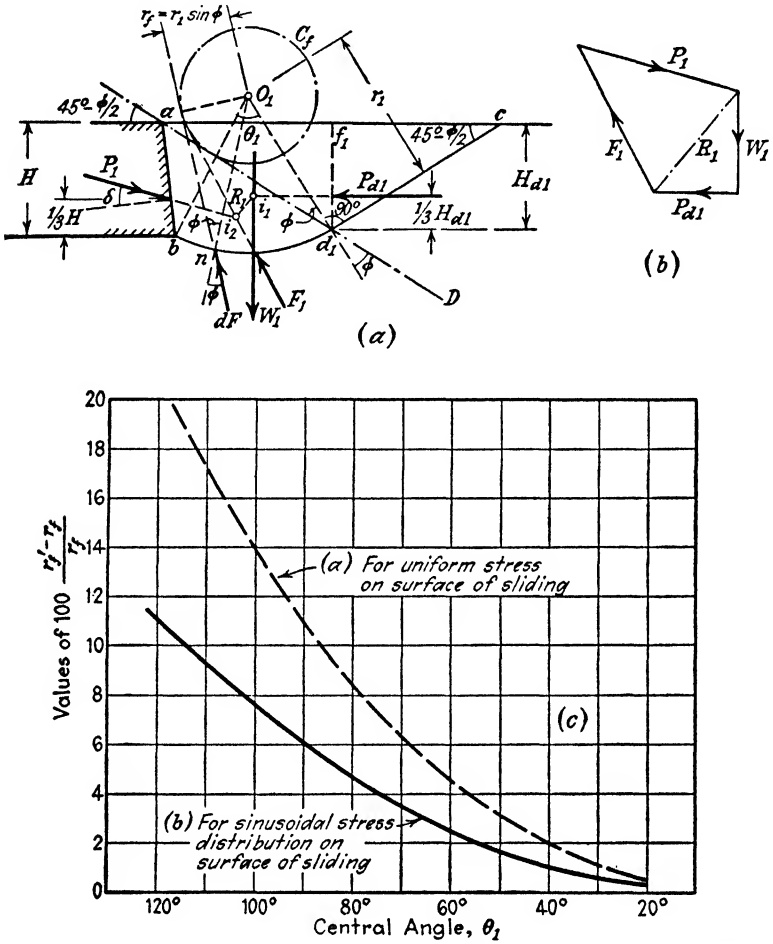

FIG. 34. (*a* and *b*) Friction circle method of determining passive earth pressure of sand; (c) correction graph to be used in connection with friction circle method. (*Diagram* c *after D. W. Taylor 1937.*)

both ends of the section and a maximum for a central angle $\theta = \theta_1/2$. Figure 34c gives the values of $100\,\frac{r_f' - r_f}{r_f}$ for both types of pressure distribution and for angles of θ_1 from 0° to 120° (Taylor 1937). If the soil is acted upon by a block of masonry such as that shown in Figures 33 and 34, the distribution of the normal pressure over the curved part of the surface of sliding is fairly uniform and the central angle seldom exceeds 90°. The central angle of the curved part of the surface of sliding shown in

Figure 34*a* is 60°. Assuming a perfectly uniform distribution of the normal stresses over this surface we obtain from curve *a* in the diagram (Fig. 34*c*) a value of 4.6 per cent for the correction factor. Hence, in order to get a more accurate result the force F_1 should be drawn tangent not to the friction circle C_f with a radius r_f as indicated in Figure 34*a* but to a circle whose radius is equal to 1.046 r_f.

If the correction graph (Fig. 34*c*) is used, the results obtained by means of the friction circle method are as accurate as those obtained by means of the spiral method described in the preceding article.

41. Passive earth pressure of a mass of cohesive earth, carrying a uniformly distributed surcharge. Figure 35 illustrates the methods of computing the passive earth pressure of a mass of cohesive soil whose shearing resistance is determined by the equation

$$s = c + \sigma \tan \phi \qquad 5(1)$$

The shearing stresses on the surface of contact between soil and masonry are

$$p_{Pt} = c_a + p_{Pn} \tan \delta$$

wherein δ is the angle of wall friction and c_a the adhesion. If the seat of the thrust consists of a mass of soil, the values c_a and δ are identical with the values c and ϕ in Coulomb's equation 5(1). The unit weight of the earth is γ. The surface of the soil is horizontal and carries a uniformly distributed surcharge, q per unit of area.

According to Article 36, the surface of sliding consists of a curved part bd_1 and a plane part d_1e_1 which rises at an angle of $45° - \phi/2$ to the horizontal. Point d_1 is located on a straight line aD which descends from point a at an angle of $45° - \phi/2$ to the horizontal. The position of point d_1 on aD has been arbitrarily selected because its real position is not yet known. Within the mass of soil represented by the triangle ad_1e_1 the soil is in a passive Rankine state (see Art. 12). The shearing stresses along vertical sections are equal to zero. The normal pressure per unit of area of the vertical section d_1f_1 (Fig. 35*a*) is determined by the equation

$$\sigma_P = 2c\sqrt{N_\phi} + \gamma\left(z + \frac{q}{\gamma}\right)N_\phi \qquad 12(5)$$

wherein $N_\phi = \tan^2(45° + \phi/2)$ is the flow value.

This pressure consists of two parts

$$\sigma'_P = 2c\sqrt{N_\phi} + qN_\phi$$

which is independent of depth and

$$\sigma''_P = \gamma z N_\phi$$

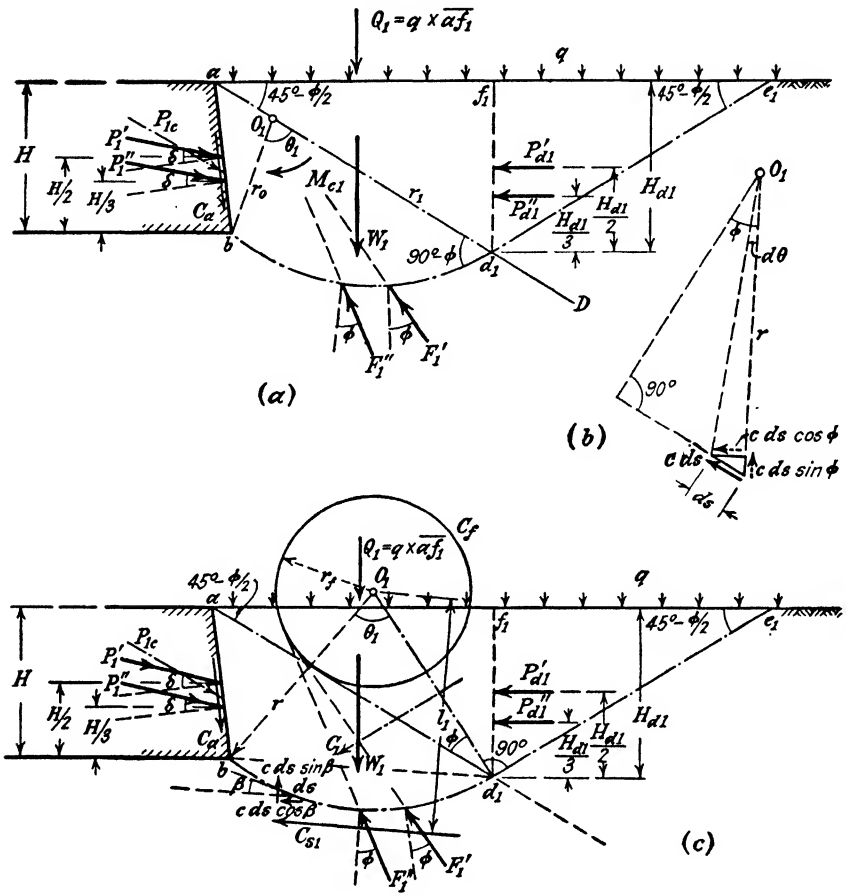

FIG. 35. Determination of passive earth pressure of cohesive soil. (*a* and *b*) Logarithmic spiral method; (*c*) friction circle method.

which increases like a hydrostatic pressure in simple proportion to depth (see Art. 37). The corresponding total pressures on the section d_1f_1 with a height H_{d1} are

$$P'_{d1} = H_{d1}(2c\sqrt{N_\phi} + qN_\phi) \qquad [1]$$

and

$$P''_{d1} = \tfrac{1}{2}\gamma H_{d1}^2 N_\phi \qquad [2]$$

The point of application of P'_{d1} is at an elevation $H_{d1}/2$ above point d_1 (Fig. 35*a*) and that of P''_{d1} is at an elevation $H_{d1}/3$ above point d_1.

For the curved part bd_1 of the surface of sliding either a logarithmic spiral or an arc of a circle can be selected. Figure 35*a* shows a loga-

rithmic spiral whose center is located at O_1. The equation of the spiral is

$$r = r_0 \epsilon^{\theta \tan \phi} \qquad 39(2)$$

The cohesion $c\,ds$ which acts on an element ds of the spiral (Fig. 35*b*) can be resolved into one component $c\,ds \sin \phi$ in the direction of the vector r through O_1 and a component $c\,ds \cos \phi$ perpendicular to this direction. The moment about the center O_1 of the spiral produced by the first component is zero and that due to the second component is

$$dM_c = rc\,ds \cos \phi = rc \frac{r\,d\theta}{\cos \phi} \cos \phi = cr^2\,d\theta = cr_0^2 \epsilon^{2\theta \tan \phi} d\theta \qquad [3]$$

Hence the total moment due to the cohesion along bd_1 is

$$M_{c1} = \int_0^{\theta_1} dM_c = \frac{c}{2 \tan \phi} (r_1^2 - r_0^2) \qquad [4]$$

In Figure 35*c* it is assumed that the curved part bd_1 of the surface of sliding is an arc of a circle with a radius r and a center angle θ_1. The cohesion $c\,ds$ which acts along an element ds of the arc can be resolved into a component $c\,ds \cos \beta$ parallel to bd_1 and a component $c\,ds \sin \beta$ perpendicular to bd_1. The resultant of the components parallel to bd_1 is parallel to bd_1 and equal to

$$C_{s1} = c\,\overline{bd_1} \qquad [5]$$

and the sum of the components perpendicular to bd_1 is equal to zero. The moment of the force C_{s1} with reference to the center O_1 of the circle must be equal to the sum of the moments of the cohesion forces $c\,ds$ with reference to the same point. Hence, if l_1 is the shortest distance from O_1 to C_{s1}

$$C_{s1} l_1 = \overline{bd_1}\, c\, l_1 = \widehat{bd_1}\, c\, r$$

or

$$l_1 = \frac{\widehat{bd_1}}{\overline{bd_1}} r \qquad [6]$$

In order to compute the passive earth pressure on ab either with the logarithmic spiral or the friction circle, we proceed as prescribed at the end of Article 37. We first assume that the unit weight γ of the soil is equal to zero and determine the force P_1' required to produce a slip along bd_1. If $\gamma = 0$ the force P_{d1}'' (eq. 2) is equal to zero. The point of application of the force P_1' is located at the midpoint of ab. The force acts at an angle δ to the normal on the surface ab. The elementary reactions dF act at an angle ϕ to the normal on the elements.

If the spiral method is used, (Fig. 35*a*), the resultant reactions F_1' for $\gamma = 0$ and F_1'' for $c = 0$ and $q = 0$ pass through the center of the spiral. The moment produced by all the cohesion forces about the center of the spiral is equal to the algebraic sum of the moment M_{c1} (eq. 4) and the moment produced by the adhesion force C_a. If the friction circle method is used, as shown in Figure 35*c*, it is necessary to establish the direction of the force F_1' for $\gamma = 0$. For this purpose we replace the cohesion force C_{s1} and the adhesion force C_a by their resultant C_1. Then we combine this resultant with the forces P_{d1}' and Q_1. Thus we obtain the resultant R_1 of the known forces C_{s1}, C_a, P_{d1}', and Q_1 (not shown in the figure). The direction of the force F_1' is obtained by tracing through the point of intersection between R_1 and P_1' a tangent to the friction circle. The intensity of the force P_1' can be determined either by means of a moment equation similar to equation 39(3) (spiral method) or by means of a polygon of forces (friction circle method), as described in Article 40.

The next step is to assume $c = 0$, $q = 0$ and to assign to the soil its unit weight γ, whereupon the force P_{d1}' (eq. 1) becomes equal to zero and the vertical section $f_1 d_1$ is acted upon only by the force P_{d1}''. The rest of the procedure is strictly identical with that described in Articles 39 and 40. It furnishes the value P_1''.

The computation must be repeated for several different assumed surfaces of sliding. Thus one obtains several sets of values $(P_1' + P_1'')$, $(P_2' + P_2'')$, $\cdots$ $(P_n' + P_n'')$. The real surface of sliding is determined by the condition that the sum $(P_n' + P_n'')$ is a minimum

$$P_P = P_P' + P_P'' = (P_n' + P_n'')_{\min.}$$

The force P_P can be determined graphically as described in Articles 39 and 40 by plotting the values of $(P_n' + P_n'')$ as ordinates above the surface of the earth. The passive earth pressure P_{Pc} is equal to the resultant of P_P and the adhesion force C_a. Since the force C_a acts along the contact face, the point of application of the passive earth pressure is identical with that of the force P_P. It is located between the midpoint and the top of the lower third of the wall.

42. Summary of the methods of computing the passive earth pressure. If the angle of wall friction δ is smaller than $\phi/3$, the passive earth pressure of cohesionless masses of soil can be computed by means of equation 38(2) or by one of its graphical substitutes. The error is on the unsafe side but it is small. For values of δ greater than $\phi/3$ the error due to Coulomb's assumption of a plane surface of sliding increases rapidly with increasing values of δ. In this case one of the methods described in Articles 39 and 40 should be used. The results obtained by means of

these methods are practically identical. The passive pressure of cohesive soil should be computed only by means of the logarithmic spiral or of the friction circle method.

The methods of computation involving the assumption of a curved surface of sliding are much more expedient than they appear to be. When dealing with the passive earth pressure of clay, the angle of shearing resistance can usually be assumed to be equal to zero. On this assumption the curved part of the surface of sliding is an arc of a circle and the plane part rises at an angle of 45° to the horizontal.

Chapter VIII

BEARING CAPACITY

43. Definitions. If a load is applied on a limited area on or below the surface of the soil, the loaded area settles. If the settlements due to a steady increase of the load are plotted as ordinates against the load per unit of area we obtain a *settlement curve*. The settlement curve

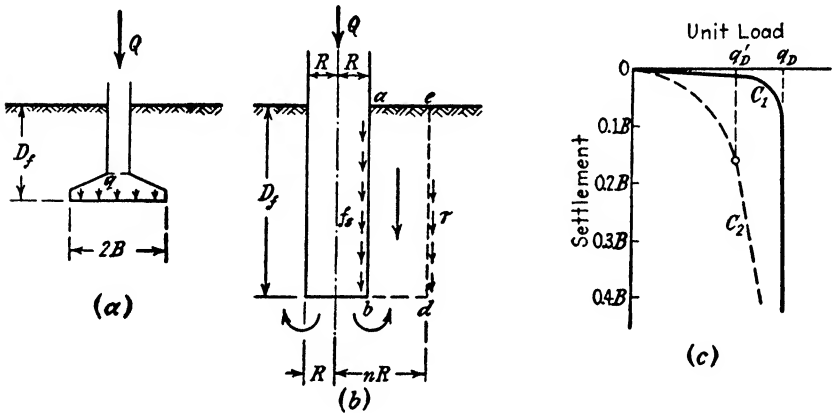

Fig. 36. (*a*) Continuous footing; (*b*) cylindrical pier; (*c*) relation between unit load and settlement on dense (C_1) and loose (C_2) soil.

may have any shape intermediate between those represented by the curves C_1 and C_2 in Figure 36c. If the curve passes fairly abruptly into a vertical tangent (curve C_1) we identify the failure of the earth support with the transition of the curve into the vertical tangent. On the other hand, if the settlement curve continues to descend on a slope, as shown by the curve C_2, we specify arbitrarily, but in accordance with current conceptions, that the earth support has failed as soon as the curve passes into a steep and fairly straight tangent.

The area covered by the load is called the *bearing area*. The load required to produce the failure of the soil support is called the *critical load* or the *total bearing capacity*. The average critical load per unit of area, q_D or q'_D (Fig. 36c), is called the *bearing capacity of the soil*. It depends not only on the mechanical properties of the soil but also on the size of the loaded area, its shape, and its location with reference to

the surface of the soil. In the following articles the investigation is limited to vertical loads acting on horizontal bearing areas.

If the load acts on a very long strip with a uniform width it is called a *strip load* in contrast to a load which acts on an area whose width is approximately equal to its length, such as a square, a rectangular, or a circular area. In engineering practice the load is transmitted to the bearing area by means of *footings* or *piers*. Figure 36*a* is a section through a footing. The length of a *continuous footing* is great compared to its width $2B$ whereas that of a *spread footing* is approximately equal to the width. A pier (Fig. 36*b*) is a cylindrical or a prismatic body of masonry whose horizontal dimensions are small compared to the depth D_f of its base below the surface. The lower end of some piers is given the shape of a truncated cone whose base has a greater area than the section through the pier (*belled-out caisson pier*).

In the following investigations it is assumed that the soil is homogeneous from the surface to a depth which is far below the level of the base of the footings or piers.

44. Failure by local and by general shear. Before the load on a footing is applied the soil located beneath the level of the base of the footing is in a state of elastic equilibrium. The corresponding state of stress will be described in Chapter XVII. When the load on the footing is increased beyond a certain critical value, the soil gradually passes into a state of plastic equilibrium. During this process of transition both the distribution of the soil reactions over the base of the footing and the orientation of the principal stresses in the soil beneath the footings change. The transition starts at the outer edges of the base and spreads as indicated in Figure 123*c* for a continuous footing which rests on the horizontal surface of a homogeneous mass of sand and in Figure 123*d* for a footing whose base is located at some depth beneath the surface. If the mechanical properties of the soil are such that the strain which precedes the failure of the soil by plastic flow is very small the footing does not sink into the ground until a state of plastic equilibrium similar to that illustrated by Figure 15*b* has been reached. The corresponding relation between load and settlement is shown by the solid curve C_1 in Figure 36*c*. The failure occurs by sliding in the two outward directions. In Figure 37*c* the line *def* represents one of these surfaces. It consists of one curved part *de* and one plane part *ef* which intersects the horizontal surface at an angle of $45° - \phi/2$ (see Art. 16). This type of failure will be called a *general shear failure*.

In practice the conditions for the general shear failure illustrated by Figure 37*c* are never completely satisfied, because the horizontal compression of the soil located immediately below the level of the base of the footing, on both sides of the base, is not

great enough to produce the state of plastic equilibrium within the entire upper part of the zone *aef*. Therefore one has to expect a failure similar to that illustrated by Figure 37*d*. On account of inadequate lateral compression the shear failure occurs while the uppermost part of the zones of potential plastic equilibrium is still in a state of elastic equilibrium. If the surface of sliding cuts across a mass of sand in a state of elastic equilibrium, it may intersect the free surface at any angle intermediate between $45° - \phi/2$ and 90°. (See Figures 17*a* and *c* and 70*c*.) In cohesive soils the surface of sliding terminates at the boundary of the zone of elastic equilibrium. In the proximity of the free surface of such soils one may find instead of a zone of shear a set of discontinuous tension cracks. In the theory of general shear failure these discrepancies between theory and reality will be disregarded. The resulting error is unimportant.

On the other hand, if the mechanical properties of the soil are such that the plastic flow is preceded by a very important strain, the approach to the general shear failure is associated with a rapidly increasing settlement and the relation between load and settlement is approximately as indicated in Figure 36*c* by the dashed curve C_2. The criterion for the failure of the soil support, represented by a conspicuous increase of the slope of the settlement curve, is satisfied before the failure spreads to the surface. Hence, this type of failure will be called *local shear failure.*

45. Conditions for general shear failure of soil support of shallow, continuous footings. The term "*shallow footing*" is applied to footings whose width $2B$ is equal to or greater than the vertical distance D_f between the surface of the ground and the base of the footing. If this condition is satisfied we can neglect the shearing resistance of the soil located above the level of the base of the footing. In other words we can replace the soil with a unit weight γ, located above this level, by a surcharge $q = D_f\gamma$ per unit of area. This substitution simplifies the computations very considerably. The error is unimportant and on the safe side. On the other hand, if the depth D_f is considerably greater than the width $2B$ (deep footings), it is necessary to take the shearing stresses in the soil located above the level of the base into consideration (see Art. 50).

If the soil located above the level of the base of a footing has been replaced by a surcharge, q per unit of area, the base of the footing represents a loaded strip with a uniform width $2B$ located on the horizontal surface of a semi-infinite mass. The state of plastic equilibrium produced by such a load is illustrated by Figure 15*b*. The figure is based on the assumption that the shearing stresses on the loaded area are equal to zero. In order to produce such a state of stress at the base of a continuous footing it would be necessary to eliminate completely the friction and the adhesion between the base and the soil. Figure 37*a* has

been plotted on the basis of the same assumption. The zone of plastic equilibrium represented in this figure by the area ff_1e_1de can be subdivided into (*I*) a wedge-shaped zone located beneath the loaded strip, in which the major principal stresses are vertical, (*II*) two zones of radial shear, *ade* and bde_1, emanating from the outer edges of the loaded strip, whose boundaries intersect the horizontal at angles of

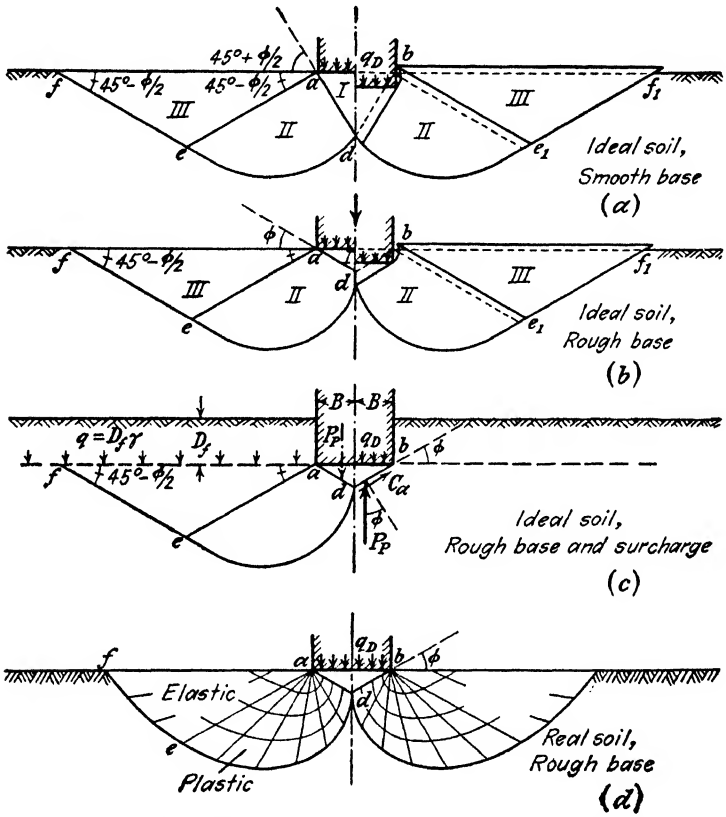

FIG. 37. Boundaries of zone of plastic flow after failure of earth support of continuous footings.

$45° + \phi/2$ and $45° - \phi/2$, and (*III*) two passive Rankine zones. The dotted lines on the right-hand side of Figure 37*a* indicate the boundaries of the zones *I* to *III* at the instant of the failure of the soil support and the solid lines represent the same boundaries while the load sinks into the ground. The soil located within the central zone *I* spreads laterally and the section through this zone undergoes the distortion indicated in the figure.

If the load is transmitted onto the ground by means of a continuous

footing with a rough base as shown in Figure 37*b*, the tendency of the soil located within the zone *I* to spread is counteracted by the friction and adhesion between the soil and the base of the footing. On account of the existence of this resistance against lateral spreading the soil located immediately beneath the base of the footing remains permanently in a state of elastic equilibrium and the soil located within the central zone behaves as if it were a part of the sinking footing. The depth of this wedge-shaped body of soil remains practically unchanged. Yet the footing sinks. This process is only conceivable if the soil located just below point *d* moves vertically downward. This type of movement requires that the surface of sliding *de* through point *d* should start from a vertical tangent. The boundary *ad* of the zone of radial shear, *ade*, is also a surface of sliding. According to Article 7 the potential surfaces of sliding in an ideal plastic material intersect each other in every point of the zone of plastic equilibrium at an angle of $90° - \phi$. Therefore the boundary *ad* (Fig. 37*b*) must rise at an angle ϕ to the horizontal, provided the friction and adhesion between the soil and the base of the footing suffice to prevent a sliding motion at the base. The right-hand side of this figure shows the deformation associated with the sinking of the footing. The sharp rise of the soil on both sides of the base of the footing has given rise to various speculations, and it has been referred to as *edge action*. It is nothing else but the visible manifestation of the existence of two zones of radial shear.

Trial computations have shown that the angle of base friction required to produce the state of plastic flow illustrated by Figure 37*b* is very much smaller than the angle of shearing resistance of the supporting soil. Hence, the lower boundary of the central zone beneath footings can always be assumed to rise at an angle ϕ to the horizontal. However, theoretically, the slope angle of these boundaries may have any value ψ intermediate between ϕ and $45° + \phi/2$.

Whatever the slope angle of the boundaries may be, the footing cannot sink into the ground until the pressure exerted by the load onto the soil adjoining the inclined boundaries of zone *I* in Figure 37*c* becomes equal to the passive earth pressure. The passive earth pressure can be computed by means of one of the methods described in Chapter VII and the ultimate bearing capacity is determined by the condition that the sum of the vertical components of the forces which act on the soil located within the central zone *I* must be equal to zero.

To illustrate the procedure we compute the ultimate bearing capacity of a shallow continuous footing whose base is located at a depth D_f below the horizontal surface of a mass of soil with a unit weight γ. Figure 37*c* is a section through the footing. Since the footing is shallow

we are justified in replacing the earth located above the level of the base of the footing by a surcharge

$$q = \gamma D_f$$

per unit of area. The shearing resistance of the soil is determined by Coulomb's equation

$$s = c + \sigma \tan \phi \qquad 5(1)$$

The shearing stresses at the contact face *ad* at the instant of failure are

$$p_{Pt} = c + p_{Pn} \tan \phi$$

wherein p_{Pn} is the normal component of the passive earth pressure per unit of area of the contact face. On account of the roughness of the base of the footing and the adhesion between the base and the soil, the contact faces *ad* and *bd* rise at an angle ϕ to the horizontal. The passive earth pressure on each one of these faces consists of two components, P_P, acting at an angle ϕ ($\phi = \delta$ = angle of wall friction) to the normal on the contact face and the adhesion component

$$C_a = \frac{B}{\cos \phi} c$$

The methods of determining the pressure P_P have been described in Article 41. In this connection it should be remembered that the surface of sliding obtained by one of these methods represents only an approximation to the real surface of sliding because the methods are not rigorous. Therefore the surface of sliding obtained by means of the spiral or the friction circle method does not necessarily start at point *d* in Figure 37*c* with a vertical tangent. However, the error due to this discrepancy between the real and the approximate surface of sliding is unimportant. The equilibrium of the mass of soil located within the zone *abd* of elastic equilibrium requires that the sum of the vertical forces, including the weight $\gamma B^2 \tan \phi$ of the earth in the zone, should be equal to zero

$$Q_D + \gamma B^2 \tan \phi - 2P_P - 2Bc \tan \phi = 0 \qquad [1]$$

Hence

$$Q_D = 2P_P + 2Bc \tan \phi - \gamma B^2 \tan \phi \qquad [2]$$

This equation represents the solution of our problem if P_P is known. If $D_f = 0$, $q = 0$ and $c = 0$, i.e., if the base of the footing rests on the horizontal surface of a mass of cohesionless sand, the pressure P_P assumes the value given by equation 38(1). Substituting in this

equation $H = B \tan \phi$, $\delta = \phi$, $K_P = K_{P\gamma}$, and $\alpha = 180° - \phi$, we get

$$P_P = \tfrac{1}{2}\gamma B^2 \frac{\tan \phi}{\cos^2 \phi} K_{P\gamma} \qquad [3]$$

wherein $K_{P\gamma}$ is the coefficient of passive earth pressure for $c = 0$, $q = 0$, $\alpha = 180° - \phi$, and $\delta = \phi$. Substituting this value and the value $c = 0$ in equation 2 we obtain for the total bearing capacity per unit of length of the footing

$$Q_D = Q_\gamma = 2 \times \tfrac{1}{2}\gamma B^2 \tan \phi \left(\frac{K_{P\gamma}}{\cos^2 \phi} - 1 \right) = 2B \times \gamma B N_\gamma \qquad [4a]$$

wherein

$$N_\gamma = \tfrac{1}{2} \tan \phi \left(\frac{K_{P\gamma}}{\cos^2 \phi} - 1 \right) \qquad [4b]$$

The value $K_{P\gamma}$ can be obtained by means of the spiral or the friction circle method (Arts. 39 and 40). Since the angle of wall friction δ and the slope angle α of the contact face are equal to ϕ and to $180° - \phi$ respectively, the values $K_{P\gamma}$ and N_γ depend only on ϕ. Therefore N_γ can be computed once for all. The relationship between N_γ and ϕ is represented by the solid line marked N_γ in Figure 38c.

46. Simplified method for computing bearing capacity. If the supporting soil has cohesion, the computation of the critical load Q_D per unit of length of a footing by means of equation 45(2) requires the determination of the component P_P of the passive earth pressure which involves several hours of work. However, in connection with practical problems we are usually satisfied with a less accurate value for the critical load. The method is based on the equation

$$P_{Pn} = \frac{H}{\sin \alpha} (cK_{Pc} + qK_{Pq}) + \tfrac{1}{2}\gamma H^2 \frac{K_{P\gamma}}{\sin \alpha} \qquad 37(4)$$

wherein P_{Pn} is the normal component of the passive earth pressure on a plane contact face with a height H, α is the slope angle of the contact face, and K_{Pc}, K_{Pq}, and $K_{P\gamma}$ are coefficients whose values are independent of H and γ. If *ad* in Figure 37c represents the contact face the values H, α, and δ contained in the preceding equation are equal to

$$H = B \tan \phi, \quad \alpha = 180° - \phi, \quad \delta = \phi, \quad \text{and} \quad c_a = c$$

Considering in addition that the total passive earth pressure P_P on the contact face is equal to $P_{Pn}/\cos \delta$, or

$$P_P = \frac{P_{Pn}}{\cos \delta} = \frac{P_{Pn}}{\cos \phi} \qquad [1]$$

we obtain from equation 37(4)

$$P_P = \frac{P_{Pn}}{\cos\delta} = \frac{B}{\cos^2\phi}\,(cK_{Pc} + qK_{Pq}) + \tfrac{1}{2}\gamma B^2 \frac{\tan\phi}{\cos^2\phi} K_{P\gamma}$$

Combining this equation with equation 45(2) we get

$$Q_D = 2Bc\left(\frac{K_{Pc}}{\cos^2\phi} + \tan\phi\right) + 2Bq\frac{K_{Pq}}{\cos^2\phi} + \gamma B^2 \tan\phi\left(\frac{K_{P\gamma}}{\cos^2\phi} - 1\right) \quad [2]$$

wherein K_{Pc}, K_{Pq}, and $K_{P\gamma}$ are pure numbers whose values are independent of the width $2B$ of the footing. The equation is valid on the condition that the soil support fails by general shear.

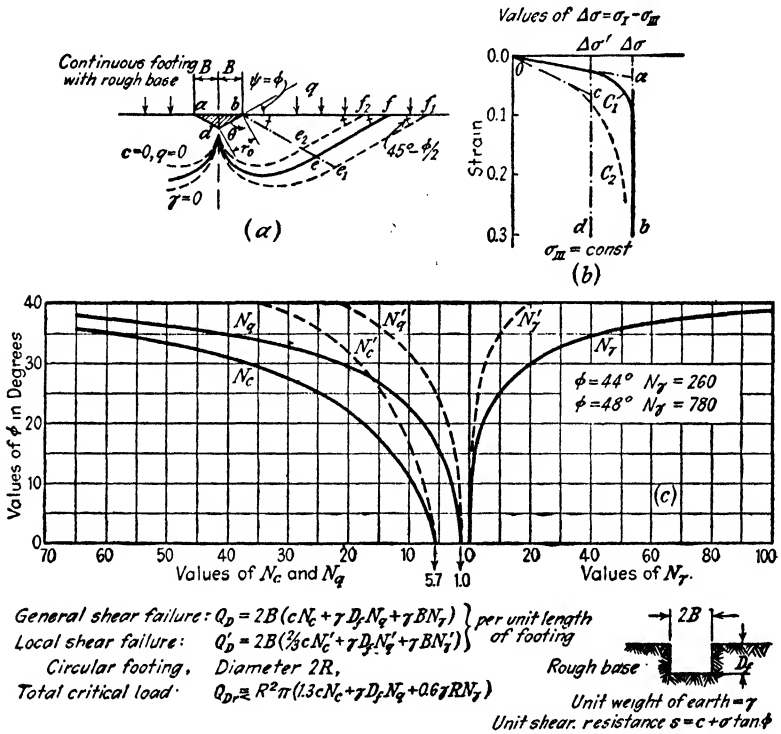

FIG. 38. Method of estimating bearing capacity by means of bearing capacity factors. (*a*) Source of error associated with the use of this method; (*b*) simplifying assumption on which computation of bearing capacity factors for dense and for loose soils is based; (*c*) relation between ϕ and the bearing capacity factors.

Figure 38*a* represents a continuous footing with a rough base. If $\gamma = 0$ failure occurs along the surface of sliding de_1f_1. The curved part de_1 of this surface is a logarithmic spiral whose center is located at

point b (Prandtl 1920). The equation of the spiral is

$$r = r_0 \epsilon^{\theta \tan \phi} \qquad [3]$$

wherein θ is the center angle in radians measured from the zero vector $r_0 = bd$ as shown in Figure 38a. For $\phi = 0$ equation 3 represents the equation of a circle with a radius r_0. Since the equation representing the surface of sliding contains neither c nor q, the shape of the surface of sliding is independent of the cohesion and the surcharge. For $\gamma = 0$ we obtain for the load required to produce a general shear failure along the surface of sliding de_1f_1 the value

$$Q_c + Q_q = 2Bc\left(\frac{K_{Pc}}{\cos^2 \phi} + \tan \phi\right) + 2Bq \frac{K_{Pq}}{\cos^2 \phi}$$

$$= 2BcN_c + 2BqN_q \qquad [4]$$

The factors N_c and N_q are pure numbers whose values depend only on the value ϕ in Coulomb's equation. The value Q_c represents the load which the weightless soil could carry if the surcharge q were equal to zero ($\gamma = 0$ and $q = 0$), and Q_q is the load which it could carry if its bearing capacity were exclusively due to the surcharge q ($\gamma = 0$ and $c = 0$).

On the other hand, if $c = 0$ and $q = 0$, while γ is greater than zero, the failure occurs along de_2f_2 (Fig. 38a). The rigorous equation of the curved part of this line is not yet known. Its approximate shape can be determined either by means of the spiral or the friction circle method (Arts. 39 and 40). The results of such investigations show that the lowest point of the curve de_2 is located well above the lowest point of de_1. The critical load required to produce a failure along de_2f_2 is determined by the equation

$$Q_\gamma = \gamma B^2 \tan \phi \left(\frac{K_{P\gamma}}{\cos^2 \phi} - 1\right) = 2B \times \gamma BN_\gamma \qquad 45(4a)$$

If the values c, D_f, and γ are greater than zero, the failure occurs along a surafce of sliding def (Fig. 38a), which is located between be_1f_1 and be_2f_2. From the results of numerical computations we know that the corresponding critical load, Q_D per unit of length of the strip, is only slightly greater than the sum of the loads $Q_c + Q_q$ (eq. 4) and Q_γ, (eq. 45(4a)). Therefore we can assume with sufficient accuracy

$$Q_D = Q_c + Q_q + Q_\gamma = 2BcN_c + 2BqN_q + 2B^2\gamma N_\gamma$$

wherein $2B$ is the width of the footing. Substituting $q = \gamma D_f$ we get

$$Q_D = Q_c + Q_q + Q_\gamma = 2B(cN_c + \gamma D_f N_q + \gamma BN_\gamma) \qquad [5]$$

The coefficients N_c, N_q, and N_γ will be called the *bearing capacity factors* for shallow continuous footings. Since their values depend only on the angle of shearing resistance ϕ in Coulomb's equation they can be computed once for all.

In order to obtain information on the importance of the error associated with equation 5, the critical load has been computed for a continuous footing with a width $2B$ whose base is located at a depth $2B$ below the horizontal surface of a mass of ideal sand. For $\phi = 34°$ we obtained bf_1 (Fig. 38*a*) $= 8.5B$, $bf = 7.0B$ and $bf_2 = 5.5B$. The corresponding values for $\phi = 38°$ are $bf_1 = 11.5B$, $bf = 8.7B$, and $bf_2 = 7.1B$. These figures show that the three surfaces of sliding indicated in Figure 38*a* are very different. Nevertheless it was found that the load Q_D required to produce a shear failure on *def* is less than 10 per cent greater than the sum of the loads Q_q and Q_γ required to produce a failure on the surfaces de_1f_1 and de_2f_2 respectively.

The problem of computing the loads Q_c and Q_q in equation 4 has been rigorously solved by means of Airy's stress function (Prandtl 1920, Reissner 1924). According to the definition of these loads the unit weight γ of the earth has been assumed equal to zero. The following equations are derived from those published by Prandtl and by Reissner:

$$N_c = \cot\phi \left[\frac{a_\theta^2}{2\cos^2(45° + \phi/2)} - 1 \right] \qquad [6a]$$

and

$$N_q = \frac{a_\theta^2}{2\cos^2(45° + \phi/2)} \qquad [6b]$$

wherein

$$a_\theta = \epsilon^{(\frac{3}{2}\pi - \phi/2)\tan\phi} \qquad [6c]$$

As stated before, the values of N_c and N_q depend only on the value of ϕ. By plotting these values as abscissa on the left-hand side of Figure 38*a* the solid curves N_c and N_q have been obtained. The values of N_γ are determined by equation 45(4*b*). They are given by the abscissa of the plain curve marked N_γ on the right-hand side of Figure 38*c*. For $\phi = 0$ we get

$$N_c = \tfrac{3}{2}\pi + 1 = 5.7, \quad N_q = 1, \quad \text{and} \quad N_\gamma = 0 \qquad [7a]$$

Introducing these values and the value $D_f = 0$ into equation 5 we get for the bearing capacity Q_D per unit of length of a continuous footing with a rough base resting on the horizontal surface of the soil the value

$$Q_D = 2B \times 5.7c \qquad [7b]$$

and for the bearing capacity per unit of area

$$q_D = 5.7c \qquad [7c]$$

For $\phi = 34°$ we get

$$N_c = 41.9, \quad N_q = 29.3, \quad \text{and} \quad N_\gamma = 36.0$$

The bearing capacity Q_D per unit of length of a continuous footing resting on the surface of the soil (depth of foundation $D_f = 0$) is

$$Q_D = 2B \times 41.9c + 2B^2 \times 36.0\gamma$$

and the average load per unit of area at the instant of failure is equal to

$$q_D = 41.9c + 36.0B\gamma$$

These results and the data shown in Figure 38*c* demonstrate that the critical load increases rapidly with increasing values of ϕ.

Equations 6 and 7 refer to continuous footings with a rough base. Beneath such footings the boundaries *ad* and *bd* of the zone of elastic equilibrium (Figure 38*a*) rise at an angle $\psi = \phi$ to the horizontal. If the resistance against sliding at the base of the footing does not suffice to reduce the angle ψ to the value ϕ the values of the bearing capacity factors are smaller than those given by the preceding equations.

The following equations represent the values of N_c and N_q on the assumption that ψ is greater than ϕ.

If $\phi < \psi < 45° + \phi/2$:

$$N_c = \tan\psi + \frac{\cos(\psi - \phi)}{\sin\phi\cos\psi}\,[a_\theta^2(1 + \sin\phi) - 1] \qquad [8a]$$

and

$$N_q = \frac{\cos(\psi - \phi)}{\cos\psi}\,a_\theta^2 \tan\left(45° + \frac{\phi}{2}\right) \qquad [8b]$$

wherein

$$a_\theta = e^{(\frac{3}{2}\pi + \phi/2 - \psi)\tan\phi} \qquad [8c]$$

If $\psi = 45° + \phi/2$ (perfectly frictionless base):

$$N_c = \cot\phi\left[a\,\tan^2\left(45° + \frac{\phi}{2}\right) - 1\right] \qquad [9a]$$

and

$$N_q = a_\theta^2 \tan^2\left(45° + \frac{\phi}{2}\right) \qquad [9b]$$

wherein

$$a_\theta = e^{\frac{1}{2}\pi\tan\phi} \qquad [9c]$$

The corresponding values of N_γ could be determined as shown in Article 45. If we take it for granted that the surface of sliding for $\gamma = 0$ (surface de_1f_1 in Figure 38*a*) is determined by equation 3, then equations 6, 8, and 9 can also be derived by elementary methods, on the basis of the condition that the pressure on the inclined boundaries of the zone of plastic equilibrium *abd* in Figures 37*c* and 38*a* must be equal to the passive earth pressure.

For a continuous footing with a perfectly smooth base the value ψ is equal to $45° + \phi/2$. If in addition $\phi = 0$ we get

$$N_c = \pi + 2 = 5.14, \quad N_q = 1, \quad \text{and} \quad N_\gamma = 0 \qquad [9d]$$

Introducing the value $N_c = 5.14$ into equation 5 and assuming that the footing rests on the surface of the ground ($D_f = 0$), we obtain for the ultimate bearing capacity Q_D per unit of length of the footing

$$Q_D = 2B \times 5.14c \qquad [9e]$$

and for the bearing capacity per unit of area

$$q_D = 5.14c \qquad [9f]$$

The corresponding value for a continuous footing with a rough base is $q_D = 5.7c$ (equation 7*c*). Both values are independent of the width of the footing.

If the point of application of the load on a footing is not located exactly at the center line (eccentric loading), the failure of the earth support will start on the side of the eccentricity. As a consequence the sinking of the footing will be associated with a tilting of its base toward the side of eccentricity. If the eccentricity is very small the load required to produce this type of failure is almost equal to the load required for producing a symmetrical general shear failure. The failure occurs on account of intense radial shear on one side of the plane of symmetry in Figure 37, while the deformations in the zone of radial shear on the other side are still insignificant. For this reason the failure is always associated with a heave on that side toward which the footing tilts.

47. Conditions for local shear failure of soil support of shallow continuous footings. The stress conditions for the failure of a cohesive soil are approximately determined by the equation

$$\sigma_I = 2c \tan\left(45° + \frac{\phi}{2}\right) + \sigma_{III} \tan^2\left(45° + \frac{\phi}{2}\right) \qquad 7(3)$$

wherein σ_I is the major principal stress and σ_{III} is the minor principal stress. The values c and ϕ represent the two constants in Coulomb's equation. Figure 38*b* shows the relation between the stress difference $\sigma_I - \sigma_{III}$ and the corresponding linear strain in the direction of the major principal stress σ_I for two different soils. If the relation for a soil located beneath a footing is such as indicated by the solid line C_1, the soil behaves under load almost like the ideal plastic material represented by the broken line $0ab$, and the soil support fails by general shear.

On the other hand, if the stress-strain relations are such as indicated by the dashed curve C_2, the lateral compression required to spread the state of plastic equilibrium as far as the outer edge f of the wedge aef (Fig. 37*c*) is greater than the lateral compression produced by the sinking of the footing. Hence, in this case the soil support fails by local shear. In order to obtain information on the lower limit for the corresponding

critical load Q_D, we replace the curve C_2 by a broken line $0cd$. It represents the stress-strain relation for an ideal plastic material whose shear values c' and ϕ' are smaller than the shear values c and ϕ for the material represented by the curve C_2. Replacing the values c and ϕ in equation 7(3) by c' and ϕ' we obtain

$$\sigma_I = 2c' \tan (45° + \phi'/2) + \sigma_{III} \tan^2 (45° + \phi'/2) \qquad [1]$$

Since the curve C_2 in Figure 38*b* is located almost entirely on the right-hand side of its ideal substitute $0cd$, the critical load Q'_D required to produce a general shear failure in the material represented by equation 1 is somewhat smaller than the load required to produce a local shear failure in the soil represented by the curve C_2. The available data on stress-strain relations suggest that we are justified in assigning to c' and ϕ' the lower limiting values

$$c' = \tfrac{2}{3}c \qquad [2a]$$

and

$$\tan \phi' = \tfrac{2}{3} \tan \phi \qquad [2b]$$

If the soil support fails by general shear, the bearing capacity is determined approximately by equation 46(5). For footings with a rough base the values of the bearing capacity factors N_c, N_q, and N_γ contained in this equation are given by equations 46(6*a* to 6*c*) and 45(4*b*). In order to compute the corresponding values N'_c, N'_q, and N'_γ for local shear failure we must replace the values ϕ and c in these equations by c' and ϕ' and the value P_P in equation 45(4*b*) must be computed on the assumption that the angle of shearing resistance of the supporting soil is equal to ϕ'. The critical load Q'_D is equal to the sum

$$Q'_D = 2B(\tfrac{2}{3}cN'_c + \gamma D_f N'_q + \gamma B N'_\gamma) \qquad [3]$$

This equation is the equivalent of equation 46(5). In Figure 38*c* the values N'_c, N'_q, and N'_γ are represented by the abscissas of the dashed curves N'_c, N'_q, and N'_γ respectively.

The bearing capacity per unit of area of the strip is

$$q'_D = \frac{Q'_D}{2B} = \frac{2}{3} cN'_c + \gamma D_f N'_q + \gamma B N'_\gamma \qquad [4]$$

If the stress-strain relations for a soil are intermediate between the two extremes represented by the curves C_1 and C_2 in Figure 38*b*, the critical load is intermediate between Q_D and Q'_D.

48. Distribution of the contact pressure over the base of continuous footings. The term *contact pressure* indicates the pressure which acts at the surface of contact between the base of a footing and the sup-

porting soil. The following investigation of the distribution of the contact pressure over the surface of contact is based on the equation

$$Q_D = 2B(cN_c + \gamma D_f N_q + \gamma B N_\gamma) \qquad 46(5)$$

This equation shows that the total bearing capacity Q_D per unit of length of a continuous footing can be resolved into two parts

$$Q_1 = 2B(cN_c + \gamma D_f N_q) \qquad [1]$$

which increases in simple proportion to the width $2B$ of the footing, and

$$Q_2 = 2\gamma B^2 N_\gamma \qquad [2]$$

which increases with the square of the width. The distribution of the pressures Q_1 and Q_2 over the base of the footing is determined by the distribution of the corresponding passive earth pressures over the inclined boundaries of the zone of elastic equilibrium, *abd* in Figure 37*c*. Figures 39*a* and 39*b* show one half of this zone.

When computing the values N_c and N_q in equation 1 it was assumed that the unit weight γ of the soil located beneath the level of the base of the footing is equal to zero. On this assumption the passive earth pressure is uniformly distributed over the inclined surface *bd* in Figure 39*a*. The shearing stresses on the vertical face *dO* are equal to zero because this face coincides with the plane of symmetry of the footing. Since the pressure on *bd* is uniform and the weight of the earth located within the zone *Obd* is assumed equal to zero, we have to expect that the normal pressure on *Od* is also practically uniform and that the resultant pressure P'_E intersects *bd* in the immediate vicinity of the midpoint, as shown in the figure. On account of the roughness of the base of the footing and of the adhesion the resultant pressure Q' on the horizontal surface *Ob* acts at an angle to the vertical direction as indicated in the figure. Equilibrium requires that the three forces, P_{Pc} (resultant of P'_P and C_a), P'_E, and Q' intersect in one point. Therefore the point of application of the vertical pressure on *Ob* is located on the right-hand side of the midpoint of *Ob*. The corresponding distribution of the normal stresses on *Ob* is represented by the ordinates of the curve *rs*. This curve shows that the normal stress on the base of the footing increases slightly from the center line toward the edges.

When computing N_γ in equation 2 it was assumed that the cohesion c and the surcharge q are equal to zero. On this assumption, the forces which act on the soil located within the zone of elastic equilibrium are as shown in Figure 39*b*. Since $c = 0$ and $q = 0$ the passive earth pressure on *db* increases like a hydrostatic pressure in simple proportion to

the distance from b. Its point of application is located at a distance $\overline{bd}/3$ from point d (see Art. 37), and its line of action passes through the center of gravity of the mass of soil, with a weight W, located within Obd. The shearing stresses on the vertical face Od are equal

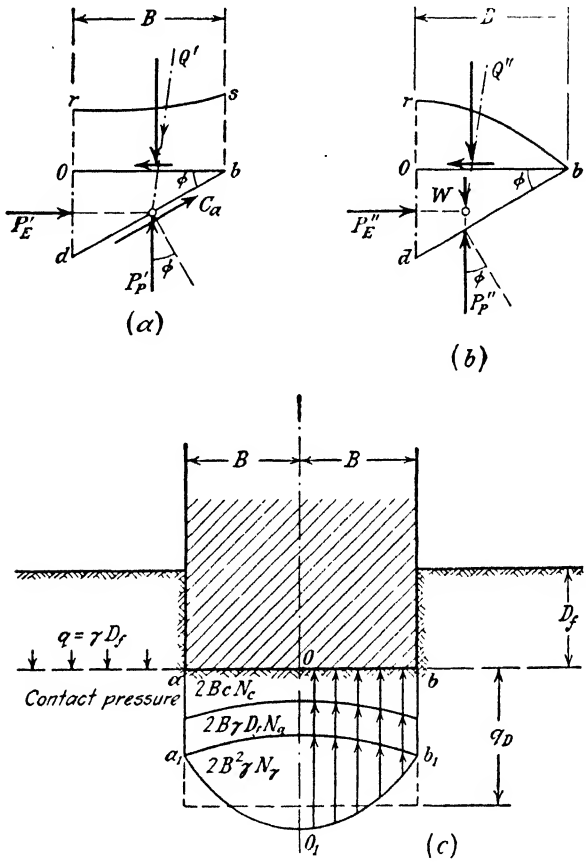

FIG. 39. Forces which act at instant of failure on boundaries of zone of elastic equilibrium beneath the rough base of continuous footings (*a*) on weightless cohesive soil; (*b*) on cohesionless soil with weight; (*c*) distribution of contact pressure on rough base of continuous footing on cohesive soil with weight at instant of failure of loaded soil.

to zero. Since the pressure on bd increases like a hydrostatic pressure with depth we have to expect that the point of application of the normal pressure P''_E on Od is located somewhere between the midpoint and the top of the lower third of Od as shown in the figure. Equilibrium requires that the resultant force Q'' acting on the horizontal surface Ob

passes through the point of intersection of P_P'' and P_E''. Since Q'' slopes toward the center line, its point of application is located at a distance slightly greater than $B/3$ from point O. At the outer edge b of the base of the footing the normal pressure on the base of the footing is equal to zero and it increases toward the center point O (see Art. 16). These conditions combined require that the distribution of the contact pressure over the base of the footing should be roughly parabolic.

The distribution of the total critical load Q_D (eq. 46(5)) over the base of the footing is shown in Figure 39c. The bearing capacity q_D is equal to the average height of the load area $aa_1O_1b_1b$.

Once the soil support has failed, the state of stress in the soil located above the surface of sliding becomes independent of strain. For this reason an elastic deformation of the footing after failure of the earth support should have no influence on the distribution of the soil reactions. On the other hand, if the load on a footing is very much smaller than the critical load, the elastic deformation of the footing is likely to have a considerable influence on the distribution of the contact pressure (see Art. 139). As the load approaches the critical load, the initial distribution of the contact pressure gradually passes into that shown in Figure 39c.

49. Bearing capacity of shallow square or circular footings. A square or circular footing is shallow if the depth of foundation D_f is smaller than the width of the footing. When dealing with shallow footings we can replace the soil (unit weight γ), located above the level of the base of the footing, by a surcharge $q = D_f\gamma$ per unit of area. (See first paragraph of Art. 45.)

If the soil support of a continuous footing yields, all the soil particles move parallel to a plane which is perpendicular to the center line of the footing. Therefore the problem of computing the bearing capacity of such footings is a problem of plane deformation. On the other hand, if the soil support of a square or circular footing yields, the soil particles move in radial and not in parallel planes.

By repeating the reasoning which led to equation 46(5) we arrive at the conclusion that the critical load for a circular footing with a radius R can be represented approximately by a general equation

$$Q_{Dr} = \pi R^2(cn_c + \gamma D_f n_q + \gamma R n_\gamma) \qquad [1]$$

wherein n_c, n_q, and n_γ are pure numbers whose values depend only on the angle of shearing resistance ϕ. Equation 1 is an analogue of equation 46(5). However, on account of the mathematical difficulties involved no rigorous method has yet been devised for computing the

coefficients. Until the results of successful theoretical or of adequate experimental investigations are available, we are obliged to estimate the bearing capacity on the basis of the limited experience we have at present. The available data will be given in a volume on applied soil mechanics (Golder 1942, Skempton 1942, and unpublished test results). Taking the most unfavorable test results as a basis for establishing a provisional equation, the author obtained from the experimental data for the bearing capacity of a circular area with a radius R

$$Q_D = \pi R^2 q_D = \pi R^2 (1.3cN_c + \gamma D_f N_q + 0.6\gamma R N_\gamma) \qquad [2]$$

wherein N_c, N_q, and N_γ represent the bearing capacity factors for continuous footings, supported by the same soil. For footings covering a square area of $2B \times 2B$ he obtained

$$Q_D = 4B^2 q_D = 4B^2 (1.3cN_c + \gamma D_f N_q + 0.8\gamma B N_\gamma) \qquad [3]$$

If the soil is loose or very compressible, the bearing capacity factors N must be replaced by the values N'. (See Figure 38c.)

Small-scale model tests have shown that the greatest heave of the ground surface surrounding a loaded circular area with a radius R occurs within a distance of about $3R$ from the center of the loaded area. Beyond a distance of about $5R$ from the center the heave is imperceptible.

Equation 2 leads to the following conclusions. If the soil support of a continuous footing with a width $2B$ on a cohesive soil ($\phi = 0$) fails under a unit load q_D by general shear, the bearing capacity of a circular footing with a diameter $2R$ is approximately equal to $1.3\,q_D$. On the other hand, if $c = 0$, $D_f = 0$, and $\phi > 0$ the circular footing fails at an average unit load of about $0.6\,q_D$ wherein q_D is the unit load required to produce a general shear failure beneath a continuous footing with a width $2R$, supported by the same material. Experiments on sand and clay have shown the approximate validity of this conclusion. An exact agreement between the computed and the measured values cannot be expected.

50. Bearing capacity of cylindrical piers. In the preceding articles the shearing resistance of the soil located above the level of the base of the footings has been disregarded, because the resulting error is small and on the safe side. However, when dealing with piers whose diameter $2R$ is small compared to the depth of foundation, no such simplification is justified because the resulting error is likely to be excessive. The effect of the shearing stresses in the soil on the bearing capacity of a pier is illustrated by the right-hand side of Figure 36*b*. The earth located beneath the annular space represented by *bd* is acted upon by

the horizontal radial pressure which is exerted by the soil located immediately beneath the base of the footing. It tends to yield in an upward direction, as indicated by arrows. This tendency is resisted not only by the weight of the soil, γD_f per unit of the annular area *bd*, but also by the skin friction f_s per unit of the area of contact between the pier and the earth and by the shearing stresses τ on the outer boundary *de* of the mass of soil located above the annular area. The effect of these stresses is twofold. First of all they reduce the total pressure on the base of the pier from Q to

$$Q_1 = Q - 2\pi R f_s D_f$$

Hence, if Q_D is the total vertical pressure on the base of the pier at the instant of failure, the load Q_{Dp} on the pier (weight of the pier included) required to produce the pressure Q_D is

$$Q_{Dp} = Q_D + 2\pi R f_s D_f \qquad [1]$$

Second, the shearing stresses in the soil located above the annular area represented by *bd* increase the vertical pressure per unit of this area, as soon as the area starts to rise, from γD_f to a higher value $\gamma_1 D_f$. Replacing γD_f in equation 49 (2) by $\gamma_1 D_f$ and substituting the value of Q_D thus obtained in equation 1 we get for the critical load on the pier the equation

$$Q_{Dp} = \pi R^2(1.3cN_c + \gamma_1 D_f N_q + 0.6\gamma N_\gamma) + 2\pi R f_s D_f \qquad [2]$$

The values N_c, N_q, and N_γ can be obtained from Figure 38*c*. The value γ_1 is determined by the vertical forces which resist a rise of the annular area *bd*. Since the outer diameter of this area is equal to $2nR$, these forces are

$$D_f[(n^2 - 1)\pi R^2 + 2\pi R f_s + 2n\pi R\tau]$$

or, per unit of the annular area

$$q_1 = D_f\left[\gamma + 2\frac{f_s + n\tau}{(n^2 - 1)R}\right] = \gamma_1 D_f \qquad [3a]$$

wherein

$$\gamma_1 = \gamma + 2\frac{f_s + n\tau}{(n^2 - 1)R} \qquad [3b]$$

The factor n in eqs. 3 should be given such a value that the critical load Q_{Dp}, eq. 2, is a minimum. This condition can be satisfied by means of a trial computation. The skin friction f_s can be introduced into the preceding equations with its full value, because the pier cannot sink into the ground before the skin friction is fully active. On the other hand, the value τ in equation 3*b* is very uncertain, because the intensity of the shearing stresses on *de* depends to a large extent on the degree of volume com-

pressibility of the earth. If the soil is practically incompressible, such as a dense sand, the shearing stresses on the lower part of *de* are likely to be very significant. On the other hand, in a loose sand, which is very compressible, the shearing stresses over the entire area *de* are likely to be insignificant, because the clearance required for a downward penetration of the pier can be produced by a lateral compression of the sand located beneath the annular area *bd* and the tendency to lift the sand located above this area is likely to be insignificant. Hence, when the value τ in equation 3*b* is selected, liberal allowance should be made for the incomplete mobilization of the shearing resistance of the soil along the cylindrical surface *de*. In any event, the volume compressibility of the soil must be taken into consideration because it has a decisive influence on the bearing capacity of the pier.

51. Bearing capacity of individual piles. The only difference between piles and slender piers is in the method of construction. Although some types of piles have a conical shape, all the foregoing comments on the bearing capacity of piers also apply to piles. One part Q_f of the total load on the pile is carried by the *skin friction*. The balance Q_p is transferred onto the soil through the base or the point of the pile and is called the *point resistance*. Hence the bearing capacity Q_s of a pile under static load can be expressed by the equation

$$Q_s = Q_p + Q_f$$

The items Q_p and Q_f correspond to the items Q_D and $2\pi R f_s D_f$ in equation 50(1), which determines the bearing capacity of piers.

For piles which are entirely embedded in uniform plastic material such as soft clay, silt, or river mud, the point resistance Q_p is likely to be negligible compared to the load Q_f which is carried by the skin friction. Such piles are known as *friction piles*. On the other hand, if the point of the pile is embedded in a firmer stratum the greater part of the load is carried by the point of the pile which, in this case, is called a *point-bearing pile*.

The ratio between the total skin friction and the point resistance depends not only on the nature of the soil and on the dimensions of the pile but also on the method which has been used for installing the pile in the ground. Certain types of piles, for instance the wood piles and the precast reinforced concrete piles, may be driven into the ground by the impact produced by a falling weight (hammer). Other types of piles are installed by driving into the ground a removable shell, whose lower end is closed during the operation of driving. While the empty space surrounded by the shell is being filled with concrete, the shell is

gradually pulled out of the ground. This process relieves part of the stresses which have been previously produced in the soil by driving the shell. In order to accelerate and facilitate the process of driving a pile or a shell through a hard stratum a water jet may be used which loosens the soil ahead of the point of the pile. Piles have also been installed by pouring or ramming the concrete into a drill hole or by driving a cylindrical shell with an open lower end into the ground. The soil which penetrates the space within the shell during the process of driving is removed by means of an air jet, whereupon the empty space is filled with concrete.

Our knowledge of the influence of the method of installing the piles on the skin friction and on the intensity of the shearing stresses in equations 50(3) is still rudimentary and the prospects for evaluating this influence by theory are very slight.

On account of the uncertainties involved in the computation of the bearing capacity of cylindrical piers (see Art. 50), it is not surprising that the attempts to compute the bearing capacity of piles (Stern 1908, Dörr 1922, and many others) have not been successful. All of them involve very arbitrary assumptions or misapplication of existing theories as illustrated by the following examples. The point resistance has been computed by means of methods which are valid only for a plane state of deformation, such as the theory of the passive earth pressure or the theory of the bearing capacity of continuous footings, described in Article 45. The pressure of the soil on the skin has been determined by means of Coulomb's theory of earth pressure, which is also valid only for a plane state of deformation and the effect of the volume compressibility of the soil on the point resistance has been consistently disregarded (Terzaghi 1925).

Since the bearing capacity of the piles cannot yet be computed on the basis of the results of soil tests performed in the laboratory we are still obliged either to estimate this value on the basis of local experience or else to determine it directly in the field by loading a test pile to the point of failure.

In order to avoid the necessity of making load tests, persistent efforts have been made for more than a century to obtain the desired information from the results of a simplified field test involving the measurement of the depth of penetration $\Delta\rho$ produced by a hammer with a known weight W_H which is allowed to drop on the head of the pile from a known elevation H. The equations which are supposed to express the relation between the distance $\Delta\rho$ of penetration of the pile and the corresponding resistance to the penetration of the pile are known as *pile formulas.*

52. Pile formulas. By analogy with the resistance to the penetration of piles under a static load, it is assumed that the relation between

the depth of penetration of a pile under a single blow of a hammer and the corresponding resistance Q of the soil is approximately as indicated by the line *oeb* in each of the two diagrams of Figure 40. The resistance of sand may increase consistently with increasing penetration, as shown in Figure 40*a*, whereas that of clay probably passes through a maximum, as shown in Figure 40*b*. Since the resistance against penetration under the blow of a hammer changes with increasing penetration the word 'dynamic resistance against penetration" has no definite meaning unless this term is applied to the final resistance, represented by the abscissa Q'_d of the vertical asymptote to the penetration curve.

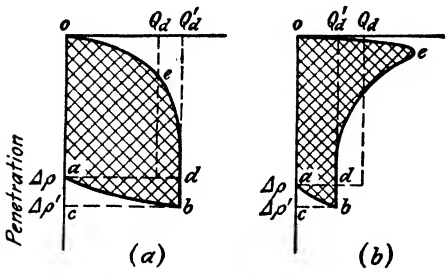

FIG. 40. Relation between resistance Q_d and penetration of pile under a blow of the hammer (*a*) into sand and (*b*) into clay. (*After A. E. Cummings 1940.*)

The blow of the hammer produces not only a permanent penetration of the pile but also a temporary elastic compression of the pile and the surrounding soil. Therefore the penetration produced by the blow is always followed by an elastic rebound involving a perceptible upward movement of the head of the pile. In Figure 40 this rebound is indicated by the line *ba*.

The product of the resistance and the corresponding increase of the penetration is equal to the work performed while the penetration is increased. In each of the diagrams shown in Figure 40, the shaded area *oba* represents the work required to overcome the skin friction and to displace the soil located below the point of the soil while the pile is being driven through a distance $\Delta\rho$ into the ground. In addition to this useful work the blow of the hammer sets up intense vibrations in the pile and in the surrounding soil and after the blow has been struck the hammer is likely to bounce conspicuously several times. The energy required to produce these dynamic effects can be classified as loss of energy, because it does not contribute toward increasing the permanent penetration of the pile. If the hammer would strike the upper end of a perfectly elastic column whose lower end rests on a perfectly elastic base, the final position of the lower end would be identical with the initial one Therefore we would classify the entire energy of the blow as a loss.

The existing pile formulas are based on the simplifying assumption that the resistance to the penetration of the pile retains a constant value Q_d during the entire movement of the pile through the distance $\Delta\rho$.

Since the total work performed by the falling hammer is $W_H H$, we can write

$$W_H H = Q_d \Delta\rho + E_l \qquad [1]$$

wherein E_l represents the total loss of energy. It is further assumed without any justification that the work performed in producing a temporary elastic compression of the pile and the adjoining soil necessarily constitutes part of the loss of energy. On the other hand the important losses of energy associated with the vibrations produced by the blow are disregarded.

In order to correlate the real resistance-penetration diagrams shown in Figure 40 with the rather artificial concept on which the pile formulas are based we must assign the lower part *abd* of the shaded areas to the loss of energy E_l and we must replace the upper part *oade* by a rectangle of equal height and area whose width

$$Q_d = \frac{\text{area } oade}{\Delta\rho} \qquad [2]$$

is assumed to represent the dynamic pile-driving resistance to which the pile formulas refer. According to Figure 40, the value Q_d can be either greater or smaller than the real dynamic resistance Q_d'.

The customary methods of estimating the loss of energy E_l in equation 1 are based on one of the following assumptions:

(*a*) the loss of energy is equal to the dynamic resistance Q_d times the temporary penetration $(\Delta\rho' - \Delta\rho)$ of the pile,
(*b*) E_l is due only to the elastic compression of the pile,
(*c*) E_l is identical with the loss of energy determined by Newton's theory of impact,
(*d*) E_l includes both the losses due to elastic compression and the Newtonian loss.

In the following analysis the different pile formulas will be written in terms of the ultimate resistance, regardless of whether or not the original equations, as published by their authors, referred to the ultimate or to the " safe " load.

Let

l = the length of the pile,
A = the area of the average cross section through the pile,
W_P = the weight of the pile,
E = the modulus of elasticity of the pile material,
n_e = the coefficient of restitution in Newton's theory of impact.

If the estimate of the loss of energy is based on assumption *a*, expressed by the equation

$$E_l = Q_d\,(\Delta\rho' - \Delta\rho) \qquad [3]$$

we obtain from equation 1

$$Q_d = \frac{W_H H}{\Delta\rho'} \qquad [4]$$

Since the evaluation of this equation requires that the maximum penetration $\Delta\rho'$ be measured in the field, the equation has not often been used.

Weisbach's theory (about 1820) is representative of the theories based on assumption *b*, which considers only the energy loss due to the elastic compression of the pile. Weisbach assumed that the resistance against penetration of the pile is concentrated at the point of the pile. The axial pressure in the pile increases from zero to Q_d. Hence the work required to produce this compression is

$$E_l = \frac{1}{2}\frac{Q_d^2 l}{AE} \qquad [5]$$

Substituting this value in equation 1 and solving for Q_d we obtain Weisbach's equation

$$Q_d = -\frac{\Delta\rho AE}{l} + \sqrt{\frac{2W_H HAE}{l} + \left(\frac{\Delta\rho AE}{l}\right)^2} \qquad [6]$$

The Newtonian equation for the loss of energy due to semi-elastic impact between hammer and pile (assumption *c*) is

$$E_l = W_H H\,\frac{W_P(1 - n_e^2)}{W_P + W_H} \qquad [7]$$

For perfectly elastic impact the coefficient of restitution n_e is equal to unity and the corresponding loss of energy is equal to zero. For $E_l = 0$ we obtain from equation 1 Sanders' (about 1850) equation

$$Q_d = \frac{W_H H}{\Delta\rho}$$

On the other hand for perfectly inelastic impact ($n_e = 0$) the Newtonian loss assumes the value

$$E_l = W_H H\,\frac{W_P}{W_P + W_H}$$

which is at the basis of Eytelwein's formula (about 1820)

$$Q_d = \frac{W_H H}{\Delta\rho\left(1 + \frac{W_P}{W_H}\right)}$$

If we replace the value $\Delta\rho\frac{W_P}{W_H}$ in this equation by an empirical constant c_p we obtain the Engineering News formula

$$Q_d = \frac{W_H H}{\Delta\rho + c_p} \qquad [8]$$

The so-called general equations based on assumption d take into consideration all the conceivable losses of energy. These include the loss due to the elastic compression of the pile (eq. 5), the Newtonian loss (eq. 7), and an additional loss E_{ls} due to the elastic compression of the soil and of the pile cap. Substituting the sum of these losses for E_l in equation 1 we obtain

$$W_H H = Q_d\Delta\rho + W_H H\frac{W_p(1 - n_e^2)}{W_p + W_H} + \frac{Q_d^2 l}{2AE} + E_{ls} \qquad [9]$$

The best-known representatives of this group of pile formulas are those of Redtenbacher (1859) and Hiley (1930).

For the same values of W_H, H, and $\Delta\rho$ the different pile formulas furnish extremely different values for the dynamic resistance Q_d. This alone should suffice to demonstrate that the theoretical evaluation of the loss of energy E_l is void of a sound scientific basis.

According to A. E. Cummings (1940) the different methods of computing the energy loss E_l are open to the following objections. Equation 5 is based on the law which governs the relation between stress and strain under static conditions. This law is not valid for deformation under impact. The equation also fails to include the loss of energy due to the deformation of the soil. The Newtonian equation 7 for the loss of energy due to impact is valid only for the impact between bodies which are not subject to an external restraint. Newton himself warned against the application of his theory to problems involving for instance the impact produced by "the stroke of a hammer" (Newton 1726). Equation 9 contains both the Newtonian impact loss and the losses due to elastic deformation. Newton's theory takes into consideration all the losses of energy including those due to the elastic deformation of the colliding bodies. This fact suffices to invalidate equation 9 regardless of whether or not the Newtonian theory of impact applies to the problem.

On account of their inherent defects all the existing pile formulas are utterly misleading as to the influence of vital conditions, such as the ratio between the weight of the pile and the hammer, on the result of the pile driving operations. In order to obtain reliable information concerning the effect of the impact of the hammer on the penetration of piles it is necessary to take into consideration the vibrations which are produced by the impact. The elements of the theory of these vibrations and the bearing of the theory on the problems of pile driving will be discussed in Article 162.

In spite of their obvious deficiencies and their unreliability, the pile formulas still enjoy a great popularity among practicing engineers, because the use of these formulas reduces the design of pile foundations to a very simple procedure. The price one pays for this artificial simplification is very high. In some cases the factor of safety of foundations designed on the basis of the results obtained by means of pile formulas is excessive and in other cases significant settlements have been experienced. The opinions regarding the conditions for the legitimate use of the formulas are still divided. In this connection the reader is referred to a recent and very illuminating discussion in the *Proceedings of the American Society of Civil Engineers* (Pile driving formulas. Progress Report of the Committee on the Bearing Value of Pile Foundations, *Proc. Am. Soc. C. E.*, May 1941; discussions in every issue from September to December 1941, from January to March 1942; closure in May 1942).

53. Dynamic and static resistance of piles. The dynamic resistance, or the resistance of the earth to rapid penetration of the pile produced by the blow of a falling hammer, is by no means necessarily identical with the static load required to produce a very slow penetration of the pile. This is due to the following reasons. The rapid penetration of the point of the pile into the soil is resisted not only by static friction and cohesion but also by the viscosity of the soil, which is comparable to the viscous resistance of liquids against rapid displacement. On the other hand a rapid succession of blows on the head of the pile loosens the grip of the soil on the sides of the pile. In extreme cases the operation of pile driving is likely to eliminate the skin friction almost completely as long as the pile driving lasts and for some time thereafter.

In connection with the design of pile foundations we are interested only in the static bearing capacity of the piles. Hence if we should succeed in obtaining reliable information on the dynamic pile driving resistance we would still face the task of investigating by systematic field tests the relation between the dynamic and the static bearing capacity under different soil conditions. Until that time the dynamic pile formulas will continue to serve only as "a yardstick to help the engineer to get reasonably safe and uniform results over the entire job" (Cummings 1940). However, since all the existing pile formulas are fundamentally deficient, it is usually preferable to use as a yardstick empirical

rules which are based on local experience or on experience with pile driving in different types of soil.

54. Resistance of piles against buckling. If a slender point-bearing pile of great length is surrounded by a very soft soil it is conceivable that the superimposed load might cause a failure of the pile by buckling. The computation of the load required to produce a buckling failure requires certain assumptions regarding the elastic properties of the surrounding soil. The problem will be discussed in Article 129, which is in the section on elasticity problems. The analysis leads to the conclusion that the danger of buckling is very remote. Hence in most cases it can be disregarded.

Chapter IX

STABILITY OF SLOPES

55. Assumptions. In every type of soil a slope can be made high and steep enough to induce a failure of the soil due to its own weight. If failure occurs by shear along a well-defined surface it is called a *slide*. It involves a downward and outward movement of a slice of earth as

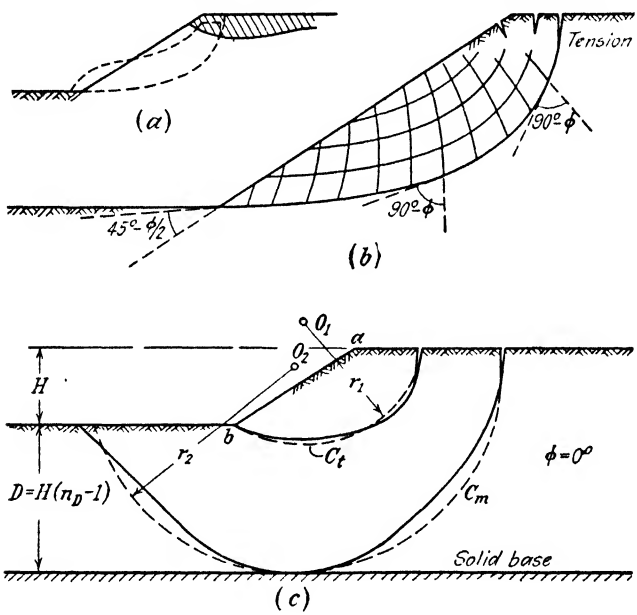

Fig. 41. (*a*) Deformation associated with slope failure; (*b*) shear pattern in sliding mass; (*c*) solid curves represent the real and dashed curves the assumed shape of surface of sliding for slope failure (upper curves) and base failure (lower curves).

shown in Figure 41*a*, and the sliding occurs along the entire surface of contact between the slice and its base. If the movement does not occur along a well-defined surface of sliding it is called a *slump* or a *flow*. Materials with a definite yield point fail only by sliding and not by slumping. Ideal soils are assumed to have a definite yield point. Therefore this chapter deals only with the conditions for stability with respect to sliding. The discussions will further be limited to slides in

cohesive materials whose shearing resistance is determined by Coulomb's equation

$$s = c + \sigma \tan \phi \qquad 5(1)$$

In this equation σ represents the total normal stress on the surface of sliding, including the neutral stress. It is assumed that the equation has been obtained by tests in the laboratory under conditions of pressure and drainage similar to those under which the shear failure is likely to occur in the field (see Art. 6). The influence of known neutral stresses on stability will be investigated independently in Chapter XII (Art. 93). This subdivision of the treatment of the subject appeared advisable for the following reason. When dealing with slopes on clay we are seldom in a position to compute with reasonable accuracy the pore-water pressure which acts in the water content of the clay at the instant of failure. In those few cases in which the pore-water pressure can be predicted, the stability of the slope can be investigated by combining the methods described in this chapter with those to be presented in Article 93.

On account of the great variety of conditions which may lead to slides, no more than a discussion of the fundamental principles of stability computations will be attempted.

Owing to the complexity of field conditions and to the important differences between the assumed and the real mechanical properties of soils, no theory of stability can be more than a means of making a rough estimate of the available resistance against sliding. If a method of computation is simple, we can readily judge the practical consequences of various deviations from the basic assumptions and modify our decisions accordingly. Complicated theories do not offer this important advantage. For this reason some of the more recent theories (Brahtz 1939, Clover and Cornwell 1941) are not included in the following discussions regardless of their academic merits. The basic assumptions of these theories and their practical implications have been summarized and commented upon by Carrillo (1942*c*).

56. Slope failure and base failure. Figure 42*a* is a section through a vertical bank consisting of cohesive soil with a unit weight γ. The shearing resistance of the earth is determined by the equation

$$s = c + \sigma \tan \phi$$

Under the influence of the weight of the soil the originally vertical section *ab* deforms during the process of excavation as indicated in the figure by a dashed line. Within the shaded area the soil is in a state of tension, which leads sooner or later to the formation of tension cracks. The conditions which determine the depth of cracks and the influence of cracks on the state of stress in the material adjoining cracks have been investigated by Westergaard (1933*d*, 1939) in connection with solid

construction materials such as concrete, but the results of the investigations are not directly applicable to the conditions which exist in the tension zone behind a vertical bank of earth. On the basis of the results of model tests on gelatine the author assumes that the depth of the

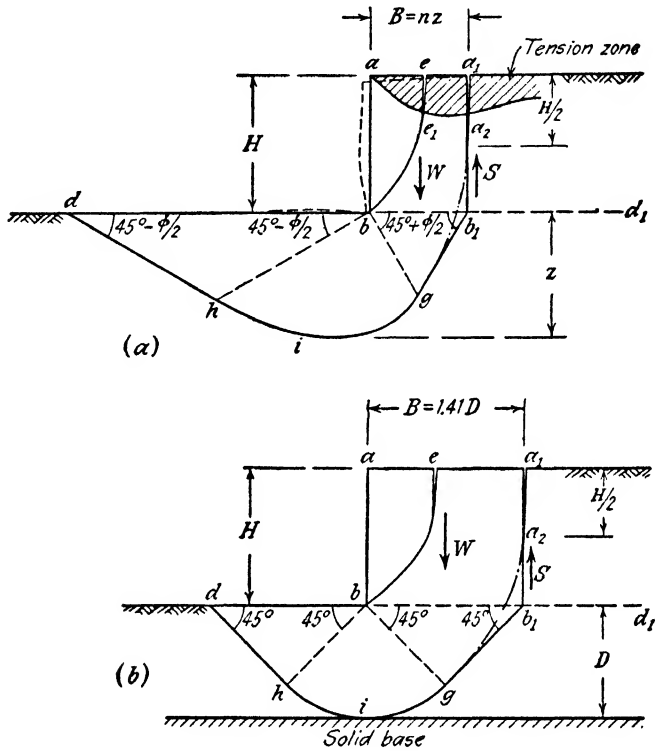

FIG. 42. Slope and base failure of vertical bank. (*a*) Angle of internal friction $\phi > 0$; (*b*) $\phi = 0$.

tension zone does not exceed one-half of the height H of the bank, provided the tension is due to gravity and not due to excessive shrinkage. On account of periodic changes in temperature and water content the earth fails sooner or later by tension, and if the shearing resistance of the soil is inadequate, the tension failure behind the upper part of the bank is followed by a shear failure along a curved and inclined surface of sliding be_1 through the lower edge b of the bank. This is a *bank* or *slope failure*. The methods of investigating the conditions for the stability of a slope with respect to a slope failure are closely related to those for computing the active earth pressure on a lateral support.

However, we must also consider the possibility of a failure of the base

of the bank. With reference to a horizontal section bd_1 through b the soil adjoining the bank acts like a uniformly distributed surcharge, γH per unit of area. If this surcharge exceeds the bearing capacity of the soil located beneath bd_1, the earth adjoining the vertical face sinks into the ground, like an excessively loaded footing. This type of failure is called a *base failure*. The soil located beneath the plane bd_1 can yield only toward the cut, and the shearing stresses on bd_1 are small, because the soil located above this plane participates in the lateral expansion of the soil located below it. Therefore the shear pattern is similar to that shown in Figure 15*a*. According to this figure and to Article 16 the lower boundary of the zone of plastic equilibrium beneath a strip adjoining the edge of the loaded area consists of two plane sections separated from each other by a curved section, as shown in Figure 41*a*. The plane sections rise to the horizontal at angles of $45° + \phi/2$ (right-hand side) and $45° - \phi/2$ (left-hand side) and the radius of curvature of the curved section increases from the surcharge side toward the side which carries no load. The deepest point of the base of the zone of plastic equilibrium is located at some depth

$$z = \frac{B}{n} \qquad [2]$$

below the plane d_1. The bearing capacity Q'_D per unit of length of a strip bb_1 with a width B adjoining the foot of the bank is roughly equal to one-half of the bearing capacity Q_D of a strip with a width $2B$, because the soil located beneath the strip can yield only to one side. The value Q_D is determined by equation 46(5). Setting D_f (depth of foundation) = 0 in this equation we obtain $Q_D = 2BcN_c + 2B^2\gamma N_\gamma$ and

$$Q'_D = \tfrac{1}{2}Q_D = BcN_c + B^2\gamma N_\gamma \qquad [3]$$

The shearing stresses along the surface of contact bb_1 between the surcharge in Figure 42*a* and the supporting earth are very small. Therefore the value of the bearing capacity factor N_c is determined by equation 46(9*a*) which applies to continuous footings with a perfectly smooth base. It is somewhat smaller than the value given by the equation 46(6*a*) and the value N_γ is somewhat smaller than that determined by the curve N_γ in Figure 38*c*.

In Figure 42*a* the surcharge which acts on the strip bb_1 with a width $B = nz$ is equal to the weight of the earth, $W = nz\gamma H$ per unit of length of the strip reduced by the shearing resistance against sliding along the vertical section a_2b_1. The upper edge of this section is located at the bottom of one of the tension cracks. Since the depth of the tension

cracks does not exceed $H/2$ the shearing resistance S per unit of length of the strip is at least equal to $0.5Hc$ and the total surcharge Q per unit of length is not greater than

$$Q = nzH\gamma - 0.5Hc \qquad [4]$$

If this surcharge is greater than Q'_D (eq. 3) the soil support of the surcharge fails by sliding along a_2b_1id. Hence the condition for the failure of the base of the bank is

$$Q'_D = nzcN_c + n^2z^2\gamma N_\gamma = nz\gamma H - 0.5Hc$$

or

$$H = \frac{N_c \frac{c}{\gamma} + nzN_\gamma}{1 - \frac{0.5}{nz}\frac{c}{\gamma}} \qquad [5]$$

The value H represents the height of the highest vertical bank whose weight can still be supported by the strip bb_1 in Figure 42*a* with a width $B = nz$. For

$$z = \frac{0.5}{n}\frac{c}{\gamma}$$

the surcharge on the strip is equal to zero and $H = \infty$. For $z = \infty$ we obtain (from eq. 5) $H = \infty$. For some intermediate value z_1, determined by the condition

$$\frac{dH}{dz} = 0 \qquad [6]$$

the height H (eq. 5) is a minimum. Combining equation 6 with equation 5 and solving for z_1 we obtain

$$z_1 = \frac{c}{2n\gamma}\left(1 + \sqrt{1 + 2\frac{N_c}{N_\gamma}}\right) \qquad [7]$$

For $\phi = 20°$ and $30°$ the value z_1 is approximately equal to $3.0\ c/\gamma$ and $2.5\ c/\gamma$ respectively. The corresponding value H_f for the height of the bank can be computed by introducing the value z_1 into equation 5. If the soil is homogeneous to a depth of more than z_1, a base failure occurs under the weight of any bank whose height is greater than H_f and the deepest point of the surface of sliding is located at a depth z_1. On the other hand, if the soil rests at a depth D of less than z_1 on a firm stratum, the base can sustain the weight of a bank whose height is greater than H_f. In order to compute this height we replace z in

equation 5 by D. The corresponding surface of sliding is tangent to the surface of the firm stratum.

For $\phi = 0$ the bearing capacity factor N_γ in equation 3 is equal to zero (see Art. 46). Introducing $N_\gamma = 0$ into equation 5 we get

$$H = \frac{N_c \frac{c}{\gamma}}{1 - \frac{0.5c}{nz\gamma}}$$

This value decreases steadily with increasing values of z. Hence, if $\phi = 0$, the surface of sliding associated with a base failure is always tangent to the surface of the firm stratum, regardless of the depth D at which this surface is located. The height H_f of the bank required to produce a base failure can be computed by substituting $z = D$. Thus we obtain

$$H_f = \frac{N_c \frac{c}{\gamma}}{1 - \frac{0.5c}{nD\gamma}} \qquad [8]$$

If $D = \infty$, the height H_f is equal to

$$H_{f\infty} = N_c \frac{c}{\gamma} \qquad [9]$$

In Figure 42*b* the surface of sliding for $\phi = 0$ is indicated by the line b_1id. It consists of two plane sections which rise at angles of 45° to the horizontal and an arc of a circle whose center is located at point b (see Art. 46). The failure occurs beneath a strip with a width

$$B = nD = D\sqrt{2} = 1.41D$$

and

$$n = 1.41$$

Since the shearing stresses along bb_1 are very small, the bearing capacity factor N_c is determined by equation 46(9*d*)

$$N_c = 5.14$$

Introducing the values $n = 1.41$ and $N_c = 5.14$ into equations 8 and 9 we get

$$H_f = \frac{5.14 \frac{c}{\gamma}}{1 - \frac{0.355c}{D\gamma}} \qquad [10]$$

and

$$H_{f\infty} = 5.14\frac{c}{\gamma} \qquad [11]$$

In the preceding investigations it was assumed that there is a sharp break in the surface of sliding at point b_1 (Figs. 42*a* and 42*b*). In reality the surface of sliding is smooth, as indicated in both figures by the dash-dotted line a_2g.

Figure 41*a* represents a slope before and after failure. Prior to the failure the soil located within the shaded area is in a state of tension and the failure of a slope is always preceded by the appearance of tension cracks. The failure occurs by sliding along a curved surface of sliding which passes through the lower edge of the slope. The slide involves a stretching of the upper part of the sliding mass in the direction of the slope and a compression of the lower part in the same direction. The corresponding shear pattern is represented in Figure 41*b*. In the lowest part of the sliding mass the shear pattern is similar to that shown on the left-hand side of the vertical section *rs* in Figure 13*a* (passive failure), and in the uppermost part it has some resemblance to that shown on the right-hand side of *rs* (active failure). The zone of transition between these two shear patterns is comparable to the zone of radial shear which separates the active and the passive Rankine zones in Figure 15*a*.

An inclined slope can also fail on account of inadequate bearing capacity of its base, as indicated in Figure 41*c* for a material whose angle of shearing resistance ϕ is equal to zero. The question whether the failure of a bank will be a slope or a base failure can only be decided on the basis of the results of a stability computation. In order to simplify the investigation we replace the surface of sliding through the lower edge *b* of the slope (slope failure) by an arc of a circle with a radius r_1, whose center is located at O_1, and the composite surface of sliding associated with a base failure by an arc of a circle with a radius r_2 whose center is located at O_2. Circles through the toe *b* are called *toe circles* in contrast to *midpoint circles*, which intersect the lower horizontal surface of the ground at some distance from the toe. The cohesion required to prevent a slip along any arbitrary toe circle is the required cohesion c_{rt} and the corresponding value for an arbitrary midpoint circle is the required cohesion c_{rm}. A slope failure occurs along that toe circle for which c_{rt} is a maximum c_{ct}, and a base failure occurs along that midpoint circle for which c_{rm} is a maximum c_{cm}. These two circles will be called the *critical toe* circle and the *critical midpoint* circle respectively. The critical toe circle can be compared to the surface of sliding in the

backfill of a yielding retaining wall and the midpoint circle to that beneath an overcharged, continuous footing. The cohesion values c_{ct} (critical toe circle) and c_{cm} (critical midpoint circle) represent the *critical cohesion values*. The methods for locating the position of the critical circles will be described in Articles 58 to 61. The critical cohesion values can be determined by means of the friction circle method (Art. 40).

If a midpoint circle similar to the circle C_m in Figure 41*c* is substituted for the real surface of sliding a_2id in Figure 42*b* we obtain for the critical height $H_{f\infty}$ corresponding to a depth factor $n_D = \infty$ instead of

$$H_{f\infty} = 5.14 \frac{c}{\gamma}$$

the value

$$H_{f\infty} = 5.52 \frac{c}{\gamma} \qquad [12]$$

involving an error of 7.4 per cent on the unsafe side. However, when dealing with inclined slopes, the error due to the assumption of a circular surface of sliding is likely to be much less important.

The ratio of the critical cohesion value c_{ct} for a toe circle to the critical cohesion value c_{cm} for a midpoint circle (c_{ct}/c_{cm}) may be greater or smaller than unity. If c_{ct}/c_{cm} is greater than unity we have to anticipate a slope failure because the cohesion c_{ct} required to prevent a slope failure is greater than c_{cm}. On the other hand a value of c_{ct}/c_{cm} smaller than unity indicates the danger of a base failure. At a given height H of a slope the value of the ratio c_{ct}/c_{cm} depends on the slope angle and on the angle of shearing resistance ϕ. In many instances it also depends on the depth D at which the soil rests on a firm stratum. The ratio $(D + H)/H$ will be called the *depth factor*, n_D. The influence of the depth factor on the stability conditions will be discussed in Articles 58 to 61.

The replacement of the real surface of sliding by an arc of a circle has been suggested for the first time by Petterson. The methods based on this substitution have been further developed by Fellenius (1927) and Taylor (1937). Rendulic (1935*b*) proposed replacing the real surface of sliding by a logarithmic spiral. However, Taylor (1937) has shown that the results obtained by means of the corrected friction circle method (Art. 40) and by the spiral method are practically identical. Since the friction circle method is more convenient than the spiral method, the latter will not be considered. Attempts to solve the problems pertaining to the stability of slopes by means of the analytical methods of the theory of plasticity have been made by Frontard (1922) and Jáky (1936). Frontard disregarded the existence of a zone of transition between the Rankine states which prevail in the vicinity of the upper and the lower edge of the sliding masses. That is, he replaced arbitrarily the

continuous shear pattern shown in Figure 41*b* by the discontinuous shear pattern shown in Figure 13*a* (Terzaghi 1936*a*). Jáky assumed that the slide occurs along an arc of a toe circle which intersects the slope at an angle of $45° - \phi/2$. The real surface of sliding intersects the slope at an angle of $45° - \phi/2$, but it is not justifiable to assume that the simplified circular one does so. The errors associated with these procedures are excessive. Furthermore neither of the two investigators considered the possibility of a base failure and their methods of computation are very complicated. For these reasons the proposed advanced methods cannot be considered satisfactory.

In order to familiarize the reader with the methods of computation, the individual problems connected with the stability of slopes will be taken up in the following sequence. First we consider the conditions for the stability of vertical banks, because they are similar to those for the stability of the backfill of a retaining wall. Then we solve in succession the following problems: (*a*) computation of the critical cohesion for plane inclined slopes; (*b*) computation of the critical cohesion for an uneven slope on a stratified mass of soil; and (*c*) computation of the factor of safety of a given slope with respect to sliding. On account of the important influence of the angle of shearing resistance ϕ on the type of failure of a slope (slope or base failure), these problems will first be solved on the assumption that $\phi = 0$ (Arts. 58 and 59) and then on the assumption that $\phi > 0$ (Arts. 60 and 61). When dealing with these problems the existence of tension cracks will be disregarded. The influence of tension cracks on the stability of inclined slopes will be discussed in Article 62.

57. Critical height of vertical banks. The uppermost part of the soil adjoining a slope is in a state of tension, provided the slope angle is greater than the angle of shearing resistance ϕ in Coulomb's equation. The *critical height* of a slope is the maximum height which the slope can have before the state of tension is relieved by the formation of tension cracks.

In the following computation of the critical height of vertical slopes it is assumed that the failure occurs along a surface of sliding through the lower edge of the bank (slope failure). Subsequently it will be shown that this assumption is justified for any value of ϕ. The shearing resistance of the earth is determined by Coulomb's equation

$$s = c + \sigma \tan \phi \qquad 5(1)$$

The crudest and simplest method of estimating the critical height of vertical banks is based on the assumption that the soil adjoining the vertical face of the bank is in an active Rankine state. On this assumption the surface of sliding *bd* in Figure 43*a* is plane and rises at an angle of $45° + \phi/2$ to the horizontal (see Art. 12). If a semi-infinite cohesive

mass is in an active Rankine state, the total horizontal pressure P_A on a vertical section between the surface and depth H is determined by the equation 14(3)

$$P_A = -2cH\frac{1}{\sqrt{N_\phi}} + \tfrac{1}{2}\gamma H^2\frac{1}{N_\phi}$$

wherein $N_\phi = \tan^2(45° + \phi/2)$ is the flow value. If

$$H = H_c = 4\frac{c}{\gamma}\sqrt{N_\phi} \qquad [1]$$

the total pressure P_A on the vertical section with depth H_c is equal to zero. For $\phi = 0$ the flow value N_ϕ is equal to unity and

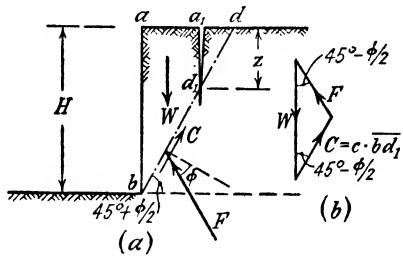

FIG. 43. Conditions for stability of vertical bank after tension cracks have developed.

$$H_c = 4\frac{c}{\gamma} \qquad [2a]$$

However, the analogy between a vertical section with a height H_c and an unsupported vertical face with a height H_c is not perfect, because the state of stress along these two vertical planes is different. The upper part of the vertical section is acted upon by tensile and the lower part by compressive stresses as indicated in Figure 11*e*, and the soil located between the section and the inclined face of the sliding wedge is in a state of plastic equilibrium. On an unsupported vertical bank the normal stresses are everywhere equal to zero and the soil located above the potential surface of sliding passing through the foot of the bank remains in a state of elastic equilibrium. This condition affects both the critical height and the shape of the surface of sliding. Experience shows that the surface of sliding is distinctly curved. Assuming a circular line of sliding, Fellenius (1927) showed that

$$H_c = 3.85\frac{c}{\gamma} \qquad [2b]$$

This value is only 5 per cent smaller than the value given by equation 2*a*, and if ϕ is greater than 0° the error is still smaller. Hence in connection with estimates, equations 1 and 2*a* are accurate enough that the curvature of the surface of sliding through the foot of a vertical bank can be disregarded. In the following investigations, which deal with the influence of tension cracks on the stability of vertical banks, it will be assumed that this surface is plane.

The upper part of the soil adjoining the face of the bank is in a state

of tension, as indicated in Figure 42*a* by a shaded area. If one of the tension cracks intersects the potential surface of sliding *bd* in Figure 43*a* at a depth z below the surface, the wedge-shaped body of soil a_1dd_1 does not participate in a slope failure. The conditions for the equilibrium of the adjoining body aa_1d_1b with a weight W per unit of length are represented by the polygon of forces shown in Figure 43*b*. The weight is

$$W = \tfrac{1}{2}\gamma(H^2 - z^2)\tan\left(45° - \frac{\phi}{2}\right) = \tfrac{1}{2}\gamma(H^2 - z^2)\frac{1}{\sqrt{N_\phi}}$$

The cohesion which acts along bd_1 is

$$C = (H - z)\frac{c}{\cos\left(45° - \frac{\phi}{2}\right)}$$

and the reaction F acts at an angle of ϕ to the normal on bd_1. From the polygon of forces we obtain

$$W = \tfrac{1}{2}\gamma(H^2 - z^2)\frac{1}{\sqrt{N_\phi}} = 2C\cos\left(45° - \frac{\phi}{2}\right) = 2c(H - z)$$

or

$$H = H_c' = 4\frac{c}{\gamma}\sqrt{N_\phi} - z = H_c - z \qquad [3]$$

wherein H_c is the critical height determined by equation 1. Under normal conditions the depth of tension cracks does not exceed about one half of the height of a vertical slope. Assuming $z = H_c'/2$ we obtain from equation 3

$$H_c' = \frac{2H_c}{3} = 2.67\frac{c}{\gamma}\sqrt{N_\phi} \qquad [4]$$

and, for $\phi = 0$ involving $N_\phi = 1$

$$H_c' = 2.67\frac{c}{\gamma} \qquad [5]$$

H_c' represents the maximum height of a bank which has been weakened by tension cracks. If the height of an unsupported vertical bank does not exceed H_c' (eqs. 4 and 5), the bank can be expected to remain stable indefinitely, unless the conditions for its equilibrium are changed, for instance by the accumulation of surface waters in the open tension cracks.

It remains to justify the initial assumption that there is no danger

of a base failure of an unsupported vertical bank. If $\phi = 0$, the base of the bank does not fail unless the height of the bank is greater than H_f (eq. 56(8)). This height decreases with increasing values of the depth factor, $n_D = (D + H)/H$. For $n_D = \infty$ it assumes its minimum value

$$H_{f\infty} = 5.14 \frac{c}{\gamma} \qquad 56(11)$$

Even this minimum value is considerably greater than the critical height $H_c = 4c/\gamma$ (eq. 2*a*).

Similar investigations have shown that the ratio H_f/H_c increases rapidly with increasing values of the angle of shearing resistance ϕ. These results are in accordance with our initial assumption.

58. Stability factor and critical circle if $\phi = 0$. In Figure 44*a* *be* is an arbitrary toe circle through the toe *b* of an inclined slope *ab*, which rises at an angle β to the horizontal. Its position with reference to the slope is determined by two angles. We select for the sake of convenience the slope angle α of the chord *be* and the center angle 2θ. Let

W = weight of the body of earth *abfe* per unit of length of the slope,
l_w = lever arm of the weight W with reference to the center O of the toe circle,
r = radius of the toe circle,
l_a = length of the arc *be*,
c_r = cohesion per unit of area required to prevent a sliding movement along *be*.

Since $\phi = 0$ a slide along *be* is resisted only by the cohesion, $c_r l_a$ per unit of length of the slope. Equilibrium requires that the sum of the moments about the center O of rotation should be equal to zero,

$$W l_w - c_r l_a r = 0$$

or

$$c_r = W \frac{l_w}{r l_a} \qquad [1]$$

A computation of the values W, l_w, and l_a from the geometrical data shown in the figure demonstrates that

$$c_r = \gamma H \frac{1}{f(\alpha,\beta,\theta)} \qquad [2a]$$

wherein γ is the unit weight of the soil and $f(\alpha,\beta,\theta)$ is a function of the angles α, β, and θ. The slope failure occurs along that toe circle for which c_r is a maximum (critical toe circle). Since the slope angle β is

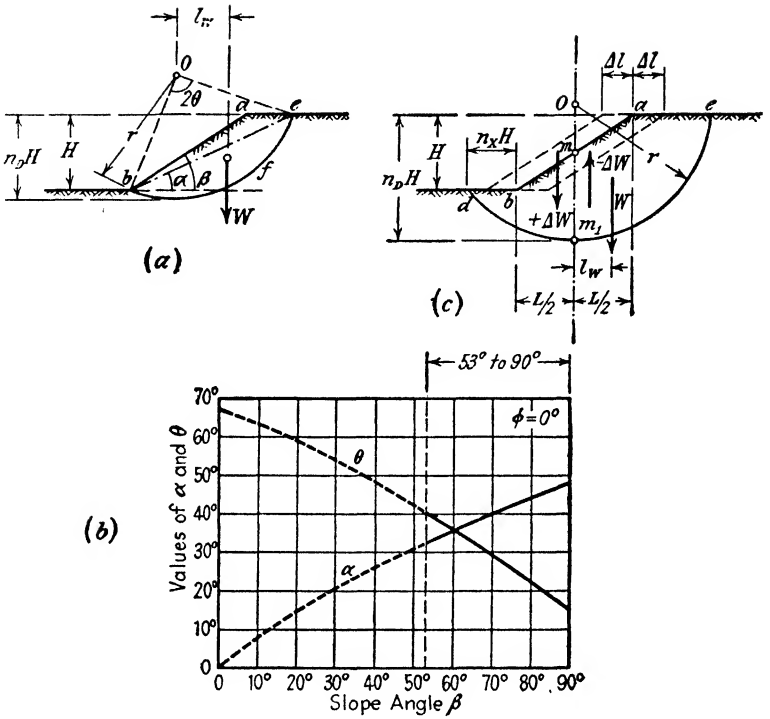

FIG. 44. (*a*) Slope failure along critical toe circle; (*b*) values of the angles α and θ in section (*a*) plotted against slope angle β; (*c*) diagram demonstrating that base failure in homogeneous soil must occur along a midpoint circle. (*After Fellenius 1927.*)

a constant, the position of the critical toe circle is determined by the condition

$$\frac{\partial c_\tau}{\partial \alpha} = 0 \quad \text{and} \quad \frac{\partial c_\tau}{\partial \theta} = 0 \qquad [2b]$$

Solving these equations and substituting the values of α and θ thus obtained in equation 1 one gets for the cohesion c_c required to prevent a slip along the critical toe circle

$$c_c = \frac{\gamma H}{f(\alpha, \beta, \theta)} = \frac{\gamma H}{N_s} \qquad [3]$$

wherein N_s is a pure number, called the *stability factor*, whose value depends only on the slope angle. If the cohesion has a given value, the *available cohesion* c, while the height of the slope is variable we obtain

from the preceding equation

$$H_c = \frac{c}{\gamma} N_s \qquad [4]$$

The height H_c is the *critical height of an inclined slope.* It corresponds to the critical height of vertical slopes, determined by equation 57(2*b*). The stability factor N_s is an analogue to the bearing capacity factor N_c (Art. 46). Fellenius (1927) has solved equations 2 for different values of β. The results of his computations are graphically represented in Figures 44*b* and 45*a*. In Figure 44*b* the values of α and θ have been plotted against the slope angle β. They determine the position of the center of the critical toe circle. If $\beta = 60°$, α is equal to θ and the tangent to the toe circle at the toe of the slope is horizontal. The values of the stability factor with respect to a failure along a critical toe circle N_s are given by the ordinates of the curve *aABb* in the diagram in Figure 45*a*. They increase from 3.85 for $\beta = 90°$ to 8.36 for $\beta = 0$. The ordinates of the plain curve, marked $\phi = 0$ in the diagram in Figure 45*c* represent the depth factor

$$n_D = \frac{D + H}{H} \qquad [5]$$

for the deepest point of the surface of sliding along a critical toe circle. For slope angles of more than 60° (right-hand side of point *C* on the curve *aAb* in Fig. 45*a*) the depth factor is equal to unity. The surface of sliding rises from the toe of the slope toward the slope. On the other hand, if $\beta < 60°$, the deepest part of the surface of sliding is located beneath the level of the toe of the slope, as shown in Figure 44*a*.

In order to investigate the conditions for the equilibrium of an inclined slope with respect to a base failure, we examine the forces which act on the body of earth $abdm_1e$ (Fig. 44*c*) located above an arbitrary midpoint circle dm_1e. The center of this circle is assumed to be located on a vertical line through the midpoint *m* of the slope. The cohesion c_r required to prevent a slide along the circle is determined by equation 1,

$$c_r = W \frac{l_w}{r l_a}$$

If we let the center *O* of the circle and the arc dm_1e be fixed while we shift the slope through a distance Δl toward the left, we increase the weight *W* by ΔW and reduce the moment by $\Delta W \Delta l/2$. On the other hand, if we shift the slope in a similar manner through a distance Δl toward the right, we reduce the weight *W* by ΔW, but at the same

time we also reduce the moment about point O by $\Delta W \Delta l/2$. In either instance the moment which tends to produce the slide decreases while the moment of the resisting forces $c\,l_a r$ remains unchanged. Hence the vertical line through the midpoint m of the slope is the locus of the centers of the circles for which the moment tending to produce sliding is a maximum. All these circles are midpoint circles. The position of a midpoint circle with reference to the slope is determined by two dimensionless quantities, for instance the depth factor $n_D = (D + H)/H$ and the ratio

$$n_x = \frac{\overline{db}}{H} \qquad [6]$$

between the horizontal distance db in Figure 44c and the height of the slope. A computation of the values W, l_w, and l_a in equation 1 from the geometrical data shown in Figure 44c shows that

$$c_r = \gamma H \frac{1}{f(\beta, n_x, n_D)} \qquad [7a]$$

wherein γ is the unit weight and $f(\beta, n_x, n_D)$ is a function of the values β, n_x, and n_D. The values n_D and n_x for the critical midpoint circle must satisfy the further condition

$$\frac{\partial c_r}{\partial n_D} = 0 \quad \text{and} \quad \frac{\partial c_r}{\partial n_x} = 0 \qquad [7b]$$

These equations are satisfied, if

$$n_D = \infty \quad \text{and} \quad H_c = 5.52 \frac{c}{\gamma} \qquad [8]$$

for any value of the slope angle β. The value H_c is identical with the value given by equation 56(12). In Figure 45a equation 8 is represented by the horizontal line cd. It intersects the N_s line for the critical toe circles at point A with an abscissa $\beta = 53°$. Hence, if the slope angle β is less than 53° there are two possibilities. If the surface of the ground adjoining the toe of the slope is horizontal one has to expect a base failure and the corresponding critical height H_c (eq. 8) is independent of the slope angle β. On the other hand, if the surface of the ground adjoining the toe rises as shown in Figure 45b, the weight of the soil located beneath the counterslope prevents a base failure and one has to anticipate a slope failure along a critical toe circle. The corresponding values of the stability factor N_s are represented by the ordinates of the curve ABb.

In the preceding discussions it has been tacitly assumed that the

entire critical circle is located within homogeneous material. In reality every mass of soil rests at some finite depth D on a firmer stratum.

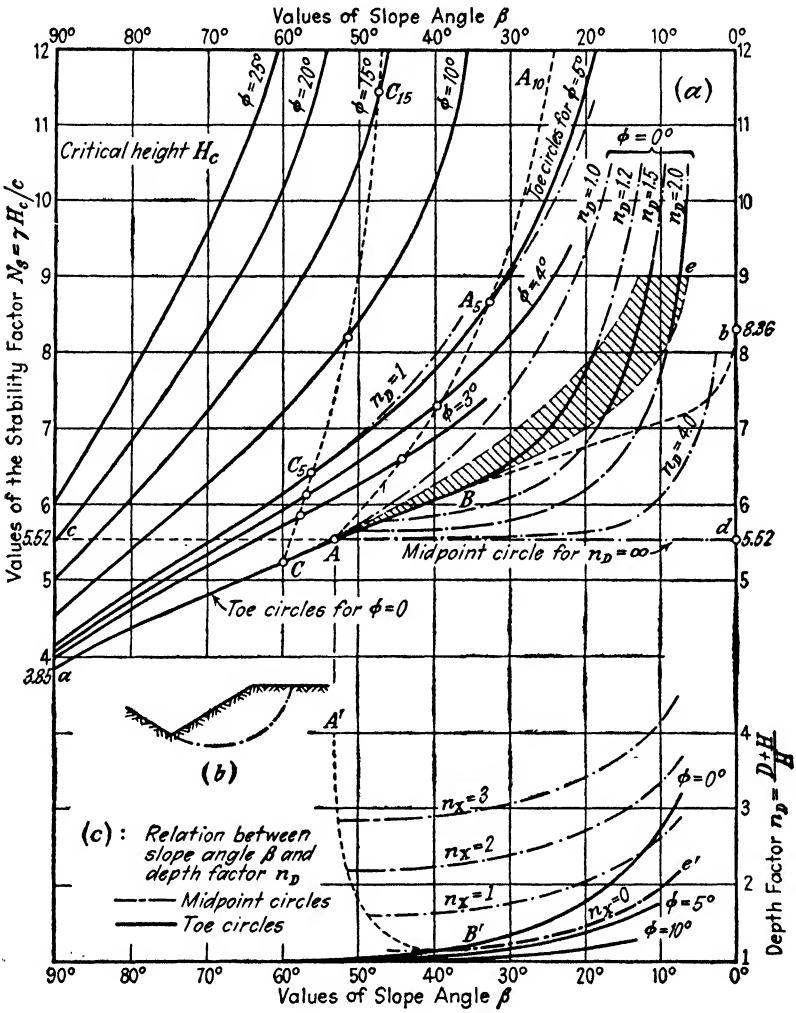

FIG. 45. (*a*) Relation between slope angle β and stability factor N_s for different values of depth factor n_D and of angle of internal friction ϕ; (*b*) diagram illustrating condition which excludes possibility of a base failure; (*c*) relation between slope angle β and depth factor n_D for different values of n_x (see Fig. 44c) and of ϕ. (*Based on data published by D. W. Taylor 1937.*)

Such a limitation to the depth of the deepest point of the surface of sliding is likely to influence the critical height with respect to both

slope and base failures. If for instance the surface of the firm stratum intersects the critical toe circle shown in Figure 45*b*, the failure will occur along some circle tangent to this surface. This circle may either be a toe circle or it may intersect the slope at some distance above the toe (*slope circle*).

The deepest point of the critical midpoint circle corresponding to equation 8 is located at depth infinity. If a firm stratum prevents the surface of sliding from extending into the ground to a depth greater than D, the critical midpoint circle is tangent to the surface of the firm stratum and the depth factor is equal to

$$n_D = \frac{H + D}{H}$$

Since the value of the depth factor is determined by the depth at which a firm stratum is located the first of the two conditions expressed by equations 7*b* becomes immaterial and the position of the critical midpoint circle with reference to the slope is determined by the second one, which is

$$\frac{\partial c_r}{\partial n_x} = 0$$

By means of this equation we obtain for the cohesion $c_c = c_{r\max}$ required to prevent a base failure at a given height of the slope the equation

$$c_c = \frac{\gamma H}{N_s}$$

The value of the stability factor N_s depends on the slope angle and the depth factor n_D. If the cohesion is given, the corresponding critical height of the slope is

$$H_c = \frac{c}{\gamma} N_s$$

This equation is identical with equation 4, but the numerical values of N_s are different, because the value N_s in equation 4 corresponds to critical toe circles and those in the preceding equation to critical midpoint circles.

The influence of the depth factor n_D on the stability factor N_s is determined by the curves marked $n_D = 1$, 1.2, etc., in Figure 45*a*. These curves have been plotted on the basis of the results of theoretical investigations by Taylor (1937). It is obvious that the influence of the depth factor on the stability conditions is limited to slopes which rise at an angle β of less than 60°, because it has been shown above that

steeper slopes fail only along critical toe circles. If $\beta > 60°$, the entire surface of sliding is located above the level of the toe and the corresponding stability factors are given by the ordinates of the curve aA in Figure 45*a*. The danger of a base failure does not exist for such slopes.

For slope angles ranging between 53° and 60°, represented by the abscissas of the points C and A respectively, there is also no danger of a base failure. However, if the depth factor n_D is very small, the critical toe circle intersects the firm stratum, which prevents a failure along this circle. Thus if $n_D = 1$ the failure occurs along a circle which intersects the slope. The corresponding values of the stability factor N_s are represented in Figure 45*a* by the ordinates of the dash-dotted line marked $n_D = 1$ which starts at point C.

If the slope angle β is smaller than 53° (abscissa of point A in Fig. 45*a*), three different possibilities must be considered independently, viz., (*a*) the depth factor n_D is greater than about 4.0, (*b*) n_D is intermediate between about 1.2 and 4.0, and (*c*) n_D is smaller than about 1.2.

(*a*) If n_D is greater than about 4.0 the stability factor N_s is practically independent of the slope angle unless the slope angle β is smaller than about 15°. For every value of β in excess of about 15°, N_s is equal to or slightly greater than 5.52, as indicated by the horizontal line Ad in Figure 45*a*. The slope fails along a midpoint circle tangent to the firm stratum.

(*b*) If n_D has a value between about 1.2 and 4.0, the curve which represents the relation between β and N_s can be obtained by interpolation between the curves marked $n_D = 1.2$, 2.0, and 4.0. Each one of these curves branches off from the plain curve AB at a point with an abscissa β_1. If the slope angle is greater than β_1, the failure occurs along a critical toe circle. For such values the stability factor is given by the ordinates of aAB. If the slope angle is smaller than β_1, N_s is determined by the ordinates of an n_D-curve. Each one of these curves, for instance the curve $n_D = 1.5$, starts almost horizontal and becomes steeper toward the right. Every point located beneath the shaded area represents failure along a midpoint circle. Every point located within the shaded area corresponds to a toe circle, and every point located above it to a slope circle. In either instance the circle is tangent to the surface of the firm stratum.

(*c*) If n_D is smaller than about 1.2, the failure occurs either along a toe or a slope circle tangent to the firm base. The curve which represents the relation between β and the stability factor N_s can be determined by interpolation between the two curves marked $n_D = 1$ and $n_D = 1.2$. Every point of such a curve located within the shaded area

represents a failure along a toe circle. Points located above this area represent failures along slope circles.

The critical midpoint circles intersect the lower horizontal surface of the ground at a distance $n_x H$ from the toe of the slope. Since the centers of the circles are located on a vertical line through the midpoint of the slope, and since the circles are tangent to the firm base, the value n_x determines the position of the circles with respect to the slope. It can be estimated by means of the diagram, Figure 45c. In this diagram the abscissas represent the slope angle and the ordinates the depth factor. Every point located above the curve $A'B'e'$ represents a critical midpoint circle tangent to a firm stratum with the depth factor n_D. For any given value of β and n_D the corresponding value of n_x can be estimated by interpolation between the curves marked $n_x = 0$ to 3.

In order to visualize the influence of the depth factor n_D on the type of failure and on the stability factor we examine the different possibilities for the failure of a slope with a slope angle $\beta = 20°$. By interpolation we find that the points with an abscissa $\beta = 20°$ of the two boundaries of the shaded area in Figure 45a are located on N_s curves corresponding to values of $n_D = 1.40$ and 1.18 respectively. For values of n_D between ∞ and 1.4 the stability factor increases from 5.52 for $n_D = \infty$ to 7.0 for $n_D = 1.4$ and the slope fails along a midpoint circle. For values of $n_D = 1.4$ to 1.18 the slope fails along a toe circle tangent to the surface of the firm bottom stratum, and the value of N_s increases from 7.0 to 7.9. For values between 1.18 and 1.0 the slope fails along a circle which intersects the slope and the value of N_s increases from 7.9 for $n_D = 1.18$ to 9.4 for $n_D = 1.0$.

59. Stability computations if $\phi = 0$. The following problems are likely to be encountered in practice: (*a*) the cohesion of a bed of soft clay is known and we want to determine the slope which should be given to the sides of a cut with a given depth; (*b*) a slide has occurred and we want to determine the average value of the cohesion of the clay prior to the slide; and (*c*) we want to determine the factor of safety of an existing slope on clay with a known but variable cohesion.

The first problem can be solved rapidly by means of the data contained in the diagram in Figure 45a. To illustrate the procedure, let us assume that we intend to make a cut with a depth of 20 feet in soft clay. The shearing resistance of the clay is $c = 500$ pounds per square foot and the unit weight is 120 pounds per cubic foot. The slope angle of the sides of the cut should be so selected that the factor of safety with respect to sliding is equal to 1.5. In order to satisfy the safety requirement the critical cohesion value should not be greater than

$$c_c = \frac{500}{1.5} = 333 \text{ lb/sq ft}$$

Substituting $H = 20$ feet, $\gamma = 120$ pounds per cubic foot and $c_c = 333$ pounds per square foot in equation 58(3) we obtain

$$c_c = 333 = \frac{\gamma H}{N_s} = \frac{120 \cdot 20}{N_s}$$

or

$$N_s = 7.18$$

This value is greater than the ordinate of point A in Figure 45*a*. Therefore the admissible slope angle depends on the depth factor. If the firm base of the bed of clay is located at the level of the bottom of the cut, the depth factor n_D equation 58(5) is equal to unity. A value of $N_s = 7.18$ corresponds on the N_s curve for $n_D = 1$ to an abscissa of $\beta = 33°$. Since the point representing $N_s = 7.18$ is located above the shaded area the critical circle intersects the slope. On the other hand, if the clay rests at a depth of 10 feet below the bottom of the cut on a stratum of hardpan, the depth factor is $n_D = 1.5$. For $N_s = 7.18$ we obtain from the N_s curve marked $n_D = 1.5$ the value $\beta = 17°30'$. The corresponding point on the curve is located a very short distance below the lower boundary of the shaded area. Therefore the critical circle is a midpoint circle which intersects the bottom of the cut in the immediate vicinity of the toe of the slope. It touches the solid base at a point located on a vertical line through the midpoint of the slope.

The preceding example demonstrates the decisive influence of the depth factor n_D on the safe value of β, if $\phi = 0$ and $N_s > 5.5$.

The second problem is illustrated by Figure 46*a*, which is a section through a slide. The unit weight of the clay is γ and the shape of the surface of sliding *efd* has been determined by means of test pits. We also know from observations in the field the approximate depth D_c of the tension cracks which had developed prior to the slide. In order to determine the cohesion c_r which resisted the slide at the instant of failure we trace an arc of a circle e_1fd_1 following as closely as possible the real curve of sliding *efd*. The radius of the circle is r and its center is located at O. The cohesion c_r is assumed to have acted over the length l_a of the arc, between d_1 and point e_2 located at a depth D_c below the upper edge of the slope. The weight of the earth located above the arc e_2fd_1 is W per unit of length of the slope. Before the slide occurred the lever arm of the weight W with respect to the center of rotation O was l_w. The cohesion is determined by the equation

$$c_r = \frac{Wl_w}{rl_a} \qquad 58(1)$$

The third problem deals with failure by sliding if the slope is uneven and the earth located beneath the slope is nonhomogeneous. Figure 46*b* illustrates the procedure. It represents a vertical section through an uneven slope on soft clay. The mechanical properties of the clay have

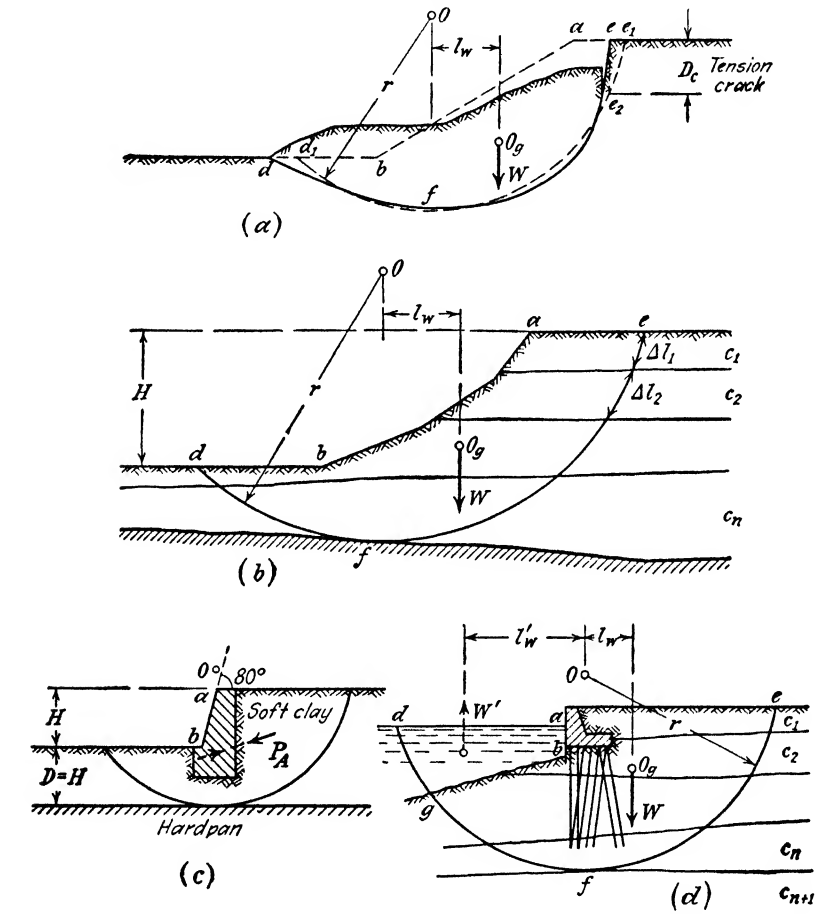

FIG. 46. (*a*) Replacement of real curve of sliding (solid line) by a circular one; (*b* to *d*) base failure in clay for which $\phi = 0$: (*b*) beneath slope on stratified, cohesive soil; (*c*) beneath retaining wall; and (*d*) beneath quay wall on pile foundation.

been investigated by means of laboratory tests on undisturbed samples. On the basis of the results of the tests we subdivide the bed of clay into several strata with an average cohesion $c_1, c_2, \cdots, c_n$. Then we trace an arc of a circle *efd* in such a manner that the sections of the arc located within the softest strata are as long as possible. The center of the circle is *O*, the center of gravity of the clay located above the arc is

O_0 and the weight of the body *aefd* is W per unit of length of the slope. The driving moment Wl_w is resisted by the moment M_c of the cohesion

$$M_c = r\sum_1^n c_n \Delta l_n$$

wherein Δl_n is the length of that part of the arc which is located within a stratum with the cohesion c_n. The factor of safety of the slope with respect to sliding along the arc *efd* is

$$G_s = \frac{M_c}{Wl_w} = \frac{r\sum_1^n c_n \Delta l_n}{Wl_w} \qquad [1]$$

This investigation must be repeated for different circles. The factor of safety of the slope is equal to the smallest value of G_s thus obtained. The procedure is entirely one of trial and error.

The preceding method of investigating the stability of slopes can also be used if a bank is supported by a structure such as a retaining wall. Figure 46c is a section through a retaining wall with a height H, supporting a vertical bank of soft homogeneous clay. The clay rests at a depth $D = H$ on a hard stratum. Hence the depth factor n_D is 2. If the retaining wall is strong enough to withstand the lateral earth pressure P_A without tilting or sliding, there is no danger of a slope failure. Hence only the possibility of a base failure needs to be considered. For the purpose of a rough estimate the difference between the unit weight of the concrete and that of the clay can be disregarded. If the two unit weights are equal, the stability conditions of the retaining wall are identical with those for an unsupported slope *ab* with respect to a base failure beneath such a slope. Since the depth factor n_D is equal to 2.0, the stability factors for failures along midpoint circles are determined by the curve $n_D = 2$ in Figure 45*a*. If we continue this curve toward the left until it intersects the left-hand boundary of the diagram (not shown in the figure) we find that the stability factor for a slope angle $\beta = 80°$ is equal to 5.60. For the corresponding critical height H_c of such a slope we obtain from equation 58(4)

$$H_c = \frac{c}{\gamma} N_s = 5.6 \frac{c}{\gamma}$$

If the retaining wall is higher than H_c the base of the wall fails along a midpoint circle tangent to the surface of the firm stratum, as shown in the figure, though the wall may be strong enough to prevent a slope failure. The movement of rotation about O involves both the wall and the adjoining mass of clay.

In order to get a more accurate value for the critical height H_c of the wall the excess of the weight of the wall over that of a body of clay with equal dimensions must be taken into account. The excess weight alters the position of the center of the critical circle and it reduces to some extent the value of the stability factor N_s. The problem of determining the corrected value of N_s can be solved by trial and error.

Figure 46*d* is a section through a quay wall on a pile foundation. On account of the shearing strength of the piles the potential surface of sliding *efd* clears the piles. The free water located on the left-hand side of the wall represents a stratum whose unit weight is equal to γ_w and whose cohesion is equal to zero. The cohesion of the other strata is c_1, c_2, etc. The weight W represents the weight of everything located above *efd*, including that of the wall and the water, per unit length of the wall. The factor of safety with respect to sliding is determined by equation 1. The location of the critical circle can be ascertained by trial and error, as described before in connection with Figure 46*b*. The earth pressure which acts on the structures shown in Figures 46*c* and 46*d* does not enter into the computations, because it represents an internal force. The only forces which need to be taken into consideration are the mass forces represented by the weight W and whatever external forces may act on the soil located above the surface of sliding.

If one of the strata shown in Figures 46*b* and 46*d* is very much softer than the others, the surface of sliding may not be even approximately circular. In this case we have to operate with composite surfaces of sliding as explained in Article 63.

As a last example we examine the effect of a draw-down of the water level in a lake or in a reservoir on the stability of the confining banks or slopes. The method of computation will be explained by means of the section shown in Figure 46*d*. In this section, W represents the total weight of the soil and the water located above the surface of sliding *efd*, per unit of length of the quay wall. The overturning moment is Wl_w and the factor of safety against sliding is determined by equation 1,

$$G_s = \frac{r\sum_1^n c_n \Delta l_n}{Wl_w}$$

When the water level is lowered to a level below that of point g in Figure 46*d*, the total weight W of the mass of soil and water located above the surface of sliding *egd* is reduced by the weight W' of the body of water *abgd*. The force W' acts at a distance l'_w from the center of rotation O. Hence the lowering of the water level increases the overturning moment from Wl_w to $Wl_w + W'l'_w$. The moment produced

by the cohesion forces, represented by the numerator on the right-hand side of the equation remains unchanged. Hence, if one disregards the influence of the draw-down on the position of the critical circle, one obtains for the factor of safety after the draw-down

$$G'_s = \frac{r\sum_1^n c_n \Delta l_n}{Wl_w + W'l'_w} \qquad [2]$$

If greater accuracy is required, it is necessary to determine independently the position of the critical circle after draw-down by trial and error, as described in the preceding paragraphs.

60. Stability factor and critical circle if $\phi > 0$. If the angle of shearing resistance ϕ is greater than zero, the shearing resistance of the soil is determined by Coulomb's equation

$$s = c + \sigma \tan \phi$$

According to Article 56 a slide may be caused by either a slope or a base failure. Slope failures occur along a critical toe circle. In Figure 44*a*, *be* represents an arc of an arbitrary toe circle. Retaining the symbols which have been used in Article 58 in connection with Figure 44*a*, we find, on the basis of the geometrical data shown in the figure, that the cohesion required to prevent a slip along *be* is

$$c_r = \gamma H \frac{1}{F(\alpha, \beta, \theta, \phi)} \qquad [1]$$

This equation is identical with equation 58(2*a*), except inasmuch as the function in the denominator contains the angle of shearing resistance ϕ. The position of the critical toe circle is determined by the condition

$$\frac{\partial c_r}{\partial \alpha} = 0 \quad \text{and} \quad \frac{\partial c_r}{\partial \theta} = 0$$

Solving these equations one gets for the cohesion $c_r = c_c$ required to prevent a slip along the critical toe circle.

$$c_c = \frac{\gamma H}{F(\alpha, \beta, \theta, \phi)} = \frac{\gamma H}{N_s} \qquad [2]$$

This equation is an analogue to equation 58(3). However, the stability factor N_s contained in equation 2 depends not only on the slope angle but also on the angle ϕ. Figure 45*a* shows the relation between the slope angle β and the stability factor N_s for $\phi = 4°$, 5°, 10°, 15° 20°, and 25° (Fellenius 1927). If the cohesion and the slope angle are

given, we replace c_e in equation 2 by c and H by the critical height H_c and obtain

$$H_c = \frac{c}{\gamma} N_s \qquad [3]$$

All the points located on the right-hand side of the dotted curve CC_{15} correspond to toe circles whose deepest point is located beneath the level of the toe. The relation between the slope angle and the corresponding depth factor n_D for the deepest point of the critical toe circle is shown by the plain curves marked $\phi = 5°$ and $\phi = 10°$ in Figure 45c. If the critical toe circle intersects the surface of a firm stratum, i.e., if the depth factor for the critical toe circle is greater than the depth factor n_D for the surface of the firm stratum on which the earth rests, the slide occurs along a circle tangent to the surface of this stratum. The smallest value which n_D can assume is unity. For $n_D = 1$ and $\phi = 5°$ the stability factors are represented by a dash-dotted curve, labeled $n_D = 1$, through point C_5. The difference between the ordinates of this limiting curve and the plain curve labeled $\phi = 5°$ is insignificant. With increasing values of ϕ this difference decreases. Therefore one is justified in disregarding the influence of the depth factor on the stability factor for values of ϕ in excess of a few degrees.

At a given value of the slope angle β, the stability factor N_s increases with increasing values of ϕ. If $N_{s\phi}$ is the value of N_s for given values of β and ϕ and N_{s0} is the corresponding value for $\phi = 0°$ on the curve $aABb$, the ratio

$$n_\phi = \frac{N_{s\phi}}{N_{s0}} \qquad [4]$$

represents the *friction index*. Its value indicates the influence of the frictional resistance on the critical height at given values of β, c, and ϕ. If H_{c0} is the critical height for $\phi = 0$, the critical height $H_{c\phi}$ for a given value ϕ is

$$H_{c\phi} = n_\phi H_{c0} \qquad [5]$$

If $\beta = \phi$, the friction index n_ϕ is equal to infinity. The cohesion required to prevent a slip along a toe circle through the toe of a slope with height H is

$$c_{c\phi} = \frac{\gamma H}{N_{s\phi}}$$

For $\phi = 0$ the value $c_{c\phi}$ becomes equal to c_{c0} and the value $N_{s\phi}$ equal to N_{s0}, whence

$$c_{c0} = \frac{\gamma H}{N_{s0}}$$

Since $N_{s\phi} = n_\phi N_{s0}$ we get

$$c_{c\phi} = \frac{N_{s\phi}}{\gamma H} \frac{1}{n_\phi} = \frac{1}{n_\phi} c_{c0} \qquad [6]$$

The influence of ϕ on the values of n_ϕ and on the location of the critical circle has been investigated by Fellenius (1927). Figure 47*a* shows the relation between ϕ and $1/n_\phi$ for different slope angles β. Figure 47*b*

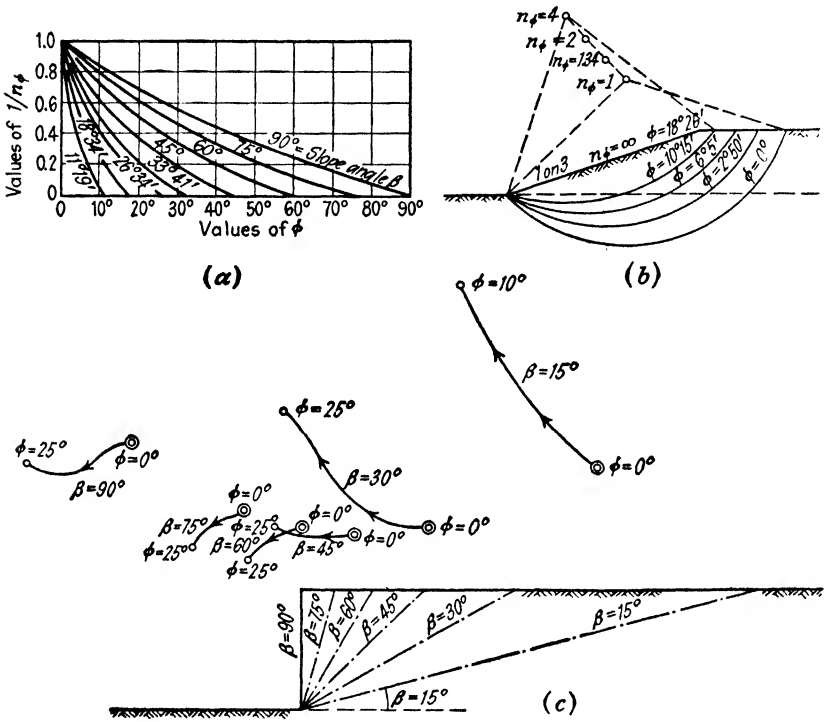

FIG. 47. (*a*) Relation between angle of internal friction ϕ and reciprocal value of friction index n_ϕ; (*b*) location of center of critical toe circle and corresponding value of n_ϕ for different values of ϕ at given slope angle; (*c*) influence of value of ϕ on position of center of critical toe circle for different values of slope angle β. (*Diagrams* a *and* b *after Fellenius 1927, and* c *after D. W. Taylor 1937.*)

illustrates the influence of n_ϕ on the position of the center of the critical toe circle for $\beta = 18°26'$ (slope 1:3). With increasing values of n_ϕ the volume of the earth located between the slope and the surface of sliding decreases and for $n_\phi = \infty$ it becomes equal to zero. Figure 47*c* shows the influence of the angle of shearing resistance on the position of the center of the critical toe circle for different values of the slope angle β, according to Taylor (1937).

The base failure of an inclined slope occurs along a midpoint circle. The center of the critical midpoint circle is always so located that the friction circle is tangent to a vertical line through the midpoint m of the

slope as shown in Figure 48. This statement can be verified by reasoning analogous to that set forth in Article 58 and illustrated by Figure 44c. The principle of the friction circle has been explained in Article 40.

If we compute the cohesion c_c required to prevent a slip along a critical midpoint circle, we arrive at an equation

$$c_c = \frac{\gamma H}{N_s}$$

which is similar to equation 2, and for the critical height H_c we obtain

$$H_c = \frac{c}{\gamma} N_s$$

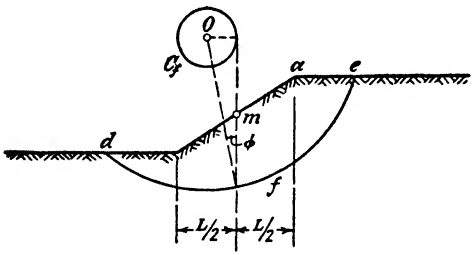

FIG. 48. Critical circle for base failure if $\phi > 0$. (*After Fellenius 1927.*)

which is similar to equation 3. The value of the stability factor N_s depends on ϕ and on the depth factor n_D. By computing the values of N_s for different values of ϕ, β, and n_D it was found that there is no danger of a base failure beneath an unsupported slope unless the angle of shearing resistance ϕ is smaller than about 5° and the slope angle is smaller than about 10°.

If the stability conditions for a given slope are represented by a point located on the right-hand side of the dotted line aA_{10} in Figure 45*a* the critical circle is likely to be a midpoint circle. Yet for any value of ϕ greater than about 5° this midpoint circle is almost identical with the critical toe circle. The corresponding stability factor for $\phi = 5°$ is represented by the ordinates of the dash-dotted curve through A_5 in Figure 45*a*. This curve is so close to the plain curve for $\phi = 5°$ that the difference can be disregarded. For greater values of ϕ it is still more insignificant.

If $\phi > 0$ typical base failures occur only beneath structures such as retaining walls on pile foundations or quay walls similar to that shown in Figure 46*d*, whose foundation excludes the possibility of a failure at a shallow depth. The essential condition of the occurrence of a typical base failure is a very low value of the angle of shearing resistance ϕ. On account of the rule illustrated by Figure 48, the center of the critical midpoint circle moves with increasing values of ϕ away from the slope. In addition it has been found that it moves with increasing values of ϕ slightly downward. For any value of ϕ the center angle 2θ ranges between about 100° and 135°.

61. Stability computations if $\phi > 0$. The following problems may be encountered in practice: (*a*) We want to determine the slope which can be given to the sides of a cut in fairly homogeneous soil with known values of c and ϕ; (*b*) we want to determine the factor of safety

of a given slope in nonhomogeneous soil; and (*c*) we inquire about the factor of safety of a retaining wall or a quay wall with respect to a base failure.

As an example of the problems in the first category we modify the problem which was solved at the beginning of Article 59 by assuming that the angle of shearing resistance ϕ is equal to 6° instead of 0°. The depth of the cut is assumed to be 20 feet, the cohesion $c = 500$ pounds per square foot, the unit weight $\gamma = 120$ pounds per cubic foot, and the factor of safety with respect to sliding $G_s = 1.5$. In order to satisfy the safety requirement we replace the available cohesion c by

$$c_c = \frac{c}{G_s} = 333 \text{ lb/sq ft}$$

and the available coefficient of shearing resistance tan ϕ by

$$\tan \phi_c = \frac{1}{G_s} \tan \phi = \frac{1}{1.5} \cdot 0.105 = 0.070$$

or $\phi_c = 4°$. Substituting the values $H = 20$ feet, $\gamma = 120$ pounds per cubic foot and $c_c = 333$ pounds per square foot in equation 60(2) and solving for N_s we obtain

$$N_s = 7.18$$

This value corresponds on the curve marked $\phi = 4°$ in Figure 45*a* to a slope angle $\beta = 42°$. For slopes as steep as 42° the danger of a base failure does not exist, and if the earth rests at a very shallow depth below the foot of the slope on a firm stratum, the safety requirement is satisfied even for a slightly steeper slope. Hence if the sides of the cut are made at an angle 42° to the horizontal, the safety requirement is satisfied regardless of the value of the depth factor n_D. On the other hand, if $\phi = 0$ (Art. 59) the admissible slope angle ranges between 33° for $n_D = 1$ and 17°30′ for $n_D = 1.5$. This example illustrates the decisive influence even of a small angle of shearing resistance on stability. This influence is chiefly due to the fact that the angle of shearing resistance required to eliminate the danger of a base failure beneath slopes with a slope angle of more than about 20° is extremely small. A slight increase of the cohesion with depth has a similar effect. Hence, if we experience a base failure in a cut in soft clay we know that the cohesion did not materially increase with depth and that the angle of shearing resistance did not exceed a few degrees.

Figure 49*a* is a section through an uneven slope on a sandy clay whose cohesion varies with depth. The average value of the angle of shearing resistance is ϕ. If ϕ is greater than about 5° the critical

circle passes through the toe of the slope, unless there is an exceptionally soft layer located beneath the level of the bottom of the cut. However, this possibility will not be considered. In order to estimate the factor of safety of this slope with respect to sliding we trace through the toe of the slope an arc of a circle *bde* in such a manner that the

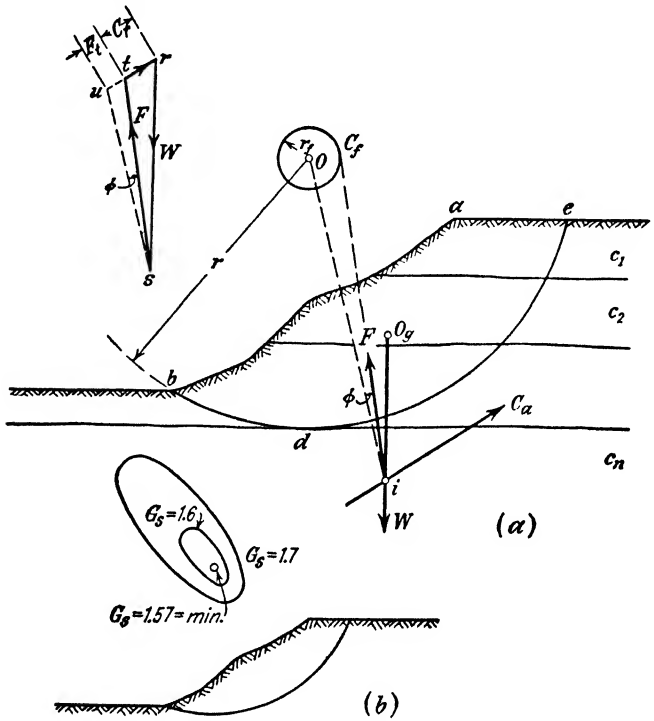

FIG. 49. (*a*) Forces which act on soil above arbitrary cylindrical section through stratified cohesive soil beneath slope; (*b*) graphic method for locating position of critical circle.

sections of the arc located within the softest strata are as long as possible. Then we determine, for instance, by means of a polygon of forces (not shown in the figure) the resultant C_a of the cohesion which acts along the circle. This is the available cohesion. The weight W of the body of earth located above the tentative surface of sliding *bde* acts along a vertical line through the center of gravity O_g of the area *bdea*. Equilibrium requires that the resultant F of the normal stresses and of the shearing stresses due to friction on the surface of sliding *bde* passes through the point of intersection i between W and C_a. If the resultant force F is tangent to the friction circle, the slope is on the verge of failure by shear along the tentative surface of sliding *bde* (see Art. 40).

Hence we obtain the direction of F for the failure state by tracing through i a tangent to the friction circle, which deviates from the vector Oi in a sense opposite to that of the direction of the potential sliding motion. By tracing the polygon of forces (Fig. 49*a*) we obtain the cohesion C_r which would be required to prevent a slide. By tracing su parallel to Oi we obtain the component F_t of the frictional resistances in the direction of the cohesion force C_a. The factor of safety with respect to sliding along the tentative surface of sliding *bde* is approximately

$$G_s = \frac{F_t + C_a}{F_t + C_r} \qquad [1]$$

This investigation must be repeated for different circles. If we assign to the center of each one of these circles the corresponding value of the safety factor G_s we can trace a set of curves of equal G_s values, as shown in Figure 49*b*. The center of the critical circle is located at the point which corresponds to a minimum of G_s.

If a vertical face is supported by a retaining wall on piles or by a quay wall on a pile foundation shown in Figure 46*d*, the danger of a base failure is very remote unless the angle of shearing resistance of the strata located beneath the foundation is smaller than about 5°. The factor of safety with respect to a base failure can be estimated by means of the friction circle method described in the preceding paragraphs. The same method has been used to determine the angle of shearing resistance from the known position of a surface of sliding along which a slide has already occurred (Fellenius 1927). However, one cannot learn from the results of such an investigation whether the deviation of the surface of sliding from the position corresponding to $\phi = 0$ was due to a value of $\phi > 0$ or due to a slight increase of cohesion with depth.

62. Correction for tension cracks. The depth of a tension crack cannot be greater than the critical height for an intact vertical bank

$$H_c = 4\frac{c}{\gamma}\sqrt{N_\phi} \qquad 57(1)$$

wherein $N_\phi = \tan^2(45° + \phi/2)$. There are, however, other limitations to the depth of tension cracks. These are illustrated by Figure 50. The arc *bde* represents a critical toe circle and the arc *ghi* a critical midpoint circle. Under normal conditions the state of stress behind a slope does not favor the formation of tension cracks with a depth in excess of $H/2$. Furthermore, the distance between the tension cracks and the upper edge a of the slope is seldom smaller than one-half of the distance between this edge and the upper end e of the critical circle. Hence the depth of tension cracks is not likely to be greater than D_c

(Fig. 50) for toe circles and $H/2$ for midpoint circles, regardless of the values of the theoretical maximum H_c (eq. 57(1)).

The effect of a tension crack (e_1f in Figure 50) on the stability of a slope is threefold. First of all the crack eliminates the resistance due to the co-

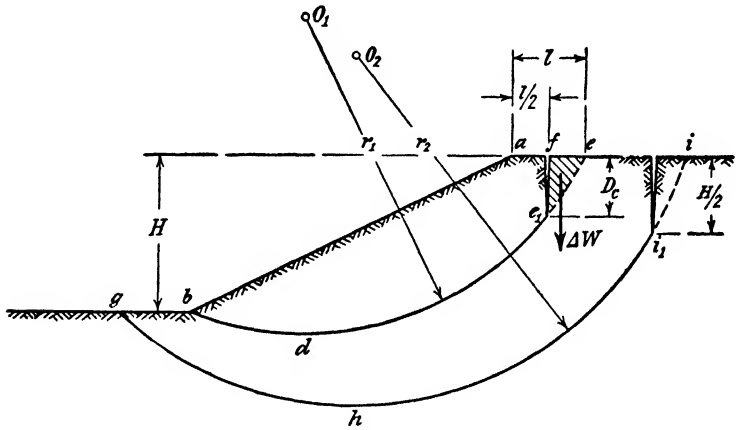

FIG. 50. Influence of tension cracks on stability of slope.

hesion along the arc e_1e. Hence, if c is the available cohesion per unit of area, the crack reduces the total cohesion per unit of length of the slope from $c \times \widehat{be}$ to $c \times \widehat{be_1}$. In order to produce the same effect, we can reduce the cohesion on $\widehat{be}$ from c to

$$c_a = c \frac{\widehat{be_1}}{\widehat{be}} \qquad [1]$$

without reducing the length of the arc. The second effect of the tension crack is to reduce the driving moment (weight of the mass of earth located above the surface of sliding $\times$ the lever arm with respect to the center of rotation) by the moment produced by the weight ΔW of the body efe_1 about O_1. The third effect is due to the hydrostatic pressure exerted by the surface water which accumulates in the cracks. This pressure increases the driving moment. However, computations have shown that the two last named effects practically compensate each other. Hence, if we replace the available cohesion c by the corrected cohesion, c_a (eq. 1), we can investigate the stability of the slope as if there were no cracks.

Applying the method of correction to a vertical slope on the assumption that the surface of sliding is plane, we find that the corrected cohesion c_a (eq. 1) is equal to one half of the available cohesion c. Replacing

c in equation 57 (2a) by $c_a = c/2$, we get

$$H_c = 4\frac{c_a}{\gamma} = 2\frac{c}{\gamma} \qquad [2]$$

This equation takes the effect of an accumulation of surface water in the cracks into consideration. On the assumption that the cracks are not filled with surface water, we obtained

$$H_c' = 2.67\frac{c}{\gamma} \qquad 57(5)$$

63. Composite surfaces of sliding. If the base of a slope contains layers of clay which are very much softer than the other strata, the surface of sliding is likely to consist of several sections joining each other at obtuse angles. In such a case no continuous curve can be substituted for the entire surface of sliding without the risk of a grave error on the unsafe side. Furthermore no slide along a broken surface is conceivable without plastic flow within at least one section of the sliding mass, because the movement along a broken surface involves a radical deformation of the superimposed material. On account of these complications the problem of estimating the degree of stability of the fill cannot be solved without taking into consideration the forces which act in the interior of the mass of soil located above the potential surface of sliding. These forces are indicated in Figure 51 which represents a section through a sand dam with a clay core prior to filling the reservoir. The dam rests on a sand stratum which contains a thin bed of clay.

Even symmetrical dams slide toward one side only and the orientation of the slide with reference to the plane of symmetry depends on accidental factors. If the dam shown in Figure 51 fails, the slip will occur along a composite surface of sliding such as *abde*. In the right-hand part of the sliding mass, corresponding to the area d_1de, active failure is to be expected because within this part the earth is merely under the influence of its own weight. The central part b_1bdd_1 of the sliding mass will move under the influence of the active pressure on dd_1 along a surface of least resistance bd toward the left. On the left side of the toe of the dam, passive failure will occur within the thin layer of sand above the clay owing to the lateral thrust exerted by the advancing central part b_1bdd_1.

In order to investigate the conditions for the stability of the dam shown in Figure 51 we first determine the passive earth pressure P_P on several tentatively selected vertical sections in the vicinity of the left toe of the dam, such as the section bb_1. It is admissible to assume that

the pressure P_P acts in a horizontal direction, because the error due to this assumption is on the safe side. The central part b_1bdd_1 of the sliding mass cannot possibly advance toward the left unless it exerts on the vertical section bb_1 a horizontal pressure equal to or greater than the passive earth pressure P_P. Then we make a vertical section dd_1 through an arbitrarily selected point d on the left side of the clay core. The

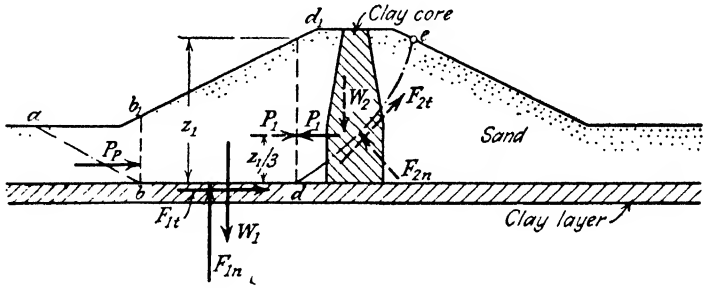

FIG. 51. Failure of fill along composite surface of sliding.

total resistance P_1 to a horizontal displacement of the body of soil bb_1d_1d with a weight W_1 is equal to the sum of P_P, the cohesion $c\,\overline{bd}$, and the frictional resistance F_{1t} against sliding along the base bd, or

$$P_1 = P_P + F_{1t} + c\,\overline{bd}$$

If the dam is on the verge of failure this resistance must be equal to or smaller than the active earth pressure exerted by the mass of earth located on the right-hand side of the section dd_1. Since the wedge d_1de can expand in a horizontal direction over its full height the distribution of the active earth pressure exerted by this wedge is hydrostatic. Therefore the point of application of the active earth pressure is located at an elevation $z_1/3$ above the surface of the clay. The shearing stresses along dd_1 can be neglected, because they increase the stability of the dam. The intensity of the active earth pressure on dd_1 can be determined by trial and error on the assumption that the surface of sliding, de, through d is an arc of a circle. The investigation must be repeated for different positions of point d (Fig. 51). The real surface of sliding satisfies the condition that the corresponding factor of safety G_s be a minimum.

64. Failure of fills by spreading. If the layer of soft clay shown in Figure 51 is located immediately beneath the base of the fill, the failure of the fill is likely to assume the character of a flow, whereby the fill spreads out laterally regardless of what the coefficient of internal friction of the fill material may be. The failure by spreading may either be

limited to the vicinity of the toes or else it may occur over the entire width of the base of the fill.

In order to determine the factor of safety of a fill with respect to a partial or a total failure by spreading it is necessary to investigate the intensity and the distribution of the shearing stresses on the base of the fill. These stresses depend to a certain degree on the state of stress in the fill. The following investigation is based on the assumption that the entire fill is on the verge of a complete failure by spreading. The shearing stresses obtained on the basis of this assumption represent the smallest stresses which are compatible with the conditions for the equilibrium of the fill.

65. Shearing stresses at the base of cohesionless fills. Rendulic (1938) has presented a simple method of determining the shearing stresses along the base of a cohesionless fill which is on the verge of active failure at every point. The shearing resistance along any section through the fill is assumed to be given by the equation

$$s = \sigma \tan \phi \qquad [1]$$

and the error due to assuming plane surfaces of sliding will be disregarded. Hence the earth pressure which acts in the fill can be determined by means of Coulomb's earth pressure theory.

Figure 52*a* shows a profile of the fill. The pressure on a vertical section *ab* produced by the fill material located on the right side of this section must be equal and opposite to the pressure exerted by the fill on the left side. This condition determines the angle δ between the resultant pressure on *ab* and its normal component. Since the angle δ is unknown it is advisable to use Engesser's graphical procedure (Art. 25) for determining the earth pressure on *ab*. According to this procedure, illustrated by Figure 21, plane sections are made through the foot *b* of the vertical section *ab* in Figure 52*a*, at different angles to the horizontal. The weights of the wedges located between *ab* and these sections are plotted on a vertical line (Fig. 52*b*) from point *r* in a downward direction. Thus for instance W_r (Fig. 52*b*) represents the weight of the wedge aba_r in Figure 52*a*, located on the right-hand side of *ab*. The slope of the base ba_r of this wedge has been arbitrarily selected. The wedge, with a weight W_r, is acted upon by the reaction F_r and by the earth pressure P_A. The reaction F_r acts at an angle ϕ to the normal on the inclined surface $a_r b$. F_r in Figure 52*b* has been traced through point *t* in Figure 52*b* parallel to F_r in Figure 52*a*. By repeating the same construction for wedges whose inclined base rises at different angles to the horizontal on the right-hand side of *ab* in

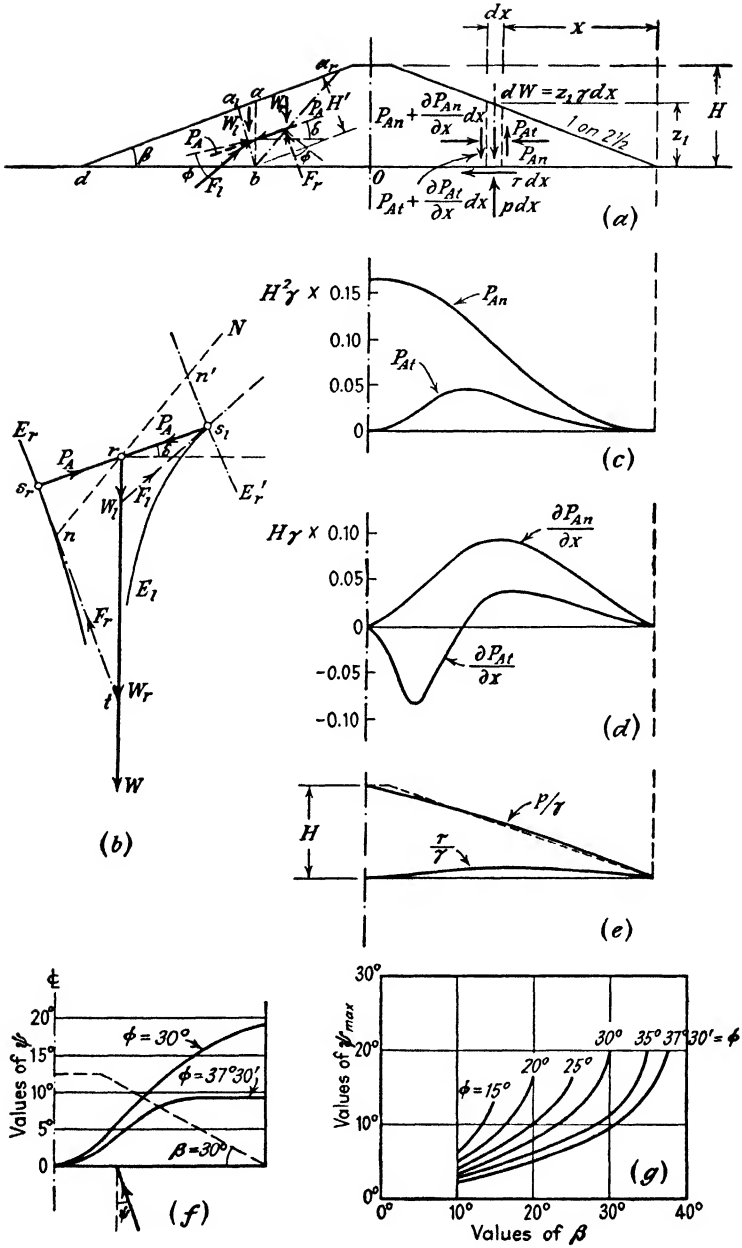

FIG. 52. (*a* and *b*) Diagrams illustrating method of computing shearing stresses at base of sand fill shown in (*a*); (*c* to *e*) results of the computation; (*f*) increase of angle ψ between resultant stress on base of sand fill and the vertical direction with increasing distance from center line of fill; (*g*) relation between ψ_{max} (ψ at toes of fill) and slope angle β for different values of ϕ. (*After L. Rendulic 1938.*)

Figure 52*a* and by tracing the envelope to the corresponding lines F in Figure 52*b* we obtain the Engesser curve E_r for the earth located on the right-hand side of ab in Figure 52*a*. By means of a similar procedure we construct in Figure 52*b* the Engesser curve E_l for the earth located on the left-hand side of ab in Figure 52*a*. According to the theory of Engesser's method (Art. 25) the earth pressure exerted on ab by the earth located on the right-hand side of ab is represented by the distance between point r and the curve E_r in Figure 52*b* measured from r in the direction of the earth pressure. In a similar manner the Engesser curve E_l determines the intensity of the pressure exerted by the earth located on the left-hand side of ab. Equilibrium requires that the pressure P_A exerted on ab by the soil located on the right-hand side of ab is equal and opposite to that exerted by the soil located on the left-hand side of ab. In order to satisfy this condition we construct in Figure 52*b* the auxiliary curve E'_r. This curve has been obtained by transferring each point n of the curve E_r along a vector such as nN through r to a distance $\overline{n'r} = \overline{nr}$ on the other side of point r. The auxiliary curve E'_r intersects the curve E_l at points s_l.

According to Article 25 and Figure 21*d* the distance rs_r in Figure 52*b* represents the active earth pressure exerted by the soil on the right side of the fill and the distance rs_l the corresponding pressure acting from the left side. Since $\overline{rs_r} = \overline{rs_l}$ these two pressures are equal and act in opposite directions.

The intensity of the pressure can be obtained by substituting $\overline{rs_r}$ for $\overline{be}$ in equation 25 (1), whereupon we obtain

$$P_A = \tfrac{1}{2}\gamma H' \overline{rs_r}$$

The line of action of P_A in Figure 52*a* is parallel to $s_r s_l$ in Figure 52*b*. The earth pressure P_A on the vertical section ab can be resolved into a normal component

$$P_{An} = P_A \cos \delta$$

and a tangential component

$$P_{At} = P_A \sin \delta$$

In Figure 52*c* the ordinates of the curve P_{An} represent the values of P_{An} for different vertical sections through the fill and the ordinates of the curve P_{At} represent the corresponding values of P_{At}. In order to determine the distribution of the shearing stresses over the base of the fill we investigate the conditions for the equilibrium of a vertical slice of the fill, shown on the right-hand side of Figure 52*a*. The weight of the

slice is $dW = z_1\gamma dx$. The external forces which act on the slice are indicated in the figure. The equilibrium of the horizontal components requires

$$\tau dx = \frac{\partial P_{An}}{\partial x}\,dx \quad \text{or} \quad \tau = \frac{\partial P_{An}}{\partial x}$$

and that of the vertical components

$$p dx = dW + \frac{\partial P_{At}}{\partial x}\,dx = \gamma z_1 dx + \frac{\partial P_{At}}{\partial x}\,dx$$

or

$$p = \gamma z_1 + \frac{\partial P_{At}}{\partial x}$$

The values $\frac{\partial P_{An}}{\partial x}$ and $\frac{\partial P_{At}}{\partial x}$ are represented in Figure 52*d*. They have been obtained graphically from the diagram, Figure 52*c*. By means of the data given in Figure 52*d* the preceding equations for p and τ can be evaluated.

In Figure 52*e* the plain lines show the distribution of the normal pressure and the shearing stresses over the base of the fill. The dashed line represents the distribution of the normal pressure on the base of the fill on the assumption that the shearing stresses on vertical sections are equal to zero. The figure shows that the normal pressure p per unit of area at any point of the base is almost directly proportional to the height of the fill above this point. The shearing stress is a maximum at some point located between the center line of the fill and the toe.

The angle ψ between the resultant stress on the base of the fill and the normal component of the stress is equal to zero at the center line, and it increases from the center line in both directions toward a maximum ψ_{max} at the toes. Figure 52*f* shows the increase of ψ from the center line toward the toe of a fill for two values of ϕ and Figure 52*g* represents the relations between the slope angle β of the sides of the fill, the angle of internal friction ϕ, and the angle ψ_{max}.

If no lateral displacement occurs along the base of a fill, the fill is not on the verge of active failure. As a consequence the lateral pressure on vertical sections and the corresponding shearing stresses on the base are likely to be considerably higher than the values obtained by means of the preceding analysis. In a fill which is not on the verge of active failure the hydrostatic pressure ratio K depends on the method of placing the fill and may be as high as 0.6. The hydrostatic pressure

ratio is determined by the equation

$$K = \tan^2\left(45° - \frac{\phi'}{2}\right) \qquad [2]$$

wherein ϕ' is the friction angle corresponding to the mobilized part of the internal friction of the fill. If K is between 0.40 and 0.60 the value of ϕ' ranges between 25° and 15°. In order to estimate the intensity of the shearing stresses at the base of a fill with a hydrostatic pressure ratio K we replace the value of ϕ in the preceding analysis by ϕ'.

If the shearing resistance along the base can be expressed by an equation

$$s = c + p \tan \phi_1$$

wherein $\phi_1 < \phi$, it may happen that the shearing resistance in the vicinity of the point at which $\tau = \tau_{max}$ (Fig. 52*e*) may be inadequate while the shearing resistance in the vicinity of the toe is excessive. Such a condition is incompatible with the assumptions on which the preceding analysis was based. It invalidates the conclusions regarding the distribution of the shearing stresses over the base of the fill, represented by Figures 52*e* to 52*g*. However, it is obvious that no failure by spreading can occur unless the active earth pressure on some vertical section through the fill is greater than the total shearing resistance along the base of the adjoining part of the fill. This condition can be used as a basis for investigating the case.

Chapter X

EARTH PRESSURE ON TEMPORARY SUPPORTS IN CUTS, TUNNELS, AND SHAFTS

66. General characteristics of shear failures behind timbered supports. The term *timbering* applies to temporary supports which are place against the face of an excavation prior to the construction of a permanent support. During the process of excavating and timbering, the area of the working face (unsupported part of the face) never exceeds a small fraction of the total area of the excavated face while the remainder is supported by relatively rigid structural members. In Chapter V it has been shown that this condition induces arching. The arching effect relieves the stresses in those parts of the mass of earth which have an opportunity to yield, and it increases the stresses in the earth adjoining the supports which tend to prevent yielding. The type of arching and its mechanical effects depend on the type of excavation and on the method of construction.

67. Earth pressure on timbering of cuts in ideal sand. The customary methods of timbering and excavating are such that the lateral yield of the soil on both sides of the cut increases from practically zero at the upper edge of the cut to a maximum at or slightly above the bottom of the cut, as shown in Figure 53*a*. Owing to the deformation condition which is imposed upon the sand by the method of construction, the surface of sliding (*bd* in Fig. 53*a*) is curved and intersects the surface of the sand approximately at right angles (see Art. 20 and Fig. 17*c*). The following computation of the lateral pressure of the sand on the timbering of a cut is based on the assumption that the lateral expansion of the sand in the lower part of the active wedge (*abd* in Fig. 53*a*) and the corresponding subsidence of the upper part is sufficient to mobilize the shearing resistance of the sand,

$$s = \sigma \tan \phi \qquad 5(2)$$

per unit of area over the entire potential surface of sliding *bd*. The point of application of the resultant pressure is located at an elevation $n_a H$ above the bottom of the cut and is assumed to act at an angle δ to the normal on the back of the support as indicated in the figure. As a result of arching, n_a is greater than one-third. Its value depends to

a certain extent on the method of construction. However, from theory as well as from experience, we know that it ranges for clean as well as for silty sand between the narrow limits of 0.45 and 0.55 provided the bottom of the cut is located above the water table (see Art. 20).

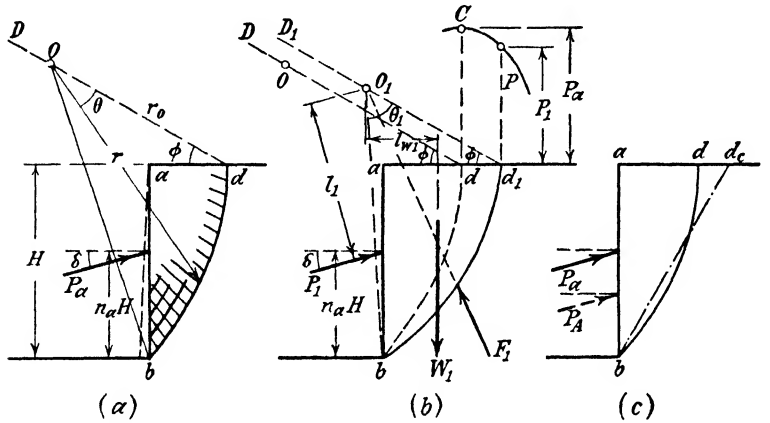

FIG. 53. (*a*) Failure by sliding in mass of sand due to yield of lateral support by tilting about upper edge; (*b*) determination of line of sliding by means of logarithmic spiral method; (*c*) the unbroken line represents surface of sliding if lateral support yields by tilting about *a* and the dash-dotted curve represents surface of sliding for retaining wall computed by means of Coulomb's theory.

A close approach to the real shape of the potential surface of sliding can be obtained by assuming that the trace of the surface on a vertical plane perpendicular to the axis of the cut is an arc of a logarithmic spiral, the equation of which is

$$r = r_0 \epsilon^{\theta \tan \phi} \qquad [1]$$

The center O of this spiral is located as shown in Figure 53*a* on a straight line dD which rises at an angle ϕ and passes through the upper rim, d, of the surface of sliding (Terzaghi 1941). In order to determine the location of point d we select arbitrarily a point d_1 on the horizontal surface in Figure 53*b* and trace, through this point and through the foot of the bank, b, a section of the spiral whose center O_1 is located on the line d_1D_1. The wedge abd_1 with a weight W_1 is acted upon by the reaction P_1 of the lateral support ab and by the reaction F_1 along the surface of sliding bd_1. The sum of the moments about the center O_1 of the spiral must be equal to zero. The reaction F_1 passes through O_1 (see Art. 39). Therefore the force P_1 is determined by the equation

$$P_1 = \frac{W_1 l_{w_1}}{l_1} \qquad [2]$$

In order to solve this equation some assumption must be made regarding the value n_a in Figure 53*b* because it determines the distance l_1. With increasing values of n_a the distance l_1 decreases and the value P_1 (eq. 2) increases. At the beginning of this article it has been stated that the value n_a for clean and for silty sands ranges between 0.45 and 0.55. Hence if for such soils it is assumed that $n_a = 0.55$ the error is most likely on the safe side.

The remainder of the investigation is practically identical with any of the graphical procedures for solving a maximum and minimum problem by trial and error. We determine the force P for spirals through different points on the horizontal surface of the sand and plot the values as ordinates above these points as shown in Figure 53*b*. Thus we obtain a P-curve. The earth pressure P_a on the timbering is equal to the ordinate of the highest point C of this curve. The surface of sliding passes through the point d located beneath point C on the horizontal surface of the deposit. The normal component P_{an} of the active earth pressure is

$$P_{an} = P_a \cos \delta$$

and the ratio

$$A_A = \frac{P_{an}}{\frac{1}{2}\gamma H^2} \qquad [3]$$

is the *earth pressure factor* for the active earth pressure on the timbering of a cut. It is a pure number. If the deformation conditions are such that the distribution of the active earth pressure of a cohesionless soil on the plane back of a lateral support is hydrostatic, the earth pressure factor A_A is identical with the coefficient of active earth pressure K_A for this soil, which is determined by equation 23(1*b*). Everything else being equal, the ratio

$$n = \frac{A_A}{K_A} \qquad [4]$$

is a measure of the influence of the deformation conditions on the active earth pressure. The greater n, the greater is the increase of the earth pressure due to the lateral confinement of the upper part of the supported mass of sand. For given values of ϕ and δ the value n increases with increasing values of the factor n_a, which determines the location of the point of application of the pressure. (See Fig. 53*a*.) If $\phi = 38°$ and $\delta = 0°$ we obtain

for $n_a = 0.45$ $n = 1.03$

and for $n_a = 0.55$ $n = 1.11$

The width of the top of the sliding wedge is always considerably smaller than the width of the top of the corresponding Coulomb wedge, represented by abd_c in Figure 53c.

With decreasing values of n_a the curvature of the surface of sliding in a mass of sand decreases and for $n_a = 1/3$ it is very slight, as shown in Figure 14c. If in addition the angle of wall friction is equal to zero, the surface of sliding for $n_a = 1/3$ is perfectly plane (see Art. 14). Hence for $n_a = 1/3$ and $\delta = 0$, the assumption that the line of sliding is a logarithmic spiral in shape (eq. 1) is not even approximately correct. Nevertheless, if on the basis of this assumption we compute the active earth pressure for $n_a = 1/3$ and $\delta = 0$ we find that the error is always considerably smaller than 10 per cent. With increasing values of n_a the percentage error decreases rapidly. For $n_a = 1/2$ the spiral method for computing the earth pressure on the timbering in cuts is at least as accurate as Coulomb's method for computing the earth pressure on retaining walls.

The distribution of the earth pressure on the timbering of cuts in sand depends to a certain degree on the details of the method of construction. In general the distribution is more or less parabolic, as shown in Figure 17c.

68. Earth pressure on the timbering of cuts in ideal cohesive soil. The method of computation described in the preceding article can also be applied to cuts in cohesive soil, the shearing resistance of which is determined by Coulomb's equation

$$s = c + \sigma \tan \phi$$

The slip along an arbitrary surface of sliding (bd_1 in Fig. 53b) is resisted not only by the friction but also by the cohesion, c per unit of area of the surface of sliding. Taking moments about the center O_1 of the spiral, equilibrium requires

$$P_1 l_1 = W_1 l_{w1} - M_c \qquad [1]$$

wherein M_c is the moment of the cohesion forces about O_1. The value of M_c can be computed by means of equation 41 (4)

$$M_c = \frac{c}{2 \tan \phi} (r_1^2 - r_0^2) \qquad 41\,(4)$$

In Figure 53b the values r_0 and r_1 are represented by the distances O_1d_1 and O_1b respectively. Introducing the value M_c into equation 1 and solving for P_1 we obtain

$$P_1 = \frac{1}{l_1}\left[W_1 l_{w1} - \frac{c}{2 \tan \phi} (r_1^2 - r_0^2) \right]$$

This force represents the lateral pressure required to prevent a slip along the arbitrary surface bd_1 (Fig. 53b). The surface of sliding must

satisfy the condition that the pressure P_1 be a maximum, P_a. Its position can be determined graphically as shown by the curve P (Fig. 53*b*) for ideal sand. Replacing P_1 in the preceding equation by the maximum value P_a and the values of W_1, r_1, etc., by those corresponding to the real surface of sliding we obtain

$$P_a = \frac{1}{l}\left[Wl_w - \frac{c}{2\tan\phi}(r_1^2 - r_0^2)\right] \qquad [2]$$

The greatest height at which the vertical sides of a cut can stand temporarily without lateral support is approximately

$$H_c = \frac{4c}{\gamma}\tan\left(45° + \frac{\phi}{2}\right) = \frac{4c}{\gamma}\sqrt{N_\phi} \qquad 57(1)$$

wherein

$$N_\phi = \tan^2\left(45° + \frac{\phi}{2}\right)$$

Hence

$$c = \frac{\gamma}{4\sqrt{N_\phi}}H_c \qquad [3]$$

Introducing this value into equation 2 we get

$$P_a = \frac{1}{l}\left[Wl_w - H_c\frac{\gamma}{8\sqrt{N_\phi}\tan\phi}(r_1^2 - r_0^2)\right]$$

The normal component of the active earth pressure is

$$P_{an} = P_a\cos\delta$$

and the earth pressure factor is

$$A_A = \frac{P_{an}}{\frac{1}{2}\gamma H^2} = \left(2\frac{W}{\gamma H^2}\frac{l_w}{l} + \frac{1}{4}\frac{H_c}{H}\frac{r_1^2 - r_0^2}{Hl}\frac{1}{\sqrt{N_\phi}\tan\phi}\right)\cos\delta \qquad [4]$$

The ratio A_A is a pure number the value of which depends only on H_c/H, δ, ϕ, and n_a. The plain curves in Figure 54 show the relation between A_A and the value n_a, which determines the position of the point of application of the earth pressure, for $\phi = 17°$, $\delta = 0°$, 10°, and 20°, and $H_c/H = 0.66$, 0.5, and 0.4. The individual values have been determined by means of the spiral method described previously.

The active Rankine pressure on the sides of the cut would be

$$P_A = P_{An} = -\frac{2cH}{\sqrt{N_\phi}} + \frac{1}{2}\gamma H^2\frac{1}{N_\phi} \qquad 14(3)$$

Replacing c by the right-hand term in equation 3 and dividing by $\frac{1}{2}\gamma H^2$ we obtain for the corresponding earth pressure factor

$$A_A = \frac{P_{An}}{\frac{1}{2}\gamma H^2} = \frac{1}{N_\phi}\left(1 - \frac{H_c}{H}\right) \qquad [5]$$

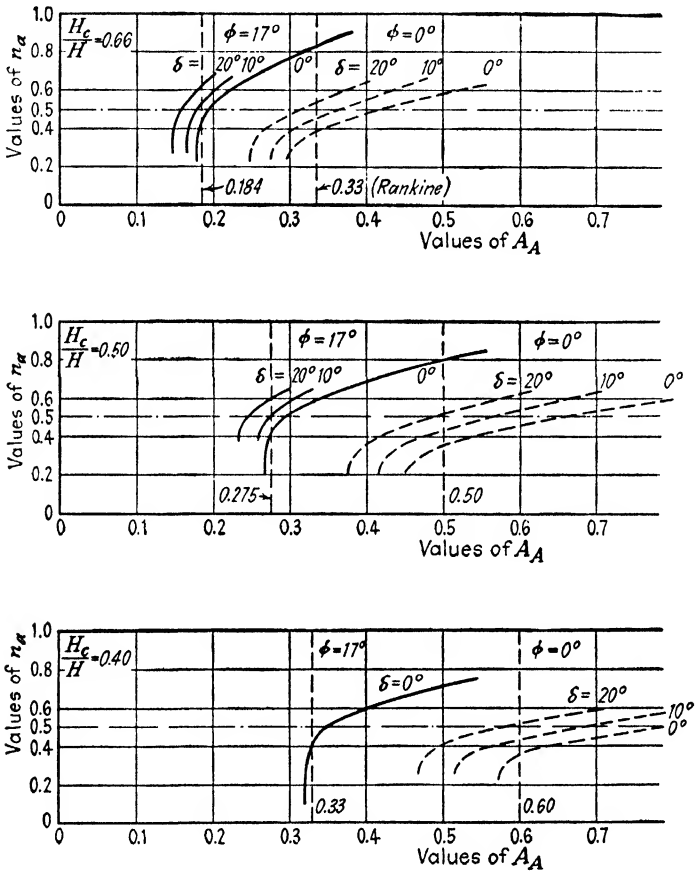

FIG. 54. Relation between earth pressure factor A_A and ratio n_a which determines position of point of application of resultant earth pressure of cohesive soil, for three different values of ratio between critical height H_c and total height H of lateral support and for different values of angle of wall friction δ.

For $\phi = 17°$ this value is represented in Figure 54 by the abscissas of the vertical dashed line which intersects the plain curves.

The dashed curves in Figure 54 show the relation between A_A and n_a for $\phi = 0$. The abscissas of the vertical dashed line which intersects

the dashed curves are equal to A_A (eq. 5) for $\phi = 0$, or

$$A_A = 1 - \frac{H_c}{H} \qquad [6]$$

For values of n_a greater than 0.5 the pressure ratio A_A represented by the abscissas of the dashed curves (Fig. 54) starts to increase rather rapidly with increasing values of n_a. Hence in attempting to estimate the earth pressure of cohesive soils on the timbering of a cut it is important to make a reasonable assumption regarding the value n_a. If $H_c/H = 0$ and $\phi = 0$, the soil adjoining the sides of the cut acts like a liquid and the corresponding value of n_a is ⅓. On the other hand, if $H_c/H = 1$, the depth of the cut is such that the sides can stand temporarily without lateral support. In this case, the struts required

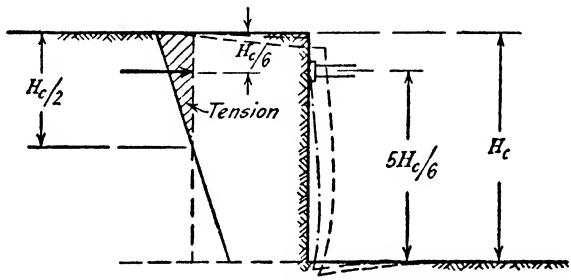

FIG. 55. Bracing required to prevent formation of tension cracks behind vertical bank whose height is equal to critical height H_c.

to prevent an ultimate failure of the sides by caving should be installed near the upper edge of the cut. The reason for the satisfactory results obtained by means of this traditional procedure is illustrated by Figure 55. In this figure is shown a vertical section through an unsupported, vertical bank, the height of which is equal to H_c. The soil adjacent to the upper part of the bank is in a state of tension. The deformation due to the weight of the soil is indicated by a dashed line. To simplify the problem, we assume that the tensile stresses are determined by Rankine's equation 12(2). On this assumption the tensile stresses decrease according to a straight line law from a maximum value at the surface to zero at a depth

$$z_0 = \frac{2c}{\gamma} = \frac{H_c}{2}$$

as shown in the figure. Hence the point of application of the tensile force is at a depth $H_c/6$ below the surface, which corresponds to a value of $n_a = 5/6$. If the bank fails the failure starts with the formation of

tension cracks parallel to the edge of the bank. In order to keep the upper part of the soil in a state of compression while excavation proceeds, struts should be installed at the elevation of the point of application of the tensile force, that means at a depth of $H_c/6$. The deformation of the supported bank is indicated by a dash-dotted line.

Thus we obtain two extreme values for n_a, viz., $n_a = 5/6$ for $H_c/H = 1$ and $n_a = \frac{1}{3}$ for $H_c/H = 0$ and $\phi = 0$. If we assume as a first approximation a linear relationship between H_c/H and n_a we obtain

$$n_a = \frac{1}{3} + \frac{H_c}{H}\left(\frac{5}{6} - \frac{1}{3}\right) = \frac{1}{3} + \frac{1}{2}\frac{H_c}{H} \qquad [7]$$

A more accurate method for estimating the value n_a is not yet available. The results of pressure measurements in open cuts in clay indicate that the real values of n_a are somewhat smaller than those determined by equation 7. However, they also indicate in accordance with the equation that the values of n_a increase with increasing values of H_c/H. The measured values of n_a are closer to n_a (eq. 7) than to $\frac{1}{3}$. In no case has a value of less than $\frac{1}{3}$ been obtained. Hence it appears that the error associated with using equation 7 is on the safe side, because a higher value of n_a involves a higher theoretical value for the earth pressure. In this connection it should be remembered that the n_a value for the Rankine pressure decreases from $\frac{1}{3}$ for $H_c/H = 0$ to $-\infty$ for $H_c/H = 1$. Hence if the point of application of the Rankine pressure goes down the point of application of the pressure on the timbering goes up.

69. Conditions for the stability of the bottom of a cut. The soil located on both sides of a cut acts, with reference to a horizontal section through the bottom of the cut, like a uniformly distributed surcharge. This surcharge tends to produce a heave of the bottom of the cut, where the surcharge is absent. This heave is comparable to the base failure on slopes. (See Art. 56.) However, no heaving failure can occur unless the load due to the weight of the soil near the sides of the cut exceeds the bearing capacity of the soil located below the level of the bottom of the cut. In the following analysis two extreme cases will be considered, viz., cuts in ideal sand and cuts in ideal cohesive soil the angle of shearing resistance of which is equal to zero.

Figure 56*a* is a vertical section through a cut of depth H in ideal sand. The bottom of the cut is located at a considerable elevation above the ground-water table. The lower ends of the vertical members of the system of bracing are located at the level of the bottom. Hence the active earth pressure P_a acts on the lateral support in a horizontal direction ($P_a = P_{an}$). The distribution of the lateral pressure on the

sides of the cut is roughly parabolic, as shown by the pressure area *rus* in Figure 56*a*. The normal pressure on a vertical section *sC* through the edge *s* of the bottom of the cut can nowhere exceed the passive earth pressure. The passive earth pressure of sand increases like a hydro-

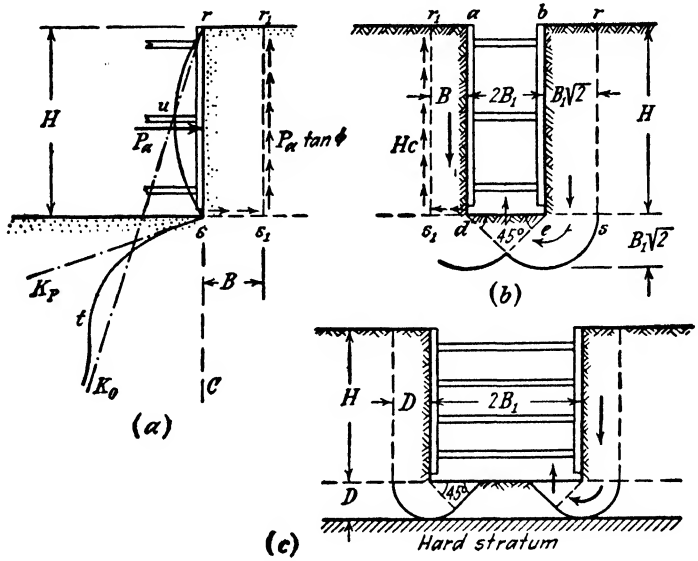

FIG. 56. (*a*) Distribution of horizontal pressure on timbering in open cut in cohesionless sand; (*b*) heave of bottom of timbered cut in soft clay if no hard stratum interferes with flow of clay; (*c*) as before, if clay rests at shallow depth below bottom of cut on hard stratum.

static pressure in simple proportion to the depth. Plotting the passive earth pressure per unit of area from *sC* to the left we obtain the straight line sK_P. Before the cut is excavated the normal stress on the vertical section *rC* at a depth *z* below the surface is

$$\sigma_{h0} = K_0 \gamma z \qquad 10(1)$$

wherein K_0 is the coefficient of earth pressure at rest. Plotting the values of σ_{h0} from *rC* to the left we obtain the straight line rK_0. Since the influence of excavating the cut on the state of stress in the soil decreases with increasing depth the line *st* which represents the distribution of the normal stresses on the vertical section *sC* must asymptotically approach the straight line rK_0 as shown in the figure.

Thus are the general characteristics of the state of stress in the vicinity of the outer edges of the bottom of the cut. In order to obtain information regarding the factor of safety of the cut with respect to a failure due to a heave of the bottom we compute the vertical pressure

Q per unit of length of a strip ss_1 (Fig. 56a) adjoining the lower edge s of the side of the cut. The strip has an arbitrary width B. The pressure on the strip is equal to the difference between the weight γHB of the prism rr_1s_1s and the total shearing force on the vertical right-hand boundary of this prism. The shearing force is approximately equal to the active earth pressure, P_a, times the coefficient of internal friction, $\tan \phi$. Hence

$$Q = \gamma HB - P_a \tan \phi = \gamma HB - \tfrac{1}{2}\gamma H^2 A_A \tan \phi$$

wherein

$$A_A = \frac{P_{an}}{\frac{1}{2}\gamma H^2} \qquad 67(3)$$

is the earth pressure factor for the active earth pressure on the timbering. The timbering prevents the soil located above the bearing area from following the lateral movement of the soil located beneath this area. Furthermore, the loaded sand can yield only toward one side. Therefore the bearing capacity Q'_D per unit of length of the strip with a width B is approximately equal to one half of the bearing capacity Q_D of a continuous footing with a width $2B$ whose rough base rests on the surface of the sand. The value Q_D is determined by equation 46(5). Setting $c = 0$ and D_f (depth of foundation) $= 0$ in this equation we get

$$Q_D = 2B^2\gamma N_\gamma$$

and

$$Q'_D = \tfrac{1}{2}Q_D = B^2\gamma N_\gamma$$

The value of the bearing capacity factor N_γ can be scaled off the diagram shown in Figure 38c (curve N_γ). The factor of safety with respect to a failure due to a heave of the bottom,

$$G_s = \frac{Q'_D}{Q}$$

is a minimum if the width B of the strip satisfies the condition

$$\frac{dG_s}{dB} = 0$$

or

$$\frac{d}{dB}\,\frac{B^2\gamma N_\gamma}{\gamma HB - \frac{1}{2}\gamma H^2 A_A \tan \phi} = 0$$

Solving this equation we get

$$B = HA_A \tan \phi$$

For $\delta = 0$ and $n_a = 0.5$ the value A_A is approximately equal to the coefficient for the active Rankine pressure,

$$K_A = \tan^2\left(45° - \frac{\phi}{2}\right)$$

Hence

$$B = H \tan^2\left(45° - \frac{\phi}{2}\right) \tan \phi = n_B H \qquad [1]$$

wherein n_B is a pure number whose value depends only on the angle of internal friction ϕ. For values of ϕ between 30° and 40° the value n_B ranges between 0.19 and 0.18. The minimum value of the factor of safety G_s is determined by the equation

$$G_s = \left[\frac{Q'_D}{Q}\right]_{B=n_B H} = 2N_\gamma n_B \qquad [2]$$

This equation shows that the factor of safety with respect to a heave of the bottom of the cut is independent of the depth of the cut. It depends only on the value of ϕ. If ϕ increases from 30° to 40°, the factor of safety increases from about 8 to about 50.

Figure 56*b* is a vertical section through a cut in an ideal cohesive soil the angle of shearing resistance ϕ of which is equal to zero. The soil is uniform to a considerable depth below the bottom of the cut and the vertical members of the system of bracing terminate at the bottom. The shearing resistance of the soil is equal to c. The vertical pressure Q per unit of length of a horizontal strip ds_1 with an arbitrary width B is approximately

$$Q = \gamma HB - Hc = BH\left(\gamma - \frac{c}{B}\right) \qquad [3]$$

which indicates that the pressure q increases with increasing values of B.

The angle ϕ of shearing resistance is equal to zero and the surcharge acts on the supporting soil like a load carried by a continuous footing with a rough base, because the timbering prevents the soil located above the level of the bottom of the cut from following the lateral yield of the soil located below this level. Therefore the bearing capacity q_D per unit of area of the strip is determined by the equation

$$q_D = 5.7c \qquad 46(7c)$$

which is independent of the width B. The ratio

$$G_s = \frac{Q_D}{Q} = \frac{Bq_D}{Q} = \frac{1}{H}\frac{5.7c}{\gamma - \frac{c}{B}}$$

represents the factor of safety with respect to a heave of the bottom of the cut. It decreases with increasing values of B. The greatest value which B can assume is determined by the shape of the surface of sliding through d (Fig. 56*b*). Since $\phi = 0$ the curved part of this surface is an arc of a circle about e, and since the section es represents the equivalent to the rough base of a footing, the surface of sliding starts at s with a vertical tangent (see Art. 45). The plane part of the surface of sliding rises at an angle of 45° to the horizontal. On account of these geometrical conditions, the width B cannot exceed $B_1\sqrt{2}$. Substituting this value in the preceding equation we get

$$G_s = \frac{1}{H}\frac{5.7c}{\gamma - \dfrac{c}{B_1\sqrt{2}}} \qquad [4]$$

For

$$H = H_1 = \frac{5.7c}{\gamma - \dfrac{c}{B_1\sqrt{2}}} \qquad [5]$$

the factor of safety becomes equal to unity. Hence if soil is excavated to a depth greater than H_1 the soil on both sides of the cut moves downward, together with the system of bracing, and the bottom of the cut rises. If $\phi = 0$ the critical height for a vertical bank is approximately

$$H_c = \frac{4c}{\gamma} \qquad 57(2a)$$

from which

$$c = \tfrac{1}{4}\gamma H_c$$

Introducing this value into equation 5 we obtain

$$H_1 = H_c\frac{5.7}{4 - \dfrac{H_c}{B_1\sqrt{2}}} \qquad [6]$$

If $B_1 = H_c/5.65$ the value H_1 becomes equal to infinity. With increasing values of B_1 the value of H_1 decreases. On the other hand, if $B_1 = \infty$ we obtain

$$H_1 = 1.42H_c \approx \tfrac{3}{2}H_c$$

This means that the bottom of a very wide cut will fail as soon as the depth becomes greater than about $\frac{3}{2}$ times the critical height H_c, provided the earth is homogeneous to a great depth. If a cut is made in a

soft soil, which is underlain at a depth D below the bottom of the cut by a hard stratum, the failure of the bottom occurs as shown in Figure 56c. The width of the strip which can sink is equal to D. Replacing $B_1\sqrt{2}$, which represents the width of the sinking strip in Figure 56b by D we obtain from equation 6 for the depth at which the cut fails by heaving the value

$$H_1 = H_c \frac{5.7}{4 - \frac{H_c}{D}} \qquad [7]$$

which is independent of the width of the cut.

If the excavation of a cut is made between sheet piles which extend to a depth D_1 below the bottom of the cut, the method for estimating the factor of safety with respect to a heave of the bottom must be modified accordingly. The simplest procedure is to compute the vertical pressure on a horizontal section through the lower edge of the sheet piles. The heave of the bottom is resisted not only by the weight of the soil located between the buried parts of the sheet piles but also by the adhesion between this body of earth and the adjoining sheet piles.

70. Tunnels through sand. Figure 57a shows a section through a bed of sand in which a tunnel is being constructed between the horizontal surface of the bed and the water table. The cohesion of the sand is assumed to be not in excess of the feeble bond produced by a trace of moisture. Yet from experience we know that this trace of cohesion is sufficient to maintain the working face in small drifts without lateral support. Part of the yield of the sand toward the tunnel occurs while the working face passes the section shown in the figure and the remainder takes place after the timbering has been constructed. Owing to the imperfect fit of the timbers at the joints and the compressibility of the supports of the footings of the vertical posts, the yield of the timbering is usually sufficient to reduce the pressure of the sand on the timbering almost to the value corresponding to the state of incipient shear failure in the sand. This state is similar to the state of stress in a mass of sand above a yielding strip. The sand adjoining the sides of the tunnel also subsides on account of the yield of its lateral support. The inclined boundaries of the zone of subsidence rise at an angle of about $45° + \phi/2$. Therefore, at the level of the roof of the tunnel, the width of the yielding strip is approximately equal to

$$2B_1 = 2\left[B_0 + H \tan\left(45° - \frac{\phi}{2}\right)\right] \qquad [1]$$

In accordance with the procedure described in Article 20 it will be assumed that the potential surfaces of sliding through the outer edges of the yielding strip b_1b_1 are vertical, as shown in the figure by dotted lines b_1e_1. On this assumption the vertical pressure on the horizontal

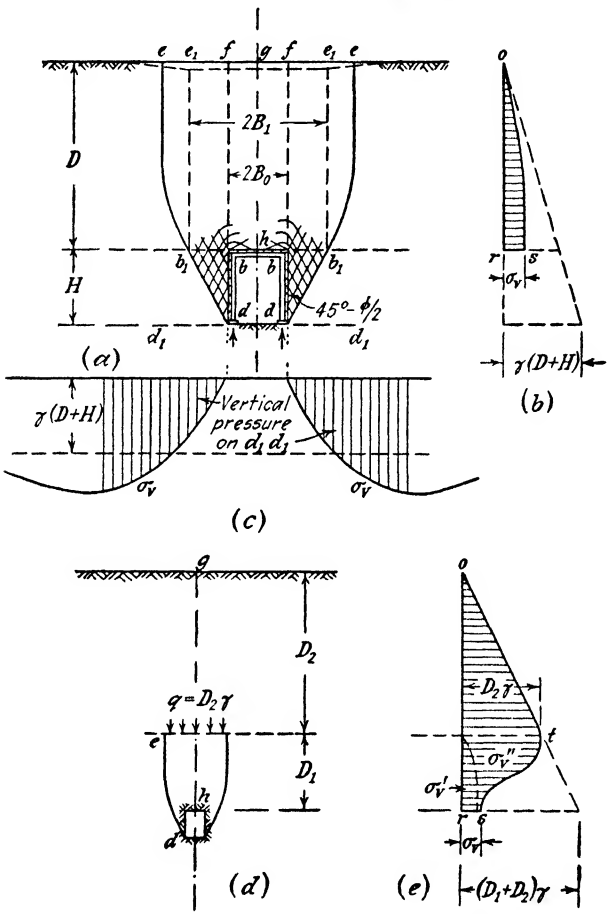

FIG. 57. (*a*) Flow of sand toward shallow tunnel at instant of failure of timbering; (*b*) vertical unit pressure in sand above center line of tunnel plotted against depth; (*c*) distribution of vertical pressure on horizontal section through bottom of tunnel. If tunnel is located at great depth, diagram (*d*) takes the place of (*a*) and (*e*) that of (*b*).

section b_1b_1 (Fig. 57*a*) with a width $2B_1$ is determined by equation 20(5). Substituting in this equation for z the value D and for B the value B_1 (eq. 1), we obtain

$$\sigma_v = \frac{\gamma B_1}{K \tan \phi} (1 - \epsilon^{-K \tan \phi \ D/B_1}) \qquad [2]$$

per unit of area of the horizontal section b_1b_1. In this equation the symbol K designates an empirical coefficient. From the results of direct measurements it has been found that the value of this coefficient is approximately unity (see Art. 20). On both sides of the tunnel the pressure σ_v acts like a surcharge on the top surface of the wedges located on both sides of the tunnel. The corresponding lateral pressure on the sides of the tunnel can be computed by means of Coulomb's theory with the assumption that the sides of the tunnel are simple retaining walls the backfill of which carries a uniformly distributed surcharge, σ_v per unit of area.

The pressure which acts on the roof of the tunnel is transferred to the sand beneath the bottom of the tunnel through the footings of the vertical posts. The remainder of the weight of the sand located above the roof is transferred by shearing stresses to the sand adjacent to the tunnel. Hence the distribution of the vertical pressure on a horizontal section through the bottom of the tunnel must be similar to the distribution shown in Figure 57*c*.

If a tunnel is located at a great depth below the surface the arching effect does not extend beyond a certain elevation D_1 above the roof of the tunnel. The sand located above this elevation, from the surface of the ground down to a depth D_2, Figure 57*d*, acts on the zone of arching like a simple surcharge with an intensity γD_2 per unit of area. In this case the pressure on the roof of the tunnel is determined by equation 20(4). Substituting $B = B_1$, $q = \gamma D_2$, and $z = D_1$, in this equation we obtain

$$\sigma_v = \frac{\gamma B_1}{K \tan \phi} (1 - \epsilon^{-K \tan \phi \ D_1/B_1}) + \gamma D_2 \epsilon^{-K \tan \phi \ D_1/B_1}$$

The angle of internal friction ϕ for a sand is at least equal to 30° and from experiments it has been found that the value K is at least equal to unity. If the roof of a deep tunnel yields, the height D_1 of the zone of arching increases while the height D_2 decreases. As soon as the height D_1 becomes equal to about 20 per cent of the total depth $D_1 + D_2$ the second term on the right-hand side of the preceding equation becomes negligible. The first term is smaller than $\gamma B_1/K \tan \phi$ for all values of D_1. Hence the pressure per unit of area of a deep tunnel through dry sand does not exceed an upper limiting value, which is equal to

$$\sigma_{v\infty} = \frac{\gamma B_1}{K \tan \phi} \qquad [3]$$

although the arching does not extend to the surface of the ground.

The vertical pressure per unit of area of horizontal sections at points located above the center line of the tunnel are represented in Figure 57*e* by the abscissas of the curve *ots*. This curve is similar to curve *odf* in Figure 18*d*.

The conditions for the stability of the bottom of tunnels in sand can be investigated by means of the method described in the preceding article. The results of such an investigation have shown that the factor of safety with respect to heaving of the bottom of a tunnel through sand is always adequate provided the deepest point of the potential surface of sliding is located above the water table.

71. Application of Rankine's theory to the computation of the pressure of sand on the lining of tunnels. Prior to the construction of a tunnel a mass of sand with a horizontal surface is laterally confined and the ratio between the horizontal and the vertical pressure is equal to the coefficient of earth pressure at rest K_0. In order to establish the active Rankine state, the sand must be allowed to expand laterally over the full width and depth of the deposit through a certain minimum distance per unit of width, which depends essentially on the density of the sand. In contrast to this fundamental requirement of Rankine's earth pressure theory the lateral expansion of the sand produced by the tunneling operations does not extend beyond narrow zones located on both sides of the tunnel. Beyond these zones the horizontal strain is practically equal to zero. This type of deformation is incompatible with Rankine's theory. There is, however, one exception to this general rule. It involves the pressure of the sand on the timbering of a tunnel at a shallow depth beneath a slope which rises at an angle equal to or slightly smaller than the angle of internal friction of the sand. To a depth not in excess of a small fraction of the total height of the slope, the sand is on the verge of active failure before the construction of the tunnel is started. This state is identical with the active Rankine state illustrated by Figures 9*b* and 9*c*. For a slope angle $\beta = \phi$ one set of potential surfaces of sliding is parallel to the slope and the other set is vertical. Since the sand was already in a state of plastic equilibrium before construction was started, the timbering in the tunnel can do no more than maintain this state. Hence the earth pressure on the upper part of the support is approximately identical with the active Rankine pressure. For example, if the section through the tunnel has the shape shown in Figure 58, the normal pressures on the section *abc* of the extrados can be estimated by means of Rankine's theory, using Mohr's diagram. In the sand adjoining this section the principal stresses σ_I and σ_{III} are oriented as shown in the figure by arrows. During the construction operations the stress in the sand at

the bottom of the tunnel is reduced to zero. On the section *ad* the construction operations reverse the direction of the shearing stresses which acted on this section prior to construction. Therefore Rankine's theory

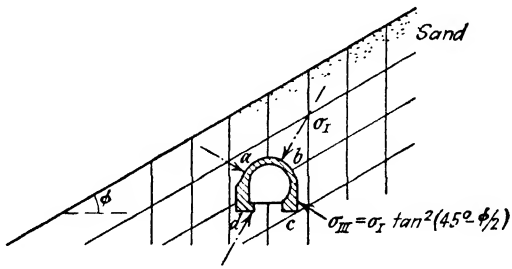

FIG. 58. Tunnel in a mass of cohesionless sand whose surface rises at the angle of repose.

should only be used for computing the pressure on the arch *abc*. The pressure on the face *ad* can be computed by means of Coulomb's theory.

In order to adapt the permanent lining of railroad tunnels to the earth pressure conditions illustrated by Figure 58, the section through the lining of some tunnels has been given an unsymmetrical shape such as that shown in the figure (Bierbaumer 1913).

If the slope angle β is slightly smaller than the angle of internal friction ϕ we can use the method illustrated in Figure 58 by assuming that the angle of internal friction is equal to the slope angle β. If the slope angle β is considerably smaller than ϕ, Rankine's theory cannot be used.

72. Tunnels through cohesive soil. The method of investigation which has been described in Article 70 can also be applied to tunnels through cohesive soil. The shearing resistance of the earth per unit of area of a potential surface of sliding is

$$s = c + \sigma \tan \phi \qquad 5(1)$$

If we retain the simplifying assumptions on which the equations in Article 70 are based we can estimate the pressure on the roof of the tunnel by means of equation 20(3). Substituting in this equation for B the value B_1 (eq. 70(1)), which represents one half of the total width of the zone of arching at the level of the roof of the gallery as shown in Figure 57*a*, and for z the depth D of the roof of the gallery below the surface we obtain

$$\sigma_v = B_1 \frac{\gamma - \dfrac{c}{B_1}}{K \tan \phi} (1 - \epsilon^{-K \tan \phi \; D/B_1}) \qquad [1]$$

According to this equation the pressure on the roof is equal to zero for any depth provided

$$B_1 \gtrless \frac{c}{\gamma} \qquad [2]$$

It should, however, be remembered that equation 20(3) is based on the simplifying assumption that the normal stresses on horizontal sections through the zone of arching are everywhere the same. In reality the surfaces of equal normal pressure are curved like arches. As a consequence the surface of zero pressure intersects the plane of symmetry of the tunnel at some distance above the roof. Within this distance the soil is in a state of tension. A tension failure along the upper boundary of the zone of tension causes a body of soil with a planoconvex cross section to drop out of the roof. In order to prevent such an accident, an unsupported roof in a tunnel through cohesive earth should always be given the shape of an arch.

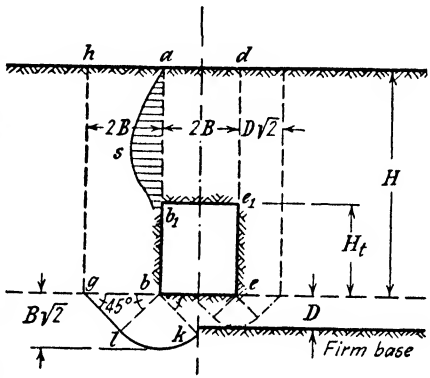

FIG. 59. Heave of bottom of tunnel in soft clay. Left-hand side of diagram shows conditions if clay extends to great depth, right-hand side the conditions if clay rests on firm base at shallow depth.

If the width of the tunnel is greater than c/γ (eq. 2) the roof must be supported. The pressure on the roof is transmitted to the bottom of the tunnel through the footings of the vertical timbers. The corresponding distribution of the normal pressure on a horizontal section through the bottom of the tunnel is similar to that shown in Figure 57*c*. In extreme cases the earth may be too weak to resist the unequally distributed load shown in Figure 57*c*, whereupon the bottom of the tunnel will rise unless it is held down by a stiff floor construction or an invert.

The conditions for the stability of the bottom of a tunnel through cohesive soil are essentially identical with those described in Article 69 and illustrated by Figures 56*b* and 56*c*. If the bottom of a tunnel is sufficiently stiff, the temporary lining of the roof can be supported by footings located on both sides of the bottom of the tunnel. Otherwise it is necessary to build the tunnel by means of a shield (Terzaghi 1942*a*). Such a method increases the cost of construction considerably. Hence

the bearing capacity of the bottom of the tunnel is a factor of great practical importance.

In Figure 59 is shown a vertical section of a shallow tunnel having a width $2B$. The unit weight of the soil surrounding the tunnel is γ, its cohesion is c, and its angle of shearing resistance is zero. The total normal pressure on the vertical sections ab and de through the sides of the tunnel is approximately equal to the earth pressure P_a on the timbering in a cut of equal width and equal depth in the same soil. The block of soil ab_1e_1d serves the function of the struts. The normal pressure on the vertical sides of this block is represented by the pressure area asb_1.

Since there are no horizontal struts below the roof of the tunnel the soil on both sides of the tunnel can yield freely toward the tunnel. Therefore the soil located above the strip gb acts like a surcharge on a perfectly smooth base. On this condition the bearing capacity of the strip is determined by the equation

$$q_D = 5.14c \qquad 46(9f)$$

It is independent of the width of the strip. The width of the yielding strip is conditioned by the limitations imposed by the width of the tunnel upon the size of the zone of plastic equilibrium in the soil located beneath the strip. Since $\phi = 0$ the boundary of the zone of plastic equilibrium consists of an arc of a circle, kl, and a straight segment, lg, which rises at an angle of 45° to the horizontal as shown on the left side of Figure 59. Hence the width of the strip bg is $2B$.

The lower limiting value of the total vertical pressure on the strip is equal to the difference between the weight of the mass of soil located between the plane of symmetry of the tunnel and the vertical section gh, which is $3\gamma BH - \gamma BH_t$, and the total shearing resistance on the vertical section gh, which is Hc. Hence the vertical pressure per unit of area of the strip bg cannot be smaller than

$$q = \frac{\gamma}{2}(3H - H_t) - \frac{Hc}{2B}$$

and the factor of safety with respect to a heave of the bottom is

$$G_s = \frac{q_D}{q} = \frac{5.14c}{\frac{\gamma}{2}(3H - H_t) - \frac{Hc}{2B}} \qquad [3]$$

For

$$H = H_1 = \frac{5.14c + 0.5\gamma H_t}{1.5\gamma - \frac{c}{2B}} \qquad [4]$$

the factor of safety becomes equal to unity. Introducing the critical height $H_c = 4c/\gamma$ (eq. 57(2a)) into this equation we get

$$H_1 = H_c \frac{5.14 + 2\dfrac{H_t}{H_c}}{6 - \dfrac{H_c}{2B}} \qquad [5]$$

If the vertical distance between the bottom of the tunnel and the surface is greater than H_1, the bottom of the tunnel will rise and the roof will subside.

The dash-dotted line on the right side of Figure 59 represents the lower boundary of the zone of plastic equilibrium on the assumption that the soft soil is underlain at a depth $D < B\sqrt{2}$ below the bottom by a hard stratum. The presence of this stratum reduces the width of the zone of subsidence from $2B$ to $D\sqrt{2}$, whereupon we obtain

$$H_1 = H_c \frac{5.14 + 2\dfrac{H_t}{H_c}}{2\left(\dfrac{D\sqrt{2}}{B} + 1\right) - \dfrac{H_c}{2B}} \qquad [6]$$

The temporary support of a tunnel may also fail as a result of inadequate support of the footings of the arch ribs or of the posts. The load on the footings per unit of length of the tunnel is at least equal to the difference between the weight of the body of soil ab_1e_1d and the greatest value $2c(H - H_t)$, which the shearing force on the vertical sections ab_1 and de_1 can assume. If the ribs are supported by continuous footings each $2b_1$ in width, the pressure per unit of area exerted on these footings will be at least equal to

$$q = \frac{\gamma B(H - H_t) - (H - H_t)c}{2b_1} = \frac{1}{2b_1}(H - H_t)(\gamma B - c)$$

Since the bases of the footings are rough, the bearing capacity is determined by the equation

$$q_D = 5.7c \qquad 46(7c)$$

The pressure q on the footings should not be greater than the bearing capacity q_D divided by an adequate factor of safety G_s. Hence

$$q = \frac{1}{2b_1}(H - H_t)(\gamma B - c) = \frac{5.7c}{G_s}$$

or

$$2b_1 = \frac{H - H_t}{5.7c}(\gamma B - c)G_s \qquad [7]$$

The method of open mining cannot be used unless it is possible to install continuous footings the widths of which are at least equal to $2b_1$ or to install equivalent square footings.

73. State of stress in the vicinity of drill holes. In dealing with problems concerning the plastic equilibrium of soil in the vicinity of cylindrical holes, a distinction must be made between small holes such as drill holes and large holes such as shafts. In contrast to a drill hole, the diameter of which does not exceed a few inches, a shaft is an excavation the width of which is at least several feet.

When a small hole is drilled in a deposit of cohesive soil, the walls of the hole may stand without any lateral support. Yet, when a shaft having a diameter of 10 feet is excavated in the same soil, the walls of the shaft may fail unless supported by timbering. The following analysis deals with the stress conditions which are likely to exist in the vicinity of small holes. The term *cylindrical section* will be used exclusively for sections whose axis coincides with the center line of the hole. Let

γ = the unit weight of the soil,

K_0 = the coefficient of earth pressure at rest the value of which depends on the nature of the soil and its geologic history,

σ_r, σ_θ, and σ_z = the horizontal radial stress, the horizontal circumferential stress, and the vertical stress respectively: all normal stresses,

τ = the shearing stress on the planes on which the normal stresses σ_r and σ_z act,

σ_I and σ_{III} = major and minor principal stress respectively which exist after the hole has been made,

σ_{r0} = the normal stress at the walls of the hole at a depth z,

r_0 = the radius of the hole, and

r_e = the outer diameter of the zone of plastic equilibrium at depth z.

The shearing resistance of the soil is determined by Coulomb's equation

$$s = c + \sigma \tan \phi$$

wherein c is the cohesion, σ the normal pressure acting on the plane of shear, and ϕ the angle of shearing resistance. The corresponding conditions for plastic equilibrium are defined by equation 7(3)

$$\sigma_I = 2c\sqrt{N_\phi} + \sigma_{III}N_\phi \qquad [1]$$

wherein σ_I designates the major and σ_{III} the minor principal stress, and

$$N_\phi = \tan^2\left(45° + \frac{\phi}{2}\right)$$

In Figure 60*a* are shown the stresses which act on an element of the soil adjoining a cylindrical section having an arbitrary radius r. Since

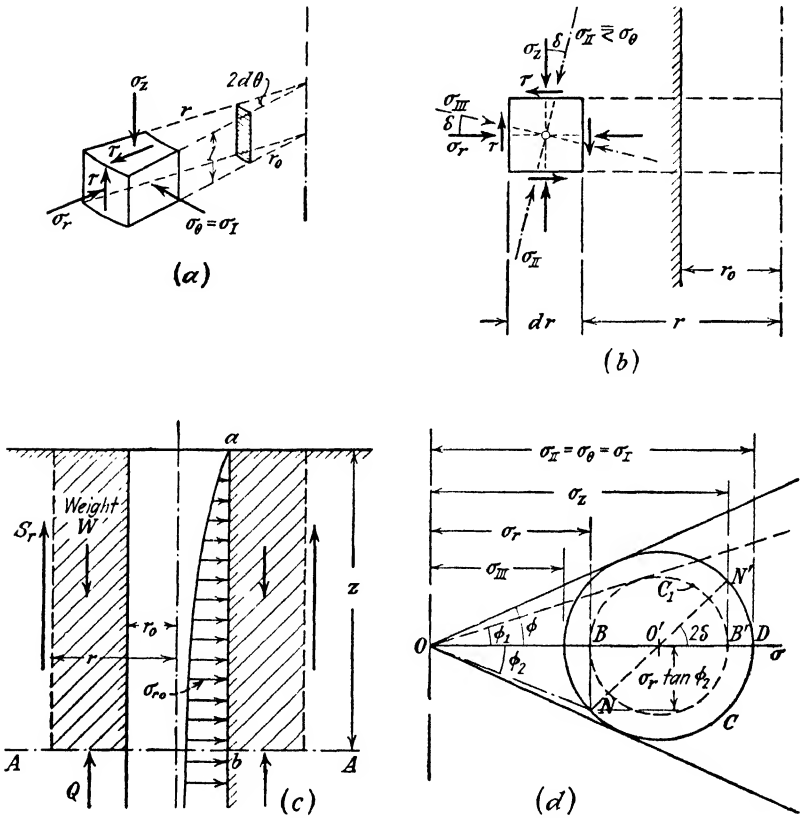

FIG. 60. (*a* and *b*) Stresses which act on the sides of a small block of soil located at an arbitrary distance r from center line of a shaft; (*c* and *d*) diagrams illustrating the assumptions on which the computation of earth pressure on lining of shaft are based.

the shearing stresses on vertical sections through the center line of the hole are equal to zero, the circumferential stress σ_θ is a principal stress.

Westergaard (1940) has demonstrated by trial computation that the shearing stress τ shown in Figure 60*a* can be negligible. If this condition is satisfied the radial stress σ_r is almost identical with the minor principal stress σ_{III}, whereupon we can replace the plasticity

condition (eq. 1) by

$$\sigma_\theta = 2c\sqrt{N_\phi} + N_\phi \sigma_r \qquad [2]$$

Since both stresses σ_θ and σ_r are horizontal a failure of the walls of the drill hole would occur by plastic flow in horizontal planes. By combining equation 2 with equations 17(3), Westergaard (1940) determined the stress function which satisfies the boundary conditions of the problem. The corresponding stresses are

$$\sigma_r = \left(\sigma_{r0} + \frac{2c\sqrt{N_\phi}}{N_\phi - 1}\right)\left(\frac{r}{r_0}\right)^{N_\phi - 1} - \frac{2c\sqrt{N_\phi}}{N_\phi - 1} \qquad [3a]$$

and

$$\sigma_\theta = N_\phi\left(\sigma_{r0} + \frac{2c\sqrt{N_\phi}}{N_\phi - 1}\right)\left(\frac{r}{r_0}\right)^{N_\phi - 1} - \frac{2c\sqrt{N_\phi}}{N_\phi - 1} \qquad [3b]$$

These equations can also be derived by elementary methods, by combining equation 2 with another equation expressing the condition that the sum of all the forces which act on the element shown in Figure 60*a* in the direction of a horizontal radius through the center of the element must be equal to zero (Terzaghi 1919).

At the boundary between the zone of plastic and elastic equilibrium, the stresses computed by means of equations 3 must also satisfy the conditions for the elastic equilibrium of the soil located beyond the boundary. The equations which determine the stresses in the elastic region will be derived in Article 145. By combining these equations with equations 3, Westergaard obtained for the radius r_e of the zone of plastic equilibrium at a depth z below the surface, on the assumption $K_0 = 1$, the equation

$$r_e = r_0\left\{\frac{2[(N_\phi - 1)\gamma z + 2c\sqrt{N_\phi}]}{(N_\phi + 1)[(N_\phi - 1)\sigma_{r0} + 2c\sqrt{N_\phi}]}\right\}^{1/(N_\phi - 1)} \qquad [4]$$

In order to apply the preceding equations to cohesionless soils we must introduce the value $c = 0$ into equations 2, 3, and 4. Thus we get

$$\sigma_\theta = N_\phi \sigma_r \qquad [5]$$

$$\sigma_r = \sigma_{r0}\left(\frac{r}{r_0}\right)^{N_\phi - 1} \qquad [6a]$$

$$\sigma_\theta = N_\phi \sigma_{r0}\left(\frac{r}{r_0}\right)^{N_\phi - 1} \qquad [6b]$$

and

$$r_e = r_0\left[\frac{2\gamma z}{\sigma_{r0}(N_\phi + 1)}\right]^{1/(N_\phi - 1)} \qquad [7]$$

The radius r_e of the zone of plastic equilibrium (eq. 7) has a finite value for every positive value of the radial stress σ_{r0} which acts at the walls of the drill hole. This conclusion is in accordance with field experience with drill holes in sand. As a rule, the insignificant lateral resistance offered by a mud jacket suffices to keep the drill hole open.

As a second case let us consider the state of stress in the vicinity of a drill hole in an ideal clay the angle of shearing resistance ϕ of which is equal to zero. Introducing into equation 2 the value

$$N_\phi = \tan^2\left(45° + \frac{\phi}{2}\right) = 1$$

we get

$$\sigma_\theta = \sigma_r + 2c \qquad [8]$$

Evaluating equations 3 and 4 for $\phi = 0$ we obtain

$$\sigma_r = 2c \ln\left(\frac{r}{r_0}\right) + \sigma_{r0} \qquad [9a]$$

$$\sigma_\theta = 2c\left[\ln\left(\frac{r}{r_0}\right) + 1\right] + \sigma_{r0} \qquad [9b]$$

and

$$r_e = r_0\, \epsilon^{(\gamma z - c - \sigma_{r0})/2c} \qquad [10]$$

If the walls of the drill hole are unsupported the normal stress σ_{r0} acting on the walls is equal to zero and the value r_e becomes equal to

$$r_e = r_0\, \epsilon^{(\gamma z - c)/2c} \qquad [11]$$

Between the surface and a depth

$$z_e = \frac{c}{\gamma} \qquad [12]$$

the value r_e is smaller than r_0. This indicates that the elastic region within this depth extends to the walls of the hole. For greater values of z the radius of the zone of plastic equilibrium increases with increasing depth. Yet, for any finite value of z the value of r_e is finite. Hence, the walls of a drill hole in clay should not require any lateral support, regardless of what the values of c and z may be. Experience has shown that the walls of drill holes in stiff or medium clay do not in fact require any lateral support. This experience agrees with the preceding conclusions. However, experience has also shown that the walls of shafts in clay are likely to fail unless they are adequately supported. This

observation indicates that the preceding analysis does not apply to shafts. The reason will be discussed in the following article in connection with the earth pressure of sand on the walls of shafts.

74. Conditions for the equilibrium of sand adjoining the walls of a shaft located above the water table. Figure 60*c* is a vertical section through a block of sand with a weight W, a height z, and an arbitrary radius r. It surrounds a cylindrical shaft with a radius r_0. The outer surface of the block is acted upon by a shearing force S_r and the base of the block by a vertical pressure Q. The equilibrium of the block requires

$$W = Q + S_r \qquad [1]$$

In the preceding article it was assumed that the shearing stresses on cylindrical sections are negligible and that the normal stresses on horizontal sections represent intermediate principal stresses. If the diameter of the hole does not exceed a few inches these conditions are almost satisfied even if the radial stresses σ_{r0} at the walls of the hole are very small. Therefore, the results of the analysis agree with experience with drill holes in sand. Since the normal stresses on horizontal sections were assumed to be intermediate principal stresses, the problem of computing the stresses in the sand surrounding the hole was a two-dimensional problem of plasticity.

When a wide shaft is excavated in sand we may expect on the basis of construction experience that the timbering has to sustain an appreciable earth pressure. If the timbering is not strong enough to sustain this pressure, it fails, whereupon the surface of the sand surrounding the mouth of the shaft subsides. This type of deformation of the sand surrounding the shaft indicates a shear failure on approximately cylindrical sections. It also indicates that the normal stresses on horizontal sections exceed the strength of the sand. Therefore the analysis contained in the preceding article cannot be applied to the computation of the earth pressure on the walls of shafts.

The intensity and the distribution of the earth pressure on the lining of shafts undoubtedly depends to a certain extent on the method of construction. Our present knowledge does not yet permit us to take this effect into consideration. In order to get at least some information concerning the influence of the diameter and the depth of the shaft and of the angle of internal friction of the sand on the earth pressure we solve by approximation the following problem. We apply on the walls of the shaft with a depth infinity a radial pressure, σ_{r0} per unit of area, as indicated on the right-hand side of Figure 60*c* and we estimate the smallest value which must be assigned to this pressure in order to pre-

vent a failure of the walls of the shaft. Since this pressure can be supplied by the resistance of an ideal lining, the pressure σ_{r0} will briefly be called the earth pressure.

Figures 60*a* and 60*b* show the stresses which act on a wedge-shaped element of the sand adjoining a cylindrical section with an arbitrary radius r. As explained in the preceding article, the circumferential stress σ_θ represents the major principal stress and the two other principal stresses act in radial planes. It has also been shown that the radial stress σ_r represents for $\tau = 0$ the smallest principal stress. In connection with shafts the shearing stress τ cannot be disregarded. Therefore the smallest principal stress σ_{III} acts at a small angle δ to the horizontal, as indicated in Figure 60*b*. The type of movement of the sand produced by a failure of the walls of the shaft indicates that the second principal stress σ_{II} has the greatest value compatible with the conditions for plastic equilibrium. According to Mohr's theory of rupture (Art. 7) this value is equal to that of the major principal stress, which in our case is equal to σ_θ. The stress conditions for failure are represented in Mohr's diagram, Figure 60*d*. Setting $\sigma_{II} = \sigma_I$ in equation 7(5) we get for the state of impending failure

$$\sigma_{II} = \sigma_\theta = \sigma_{III} N_\phi$$

wherein $N_\phi = \tan^2\left(45° + \frac{\phi}{2}\right)$. Hence

$$\frac{\sigma_{II}}{\sigma_{III}} = N_\phi \qquad [1]$$

Since σ_r and σ_z in Figure 60*d* are not principal stresses the ratio $\sigma_z/\sigma_r = a$ is smaller than the ratio $\sigma_{II}/\sigma_{III} = N_\phi$. By geometry we obtain from Mohr's diagram

$$\frac{\sigma_z}{\sigma_r} = a = \tan^2\left(45° + \frac{\phi_1}{2}\right) \qquad [2]$$

The value of the angle ϕ_1 depends on that of δ. It is smaller than ϕ. The diagram further shows that the shearing stress which acts on the cylindrical section at a given value of ϕ_1 cannot be greater than

$$s = \sigma_r \tan \phi_2 \qquad [3]$$

Finally we learn from Figure 60*d* that the ratio σ_θ/σ_r is somewhat greater than the ratio $\sigma_z/\sigma_r = a$. Hence, if we assume $\sigma_\theta \approx \sigma_z$ or

$$\frac{\sigma_\theta}{\sigma_r} \approx \frac{\sigma_z}{\sigma_r} = \tan^2\left(45° + \frac{\phi_1}{2}\right) = a \qquad [4a]$$

we introduce a slight error on the safe side into our computation. In the following analysis the value $a = \sigma_\theta/\sigma_r$ represents the equivalent of the value $N_\phi = \sigma_\theta/\sigma_r$ which appears in equations 73(6).

The relation between σ_θ, σ_r, and σ_{r0} is determined by equations 73(6). If we replace the value N_ϕ in these equations by a, we obtain for the radial and circumferential stress respectively the values

$$\sigma_r = \sigma_{r0}\left(\frac{r}{r_0}\right)^{a-1} \qquad [4b]$$

and

$$\sigma_\theta = a\sigma_{r0}\left(\frac{r}{r_0}\right)^{a-1} \qquad [4c]$$

These equations show that both the radial and the circumferential stresses decrease with decreasing values of r/r_0. In other words, the intensity of all the stresses decreases in radial directions toward the shaft. This stress condition will be referred to as *ring action.*

From equations 2 and 4*b* we get

$$\sigma_z = a\sigma_r = a\sigma_{r0}\left(\frac{r}{r_0}\right)^{a-1} \qquad [4d]$$

Figure 61*a* is a vertical section through the center line of a shaft. If there were no ring action, the lateral pressure on the walls of the shaft would not be smaller than the active Rankine pressure. At a depth z below the surface this pressure is equal to

$$\sigma_A = \gamma z \tan^2\left(45° - \frac{\phi}{2}\right) = \gamma z \frac{1}{N}$$

per unit of area. In Figure 61*a* this pressure is represented by the horizontal distances between the lines *ib* and iK_A. However, as a result of the ring action the lateral pressure on *ib* is very much smaller than the active Rankine pressure. It is represented by the pressure area *ibd.* At point *i* at the upper edge of the shaft, the pressure line *id* should be tangent to the line iK_A. The pressure area *efg* on the right-hand side of the center line of the shaft shown in Figure 61*a* shows the distribution of the lateral pressure on a cylindrical section with an arbitrary radius r. Before the shaft is constructed, the pressure per unit of area acting on this section at any depth z is equal to

$$\sigma_0 = K_0\gamma z$$

wherein K_0 is the coefficient of earth pressure at rest. The stress σ_0 is represented in Figure 61*a* by the horizontal distance between the lines *ef*

and eK_0. After the shaft has been excavated, the pressure line shifts from its original position to position *eg*.

Figure 61*b* represents the stresses which act in the vicinity of the shaft at any depth z below the surface. The scale of the stress diagrams shown in this figure is smaller than that used in Figure 61*a*. The abscissas give the distances r from the center line, the ordinates of the lower curve represent the radial stress, and those of the upper curve the circumferential stress and the vertical stress. The boundary between the plastic and the elastic zone is indicated by a break in the stress curves. Within the plastic zone, the stresses σ_r and σ_θ are determined by equations 4*b* and 4*c* respectively.

The total weight of the sand above the horizontal section at depth z, between the walls of the shaft and a distance r from the center line is

$$W = \pi(r^2 - r_0^2)\gamma z$$

The total pressure on the annular area $\pi(r^2 - r_0^2)$ is equal to

$$Q = \int_{r_0}^{r} 2\pi r \sigma_z dr$$

In Figure 61*b* the pressure Q is represented by the shaded area. The difference between the forces W and Q must be carried by the shearing stresses acting on the cylindrical surface *ef* in Figure 61*a*. The following investigations will show that the rate of increase of the radial stress on a cylindrical section decreases as the depth below the surface increases, as indicated by the curvature of the pressure line *eg* in Figure 61*a*. Therefore the average radial pressure per unit of area acting on the

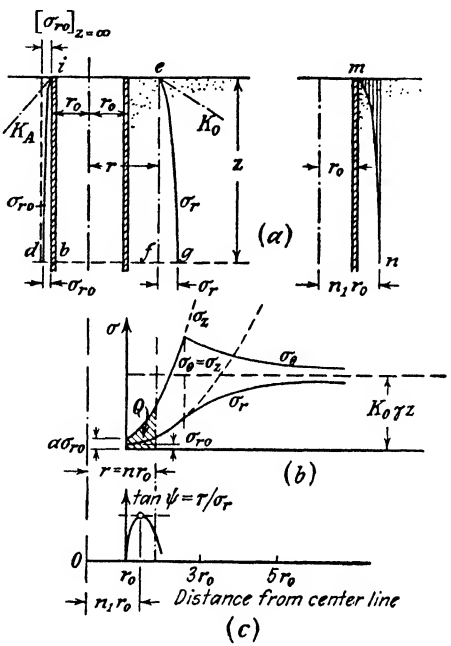

FIG. 61. (*a*) Distribution of radial pressure σ_{r0} on lining of shaft in sand and of radial stresses σ_r on cylindrical section with radius r; shaded area in right-hand diagram indicates zone in which shearing stresses on cylindrical section are almost equal to shearing resistance of sand; (*b*) approximate distribution of radial, circumferential, and vertical normal stresses (σ_r, σ_θ, and σ_z) along horizontal section at depth z; (*c*) relation between radius of a cylindrical section and average value of tangent of angle ψ between resultant stresses on this section above depth z and the radial direction.

cylindrical section ef is intermediate between the value σ_r, which represents the normal pressure on the section at depth z, and the value $\frac{1}{2}\sigma_r$, which represents the average normal pressure on the assumption that the pressure increases in simple proportion to depth. The corresponding average shearing resistance s_a on the cylindrical section is intermediate between $\sigma_r \tan \phi_2$ and $\frac{1}{2}\sigma_r \tan \psi$. In the following computations we assign to s_a the lower limiting value

$$s_a = \tfrac{1}{2}\sigma_r \tan \phi_2 \qquad [5]$$

which involves an error on the safe side.

If only a part of the shearing resistance is required to maintain a state of equilibrium, the average shearing stress on ef will be equal to $\frac{1}{2}\sigma_r \tan \psi$, wherein $\tan \psi$ is smaller than $\tan \phi_2$. The value of $\tan \psi$ is determined by the condition that the total shearing force on ef should be equal to the difference between the forces W and Q, or

$$W - Q = \pi(r^2 - r_0^2)\gamma z - \int_{r_0}^{r} 2\pi r \sigma_z dr = 2\pi r z \tfrac{1}{2}\sigma_r \tan \psi$$

Combining this equation with equation 4d, and setting

$$\frac{r}{r_0} = n \quad \text{and} \quad m_\sigma = \frac{\sigma_{r0}}{\gamma r_0} \qquad [6a]$$

we get

$$\tan \psi = \frac{n^2 - 1}{m_\sigma n^a} - \frac{2a}{a+1}\frac{r_0}{z}\frac{n^{a+1} - 1}{n^a} \qquad [6b]$$

The value n_1 for which $\tan \psi$ is a maximum is determined by the condition

$$\frac{d \tan \psi}{dn} = 0$$

Solving this equation for m_σ we obtain

$$m_\sigma = \frac{z}{r_0}\frac{a+1}{2a}\frac{a - (a-2)\, n_1^2}{a + n_1^{a+1}} \qquad [7]$$

The angle ψ represents the angle between the resultant stress on a cylindrical section and the corresponding normal stress σ_r. According to Mohr's diagram, Figure 60d, the greatest value which this angle can assume at a given value of the angle ϕ_1 is ϕ_2. Replacing n in equation 6b by n_1 and $\tan \psi$ by $\tan \phi_2$ we obtain

$$\tan \phi_2 = \frac{n_1^2 - 1}{m_\sigma n_1^a} - \frac{2a}{a+1}\frac{r_0}{z}\frac{n_1^{a+1} - 1}{n_1^a} \qquad [8]$$

If $z = 0$, equation 8 is not satisfied unless $n_1 = 1$, whence

$$z = 0, \quad n_1 = 1, \quad \text{and} \quad m_\sigma = \frac{z}{ar_0} \qquad [9]$$

With increasing values of z, both n_1 and m_σ increase. For $z = \infty$ we get from equation 8

$$m_\sigma = \frac{n_1^2 - 1}{n_1^a \tan \phi_2}$$

Introducing this value into equation 7 and solving for n_1 we get

$$n_1 = \sqrt{\frac{a}{a-2}}$$

Hence

$$z = \infty, \quad n_1 = \sqrt{\frac{a}{a-2}}, \quad \text{and} \quad m_\sigma = 2\frac{(a-2)^{(a-2)/2}}{a^{a/2} \tan \phi_2} \qquad [10]$$

The value a contained in the preceding equations is equal to $\tan^2 (45° + \phi_1/2)$ (eq. 2). If ϕ_1 is known the angle ϕ_2 can be determined graphically by means of Mohr's diagram as shown in Figure 60*d*. In Figure 62*a* the values of ϕ_1 and ϕ_2 have been plotted against $\phi - \phi_1$ for $\phi = 30°$ (dashed curves) and $\phi = 40°$ (plain curves). In Figure 62*b* the abscissas represent the values of $\phi - \phi_1$ and the ordinates the corresponding values of m_σ computed by means of equation 10 for $\phi = 30°$ (dashed curve) and $\phi = 40°$ (plain curve). For $\phi_1 = \phi$ or $\phi - \phi_1 = 0$, ϕ_2 is equal to zero, whence m_σ for $z = \infty$ (eq. 10) is equal to infinity. If the radial pressure σ_{r0} acting on the walls of the shaft at depth infinity is smaller than infinity the sand surrounding the shaft starts to yield toward the shaft. During this process shearing stresses develop along cylindrical sections and the radial stresses σ_r (Fig. 60*b*) which act on these sections cease to be principal stresses. As the shearing stresses increase the angle ϕ_1 decreases, the angle ϕ_2 increases and the value $m_\sigma = \sigma_{r0}/\gamma r_0$ decreases as shown in Figure 62*b*. Hence the radial pressure $\sigma_{r0} = \gamma r_0 m_\sigma$ required to stop the yield also decreases. As soon as ϕ_1 becomes approximately equal to $\phi - 5°$ this pressure becomes a minimum. This minimum pressure value satisfies the requirements of our problem because we inquired about the smallest radial pressure σ_{r0} which suffices to maintain in the vicinity of the shaft a state of plastic equilibrium. According to Figure 62*a* the value of ϕ_2 corresponding to a value of $\phi_1 = \phi - 5°$ is approximately equal to $\phi - 5°$. For $\phi_1 = \phi - 5°$ the angle δ (slope angle of the direction of

the smallest principal stress σ_{III} in Fig. 60*a*) is roughly equal to 15° for any value of ϕ between 30° and 40°.

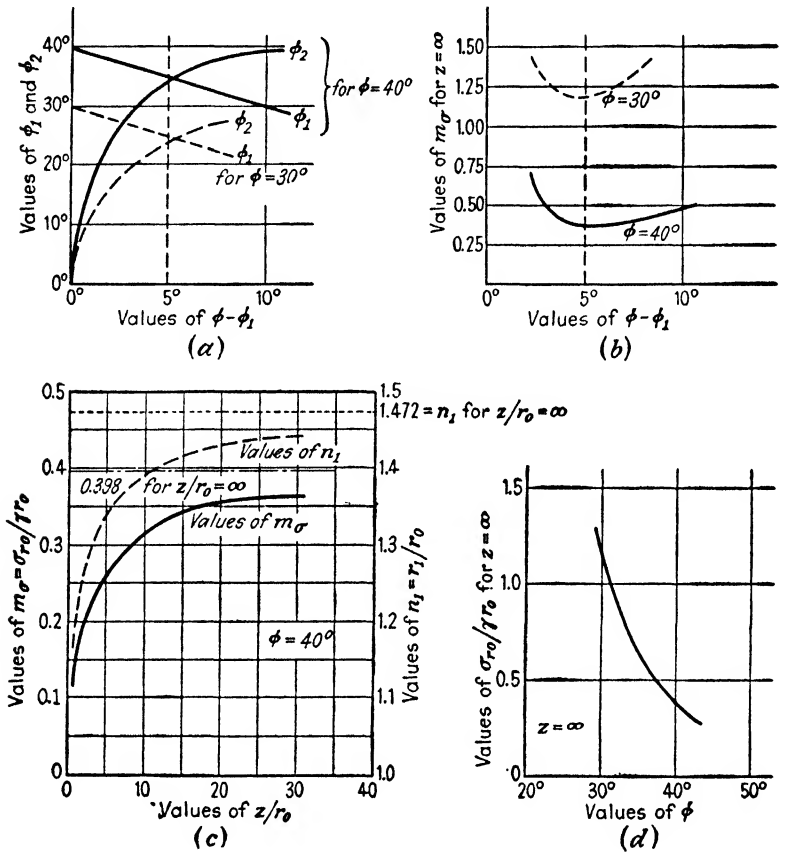

FIG. 62. (*a*) Values of angles ϕ_1 and ϕ_2 in Mohr's diagram, Fig. 60*d*, plotted against $\phi - \phi_1$; (*b*) influence of $\phi - \phi_1$ on value of $m_\sigma = \sigma_{r0}/\gamma r_0$ for $z = \infty$; (*c*) relation between m_σ and the depth ratio z/r_0 for $\phi = 40°$; (*d*) relation between $m_\sigma = \sigma_{r0}/\gamma r_0$ and ϕ for $z = \infty$.

Thus the smallest radial pressure $\sigma_{r0} = \gamma r_0 m_\sigma$ required to prevent a failure of the walls of the shaft can be computed for any given value of z by combining equations 7 and 8 with the equation

$$\phi_1 = \phi_2 = \phi - 5° \qquad [11]$$

provided the angle ϕ ranges between the limits of 30° and 40°, representing the extreme values which the angle of internal friction of a sand is likely to assume. The following table contains the numerical values

of m_σ and n_1 for $\phi = 40°$ ($\phi_1 = 40° - 5° = 35°$) and different values of z/r_0.*

z/r_0	0	3.1	8.3	11.8	18.2	29.4	76.0	∞
$m_\sigma = \frac{\sigma_{r0}}{\gamma r_0}$	0	0.23	0.30	0.33	0.35	0.36	0.37	0.398
n_1	1	1.30	1.38	1.40	1.42	1.44	1.46	1.472

In Figure 62*c* the abscissas represent the values z/r_0, the ordinates of the plain curve the corresponding values of m_σ, and those of the dashed curve the values of n_1. With increasing values of z/r_0 both curves approach horizontal asymptotes with ordinates of 0.398 and 1.472. For depths greater than about $8r_0$ (four times the diameter of the shaft), the unit earth pressure on the walls of a shaft with a given radius r_0 increases very slowly with increasing depth. The radius $n_1 r_0$ of the space within which the sand would subside in a vertical direction in case of a failure of the lateral support of the walls of the shaft is approximately equal to 1.5 times the radius r_0 of the shaft.

Similar graphs can be plotted for any given value of ϕ. By means of such graphs the earth pressure on the walls of a shaft can be computed rapidly. Let us assume that a cylindrical shaft having a diameter of $2r_0 = 20$ feet is to be excavated in a bed of sand with a unit weight $\gamma = 110$ pounds per cubic foot. We wish to determine the lateral pressure on the walls of the shaft at a depth $z = 100$ feet below the surface. For $z/r_0 = 100/10 = 10$, we obtain from Figure 62*c* $m_\sigma = 0.315$. Since

$$m_\sigma = \frac{\sigma_{r0}}{\gamma r_0} = 0.315 = \frac{\sigma_{r0}}{110 \times 10}$$

the pressure per unit of area acting on the walls of the shaft at a depth of 100 feet is

$$\sigma_{r0} = 0.315 \times 110 \times 10 = 345 \text{ lb/sq ft}$$

According to Figure 62*c* a value of $z/r_0 = 10$ is associated with a value of $n_1 = 1.39$. Hence, the ratio between shearing stresses and normal stresses on cylindrical sections will be greatest at a distance of about $n_1 r_0 = 14$ feet from the center line of the shaft or of 4 feet from the walls of the shaft. If the values of $n_1 r_0$ are plotted as a function of the depth, we obtain a dome-shaped surface. On the right-hand side of Figure 61*a* the generatrix of this surface is represented by the line *mn*. Above this surface, within the space represented by the shaded

* The numerical values in the table were obtained by introducing $\tan \phi_2 - \tan \phi_1 = \tan 35°$ into eq. 8, computing from this equation the values m for different values of n_1 and by computing the corresponding values of z/r_0 by means of eq. 7.

area, the shearing resistance of the sand acting on cylindrical sections is fully active. Beyond the boundaries of this space the shearing stresses on cylindrical sections rapidly drop below the maximum value which they could assume.

If the walls of the shaft are located entirely below the water table and if the shaft is perfectly sealed, the walls are acted upon by the sum of the full water pressure and the pressure exerted by the sand. At a depth of 100 feet below water table, the pressure of the water is equal to 100 times 62.5 = 6250 pounds per square foot. In order to calculate the pressure exerted by the sand, we must replace in the preceding equations the unit weight γ of the sand by the submerged unit weight γ'. Assuming $\gamma' = 70$ pounds per cubic foot, we get

$$\sigma_{r0} = 0.315 \times 70 \times 10 = 221 \text{ lb/sq ft}$$

which is negligible compared with the pressure exerted by the water.

Figure 62*d* shows the relation, given by equation 10, between the angle of internal friction ϕ of the sand and the values of $m_\sigma = \sigma_{r0}/\gamma r_0$ for $z = \infty$. The corresponding value of σ_{r0} represents the highest value which the unit pressure of a given sand on the walls of a shaft with a given diameter can assume.

Figure 62*c* shows that the ratio n_1 for $\phi = 40°$ and $z/r_0 = \infty$ is equal to 1.47. For $\phi = 30°$ we obtain from equations 10 $n_1 = 2.30$. These results indicate that the zone in which the shearing resistance of the sand on cylindrical sections is fully active is very narrow. For this reason we were justified in disregarding the abnormal stress conditions which prevail in the vicinity of the bottom of the shaft. At a short distance above the bottom of the shaft they must be practically normal.

So far we have no evidence of any contradiction between the results of the preceding computations and the earth pressure on the lining of real shafts in sand. This fact seems to indicate that the customary methods of constructing such shafts permit the full mobilization of the shearing resistance of the sand while excavation proceeds. In accordance with the results of the preceding computations the earth pressure on the lining of shafts in sand approaches a finite and relatively small value with increasing depth.

75. Pressure of clay on the walls of shafts. The method of computation described in the preceding article could also be applied with minor modifications to the computation of the earth pressure on the walls of shafts in clay. However, a study of the problem on this basis showed that the errors are likely to be excessive. They are primarily due to the influence of the soil located beneath the bottom of the shaft on the intensity and distribution of the stresses. The theory described in the preceding article is based on the assumption that the depth of the shaft is infinity. If the depth of a shaft is finite, part of the radial pressure exerted by the soil around

the lower part of the shaft is transferred by shearing stresses to the soil located beneath the bottom. Up to a height above the bottom which is roughly equal to the width of the zone of plastic equilibrium, the relief of pressure due to this pressure transfer is very important. If a shaft is surrounded by sand the width of this zone is very small. Therefore at a short distance above the bottom the pressure on the walls of the shaft is practically identical with that on the walls of a shaft with infinite depth. On the other hand, at the level of the bottom of a shaft in clay the width of the zone of plastic equilibrium is roughly equal to the depth of the shaft. Therefore the relief of the earth pressure due to the pressure transfer described above extends over the major part of the depth of the shaft. On account of this influence the earth pressure on the walls of a shaft with finite depth in clay should be very much smaller than the computed pressure. As a matter of fact, a comparison of the results of one such computation with the results of pressure measurements in the field showed that the measured pressure did nowhere exceed about one half of the computed pressure. More accurate methods of computation are not yet available.

Chapter XI

ANCHORED BULKHEADS

76. Definitions and assumptions. Anchored bulkheads serve the same purpose as retaining walls. However, in contrast to retaining walls whose weight always represents an appreciable fraction of the weight of the sliding wedge, bulkheads consist of a single row of relatively light sheet piles of which the lower ends are driven into the earth.

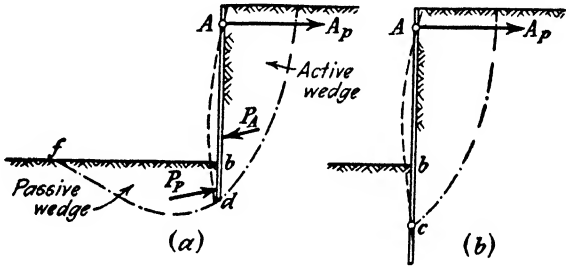

FIG. 63. Anchored bulkhead with (*a*) free and (*b*) fixed earth support. Dash-dotted lines indicate potential surfaces of sliding.

The active earth pressure is taken up partly by anchor rods which are tied to the sheet piles at A in Figure 63, at a short distance below the upper edge a of the bulkhead and partly by the passive resistance of the soil located on the left side of the lower part of the sheet piles. The anchor rods are held in place by anchors which are buried in the backfill at a considerable distance from the bulkhead.

In further contrast to retaining walls, bulkheads are flexible. On account of the anchorage of the uppermost part and the passive resistance of the soil adjoining the lowest part of the bulkhead, the upper and the lower edges of a bulkhead are practically fixed. Therefore a bulkhead yields only by bending in a horizontal direction and the maximum deflection occurs approximately at midheight of the bulkhead. This type of yield is essentially different from that of any of the lateral supports which have been discussed in the preceding chapters. When a cut is made in sand the lateral yield of the sand adjoining the cut increases from almost zero at the upper rim to a maximum at the bottom and the distribution of the lateral pressure of the sand on the

timbering is roughly parabolic. A retaining wall usually yields by tilting about its base and the distribution of the active earth pressure of sand on such a wall is hydrostatic. The lateral yield of the upper part of the soil adjoining a bulkhead resembles that of the soil adjoining a cut and the lateral yield of the lower part is similar to that of the backfill of a tilting retaining wall. On account of this deformation condition the distribution of the active earth pressure on a bulkhead represents a combination between that on the timbering of cuts and that on the back of retaining walls, as indicated by the pressure area $ab_1t_1s_1$ in Figure 64.

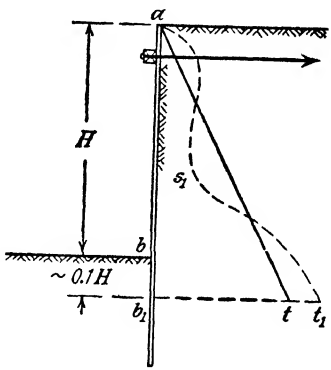

FIG. 64. Assumed (unbroken line) and real (dashed line) distribution of active earth pressure on anchored bulkhead with fixed end support.

In connection with bulkhead problems it is always assumed that the lateral yield of the middle part of the bulkhead is important enough to mobilize the full shearing resistance of the supported soil along the potential surface of sliding, for instance the surface *de* in Figure 63*a*. The intensity and the distribution of the earth pressure on the buried part of the bulkhead depends on the depth to which the sheet piles have been driven into the ground.

In connection with the design of bulkheads we have to answer the following questions: What is the depth to which the sheet piles must be driven in order to insure an adequate lateral support for the lower part of the bulkhead? What is the intensity of the force which acts on the anchor rods? What is the value of the greatest bending moment in the sheet piles?

In order to simplify the presentation of the subject the discussions will be limited to vertical bulkheads acted upon by the earth pressure of a homogeneous mass of ideal sand whose shearing resistance is determined by the equation

$$s = \sigma \tan \phi \qquad 5(2)$$

The anchor pull is assumed to be horizontal. It is also assumed that the water table is located below the lower edge of the sheet piles and that the surface of the mass of sand which is supported by the bulkhead does not carry any surcharge. However, the methods of computation described in the following articles can also be used without essential modification even if the soil adjoining the bulkhead is partly or wholly submerged, or stratified, or cohesive, or if the anchor pull acts at an

angle to the horizontal. The influence of seepage forces on the stability of bulkheads will be discussed in Article 92.

77. Conditions of end support. If the sheet piles have been driven only to a shallow depth, the deflection of the bulkhead is somewhat similar to that of a vertical elastic beam whose lower end d is simply supported without being fixed, as shown in Figure 63*a*. Bulkheads which satisfy this condition are called *bulkheads with free earth support.* On the other hand, if sheet piles have been driven to a considerable depth, as indicated in Figure 63*b*, the lower end of the bulkhead is practically fixed in its position, because the resistance of the sand adjoining the end does not permit more than an insignificant deviation of the piles from their initial, vertical position. Therefore bulkheads of this type will be called *bulkheads with fixed earth support.* An adequately anchored bulkhead with free earth support can fail either by bending or, on account of a failure of the sand adjoining the contact face bd, by shear along a curved surface of sliding df. A securely anchored bulkhead with fixed earth support can fail only by bending.

78. Distribution of active earth pressure on bulkheads. On account of the boundary deformation conditions described in Article 76 the distribution of the active earth pressure on a bulkhead is nonhydrostatic. The results of theoretical investigations (Schoenweller 1929, Ohde 1938) and experience indicate that the distribution of the active earth pressure is similar to the distribution indicated by a dashed curve as_1t_1 in Figure 64. It is also known from both theory and experience that the total active earth pressure on the bulkhead is approximately equal to the Coulomb pressure on the back of a retaining wall, which is determined by equations 23(1). However, the methods which have been worked out for determining the distribution of the pressure do not take the elastic properties of the soil into consideration. The importance of the error due to disregarding this vital factor is not yet known. Furthermore, the elaborate character of the procedures conceals the manifold arbitrary assumptions on which the procedures are based and inspire an unwarranted confidence in the reliability of the results. Hence, pending further increase of our knowledge of this subject, the author suggests that the influence of the nonhydrostatic distribution of the pressure on the maximum bending moment M_0 should be estimated on the basis of our purely empirical knowledge of earth pressure phenomena, as explained in the following paragraph.

Figure 64 is a vertical section through a bulkhead with fixed earth support. Below point b_1 the lateral deflection of the bulkhead is insignificant. Above b_1 the right-hand face of the bulkhead is acted

upon by the active earth pressure P_A. The distribution of the earth pressure on the bulkhead depends to a large extent on the elastic properties of the soil supported by the bulkhead. If the soil consists of a semi-liquid, fine-grained hydraulic fill, the pressure distribution is hydrostatic as indicated by the triangular area ab_1t which represents the pressure P_A. As a consequence, the maximum bending moment M_0 computed on the assumption of a hydrostatic pressure distribution is practically identical with the real maximum bending moment M. On the other hand, if the bulkhead supports a mass of clean sand as assumed in this chapter the distribution of the lateral pressure is indicated by the pressure area $as_1t_1b_1$ and the real maximum bending moment M in the sheet piles does not exceed about one half of the maximum bending moment M_0 computed on the basis of a hydrostatic pressure distribution.

79. General procedure. The customary methods of bulkhead design (Lohmeyer 1930, Blum 1930) ignore the nonhydrostatic distribution of the active earth pressure on the bulkhead. Therefore the computed value of the maximum bending moment in the sheet piles is considerably greater than the real one as demonstrated in the preceding article. On the other hand, the influence of the pressure distribution on the depth of penetration required to obtain an adequate lateral support for the buried part of the bulkheads is very small. Therefore this depth can be determined without appreciable error by means of the usual methods.

In accordance with this general procedure it will be assumed that the horizontal component of the active earth pressure, p_{An} per unit of area of the back of the bulkhead, is determined by the equation

$$p_{An} = \gamma z K_A \qquad 15(1)$$

wherein K_A is the coefficient of active earth pressure. The horizontal component of the passive earth pressure p_{Pn} per unit of area of the contact face of the buried part of the sheet piles is equal to

$$p_{Pn} = \gamma z' K_P \qquad 15(3)$$

wherein K_P is the coefficient of the passive earth pressure and z' is the depth below the lower ground surface. The methods for computing the values of K_A and K_P have been discussed in Chapters VI and VII respectively. These values depend on the angle of internal friction ϕ and the angle of wall friction δ. The angle δ must be selected in accordance with the conditions of the problem. Since the weight of the sheet piles is negligible compared to the external forces which act on the

bulkhead the friction component of the passive earth pressure cannot be appreciably greater than that of the active earth pressure. For $\delta = 0$ the values K_A and K_P become identical with the Rankine values

$$K_A = \tan^2\left(45° - \frac{\phi}{2}\right) = \frac{1}{N_\phi} \qquad 15(2)$$

and

$$K_P = \tan^2\left(45° + \frac{\phi}{2}\right) = N_\phi \qquad 15(4)$$

respectively.

80. Bulkheads with free earth support. Figure 65 is a section through a bulkhead with free earth support. The distribution of the active earth pressure over the right-hand face of the bulkhead is assumed

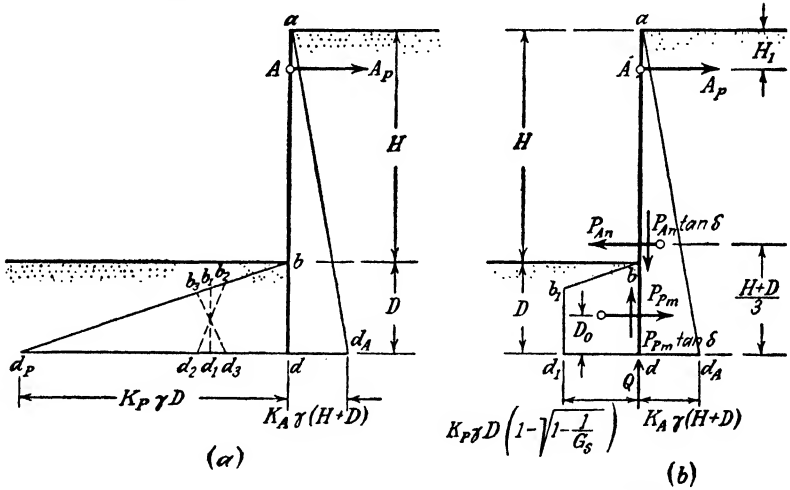

FIG. 65. (*a*) Various assumptions regarding distribution of passive earth pressure on buried part of bulkhead with free earth support; (*b*) customary assumptions concerning the forces which act on such a bulkhead.

to be hydrostatic, as indicated by the triangular pressure area add_A. The depth D of penetration of the sheet piles is determined by the condition that the passive resistance of the earth required to support the lower end of the sheet piles should not exceed a certain fraction $1/G_s$ of the passive earth pressure represented by the triangular pressure area bdd_P (Fig. 65). The value G_s is called the factor of safety with respect to failure of the lower support of the bulkhead.

The lines d_1b_1, d_2b_2, and d_3b_3 (Fig. 65*a*) indicate different opinions

concerning the left-hand boundary of the pressure area which represents the mobilized fraction of the total passive earth pressure bdd_P. Most investigators prefer the vertical line d_1b_1 because it simplifies subsequent computations (Krey 1936).

Assuming that the mobilized part of the passive earth pressure can be represented by a trapezoid bb_1d_1d (Fig. 65*a*), the bulkhead is acted upon by the forces indicated in Figure 65*b*. Let

$P_{An} = \dfrac{(H+D)^2}{2}\gamma K_A$ = horizontal component of the active earth pressure,

$P_{Pm} = \dfrac{1}{G_s}P_{Pn} = \dfrac{1}{G_s}\dfrac{D^2}{2}\gamma K_P$ = mobilized part of the horizontal component of the passive earth pressure,

$\tan\delta$ = coefficient of wall friction,

A_p = tension in the anchor rods per unit of length of the bulkhead,

Q = vertical soil reaction at lower edge of sheet piles, per unit of length,

D_0 = the elevation of the center of gravity of the pressure area bb_1d_1d above the lower edge of the sheet piles.

The equilibrium of the system requires that the sum of the vertical components, that of the horizontal components, and that of the moments around any point, for instance point A, should be equal to zero. Hence

$$P_{An}\tan\delta_A - P_{Pm}\tan\delta_P - Q = 0 \qquad [1a]$$

$$A_p + P_{Pm} - P_{An} = 0 \qquad [1b]$$

and

$$P_{An}[\tfrac{2}{3}(H+D) - H_1] - P_{Pm}(H + D - H_1 - D_0) = 0 \qquad [1c]$$

Equations 1*b* and 1*c* can be solved for D, the required depth of penetration of the sheet piles, and for A_p, the pull in the anchor rods. The specifications usually require a factor of safety $G_s = 2$. Nothing is known regarding the intensity of the soil reaction Q in equation 1*a*. Yet this reaction has a considerable influence on the values K_A and K_{Pm}. If $Q = 0$ the condition expressed by equation 1*a* is not satisfied unless the angle of wall friction for the passive pressure is greater than that for the active pressure or unless both values are equal to zero. In order to keep the errors on the safe side, it is often assumed that $\delta = 0$. On this assumption the Coulomb values for the earth pressures become identical with the Rankine values, provided the bulkhead is vertical. The Rankine values are given by equations 15(2) and (4).

81. Bulkheads with fixed earth support. The lower end of a bulkhead is assumed to be fixed if the depth of penetration of the sheeting is sufficient to produce an elastic line of the type represented in Figure 66*a* by the dashed line *E*. The S-shape of this line represents the combined result of the flexibility and of the deep penetration of the sheet piles. Owing to the fact that the active earth pressure produces bend-

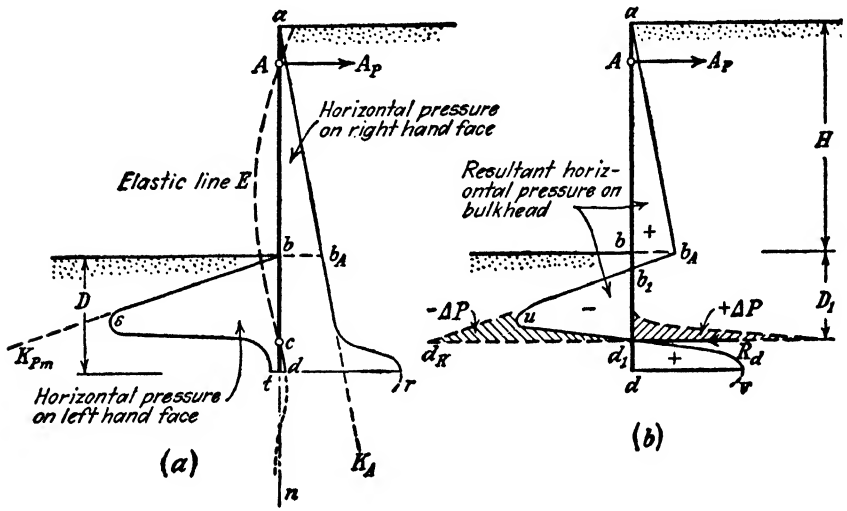

FIG. 66. (*a*) Real and (*b*) assumed distribution of horizontal pressures on the two sides of a bulkhead with fixed earth support.

ing between the anchorage and the earth support, the bulkhead yields toward the left. As a result, passive earth pressure sufficient to maintain the equilibrium of the system is mobilized in the sand adjoining the upper part *bc* of the section *bd* of the sheet piles.

On the other hand, at a greater depth, below some point *c* located between *b* and *d* the sheet piles must deflect to the right of their original position, because if the sheet piles were long enough the elastic line *E* would ultimately become identical with the straight vertical line *an*. This asymptotic approach to *an* can only be accomplished by successive deviations of the elastic line to the left and to the right of *an*, which gradually die out with depth. A deflection of the elastic line toward the left of its original position involves the mobilization of the passive earth pressure on the left side of the sheet piles while the right face is acted upon by the active earth pressure. A deflection toward the right has the opposite effect. In order to ascertain the extreme boundaries for the values which the earth pressure can assume at different depths

below the surface the designers reasoned in the following manner. The smallest value which the earth pressure on the right-hand face of the bulkhead can assume is equal to the active earth pressure. The horizontal component of this pressure is represented by the pressure area anK_A (Fig. 66*a*). The horizontal pressure exerted by the buried part bd of the bulkhead on the adjoining soil should nowhere exceed the horizontal component p_{Pn} of the passive earth pressure divided by the safety factor G_s. At any depth z' below point b the pressure p_{Pn} is

$$p_{Pn} = \gamma z' K_P$$

wherein K_P is the coefficient of passive earth pressure. In order to satisfy the safety requirement the horizontal unit pressure should not exceed

$$p_{Pm} = \frac{1}{G_s} p_{Pn} = \gamma z' K_{Pm}$$

wherein

$$K_{Pm} = \frac{1}{G_s} K_P$$

As a rule it is assumed $G_s = 1$ because there is hardly any danger that a bulkhead with fixed earth support may fail on account of inadequate passive earth pressure. However, the numerical value of G_s has no influence on the following analysis. Therefore the distinction between K_P and K_{Pm} will be retained.

In Figure 66*a* the pressure p_{Pm} is represented by the abscissas of the line bK_{Pm}. No limiting values are needed for the lateral pressure exerted by the section cd of the bulkhead, because this pressure is always very small compared with what the soil can stand.

The effect of the deflection of the bulkhead on the intensity and distribution of the horizontal pressure on the two sides of the bulkhead is shown in Figure 66*a* by the pressure area located between the bulkhead and the line ab_Ard for the right-hand side and by the pressure area $bstd$ for the left-hand side. The resultant pressure per unit of area of the bulkhead is given by the abscissas of the line ab_Auv in Figure 66*b* with reference to the vertical line ad. These abscissas are equal to the algebraic sum of the abscissas of the lines ab_Ar and bst in Figure 66*a*.

Our first problem is to determine the depth to which the piles must be driven in order to get an elastic line similar to that shown in Figure 66*a*. In order to simplify this problem we add to the pressures indicated by the abscissas of the curve b_Auv (Fig. 66*b*) two equal and opposite pressures represented by shaded areas and we replace the entire positive pressure which acts on the lower end of the bulkhead, including the pressure $+\Delta P$ represented by a shaded area, by its resultant R_d per

unit of length of the bulkhead. The point of application of the resultant pressure R_d is located approximately at point d_1. Thus we replace the two real pressure areas b_1ud_1 and d_1vd with curved boundaries by one triangular area $b_1d_Rd_1$ located on the left-hand side of the bulkhead section bd and one concentrated force R_d acting on the right-hand side of this section. The section d_1d of the bulkhead located below the point of application of R_d is assumed to be fixed. The graphical solution of the problem of determining the required depth of penetration of the piles is illustrated by Figure 67.

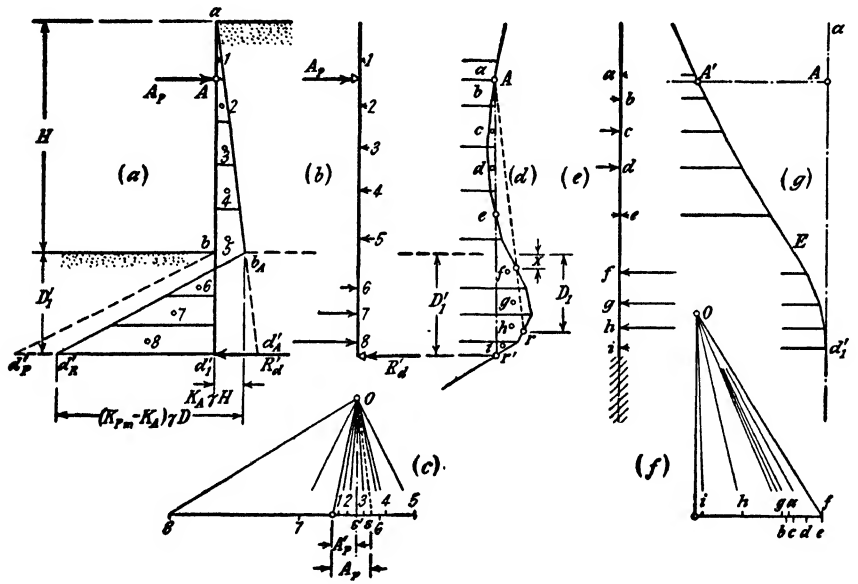

FIG. 67. Elastic line method for computing anchor pull and maximum bending moment in anchored bulkhead with fixed earth support.

At the outset of our investigation the depth D_1 at which point d_1 (Fig. 66*b*) is located is unknown. Hence we are obliged to make a first guess, represented by the value $D_1' = bd_1'$ in Figure 67*a*. Then we replace the continuous system of forces which acts on the bulkhead by a system of individual forces 1 to 8 as shown in Figure 67*b*, draw the polygon of forces shown in Figure 67*c* and the corresponding funicular polygon, Figure 67*d*. The elastic line corresponding to the system of forces shown in Figure 67*a* should intersect the line $d_1'a$ at point A where the anchor rods are attached. In order to find out whether or not this condition is satisfied it is necessary to construct the elastic line. This may be done by the methods of graphic statics. (See for instance

Malcolm 1909). We assume that the areas enclosed by the funicular polygon (Fig. 67*d*) represent horizontal pressures. The area which is located on the left side of the closing line Ar' represents a positive pressure and the area on the right side represents a negative pressure. It is not necessary to make an assumption concerning the absolute value of these pressures because the scale of the forces has no influence on the position of the point of zero deflection. We replace these continuous pressures by a system of individual forces *a* to *i*, as shown in Figure 67*e*, and construct the corresponding funicular polygon shown in Figure 67*g*. This funicular polygon represents the elastic line of the sheet piles. Since the elastic line thus obtained does not pass through point *A* (Fig. 67*g*) we repeat the construction with smaller values of D_1' until we find a value which satisfies the condition that the elastic line passes through point *A* (Fig. 67*g*). The final solution is represented by the closing line *Ar* in the funicular polygon, Figure 67*d*, and by the vector *Os* in the polygon of forces (Fig. 67*c*). The position of point *s* (Fig. 67*c*) also determines the intensity of the anchor pull A_p.

For active earth pressure the angle of wall friction is usually assumed to be equal to zero. In connection with the passive earth pressure of material whose angle of internal friction ϕ is greater than 25°, it is generally assumed that the coefficient of passive earth pressure K_P is equal to twice the corresponding Rankine value, $\tan^2(45° + \phi/2)$. If the angle of internal friction is smaller than 25°, it is assumed that K_P equals the Rankine value. These assumed values are based on the fact that the existence of wall friction more than doubles the value K_P provided that ϕ is greater than 25°. If ϕ is less than 25° the influence of wall friction on the value K_P decreases rapidly with decreasing values of ϕ.

The value D_1 obtained by means of the graphical procedure shown in Figure 67 determines the position of point d_1 in Figure 66*b*. The lower end of the sheet piles is located at point *d*, which is below the point of application d_1 of the pressure R_d. For practical purposes it is admissible to assume without any further investigation that $\overline{dd_1} = 0.2D_1$. Hence the sheet piles should be driven to a depth $D = 1.2D_1$.

82. Equivalent beam method. The equivalent beam method represents a simplification of the elastic line method described in the preceding article. It involves a considerable saving in time and labor at a small sacrifice of accuracy. Figures 68*a* and 68*b* illustrate the principle on which this method is based. Figure 68*a* represents a loaded beam of which one end (*b*) is fixed and the other end (*a*) is simply supported. The corresponding moment curve is shown in Figure 68*b*. The point of inflection of the elastic line is at *c*. If we cut the beam at point *c* and provide a free support at *c* for the left section *ac* of the beam, the bending moments in the section *ac* remain unaltered. The beam *ac* is called the equivalent for the section *ac* of the beam *ab* (Blum 1930).

The application of this reasoning to the design of bulkheads with fixed earth support is illustrated by Figures 68*c* and 68*f*. Figure 68*c* represents the system of forces which act on the bulkhead according to Figure 67*a* and Figure 68*f* shows the corresponding moment curve.

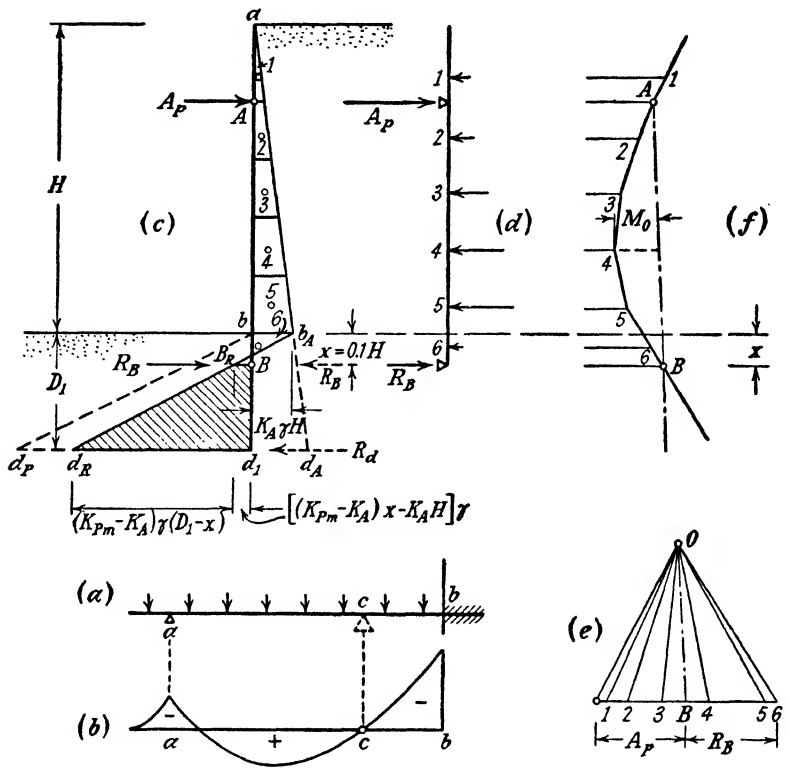

FIG. 68. Equivalent beam method for computing anchor pull and maximum bending moment in anchored bulkhead with fixed earth support.

In order to apply the equivalent beam method to our problem we must ascertain the location of the point at which the bending moment in the sheet piles is equal to zero. This point is identical with the point B in Figure 68*f* at which the closing line intersects the moment curve. It is located at a certain depth x below the original surface of the ground. The bulkhead analysis by means of the elastic line method (Fig. 67) furnishes the following values of x for different values of ϕ:

$\phi =$	20°	30°	40°
$x =$	$0.25H$	$0.08H$	$-0.007H$

The angle of internal friction ϕ of sandy backfills is approximately 30° corresponding to a value of x of about $0.1H$. Hence if both the backfill and the earth on the left-hand side of bd_1 in Figure 68*c* are sandy we are entitled to assume $x = 0.1H$ without risking a serious error. This assumption makes it possible to solve our problem by means of the equivalent beam method, illustrated by Figures 68*a* and 68*b*. After tracing the boundaries $ab_A d_R d_1$ of the pressure areas, we cut the sheet piles at B (Fig. 68*c*) at a depth $x = 0.1H$ below point b. We replace the shearing force at B by a reaction R_B per unit of length of the bulkhead and replace the earth pressure acting on aB by a system of individual forces 1 to 6 as shown in Figure 68*d*. We then construct the polygon of forces (Fig. 68*e*) and the corresponding funicular polygon (Fig. 68*f*) with the closing line AB. By tracing the ray OB in the polygon of forces (Fig. 68*e*) parallel to the closing line AB in Figure 68*f* we obtain the magnitude of the reaction R_B as well as that of the anchor pull A_p as shown in Figure 68*e*. The maximum bending moment M_0 in the sheet piles is determined by the funicular polygon (Fig. 68*f*).

The lower part Bd_1 of the sheet piles (Fig. 68*c*), with a depth $D_1 - x$, is acted upon by the upper reaction R_B, by the earth pressure represented by the pressure area located between $B_R d_R$ and Bd_1 (Fig. 68*c*), and by the lower reaction R_d. The moments about any point, for instance point d_1 in Figure 68*c*, must be equal to zero. This condition requires that

$$\frac{(D_1 - x)^2}{2}(K_{Pm} - K_A)\frac{D_1 - x}{3}\gamma + [(K_{Pm} - K_A)x - K_A H]\frac{(D_1 - x)^2}{2}\gamma = R_B(D_1 - x)$$

Solving this equation we obtain

$$D_1 = \tfrac{3}{2}H\frac{K_A}{K_{Pm} - K_A} - \frac{x}{2} + \sqrt{\frac{6R_B}{(K_{Pm} - K_A)\gamma} + \frac{9}{4}\left(x - H\frac{K_A}{K_{Pm} - K_A}\right)^2} \quad [1]$$

The second term under the root is very small compared with the first one and can be neglected. Hence we can write

$$D_1 = \tfrac{3}{2}H\frac{K_A}{K_{Pm} - K_A} - \frac{x}{2} + \sqrt{\frac{6R_B}{(K_{Pm} - K_A)\gamma}} \quad [2]$$

The sheet piles are driven to a depth $D = 1.2D_1$. The reason has been explained in the preceding section.

83. Comparison of methods of bulkhead computation. When computing the required depth D of penetration by means of the elastic line or the equivalent beam method (Arts. 81 and 82), one obtains for D very much higher values than those corresponding to bulkheads with free earth support (Art. 80). The data contained in the following table serve as an example (Rimstad 1937).

TABLE 1

Method of computation	Depth of penetration D (ft.)	Anchor pull (lbs./ft.)	Max. bending moment (ft.-lbs.)
1. Free earth support (method Fig. 65)	6.0	6300	18,550
2. Fixed support (elastic line method, Fig. 67)	12.0	5180	14,000
3. Fixed support (equivalent beam method, Fig. 68)	12.2	5180	14,000

The height H of the bulkhead to which the data in the table refer is 23 feet and the backfill is supposed to carry a continuous surcharge whose weight is equal to that of a layer of soil 8 feet deep. The results obtained by the elastic line and the equivalent beam method are practically identical. When computing the quantity of steel per linear foot one usually finds that the bulkheads with free earth support require somewhat less steel than those with fixed earth support provided the computation has been made on the basis of the customary assumptions regarding the factor of safety of these two types of bulkheads. However, the fixed earth support has the advantage that it eliminates the possibility of a failure of the bulkhead due to inadequate lateral resistance of the soil adjoining the buried part of the bulkhead.

The nonhydrostatic pressure distribution on bulkheads seems to be associated with a displacement of the point of application of the active earth pressure in an upward direction. Hence when computing the anchor pull on the assumption of a hydrostatic pressure distribution, as was done in Articles 80 to 82, one is likely to underestimate the anchor pull. As a matter of fact, most of the bulkhead failures which came to the author's attention were due to inadequate anchorage. Unfortunately no reliable data regarding the position of the point of application of the earth pressure are available. Pending further advance in our knowledge, it appears advisable to increase the theoretical value of the anchor pull by at least 20 per cent.

84. Anchorage of bulkheads and the resistance of anchor walls. The anchor rods of the bulkheads shown in Figure 63 can be tied to individual blocks supported by battered piles or to walls or plates which are buried in the ground and maintained in their position by the resistance of the adjoining earth against lateral displacement. Figure 69*a* shows an anchor block supported by two battered piles. The force A_p exerted by the tie rod tends to force the left pile deeper into the ground and to pull the right pile out of the ground. The forces P_1 and

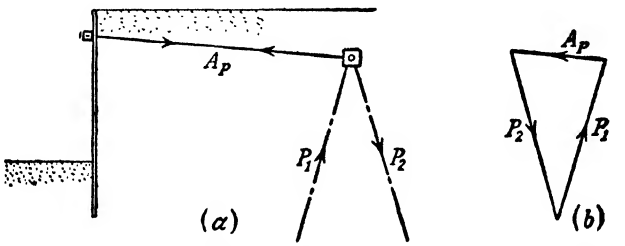

FIG. 69. Anchorage of bulkhead by means of groups of batter piles.

P_2 which act on these piles can be determined by means of the polygon of forces (Fig. 69*b*). The bearing capacity of piles has been discussed in Article 51.

Anchors such as anchor walls and anchor plates which depend for their resistance entirely on the passive earth pressure must be given such dimensions that the anchor pull does not exceed a certain fraction of the pull required to produce failure. The ratio between the anchor pull A_p and the maximum pull which the anchor can stand is called the factor of safety of the anchor.

Figures 70*a* and 70*c* represent vertical sections through anchor walls. If the upper edge of the wall is located at the surface of the ground as shown in Figure 70*a* the failure of the wall due to an excessive pull on the anchor is associated with the rise of a wedge-shaped body of sand *abc* along an inclined surface of sliding *bc*. At the same time active failure occurs behind the wall, involving a slip along an inclined surface of sliding. Since the sand on the left side of the wall yields in an upward direction the vertical component of the passive earth pressure tends to lift the wall out of the ground. This force cannot possibly assume a value greater than the sum of the weight of the wall and its friction along the surface of contact with the active wedge on the right side of the wall. Both the weight and the friction are very small. Hence we assume that the vertical component of the passive earth pressure $P_P \tan \delta$ is almost equal to zero or $\delta = 0$. The corresponding

surface of sliding is almost plane, as shown in Figure 70*a*. If the wall is vertical and δ is equal to zero, the passive earth pressure is determined by the equation

$$P_P = \tfrac{1}{2}\gamma H^2 \tan^2\left(45° + \frac{\phi}{2}\right)$$

If the wall is inclined we can compute the value P_P by means of Coulomb's theory.

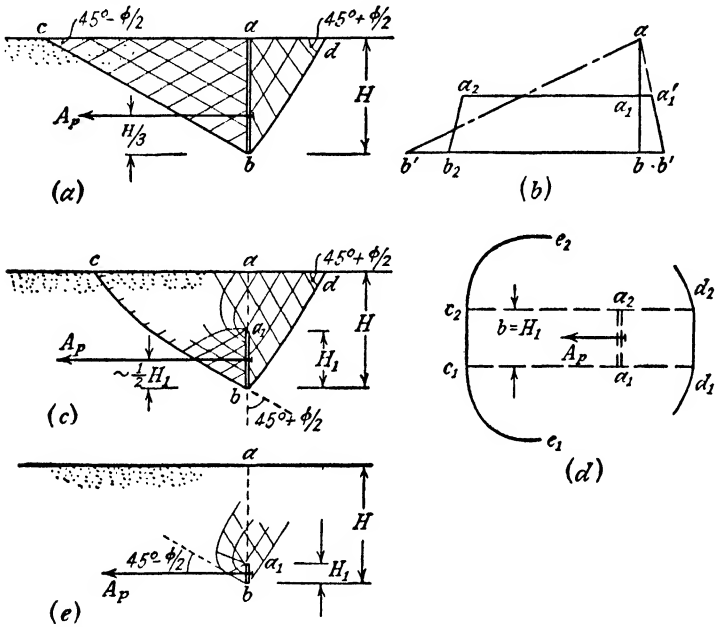

FIG. 70. (*a*) Shear pattern in sand adjoining an anchor wall; (*b*) distribution of pressure on the two sides of *ab* representing the anchor wall in (*a*) and of a_1b representing the wall in (*c*); (*c*) shear pattern in soil adjoining an anchor wall whose upper edge is below the surface of the sand; (*d*) traces of surfaces of sliding on surface of sand after failure of square anchor plate; (*e*) shear pattern in sand adjoining an anchor beam.

In both cases the distribution of the passive earth pressure over the left face of the anchor wall is hydrostatic, provided the anchor rods are tied to the anchor wall at the top of the lower third of its height. For the active earth pressure P_A we can also assume, at least as a first approximation, that δ equals zero, whereupon we obtain for a vertical anchor wall

$$P_A = \tfrac{1}{2}\gamma H^2 \tan\left(45° - \frac{\phi}{2}\right)$$

If A_p is the pull on the tie rods per unit of length of the bulkhead and G_s the specified factor of safety for the anchorage, the depth H of the anchor wall must be chosen so as to satisfy the equation

$$A_p = \frac{1}{G_s}(P_P - P_A) \qquad [1]$$

Figure 70c is a section through an anchor wall whose height is equal to about one half of the depth at which its lower edge is located. The distribution of the earth pressure over the left-hand side of the anchor wall a_1b is shown by the pressure area $a_1a_2b_2b$ in Figure 70b. The anchor pull required to produce a failure of the anchorage is equal to the difference between the passive and active pressure areas, $a_1a_2b_2b$ and $a_1a_1'b'b$ respectively. In Article 15 it has been shown that a plane surface of sliding is associated with a hydrostatic pressure distribution. Since the distribution of the lateral pressure on the sand located on the left side of the vertical section ab in Figure 70c has no resemblance to a hydrostatic pressure distribution, the surface of sliding bc through the lower edge b of the wall cannot be even approximately plane, although the angle of wall friction is practically equal to zero.

Figure 70c also shows the orientation of the surfaces of sliding within the zones of plastic equilibrium on both sides of the anchor wall a_1b. It has no similarity to the shear pattern represented in Figure 70a. An accurate method for computing the ultimate resistance of an anchor wall whose upper edge is located below the surface of the ground is not yet available. However, experience has shown that the difference between the resistance of the two walls shown in Figures 70a and 70c is unimportant provided H_1 (Fig. 70c) is equal to or greater than $H/2$.

As a last case we consider the resistance of an anchor wall (Fig. 70e) whose height is small compared with the depth H. In this case the anchor must be expected to yield by ploughing through the ground without producing a shear failure extending to the surface of the ground. The displacement occurs along curved surfaces of sliding (Fig. 70e) toward the zone of expansion on the right side of the section aa_1 because this is the zone of least resistance against the inflow of displaced material. The force required to pull such an anchor beam with a height H_1 is approximately equal to the bearing capacity of a continuous footing with a width H_1 whose base is located at a depth $H - H_1/2$ below the ground surface. The method of computing the bearing capacity has been described in Article 46.

85. Spacing between bulkhead and anchor wall. The minimum distance between the bulkhead and the anchor wall is determined by the condition that the base fc_2 of the passive wedge adjoining the anchor

wall (Fig. 71*a*) should not intersect the base dc_1 of the active wedge adjoining the bulkhead. If, as shown in Figure 71*c*, this condition is not satisfied, one part of the passive wedge c_1c_2g is located within the active wedge. Within this zone the sand is expanding in a horizontal direction which is incompatible with the passive state. In order to estimate the effect of the superposition of the two zones on the resistance

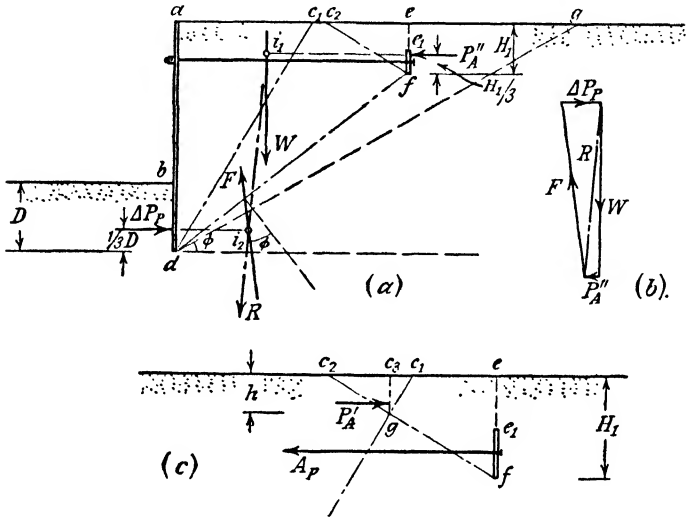

FIG. 71. (*a* and *b*) Conditions for equilibrium of bulkhead anchored to a wall located above the line *dg*, which represents natural slope of sand; (*c*) conditions for equilibrium of anchor wall, if surface of sliding passing through lower edge of anchor wall intersects surface of sliding through lower edge of bulkhead.

of the anchor we investigate the stress conditions on the vertical section c_3g (Fig. 71*c*). If the wedge c_2ef were located entirely outside of the active wedge, the section c_3g would be acted upon by the passive earth pressure.

$$P'_P = \tfrac{1}{2}h^2\gamma \tan^2\left(45° + \frac{\phi}{2}\right) \qquad [1]$$

However, in the case illustrated by Figure 71*c* the pressure on c_3g will not be far from the active pressure.

$$P'_A = \tfrac{1}{2}h^2\gamma \tan^2\left(45° - \frac{\phi}{2}\right) \qquad [2]$$

Hence the inadequate distance between the bulkhead and the anchor wall reduces the resistance of the anchorage approximately by the amount $P'_P - P'_A$.

It is also frequently specified that the upper edge of the anchor wall should be located beneath the slope line dg (Fig. 71a) which rises from the lower edge d of the bulkhead at an angle ϕ to the horizontal. The anchor wall shown in Figure 71a does not satisfy this condition. As a consequence the body of sand $adfe$ has a tendency to slide in a downward direction along the inclined surface of sliding df. This tendency increases the pressure on the earth adjoining the section bd of the bulkhead by an amount ΔP_P over the pressure exerted on this section by a bulkhead with adequate anchorage. The body $adfe$ with a weight W is acted upon by the active earth pressure P_A'', by the supplementary force ΔP_P and by a reaction F which acts on df at an angle ϕ to the normal on df. It is assumed that the force ΔP_P acts in a horizontal direction at a height $D/3$ above the lower edge d of the bulkhead. We also assume that P_A'' acts in a horizontal direction, at $H_1/3$ above f. On these assumptions the intensity of ΔP_P is determined by the polygon of forces shown in Figure 71b (Krey 1936).

If the anchor wall were buried on the right side of the slope line dg (Fig. 71a) the sand on the left side of bd would be acted upon only by the pressure P_{Pm} (Fig. 65b). The inadequate length of the anchorage shown in Figure 71a increases this pressure by ΔP_P.

86. Resistance of anchor plates. If the anchorage shown in Figure 70c consists not of a continuous wall but of individual plates whose width b is equal to their height H_1 the passive failure in the sand adjoining the plate spreads over a width in excess of the width b, as shown in Figure 70d by the line e_1e_2. Before the anchor pull is applied the sand is in a state of rest. The corresponding coefficient of earth pressure is approximately 0.5 and the frictional resistance along any section through the fill is equal to the normal component of the earth pressure at rest times the coefficient of internal friction, tan ϕ. As soon as the anchor pull is applied the horizontal pressure in the sand increases within a roughly cone-shaped zone extending from the anchor plate toward the left. Prior to the application of the anchor pull the total horizontal pressure on the vertical sections represented by the lines a_1c_1 and a_2c_2 through the passive wedge in Figure 70d is equal to the earth pressure at rest, P_0, and the corresponding resistance against sliding along these surfaces is $P_0 \tan \phi$. As the anchor pull increases, the pressure on these two sections and the corresponding resistance to sliding also increases very considerably. Therefore the slip occurs along the outer boundaries of the zone of compression produced by the anchor pull, and the surface of sliding intersects the surface of the fill along a crescent-shaped line e_1e_2 (Fig. 70d). The resistance to sliding along the wide inclined sides of such a surface is undoubtedly greater than

the original resistance against sliding, $2P_0 \tan \phi$, along the vertical sections a_1c_1 and a_2c_2. Hence the admissible pull A_P for each anchor plate is

$$A_P = A_p b + \frac{2P_0}{G_s} \tan \phi \qquad [1]$$

wherein A_p is the admissible anchor pull per unit of length of an anchor wall (eq. 84(1)), G_s is the required factor of safety, and P_0 is the earth pressure at rest on a vertical section through the passive wedge.

Section C

MECHANICAL INTERACTION BETWEEN SOLID AND WATER IN SOILS

Chapter XII

EFFECT OF SEEPAGE ON THE CONDITIONS FOR EQUILIBRIUM IN IDEAL SAND

87. Shearing resistance of saturated sand. The shearing resistance of saturated sand is determined by the equation

$$s = (\sigma - u_w) \tan \phi \qquad 6(5)$$

wherein σ is the total normal stress on the surface of sliding at a given point and ϕ is the angle of internal friction. The neutral stress u_w is equal to the unit weight γ_w of the water times the height h_w to which the water rises in a piezometric tube above the point, or

$$u_w = \gamma_w h_w \qquad 6(1)$$

If the water which occupies the voids of the sand is stationary, it rises at every point to the same level and the piezometric head h_w is equal to the depth of the point below that level. The influence of neutral stresses acting in stationary water on the effective stresses and on the stability of a mass of sand has been described in Articles 8 and 11. On the other hand, if the water percolates through the voids of a sand it rises in piezometric tubes at different points to different levels. In order to determine the neutral stresses due to flowing water it is necessary to take into consideration the hydrostatic conditions which exist along the boundaries of the mass of sand subject to seepage. This is a problem of applied hydraulics. The effect of neutral stresses due to capillary action on the stress conditions for the failure of soils will be discussed in Chapter XIV. In this chapter the capillary forces will be disregarded.

88. Flow of water through soils. The path along which a water particle travels through a mass of soil is called a *flow line.* If the flow lines are straight and parallel the flow is a *linear flow.* The flow of water in a downward direction through a horizontal bed of sand is an

example of this type. If the water particles travel along curves in parallel planes, the flow is two-dimensional. All other types of flow, such as the flow toward wells, are three-dimensional. In connection with foundation problems we are primarily interested in two-dimensional types of flow. The flow of water out of a storage reservoir through the soil located beneath the foundation of a dam belongs in this category.

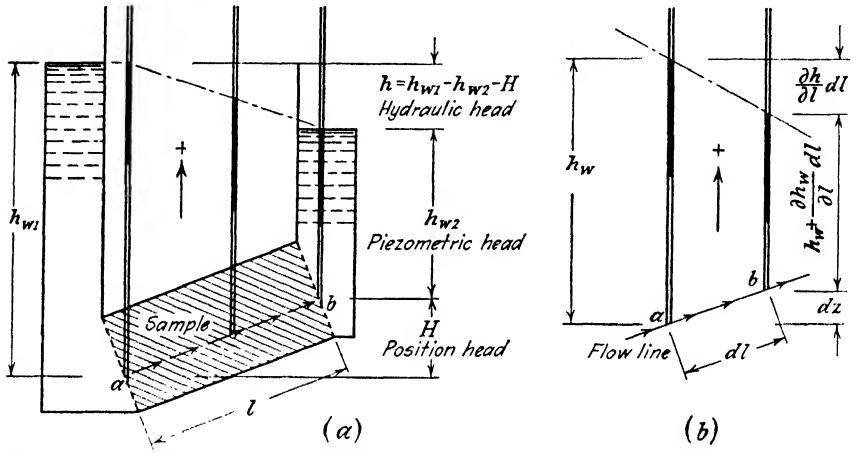

FIG. 72. Meaning of terms and symbols used in theory of seepage if used in connection with (*a*) linear flow and (*b*) two- or three-dimensional flow involving curved flow lines of which *dl* is an element.

Figure 72*a* is a section through one of several types of an apparatus which could be used to establish a linear flow in a soil sample with finite dimensions. The sample is contained in a prismatic box with a length l and a cross-sectional area A. The sides of the box are impermeable. The two ends are perforated to permit free communication between the soil and the adjoining columns of free water. The line ab represents one of the flow lines. The neutral stress at point a is

$$u_{w1} = \gamma_w h_{w1} \qquad [1]$$

and at point b

$$u_{w2} = \gamma_w h_{w2} \qquad [2]$$

If the water stands at the same level in the two piezometric tubes at a and b the water is in a state of rest, although the neutral stresses u_{w1} and u_{w2} may be very different. In order to cause the water to flow through the sand it is necessary to establish a hydraulic head h (Fig. 72*a*) which increases the hydrostatic pressure in one tube by $\gamma_w h$ in excess of the hydrostatic pressure in the other tube at the same level.

This *excess hydrostatic pressure* $\gamma_w h$ represents the force which drives the water through the sand. The ratio

$$i_p = \gamma_w \frac{h}{l} \qquad [3]$$

represents the *pressure gradient* between the points a and b. It has the dimension of a unit weight, gm cm^{-3}. The ratio

$$i = \frac{i_p}{\gamma_w} = \frac{h}{l} \qquad [4]$$

is the *hydraulic gradient.* It is a pure number.

The quantity of water which percolates per unit of time through the unit of area of a section at right angles to the direction of the flow is called the *discharge velocity* v. For fine sands and for soils finer than sand the relation between the pressure gradient i_p, equation 3, and the corresponding discharge velocity v can be expressed almost exactly by the equation

$$v = \frac{K}{\eta} i_p \qquad [5]$$

wherein η (gm cm^{-2} sec) is the coefficient of viscosity of the liquid and K (cm^2) an empirical constant. The value η depends to a certain extent on the temperature of the liquid and the value K on the porosity and on the shape and size of the voids in the porous material. In physics the value K is called the coefficient of permeability. By combining equations 4 and 5 we get

$$v = \frac{K}{\eta} \gamma_w i$$

The only liquid with which the civil engineer has to deal in connection with seepage problems is water. Within the range of temperatures to be encountered under field conditions the values η (viscosity) and γ_w (unit weight) of water are almost constant. Therefore it is customary in civil engineering to assume that both values are constant and to substitute in the preceding equation the value

$$k = \frac{K}{\eta} \gamma_w \qquad [6]$$

whence

$$v = ki = k \frac{h}{l} \qquad [7]$$

The value k is also called the *coefficient of permeability.* However, in

contrast to the value K used by the physicists it has the dimension of a velocity, cm per sec. It represents the discharge velocity for a hydraulic gradient i equal to unity, and the law expressed by equation 7 is called *Darcy's law* (Darcy 1856). According to this law the quantity of water which flows per unit of time through the sample shown in Figure 72*a* is

$$q = Av = Aki$$

In connection with equation 6 it should be emphasized that the permeability characteristics of a porous material are expressed by K (cm^2) and not by k (cm sec^{-1}), because K is independent of the unit weight and the viscosity of the percolating liquid whereas k depends on these factors. The exclusive use of k in this book and in civil engineering in general is justified only by convenience.

Within the sample the water occupies only a volume n per unit of volume of the soil. Therefore the average velocity with which the water particles travel in a direction parallel to the flow lines is

$$v_s = \frac{1}{n} v \qquad [8]$$

which is called the *seepage velocity.*

From the data shown in Figure 72*a* we obtain the following relations. If h_{w1} and h_{w2} represent the piezometric heads at a and b respectively, the hydrostatic head h is equal to

$$h = h_{w1} - h_{w2} - H \qquad [9]$$

and the hydraulic gradient is

$$i = \frac{h}{l} = \frac{h_{w1} - h_{w2}}{l} - \frac{H}{l} \qquad [10]$$

Since $h_{w1} = u_{w1}/\gamma_w$ (eq. 1) and $h_{w2} = u_{w2}/\gamma_w$ (eq. 2), equation 10 can be replaced by

$$i = \frac{1}{\gamma_w} \frac{u_{w1} - u_{w2}}{l} - \frac{H}{l} \qquad [11]$$

If the flow occurs in a vertical direction, H in equations 10 and 11 is equal to l, whence

$$i = \frac{h_{w1} - h_{w2}}{H} - 1 = \frac{1}{\gamma_w} \frac{u_{w1} - u_{w2}}{H} - 1 \qquad [12]$$

A positive value of i indicates that the hydraulic gradient produces a flow in an upward direction.

In Figure 72*b* the line ab represents an element of an arbitrarily curved flow line. The length of the element is dl. At one end a of the element the water rises in a piezometric tube to a height h_w above a and at the other end b it rises to an elevation

$$h_w + \frac{\partial h_w}{\partial l} dl$$

The difference between the elevation of the observation points a and b is dz. Substituting in equation 10

$$l = dl, \quad \frac{h}{l} = -\frac{\partial h}{\partial l}, \quad h_{w1} = h_w, \quad h_{w2} = h_w + \frac{\partial h_w}{\partial l} dl$$

and

$$H = dz$$

we obtain

$$i = -\frac{\partial h}{\partial l} = -\frac{\partial h_w}{\partial l} - \frac{\partial z}{\partial l} \qquad [13]$$

Since

$$u_w = h_w \gamma_w \quad \text{or} \quad h_w = \frac{u_w}{\gamma_w} \quad \text{and} \quad \frac{\partial h_w}{\partial l} = \frac{1}{\gamma_w} \frac{\partial u_w}{\partial l}$$

we can also write

$$i = -\frac{1}{\gamma_w} \frac{\partial u_w}{\partial l} - \frac{\partial z}{\partial l} \qquad [14]$$

The pressure gradient is equal to

$$i_p = -\gamma_w \frac{\partial h}{\partial l} = \gamma_w i \qquad [15]$$

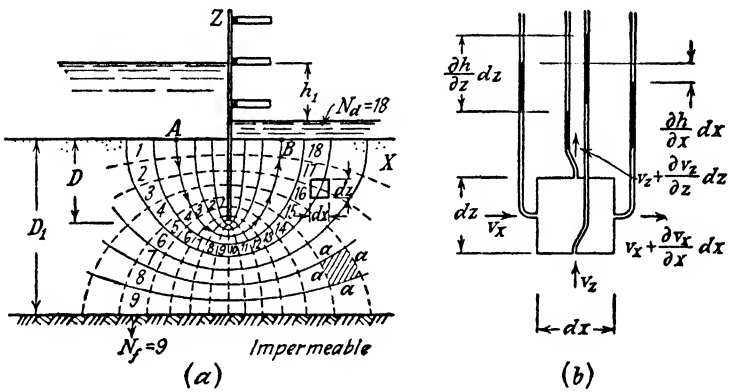

FIG. 73. (*a*) Flow of water through homogeneous sand around lower edge of single row of sheet piles; (*b*) hydrostatic pressure conditions on four sides of prismatic element of sand shown in (*a*).

89. Flow net. Figure 73*a* illustrates the flow of water along curved lines which are parallel to the section shown in the figure. The figure represents a section through an impermeable diaphragm extending to a depth D below the horizontal surface of a homogeneous stratum of soil which rests at a depth D_1 below its surface on an impermeable horizontal base. It is assumed that the difference h_1 between the water levels on the two sides of the diaphragm is constant. On account of the existence of the hydraulic head h_1 the water enters the soil on the upstream side of the diaphragm, flows in a downward direction, and

rises on the downstream side toward the surface. Figure 73*b* shows a prismatic element of the soil on a larger scale. The element is a parallelepiped with sides dx, dy, dz. The flow of the water occurs parallel to the section represented by the figure. Let

v_x = the component of the discharge velocity v in a horizontal direction,

$i_x = -\dfrac{\partial h}{\partial x}$, the hydraulic gradient in a horizontal direction, and

v_z and $i_z = -\dfrac{\partial h}{\partial z}$, the corresponding values for the vertical direction.

The total quantity of water which enters the element per unit of time is equal to $v_x\,dz\,dy + v_z\,dx\,dy$ and the quantity which leaves it is

$$v_x\,dz\,dy + \frac{\partial v_x}{\partial x}\,dx\,dz\,dy + v_z\,dx\,dy + \frac{\partial v_z}{\partial z}\,dz\,dx\,dy$$

If we assume that the water is perfectly incompressible and that the volume occupied by the water within the element remains constant, the quantity of water which enters the element must be equal to the quantity which leaves it. Hence

$$\frac{\partial v_x}{\partial x}\,dx\,dz\,dy + \frac{\partial v_z}{\partial z}\,dz\,dx\,dy = 0$$

or

$$\frac{\partial v_x}{\partial x} + \frac{\partial v_z}{\partial z} = 0 \qquad [1]$$

This equation expresses the condition for the continuity of the flow. According to Darcy's law (equation 88 (7)) the two components of the discharge velocity are

$$v_x = -k\frac{\partial h}{\partial x} \quad \text{and} \quad v_z = -k\frac{\partial h}{\partial z}$$

wherein $-\dfrac{\partial h}{\partial x}$ and $-\dfrac{\partial h}{\partial z}$ represent the hydraulic gradient i in the X and Z directions, respectively.

The product kh is called the *potential* and it is designated by

$$\Phi = kh$$

Hence $v_x = -\dfrac{\partial \Phi}{\partial x}$ and $v_z = -\dfrac{\partial \Phi}{\partial z}$.

Substituting these values in equation 1 we obtain

$$\frac{\partial^2 \Phi}{\partial x^2} + \frac{\partial^2 \Phi}{\partial z^2} = 0 \qquad [2]$$

The solution of this equation can be represented by two sets of curves which intersect each other in every point at right angles. The curves of one set are called the *flow lines* and those of the other one the *equipotential lines*. At every point of an equipotential line the water rises in an observation well to the same elevation. In accordance with this definition the horizontal surface of the ground on the upstream side of the diaphragm represents one equipotential line and that on the downstream side another.

Furthermore the contours of the embedded part of the diaphragm and the section through the base of the permeable stratum represent flow lines. These data constitute the *hydraulic boundary conditions* for the flow of seepage and permit the solution of equation 2. In Figure 73*a* this solution is graphically represented by a flow net which satisfies both equation 2 and the boundary conditions (Forchheimer 1917). In complicated cases the flow net can also be determined graphically, by trial and error, by a hydraulic model test or on the bases of the electric analogue to the process of the flow of seepage. A brief review of all these methods has recently been published (A. Casagrande 1937). Complete treatises on this subject are also available (Muskat 1937).

Figure 74 represents several flow nets to be used as a guide when using the graphical method. For reasons which will be explained in the following article the individual curves which constitute the flow nets are always selected in such a manner that all the fields enclosed between the two sets are approximately square.

Figures 74*a* to 74*d* represent the seepage through a uniformly permeable stratum beneath the base of concrete storage dams with different cross sections. The permeability of the graded filters indicated in Figures 74*c* and 74*d* is assumed to be very great compared with that of the natural soil. Hence the area of contact between the soil and the filters represents the equivalent of a free exit surface. In each of the cases represented by Figures 74*a* to 74*d* the boundaries of the zone of seepage are identical with the boundaries of the permeable stratum. Hence the hydraulic boundary conditions are determined by the section through this stratum and by the position of the free-water levels above it.

Figure 74*e* is a section through a homogeneous earth dam which serves as a storage dam. On the downstream side the embankment rests on a horizontal layer of sand and gravel whose permeability is very great compared with that of the construction material of the dam.

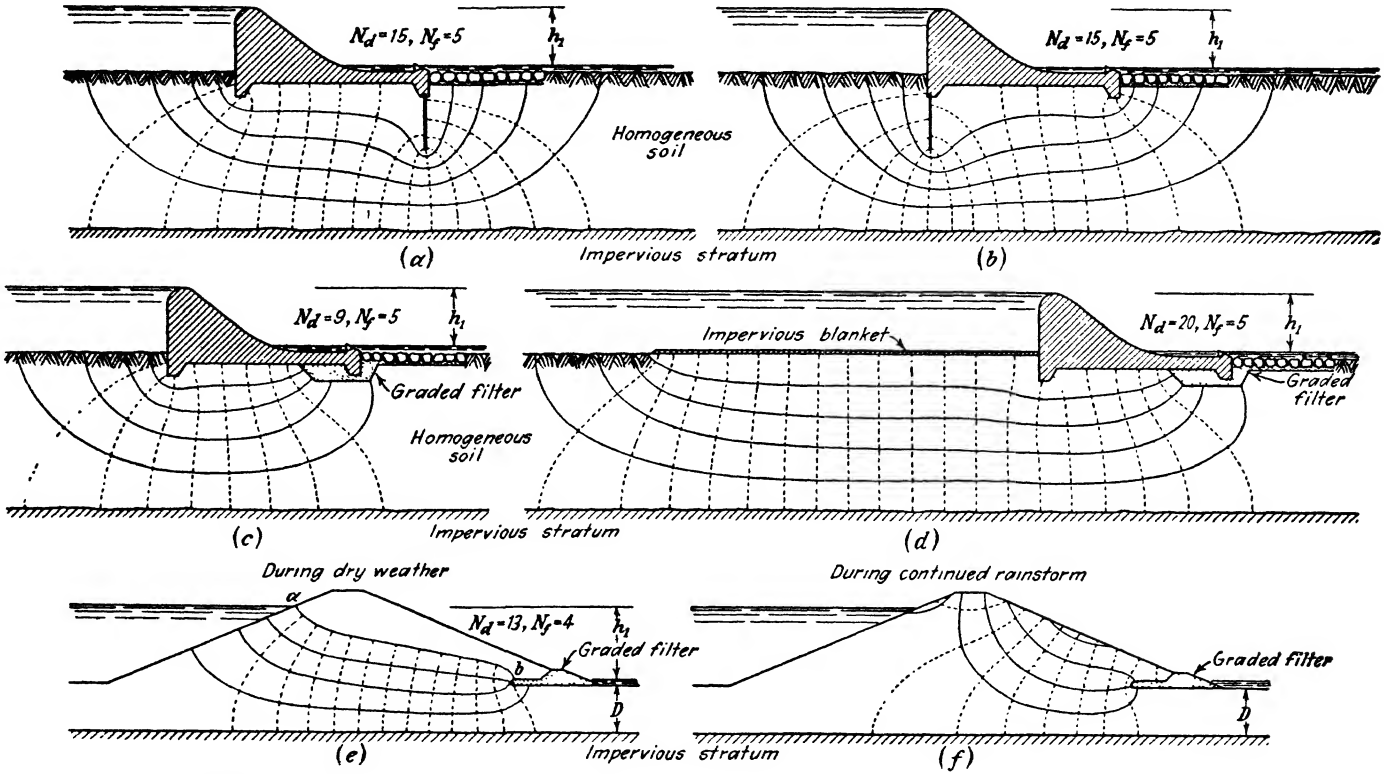

FIG. 74. **(*a* to *d*)** Seepage through homogeneous sand beneath base of concrete dams; (*e* and *f*) seepage through homogeneous dam consisting of very fine, clean sand. (*After C. Casagrande, Trans. Am. Soc., Civil Engrs.*)

Therefore this layer acts as a toe drain. The uppermost flow line *ab* is commonly known as *line of saturation* or *line of seepage.* It represents the upper boundary of the zone of seepage.

The seepage water enters the dam through the upstream slope and it flows toward the left boundary of the drainage layer. The fact that the position of the boundary *ab* is not known in advance complicates the problem of constructing the flow net. However, since this boundary coincides with a flow line, it can be determined graphically, by trial and error (A. Casagrande 1937). The method is based on the assumption that the capillary forces have no influence on the position of the uppermost flow line. In connection with fine-grained soils this assumption is not even approximately justified (see Art. 111). If a homogeneous earth dam consisting of sandy soil is sufficiently watertight to retain the water in a reservoir, a rainstorm is likely to establish a flow of seepage within the entire body of the dam as shown in Figure 74*f*. During the rainstorm the dam is less stable than during a dry spell.

All the flow nets represented in Figure 74 were constructed on the assumption that the soil located within the zone of seepage is hydraulically homogeneous. In other words, it has been assumed that the permeability of the stratum is the same in every direction. In nature almost all accumulations of soil are stratified, i.e., they are composed of successive layers with different coefficients of permeability. Let

$k_1, k_2, \cdots k_n$ = the coefficients of permeability of the individual layers,

$H_1, H_2, \cdots H_n$ = their thickness,

$H = H_1 + H_2 + \cdots + H_n$ the total thickness of the deposit,

k_I = the average coefficient of permeability parallel to the bedding planes, and

k_{II} = the average coefficient of permeability perpendicular to the bedding planes.

If a flow occurs parallel to the bedding planes the flow lines are also parallel to these planes and the hydraulic gradient has at every point of every bed the same value i, which is independent of the coefficient of permeability of the beds. Hence the average discharge velocity is

$$v = ik_I = \frac{i}{H}(k_1H_1 + k_2H_2 + \cdots + k_nH_n)$$

or

$$k_I = \frac{1}{H}(k_1H_1 + k_2H_2 + \cdots + k_nH_n) \qquad [3]$$

On the other hand, if a flow occurs at right angles to the bedding planes every water particle passes in succession through every one of the layers. Since the flow is continuous the discharge velocity v must be the same in every layer, whereas the coefficient of permeability of the layers is different. Hence the hydraulic gradient must also be different in the different layers. Let

$i_1, i_2, \cdots i_n$ = the hydraulic gradient in the individual layers and
h = the total loss of hydraulic head corresponding to a total distance of percolation $H = H_1 + H_2 + \cdots + H_n$.

On the basis of equation 88(7) we obtain

$$v = \frac{h}{H}k_{II} = k_1i_1 = k_2i_2 = \cdots = k_ni_n$$

The solution of these equations is

$$k_{II} = \frac{H}{\frac{H_1}{k_1} + \frac{H_2}{k_2} + \cdots + \frac{H_n}{k_n}} \qquad [4]$$

Comparison of equations 3 and 4 shows that the coefficient of permeability k_{II} of a stratified deposit perpendicular to the bedding planes must always be smaller than the coefficient k_I.

This can be demonstrated in the following manner. We assume that the permeable layer with a total thickness D consists of two homogeneous layers each with a thickness of $\frac{1}{2}D$ and with different coefficients of permeability k_1 and k_2. By means of equations 3 and 4 we obtain

$$k_I = \tfrac{1}{2}(k_1 + k_2), \quad k_{II} = \frac{2k_1k_2}{k_1 + k_2}$$

and

$$\frac{k_{II}}{k_I} = \frac{4k_1k_2}{(k_1 + k_2)^2} = 1 - \left(\frac{k_1 - k_2}{k_1 + k_2}\right)^2$$

Hence k_{II} must be smaller than k_I. Similar results are obtained if the stratum consists of more than two layers with different permeabilities.

All the theoretical methods of computing the flow of seepage through stratified masses of soil are based on the simplifying assumptions that the values k_{II} and k_I are constant but not identical throughout the stratum; in other words, that the stratum is characterized by trans-

verse anisotropy. On this assumption the anisotropy merely causes a linear distortion of the flow net. In order to construct the flow net for an anisotropic medium of this type it suffices to reduce the dimensions of the zone of seepage in a direction parallel to the beds of stratification in the ratio $\sqrt{\frac{k_{II}}{k_I}}$ (Samsiöe 1931). For this distorted section the flow net can be constructed as if the permeable stratum were isotropic. After the construction is finished, we restore to the original scale all

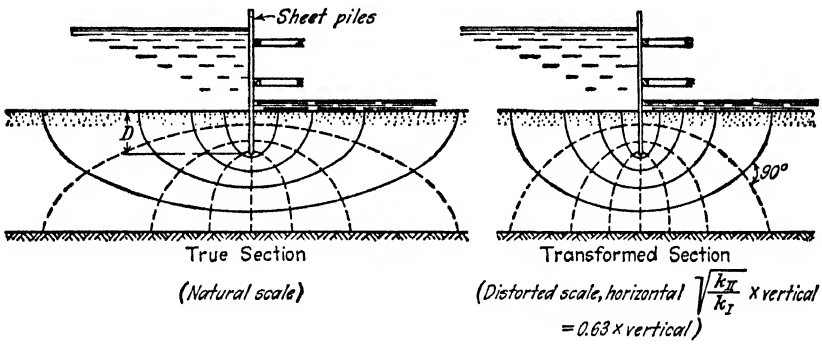

FIG. 75. Construction of flow nets by means of transformed section, if coefficients of permeability of sand in horizontal and vertical directions (k_I and k_{II}) are different.

the dimensions, including those of the flow net. Figure 75 illustrates the procedure. This figure represents a section through a row of sheet piles in a stratified bed of fine sand whose coefficient of permeability k_I in a horizontal direction is equal to 2.5 times the corresponding value k_{II} for a vertical direction. In order to construct the flow net for seepage from a body of free water on the left side of the sheet piles toward the right we multiply the horizontal dimensions of the section by the factor $\sqrt{\frac{k_{II}}{k_I}} = 0.63$ and construct the flow net for the transformed section by means of one of the methods mentioned above. Then we multiply the horizontal dimensions of the net by $\sqrt{\frac{k_I}{k_{II}}} = 1.58$. Thus we obtain the flow net on the left-hand side of Figure 75. The two sets of curves which constitute this flow net do not intersect at right angles.

The reasoning which led to the differential equation 2 can also be applied to the three-dimensional flow of water through a homogeneous,

porous material. Thus one obtains

$$\frac{\partial^2\Phi}{\partial x^2}+\frac{\partial^2\Phi}{\partial y^2}+\frac{\partial^2\Phi}{\partial z^2}=0 \qquad [5]$$

The solution of this equation can be represented by three sets of curved surfaces. The surfaces of one set are surfaces of equal hydrostatic head and correspond to the equipotential lines in the flow net. The water percolates along the lines of intersection between the members of the two other sets. Equation 5 can be solved only in exceptionally simple cases, and there are no convenient graphic or experimental methods comparable to the methods for constructing flow nets. Therefore most of the practical problems involving three-dimensional flow can be solved only by crude approximation, on the basis of more or less arbitrary, simplifying assumptions. Fortunately most of the problems in civil engineering deal with the flow of water parallel to a plane.

90. Rate of percolation. After the flow net has been obtained by means of one of the methods mentioned in the preceding article the rate of percolation can be determined rapidly on the basis of Darcy's law

$$v = ki \qquad 88(7)$$

wherein v is the discharge velocity, k is the coefficient of permeability, and i is the hydraulic gradient. In order to facilitate the procedure the flow net should be plotted in such a manner that the potential drop between two adjacent equipotential lines is a constant

$$\Delta h = \frac{h_1}{N_d} \qquad [1]$$

In this equation, h_1 is the total hydraulic head and N_d is the number of potential drops. The value N_d may be arbitrarily selected. In Figure 73*a* the value N_d was made equal to 18. The successive potential drops are marked 1 to 18.

The flow lines intersect the equipotential lines at right angles. The space between two flow lines is known as a *flow channel.* Since the water particles travel along the flow lines, water neither enters nor leaves a flow channel except through the entrance and the discharge end. However, the width of the channel and the corresponding rate of flow vary throughout the length of the channel.

A section of a flow channel located between two adjacent equipotential lines is a *field* of the flow net. One of these fields, located within the zone of the potential drop No. 15, is marked by a shaded area. If a is the average distance between the two equipotential lines at the site of this field, the average hydraulic gradient within the field is $i = \Delta h/a$

and the quantity of water which flows through the field per unit of time and unit of width of the flow channel is

$$ki = k\frac{\Delta h}{a}$$

If b were the average distance between the boundary flow lines of the field instead of a as shown in Figure 73*a* the quantity of water which flows through the field would be

$$bki = k\Delta h\frac{b}{a}$$

Since the quantity of discharge is the same over the whole length of the flow channel, the ratio b/a must also be a constant. In order to simplify the computation of the rate of percolation we plot the flow net in such a way that the fields are square. As a result, $b/a = 1$. On this condition the discharge per flow channel is equal to

$$\Delta Q = k\Delta h\frac{a}{a} = k\frac{h_1}{N_d} \qquad [2]$$

If N_f is the total number of flow channels, the rate of discharge Q per unit of width of the section shown in Figure 73*a* is

$$Q = kh_1\frac{N_f}{N_d} \qquad [3]$$

Since the fields of the flow net are square the number N_f depends on the number N_d. If we double N_d we also double N_f. In Figure 73*a* the number N_f is equal to 9.

If the stratum is anisotropic, that is, if the coefficient of permeability parallel to the bedding planes is k_I and that perpendicular to the bedding planes is k_{II} we construct the flow net as shown in Figure 75 by means of a transformed section. On the basis of such a flow net the rate of discharge can be computed (Samsiöe 1931) by means of the equation

$$Q = h_1\frac{N_f}{N_d}\sqrt{k_I k_{II}} \qquad [4]$$

The following articles contain examples of the computation of the effect of seepage on earth pressure and on the stability of slopes. For the sake of simplicity the examples will be limited to soils with a negligible cohesion.

91. Effect of rainstorms on the earth pressure on retaining walls. Figure 76*a* represents a section through a gravity retaining wall. The backfill rests on a horizontal impermeable base and is separated from

the back of the wall by a coarse-grained filter layer communicating with weep holes at the foot of the wall. During a rainstorm part of the water which falls on the surface of the backfill enters the backfill and flows through it toward the filter. In the section shown in the figure

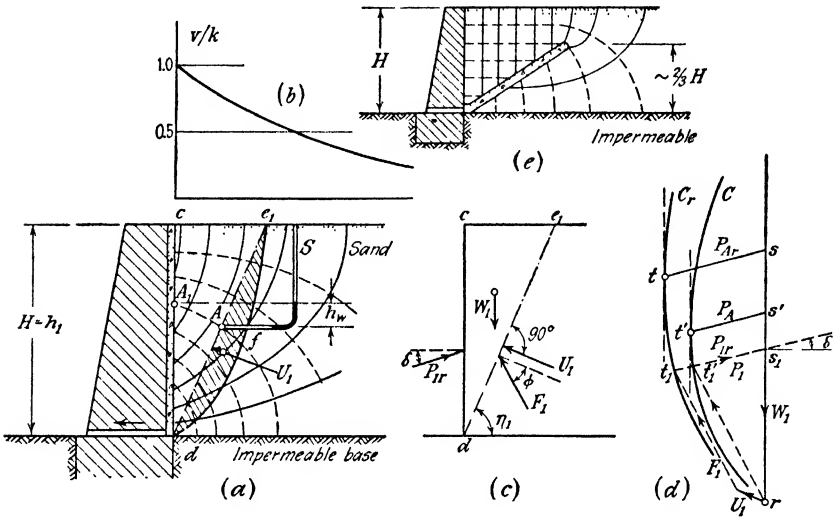

FIG. 76. (*a*, *c*, and *d*) Graphic determination of earth pressure of fine sand during rainstorm on vertical back of retaining wall covered with a coarse sand drainage layer; (*b*) distribution of ratio between seepage velocity at surface and coefficient of permeability over surface of backfill; (*e*) inclined filter layer designed to eliminate increase of earth pressure during rainstorm.

the surface of the backfill represents an equipotential line and the base of the backfill a flow line. At every point of the vertical surface of contact between the backfill and the filter the neutral stress in the water is equal to zero. The flow net shown in Figure 76*a* satisfies all these hydraulic boundary conditions.

According to equation 90(2) the discharge ΔQ per unit of time is the same for every flow channel. The discharge velocity is

$$v = ki = k\frac{\Delta h}{a}$$

wherein Δh is the loss of head during the flow from one equipotential line to the next one and a is the length of the side of a square in the flow net. The water which enters the fill next to point c (Fig. 76*a*) flows almost vertically downward and leaves the ground again at an infinitely small distance dl below c (not shown in the figure). The loss of head is equal to dl and the distance through which the water travels

is also equal to dl. Therefore the hydraulic gradient i is equal to unity and the discharge velocity is

$$v_0 = ki = k$$

wherein k is the coefficient of permeability of the backfill. From point c toward the right the distance between successive equipotential lines increases while the potential drop Δh remains unchanged. The corresponding discharge velocity decreases toward the right, as shown in Figure 76*b*. Therefore, as soon as the intensity v_r of a rainstorm (depth of precipitation per unit of time) approaches the value of the coefficient of permeability k, there will be a continuous flow of water through the backfill toward the filter, and the intensity of the neutral stress u_w in the water is determined for every point of the backfill by the flow net shown in the figure. In humid climates the aforementioned condition is satisfied during every severe rainstorm, provided the value k is equal to or smaller than about 0.002 cm per sec or 2.84 in. per h.

The intensity of the earth pressure exerted by the backfill during the rainstorm can be estimated by adapting Coulomb's method to the problem under consideration (Terzaghi 1936*d*). The unit weight of the backfill, water, and soil combined is γ, and the shearing resistance of the fill is determined by the equation

$$s = (\sigma - u_w) \tan \phi \qquad 6(5)$$

In accordance with Coulomb's procedure we also assume that the surface of sliding is plane. To solve our problem we select an arbitrary plane section de_1 (Figs. 76*a* and 76*c*) through the foot of the fill. The weight of the wedge is W_1, soil and water combined. The wedge is acted upon by the water pressure U_1 perpendicular to the section de_1 by a reaction F_1 at an angle ϕ to the normal on de_1 and by a reaction P_{1r} at an angle δ to the normal on the back of the wall.

The water pressure U_1 represents the resultant of the neutral stresses u_w along the section de_1. According to equation 6(1)

$$u_w = \gamma_w h_w$$

the neutral stress at any point A (Fig. 76*a*) of the section is equal to the unit weight γ_w of the water times the height h_w to which the water rises above that point in a piezometric tube S. This height is equal to the difference in elevation between the point A and the point A_1 where the equipotential curve through A meets the vertical face of the backfill. By plotting the neutral stress u_w at each point of e_1d at right angles to e_1d one obtains the hydrostatic pressure line dfe_1. The pres-

sure area dfe_1 represents the neutral force U_1 and the resultant of this force passes through the center of gravity of the pressure area.

The reaction F_1 (Fig. 76*c*) represents the resultant of the effective stresses on de_1. Therefore it acts at an angle ϕ to the normal on the section de_1. Since the wedge cde_1 is in a state of equilibrium the corresponding polygon of forces (Fig. 76*d*) must be closed. This condition, together with the known direction of the unknown forces F_1 and P_{1r}, determines the intensity of the reaction $P_{1r} = \overline{s_1 t_1}$ (Fig. 76*d*) which is required to prevent a slip along the section de_1 (Fig. 76*a*). After the rainstorm the neutral force U_1 decreases rapidly. Finally, on account of capillary action (see Chapter XV) it becomes negative. If one disregards both the capillary forces and the decrease of the unit weight of the sand due to partial drainage, the lateral force required to prevent a slip along de_1 in Figure 76 becomes equal to $P_1 = \overline{s_1 t_1'}$ in Figure 76*d*.

The position of the surface of sliding can be determined by repeating the construction for different arbitrary sections de_2, de_3, etc., not shown in the figure. The corresponding weights W_2, W_3, etc., are plotted in Figure 76*d* from point r in an upward direction. All the points t_2, t_3, etc., thus obtained (not shown in the figure) are located on a curve C_r. By tracing a tangent to this curve parallel to rs we obtain point t. The distance st represents the active earth pressure on the wall during the rainstorm. The point of application of the earth pressure P_{Ar} is located at an elevation slightly greater than $H/3$ above the base of the fill. The active earth pressure P_A on the retaining wall after the rainstorm can be determined by means of Culmann's method as shown in Figure 76*d*. (See Art. 24.) According to the results of numerical computations the effect of a rainstorm on the intensity of the lateral pressure can be very important in spite of effective drainage of the back of the wall. It has also been found that the rainstorm reduces the slope angle of the potential surface of sliding. If $\gamma = 125$ pounds per cubic foot, $\phi = 38°$, $\delta = 15°$, and $H = 24$ feet, the computation furnishes the following results:

Before rainstorm	$P_A = 3.6$ tons per ft	$\eta = 62°$
During rainstorm	$P_A = 4.8$ tons per ft	$\eta = 54°30'$

The customary methods of computing retaining walls disregard the effect of rainstorms on the earth pressure. Yet, as shown by the above data, a rainstorm may increase the earth pressure by as much as 33 per cent. Hence it is not surprising that the failure of retaining walls usually occurs during heavy rainstorms. The preceding analysis shows the fallacy of the current opinion that such failures are necessarily due to inadequate drainage of the back of the wall.

According to Figure 76*a* the effect of the rainstorm on the earth pressure is due to the curvature of the equipotential lines which in turn produces during the rainstorm a hydrostatic pressure along the potential surfaces of sliding through the foot of the wall. If the filter is inclined as shown in Figure 76*e*, all the equipotential lines within the sliding wedge are horizontal. Hence the hydrostatic pressures are eliminated and the earth pressure during rainstorms is reduced to the value obtained by means of the customary methods of computation.

92. Effect of rainstorms and of tides on the stability of anchored bulkheads. The methods of designing bulkheads described in Chapter XI are based on the assumption that the shearing resistance of the soil is determined by the equation

$$s = \sigma \tan \phi \qquad 5(2)$$

wherein σ is the effective normal stress on the potential surfaces of sliding. In other words it has been assumed that the neutral stresses are negligible. If a bulkhead is fairly permeable, owing, for instance, to the existence of open joints between the individual sheet piles, a rainstorm may cause an increase of the active earth pressure on the upper part of the bulkhead, but it does not reduce the passive resistance of the soil which supports the lower part. On the other hand, if the bulkhead is practically watertight because the joints between the sheet piles have been silted up or because the bulkhead is made of reinforced concrete members with grouted interstices a rainstorm causes a flow of water from the backfill through the soil beneath the sheet piles into the soil which supports the lower part of the bulkhead. Such a case is illustrated by Figure 77*a* representing a section through a bulkhead driven into a stratum of very fine sand which rests on an impermeable base at some depth below the lower edge of the sheet piles. Before the rainstorm the water table is located at the level of the plane *ed*. The flow net represents the hydraulic conditions which prevail during the storm. It has been constructed on the assumption that the permeability of the backfill is identical with that of the natural sand stratum and that the bulkhead is perfectly watertight.

The shearing resistance of the sand is determined by the equation

$$s = (\sigma - u_w) \tan \phi \qquad 6(5)$$

The neutral stresses u_w can be determined from the flow net as explained in the preceding article in connection with the backfill of a retaining wall. They increase the active earth pressure on the upper part of the bulkhead and reduce the resistance of the sand against the lateral pressure exerted by the lower part of the bulkhead. At every

point the neutral stress u_w is equal to the unit weight of the water, γ_w, times the height to which the water rises at that point in a piezometric tube. As an example of the application of this method we determine the neutral stress at the points a_1 and a_2 located on the second equipotential curve (Fig. 77*a*). If N_d is the total number of potential drops between the entrance and the exit surface, the loss of head associated with the flow from one equipotential line to the next is

$$\Delta h = \frac{h_1}{N_d} = \frac{h_1}{10} = \frac{H}{10}$$

and the loss of head between the surface and the line a_1a_2 is $2\Delta h$. Hence the neutral stress at point a_1 is $\gamma_w(z_1 - 2\Delta h)$ and at point a_2 is

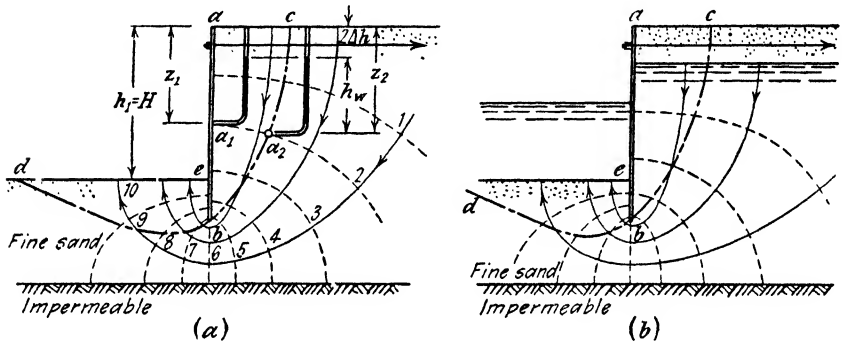

FIG. 77. (*a*) Seepage through mass of fine sand supported by watertight bulkhead, during rainstorm; water table is located at *ed*; (*b*) flow of water through sand behind bulkhead at seacoast during receding tide.

$\gamma_w(z_2 - 2\Delta h)$. In this manner we can determine the neutral stress along any section through the sand, for instance along the potential surfaces of sliding *bc* and *bd* (Fig. 77*a*). These stresses increase the active earth pressure on the upper part of the bulkhead and reduce the resistance of the lateral sand support on the lower part. Both effects tend to reduce the factor of safety of the bulkhead. The computation of the factor of safety can be accomplished by combining one of the methods described in Chapter XI with the method explained in the preceding article.

Figure 77*b* is a section through an impermeable bulkhead located at a seacoast with considerable tidal variations. The soil conditions are assumed to be identical with those shown in Figure 77*a*. While the tide is rising, the water flows from the sea into the backfill through the space between the bottom of the sheet piles and the impermeable base of the sand stratum. This flow increases the resistance of the earth

support and the factor of safety of the bulkhead. On the other hand, while the tide recedes, the opposite phenomenon takes place, as indicated in the figure. It increases the active pressure on the upper part of the bulkhead and reduces the resistance of the earth support of the lower part.

On account of the decisive influence of the aforementioned flow phenomena on the factor of safety of bulkheads, no bulkhead should be designed without a previous investigation and analysis of the possible sources and the mechanical effects of a temporary flow of water from the backfill toward the seat of the sand support of the lower part of the bulkhead. At a given section through the bulkhead the flow pattern depends to a large extent on the details of the stratification of the natural sand deposit and on the ratio between the average coefficient of permeability of the natural deposit and of the backfill. Neither one of these data can accurately be ascertained. Hence the analysis should be based on the most unfavorable possibilities which are compatible with the results of the soil investigations. In most cases it will be possible to eliminate the major part of the harmful effects of rainstorms or of tidal variations by measures of drainage, as illustrated for retaining walls by Figure 76*e*.

93. Effect of seepage on the stability of slopes. Figure 78*a* is a section through a homogeneous earth embankment consisting of a fine-grained soil with a negligible cohesion. The shearing resistance of the soil is determined by the equation

$$s = (\sigma - u_w) \tan \phi \qquad 6(5)$$

wherein σ is the total normal stress and u_w the neutral stress on the potential surface of sliding. The embankment is assumed to rest on the surface of a practically impermeable stratum. Fine-grained soils remain almost saturated for long periods of time, with the result that the unit weight γ of soil and water combined has a practically constant value. During the dry season the water is held in the voids by capillary forces, associated with negative values of the neutral stresses u_w (see Chapter XIV). Since negative stresses in the water raise the factor of safety of the embankment over the value corresponding to $u_w = 0$, the neutral stresses in existence during the dry season will be disregarded in the following analysis.

During heavy rainstorms rain water enters the embankment through the crest and the upper part of the slopes and leaves the embankment through the lower part of the slopes. The excess over the quantity which can seep through the voids of the soil flows down on the surface of the slopes. The hydraulic boundary conditions for con-

structing the flow net shown in Figure 78*a* are as follows: The base of the section through the embankment and the line of symmetry of the section are flow lines. The crest is an equipotential line, and at any point along the slopes the neutral stress is equal to zero.

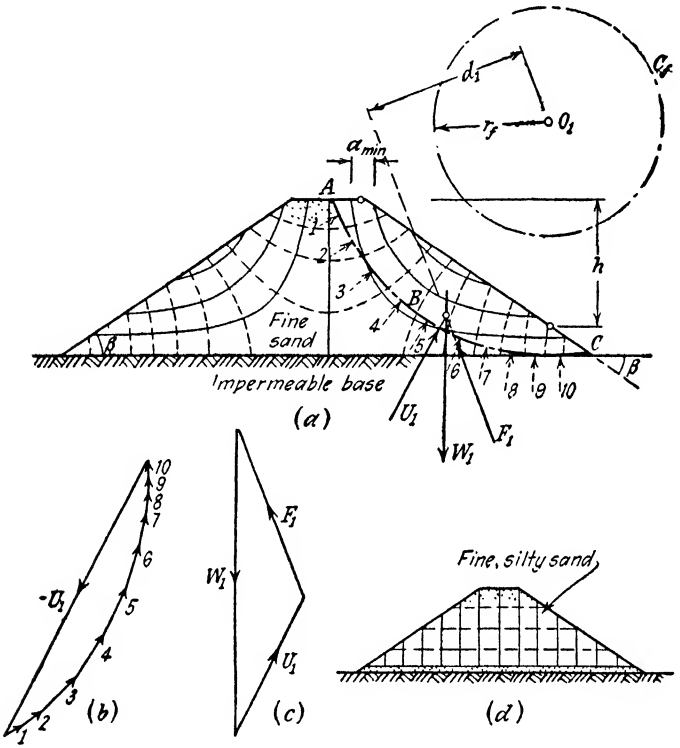

FIG. 78. (*a*) Seepage through fill made of fine sand, during heavy rainstorm; (*b* and *c*) polygons of forces required for stability computation by means of friction circle method; (*d*) method of preventing failure during rainstorm by means of a coarse-grained filter covering the base of the fill.

In order to maintain a stationary flow through the embankment, the intensity v_r of the rainstorm (quantity of precipitation per unit of time and unit of area of a horizontal surface) must be sufficient to maintain the stationary flow determined by the flow net. The quantity of water, ΔQ, which flows between two adjoining flow lines is the same for every flow channel (see Art. 90). Hence the quantity of rain water which must be fed into the channels per unit of time and per unit of area of the intake surface is greatest where the width of the channels at the surface is smallest. This condition is realized along the edges of the crest of the embankment, where the distance between two adjoining

flow lines is smallest and equal to $a_{\min}$. The total loss of head for the corresponding flow channel is equal to h as shown in Figure 78*a*, and the potential drop is

$$\Delta h = \frac{h}{N_d} \qquad 90(1)$$

wherein N_d is the number of drops within the channel. At the entrance to the channel, with a width $a_{\min}$, the hydraulic gradient is

$$i = \frac{\Delta h}{a_{\min}}$$

and the quantity of water which must be fed into the channel per unit of time and unit of area is

$$v = ki = k\frac{\Delta h}{a_{\min}} = \frac{k}{a_{\min}}\frac{h}{N_d}$$

Hence the condition for maintaining the flow indicated in Figure 78*a* is

$$v_r \leqq \frac{k}{a_{\min}}\frac{h}{N_d} \qquad [1]$$

In humid climates this condition is satisfied for every embankment whose coefficient of permeability k is smaller than that of a very fine sand.

The influence of the rainstorm on the factor of safety of the slopes can be determined by means of the friction circle method described in Chapter IX. Prior to the rainstorm the neutral stresses are assumed to be equal to zero. Since the cohesion is negligible the critical circle in that state is identical with the slope line (see Art. 60) and the factor of safety with respect to sliding is

$$G_s = \frac{\tan\phi}{\tan\beta}$$

wherein β is the slope angle, Figure 78*a*.

During the rainstorm the radius of the critical circle assumes a finite value and the position of the circle with reference to the slope can only be determined by trial and error. For this purpose we assume an arbitrary circle tangent to the firm base of the embankment. The center of this circle is located at O_1 and the corresponding friction circle, with a radius r_f, is marked C_f. The tentative surface of sliding ABC (Fig. 78*a*) represents the seat of neutral stresses

$$u_w = \gamma_w h_w \qquad 6(1)$$

wherein h_w is the height to which the water rises in a piezometric tube

at the point of observation as shown for instance in Figures 76*a* and 77*a*. The resultant U_1 of the neutral stresses on ABC can be determined by means of a polygon of forces (Fig. 78*b*). The line of action of U_1 passes through the center O_1 of the circle, parallel to U_1 in the polygon in Figure 78*b*. The weight W_1 of the body of soil (solid and water combined) is counterbalanced by two forces, U_1 and F_1, as shown in the polygon of forces in Figure 78*c*. One of them, U_1, is known. It represents the resultant of the water pressure which acts on the surface ABC. The second force, F_1, represents the resultant of the effective stresses on ABC. In Figure 78*a* the force F_1 must pass through the point of intersection between the forces U_1 and W_1. The distance between the prolongation of the line representing the force F_1 and the center O_1 is d_1. Since the tendency of the slope to slide increases with increasing values of d_1 the ratio r_f/d_1 can be regarded as a measure of the safety of the slope with respect to sliding. If $d_1 = r_f$ the reaction is tangent to the friction circle and the corresponding factor of safety is equal to $r_f/d_1 = 1$. For $d_1 = 0$ the factor of safety is equal to infinity. Hence we can assume that the factor of safety during the rainstorm, with respect to a slip along ABC, is

$$G_{sr} = \frac{r_f}{d_1}$$

In the case illustrated by Figure 78*a* the value G_{sr} is smaller than unity, although the surface ABC does not necessarily correspond to a critical circle. Hence along the critical circle a slide is likely to occur before the rainstorm has established the state of stationary flow represented by the flow net shown in Figure 78*a*. On the other hand, if G_{sr} is found to be greater than unity we must repeat the investigation for other circles. The position of the critical circle is determined by the condition

$$G_{sr} = \frac{r_f}{d_1} = \text{minimum}$$

If we insert a coarse-grained filter immediately beneath the base of the embankment all the equipotential lines become horizontal and the flow lines vertical, as shown in Figure 78*d*; consequently the neutral stress at every point of the embankment is equal to zero. Hence the presence of the filter layer prevents rainstorms from reducing the stability of the slopes. This arrangement is a cheap and simple measure to increase the stability of road or railroad fills.

The graphic method of computation illustrated by Figure 78*a* can also be used without modification for determining the factor of safety

of earth dams acted upon by seepage flowing out of a storage reservoir (Fig. 74*e*) or of earth dams consisting of sandy soils with some cohesion provided the clay content of the soil is very low. Once the flow net is constructed it suffices to determine the neutral force U_1 (Fig. 78*a*), and to combine it with the weight W_1 of the earth located above the potential surface of sliding.

The preceding method of computation is based on the assumption that the water content of the soil adapts itself almost instantaneously to a change in the state of stress in the embankment. Therefore it cannot be applied to dams or fills made out of a compressible material with a low permeability such as clay.

94. Mechanics of piping and the critical head. Figure 79*a* is a section through a single-wall cofferdam. It consists of a row of sheet piles which are supported laterally by wales and struts. The subsoil is assumed to consist of a stratum of gravel with a thickness D_1 and a stratum of fine, dense, homogeneous sand with a thickness D_2. The coefficient of permeability of the upper stratum is very large compared to that of the lower one. The sheet piles penetrate the lower stratum

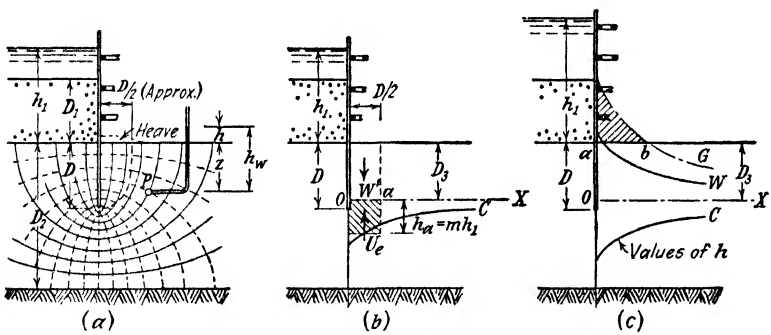

FIG. 79. Graphic determination of factor of safety of homogeneous sand with respect to piping. Danger of piping is produced by pumping from excavation pit which is surrounded by single-wall cofferdam. (*a*) Flow net; (*b*) neutral and effective forces which act on sand within zone of potential heave; (*c*) method of determining filter load required to maintain a given degree of safety.

to a depth D below its surface. After the sheet piles are driven, the soil located within the cofferdam above the surface of the lower stratum is removed by dredging and the water is pumped out of the space surrounded by the cofferdam. Outside the cofferdam the water level retains its original position. Therefore the pumping causes a flow of water through the soil toward the bottom of the excavation. On account of the high permeability of the top stratum, with a thickness D_1, the flow occurs as if this stratum were non-existent. The flow net shown

in Figure 79*a* was constructed on the assumption that the flow of seepage toward the bottom of the excavation is approximately two-dimensional.

From model tests we know that the sand adjoining the sheet piles remains in equilibrium provided the hydraulic head h_1 is smaller than a certain critical value (Terzaghi 1922). However, as soon as this critical value is approached the discharge increases more rapidly than the head, indicating an increase of the average permeability of the sand. Simultaneously the surface of the sand rises within a belt with a width of approximately $D/2$, as shown in Figure 79*a*, and finally a mixture of sand and water breaks through the space located below the sheet piles. This phenomenon is called *piping*, and the hydraulic head at which piping takes place is *the critical head* h_p. Piping beneath a cofferdam is likely to cause a failure of the cofferdam. Our problem is to determine the factor of safety with respect to piping of the cofferdam shown in Figure 79*a* after the water level has been lowered within the cofferdam to a depth h_1 below the outside water level.

The process described in the preceding paragraph suggests that the piping is initiated by an expansion of the sand between the buried part of the sheet piles and a distance of about $D/2$ downstream from the sheet piles. This expansion is followed by an expulsion of the sand out of this zone. No such phenomenon could occur unless the water pressure overcame the weight of the sand located within the zone of expulsion. With sufficient accuracy we can assume that the body of sand which is lifted by the water has the shape of a prism with a width $D/2$ and a horizontal base at some depth D_3 below the surface. The rise of the prism is resisted by the weight of the prism and by the friction along the vertical sides of the prism. At the instant of failure the effective horizontal pressure on the sides of the prism and the corresponding frictional resistance are practically zero. Therefore the prism rises as soon as the total water pressure on its base becomes equal to the sum of the weight of the prism, sand and water combined. The head h_p at which the body is lifted is the critical head. The elevation of the base of the body is determined by the condition that h_p should be a minimum because piping occurs as soon as the water is able to lift a prism of sand regardless of where its base is located. Figure 79*b* shows the base at an arbitrary depth D_3.

In order to determine the water pressure which acts on the base of the prism we begin by investigating the state of stress in the water at an arbitrary point P (Fig. 79*a*). The stress in the water or the neutral stress at point P is equal to the height h_w to which the water rises above that point in a piezometric tube multiplied by the unit weight γ_w of the

water. The height h_w can be divided into two parts, z and h, and the neutral stress at P is

$$u_w = z\gamma_w + h\gamma_w \qquad [1]$$

The first part, $z\gamma_w$, represents the hydrostatic uplift (Art. 8). Its mechanical effect consists in reducing the effective unit weight of the sand from γ to the submerged unit weight γ'. The second part, $h\gamma_w$, is the excess hydrostatic pressure in the water with reference to the free-water level on the downstream side and h is the hydrostatic head at point P with reference to this level. Therefore the condition for the rise of the prism of sand shown in Figure 79*b* is that the total excess hydrostatic pressure on the base of the prism should be greater than the submerged weight of the prism, which in turn is equal to $\frac{1}{2}DD_3\gamma'$.

The excess hydrostatic pressure at any point P (Fig. 79*a*) within the zone of seepage can be determined from the flow net. According to the theory of flow nets (Art. 89) the potential drop Δh representing the loss of head associated with flow of water from one equipotential line to the next one is

$$\Delta h = \frac{h_1}{N_d}$$

wherein N_d is the total number of fields in one flow channel. Hence the hydrostatic head h at point P is equal to

$$h = n_d \Delta h = \frac{n_d}{N_d} h_1 \qquad [2]$$

wherein n_d is the number of fields in the flow channel through point P between the point P and the discharge end of the channel. By means of this equation we are able to determine the distribution of the hydrostatic head h over the base of the prism shown in Figure 79*b*. It is represented in the scale of the drawing by the ordinates of the curve C. The average hydrostatic head on the base Oa of the prism is h_a and the total excess hydrostatic pressure on this base is

$$U_e = \tfrac{1}{2}\gamma_w D h_a$$

The hydrostatic head h at any point in the sand is determined by equation 2

$$h = \frac{n_d}{N_d} h_1 = h_1 \times \text{constant}$$

wherein the constant factor n_d/N_d merely depends on the position of the point in the flow net. Therefore the ordinates of the curve C

increase in simple proportion to the head h_1 and the corresponding average head h_a can be expressed by a product

$$h_a = mh_1 \qquad [3]$$

wherein m is independent of the head. The values h_a and h_1 can be measured in the drawing. Hence the value of the ratio $m = h_a/h_1$ can be computed.

In order to lift the prism the excess hydrostatic pressure U_e on the base Oa of the prism must be equal to the submerged weight of the prism, $\frac{1}{2}DD_3\gamma'$ or

$$\tfrac{1}{2}Dh_a\gamma_w = \tfrac{1}{2}DD_3\gamma'$$

whence

$$h_a = D_3\frac{\gamma'}{\gamma_w} \qquad [4]$$

At the instant when the prism rises, the head h_1 in equation 3 is equal to the critical head h_p. Substituting mh_p for h_a in equation 4 we get

$$mh_p = D_3\frac{\gamma'}{\gamma_w}$$

or

$$h_p = \frac{D_3}{m}\frac{\gamma'}{\gamma_w} \qquad [5]$$

The investigation can be repeated for different horizontal sections through the sand, which are located at different depths D_3 below the bottom of the pit. The critical head is determined by the condition h_p = minimum, and the horizontal section to which this minimum refers is the critical section. It represents the lower boundary of the mass of sand subject to lifting in the initial state of the piping phenomenon. For the simple row of sheet piles represented in Figure 79*b* an investigation has shown that the critical section passes almost exactly through the lower edge of the sheet piles, or $D_3 = D$. On the other hand, if the buried part of a water-retaining structure consists of several rows of sheet piles or of one row of sheet piles located at the downstream edge of a concrete dam as shown in Figures 74*a* to 74*d* the location of the critical section must be determined by trial, which requires repetition of the construction represented in Figure 79*b* for different horizontal sections.

According to equation 4 the critical head h_p for a given water-retaining structure is practically independent of the angle of internal friction

of the sand, and it increases in simple proportion to the submerged unit weight of the sand. The agreement between the computed values of h_p and the values obtained by experiments with clean sand is very satisfactory.

At a given hydraulic head h_1 the factor of safety G_s against piping is determined by the ratio between the submerged weight W' of the body of sand located above the strip Oa (Fig. 79*b*) and the water pressure U_e or

$$G_s = \frac{W'}{U_e} = \frac{\frac{1}{2}DD_3\gamma'}{\frac{1}{2}h_aD\gamma_w} = \frac{h_p}{h_1} \qquad [6]$$

The preceding analysis was based on the assumption that the subsoil of the water-retaining structure is hydraulically isotropic. In practice it is always necessary to take the stratification of the subsoil into consideration. Since the stratification has a decisive influence on the flow net it also determines to a large extent the factor of safety.

95. Effect of loaded filters on the critical head and on the factor of safety. If the factor of safety of a proposed dam foundation with respect to piping through a permeable substratum is inadequate we are compelled to increase the factor of safety by constructive measures. This can be accomplished simply and cheaply by utilizing the relation expressed by the equation

$$G_s = \frac{W'}{U_e} \qquad 94(6)$$

According to this equation the factor of safety is equal to the ratio between the submerged weight of the body of sand adjoining the downstream face of the sheet piles in Figure 79*b* and the excess hydrostatic pressure U_e which tends to lift this body. In order to increase the factor of safety it is sufficient to increase the weight W' without changing the pressure U_e. The increase of W' can be obtained by applying a surcharge on the surface through which the water flows out of the sand. In order to prevent the surcharge from producing a change in the flow net and a corresponding increase of the pressure U_e we must introduce an inverted filter between the sand and the base of the surcharge. The filter should be coarse enough to permit a practically unrestricted escape of the water out of the sand and yet fine enough to prevent the escape of soil particles through the bottom layer of the filter. If these two conditions are satisfied the surcharge has no influence on the pressure U_e.

The method of determining the magnitude and the distribution of the surcharge required to obtain a given factor of safety is illustrated by Figure 79*c* for the single-wall cofferdam shown in Figure 79*a*. Our

problem is to determine the surcharge required to prevent the factor of safety from dropping below a given value G_s while the water level rises during the highwater period to an elevation h_1 above the water level within the cofferdam. OX represents the critical section, and the ordinates h of the curve C represent the height of a layer of water whose weight is equal to the excess hydrostatic pressure on the critical section. By plotting above the line OX the values $h\gamma_w/\gamma'$ we obtain the curve W. This curve represents the upper boundary of an imaginary mass of earth with a unit weight γ' whose weight is equal to the excess hydrostatic pressure on the critical section. In order to establish a factor of safety G_s with respect to piping, the pressure on the critical section due to the submerged weight of the earth and the surcharge should be equal to G_s times the total excess hydrostatic pressure on the base of the prism. By multiplying the ordinates of the curve W by G_s we get the curve G (Fig. 79c). In order to obtain a factor of safety G_s we must charge the section ab of the surface of the sand with a weight equal to the shaded area times the submerged weight γ' of the sand.

Experiments have shown that a uniformly distributed surcharge has practically the same effect on the critical head as the surcharge represented by the shaded area in Figure 79c provided that the width of the uniform surcharge is approximately equal to the width ab of the base of the shaded area. Since the surcharge is located above the water level the effective unit weight of the surcharge is roughly equal to twice the submerged unit weight γ'. Hence the cross-sectional area of the required surcharge would be approximately equal to about one half that of the shaded area.

96. Lateral pressure on sheet pile cut-offs. Figure 80a is a section through the lowest part of the row of sheet piles shown in Figure 79. The abscissas of the curve cd with reference to the vertical line ab represent the water pressure on the left face of the sheet piles and those of the curve ac_1 the water pressure on the right side. The figure demonstrates that the buried part of the sheet piles is acted upon by an unbalanced water pressure ΔU represented by the shaded area in Figure 80b tending to bend the sheet piles toward the right. This water pressure combines with the active earth pressure $\overline{P}_A$ exerted by the sand located on the left side of the sheet piles. The curves ac and de can be constructed by means of the flow net as described in Article 94, and the active earth pressure $\overline{P}_A$ can be computed graphically by means of the method described in Article 91. The resistance of the sand to a yield of the sheet piles by tilting about point a in Figure 80a cannot exceed the effective part $\overline{P}_P$ of the passive earth pressure of the sand located on the right-hand side of ab in Figure 80a. This pressure can

be estimated by means of equation 14(2). Setting $P_P = \overline{P}_P$, $H = D$, $\gamma = \gamma''$, and $N_\phi = \tan^2 (45° + \phi/2)$ in this equation we obtain

$$\overline{P}_P = \tfrac{1}{2}\gamma'' D^2 \tan^2 \left(45° + \frac{\phi}{2}\right)$$

The quantity γ'' contained in this equation represents the submerged unit weight γ' of the sand reduced by the average seepage pressure per unit of volume of the mass of sand adjoining the right-hand face of the sheet piles.

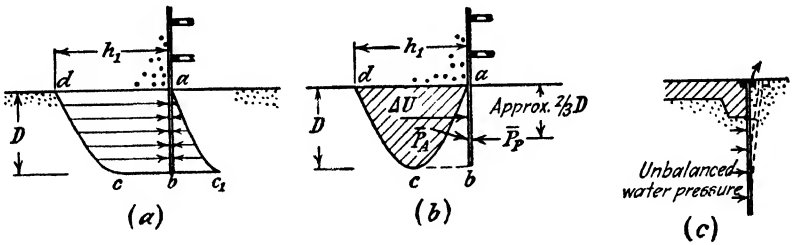

FIG. 80. (*a*) Water pressure on the two sides of buried part of single-wall cofferdam during pumping; (*b*) unbalanced water pressure, equal to difference between water pressures indicated in (*a*); (*c*) conditions for failure due to piping on account of inadequate bond between concrete apron of a dam and the adjoining sheet piles.

As soon as the hydraulic head h becomes equal to the critical head h_p the effective weight of the prism of sand located above *Oa* in Figure 79*b* becomes equal to zero and the average unit weight γ'' of the sand located within this prism also becomes equal to zero. The height D_3 of the prism is approximately equal to D. Therefore the condition $\gamma'' = 0$ prevails practically throughout the mass of sand located in the vicinity of the sheet piles on the right-hand side of *ab* in Figure 80*a*. Setting $\gamma'' = 0$ in the preceding equation we get

$$\overline{P}_P = 0$$

Hence, as the hydraulic head approaches the critical value h_c the passive earth pressure of the sand on the right side of the sheet piles approaches the value zero; whereupon the forces $\overline{P}_A$ and ΔU on the left-hand side of the sheet piles are resisted only by the bending strength of the sheet piles. On account of this condition it is conceivable that the sheet piles fail by bending before the sand on the right side of the sheet piles is actually lifted by the water pressure.

If a sheet pile cut-off is located at the downstream toe of a concrete structure, as shown in Figure 80*c*, the unbalanced water pressure on the upstream face of the sheet piles combined with the active earth pressure

on this face is likely to push the sheet piles away from the concrete unless the upper part of the sheet piles is firmly anchored in the concrete. If a gap opens up between the sheet piles and the concrete a mixture of sand and water escapes through this gap and the structure fails at a hydraulic head which is very much smaller than that required to lift the sand located on the downstream side of the sheet piles. Since the connection between the sheet piles and the concrete has seldom received the attention which it deserves, it is by no means impossible that some dams have failed owing to a break in this connection and the consequent piping through the gap. Failures due to piping usually occur within a very short time, and the destruction is so complete that it is practically impossible to reconstruct after the accident the real cause of events.

The value $\overline{P}_P$ of the passive earth pressure also determines the bearing capacity of the sand which supports the dam. As the value $\overline{P}_P$ approaches zero the ultimate bearing capacity of the sand located on the left side of the sheet piles also approaches the value zero, and it is conceivable that a dam may fail on account of inadequate support although the sand beneath the dam may be firm and dense.

The preceding examples illustrate the various mechanical effects of seepage which tend to produce failure of dams on permeable foundations. On account of the variety of conditions which are likely to be encountered in actual practice no general rules can be established. Yet, in every special case the effect of the flow of seepage on the theoretical factor of safety of the structure can be estimated on the basis of the general principles established in Articles 87 to 94. The real factor of safety depends on details of stratification and other minor geologic factors which cannot be determined in advance. Therefore the results of an analysis pertaining to the safety of a structure with respect to piping always requires subsequent verification or modification on the basis of the results of water pressure measurements to be performed during construction or during the period when hydraulic head is applied for the first time. Whatever the results of such an investigation may be, it is usually possible to eliminate the existing sources of danger by appropriate measures of drainage or by means of the loaded filters described in the preceding article.

Chapter XIII

THEORY OF CONSOLIDATION

97. Fundamental conceptions. In the preceding chapter on seepage and seepage effects it was assumed that the volume occupied by the water per unit of volume of the soil is independent of the state of stress in the soil. If this condition is satisfied the quantity of water which flows out of an element of the soil such as that shown in Figure 73*b* is equal to the quantity of water which enters the element, regardless of whether or not the state of stress in the soil changes. This condition, known as the continuity condition, is expressed in mathematical terms by the differential equation 89(1). There is no real soil which strictly satisfies the continuity condition, because every change in the state of stress produces a certain change in the volume of voids, Δn, per unit volume of the soil. Yet, if the soil is very permeable and not very compressible, the change of the porosity due to a change in the state of stress in the soil can usually be disregarded.

A change in the effective stresses in a highly compressible soil, such as a clay or a sand-mica mixture, is likely to produce an important change Δn in the volume of voids n. Hence if the voids of such a soil are completely filled with water and remain in that state a change in the effective stresses involves a change in the water content of the soil. Every process involving a decrease of the water content of a saturated soil without replacement of the water by air is called a *process of consolidation.* The opposite process is called a *process of swelling*, which involves an increase of the water content due to an increase of the volume of voids.

A further complication arises if a soil combines high compressibility with low permeability. Both of these properties are exhibited to a high degree by fat clays. In soils with such characteristics, changes in the water content due to changes in the state of stress take place very slowly, because the low permeability of the soil does not permit a rapid transfer of the water from one part of the mass of soil to another or to an adjoining highly permeable stratum. This phenomenon produces a time lag between a change of the external forces which act on a feebly permeable, compressible stratum and the corresponding change of the water content of the soil. It is the principal cause of the pro-

gressive settlement of foundations on clay and of many other processes of outstanding practical importance. The theories which deal with these processes are called *theories of consolidation.* Like all the other theories of soil mechanics and of structural engineering they are based on simplifying assumptions. Hence the results represent only approximations to reality.

98. Assumptions involved in the theories of consolidation. With few exceptions all the existing theories of consolidation are based on the following assumptions: the voids of the soil are completely filled with water; both the water and the solid constituents of the soil are perfectly incompressible; Darcy's law is strictly valid; the coefficient of permeability k is a constant; and the time lag of consolidation is due entirely to the low permeability of the soil. The theories contained in the following articles are based on the following supplementary assumptions, unless a departure from these assumptions is specifically mentioned. The clay is laterally confined; both the total and the effective normal stresses are the same for every point of any horizontal section through the clay and for every stage of the process of consolidation; an increase in the effective pressure from an initial value $\bar{p}_0$ to a final value $\bar{p}$ reduces the void ratio of the clay from an initial value e_0 to a final value e; the ratio

$$a_{vc} = \frac{e_0 - e}{\bar{p} - \bar{p}_0} \text{ gm}^{-1}\text{cm}^2 \qquad [1]$$

is assumed to be a constant for the range of pressure $\bar{p}_0$ to $\bar{p}$. It is called the *coefficient of compressibility.* If the effective pressure is reduced from an initial value $\bar{p}$ to a final value $\bar{p}'$ the void ratio increases from an initial value e to a final value e'. The ratio

$$a_{vs} = \frac{e' - e}{\bar{p} - \bar{p}'} \qquad [2]$$

is also assumed to be a constant for the range of pressure $\bar{p}$ to $\bar{p}'$. It is called the *coefficient of elastic recovery.*

From equation 1 we obtain

$$e_0 - e = a_{vc}(\bar{p} - \bar{p}_0) \qquad [3]$$

The quantity $e_0 - e$ represents the decrease of the volume of the voids in a block of soil with the initial volume $1 + e_0$. The initial void ratio e_0 corresponds to a volume of voids per unit of volume of soil $n_0 = e_0/(1 + e_0)$ and the final void ratio e to $n_{01} = e/(1 + e_0)$. Therefore the decrease Δn of the volume of voids per unit of the initial

volume of the soil is

$$\Delta n = n_0 - n_{01} = \frac{a_{vc}}{1 + e_0} (\bar{p} - \bar{p}_0) = m_{vc} (\bar{p} - \bar{p}_0) = m_{vc} \Delta \bar{p} \qquad [4]$$

wherein $\Delta \bar{p}$ is the increase of the effective unit pressure. The value

$$m_{vc} = \frac{a_{vc}}{1 + e_0} \text{ gm}^{-1}\text{cm}^2 \qquad [5]$$

is the *coefficient of volume decrease.* The corresponding value for a process of swelling due to a reduction of the effective pressure is

$$m_{vs} = \frac{a_{vs}}{1 + e_0} \qquad [6]$$

which is called the *coefficient of volume expansion.* If there is no possibility of a misunderstanding the second subscript on the symbols a_v and m_v will be omitted.

The preceding assumptions determine the physical properties ascribed to the ideal clay which constitutes the subject of the subsequent theoretical investigations. Equations 1 to 3 represent a crude approximation of the relation between the effective pressure on a real clay in a state of complete lateral confinement and the corresponding void ratio. For this reason the theories based on equations 1 to 3 can be applied only to processes in which the lateral deformation of the consolidating bed of clay is small compared with the strain in a vertical direction. Owing to the assumed absence of stress variations on horizontal sections the flow of water within the clay takes place only along vertical lines and is therefore an example of linear flow. In actual practice the stress distribution over horizontal sections is never perfectly uniform, but in many cases the resulting error can be disregarded.

99. Differential equation of the process of consolidation of horizontal beds of ideal clay. Figure 81 is a section through a stratum of ideal clay on an impermeable horizontal base. Let

e_0 = the initial void ratio,
a_{vc} = the coefficient of compressibility (eq. 98(1)),
m_{vc} = the coefficient of volume decrease (eq. 98(5)),
k = the coefficient of permeability,
γ_w = the unit weight of the water, and
H = the initial thickness of the bed of clay.

The clay is buried beneath a bed of highly permeable sand, and the water table is located at an elevation h_0 above the surface of the clay. At the outset of our investigation the clay is assumed to be in a

state of hydraulic equilibrium. On this assumption the water would rise in a piezometric tube I from any point of any horizontal section mn in the clay up to the water table at a height h_0 above the surface of the clay. For the corresponding neutral stress u_w we obtain

$$u_w = \gamma_w(H + h_0 - z)$$

wherein $H + h_0 - z$ represents the piezometric head which is equal to the vertical distance between the section mn and the water table. By

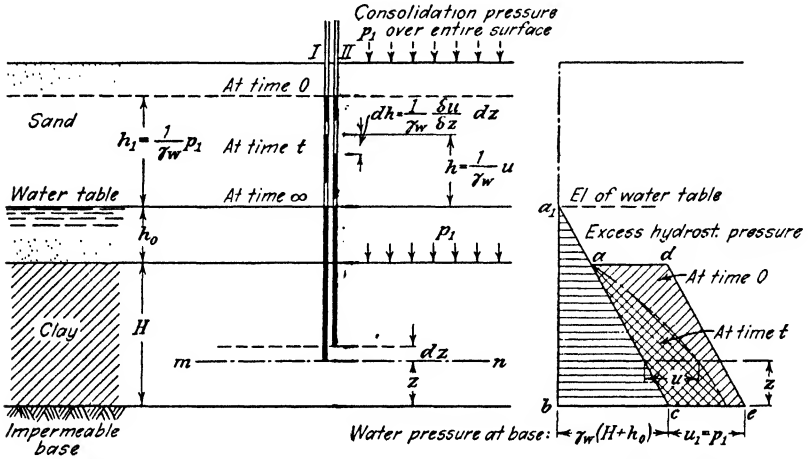

FIG. 81. Excess hydrostatic pressure in pore water of clay due to sudden application of uniformly distributed surcharge.

plotting this stress horizontally from the reference line a_1b the line a_1c has been obtained. The total normal stress on mn is equal to the weight p_0 of the clay, sand and water located above a unit area of mn. The effective normal stress on mn is

$$\bar{p}_0 = p_0 - u_w$$

If we apply a uniformly distributed surcharge p_1 per unit of area of the surface of the sand which extends in every direction to infinity, the total normal stress on the surface of the clay and on any horizontal section mn through the clay increases by p_1. This increase of the total stress is represented in the Figure 81 by the shaded area *aced*, whose width $ad = ce$ is equal to p_1. The supplementary pressure p_1 consolidates the clay. At the end of the process of consolidation the entire surcharge p_1 is transmitted from grain to grain and the neutral stresses are identical with those represented by the abscissas of ac. This means that the surcharge ultimately increases the effective normal stress on every horizontal section by p_1. The normal stress p_1 is called the *consolidation*

stress or the *consolidation pressure* because it is responsible for the process of consolidation.

If the consolidation pressure is due to some cause other than a uniformly distributed surcharge, it may change with depth within the clay. In any event, for any horizontal section through the clay the consolidation pressure is equal to the difference between the effective normal stress on the section after consolidation and the effective normal stress on the same section prior to the application of the surcharge.

However, on account of the low permeability of the clay the process of consolidation proceeds very slowly. Immediately after the surcharge p_1 is applied, the void ratio of the clay is still equal to e_0, which indicates that the effective stresses remain equal to $\bar{p}_0$; yet the total normal stress on the horizontal section has been increased by p_1. Hence, at the outset of the process of consolidation the entire surcharge p_1 per unit of area is carried by a neutral stress of equal intensity which indicates that the pressure in the water has increased from its initial value u_w to $u_w + p_1$. The temporary increase u of the hydrostatic pressure represents the excess hydrostatic pressure (see Art. 88). At the instant when the load p_1 is applied the excess hydrostatic pressure on any horizontal section mn through the clay is equal to p_1. As a consequence the water rises in a piezometric tube (I in Fig. 81) to a height

$$h_1 = \frac{p_1}{\gamma_w}$$

above the water table. As time goes on, the excess hydrostatic pressure decreases and the water level in the piezometric tube goes down. If, at a time t, the excess hydrostatic pressure is equal to u, the water stands in the piezometric tube at a height

$$h = \frac{u}{\gamma_w} \qquad [1]$$

above the water table. Finally the excess hydrostatic pressure becomes equal to zero and the surface of the water in the piezometric tube arrives at the elevation of the free ground water level. Yet, at any time the sum of the added effective normal stress $\bar{p} - \bar{p}_0$ produced by the surcharge and the excess hydrostatic pressure u is equal to p_1 or

$$u + \bar{p} - \bar{p}_0 = p_1$$

whence

$$u = p_1 - \bar{p} + \bar{p}_0 \qquad [2]$$

The decrease of the excess hydrostatic pressure per unit of time is equal to

$$\frac{\partial u}{\partial t} = -\frac{\partial \overline{p}}{\partial t} \qquad [3]$$

The increase of the effective normal stress by $\partial \overline{p}/\partial t$ per unit of time involves a corresponding decrease in the volume of voids n of the clay. The relation between $\overline{p}$ and n is determined by equation 98(4)

$$n_0 - n = m_{vc}\,(\overline{p} - \overline{p}_0)$$

from which we obtain

$$\frac{\partial \overline{p}}{\partial t} = -\frac{1}{m_{vc}}\frac{\partial n}{\partial t}$$

Combining this equation with equation 3 we get

$$\frac{\partial n}{\partial t} = m_{vc}\frac{\partial u}{\partial t}$$

Since the voids of the clay are assumed to be completely filled with water the value $-\partial n/\partial t$ represents the quantity of water which is squeezed out of the clay at depth $H - z$ per unit of time and per unit of volume. The quantity which is squeezed out of a slice with thickness dz is equal to

$$-\frac{\partial n}{\partial t}dz = -m_{vc}\frac{\partial u}{\partial t}dz$$

per unit of time and unit of the area of the slice. It joins the quantity which enters the slice through its base mn. Hence, if v is the discharge velocity at the section mn, the velocity v increases in an upward direction over the distance dz by

$$\frac{\partial v}{\partial z}dz = -\frac{\partial n}{\partial t}dz = -m_{vc}\frac{\partial u}{\partial t}dz \qquad [4]$$

This equation is nothing more than a mathematical expression of the fact that the difference $\frac{\partial v}{\partial z}dz$ between the quantity of water which leaves the element per unit of time and that which enters it must be equal to the quantity $-\frac{\partial n}{\partial t}dz$ which is squeezed out of the element per unit of time.

The discharge velocity v is determined by the hydraulic gradient i and by the coefficient of permeability, k, of the clay. At the surface of the

clay the excess hydrostatic pressure is always equal to zero. This means that the water in a piezometric tube at the surface of the clay never rises higher than h_0. On the other hand, in the piezometric tubes shown in Figure 81, the water rises immediately after the application of the surcharge to an elevation h_1 and as consolidation proceeds the water level goes down again. At any time t it stands at an elevation h above the initial level. With increasing values of z, h decreases and for $z = H$, h is equal to zero. At depth $H - z$ and at a time t the corresponding hydraulic gradient is

$$i = -\frac{\partial h}{\partial z} = -\frac{1}{\gamma_w}\frac{\partial u}{\partial z}$$

Darcy's law requires that the discharge velocity v be equal to

$$v = ik = -\frac{k}{\gamma_w}\frac{\partial u}{\partial z} \qquad [5]$$

The rate of change of v in a vertical direction is

$$\frac{\partial v}{\partial z} = -\frac{k}{\gamma_w}\frac{\partial^2 u}{\partial z^2}$$

Combining this equation with equation 4, we obtain

$$\frac{\partial u}{\partial t} = \frac{k}{\gamma_w m_{vc}}\frac{\partial^2 u}{\partial z^2} \qquad [6]$$

This is the differential equation of the process of consolidation of horizontal beds of clay on the assumptions specified in the preceding article. (Terzaghi 1923.) To simplify this equation we substitute

$$\frac{k}{\gamma_w m_{vc}} = c_{vc} \qquad [7]$$

and obtain

$$\frac{\partial u}{\partial t} = c_{vc}\frac{\partial^2 u}{\partial z^2} \qquad [8]$$

The coefficient c_{vc} is called the *coefficient of consolidation*. A reduction of the load on a bed of clay causes the clay to swell. In this case the coefficient c_{vc} must be replaced by the *coefficient of swelling*

$$c_{vs} = \frac{k}{\gamma_w m_{vs}} \text{ cm}^2 \text{ sec}^{-1} \qquad [9]$$

where m_{vs} is the coefficient of volume expansion (eq. 98(6)). If there is no doubt whether the coefficient of consolidation applies to a process of compression (c_{vc}) or of swelling (c_{vs}), the second subscript will be omitted.

All the quantities contained in this equation are independent of the initial hydrostatic head h_0. Therefore it will be assumed in each of the following investigations that the initial hydrostatic head h_0 is equal to zero.

Every process of consolidation involves the transition of the excess water from a state of rest into a state of movement. In the derivation of equation 8 the energy required to overcome the inertia of the water was neglected. One investigator objected to this omission and claimed that it invalidates the results, whereupon a rigorous solution was found which takes the forces of acceleration into account (Heinrich 1938). This solution demonstrated that the error involved in the original solution does not exceed a few tenths of one per cent.

100. Thermodynamic analogue to the process of consolidation. If we assume $\gamma_w = 1$, equation 99(6) becomes identical with the differential equation for the non-stationery, one-dimensional flow of heat through isotropic bodies, provided we assign to the symbols in the equation the following physical meaning:

Theory of consolidation	*Symbol*	*Thermodynamics*
Excess hydrostatic pressure	u	Temperature
Time	t	Time
Coefficient of permeability	k	Coefficient of heat conductivity
Coefficient of volume change	$\frac{a_v}{1+e_0} = m_v$	Heat capacity times unit weight
Coefficient of consolidation or swelling	c_v	Diffusivity

The loss of water (consolidation) corresponds to the loss of heat (cooling) and the absorption of water (swelling) to an increase of the heat content of a solid body. The existence of the thermodynamic analogue is useful in two different ways. First of all it eliminates in some cases the necessity of solving the differential equation 99(6) because a great variety of solutions has already been obtained in connection with thermodynamic problems. Second, in contrast to the phenomena of consolidation and swelling, the processes of cooling and heating are familiar to everybody from daily experience. Therefore the knowledge of the existence of the analogue facilitates the visualization of the mechanics of consolidation and swelling.

The case represented by Figure 81 may serve as an example. It involves the consolidation of a bed of clay on an impermeable base due to the sudden application of a surcharge p_1 per unit of area. At the instant of the load application the excess hydrostatic pressure in the water content of the clay rises in every point of the loaded stratum from its initial value zero to a value $u_0 = p_1$ represented by the width of the

cross-shaded area *aced*. As time goes on the excess hydrostatic pressure gradually decreases and finally becomes equal to zero. The thermodynamic analogue to this case is the gradual cooling of a plate with a thickness H after the temperature has been raised at every point from zero degrees to u_0 degrees. The base of the plate is insulated and the surface remains in contact with air whose temperature is maintained at zero degrees. The cooling of the plate proceeds at a decreasing rate from the exposed surface toward the insulated bottom. On the basis of the thermodynamic analogue we may conclude that the consolidation of the bed of clay will proceed at a decreasing rate from the surface toward the impermeable base of the stratum. The equations which describe this process will be derived in the following article.

Mathematical analogues also exist between consolidation processes in general and the following physical processes: Diffusion of substances dissolved in liquids, diffusion of gases, propagation of electric currents in cables, and movement of solid bodies through a stationary viscous liquid (Terzaghi and Fröhlich, 1936).

101. Excess hydrostatic pressures during consolidation. The excess pressure u in the water contained in consolidating beds of clay is determined by the differential equation 99(8). Solving this equation for u we obtain u as a function of the time t and the elevation z,

$$u = f(t, z) \qquad [1]$$

The character of this function depends on the type and the rate of the change of stress which causes the consolidation and on the location of the surface or surfaces through which the excess water can escape from the clay. In their totality these factors determine the conditions to be satisfied by the solution of equation 99(8). Figure 81 illustrates the consolidation of a bed of clay with a thickness H due to a suddenly applied surcharge p_1 per unit of area. This surcharge instantaneously produces on every horizontal section through the clay a consolidation stress with the intensity p_1. The excess water can escape through the upper surface only. At the instant of load application, $t = 0$, the void ratio of the clay has not yet changed, but the total normal pressure on every horizontal section has increased by p_1. Therefore at time $t = 0$ the excess hydrostatic pressure is equal to $u = p_1$ throughout the layer. At any time t, such that $0 < t < \infty$, the excess hydrostatic pressure at the surface, where $z = H$, is equal to zero because there is no obstruction against the escape of the excess water out of the clay adjoining the surface. At the bottom of the layer, where $z = 0$, the discharge velocity v is always equal to zero, because no water comes

out of the impermeable base of the clay. Since

$$v = -\frac{k}{\gamma_w}\frac{\partial u}{\partial z} \qquad 99(5)$$

we obtain for the bottom of the layer ($z = 0$)

$$\frac{\partial u}{\partial z} = 0$$

After a time infinity the excess pressure in the water is everywhere equal to zero. These conditions can be condensed into the following set of equations. For

$$t = 0 \quad \text{and} \quad 0 \leqq z < H, \qquad u = p_1 \qquad [2a]$$

$$0 \leqq t \leqq \infty \quad \text{and} \quad z = 0, \qquad \frac{\partial u}{\partial z} = 0 \qquad [2b]$$

$$0 \leqq t \leqq \infty \quad \text{and} \quad z = H, \qquad u = 0 \qquad [2c]$$

$$t = \infty \quad \text{and} \quad 0 \leqq z \leqq H, \qquad u = 0 \qquad [2d]$$

On the basis of these conditions the solution of the differential equation can be accomplished by means of Fourier's series.

The solution of the problem illustrated by Figure 81 led to the following results:

$$u = \frac{4}{\pi} p_1 \sum_{N=0}^{N=\infty} \frac{1}{2N+1} \sin\left[\frac{(2N+1)\,\pi z}{2H}\right] \epsilon^{-(2N+1)^2\pi^2 T_v/4} \qquad [3a]$$

wherein ϵ is the base of natural logarithms and

$$T_v = \frac{c_v}{H^2} t = \frac{k}{\gamma_w m_v}\frac{t}{H^2} \qquad [3b]$$

represents an independent variable, called the *time factor*. It has the dimension of a pure number.

In order to visualize the distribution of the excess hydrostatic pressure u (eq. 3*a*) within the consolidating bed of clay we make an inclined section *ab* (Fig. 82) through the clay which rises at an angle of 45° to the horizontal and establish at some point m of this section a piezometric tube. If u is the excess hydrostatic pressure at point m, the water rises in the tube to an elevation $h = u/\gamma_w$ (eq. 99(1)) above the original ground-water level at elevation h_0, as shown in Figure 81. Since h is independent of the position of the ground-water table, we assume $h_0 = 0$ and plot the value h from the top surface of the clay in an upward direction. The point thus obtained is located on a curve which is

called an *isochrone*. An isochrone is the locus of the levels to which the water rises in piezometric tubes from different points of the inclined section *ab* at any one time. The difference between the elevation of any point *m* on the section *ab* and that of the corresponding point *i* on an isochrone labeled *t* is the piezometric head at point *m* at time *t* and the neutral stress at point *m* is

$$u_w = \gamma_w \overline{mi} = \gamma_w(H + h - z) \qquad [4]$$

The hydraulic head *h* at point *m* with reference to the initial water table is equal to

$$h = \frac{u}{\gamma_w} \qquad [5]$$

wherein *u* is the excess hydrostatic pressure at time *t*. The value of *u* is determined by equations 3, which represent the solution of equation 99(8). The hydraulic gradient at point *m* at time *t* is equal to

$$i = -\frac{\partial h}{\partial z} = -\frac{1}{\gamma_w}\frac{\partial u}{\partial z} \qquad [6]$$

A negative value of *i* indicates a gradient in a downward direction. Since $\overline{cm}_1 = z$, the gradient at point *m* at time *t* is identical with the slope of the isochrone labeled *t* at point *i*. If the slope is toward point *a*, as shown in the figure, the gradient at point *m* is positive, which indicates that the excess water at the elevation of point *m* flows in an upward direction.

At the instant of the application of a uniformly distributed load p_1 per unit of area of the surface of the bed of clay shown in Figure 82 the isochrone consists of a broken line *ade* whose horizontal part *de* is located at an elevation p_1/γ_w above the horizontal surface of the clay. This is the *zero isochrone*. During the first stage of the process of consolidation the isochrones are tangent to *de*. This fact indicates that the consolidation is still limited to the upper part of the clay deposit while the void ratio in the lower part is unchanged. At a later stage, represented by the isochrone af_2, the isochrones meet the vertical line *ec*. The distance ef_2 represents the increase of the effective normal stress in the clay at the base of the clay deposit since the instant of load application. Because the rate of percolation through a horizontal section increases with the elevation *z* of the section the slope of the isochrones increases from the right to the left. At the base of the zone in process of consolidation the discharge velocity is equal to zero, which requires $\partial u/\partial z = 0$. Therefore at any time the tangent to the right-hand end of the isochrones must be horizontal. After consoli-

dation is complete the water level in each of the tubes is located on the line *ac*. This is the *final isochrone*. If the external hydraulic conditions, such as the position of the water table, remain unchanged, the

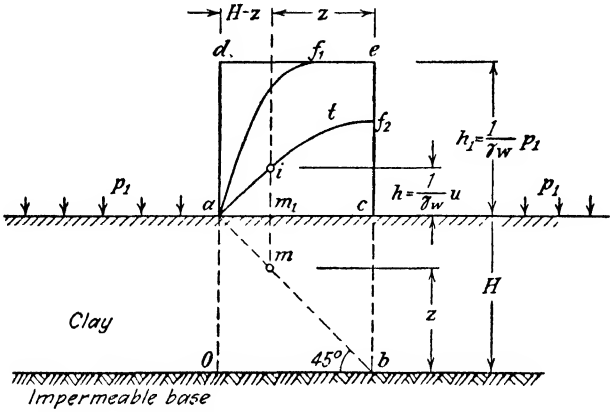

FIG. 82. Consolidation of layer of clay after sudden application of uniformly distributed surcharge. Isochrones (plain curves) represent locus of water level in vertical piezometric tubes whose lower ends are located on section *ab*.

final isochrone is identical with the locus of the water levels in the tubes before the application of the consolidation stresses.

In the thermodynamic analogue the ordinates of the isochrones with reference to the surface of the bed of clay represent the temperatures. In an early stage of cooling, indicated by the isochrone af_1, the temperature of the lower part of the hot plate is still unchanged whereas the upper part has already cooled off.

The diagrams which represent the successive stages of a process of consolidation by means of isochrones, such as the diagram in Figure 82, will briefly be called *piezographs*. They facilitate the determination of the state of stress at any time in every point of the bed of clay. The total normal stress at time t on a horizontal section at elevation z is

$$p_t = p_1 + \gamma (H - z) \qquad [7]$$

wherein γ is the unit weight of the clay and water combined. The total neutral stress is

$$u_w = u + \gamma_w (H - z) \qquad [8]$$

Therefore the effective normal stress is

$$\bar{p}_t = p_t - u_w = (p_1 - u) + (H - z)(\gamma - \gamma_w) \qquad [9]$$

In this equation the difference $(p_1 - u)$ represents the increase of the effective stress due to the surcharge and $(H - z)(\gamma - \gamma_w)$ is the

effective stress at elevation z due to the submerged weight of the clay. This part of the total effective stress $\bar{p}_t$ existed before the surcharge was applied.

The validity of the preceding equations requires that the initial surcharge on the surface of the clay be equal to zero and that the water table coincide with the surface of the clay. If these two conditions are not satisfied, the total surcharge per unit of area must be added to the total normal stress p_t, equation 7, and the initial neutral stress which acted on the surface of the clay must be added to the neutral stress u_w, equation 8.

Figures 83*a* to 83*f* show the isochrones for several other important cases of consolidation of horizontal beds of clay. In Figure 83*a* the bed of clay with a thickness $2H$ is assumed to rest on a permeable base. Hence the excess water can escape toward both the upper and lower surfaces of the clay stratum. Since the flow of the excess water out of the clay is symmetrical with reference to a plane at midheight of the bed of clay, the isochrones are also symmetrical, as shown in the figure. In the case represented by Figure 83*b* the bed of clay with a thickness $2H$ also rests on a permeable base but the consolidation stresses are assumed to decrease from a value p_1 at the top to a smaller value p_2 at the bottom, as shown in the figure by the straight line de. This assumption approximates the stress conditions produced by a surcharge acting on a strip on the surface of the clay because the normal stress on horizontal sections due to a local surcharge decreases with increasing vertical distance between the surface and the section. The isochrones resemble those in Figure 83*a*, but they are not symmetrical. During every stage of the process the point of contact between the corresponding isochrone and a horizontal tangent to this isochrone determines the elevation of the boundary between the zones of upward and downward drainage. This boundary passes through the point of intersection between the vertical through the point of contact and the inclined section ab, as shown in Figure 83*b*. At time zero the boundary is identical with that surface of the clay where the excess pressure is greatest. As time goes on the boundary gradually approaches a horizontal plane at midheight of the bed of clay. These statements also apply to every other process of consolidation involving drainage in two directions such as the process illustrated by Figures 83*c* and 83*e*.

In Figure 83*c* the consolidation stresses are assumed to decrease from p_1 at the upper surface to zero at the lower, and the excess water can escape through both upper and lower surfaces. If the base of the clay is impermeable, the isochrones corresponding to the system of stresses indicated in Figure 83*c* intersect the zero isochrone dc, as shown in Figure 83*d*. The physical meaning of this result obtained by compu-

tation can be recognized on the basis of the thermodynamic analogue to this case. This analogue consists of a plate with an insulated base whose initial temperature increases from T_0 at the base to $T_0 + T = T_0 + \gamma_w \overline{ad}$ at the top. The surface remains in contact with air

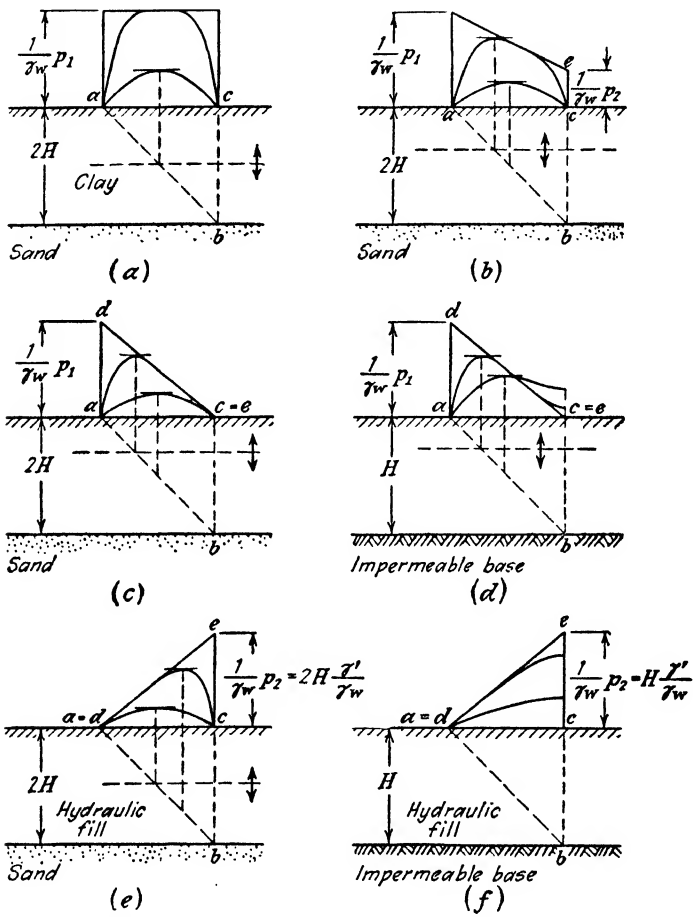

FIG. 83. Isochrones representing progress of consolidation of a layer of ideal clay for different types of drainage and different distributions of consolidation pressure in a vertical direction. (*After Terzaghi and Fröhlich, 1936.*)

at temperature T_0. During the subsequent process of cooling the temperature of the lower part of the plate temporarily increases. In the theory of consolidation, an increase of the temperature corresponds to a swelling of the clay.

Figure 83*e* shows the piezograph for a hydraulic fill on a permeable

base. This graph was drawn on the assumption that the consolidation during the process of placing the fill and the change of the unit weight of the fill due to consolidation can be neglected. The total normal stress on a horizontal section through the fill at a depth $2H-z$ is $(2H - z)\,\gamma$ wherein γ is the unit weight of the fill, water and clay combined. Yet immediately after the fill has been placed the effective stress is equal to zero, because consolidation has not yet started. Hence at a time $t = 0$ the neutral stress at any depth $2H - z$ is equal to the total stress $(2H - z)\,\gamma$ which causes the water to rise in a piezometric tube from depth $2H - z$ to an elevation $(2H - z)\,\gamma/\gamma_w$ above this depth or to an elevation

$$h = \frac{1}{\gamma_w}(2H - z)\,\gamma - (2H - z) = (2H - z)\frac{\gamma - \gamma_w}{\gamma_w} = (2H - z)\frac{\gamma'}{\gamma_w}$$

above the surface of the fill. In Figure 83*e* these initial values of the hydrostatic head are represented by the ordinates of the straight line *ae*. During the following process of consolidation the hydrostatic

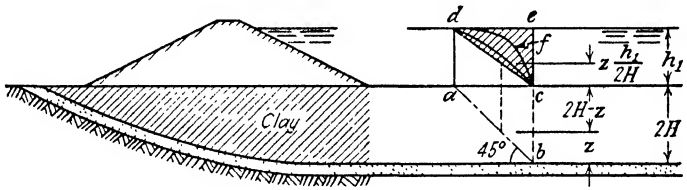

FIG. 84. Consolidation of bed of clay due to seepage in vertical downward direction from reservoir into sand stratum whose outcrops are located on downstream side of storage dam.

head gradually approaches the value zero and the boundary between the zones of upward and of downward drainage gradually rises from the base of the fill toward a horizontal plane at midheight of the consolidating stratum. If the fill rests on an impermeable base the isochrones slope only toward the left, as shown in Figure 83*f* and intersect the line *ec* at right angles, because at the impermeable base the hydraulic gradient is equal to zero.

It should be noted that the thickness of all those layers of clay in Figure 83 from which the excess water escapes through both surfaces of the layer is indicated by $2H$ (Fig. 83*a*, 83*b*, 83*c*, and 83*e*), whereas that of the others is indicated by H. The reason for this important distinction will be explained in the following article.

The consolidation of a bed of clay can also be produced by a flow of water through the clay in a downward direction. Figure 84 illustrates the mechanics of this process. It represents a section through a reser-

voir located above a bed of clay with a thickness $2H$ which in turn rests on a layer of sand. Prior to filling the reservoir the water table is assumed to be located at the surface of the ground. By filling the reservoir to a depth h_1 with water we increase the total normal stress on every horizontal section through the clay by $h_1\gamma_w$. If the hydrostatic head in the bed of sand beneath the clay is also increased by h_1 the increase of the neutral stress is everywhere equal to the increase of the total stress and both the effective stresses and the void ratio of the clay remain unaltered. On the other hand, if the hydrostatic head in the sand is maintained at its original value, for instance, because the sand layer intersects the surface of the ground on the downstream side of the dam, as shown in the figure, the filling of the reservoir creates a flow of water from the reservoir through the clay into the sand. Once this flow has become stationary, the hydrostatic head of the water at any point of the section *ab* (Fig. 84) through the clay is equal to the ordinates of the straight line *dc* with reference to the base of the fill. These ordinates also determine the permanent increase $\gamma_w h_1 z/2H$ of the neutral stress in the clay. However, owing to the filling of the reservoir the total normal stresses on every horizontal section have increased by $h_1\gamma_w$. Hence the filling of the reservoir ultimately increases the effective normal stresses on horizontal sections through the clay by

$$p = \gamma_w h_1 \left(1 - \frac{z}{2H}\right)$$

This potential increase of the effective stresses produces consolidation. Immediately after the reservoir has been filled the void ratio of the clay is still unchanged. Hence at that time the increase of the effective pressure is still equal to zero and the entire excess stress $\gamma_w h_1$ is added to the neutral stress. The corresponding isochrone is represented by the horizontal line *de*. As time goes on the clay consolidates, the hydrostatic head becomes smaller, as indicated by the isochrone *dfc*, and finally it assumes the values determined by the ordinates of the straight line *dc*. The process of consolidation is identical with that represented by Figure 83*e*.

The line *dc* is an example of a final isochrone located above the level *ac* to which the water rose in the piezometric tubes prior to the application of the consolidation stresses. If the final isochrone is located above or below the original water table, the excess hydrostatic pressure u in the differential equation of the process (eq. 99 (8)) represents the difference between the hydrostatic pressure at a given point at a given time and either the initial or the final hydrostatic pressure at the same

point. Therefore one has the choice between two different reference pressures. However, the choice has no influence on the results of the computation. The author always uses the final pressure as a reference pressure. In accordance with this arbitrary convention the final isochrone represents the base line for measuring the hydraulic heads.

102. Settlement due to consolidation. During the process of consolidation of a bed of clay the thickness of the bed decreases on account of the decrease of the void ratio. The corresponding downward movement of the surface of the layer is called the *settlement due to consolidation.* The final decrease of volume Δn_1 per unit of the initial volume of the clay is determined by equation 98(4). By means of this equation we obtain

$$\Delta n_1 = \frac{a_v}{1 + e_0} p_1 = m_v p_1 \qquad [1]$$

wherein p_1 denotes the consolidation pressure (see Article 99). In the process illustrated by Figure 82 the consolidation pressure p_1 is the same throughout the bed of clay. Therefore the final settlement of the surface of the bed of clay shown in Figure 82 due to consolidation is

$$\rho_1 = H \Delta n_1 = H m_v p_1 \qquad [2]$$

If the consolidation pressure changes with depth according to a straight line law, as for instance in the processes illustrated by Figures 83*b* to 83*f* and Figure 84, the final settlement is equal to

$$\rho_1 = m_v H \frac{p_1 + p_2}{2} \qquad [3]$$

wherein p_1 is the consolidation pressure on the upper surface of the clay and p_2 the consolidation pressure on the lower surface.

A surcharge p_1 per unit of area of the entire surface of a bed of clay with a thickness H produces a consolidation pressure which has the same intensity p_1 throughout the layer and the final settlement is determined by equation 2. During the period between the instant when the surcharge is applied and an arbitrary time t the effective pressure produced by the consolidation pressure p_1 at a given depth $H - z$ increases from zero to

$$\bar{p} = p_1 - u$$

The decrease Δn of the porosity of the consolidating clay due to an increase of the effective pressure by $\bar{p}$ can be computed by means of equation 98(4). Setting $\Delta \bar{p} = \bar{p}$ in this equation we get

$$\Delta n = m_v \bar{p} = m_v (p_1 - u) \qquad [4]$$

The decrease $d\rho$ of the thickness of a horizontal layer with the original thickness dz is

$$d\rho = \Delta n\, dz = m_v(p_1 - u)\, dz \qquad [5]$$

and the settlement ρ at the time t is

$$\rho = \int_0^H \Delta n\, dz = m_v\left(p_1 H - \int_0^H u\, dz\right) \qquad [6]$$

For the bed of clay shown in Figure 82 the value u is determined by equations 101 (3). Substituting this value in equation 6 and integrating we have

$$\rho = m_v p_1 H\left[1 - \frac{8}{\pi^2}\sum_{N=0}^{N=\infty}\frac{1}{(2N+1)^2}\epsilon^{-(2N+1)^2\pi^2 T_v/4}\right] \qquad [7]$$

wherein

$$T_v = \frac{c_v}{H^2}t \qquad 101(3b)$$

represents the time factor.

The factor outside the brackets represents the ultimate settlement ρ_1 (eq. 2). If the boundary conditions are different from those shown in Figure 82 the term in brackets will also be different. Yet, in any event, the first term on the right-hand side of the equation represents the final settlement and the term in brackets represents always some function, $f(T_v)$, of the time factor. Hence we can write

$$\rho = \rho_1 f(T_v) = \rho_1 \frac{U\%}{100} \qquad [8a]$$

The value

$$U\% = 100\frac{\rho}{\rho_1} = 100 f(T_v) \qquad [8b]$$

is called the *degree of consolidation.* It depends only on the boundary conditions and on the time factor T_v. The character of the function $f(T_v)$ depends on the conditions of the problem. For a great number of different conditions the function $f(T_v)$ is already known (Terzaghi and Fröhlich, 1936). Hence there is no need to determine this function in any but exceptional cases. In Figure 85, curve C_1 represents the function $100 f(T_v) = U\%$ for the processes illustrated by Figures 82, 83*a*, 83*b*, 83*c*, and 83*e*. All these processes with the exception of the first involve the drainage of beds of clay with a thickness $2H$ in two opposite directions due to an excess pressure which is a linear function of depth. The identity of the time factor-consolidation curves for all these processes demonstrates that the shape of these curves is inde-

pendent of the slope of the zero isochrone *ed*, provided this isochrone is straight, and the excess water can escape through both the upper and the lower surfaces of the consolidating layer. A layer of clay which permits drainage through both surfaces is called an *open layer*. The thickness of such a layer is always represented by the symbol $2H$, in contrast to the symbol H used for the thickness of *half-closed* layers which can discharge their excess water only through one surface.

The shape of the time factor-consolidation curve for half-closed layers of clay with a thickness H depends on the distribution of the consolidation pressure. Figures 83*d* and 83*f* represent two different distributions which are frequently encountered. The corresponding time factor-consolidation curves shown in Figure 85*a* are C_2 and C_3

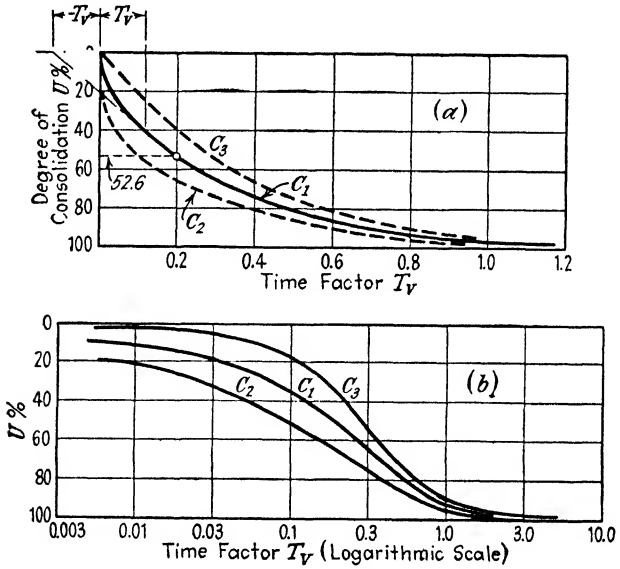

FIG. 85. Relation between time factor and degree of consolidation. In (*a*) the time factor is plotted on an arithmetic and in (*b*) on a logarithmic scale. The three curves C_1 to C_3 correspond to three different cases of loading and drainage, represented by Figure 83 (*a*, *d*, and *f*). (*After Terzaghi and Fröhlich, 1936.*)

respectively. For a half-closed layer acted upon by a uniformly distributed consolidation pressure, such as the layer shown in Figure 82, the time factor-consolidation curve is identical with the curve C_1 for open layers, because the process of consolidation in such a layer is identical with that in each one of the two halves of the open layer illustrated by Figure 83*a*.

The curves C_1, C_2, and C_3 (Fig. 85*a*) represent the solution of the

most common consolidation problems. The solutions of many others have also been published (Terzaghi and Fröhlich, 1936). If we want to determine the settlement of the surface of a bed of clay at a time t after consolidation started we determine first of all the ultimate amount of settlement ρ_1 by means of equations 2 or 3. Then we determine the time factor by means of equation 101 (3*b*)

$$T_v = \frac{k}{\gamma_w m_v} \frac{t}{H^2} = \frac{c_v}{H^2} t$$

and finally we take the value of the corresponding degree of consolidation from the graph (Fig. 85*a*). From equation 8*a* we obtain for the settlement at time t the value

$$\rho = \rho_1 \frac{U\%}{100}$$

For open beds of clay the value H in the equation for computing the time factor T_v is always equal to one half of the initial thickness of the bed of clay. On the other hand, if the clay rests on an impermeable base (Figs. 83*d* and 83*f*) the value H is equal to the total thickness.

In engineering practice by far the most important processes of consolidation are those represented by the curve C_1 in Figure 85. They include the consolidation of half-closed beds of clay due to a uniformly distributed consolidation pressure (Fig. 82) and of open beds of clay under the influence of any consolidation pressure which is a linear function of depth, such as the processes illustrated by Figures 83*a*, 83*b*, 83*c*, and 83*e*. The curve C_1 also represents the relation between the time factor and the degree of consolidation for the small-scale consolidation tests which are performed in the laboratory for the purpose of determining the coefficient of consolidation c_v in equation 101 (3*b*). For values of $U\%$ between 0 and 52.6 the curve C_1 can be represented almost exactly by the equation

$$T_v = \frac{\pi}{4}\left(\frac{U\%}{100}\right)^2 \qquad [9]$$

which is the equation of a parabola. Substituting for T_v the value given by equation 101 (3*b*) we obtain

$$\frac{U\%}{100} = \sqrt{\frac{4c_v}{\pi H^2}}\sqrt{t} \qquad [10]$$

The values c_v and H are constant. Hence for values of $U\%$ smaller than 52.6 the degree of consolidation produced by a suddenly applied

load increases in direct proportion to the square root of the time. For values of $U\%$ greater than 52.6 the curve C_1 is almost identical with a curve with the equation

$$T_v = 1.781 - 0.933 \log_{10}(100 - U\%) \qquad [11]$$

It should be noted that the radius of curvature of the curve C_1 in Figure 85*a* increases steadily until $U\%$ becomes approximately equal to 50, then decreases once more and assumes a second minimum at about $U\% = 85$. On account of the parabolic shape of the first section of the curve (see eq. 10) the tangent to the curve at any point of that section with the abscissa T_v intersects the horizontal axis at a distance $-T_v$ from the origin.

In Figure 85*b* the relation represented by the curve C_1 in Figure 85*a* has been shown on a semilogarithmic plot. The curve thus obtained has a point of inflection at about $U\% = 75$. In the vicinity of $U\% = 95$ it flattens rapidly and approaches a horizontal asymptote corresponding to $U\% = 100$. The curve represents an equation

$$\log_{10} T_v = F(U\%)$$

Substituting for T_v the value given by equation 101(3*b*) we obtain

$$\log_{10} T_v = \log_{10} t + \log_{10} \frac{c_v}{H^2} = \log_{10} t + \text{const.} = F(U\%)$$

This equation leads to the following conclusion. If the degree of consolidation of two beds of clay with different values of c_v/H^2 is plotted against the logarithm of time, the time-consolidation curves thus obtained have the same shape but they are separated from each other by a horizontal distance $\log_{10}(c_v/H^2)$. For $T_v/t = 1$ the time-consolidation curve becomes identical with the time factor-consolidation curve shown in the figure. This important property of the semilogarithmic time-consolidation graph facilitates comparison of empirical consolidation curves with the theoretical standard curve for the purpose of detecting deviations of the real process from the theoretical one. Therefore in many cases the semilogarithmic plot is preferable to the arithmetic plot.

103. Approximate methods of solving consolidation problems. Solutions which have been obtained by solving the differential equations 99(8) are called *rigorous solutions* because they comply strictly with the fundamental assumptions (see Art. 17). If the conditions of the problem exclude the possibility of obtaining a relatively simple rigorous solution it is always possible to obtain satisfactory approximate solutions. Approximate solutions can be obtained by substituting for the

real isochrones such as those shown in Figures 82 and 83 a family of simpler curves with similar general characteristics.

For instance the isochrones shown in Figure 82 have approximately the shape of parabolas because the drainage of the excess water toward the top surface of the clay requires an increase of the hydraulic gradient from zero at the base of the zone of consolidation toward a maximum at the surface (see Art. 101). Hence the simplified method of computation is based on the assumption that the isochrones are parabolas. As time goes on the apex of the parabolic isochrones advances first from *d* in Figure 82 in a horizontal direction toward *e* and then in a vertical downward direction from *e* toward *c*. The rate at which the apex travels determines the quantity of excess water which drains out of the clay per unit of time. At the surface the hydraulic gradient must always be equal to the gradient required to maintain the flow of the excess water toward the surface. This condition makes it possible to determine the rate of displacement of the isochrones and the corresponding rate of consolidation. The time factor-consolidation curve obtained by means of this procedure is almost identical with the curve representing the rigorous solution.

The replacement of the real isochrones by simpler curves is strictly comparable to Coulomb's method of substituting plane surfaces of sliding in the backfill of retaining walls for the real surfaces, which are slightly curved. (See Art. 23.) Many approximate solutions of consolidation problems have already been published (Terzaghi 1925, Terzaghi and Fröhlich, 1936), and the method can easily be adapted to problems which have not yet been solved.

104. Consolidation during and after gradual load application. In practice the most important causes of consolidation are the construction of buildings or embankments above beds of clay and the deposition of clay in a semi-liquid state by hydraulic fill processes. In both cases the consolidation of the clay under constant load is preceded by a period of transition during which the consolidation occurs simultaneously with an increase of the load. The consolidation due to every load increment proceeds independently of the consolidation due to the preceding and the succeeding load increments. Therefore the rate of consolidation during the period of transition can be computed with any desired degree of accuracy by a simple process of superposition.

As an example of this method we compute the rate of consolidation of a bed of clay with a thickness $2H$ located between two layers of sand. The upper layer of sand serves as a base for a building under construction. The ordinates of the broken line *Oab* in Figure 86*a* represent the average normal pressure p due to the weight of the building on hori-

zontal sections through the clay plotted against the time t. Construction is started at time $t = 0$ and it is finished at time t_1. After time t_1 the pressure p is constant and equal to p_1. The curve C_1 represents the time-consolidation curve on the assumption that the entire weight of the building was suddenly applied at time $t = 0$. It was obtained from the curve C_1 in Figure 85a by substituting the time scale of Figure 86 for the time-factor scale of Figure 85a. The substitution is accomplished by means of equation 101 (3b)

$$T_v = \frac{c_v}{H^2} t$$

At a time t smaller than t_1 the average pressure on the clay is p. For practical purposes we can assume that the state of consolidation at time t is the same as if the pressure p had acted on the clay during a

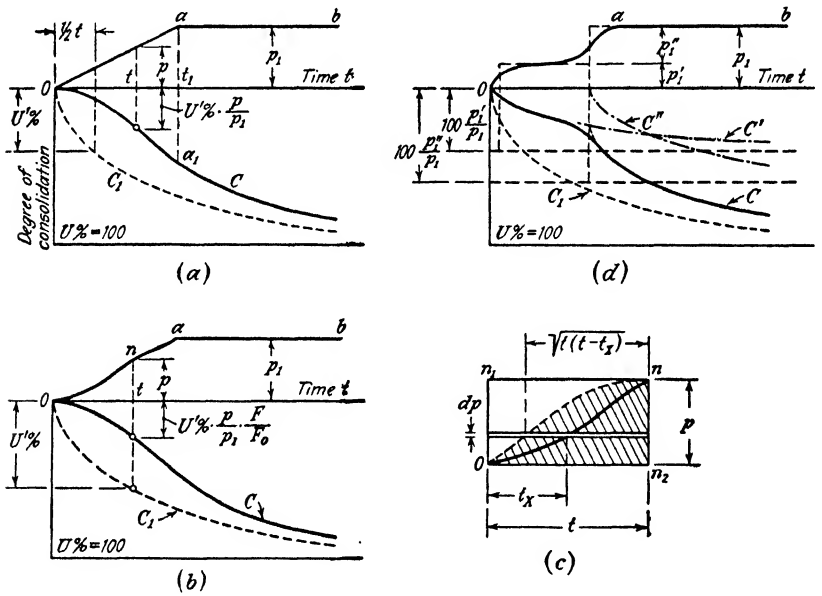

FIG. 86. Graphic methods of constructing time-consolidation curve, if consolidation pressure is applied gradually. (*After Terzaghi and Fröhlich, 1936.*)

period $t/2$. At a time $t/2$ after sudden application of a pressure p the degree of consolidation would be U' (Fig. 86a). Hence the degree of consolidation at time t is equal to

$$U\% = U'\% \frac{p}{p_1}$$

in per cent of the final settlement due to consolidation under load p_1. The theoretical justification of this approximate method of computation has been published elsewhere (Terzaghi and Fröhlich, 1936).

Plotting this value against an abscissa t we obtain one point of the consolidation curve C. Other points can be determined by repeating the procedure for other values of t. Beyond point a_1 with an abscissa t_1 consolidation proceeds as if the final pressure p_1 had been suddenly applied at a time $t_1/2$.

If the rate of application of the load p_1 is variable as indicated by the time-load curve Oa in Figure 86*b*, the time-consolidation curve can be obtained by means of the graphical method illustrated by Figures 86*b* and 86*c*. The curve C_1 in Figure 86*b* is identical with the curve C_1 in Figure 86*a*. It represents the relation between time and the degree of consolidation on the assumption that the final pressure p_1 had been suddenly applied at a time $t = 0$. The degree of consolidation at time t due to the sudden application of the smaller pressure p at a time $t = 0$ is equal to

$$U''\% = U'\% \frac{p}{p_1} \qquad [1]$$

in per cent of the final consolidation under a pressure p_1. The influence of the gradual application of the pressure p remains to be investigated. In order to ascertain this influence we reproduce in Figure 86*c* the section On of the time-load curve Oa of Figure 86*b*, on a larger scale. If we choose the scale in this figure in such manner that the area F_0 of the rectangle On_1nn_2 represents the settlement at a time t after sudden application of the pressure p, the settlement due to the sudden application of a load increment dp at a time $t = 0$ is equal to the area of the slice shown in the figure with a length t. In reality the increment dp acted on the clay only during a time $t - t_x$. From equation 102(10)

$$\frac{U\%}{100} = \sqrt{\frac{4c_v}{\pi H^2}}\sqrt{t}$$

we learned that the settlement due to a suddenly applied load increases with the square root of the time. Therefore the length of the strip which represents the settlement due to the load increment dp in Figure 86*c* is equal to

$$t \cdot \sqrt{\frac{t - t_x}{t}} = \sqrt{t(t - t_x)}$$

By plotting the values $\sqrt{t(t - t_x)}$ corresponding to different points on the load curve On (Fig. 86*c*) from nn_2 to the left we obtain the dashed

line On. The shaded area $F = Onn_2$ represents the real settlement at the time t in the scale of the figure. If p had been applied at $t = 0$ the settlement would be equal to the area $On_1nn_2 = F_0$ and the corresponding degree of consolidation would be equal to $U''\%$ (eq. 1). Hence the real degree of consolidation at a time t due to a load applied as indicated by the curve On (Figs. 86*b* and 86c) is

$$U\% = U''\% \frac{F}{F_0} = U'\% \frac{p}{p_1} \frac{F}{F_0}$$

This value determines one point on the line of consolidation C. Other points can be determined by repeating the procedure for other values of t. Equation 102(10) on which the procedure is based is strictly valid for values of $U\%$ between 0 and 52.6. Yet, even for somewhat higher values of $U\%$ the approximation obtained by the method described before is very satisfactory.

If the load curve rises in irregular steps (see load curve shown in Fig. 86*d*) the problem of estimating the rate of consolidation can be solved by substituting for the curve a set of two or more sharp steps (dashed load lines in Fig. 86*d*). Each one of these steps represents the sudden application of one part of the final pressure. Each one of these increments contributes one share, $100 \frac{p_1'}{p_1}$, $100 \frac{p_1''}{p_1}$, $\cdots$ to the final consolidation of 100 per cent. The consolidation produced by each increment proceeds independently of the others. The corresponding consolidation curves are represented in Figure 86*d* by C' and C''. At any time t the degree of consolidation is equal to the sum of the ordinates of these curves for a time t. By performing this operation we obtain a curve with sharp breaks. These breaks are due to the preceding substitution of a broken line for the real load curve which is smooth. The real consolidation curve is also smooth, as shown by the plain curve C in Figure 86*d*.

The general procedures illustrated by Figure 86 can also be adapted to the solution of all the other problems involving consolidation during a gradual change of the load on the clay.

105. Effect of gas content of the clay on the rate of consolidation. If one part of the voids of a clay is occupied by gas bubbles the application of a surcharge on the clay causes a simultaneous compression of the gas which in turn involves a decrease of the void ratio in advance of the subsequent consolidation of the clay. In the diagram in Figure 87 this sudden decrease of the void ratio prior to the consolidation is indicated by the initial consolidation $U_0\%$. The value $U_0\%$ depends on the initial gas pressure, on the volume occupied by the gas prior to

the application of the surcharge, and on the intensity of the surcharge.

During the following process of consolidation the temporary excess hydrostatic pressure in the water content of the clay disappears and the gas pressure in the bubbles approaches its original value p_g. Therefore the quantity of water which leaves the clay during the process of consolidation is exactly the same as if the gas bubbles were not present. The coefficient of permeability of the clay is also practically independent of the gas content of the clay unless the gas occupies an appreciable percentage of the voids. Therefore we can conclude that the pressure of the gas in the clay has very little effect on the rate of consolidation. In a clay without gas the degree of consolidation for $t = 0$ is equal to zero and the subsequent consolidation proceeds as shown by the curve C (Fig. 87). If the clay contains gas bubbles the degree of consolidation for $t = 0$ is equal to $U_0\%$. Yet, according to the preceding reasoning the rate at which the final state is approached is independent of the gas content. Hence we obtain the consolidation curve C_g for clay which contains gas by reducing the ordinates of the curve C (Fig. 87) with reference to the lower boundary of the diagram at a ratio $\dfrac{100 - U_0\%}{100}$.

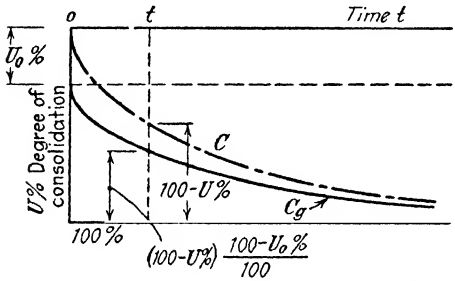

FIG. 87. Influence of incomplete saturation of clay on shape of time-consolidation curve (plain curve C_g).

106. Two- and three-dimensional processes of consolidation. In consolidation processes involving two-dimensional flow, the excess water drains out of the clay in parallel planes. In a three-dimensional process of consolidation the flow occurs in radial planes or else the water particles travel along flow lines which do not lie in planes.

The differential equation for one-dimensional flow has been derived in Article 99. By means of a similar method of approaching the problem one obtains for the three-dimensional flow the equation

$$\frac{\partial u}{\partial t} = c_v\left(\frac{\partial^2 u}{\partial x^2} + \frac{\partial^2 u}{\partial y^2} + \frac{\partial^2 u}{\partial z^2}\right) \qquad [1]$$

wherein u is the excess hydrostatic pressure in the water, t the time, and c_v the coefficient of consolidation (eq. 99(7)). If the flow occurs only in one direction, for instance in the direction of the Z axis, two of the three terms in brackets become equal to zero and equation 1 becomes identical with equation 99(8). The differential equation for the two-dimensional process of consolidation, parallel to the XZ

plane is

$$\frac{\partial u}{\partial t} = c_v\left(\frac{\partial^2 u}{\partial x^2} + \frac{\partial^2 u}{\partial z^2}\right) \qquad [2]$$

If a three-dimensional process of consolidation is symmetrical about an axis, it is more convenient to replace the Cartesian coordinates by polar coordinates, r in a radial and z in an axial direction. By means of this substitution one obtains from equation 1

$$\frac{\partial u}{\partial t} = c_v\left(\frac{\partial^2 u}{\partial r^2} + \frac{1}{r}\frac{\partial u}{\partial r} + \frac{\partial^2 u}{\partial z^2}\right) \qquad [3]$$

If the radial flow takes place in planes at right angles to the Z axis, the term $\partial^2 u/\partial z^2$ is equal to zero and one gets

$$\frac{\partial u}{\partial t} = c_v\left(\frac{\partial^2 u}{\partial r^2} + \frac{1}{r}\frac{\partial u}{\partial r}\right) \qquad [4]$$

Carrillo (1942*b*) has shown that the three-dimensional radial flow, described by equation 3, can be resolved into a plane, radial flow (eq. 4) and into a linear flow (eq. 99(8)). If $U_r\%$ is the average degree of consolidation of a layer of clay due to the plane radial drainage at a given time t and $U_z\%$ the degree of consolidation due to the linear drainage at the same time, the degree of consolidation $U\%$ due to the combined linear and radial drainage is determined by the equation

$$100 - U\% = \frac{1}{100}(1 - U_r\%)\,(1 - U_z\%) \qquad [5]$$

The coefficient of consolidation c_v in equation 3 is given by the equation

$$c_v = \frac{k}{\gamma_w m_v} \qquad 99(7)$$

wherein k is the coefficient of permeability, γ_w the unit weight of the water, and m_v the coefficient of volume decrease (eq. 98(5)). If the coefficient of permeability k for the axial direction is equal to n times the coefficient of permeability k_r for radial directions the ratio between the corresponding values of c_v is also equal to n, or

$$\frac{k}{k_r} = n \quad \text{and} \quad \frac{c_v}{c_{vr}} = n \qquad [6]$$

If k is different from k_r, it can be shown that equation 3 must be replaced by

$$\frac{\partial u}{\partial t} = c_{vr}\left(\frac{\partial^2 u}{\partial r^2} + \frac{1}{r}\frac{\partial u}{\partial r}\right) + c_v\frac{\partial^2 u}{\partial z^2} \qquad [7]$$

However, the general relation expressed by equation 5 retains its validity.

In engineering practice one of the most important two-dimensional processes of consolidation occurs in the core of hydraulic fill dams during and after the period of construction. Figure 88*a* is a section through such a fill during construction. The central part of the fill occupied by the finest soil constituents is called the *core* of the fill. One part of the excess water drains out of the core through the top surface in a vertical upward direction into the core pool P and the remainder escapes in a horizontal direction through the slopes of the core. Both types of flow take place simultaneously and parallel to the section shown in the figure. G. Gilboy (1934)

computed the rate of consolidation of such fills on the simplifying assumptions that the excess water escapes out of the core only in a horizontal direction. At least during the first period of construction the drainage through the top surface is likely to be important. Therefore the real rate of consolidation should be expected to be appreciably higher than the computed one.

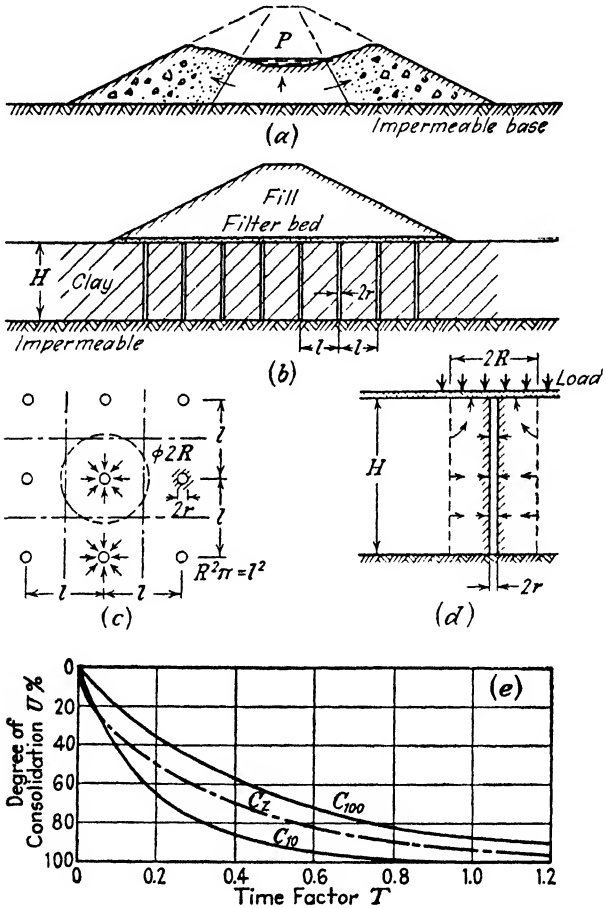

FIG. 88. Two- and three-dimensional processes of consolidation. (*a*) Hydraulic fill dam; (*b* to *d*) drainage of bed of clay beneath fill by means of sand wells; (*e*) relation between time factor and degree of consolidation of cylindrical body shown in (*d*) due to drainage toward central well for $R/r = 1$, 10, and 100.

As a simple example of a three-dimensional process of consolidation we consider the process illustrated by Figure 88*b*. This figure represents a section through an embankment resting on the horizontal surface of a stratum of soft clay or silt. In order to accelerate the consolidation of the loaded stratum, filter wells have been established which permit the escape of part of the excess water in a horizontal direc-

tion into the wells, which in turn deliver the water into a filter bed located between the clay and the base of the fill. The rest of the excess water flows in an upward direction from the clay into the filter bed. Figure 88*c* shows the layout of the system of wells. The vertical sections indicated by dash-dotted lines divide the consolidating layer of clay into prismatic blocks. Within each block the drainage proceeds as if the vertical sides of the block were lined with an impermeable membrane, because the excess water in the clay located on either side of each vertical section escapes in opposite directions. The problem of computing the rate of drainage can be simplified without appreciable error by assuming that each block is cylindrical. On this assumption the flow is symmetrical about the axis of the block. Within the block the flow of the water toward the exit surfaces proceeds as if the cylindrical surface of the block were covered with an impermeable material.

If the permeability of the clay in a vertical direction is different from that in a radial direction the consolidation of the cylindrical block is represented by equation 7. Rapid application of the weight of the fill produces throughout the block an excess hydrostatic pressure equal to the weight of the fill q per unit of area of the top surface of the block. As time goes on this excess pressure gradually approaches zero. Simultaneously the effective stresses in the clay increase and approach a constant value which is equal to the total increase of the stress in the clay produced by the weight of the fill. The outer cylindrical surface and the base of the block are impermeable and the excess water escapes through the top surface and the walls of the well. These are the boundary conditions. The flow of the excess water through the block can be resolved into two components, one vertical component in the direction of the centerline of the filter well (direction of the Z axis) and one horizontal, radial component directed toward the filter well. The boundary conditions for the vertical linear flow are identical with those for the consolidation due to sudden application of a surcharge q per unit of area on a bed of clay with a thickness H which rests on an impermeable base (half-closed layer). (See Art. 102.) The relation between the time t and the degree of consolidation $U_z\%$ is determined by the equation

$$U_z\% = 100 f(T_v) \qquad 102(8b)$$

wherein

$$T_v = \frac{c_v}{H^2} t \qquad 101(3b)$$

is the time factor. The function $f(T_v)$ depends only on the boundary conditions. For the boundary conditions described before, the relation between $U_z\%$ and T_v is represented by the curve C_1 in Figures 85*a* and 88*e*.

The second component of the flow of the excess water represents a process of consolidation involving the flow of the water in horizontal radial directions from the vertical outer surface of a cylindrical body toward the filter well which occupies the central part of the body. This type of flow is represented by equation 4. The equation has been solved by Rendulic (1935*a*) who showed that the relation between the time t and the degree of consolidation $U_r\%$ can be expressed by an equation

$$U_r\% = 100 F(T) \qquad [8a]$$

wherein

$$T = \frac{c_{vr}}{4R^2} t \qquad [8b]$$

is the time factor for consolidation involving horizontal radial flow out of a cylindrical

body with an outer diameter $2R$ toward a central filter well with a diameter $2r$. The relation between the degree of consolidation $U_r\%$ and the time factor T depends on the value of the ratio R/r. In Figure 88*e* this relation is represented by the curves C_{10} and C_{100} for values of $R/r = 10$ and 100 respectively. If the values $U_z\%$ and $U_r\%$ have been determined for a given time t one obtains the average degree $U\%$ of consolidation of the block for the time t by introducing these values into equation 5.

In order to illustrate the influence of the filter wells on the rate of consolidation we assume that the depth H of the bed of clay shown in Figure 88*b* is 20 feet. The wells have a diameter of 1 foot and they are spaced 9 feet in either direction. Replacing the vertical prismatic blocks which surround the wells by cylindrical blocks with equal horizontal cross-sectional area we obtain for the diameter of these blocks $2R = 10$ feet. We want to determine the influence of the wells on the average degree of consolidation at the time when the degree of consolidation in the clay without wells would be equal to 30 per cent. The computation will be made on two different assumptions regarding the permeability. First it will be assumed that the clay is isotropic,

$$k_r = k \quad \text{or} \quad c_{vr} = c_v \quad \text{and} \quad n = 1$$

and then it will be assumed that

$$k_r = 10k \quad \text{or} \quad c_{vr} = 10c_v \quad \text{and} \quad n = 10$$

From curve C_1 (Fig. 88*e*) we obtain for $U_z\% = 30$ the value $T_v = 0.07$. Introducing this value into equation 101(3*b*) we get

$$T_v = 0.07 = \frac{c_v}{H^2} t$$

whence

$$t = \frac{0.07H^2}{c_v}$$

The time factor for radial flow at time t is

$$T = \frac{c_v}{4R^2} t = \frac{c_v}{4R^2} \frac{0.07H^2}{c_v} = \frac{0.07 \cdot 20^2}{4 \cdot 5^2} = 0.28$$

Since $R/r = 10$, the degree of consolidation $U_r\%$ at time t is equal to the ordinate of that point on curve C_{10} in Figure 88*e*, whose abscissa is equal to 0.28, or $U_r\% = 29$. Introducing the values $U_z\% = 30$ and $U_r\% = 29$ into equation 5, we obtain

$$100 - U\% = \frac{1}{100} 70 \times 71 = 50$$

or

$$U\% = 50$$

Hence the presence of the wells increases the degree of consolidation at time t from 30 to 50 per cent.

If $k_r = 10k_z$ or $c_{vr} = 10c_v$ the time factor for radial flow at time t is

$$T = \frac{c_{vr}}{4R^2} t = \frac{10c_v}{4R^2} \frac{0.07H^2}{c_v} = 2.8$$

A value of $T = 2.8$ corresponds on curve C_{10} to a degree of consolidation $U_r\%$ of almost 97.5 per cent.

Every sedimentary bed of clay is far more permeable in a horizontal direction than in a vertical direction. Therefore the filter wells are much more effective than one should expect from a computation of the influence of the wells on the rate of consolidation on the assumption that the bed is hydraulically isotropic $k = k_r$ or $n = 1$.

Filter wells have also been used to accelerate the consolidation of beds of clay or silt which have been artificially deposited by some hydraulic process. If such a fill is located above a highly permeable layer one can further increase the efficacy of the wells by maintaining the water level in the wells at the level of the base of the fill by pumping. In either case the rate of consolidation can be estimated by means of a procedure similar to that described above.

Another, less important but more difficult, problem involving a three-dimensional flow of the excess water out of a consolidating clay presents itself in connection with the computation of the rate of settlement of a local surcharge on the horizontal surface of a bed of clay whose thickness is great compared with the width of the area covered by the surcharge. A first attempt to solve the problem was made by Biot (1935*b*) on the assumption that the clay obeys Hooke's law and that the excess water escapes only in a vertical direction.

At a later date the same investigator formulated a general theory of three-dimensional consolidation (Biot 1941*a*). On the basis of this theory he computed the consolidation settlement under a uniformly distributed load covering a rectangular area on the surface of a bed of clay (Biot 1941*b*) and the consolidation due to a load acting on a bed of clay whose top surface is impermeable (Biot and Clingan, 1941). He also investigated the progressive settlement of loaded, elastic slabs resting on a bed of ideal clay (Biot and Clingan, 1942).

All these investigations were based on the assumption that the coefficient of consolidation c_v contained in equation 1 is a constant. For processes of consolidation involving linear flow this assumption is known to be reasonably accurate. However, in connection with two- and three-dimensional processes of consolidation, the same assumption should be regarded as a potential source of errors whose importance is not yet known. Biot also assumed that c_v has the same value for both compression and swelling. This assumption is never justified. A better approximation could be obtained by assuming that c_v for swelling is equal to infinity.

Based on experimental data obtained from triaxial compression tests Rendulic (1936) showed that the process of consolidation of the clay located beneath a finite loaded area can be expressed by the differential equation

$$\frac{\partial u}{\partial t} = \frac{k}{\gamma_w f(x, y, z)}\left(\frac{\partial^2 u}{\partial x^2} + \frac{\partial^2 u}{\partial y^2} + \frac{\partial^2 u}{\partial z^2}\right) \qquad [9]$$

provided the process does not involve a local swelling of the clay. In this equation, k is the coefficient of permeability, and $f(x, y, z)$ is a function which depends on the relation between a change in the effective state of stress in the clay and the corresponding change of the volume of voids. The factor

$$\frac{k}{\gamma_w f(x, y, z)}$$

corresponds to the coefficient of consolidation c_v mentioned above. The function $f(x, y, z)$ represents the equivalent of the coefficient of volume decrease m_{vc} in equation 99(7). According to the results of the tests made by Rendulic, this function

is very complicated. The error due to replacing this function by a constant could be estimated only by means of a theoretical analysis based on the test results which Rendulic has published or by a comparison of computed and observed rates of consolidation. Up to this time no such investigations have been made. Therefore the existing theoretical methods for dealing with two- or three-dimensional problems of the consolidation of clay under load are not yet ready for practical application.

Chapter XIV

CAPILLARY FORCES

107. Capillary phenomena. In fine-grained soils water is capable of rising to a considerable elevation above the water table and remaining there indefinitely. In order to explain this phenomenon physicists have been obliged to assume the existence of a force which is capable of compensating the weight of the water located above the water table. This force is known as *capillary force.* Although the physical nature of this force is still controversial all its mechanical effects can be accurately computed on the basis of the assumption that the locus of the force is the line along which water, air, and solid meet.

108. Surface tension. In order to visualize the mechanics of the capillary rise of the water in the voids of a dry, cohesionless sand, we simplify the problem by considering the rise of the water in a capillary tube. Figure 89 is a section through such a tube. Every part of the body of water contained in the tube, such as the cylindrical element shown in the figure, with a diameter $2x$, a height h_c and a weight $\pi x^2 \gamma_w h_c$ is in a state of equilibrium. At the base of the element, at the elevation of the free water level outside the tube, the hydrostatic pressure in the water is equal to zero. The pressure on the top surface of the element is also equal to zero. The shearing stresses along the cylindrical surface of the element are equal to zero. Yet the element has a weight $\pi x^2 \gamma_w h_c$. Hence it cannot be in equilibrium unless the outer rim of the top surface of the element is acted upon by a force whose vertical component F is equal to the weight $\pi x^2 \gamma_w h_c$. No such force could exist unless the mechanical properties of the uppermost layer of the column of water are different from those of ordinary water. This uppermost layer is called the *surface film* of the water. The force which keeps the element from sinking downward must have its seat within this film, because there is no other conceivable seat for this force. Up to this point our reasoning does not contain any assumption and

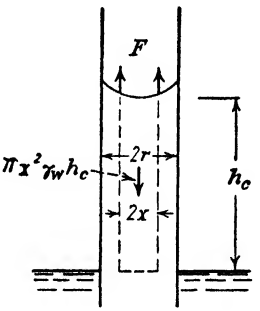

FIG. 89. Forces acting on water contained in a capillary tube.

the conclusion is as strictly valid as any statement regarding the conditions for the equilibrium of a solid body.

The next step is to ascertain the state of stress within the surface film, because the preceding analysis merely informed us concerning the vertical component F of the stresses. Experimental investigations made more than a hundred years ago have shown that the surface film is in a state of two-dimensional tension parallel to its surface and that the force F, shown in Figure 89, represents the vertical component of these tensile stresses. This tension is called the *surface tension* of the water. The thickness of the surface film which represents the seat of the surface tension is of the order of magnitude of 10^{-7} centimeters. The views concerning the molecular mechanism which produces the surface tension are still controversial. Yet the existence of surface tension as a stress acting within the surface film was established during the last century beyond any doubt, and the intensity of this stress has repeatedly been determined by independent methods with consistent results.

Hence, the mathematical concept of this phenomenon involves no hypothesis, because it is valid regardless of the physical causes of surface tension.

A few investigators in the field of soil mechanics have been misled by the differences in opinion concerning the physical causes of surface tension to the conclusion that the existence of surface tension as such is a matter of opinion. This conclusion can be compared to doubts concerning the validity of the laws of electric conductivity based on the fact that our conceptions regarding the nature of electricity are still in a controversial state. In this connection it should be emphasized that no capillary phenomenon has ever been observed which is incompatible with the mathematical concept of surface tension.

The following table contains the tension T_s in the surface film of water in contact with air for different temperatures T. (Smithsonian Physical Tables 1934.)

T(°C.) =	0°	10°	20°	30°	40°
T_s (gr. per cm.) =	0.0756	0.0742	0.0727	0.0711	0.0695

109. Rise of water in capillary tubes and grooves. A tube is called a capillary tube if its diameter is sufficiently small to induce a visible rise of the water within the tube above the free water surface outside the tube. Figure 90*a* is a section through such a tube. The surface of the water in the tube assumes the shape of a cup, called the *meniscus*. The surface of the water intersects the vertical wall at an angle α called the *contact angle*.

The value α depends on the chemical composition of the walls of

the tube and on the type of impurities which cover the walls. If the walls of a glass tube have been cleaned and moistened prior to the test, α is equal to zero. On the other hand, if the walls are covered with a greasy film, α may even be greater than 90°. In this case, the meniscus

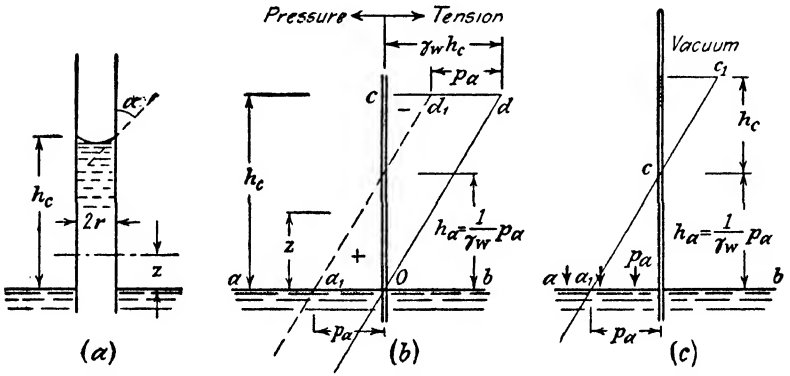

FIG. 90. (*a*) Water contained in a capillary tube; α denotes contact angle at boundary between meniscus and tube; (*b*) state of stress in water in capillary tube with open upper end; (*c*) rise of water in capillary tube whose upper part is evacuated, while free water surface is acted upon by atmospheric pressure p_a.

is convex upward and the apex of the meniscus is located below the level of the water outside the tube. Usually the impurities which cover the walls of capillary tubes are such that the value α ranges between 0° and 80°.

The equilibrium of the column of water which occupies the tube (Fig. 90*a*) above the free water level requires that

$$\pi r^2 \gamma_w h_c = T_s 2\pi r \cos \alpha$$

or

$$h_c = \frac{2T_s}{r\gamma_w} \cos \alpha \qquad [1a]$$

If r is given in centimeters, $\gamma_w = 1$ gram per cubic centimeter and $T_s = 0.075$ gram per centimeter

$$h_c = \frac{0.15}{r} \cos \alpha \qquad [1b]$$

The state of stress in the water contained in a capillary tube depends on the pressure, p_a, in the air located above the water. If the test illustrated by Figure 90*b* is made in a perfect vacuum the entire column of water located above the free water level is in a state of tension for the

following reasons. Since the water is in a state of equilibrium, the pressure in the water is the same in every point of a horizontal section. At the level of the free water surface the pressure is equal to zero. The weight of a column of water located within the capillary tube between the free water level and an elevation z above this level is equal to $\gamma_w z$ per unit of area of a horizontal section. The pressure on the base is equal to zero and the unit pressure on the upper surface is u_z. Since the sum of all the forces which act on the column is equal to zero, we obtain

$$u_z + \gamma_w z = 0$$

or

$$u_z = -\gamma_w z \qquad [2]$$

In Figure 90*b* the values u_z are represented by the abscissas of the straight line *Od*.

If the space located above the water is invaded by air under a pressure p_a the pressure in the water increases everywhere by p_a. Hence, in this case the pressure in the water will be as shown by the abscissas of the dotted line $a_1 d_1$ (Fig. 90*b*). The height h_c of capillary rise remains unaltered. According to Figure 91*b* no tension exists in the water unless the height h_c of capillary rise is greater than $h_a = p_a/\gamma_w$ or approximately 10 meters. Finally, if we dip the lower end of an evacuated capillary tube (Fig. 90*c*) into water in contact with air under a pressure p_a, the water will rise in the tube to a height of

$$h_a + h_c = \frac{p_a}{\gamma_w} + \frac{0.15}{r} \cos \alpha \qquad [3]$$

For glass tubes with perfectly clean walls, $\alpha = 0$.

If we lift the lower end of a capillary tube out of the water and maintain the vertical position of the tube, the flow of the water out of the tube will stop as soon as the water level in the tube arrives at an elevation of about h_c above the lower end of the tube. At the same time a permanent droplet will be formed at the lower end of the tube, as shown in Figure 91*a*. The weight of the column of water contained in the tube is carried by the surface tension of the film at the upper boundary of the column. In the vicinity of the lower end of the tube the stress in the water changes from tension in the column to pressure in the drop and the surface film of the drop can be compared to a minute rubber bag which acts as a container and transfers the weight W of the drop to the lower end of the tube.

Thus far we have considered only the capillary rise of continuous columns of water in a tube and the column of water retained in capillary

tubes after drainage. However, in connection with the origin of soil moisture we are also interested in the capillary rise of water in slits and grooves and in the droplets which are retained at the points of contact between uneven surfaces.

If we immerse the lower edge of two glass plates which are separated from each other by a very narrow air space, the water rises within this space as it does in a capillary tube although the sides of the air space are open. If we adjust the position of the glass plates in such a fashion that they touch each other along a vertical line of contact, the height of the capillary rise in the groove thus obtained decreases from the contact toward the open side. Very narrow grooves can even be used as capillary siphons for transporting water out of a container, provided they are given the shape of a hook whose outer end is located below the surface of the water in the container as shown in Figure 91*b*.

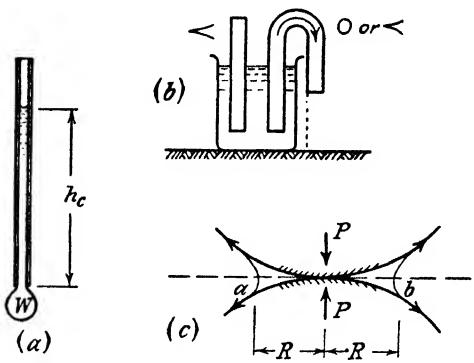

FIG. 91. (*a*) Permanent droplet at lower end of water-filled capillary tube; (*b*) experiment to demonstrate capillary movement in V-shaped grooves; (*c*) adhesion between sand grains produced by contact moisture.

In an accumulation of solid particles such as sand every point of contact between two adjoining particles is surrounded by an annular groovelike space having a V-shaped cross section. The width of this space increases from zero at the contact in every direction. When sand is drained by gravity or by centrifuging, each of these grooves retains a minute quantity of water held in place by capillary forces as shown in Figure 91*c*. The forces exerted by the solid onto the surface film are indicated by arrows. Since they tend to increase the diameter of the particle of water surrounding the point of contact, the water is maintained in a state of tension and the solid particles located on both sides of the point of contact are forced together with a pressure equal and opposite to the tension on the section *ab* through the water.

110. Capillary movement of water in a column of dry sand. If we immerse the lower end of a column of dry sand contained in a cylindrical vessel with a perforated bottom, the water rises in the voids of the sand in the same manner as it rises in a bundle of capillary tubes. In both the sand and the tubes the rate of capillary rise decreases rapidly and finally becomes equal to zero.

In order to simplify the analysis we assume arbitrarily that the water level within the sand represents the boundary between a zone of complete capillary saturation and a zone in which the sand is completely dry. On this assumption the rate of capillary rise is governed by Darcy's law

$$v = ki \qquad [1]$$

wherein v is the discharge velocity, k the coefficient of permeability, and i the hydraulic gradient.

In reality the uppermost part of the moistened zone is in a state of partial and not of complete capillary saturation. Within this zone the rate of flow of the water is determined by the *capillary potential*, which is a function of the degree of saturation of the sand (see, for instance, Baver 1940). However, the methods of computation which are based on the concept of the capillary potential have not yet reached a stage in which they could be advantageously applied to the solution of engineering problems.

Since the cross-sectional area of the column of sand is the same for every elevation, the rise of the water into the column represents a linear flow in a vertical upward direction. At a given time t the water level stands in the sand at an elevation z above the free water level outside the column. Assuming that the vertical component of the surface tension at the upper boundary of the saturated section is a constant, the hydraulic head with respect to the base of the column, located at the free water level is $h_c - z$ and the hydraulic gradient is

$$i = \frac{h_c - z}{z} \qquad [2]$$

The rate dz/dt at which the upper boundary of the saturated zone rises in a vertical direction is identical with the seepage velocity v_s, i.e., with the vertical component of the average velocity of the water in the capillary passage ways. If n is the volume porosity of the sand, v_s is equal to v/n (eq. 88(8)).
Hence

$$v_s = \frac{v}{n} = \frac{dz}{dt}$$

If we combine this equation with equations 1 and 2 we obtain

$$\frac{dz}{dt} = \frac{k}{n}\,\frac{h_c - z}{z}$$

whence

$$h_c - z - h_c \log (h_c - z) = \frac{k}{n} t + C$$

At $t = 0$ the height of capillary rise z is equal to zero. This condition is satisfied, if

$$C = h_c - h_c \log h_c$$

Thus we get

$$t = \frac{nh_c}{k}\left[\log \frac{h_c}{h_c - z} - \frac{z}{h_c}\right] \qquad [3]$$

In the preceding analysis it was assumed that the water is allowed to rise in the voids of a dry sand until a state of equilibrium is reached. However, a state of final capillary equilibrium can also be established by permitting the excess water to drain out of a column of sand which, at the outset, has been completely saturated. In this case the process which leads to the final state of capillary equilibrium is called *drainage*. As soon as the excess water is given an opportunity to escape through the base of the column of sand, air invades the upper part of the column. Thus the water content of the upper part is transformed into a system of threads and streaks of water interwoven with a network of air channels. The water contained in such a network is called *semi-continuous capillary water*. It occupies the narrowest pore channels and the grooves between the grains. If the column of sand is very high, the streaks and threads of water contained in the uppermost part of the column are likely to break up into individual droplets which surround the points of contact between the individual grains, as shown in Figure 91c. Capillary water of this type is in a *discontinuous* state, because each one of the droplets is hydrostatically independent of its neighbors. It is acted upon by its own weight and by surface tension only. Water in this category can remain in the sand forever, at any elevation above the ground-water level provided there is no loss of water due to evaporation.

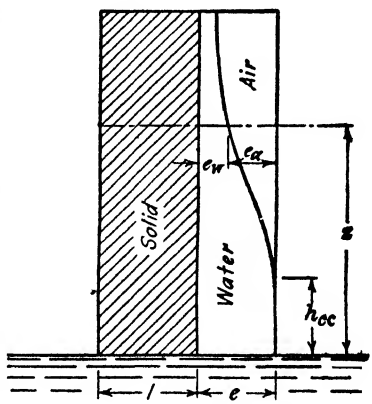

FIG. 92. Vertical distribution of air space after drainage of column of wet sand.

Hence in a final state of capillary equilibrium the uppermost part of the column is moistened by discontinuous soil moisture, whereas the lowest part is completely saturated. The zone of transition contains the capillary moisture in the semi-continuous state as described above. Figure 92 illustrates a method of expressing the degree of saturation in

different parts of a drained column of sand in quantitative terms. In this figure the width of the right-hand rectangle represents the total volume of voids, e, per unit of volume of the solid constituents. The curve shown in the figure divides this rectangle into two parts. At any elevation z above the free water level the width e_w of the left-hand part indicates the volume occupied by the water and the width $e_a = e - e_w$ the volume occupied by the air. The ratio

$$S\% = 100 \frac{e_w}{e} \qquad [4]$$

is called the *degree of saturation* and the ratio

$$G_a = \frac{e_a}{e} = 1 - \frac{S\%}{100} \qquad [5]$$

the *air space ratio*. The height of the zone of complete capillary saturation ($S\% = 100$) will be designated by the symbol h_{cc}. It seems to be smaller than the height h_c to which the water rises by capillarity in a column of perfectly dry sand.

111. Capillary siphon effect. Figure 93*a* is a section through an earth dam with a core made of relatively impermeable material. The crest of the core is located at an elevation ΔH above the free water level. If ΔH is smaller than the height of capillary rise for the material which constitutes the more permeable part of the dam, the capillary siphon effect illustrated by Figure 91*b* causes the water to flow over the crest of the core and to discharge into the downstream part of the dam. A method of computing the rate of discharge is not yet available. However, from both laboratory experiments and field experience it is known that the loss of water due to the siphon effect can be rather important (see, for instance, Terzaghi 1942*b*).

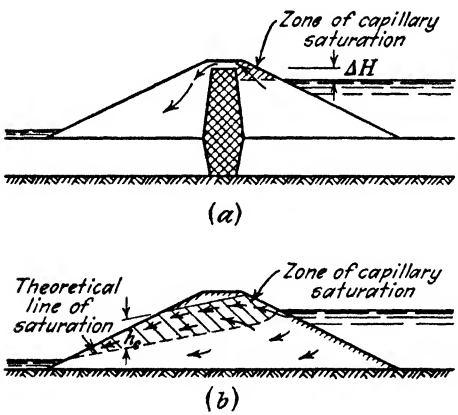

FIG. 93. Capillary flow of water out of a reservoir (*a*) through the soil located above a watertight core, and (*b*) through soil located above the theoretical line of saturation in a homogeneous earth dam.

A similar siphon effect takes place in homogeneous earth dams, as shown in Figure 93*b*. On account of capillary action the water perco-

lates through the dam not only below the so-called line of saturation (see Art. 89) but also within the zone of capillary saturation. In the construction of a flow net for a dam as described in Article 89 this source of movement is not considered. Therefore the real flow net is not perfectly identical with the theoretical flow net and the real discharge is likely to be somewhat greater than the computed discharge.

112. Gas pressure in bubbles and voids. In many soils the zone of complete saturation (capillary or gravity saturation) contains a certain amount of free gas in a discontinuous state. If a gas particle is entirely surrounded by water it is called a *bubble*. Bubbles in soils always adhere to the surface of a soil particle, but the area of contact is insignificant compared with the total surface area of the bubble. On the other hand, if a gas particle occupies a space whose outer boundaries consist of independent menisci separated from each other by the surface of soil grains the gas particle is said to occupy a *void*. Gas bubbles are always almost spherical, whereas the voids may have any shape.

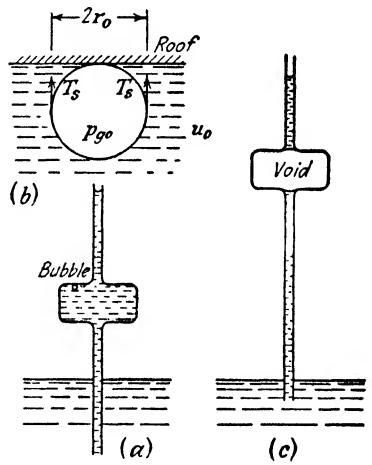

FIG. 94. Diagrams illustrating the conditions which determine the expansion of bubbles into voids.

The gas particles in a soil may represent the remnants of the air which occupied the voids before the water invaded the soil. They may also represent air or some other gas which has previously been dissolved in the water or a gas which developed as the result of chemical processes in the soil. At a given temperature the gas pressure in a bubble depends exclusively on the weight of the gas contained in the bubble and on the stress in the water. The gas pressure in voids also depends on the arrangement of the soil particles which surround the void.

In order to illustrate the difference between the conditions for the equilibrium of a gas bubble and of a gas particle contained in a void we compute the gas pressure in a bubble which adheres to the roof of the water-filled container shown in Figure 94*a*. The bottom of the container communicates through a capillary with an open body of water. Another capillary rises from the roof. By changing the distance between the outside water level and the bottom of the container one can change the stress in the water within the limits determined by the diameter of the upper capillary. The computation will be based on the simpli-

fying assumption that the weight of the gas in the bubble is independent of the state of stress in the water. At the outset of the experiment the diameter of the bubble is equal to $2r_0$. Since the bubble is located above the free water level, the hydrostatic pressure u_{w0} in the water next to the bubble is negative. The real pressure u_0 in the water is equal to the algebraic sum of u_{w0} and the atmospheric pressure p_a, or

$$u_0 = u_{w0} + p_a \qquad [1]$$

The pressure u_0 can be either positive or negative. The gas pressure is p_{g0} and the surface tension T_s. Figure 94*b* is an enlarged vertical section through the bubble. The equilibrium of the forces which act on the lower half of the bubble requires

$$\pi r_0^2 p_{g0} = \pi r_0^2 u_0 + 2\pi r_0 T_s$$

or

$$p_{g0} = u_0 + \frac{2T_s}{r_0} = u_{w0} + p_a + \frac{2T_s}{r_0} \qquad [2]$$

If r_0 approaches zero, the gas pressure p_{g0} approaches infinity. However, within the range of molecular dimensions, equation 2 loses its validity.

By raising the position of the container shown in Figure 94*a* one can reduce the pressure in the water from u_0 to u, whereupon the gas pressure changes from p_{g0} to p_g and the radius of the bubble changes from r_0 to r. According to Boyle's law the product of the volume and the pressure is a constant for every gas at a constant temperature. The volume occupied by the gas before and after the change of the pressure in the water is equal to $\frac{4}{3}\pi r_0^3$ and $\frac{4}{3}\pi r^3$ respectively. Therefore, if r_0 is known, the radius r can be computed from the equation

$$\tfrac{4}{3}\pi r_0^3 \left(u_0 + \frac{2T_s}{r_0}\right) = \tfrac{4}{3}\pi r^3 \left(u + \frac{2T_s}{r}\right)$$

or

$$r_0^3 \left(u_0 + \frac{2T_s}{r_0}\right) = r^3 \left(u + \frac{2T_s}{r}\right) \qquad [3]$$

Solving this equation for u one gets

$$u = \frac{r_0^3}{r^3}\left(u_0 + \frac{2T_s}{r_0}\right) - \frac{2T_s}{r}$$

The rate at which the bubble expands with decreasing value of the

pressure u in the water is determined by the equation

$$-\frac{dr}{du} = \frac{r^2}{\frac{3r_0^3}{r^2}u_0 + 2T_s\left(\frac{3r_0^2}{r^2} - 1\right)}$$

For

$$r = r_1 = r_0\sqrt{3}\sqrt{\frac{r_0 u_0}{2T_s} + 1} \qquad [4]$$

the rate of increase of the radius of the bubble becomes equal to infinity. At that state the real pressure in the water is u_1. By combining equations 3 and 4 we get

$$u_1 = -\frac{4}{3}\frac{T_s}{r_1} \qquad [5]$$

The corresponding hydrostatic pressure (see eq. 1) is

$$u_{w1} = u_1 - p_a = -\left(\frac{4}{3}\frac{T_s}{r_1} + p_a\right) \qquad [6]$$

For the gas pressure one obtains by means of equation 2

$$p_{g1} = u_1 + \frac{2T_s}{r_1} = \frac{2}{3}\frac{T_s}{r_1} \qquad [7]$$

As soon as the hydrostatic pressure in the water becomes equal to u_{w1} (eq. 6) the gas bubble expands and continues to expand until the container is empty. As soon as this state is reached, the gas particle ceases to represent a bubble. It occupies a void, as shown in Figure 94*c*. The boundaries of this void consist of the walls of the container and of two menisci, located at the bottom and the roof of the container respectively. If V is the volume of the container, the gas pressure p_{gv} is determined by the equation

$$\tfrac{4}{3}\pi r_0^3 p_{g0} = V p_{gv}$$

or

$$p_{gv} = \frac{4\pi r_0^3}{3V} p_{g0}$$

In contrast to the gas pressure for the bubble state determined by equation 2, the preceding equation for the gas pressure in the void state contains the volume of the void into which the gas particle expanded. Hence, as soon as the gas particle passes into the void state, as shown in Figure 94*c*, the gas pressure depends chiefly on the initial conditions

and on the volume of the void into which the particle expanded. All the other factors, such as the stress in the water and the surface tension, are of minor importance. The curvature of the menisci which form part of the boundary of the gas-filled void depends on the gas pressure and on the height of the column of water located above and below the container. It can easily be computed on the basis of these data.

In order to illustrate the influence of the size of a bubble on the stress in the water at which the bubble expands into a void we compute the radius r_1 (eq. 4) and the corresponding values u_1 (eq. 5) and u_{w1} (eq. 6) for two different values of r_0 on the assumption that the bubble is located at the outset of the test at the elevation of the free water level. As a consequence u_{w0} in equation 1 is equal to zero. The atmospheric pressure p_a is equal to 1000 grams per square centimeter. On these assumptions u_0 is equal to 1000 grams per square centimeter.

If $r_0 = 5 \times 10^{-5}$ centimeters (radius of a medium-sized clay particle) we obtain $r_1 = 10 \times 10^{-5}$ centimeters, $u_1 = -1000$ grams per square centimeter, and $u_{w1} = -2000$ grams per square centimeter. Hence the bubble expands into a void after it doubles its size, and the corresponding stress in the water is equal to that in the water in a capillary tube at an elevation of 2000 centimeters or 20 meters above the free water level. On the other hand, if $r_0 = 0.05$ centimeter (size of a fine sand particle), we obtain $r_1 = 1.6$ centimeters, $u_1 = -.06$ gram per square centimeter, and $u_{w1} = -1000.06$ grams per square centimeter. Hence, in this case, the expansion of the bubble which precedes the expansion into a void is very important and the stress in the water at which the expansion occurs is numerically almost equal to the atmospheric pressure. It should be remembered that all the equations from which the preceding data were obtained were based on the assumption that the weight of the air contained in the bubbles remains constant. In reality the decrease of the pressure in the water is always associated with a release of air. Therefore the results of the computations are only approximately correct.

The results of the preceding analysis make it possible to visualize the influence of tension in the water contained in the voids of a soil on the space occupied by the gas particles. A void in a soil can be compared to the container shown in Figure 94. The gas content of an almost saturated soil is likely to consist of very small gas bubbles, which adhere to the walls of the voids. If tension develops in the water the largest bubbles expand into voids and as the tension increases the smaller bubbles follow. The tension required to start this process depends on the initial state of stress in the water and on the size of the largest gas bubbles. Once a gas bubble has expanded the relation between gas pressure and surface tension, expressed by equation 2, loses its validity for this gas particle.

Chapter XV

MECHANICS OF DRAINAGE

113. Types of drainage. The term *drainage* is applied to the process of artificial withdrawal of water from a body of soil. In connection with engineering operations drainage is used to increase the stability of the soil prior to excavation or prior to the application of loads. In either case the increase of stability is due to the reduction of the neutral stresses in the soil at practically unaltered total stresses. In order to drain a soil it is necessary to lower the water table. The terms *ground-water level, phreatic water level, water table,* or *ground-water surface* indicate the level to which the water rises in piezometric tubes whose lower end is located immediately below this level. If the ground water is stationary, the water rises in every tube to the same elevation regardless of the location of the lower end of the tubes.

If the water flows through the soil, the ground-water surface is also sometimes called the line of saturation. However, this term is misleading, because every soil is in a state of complete capillary saturation up to some elevation above the water table. At the upper boundary of the zone of complete capillary saturation the piezometric head is always negative, whereas the water table is the locus of all those points in a mass of soil for which the piezometric head is equal to zero.

The lowering of the water table can be accomplished by constructing within the soil a system of ditches or tunnels with a gravity outlet (drainage by gravity), by pumping from wells or ditches (drainage by pumping), or by surface evaporation (drainage by desiccation). The excess water may escape along straight, parallel lines (linear drainage), by flow along curves in parallel planes (two-dimensional drainage), in radial planes (radial drainage), or by flow along lines having a three-dimensional curvature (general case of a three-dimensional drainage).

In connection with the practical application of drainage it is often useful or necessary to know in advance the approximate time required to drain the major part of the excess water out of the soil. The rate at which the water escapes is called the *rate of drainage.* For a given layout of the drainage system both the rate and the effect of drainage depend on the physical characteristics of the soil subject to drainage, such as grain size and compressibility. These characteristics range

between the two limits represented by those of ideal sand and ideal clay.

In connection with drainage the term *ideal sand* indicates an ideal granular material which is perfectly incompressible. Hence the water which drains out of such an ideal sand must be replaced by air occupying the same volume (drainage by air replacement).

The term *ideal clay* indicates a highly compressible soil whose voids are so small that they remain completely filled with water during the entire process of drainage, provided the surface of the soil is protected against evaporation. Hence the total volume of the water which drains out of the ideal clay is equal to the simultaneous decrease in the total volume of the voids. A process of this type is essentially identical with the processes of consolidation under the influence of an external load, and the rate of consolidation can usually be computed by means of the methods described in Chapter XIII.

While the drainage of a mass of sand proceeds the drained part of the mass is separated from the saturated part by a broad zone of transition in which some of the voids are occupied by air and the remainder by flowing water. Within the zone of transition the rate of flow depends not only on the hydraulic gradient and on the size of the voids but also on the degree of saturation and on several other factors. The theories which take these factors into consideration (Gardner 1936; see also Wilson and Richards, 1938, and Baver 1940) are so involved that they are not yet fit for practical application. The computations contained in the following articles are based on the traditional assumption that the drained and the saturated parts of the sand are separated by sharp boundaries. Therefore the results provide us only with a very crude approximation to the real processes of drainage in sands.

114. Drainage of a stratum of ideal sand through its base. Figure 95*a* is a section through a bed of ideal sand with a depth H resting on a layer of gravel which is much more permeable than the sand. Prior to the drainage of the sand, the water table is located at the surface of the sand. At that stage the water stands in piezometric tubes at the level of the surface of the ground. At any depth $H - z$ below the surface the neutral stress (see Art. 6) is equal to

$$u_w = \gamma_w(H - z)$$

Drainage is accomplished by pumping water out of the gravel through wells with a watertight lining. On account of the lining the drainage occurs only in a vertical direction (vertical drainage). The pumping operations maintain the water level in the wells at the level of the base of the sand stratum. After drainage is complete, the lowest part of the sand remains in a state of complete capillary saturation whereas

the voids in the remainder of the sand are occupied by discontinuous soil moisture (see Art. 110). In nature there is a gradual transition between these two zones, but in the following analysis it will be assumed that they are separated by a sharp boundary.

If the sand were dry the water would rise by capillarity within a few days to an elevation h_c above the water table. Therefore it will be assumed that the boundary between the saturated and the drained part of the fill is located at an elevation h_c above the water table, at every state of drainage. Let

n = the volume of voids in the sand per unit of total volume,
G_a = the air space ratio of the sand after drainage (eq. 110(5)),
k = the coefficient of permeability of the sand,
γ_w = the unit weight of the water,
γ = the unit weight of the saturated sand (sand and water combined),
γ_d = the unit weight of the sand after drainage, and
γ' = the submerged unit weight of the sand.

Drainage is performed by rapidly lowering the water level in the wells to the level of the base of the sand and maintaining it at that level by pumping. As a consequence, the water table is transferred from the surface to the base of the bed of sand, whereupon the water tends to flow out of the sand. This tendency is resisted by the surface tension of the water which is capable of carrying the weight of a layer of water with a depth h_c. In order to visualize the effect of the surface tension on the state of stress in the water we make an inclined section ab at an angle of 45° to the horizontal through the sand and establish at different points of this section piezometric tubes, such as the tube S at point m in Figure 95*a*. These tubes are given the shape of a U, which makes it possible to measure both positive and negative neutral stresses. Before pumping starts the water in every tube stands at the level of the surface of the ground. If there were no surface tension the hydraulic head with reference to the lowered water table at time $t = 0$ would be equal to H and the hydraulic gradient equal to $H/H = 1$. However, as soon as the pumping from the wells produces a tendency of the water to flow out of the sand, the surface tension of the water becomes fully active, whereupon the piezometric level for points located close to the surface descends from the surface to a depth h_c below the surface. This event reduces the initial head at the surface with reference to the lowered water table from H to $H - h_c$ and the initial hydraulic gradient from unity to

$$i_0 = \frac{H - h_c}{H} \qquad [1]$$

In Figure 95*a* this gradient is given by the slope of the straight line a_0b, which represents the locus of the piezometric levels for different points on

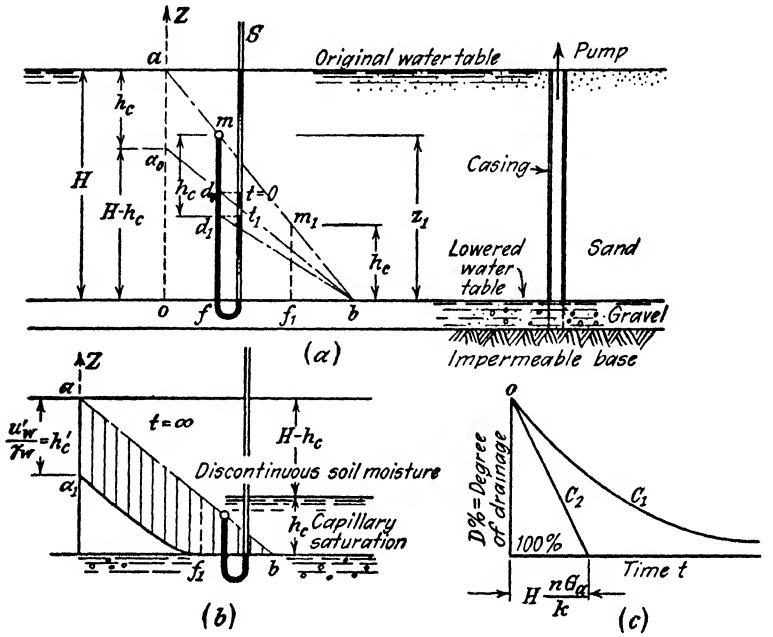

FIG. 95. (*a*) Drainage of bed of sand by pumping from underlying layer of gravel; (*b*) state of stress in the sand after drainage; (*c*) retarding influence of surface tension on rate of drainage. If surface tension were negligible, drainage would proceed as indicated by C_2 in (*c*).

the plane ab at time zero. At any point m of this plane at depth $H - z_1$ below the surface the initial head with reference to the lowered water table is

$$h_0 = \overline{d_0 f} = (H - h_c)\frac{z_1}{H}$$

the initial excess hydrostatic pressure is

$$u_0 = \gamma_w \times \overline{d_0 f} = \gamma_w (H - h_c)\frac{z_1}{H}$$

and the neutral stress is

$$u_{w0} = \gamma_w \times \overline{m d_0} = -\gamma_w h_c \frac{z_1}{H}$$

The line a_0b, as well as any other line in the diagram which connects

simultaneous piezometric levels for the section ab, has the same physical significance as the isochrones shown in Figures 82 and 83. Since the isochrone a_0b (Fig. 95a) is located entirely beneath the section ab the neutral stress at every point of this section is already negative at $t = 0$.

As drainage proceeds the upper boundary of the zone of complete capillary saturation moves downward. At this boundary the piezometric head is always equal to $-h_c$. Hence, if the boundary is located at an elevation z above the lowered water table, the hydraulic head at the boundary is equal to $z - h_c$ and the hydraulic gradient

$$i = \frac{z - h_c}{z} \qquad [2]$$

While z decreases, the water level in the tube S goes down; and as soon as $z = z_1$ the water level stands in S at a distance h_c below point m, as shown in the figure. Further descent of the boundary causes the column of water in the U-tube to break, because m is no longer surrounded with saturated sand.

As soon as the boundary arrives at the elevation h_c of the point m_1 the hydraulic gradient i (eq. 2) becomes equal to zero, whereupon the drainage is complete. The stress conditions for this final state are shown in Figure 95b. In this figure the vertical distance between any point on the plane section ab and the corresponding point on the final isochrone bf_1a_1 represents the piezometric head at that point. The reason for the curvature of the lower part of a_1f_1 will be explained below. Since the isochrone is located entirely below ab the piezometric head is negative at every point of the section. Below elevation h_c the sand remains completely saturated. Above this elevation the water merely occupies the vicinity of the points of contact between the soil grains. It constitutes the discontinuous soil moisture (Art. 110). At any elevation $z < h_c$ the total normal stress on a horizontal section is

$$p = \gamma\,(h_c - z) + \gamma_d\,(H - h_c) \qquad [3]$$

and the effective normal stress is

$$\bar{p} = p + \gamma_w z \qquad [4]$$

At any elevation $z > h_c$ the total normal stress is

$$p = \gamma_d\,(H - z)$$

The neutral stress in the water contained in the voids of the sand above the zone of saturation cannot be measured by any direct means, because the column of water contained in the piezometric tubes breaks as soon as

air enters the end of the tube located at the observation point. However, laboratory determinations of the apparent cohesion of drained sand indicate that the stress in the water contained in the zone of discontinuous soil moisture represents the equivalent of a neutral stress

$$u'_w = -\gamma_w h'_c \qquad [5]$$

which is practically independent of the depth below the surface. The value h'_c is somewhat greater than h_c. In Figure 95*b* the value h'_c is represented by the vertical distance between ab and the upper part of $a_1 f_1$. Hence, for $z > h_c$ the effective normal stress on a horizontal section is

$$\overline{p} = p + \gamma_w h'_c \qquad [6]$$

Since h'_c is greater than h_c there is a gradual transition between the straight upper part of the final isochrone $a_1 f_1 b$ and the straight lower part $f_1 b$. The rate at which the top of the zone of saturation descends from any elevation z toward its final position at elevation h_c is $-dz/dt$ per unit of time. The quantity of water per unit of time which flows out of the layer of sand per unit of area of its base is

$$v = -\frac{dz}{dt} nG_a \qquad [7]$$

In this equation the product nG_a represents that part of the voids of the sand, n per unit volume, which is invaded by air. The quantity v represents the discharge velocity. Darcy's law requires

$$v = ki$$

Combining this equation with equations 2 and 7 we obtain

$$k \frac{z - h_c}{z} = -\frac{dz}{dt} nG_a \qquad [8]$$

The solution is

$$t = \frac{nG_a}{k}\left[h_c - z - h_c \log (h_c - z)\right] + C$$

The value of the constant of integration C is determined by the condition $z = H$ for $t = 0$. Thus we obtain

$$t = \frac{h_c nG_a}{k}\left[\log \frac{H - h_c}{z - h_c} - \frac{z}{h_c} + \frac{H}{h_c}\right] \qquad [9]$$

This equation determines the rate at which the drainage of the ideal sand proceeds. At any time t the quantity of water which has left the

sand per unit of area of its base is

$$(H - z)nG_a$$

The total quantity of water which drains out of the sand is $(H - h_c)nG_a$. The ratio

$$D\% = 100\,\frac{H - z}{H - h_c} \qquad [10]$$

represents the *degree of drainage* of the sand in per cent. It corresponds to the degree of consolidation $U\%$ defined by equation 102(8*b*). By plotting the value $D\%$ against time we obtain the drainage curve C_1 (Fig. 95*c*). It approaches the value $D\% = 100$.

If the height of capillary rise h_c is negligible we obtain for i (eq. 2) the value $i = 1 =$ constant. Instead of equations 8 and 9 we get

$$k = -\frac{dz}{dt}nG_a$$

$$-\frac{dz}{dt} = \frac{k}{nG_a} = \text{constant}$$

and

$$z = H - \frac{k}{nG_a}t$$

Substituting $h_c = 0$ into equation 10, we obtain for the degree of drainage at any time t

$$D(\%) = 100\,\frac{H - z}{H} = 100\,\frac{kt}{nG_aH} \qquad [11]$$

This is the equation of a straight line C_2 in Figure 95*c*, which intersects the lower boundary of the diagram at a point with the abscissa

$$t = \frac{nG_a}{k}H$$

For given values of k, n and G_a the curve C_1 for $h_c > 0$ is always located entirely on the right-hand side of the straight line C_2 for $h_c = 0$. Hence the capillary forces not only reduce the total quantity of water which drains out of the sand but they also retard the process of drainage.

115. Drainage of ideal sand by pumping from well. The drainage of sand prior to excavation operations is frequently accomplished by pumping from wells. Figure 96 shows a layer of sand underlain by an impermeable base at a depth H below the original water table. The

water is pumped out of a single well at a constant rate Q per unit of time. The pumping produces a funnel-shaped depression in the water table, whose radius R increases with time. The computation of the radius R as a function of time is a problem of applied hydraulics, which has been solved only on the simplifying assumption that the capillary

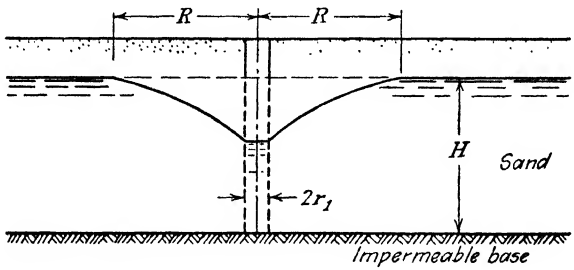

FIG. 96. Drainage of sand by pumping from single well.

suction head h_c is negligible. If h_c is equal to zero the lowered groundwater surface is identical with the boundary between the moist and the saturated part of the sand. Above this boundary the volume occupied by the water is equal to $n(1 - G_a)$ per unit of volume of the sand. The coefficient of permeability of the sand is k. At an arbitrary time t after the pump has been started the vertical distance z between the original and the lowered water table at an arbitrary distance r from the centerline of the well is

$$z = \frac{Q}{4\pi kH}\left(\log\frac{1.5^2}{a} + \frac{a}{4 \times 1!} - \frac{a^2}{4^2 \times 2 \times 2!} + \cdots\right)$$

wherein

$$a = \frac{nG_a r^2}{kHt}$$

If a is small one can neglect all the terms in the parentheses on the right-hand side of the equation except for the first one, whence

$$z = \frac{Q}{4\pi kH}\log\left(\frac{1.5^2}{a}\right)$$

The radius R of the funnel-shaped drained zone in Figure 96 is determined by the condition $z = 0$, which requires that

$$\log(1.5^2/a) = 0 \quad \text{or} \quad a = 1.5^2$$

On the basis of this condition we get

$$R = 1.5\sqrt{\frac{Hkt}{G_a n}} \qquad [1]$$

and

$$z = \frac{Q}{2\pi kH} \log\left(\frac{R}{r}\right) \qquad [2]$$

(Steinbrenner 1937). According to these approximate equations and to several other independent solutions of the problem (Weber 1928, Kozeny 1933) the radius R at a given time t is independent of both the radius of the well and the quantity of water Q which is pumped out of the well. (See also Theis 1940.)

116. Drainage of sand embankments after drawdown. In order to visualize the process of drainage induced by lowering the free water level adjoining an embankment consisting of ideal sand we analyze the simple case illustrated by Figure 97. This figure represents a section

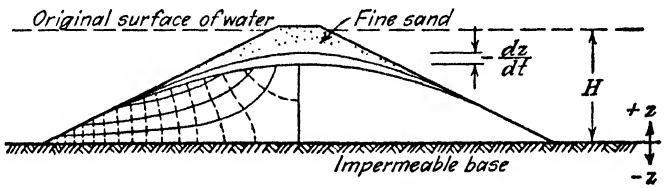

FIG. 97. Flow net for sand embankment, corresponding to an intermediate state of drainage after sudden drawdown.

through a road fill across a pond. The free water level is located immediately below the crest of the fill at an elevation H above the impermeable base of the fill. If the pond is suddenly and completely emptied the excess water, nG_a per unit of volume of the fill, drains out through the slopes of the fill. The height of capillary rise h_c is assumed to be negligible. Since the excess water contained in the sand adjoining the slopes can drain out of the fill more easily than that in the center, the upper boundary of the zone of saturation very soon assumes the shape of a rounded ridge. As time goes on, the crest of the ridge descends at a rate $-dz/dt$ per unit of time, which approaches the value zero. At the crest the discharge velocity is

$$v = -\frac{dz}{dt} nG_a \qquad 114(7)$$

Below the upper boundary of the zone of drainage the continuity condition (eq. 89(1)) is satisfied. Therefore the flow net can be constructed by means of one of the methods cited in Article 89. Immediately after the drawdown, at time $t = 0$, the flow net is similar to that shown in Figure 78*a*, representing the seepage through an embankment during a rainstorm. As time goes on the average hydraulic

gradient within the zone of saturation steadily decreases. Therefore the final state is asymptotically approached. Figure 97 shows the flow net for an arbitrary time t after the drawdown has been accomplished. At any time $t > 0$ the crest of the zone of seepage is located below the crest of the embankment. Hence the corresponding stability conditions are more favorable than those produced by heavy rain provided that the rain establishes a state of complete saturation.

The effect of a sudden drawdown on the stability of fills consisting of cohesive soils will be discussed in Article 122.

117. Drainage of a bed of ideal clay through its base. Figure 98*a* is a section through a stratum of ideal clay whose thickness H is less than the height of capillary rise of the water in the clay. The surface

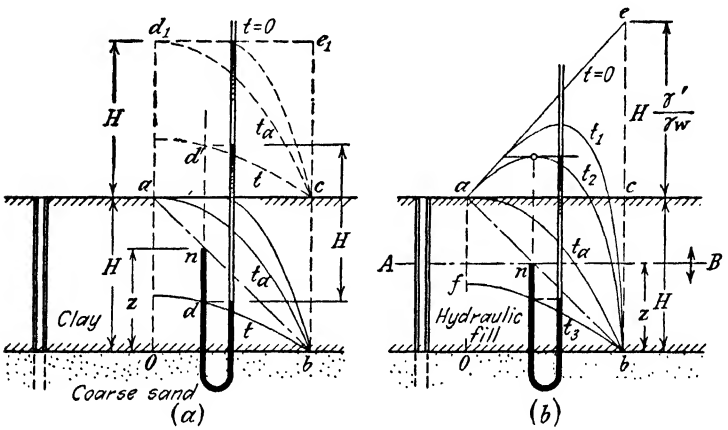

FIG. 98. Consolidation (*a*) of an existing bed of clay and (*b*) of a freshly deposited hydraulic fill by suddenly lowering the water table to the base of the clay and maintaining it at that level by pumping from a well.

of the stratum is permanently protected against evaporation. Prior to drainage the water table is located at the surface of the clay. In this state the water rises from every point of both the clay and the sand in a piezometric tube to the surface of the clay and the neutral stress u_{w0} at a point n at an elevation z above the base of the clay is

$$u_{w0} = \gamma_w(H-z)$$

Drainage is accomplished by sinking a well through the clay into the sand and by maintaining the water level in the well by pumping at the level of the base of the clay. The time required to lower the water level in the well is assumed to be negligible. In accordance with the properties which have been assigned to the ideal clay (Art. 113)

the clay remains in a saturated state throughout the process of drainage. In other words, the volume of the water removed by drainage is equal to the decrease in the volume of the voids of the clay. The excess water escapes out of the clay in a downward direction into the sand. After drainage is complete the piezometric head at any point n of the clay at an elevation z above its base is equal to

$$u_{w1} = -\gamma_w z$$

Hence drainage reduced the neutral stress at elevation z by

$$u_{w0} - u_{w1} = \gamma_w(H - z) + \gamma_w z = \gamma_w H \qquad [1]$$

which is independent of depth.

The total normal unit pressure on a horizontal section through that point remains almost unaltered during the process of drainage, because the weight of the water which drains out of the clay is negligible compared to the total weight of the clay. Therefore the effective normal pressure on horizontal sections increases during the process of drainage by an amount p_1 equal to the simultaneous decrease of the neutral stress (eq. 1) or

$$p_1 = \gamma_w H \qquad [2]$$

The same effect can be produced by loading the surface of the clay with p_1 per unit of area while maintaining the water table at its original position at the surface of the clay. In order to realize the intimate relationship which exists between drainage and consolidation under load, we first consider the consolidation of the clay under the influence of a surcharge $p_1 = \gamma_w H$ without any change in the position of the water table. The surface of the clay is assumed to be covered with an impermeable membrane. Owing to the presence of this membrane the excess water can escape only in a downward direction into the sand. Immediately after the application of the load, the water in every tube stands at the level d_1e_1 at an elevation $p_1/\gamma_w = H$ above the surface of the clay (Fig. 98a). At time $t = \infty$ the water stands in every tube at the level of the surface of the clay. Therefore the lines d_1e_1 and ac represent the zero and the final isochrones respectively. The excess hydrostatic pressure u for intermediate stages is determined by

$$\frac{\partial u}{\partial t} = c_v \frac{\partial^2 u}{\partial z^2} \qquad 99(8)$$

The procedure for establishing the boundary conditions has been explained in Article 101. These conditions are:

for

$$t = 0 \quad \text{and} \quad 0 < z \leqq H, \qquad u = p_1 = \gamma_w H \qquad [3a]$$

$$0 \leqq t \leqq \infty \quad \text{and} \quad z = H, \qquad \frac{\partial u}{\partial z} = 0 \qquad [3b]$$

$$0 \leqq t \leqq \infty \quad \text{and} \quad z = 0, \qquad u = 0 \qquad [3c]$$

$$t = \infty \quad \text{and} \quad 0 \leqq z \leqq H, \qquad u = 0 \qquad [3d]$$

The solution of equation 99(8) which satisfies these boundary conditions is similar to equation 101(3*a*). It can be written in the form

$$u = f(t, z) \qquad [4]$$

In Figure 98*a* this equation is represented by the dashed isochrones. They are a mirror image of those shown in Figure 82. At any time t the water level stands in a piezometric tube at an observation point n at the level of the corresponding point d' on the isochrone for time t, as shown in the figure. The corresponding neutral stress is

$$u_w = \gamma_w \times \overline{nd'} \qquad [5]$$

The process of consolidation due to drainage is also determined by the differential equation 99(8). The boundary conditions are identical with those given in equations 3, except that the head representing the excess hydrostatic pressure u is measured not from the surface but from the base of the bed of clay, at a depth H below the surface. Therefore the solution of equation 99(8) which satisfies the conditions of the problem is identical with equation 4, but the final isochrone *Ob* is located at the base of the layer of clay and not at its surface. Hence, if a set of dashed isochrones, representing a process of consolidation under a surcharge $\gamma_w H$, is given, the corresponding plain isochrones can be obtained by shifting the dashed isochrones through a distance H vertically downward. In other words, the vertical distance dd' between two isochrones corresponding to the same time t is a constant, H. If the consolidation at a given time t at a given point n is due to a surcharge, the neutral stress u'_w at time t is $\gamma_w \overline{nd'}$ and if it is due to drainage the neutral stress u_w is $-\gamma_w \overline{nd}$. Since

$$\overline{nd'} + \overline{nd} = H$$

the difference $u'_w - u_w$ is a constant

$$u'_w - u_w = \gamma_w H$$

or

$$u_w = u'_w - \gamma_w H$$

The neutral stress u_w can either be positive or negative whereas u'_w is always positive.

For both processes, represented by the dashed and the plain isochrones respectively, the relation between time and excess hydrostatic pressure u is determined by the same equation (eq. 4). Therefore the relation between the time factor T_v and the degree of consolidation $U\%$ (eq. 102(8*b*)) is also the same for both processes. It is shown by the curve C_1 in Figure 85*a*.

Figure 98*b* represents the piezograph for a hydraulic fill located above a bed of sand. The piezograph has been plotted on the following assumptions. The consolidation during the construction of the fill can be disregarded. The maximum height of capillary rise is greater than the depth H of the fill, and the hydrostatic head at the base of the fill is maintained at zero with reference to the base of the fill by pumping from a well which extends into the sand. The line *ae* is the zero isochrone, which represents the locus of the piezometric levels for every point of the plane section *ab* for time $t = 0$. At time $t = \infty$ the piezometric level coincides everywhere with the level of the base of the fill. Hence the line *Ob* represents the final isochrone. The zero isochrone is identical with the zero isochrones *ae* in Figures 83*e* and 83*f* respectively, but the final isochrone is different. The process of consolidation is determined by the differential equation 99(8), given before. However, in contrast to the process illustrated by Figure 98*a*, that represented by Figure 98*b* cannot be reproduced by any system of external loading. Therefore it is necessary to solve the equation independently of the solutions given in Article 101. Since *ae* and *Ob* represent the zero and the final isochrones respectively, the boundary conditions are

$$t = 0 \quad \text{and} \quad 0 < z \leqq H, \qquad u = H\frac{\gamma'}{\gamma_w}\frac{H - z}{H} + \gamma_w H$$

$$0 \leqq t \leqq \infty \quad \text{and} \quad z = 0, \qquad u = 0$$

$$t = \infty \quad \text{and} \quad 0 \leqq z \leqq H, \qquad u = 0$$

In Article 101 it has been shown that the hydraulic gradient (eq. 101(6)) at a given point n is identical with the slope of the isochrone at the point of intersection between the isochrone and a vertical through the point. A slope in a direction opposite to that of the reference line *ab* indicates a gradient in an upward direction, whereas a slope in the

same direction indicates a gradient in a downward direction. For $t = 0$, the isochrone is represented by the line ae with a uniform slope toward the left. As a consequence, at time $t = 0$, the water flows at every point of the fill in an upward direction. At time t_2 the flow across the horizontal section AB through point n changes from upward into downward. After time t_a corresponding to the isochrone marked t_a in Figure 98*b* the excess water escapes only in a downward direction and the gradient at the surface remains equal to zero, as shown in Figure 98*b*. Therefore one must supplement the preceding boundary conditions by

$$0 \leqq t \leqq t_a \quad \text{and} \quad z = H, \qquad u = \gamma_w H$$

$$t_a \leqq t \leqq \infty \quad \text{and} \quad z = H, \qquad \frac{\partial u}{\partial z} = 0$$

On the basis of these boundary conditions, the shape of the isochrones shown in Figure 98*b* has been computed by means of an approximate method. During the first stage of drainage, $t < t_a$, the isochrones slope both ways, indicating that part of the water escapes in an upward direction through the surface of the fill and temporarily accumulates on the surface. This phenomenon is called *water-logging*, and it has been observed repeatedly. The elevation of the boundary between the zone of upward and that of downward drainage is determined by the position of the point of contact between the corresponding isochrone and a horizontal tangent to this isochrone as described in Article 101. After the tangent to the isochrones at point a becomes horizontal ($t = t_a$) further drainage occurs only in a downward direction and the water which has previously accumulated on the surface disappears quite rapidly and percolates through the fill into the sand. This part of the excess water is small compared with the total quantity of water which drains out of the fill. Therefore when establishing the boundary conditions we were justified in assuming that the hydraulic gradient at the surface is equal to zero at any time greater than t_a.

Solving the problem on this assumption we obtain a time-consolidation curve which is always located entirely between the curves C_1 and C_2 shown in Figure 85*a*. Since the space between these two curves is rather narrow it suffices for the purpose of an estimate to assign to the time-consolidation curve for the process represented in Figure 98*b* a position intermediate between C_1 and C_2 in Figure 85*a*. If the process of drainage is not assisted by pumping from wells the relation between the degree of consolidation U and the time factor T_v is represented by the curve C_1 (Fig. 85*a*) and at the end of the process of consolidation the hydrostatic excess pressure is equal to zero throughout the fill.

During pumping, the fill acts as a half-closed layer because most of the excess water leaves the fill only through its base. Therefore the symbol H in the equation for the time factor T_v (eq. 101 (3*b*)) represents the entire thickness of the fill. If the consolidation is not assisted by pumping it proceeds as shown in Figure 83*e* and the symbol H represents one half of the thickness of the layer. Since the process of pumping almost triples the average effective vertical pressure in the fill, it causes a very considerable increase of the density of the fill.

118. Effect of gas bubbles on the rate of drainage of a bed of ideal clay through its base. The drainage of a clay always involves a decrease of the neutral stress in the clay. In the process illustrated by Figure 98*a* the ultimate decrease at every point of the bed of clay is equal to $\gamma_w H$ (eq. 117(1)) wherein H is the thickness of the bed of clay which in turn is equal to the vertical distance between the zero isochrone *ac* and the final isochrone *Ob*. If one part of the voids of the clay is occupied by gas bubbles under a gas pressure p_{g0} the decrease of the neutral stress is associated with a lowering of the gas pressure, which in turn involves an expansion of the bubbles. Hence the volume of the water which drains out of the clay is greater than the decrease of voids of the clay. Let

r_0 = average radius of the bubbles prior to drainage,
r = average radius of the bubbles after drainage,
u_w = average neutral stress in the clay before drainage,
$u_w - \gamma_w H$ = average neutral stress in the clay after drainage,
p_a = atmospheric pressure,
e_0 = the average initial void ratio of the clay,
e_1 = the average final void ratio,
a_v = the coefficient of compressibility of the clay,
m_v = the coefficient of volume decrease,
G_a = initial air space ratio, equal to the ratio between the space occupied by the gas prior to drainage, and the initial volume of voids, and
Δe = the final increase of the volume occupied by the gas per unit of volume of solid.

By means of equations 112 (1 and 2) one obtains for the average initial gas pressure in the bubbles the value

$$p_{g0} = u_w + p_a + \frac{2T_s}{r_0} \qquad [1]$$

Drainage reduces the gas pressure to

$$p_g = u_w - \gamma_w H + p_a + \frac{2T_s}{r} \qquad [2]$$

If r_0 is known the radius r of the bubbles after drainage can be computed by means of equation 112(3). Prior to drainage the volume occupied by the bubbles per unit of volume of the solid is equal to $G_a e_0$. Drainage increases this volume to $G_a e_0 + \Delta e$. Boyle's law requires that

$$e_0 G_a p_{g0} = (e_0 G_a + \Delta e) p_g$$

whence

$$\Delta e = e_0 G_a \frac{p_{g0} - p_g}{p_g} \qquad [3]$$

The total quantity of water which leaves the clay during the process of drainage is equal to

$$e_0 - e_1 + \Delta e$$

per unit of volume of solid. In a clay without any bubbles the quantity of water which drains out of the clay due to an increase of the effective pressure by $\bar{p}$ is equal to $e_0 - e_1 = a_v p$ per unit of volume of solid. In a clay with gas bubbles it is equal to

$$e_0 - e_1 + \Delta e = a_v \bar{p} + \Delta e = \bar{p}\left(a_v + \frac{\Delta e}{\bar{p}}\right) = a_v' p$$

wherein

$$a_v' = a_v + \frac{\Delta e}{\bar{p}} \qquad [4]$$

The corresponding coefficient of volume decrease (eq. 98(5)) is

$$m_v' = \frac{a_v'}{1 + e_0} = \frac{a_v + \frac{\Delta e}{\bar{p}}}{1 + e_0} \qquad [5]$$

Hence the rate of consolidation of the clay with gas bubbles can be computed by substituting m_v' for m_v in equation 101(3*b*) which defines the time-factor T_v. Thus we obtain

$$T_v' = \frac{k}{\gamma_w m_v' H^2} t \qquad [6]$$

In the case under discussion the value $\bar{p}$ in equation 5 is equal to $\gamma_w H$ and the value Δe is determined by equation 3. On account of the relations expressed by equations 5 and 6 the drainage of a fine-grained,

practically incompressible sediment may proceed as slowly as that of a highly compressible one, provided its voids are partly filled with gas. The apparent coefficient of compressibility of such a sediment is identical with a_v' (eq. 4) for clays,

$$a_v' = a_v + \frac{\Delta e}{\bar{p}}$$

In Article 105 it has been shown that the presence of gas bubbles in a clay accelerates the rate of consolidation. According to the preceding analysis the gas content has the opposite effect on the rate of drainage.

119. Drainage of ideal clay through the walls of a shaft. Figure 99 is a section through a bed of clay in a state of hydrostatic equilibrium. The water table is assumed to be located at the surface of the bed.

The excavation of a shaft in such a deposit changes the total stresses in the clay adjoining the shaft, thus causing a migration of the water

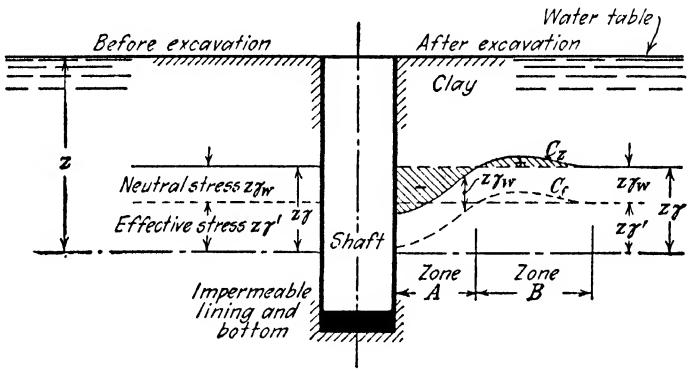

FIG. 99. State of stress in ideal clay surrounding a shaft with watertight lining. Shaded areas on right-hand side indicate temporary change in pore water pressure due to stress relaxation in clay during excavation.

in the clay toward the zone of stress relaxation. We also establish a hydraulic gradient between the clay and the walls of the shaft, involving a gravity flow of water toward the shaft comparable to the flow of water through sand toward a well. In order to perceive the mechanics of this compound process we investigate both components independently. In order to isolate the first component we assume that the bottom and the walls of the shaft are lined with an impermeable membrane and that the shaft is completely filled with water immediately after excavation. Thus we eliminate the source of gravity drainage toward the shaft, and the effect of sinking the shaft is limited to a change in the

state of the stress in the clay. Prior to the construction of the shaft the neutral stress along a horizontal section at a depth z was equal to $z\gamma_w$, the effective normal stress $z\gamma'$ (γ' = submerged unit weight of clay) and the total normal stress $z\gamma$ (γ = unit weight of clay, solid and water combined). In Figure 99 these initial stresses are indicated by the ordinates of horizontal lines. However, the normal stress on horizontal sections in the undisturbed bed of clay is very much higher than the clay can stand without being laterally confined. Therefore the excavation of the shaft causes a plastic yield of the clay toward the shaft, which continues until the state of stress in the clay becomes compatible with the conditions of plastic equilibrium. During this process of stress relaxation, which has been referred to as ring action (Art. 74), the total normal stress on horizontal sections changes from its original value to the values represented by the ordinates of the curve C_z (Fig. 99). (See also Fig. 61*b*.) Within zone A these stresses are lower and in zone B they are higher than the initial total stress γz. Yet, the effective pressures in the clay do not change appreciably unless the void ratio changes. Hence, immediately after the construction of the shaft the change of stress indicated by the shaded areas (Fig. 99) merely involves a change of the neutral stresses. Within zone A the neutral stress has been reduced and within zone B it has been increased. The corresponding hydrostatic pressure gradient causes a migration of water from zone B into zone A. Hence in zone B the clay consolidates and in A it swells. This process continues until the water content of the clay has adapted itself to the modified stress conditions. In the final state the neutral stress is again equal to what it was before the construction of the shaft, or $\gamma_w z$, and the effective normal stresses on a horizontal section at depth z are equal to the ordinates of the curve C_f (Fig. 99) which is located at a distance $z\gamma_w$ below the curve C_z.

It should be emphasized that the swelling of the clay in zone A occurs in spite of the impermeable membrane which is assumed to cover the bottom and the walls of the shaft. This fact indicates the fallacy of the widespread opinion that the swelling of the clay in shafts and in tunnels is exclusively due to the absorption of moisture out of the atmosphere.

If the shaft is not provided with a watertight lining and if no free water is allowed to accumulate in the shaft, the piezometric head at any point of the walls of the shaft at a depth z below the surface cannot be greater than zero. It can, however, be temporarily negative. On the other hand, at the same depth z, at a considerable distance from the shaft the piezometric head is equal to z. Therefore the construction of the shaft produces a tendency for the water to drain toward

the shaft. However, as long as the clay located within zone A tends to swell not a drop of water can get out of the clay into the shaft, because all the water which flows toward the shaft is retained within the zone of swelling A. The flow of water into the shaft cannot begin until the water content of the clay has adapted itself to the modified stress conditions. If the recharge of the clay by rain water balances the loss of water by drainage toward the shaft the existence of the shaft gives rise to a stationary, radial flow of water toward the shaft. The piezometric head at any point of the walls of the shaft remains equal to zero. In practice it is unlikely that water will ever flow out of the clay into the shaft because the rate of evaporation is likely to be higher than the quantity of water which drains toward the shaft by gravity. The influence of evaporation on the state of stress in the clay will be discussed in Article 121.

The excavation of a tunnel in a bed of homogeneous clay also produces a very substantial reduction of the stresses in the clay adjoining the tunnel combined with an increase in the pressure at a greater distance (see Fig. 57*c*). Therefore the excavation of the tunnel must also be followed by a swelling of the clay adjoining the tunnel, regardless of whether or not the atmosphere contributes any moisture to the clay. The rate of swelling of the clay adjoining a shaft can be estimated by means of equation 106 (4) on the simplifying assumptions that the flow of the water occurs in horizontal planes and that the radial and circumferential normal stresses are principal stresses.

120. Drainage of an ideal clay embankment after a sudden drawdown. Figure 100*a* shows a cross-section through an embankment made of ideal clay whose unit weight is γ. The submerged unit weight is γ' and the height H of the embankment is smaller than the height of capillary rise. The embankment rests on an impermeable base and it is almost completely submerged in a pond. The clay is assumed to be in a state of hydrostatic equilibrium. Hence the water rises at every point of the embankment in a piezometric tube to the level of the water in the pond. If we suddenly empty the pond the piezometric head becomes temporarily equal to zero at every point of the slopes of the embankment. As time goes on the water content of the clay adapts itself to the new hydraulic boundary conditions. However, immediately after the drawdown the water content is practically identical with what it was before.

In order to visualize the influence of this condition on the state of stress in the fill immediately after a drawdown we investigate the state of stress on a horizontal section through the fill at an elevation z above its base. The left-hand side of Figure 100*a* shows the approximate

distribution of the stresses on the section before the drawdown. The total normal stresses $u_w + \bar{\sigma}$ on the section are approximately represented by the ordinates of the line $rr_1t_1o_1$ and the effective normal stresses $\bar{\sigma}$ by those of the line rto. The ordinates of these lines have been

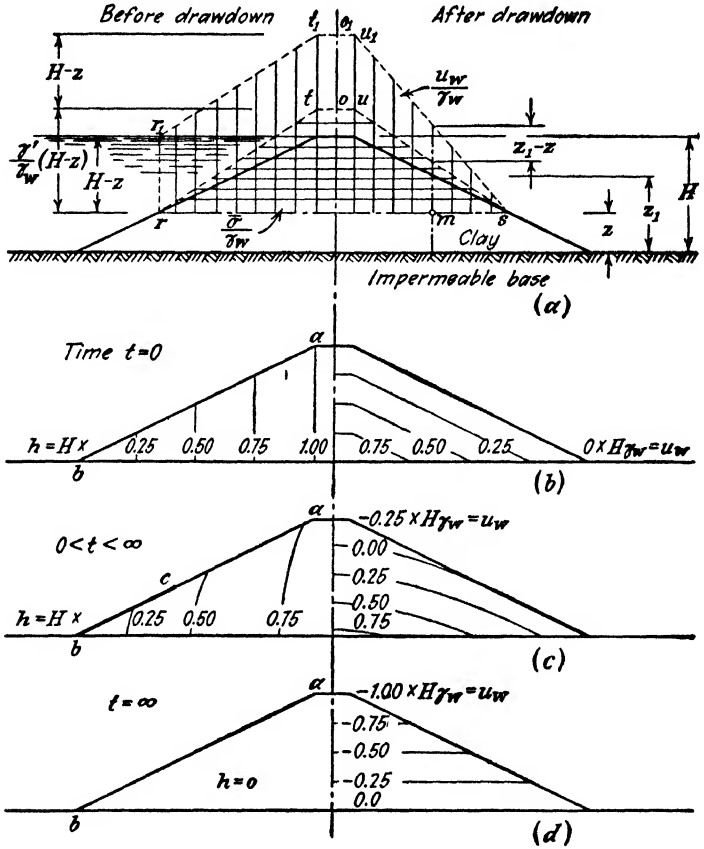

FIG. 100. (*a*) Left-hand side: approximate distribution of effective and neutral pressure on horizontal section through completely immersed clay fill; right-hand side: the corresponding pressures immediately after sudden drawdown; (*b* to *d*) hydraulic conditions at times 0, *t*, and ∞. Left-hand sides show lines of equal hydrostatic head and right-hand sides the lines of equal neutral stress.

obtained by dividing the normal stresses by the unit weight γ_w of the water. The drawdown reduces the total normal stresses to the values which are determined by the line su_1o_1 on the right-hand side. Yet the water content of the clay remains unchanged. Hence, if the fill material were laterally confined, the effective normal stresses would

also remain unchanged, and the neutral stress u_w at any point m of the horizontal section would be equal to

$$u_w = \gamma_w(z_1 - z,$$

The piezometric head is $z_1 - z$ and the hydrostatic head with reference to the toe of the fill would be

$$h = z_1$$

which is the same for every point on a vertical line through m. The right-hand side of Figure 100*b* shows the lines of equal neutral stress and the left-hand side the lines of equal head for the state immediately after the drawdown.

In reality the fill material is not laterally confined. As a consequence the drawdown changes not only the total normal stress on horizontal sections but also the shearing stresses. This change is associated with a change of the effective principal stresses at unaltered water content, which in turn produces a supplementary change in the neutral stresses. This change can either be positive or negative. It depends on the relation between stress and volume change for the fill material and cannot yet be computed. Hence at the very best, the state of stress represented by Figure 100*b* is approximately correct.

During the subsequent process of drainage the clay remains in a state of complete capillary saturation and the total quantity of water which flows out of the embankment is equal to the total decrease of the volume of the voids due to consolidation. Since the hydraulic head decreases from the central part of the fill in both directions the excess water drains toward the lowest parts *bc* of the slopes, as shown in Figure 100*c*. At every point of the discharge area the hydraulic head with reference to the toes of the embankment remains equal to its initial value. Within the upper and the central parts of the embankment the neutral stress and the corresponding hydraulic head decrease. The equations of the curves of equal head and of equal neutral stress could be derived by means of the differential equation 106(2). However, on account of the involved boundary conditions, the problem has not yet been solved. The author assumes that the curves would look about like those shown on the left-hand side of Figure 100*c*.

On the upper part *ac* of the slopes the piezometric head is negative, because the flow of the water from *ac* through the clay toward *bc* is resisted by the surface tension of the water. As time goes on the width of the exit area *bc* decreases and approaches zero. In this final state the water in every piezometric tube stands at the level of the

base of the embankment and the hydrostatic head with reference to this base is at every point equal to zero, as shown in Figure 100*d*.

Since the ultimate neutral stress is negative in every point of the embankment, subsequent immersion of the embankment causes the clay to swell. A similar condition exists in earth dams for storage purposes which have been built out of cohesive soil in a semi-desiccated state because this state is associated with a negative neutral stress in the soil. While the reservoir is being filled for the first time, the soil swells, its shearing resistance decreases, and the factor of safety with respect to sliding decreases. The process begins on the upstream side of the fill.

121. Drainage by desiccation. We know from experience that a specimen of saturated clay in contact with the atmosphere gradually dries out from the surface toward the interior. This process involves a continuous flow of water from the interior of the clay toward the surface of evaporation. At the surface the discharge velocity is equal to the rate of evaporation, v_e per unit of area and per unit of time. The neutral stress due to the weight of the water contained in the specimen is negligible. Therefore, as long as the water contained in the clay is in a state of equilibrium, the neutral stress throughout the specimen is either almost equal to zero or else it is everywhere negative. Yet, as soon as one exposes the surface of the clay to evaporation, the water drains from the interior of the specimen toward the surface which in turn requires the existence of a hydraulic gradient. Since the neutral stress in the interior of the specimen did not increase, the existence of the hydraulic gradient indicates a decrease in the neutral stress at the surface. The only one known agent which can produce such a decrease without any change in the external conditions is the surface tension of the water.

If we eliminate further evaporation before air has entered the voids of the clay, the clay is still in a saturated state. Yet its void ratio is appreciably smaller than the initial void ratio and subsequent immersion causes the clay to swell. The inflow of water into the clay requires a hydraulic gradient, which is directed toward the interior of the clay. Since the surface of the swelling specimen is in direct contact with free water we are obliged to assume that the water contained in the clay is in a state of tension.

In order to visualize the state of stress in a partly desiccated mass of clay and its relation to the surface tension we analyze the forces which act on a bundle of highly compressible capillary tubes whose radii are equal to r. The tubes are completely filled with water as shown in Figures 101*a* and 101*b*. Pressures due to the weight of the water are considered negligible compared to the forces produced by the surface tension, and the area of the section through the walls of the

capillaries is assumed to be negligible compared to the total area of the section through the tubes. The minimum value of the angle of contact α is assumed equal to zero. Figure 101*a* shows the tubes before evaporation starts. At this stage the total normal stress on a section through the bundle is practically equal to zero and the angle of contact of the

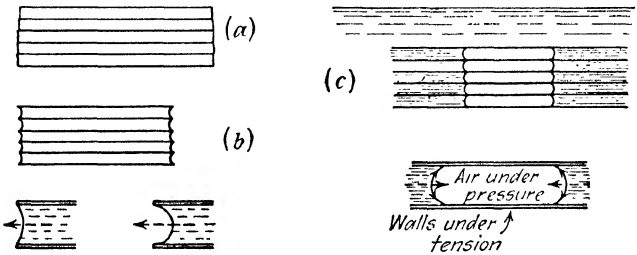

FIG. 101. (*a* and *b*) Axial compression of capillary tubes due to evaporation of water at their open ends; (*c*) tension in middle part of air-filled capillary tubes after immersion.

menisci is 90°. As evaporation proceeds the surface of the water tends to withdraw into the interior of the tubes. This tendency is resisted by the surface tension of the water which causes the surface layer of the water to adhere to the outer ends of the tubes. Hence the menisci assume a cuplike shape. With increasing curvature the axial component of the surface tension, indicated by a dashed arrow, increases. It produces a tension in the water and a pressure of equal intensity in the walls of the tubes. The smallest value which the radius of curvature of the menisci can assume is equal to the radius of the tubes. In this stage the contact angle α which was originally equal to 90° is equal to zero. For $\alpha = 0$ the total pull exerted by the surface tension on the water contained in one tube is $2\pi r T_s$. The tensile stress u_w in the water is determined by the equation

$$2\pi r T_s \cos \alpha + \pi r^2 u_w = 0$$

or

$$u_w = -\frac{2T_s}{r} \cos \alpha \qquad [1]$$

This value represents the neutral stress in the system. The total normal stress on every section through the tubes remained equal to zero. Therefore the solid walls must be acted upon by an effective stress

$$\bar{p} = 0 - u_w = \frac{2T_s}{r} \cos \alpha \qquad [2]$$

per unit of area of the total section through the tubes. The value $\bar{p}$ is called the *capillary pressure*, because it is exerted by the capillary forces. If the walls of the tubes are highly compressible the capillary pressure produces a visible shortening of the tubes, as indicated in Figures 101*a* and 101*b*. By combining equations 2 and 109(1*a*) we get

$$p = \gamma_w h_c \cos \alpha$$

wherein h_c is the height of capillary rise.

When a bundle of empty capillary tubes is immersed in a horizontal position to a depth z below the surface of the water the surface tension pulls the water into the tubes and compresses the air which remained in the tubes as shown in Figure 101*c*. The force with which the surface tension pulls the water toward the air is determined by equation 2. It combines with the water pressure $\gamma_w z$ and the atmospheric pressure p_a. For $\alpha = 90°$ the total pressure in the air is

$$p_g = \gamma_w z + p_a + \frac{2T_s}{r} = \gamma_w (z + h_c) + p_a$$

This equation can also be obtained by substituting $u_{wo} = \gamma_w z$ in equation 112(2).

The average normal pressure per unit of the total area of a vertical section through the bundle is equal to the pressure in the water at the same elevation, which is $\gamma_w z + p_a$; the pressure in the air which occupies the tubes is p_g, and the cross-sectional area of the walls of the tubes was assumed to be very small compared to that of the bundle. Therefore equilibrium requires that the solid walls carry a stress

$$\bar{p} = \gamma_w z + p_a - p_g = \frac{2T_s}{r} = \gamma_w h_c$$

per unit of the area of the total cross section of the bundle. This stress is a tensile stress. If the walls are weak it may cause a failure of the walls by tension.

Every soil, including clay, comprises a system of capillary channels which communicate through the surface with the surrounding space. If these capillaries are filled with water the process of evaporation must necessarily produce the mechanical effects illustrated by Figures 101*a* and 101*b*, including the development of tensile stresses in the water combined with shrinkage due to the capillary pressure. Subsequent immersion causes the soil to swell.

The preceding account of capillary pressure and of swelling is based on the assumption that the flow of water into or out of a soil is exclusively due to the existence of a hydraulic gradient with a purely mechanical origin. This is the mechanical concept of swelling. In exceptionally fine grained soils, such as bentonites, the swelling assumes the characteristics of a penetration of water into a solid by diffusion. The relation between swelling due to mechanical causes and to diffusion will be discussed in a volume on applied soil mechanics. Since the fundamental equations for consolidation and for diffusion are identical it makes no difference to which of these two causes the observed phenomena may be ascribed.

The greatest value $\bar{p}_s$ which the capillary pressure in a soil can assume is numerically equal to the greatest tension u_s which can develop in the water contained in the soil. This tension is equal to

$$u_s = -\gamma_w h_c = -\bar{p}_s \qquad [3]$$

wherein h_c is the height of capillary rise (see Arts. 109 and 110). As soon as the neutral stress in the water becomes equal to u_s further evaporation causes the surface of the water to recede into the interior of the soil while the stress in the water retains its value u_s.

In practice it may occasionally be necessary to estimate in advance the rate of consolidation of a bed of clay by drying. After the desiccation is complete the neutral stress throughout the clay is equal to $u_s = -\gamma_w h_c$ (eq. 3). Since the weight of the water which evaporates is small compared with the total weight of the clay the total normal stress on horizontal sections through the clay remains practically constant. Therefore the process of drying increases the vertical effective pressure of the clay by $p_s = -u_s$. The same ultimate effect can be obtained by consolidating the clay under a surface load $p_s = \gamma_w h_c$ per unit of area. If the clay rests on an impermeable base as assumed in the computation illustrated by Figure 82, the excess water escapes during both processes in an upward direction through the surface of the clay. Yet, though the final effect of both processes is the same, the rate of consolidation is governed by different laws, because the boundary conditions are different. In order to visualize this difference we make a vertical section (Fig. 102*a*) through the clay, similar to the section shown in Figure 82 and plot the piezograph for the state of stress on a plane *ab* which rises at an angle of 45° to the horizontal. The dashed curves above *ac* are the isochrones for consolidation under a surface load p_s per unit of area and are identical with those shown in Figure 82. At any time t' the water stands in a piezometric tube above an arbitrary point m of the plane *ab* at the level of the point l' which is located at the intersection between a vertical line through m and the isochrone for time t'. The corresponding hydraulic gradient is equal to the slope of the isochrone at point l'. A slope toward the left indicates a gradient

in an upward direction. At the surface, represented by point a, the piezometric level remains permanently at the level of the surface of the

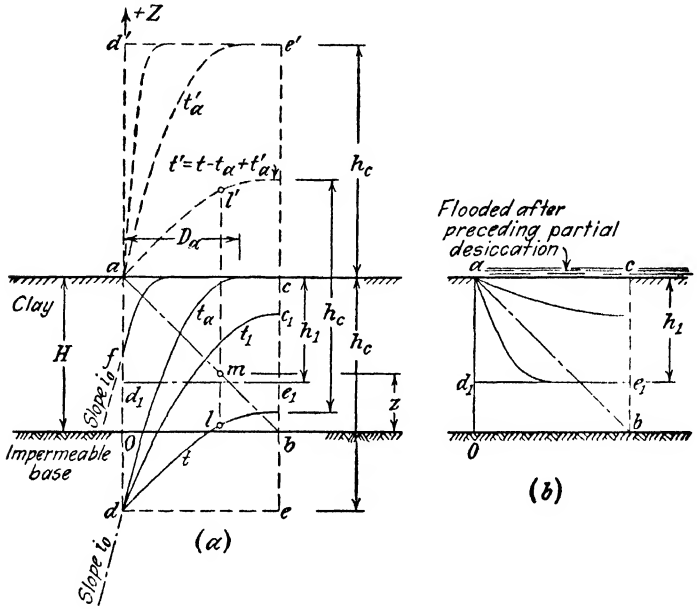

FIG. 102. (a) Consolidation of bed of clay due to surface evaporation; (b) swelling of partly desiccated bed of clay after flooding of its surface.

clay. As time goes on the hydraulic gradient i at the surface steadily decreases and approaches zero. Therefore the discharge velocity

$$v = ki$$

also decreases and approaches zero.

If the consolidation is due to desiccation, the line ac represents the zero isochrone and the line de the final isochrone. At any time t the excess hydrostatic pressures u are equal to the ordinates of the isochrone for time t with reference to the final isochrone de multiplied by the unit weight of the water γ_w. The tension in the pore water at the surface increases with increasing loss of water by evaporation. Therefore the left-hand end f of the isochrones (Fig. 102a) whose ordinate represents the hydraulic head at the surface gradually moves from its initial position a toward its final position d, where it arrives at time t_a. At any time during this period the slope i_0 at the left-hand end f of the isochrones is determined by the rate of evaporation v_e. The process which takes place between time zero and t_a constitutes the first stage of the process of consolidation due to desiccation. Dur-

ing the same period all the dashed isochrones pass through a. Hence the first stage of desiccation has no resemblance to the corresponding consolidation under the load p_s.

The second stage begins as soon as the stress in the water assumes the greatest value compatible with the shape and size of the voids in the clay. This value is equal to $u_s = -\gamma_w h_c$, equation 3. During the second stage the stress in the water at the surface remains constant, while the quantity of water which leaves the clay through the surface decreases. During this stage the isochrones pass through the left-hand end d of the final isochrone de and at their right-hand ends their slope is equal to zero. Hence in this stage the boundary conditions for the plain isochrones are identical with those for the dashed ones.

In order to compute the rate of consolidation during the first stage one must know the rate of evaporation. Everything else being equal the rate of evaporation decreases with increasing tension in the water. However, to simplify the computation we assume that the rate of evaporation remains constant during this stage and equal to v_e. A constant rate of evaporation is necessarily associated with a constant rate of flow of water through the surface and a constant hydraulic gradient i_0 at the surface. This condition can be expressed by the equation

$$v_e = ki_0$$

wherein i_0 is the hydraulic gradient at the surface. Therefore the hydraulic gradient

$$i_0 = \frac{v_e}{k} = -\frac{1}{\gamma_w}\frac{\partial u}{\partial z} \qquad [4]$$

which is equal to the slope of the left-hand end of the isochrones is also a constant. This condition prevails until the time t_a when the left-hand end of the isochrones arrives at point d corresponding to a neutral stress $u_s = -\gamma_w h_c$. Until this time the boundary conditions for the process of desiccation are

$t = 0$	and	$0 \leqq z \leqq H,$	$u = \gamma_w h_c$
$0 \leqq t \leqq t_a$	and	$z = H,$	$\frac{\partial u}{\partial z} = -\frac{\gamma_w}{k} v_e$
$0 \leqq t \leqq t_a$	and	$z = 0,$	$\frac{\partial u}{\partial z} = 0$
$t = t_a$	and	$z = H,$	$u = 0$

After time t_a (second stage), the piezometric head h_c remains constant, but the quantity of water which flows toward the surface decreases and approaches zero. Thus the quantity of water which flows toward the surface becomes smaller than the quantity which evaporates as long as the surface of the water remains at the surface of the clay. Therefore, the surface of evaporation withdraws into the interior of the clay. With increasing distance between these two surfaces the rate of evaporation decreases very rapidly. Hence a slight downward movement of the surface suffices to maintain equality between the loss due to evaporation and the decreasing recharge from below.

In the second stage the isochrones pass through point d because at the surface represented by point a the excess hydrostatic pressure u attained its final value zero at the beginning of this stage. At time $t = \infty$ the isochrone becomes identical with the horizontal line de. Therefore between the time t_a and $t = \infty$ the slope of the isochrones at d decreases and approaches zero. For this second stage of desiccation the boundary conditions are

$$t_a \leqq t \leqq \infty \quad \text{and} \quad z = H, \quad u = 0$$

$$t_a \leqq t \leqq \infty \quad \text{and} \quad z = 0, \quad \frac{\partial u}{\partial z} = 0$$

$$t = \infty \quad \text{and} \quad 0 \leqq z \leqq H, \quad u = 0$$

The isochrones for this second stage are similar to the dashed isochrones in Figure 102*a* because the boundary conditions are similar.

The rate of consolidation is determined by the differential equation 99(8). The problem of computing this rate has been solved by approximation for $H = \infty$ (Terzaghi and Fröhlich, 1936), with the following results. Between time $t = 0$ and a time

$$t_a = \frac{\pi}{4} \frac{1}{c_v} \left(\frac{k p_s}{\gamma_w v_e} \right)^2 \qquad [5]$$

in which c_v = coefficient of consolidation (eq. 99(7)), the perceptible consolidation of the clay due to desiccation is limited to the upper part of the layer of clay. For any time $t > t_a$ the thickness of the consolidated crust is determined by the equation

$$D = 2\sqrt{3 c_v t} \qquad [6]$$

For $t = t_a$, D is equal to

$$D_a = \frac{k p_s}{\gamma_w v_e} \sqrt{3\pi} \qquad [7]$$

If the depth H of a bed of clay is greater than D_a the foregoing equations also apply to such a bed. In either case the isochrone corresponding to time t_a is a parabola

whose vertex is located in Figure 102*a* on *ac* at a distance D_a from *a*. At any time $t < t_a$ the neutral stress at the surface is

$$u_w = 2\gamma_w \frac{v_e}{k}\sqrt{\frac{tc_v}{\pi}}$$

At time $t = t_a$ the degree of consolidation is

$$U_a = \frac{D_a}{3H} \qquad [8]$$

In the process of consolidation under load represented by the dashed isochrones the same degree of consolidation would be reached at a time t'_a. After the time t_a the relation between the time factor and the degree of consolidation is the same for both processes, provided we apply the load $p_s = \gamma_w h_c$ on the surface of one bed of clay at a time $t_a - t'_a$ after the process of desiccation has been started on another similar bed of clay. In order to obtain a plain isochrone in Figure 102*a* for $t > t_a$ we construct the dashed isochrone for $t' = t - t_a + t'_a$ after the load was applied and shift the dashed isochrone through a distance h_c in a downward direction as shown in the figure.

If we stop further evaporation at a time t_1 represented by an isochrone dc_1 (Fig. 102*a*) the water in the clay is the seat of a hydraulic gradient directed toward the surface of the clay. Since such a gradient is incompatible with the hydraulic equilibrium in the clay for $v_e = 0$, water flows from the lower part of the bed of clay into the upper one until the hydraulic gradient becomes equal to zero. This process involves a consolidation of the lower part and a swelling of the upper part of the clay. At the end of this process the excess hydrostatic pressure is equal to $-\gamma_w h_1$ throughout the bed of clay. Such a process is called an *adiabatic process*. The value h_1 is determined by the condition that the average water content of the clay remains constant during the entire process. At time $t = \infty$ the water stands in every piezometric tube on the line d_1e_1 at a depth h_1 below the surface. Therefore the line d_1e_1 represents the final isochrone for this process.

In the thermodynamic analogue this process corresponds to the upward migration of heat in a horizontal layer with insulated surfaces, whose initial temperature decreases from the base toward the top. As time goes on the temperature gradient gradually disappears and the temperature of the layer becomes everywhere equal to the average of the initial temperatures.

If the surface of the clay is flooded at the stage represented by the final isochrone d_1e_1 (Fig. 102*a*) the hydrostatic head at the surface becomes equal to zero against $-h_1$ in the interior of the clay. The corresponding hydraulic gradient causes an infiltration of free water into the interior of the clay. The zero isochrone for this process is d_1e_1 in Figure 102*b* and the final isochrone is *ac*. The isochrones for this process of swelling

resemble a mirror image of the dashed isochrones shown in Figure 102*a* with reference to the surface of the clay and the equation of the time-swelling curve is identical with the equation of the time-consolidation curve C_1 in Figure 85*a*. However, in order to compute the rate of swelling we must replace the coefficient of volume compression m_v in the equation for the time-factor T_v (eq. 101(3*b*)) by the coefficient m_{vs} of volume expansion (eq. 98(6)).

122. Effect of drainage on earth pressure and stability. Every process of drainage reduces the stress in the pore water of the soil without appreciably changing the total stress. This change in the neutral stress involves an increase in the effective stresses on every potential surface of sliding within the soil, although the weight of the soil located above

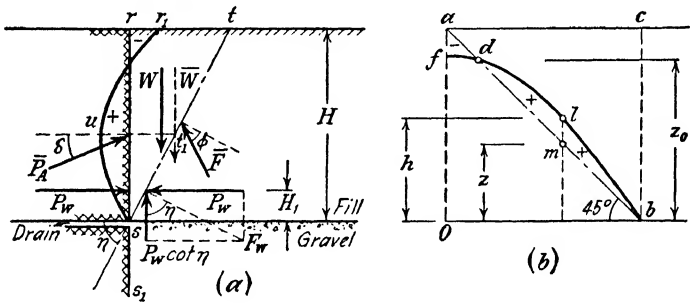

FIG. 103. Hydraulic fill with negligible cohesion deposited behind retaining wall. Water table is located at base of fill and height of capillary rise is greater than the depth H of the fill. (*a*) shows forces which act on sliding wedge at intermediate state of consolidation of fill; (*b*) isochrone for the same state.

this surface is unaltered. Drainage therefore increases the factor of safety with respect to sliding, provided the external conditions for equilibrium remain unchanged. This statement is valid regardless of whether or not the lateral face of the earth is held by an artificial support.

The neutral stress in the soil during and after drainage can be computed for any potential surface of sliding on the basis of the information contained in the preceding articles of this chapter. Once these stresses have been determined the factor of safety against sliding or the conditions for equilibrium can be ascertained by means of the methods described in Chapter XII. If the drainage occurs in a vertical direction toward the base of a stratum the computation is substantially simplified by the fact that the neutral stress at a given time is the same for every point of a horizontal section through the stratum. As an example we compute the lateral pressure exerted on the section rs of the back rs_1 (Fig. 103*a*) of a retaining wall by a sluiced backfill in an intermediate

state of consolidation. At the elevation of point s the backfill rests on a bed of gravel. The water table is assumed to be located at the elevation of the base of the fill. The excess water drains through the base of the fill into the gravel and escapes through openings in the wall, below the level of point s, toward an open space located on the left side of the wall.

The process of consolidation of the fill is graphically represented by the plain isochrones in Figure 98*b*. The isochrones represent the locus of the piezometric levels for different points of an inclined section ab for a given time t. The curve bdf in Figure 103*b* is a duplicate of one of these isochrones. It intersects the inclined section ab at point d with the ordinate z_0. Above the level of point d the piezometric head is negative and below this level it is positive. If z is the elevation of any point m on the section ab and h is the ordinate of the corresponding point l on the isochrone, the neutral stress u_w at point m at time t is

$$u_w = \gamma_w(h - z)$$

If $z < z_0$ the neutral stress u_w is positive and if $z > z_0$ it is negative. Plotting the positive values of u_w to the left of rs in Figure 103*a* and the negative values toward the right we obtain the hydrostatic pressure area rr_1us, which represents the total neutral pressure on the vertical face rs of the sliding wedge rst. The resultant P_w of this pressure passes through the center of gravity of the pressure area at an elevation H_1 above the base of the fill. Since the neutral stress at a given time is the same for every point on a horizontal section through the fill the total neutral pressure F_w on the inclined surface st of the sliding wedge is

$$F_w = \frac{P_w}{\sin \eta}$$

The point of application of this pressure is also at an elevation H_1 above the base of the fill. The horizontal component of F_w is equal to P_w and the vertical component is $P_w \cot \eta$. The horizontal component is equal and opposite to the water pressure on rs. Therefore the resultant of all the neutral forces which act on the sliding wedge rst is equal to $P_w \cot \eta$ and it acts in a vertical direction as shown in the figure. The neutral force $P_w \cot \eta$ reduces the effective weight of the sliding wedge from W (weight of solid and water combined) to

$$\overline{W} = W - P_w \cot \eta = \tfrac{1}{2}\gamma H^2 \cot \eta - P_w \cot \eta$$

$$= \tfrac{1}{2}\gamma H^2 \cot \eta \left(1 - \frac{2P_w}{\gamma H^2}\right) = \tfrac{1}{2}\gamma_r H^2 \cot \eta$$

wherein

$$\gamma_r = \gamma\left(1 - \frac{2P_w}{\gamma H^2}\right) \qquad [1]$$

The value γ_r is independent of the slope angle of the potential surface of sliding *st*. Hence the neutral pressure reduces the effective unit weight of the fill from γ to γ_r. It also shifts the position of the effective weight toward the right-hand side as shown in the figure. The effective reaction $\overline{F}$ acts at an angle ϕ to the normal on the surface of sliding and the effective part $\overline{P}_A$ of the active earth pressure acts at an angle δ to the normal on the back of the wall. The pressure $\overline{P}_A$ can be determined by any one of the methods described in Chapter VI, after substituting the value γ_r (eq. 1) for the unit weight γ of the fill. When assuming that the point of application of $\overline{P}_A$ is located at the elevation of the point of intersection t_1 between the effective weight $\overline{W}$ and the potential surface of sliding *rs* one makes a slight error on the safe side.

Another group of problems of practical importance deals with the effect of a rapid drawdown on the stability of embankments. The drawdown initiates a process of drainage. During drainage the factor of safety with respect to sliding increases; and after drainage is complete it is even higher than it was before drainage, because the surface tension of the water reduces the danger of sliding. Therefore the greatest danger exists immediately after the drawdown, and the subsequent stages do not need to be taken into consideration.

If a completely immersed embankment consists of fine sand the distribution of the neutral stresses immediately after a sudden drawdown was found to be slightly more favorable than the corresponding state of stress in the water during a heavy rainstorm which produces a state of complete saturation. (See Art. 116.) Hence, if the slopes of such an embankment are stable during long wet spells before the slopes were submerged they are also stable after a sudden drawdown.

In connection with an investigation of the effect of a sudden drawdown on the stability of slopes on cohesive soil such as clay it is necessary to consider the incapacity of the clay to adapt its water content rapidly to a change in the state of stress. To illustrate the method of investigation we determine the factor of safety with respect to sliding of the upstream slope of the earth dam shown in Figure 74*e* immediately after a sudden drawdown of the water level in the reservoir to the level of the foot of the slope. Figure 104*a* is a duplicate of the section represented by Figure 74*e*. As indicated in the discussion of Figure 74*e*, in

Article 89, it is assumed that the soil located between the base of the dam and a depth D below the base is identical with the construction material of the dam and that the water content of the soil has adapted itself to

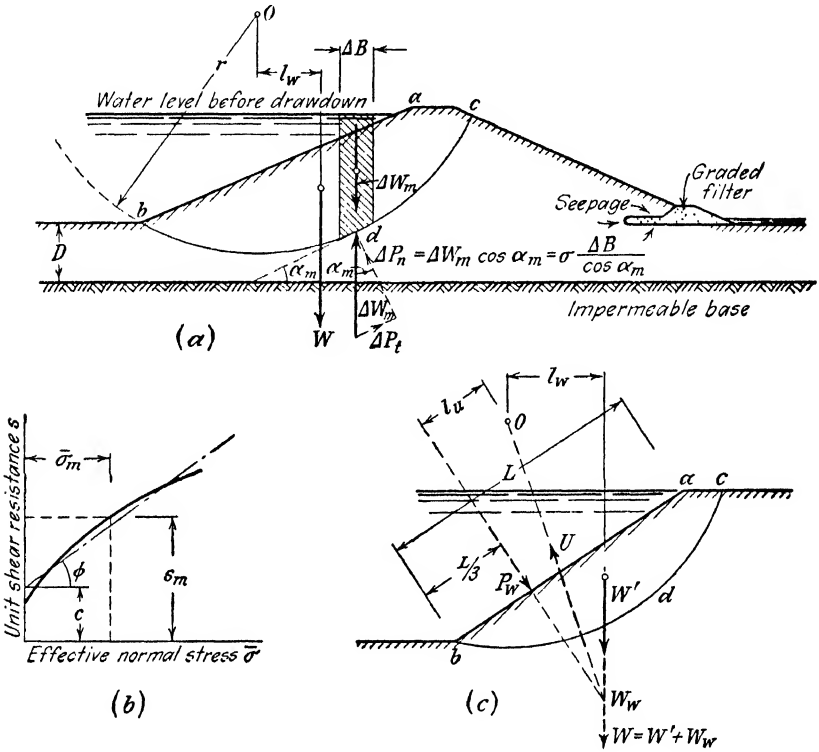

FIG. 104. (*a*) Diagram illustrating method of estimating factor of safety of homogeneous earth dam with respect to sliding after sudden drawdown; (*b*) relation between effective normal stress and shearing resistance for the construction material of the dam; (*c*) a simplified method of investigating stability of completely submerged slope after sudden drawdown.

the state of stress which existed before the drawdown. If the drawdown was preceded by a long wet spell the neutral stresses are determined by the flow net shown in Figure 74*f*. Otherwise they are determined by that shown in Figure 74*e*.

In order to estimate the factor of safety with respect to sliding along an arbitrarily selected toe circle *bdc* in Figure 104*a* we divide the total mass of soil and water which is located above the surface *bdc* before the drawdown into n vertical slices with a width ΔB. The weight of the arbitrary slice shown in the figure is ΔW_m per unit of length of the dam and its base rises at an angle α_m to the horizontal.

If we disregard the stresses on the vertical boundaries of the slice the total reaction on the base of the slice is equal to ΔW_m. It can be resolved into a tangential component ΔP_t and a normal component $\Delta P_n = \Delta W_m \cos \alpha_m$. Since the width of the base of the slice is $\Delta B/\cos \alpha_m$, the total normal stress on the base is

$$\sigma = \frac{\Delta P_n}{\Delta B} \cos \alpha_m = \frac{\Delta W_m}{\Delta B} \cos^2 \alpha_m \qquad [2]$$

The neutral stress u_w at the base can be determined from the flow net (Figs. 74*e* or 74*f*) by means of the method described in Article 91. Prior to the drawdown the base of the prism is acted upon by an effective normal stress

$$\bar{\sigma}_m = \sigma - u_w \qquad [3]$$

In this manner the intensity and the distribution of the effective normal stresses can be determined for any point of the surface *bdc*.

During the drawdown the water content of the soil remains practically unaltered. Therefore the effective pressure on the surface *bdc* also remains practically the same, while the shearing stresses increase. The relation between the effective normal stress $\bar{\sigma}_m$ (eq. 3) and the corresponding shearing resistance s_m per unit of area under conditions which do not permit a change in the water content during failure can be determined by laboratory tests. The results of a typical series of such tests are shown in Figure 104*b*. By means of this figure and equation 3 we can determine the shearing resistance s_m per unit of area of the slice shown in Figure 104*a*. The total shearing resistance along the inclined base of the slice is $s_m \Delta B/\cos \alpha_m$. The total moment of the shearing resistance about 0 is

$$M_r = \Delta B\, r \sum_1^n \frac{s_m}{\cos \alpha_m}$$

and the moment which tends to produce the slide is

$$M_d = W l_w$$

wherein W is the weight of the soil and the water located above the surface *bdc* after the drawdown. The factor of safety with respect to sliding along *bdc* is

$$G_s = \frac{M_r}{M_d} = \frac{\Delta B\, r \sum_1^n \frac{s_m}{\cos \alpha_m}}{W l_w} \qquad [4]$$

If the results of the shear tests represented in Figure 104*b* can be replaced with sufficient accuracy by a straight line, the value of s_m is

given by the equation

$$s_m = c + \bar{\sigma}_m \tan \phi \qquad [5]$$

which corresponds to Coulomb's equation, 5(1). Introducing the value for s_m (eq. 5) into equation 4 we obtain

$$G_s = \frac{\Delta B\, r \sum_1^n (c + \bar{\sigma}_m \tan \phi) \frac{1}{\cos \alpha_m}}{W l_w}$$

$$= \frac{r}{W l_w}\left[c l_s + \Delta B \tan \phi \sum_1^n \frac{\bar{\sigma}_m}{\cos \alpha_m} \right] \qquad [6]$$

wherein l_s is the length of the arc bdc. The investigation must be repeated for several different toe circles. The slide occurs along that circle for which G_s is a minimum.

In practice the drawdown of the water level in the reservoir never occurs suddenly. While the water level goes down the dam starts to consolidate and hence the stability with respect to sliding is increased. Therefore the real factor of safety is somewhat higher than the factor obtained by means of the procedure described above.

In the preceding investigations the effect of deformation at constant water content on the neutral stresses has been disregarded. At the present state of our knowledge the error due to this simplification cannot yet be avoided. If an embankment is well compacted the error is likely to be on the safe side. For loose embankments it is on the unsafe side.

If the soil behind a slope is completely immersed in standing water, as shown in Figure 104*c*, the effect of a sudden drawdown on the stability of the slope can be estimated without computing the neutral stresses along the surface of sliding (Taylor 1937). In order to visualize the principle of the method let us assume that the resistance of a body against sliding on a plane surface is determined by the empirical equation

$$S = C + W \tan \phi \qquad [7]$$

where C is the adhesion between the body and its base and W is the effective weight of the body. If we immerse the body its effective weight becomes equal to

$$W' = W - W_w$$

wherein W_w is the weight of the water displaced by the body. After immersion its resistance against sliding is

$$S' = C + (W - W_w) \tan \phi = C + W\left(\frac{W - W_w}{W} \tan \phi\right)$$

$$= C + W \tan \phi_1 \qquad [8a]$$

wherein

$$\tan \phi_1 = \frac{W - W_w}{W} \tan \phi \qquad [8b]$$

is a fictitious angle of shearing resistance. Hence the effect of immersion on the sliding resistance can be computed by replacing the value tan ϕ in equation 7 by tan ϕ_1 in equation 8*b*. In order to apply this method to the case illustrated by Figure 104*c* we resolve the total weight of the body *abdc* (Fig. 104*c*), W per unit of length of the slope, into the submerged weight W' and the weight W_w of the water displaced by the body *abdc*. Before the drawdown, the slope *ab* is acted upon by a water pressure P_w per unit of length of the slope. Since the moment of the neutral forces about O is equal to zero, the resultant U of the neutral stresses on *bdc*, Figure 104*a*, passes through O and

$$P_w l_u = W_w l_w$$

The moment which tends to produce a slide is $W' l_w$. The drawdown eliminates the resisting moment $P_w l_u = W_w l_w$. Therefore it increases the driving moment from $W' l_w$ to

$$M_d = (W' + W_w) l_w$$

Yet the effective pressure on the surface of sliding remains unchanged. As a consequence the resistance against sliding along *bdc* is the same as if the body *abdc* were still in a state of complete immersion. If the shearing resistance is determined by Coulomb's equation

$$s = c + \bar{\sigma} \tan \phi$$

the effect of complete immersion can be compensated for by replacing the value tan ϕ by the value given by equation 8*b*

$$\tan \phi_1 = \frac{W - W_w}{W} \tan \phi$$

After this substitution has been made the neutral forces can be disregarded, whereupon the factor of safety with respect to sliding can be determined by means of any one of the methods described in Articles 57 to 65.

Section D

ELASTICITY PROBLEMS OF SOIL MECHANICS

Chapter XVI

THEORIES INVOLVING A COEFFICIENT OF SUBGRADE, SOIL, OR PILE REACTION

123. Definition of subgrade reaction. If a load or a system of loads is transmitted onto the soil either by rigid or by elastic footings the base of the footings is acted upon by the contact pressure whose total magnitude is equal to the total load on the bearing area. The distribution of the contact pressure over the bearing area depends on both the physical properties of the supporting earth and on the elastic properties of the footing. A computation of the contact pressure shows, in agreement with experience, that the ratio between the unit contact pressure at a given point of the base of a footing and the settlement of that point is different for different points of the contact area. For instance, every point of the base of a rigid footing which carries a centric load settles through the same distance. Yet the distribution of the contact pressure over the bearing area is non-uniform.

Since the rigorous methods of computing the distribution of the contact pressure are too complicated for application to routine problems it is customary to simplify the computation by the arbitrary assumption that the ratio between the unit contact pressure and the settlement is the same for every point of the bearing area. In other words it is assumed that the settlement of any fraction of a loaded area is independent of the size of the area and of the load which acts on the balance of the area.

This assumption is incompatible with the mechanical properties of solids and soils in general. In order to establish agreement between assumption and reality it would be necessary to replace the soil support of the footing by a bed of equally spaced and equally compressible springs each one of which is independent of the others, as shown in Figure 141*a*. This is a highly artificial concept. Therefore the results of computation based on this concept must be considered crude estimates. Nevertheless most of the current methods for computing

the pressure on the base of footings and on the individual members of a group of piles belong in this category. The present chapter deals only with these methods. In order to distinguish between the pressure computed by means of one of these methods and the real contact pressure or the contact pressure computed by means of the theory of plasticity or the theory of elasticity, the former will be called the *subgrade reaction.* The ratio between the unit subgrade reaction and the corresponding settlement is known as the *coefficient of subgrade reaction.* The methods of computing the contact pressure by means of the theory of elasticity will be discussed in the next chapter.

124. Coefficients of soil and pile reaction. The coefficient of subgrade reaction is defined as the ratio p/ρ between a load p per unit of area of the horizontal surface of a mass of soil and the corresponding settlement ρ of the surface. The ratio between a horizontal pressure p per unit of area of a vertical surface and the corresponding horizontal displacement is called the *coefficient of horizontal soil reaction.* The ratio Q/ρ between the load Q on a foundation pile and the settlement ρ of the pile represents the *coefficient of vertical pile reaction.*

In order to secure the data required to assign a reasonable value to these coefficients we may apply a uniform pressure on an exposed surface of the soil; then we measure the deflection at different points, divide the unit pressure by the deflection at different points, and take the average of the values thus obtained. Or we transmit a known total pressure onto the soil by means of a rigid body, such as a block of concrete, measure the displacement, and compute the ratio between unit pressure and displacement. When dealing with piles we may apply a load Q on each member of a group of uniformly spaced piles, measure the settlement of each pile, and take the average. Or we apply a given total load by means of a block of concrete onto the group of piles and divide the load per pile by the settlement of the block. In either case both procedures involve an arbitrary element inasmuch as we replace a variable ratio by an average value, the fictitious coefficient of subgrade reaction. The importance of the error due to this substitution will be discussed in the next chapter.

From experience it is known that a uniformly distributed load on a circular or rectangular area of the horizontal surface of a cohesive soil produces a bowl-shaped depression, as shown in Figure 105*a*. In other words the settlement decreases from the central part of the loaded area toward the periphery. The average settlement is ρ. Experience has also shown that the average settlement increases at a higher rate than the unit load. Disregarding the non-uniform settlement of the loaded area and the absence of strict proportionality between load and

average settlement one can write

$$\frac{p}{\rho} = k_s \text{ (gm cm}^{-3}\text{)} \qquad [1]$$

The value of the coefficient of subgrade reaction k_s depends not only on the nature of the soil but also on the size and the shape of the area which carries the load. Furthermore it decreases with increasing unit load, everything else being equal. Therefore the value k_s is not a constant for a given soil and the relation expressed by equation 1

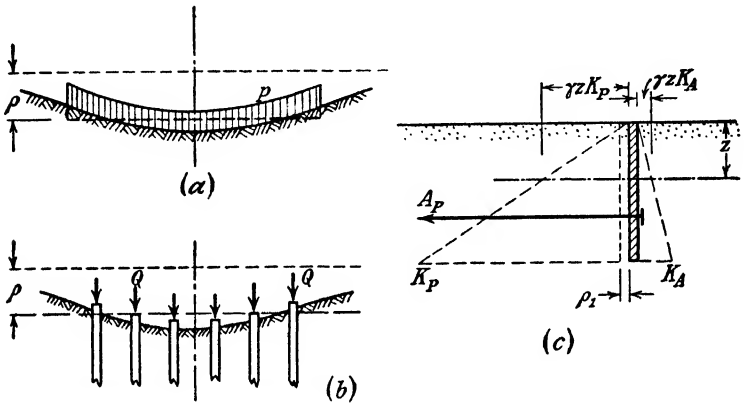

FIG. 105. (*a*) Real settlement of uniformly loaded area; (*b*) real settlement of uniformly loaded group of equally spaced piles; (*c*) simplifying assumptions on which the theory of anchor walls embedded in sand is based.

represents only a crude substitute for the real relation. Hence when the value k_s is selected all the factors which are likely to influence this value must be taken into consideration.

If every pile in a group of uniformly spaced piles carries the same load Q per pile, the settlement of the piles also decreases from the center of the group toward the periphery as shown on Figure 105*b*, unless the points of the piles rest on a very rigid stratum. Therefore the ratio Q/ρ increases from the center of the group toward the periphery. Yet, when computing the distribution of a total load on the piles in a group we always assume that the ratio

$$\frac{Q}{\rho} = k_p \text{ (gm cm}^{-1}\text{)} \qquad [2]$$

is a constant. The value k_p represents the *coefficient of vertical pile reaction.*

The concept of subgrade reaction has also been applied to the com-

putation of the horizontal pressure on piles and on sheet piles. In order to visualize the fundamental principles of this method we consider the relation between pressure and displacement for a vertical anchor wall (Fig. 105*c*) buried in sand. The wall is acted upon by a horizontal anchor pull A_p. At the instant of failure the right-hand face is acted upon by the active and the left-hand face by the passive earth pressure. Assuming a hydrostatic distribution of the earth pressure one obtains for the resultant horizontal unit pressure at depth z below the surface

$$p_1 = \gamma z(K_P - K_A)$$

wherein K_P and K_A are the coefficients of passive and active earth pressure respectively and γ is the unit weight of the sand (see Art. 84). It is further assumed that the horizontal displacement ρ_1 required to increase the resultant unit pressure from its initial value zero to p_1 is independent of depth. Finally it is assumed, in contradiction with experience, that the resultant unit pressure p increases in simple proportion to the horizontal displacement ρ. On the basis of all these assumptions one obtains for the pressure p the equation

$$p = p_1 \frac{\rho}{\rho_1} = \frac{\rho}{\rho_1} \gamma z\ (K_P - K_A) = \rho \gamma z \frac{K_P - K_A}{\rho_1} = \rho \gamma z n_h$$

or

$$\frac{p}{\rho} = \gamma z n_h \qquad [3a]$$

wherein

$$n_h = \frac{K_P - K_A}{\rho_1}\ (\text{cm}^{-1}) \qquad [3b]$$

However, in most publications the relation expressed by equation 3*a* is given in the form

$$\frac{p}{\rho} = m_h z \qquad [4]$$

wherein

$$m_h = \gamma \frac{K_P - K_A}{\rho_1}\ (\text{gm cm}^{-4})$$

is an empirical constant, which is independent of depth. It should be noted that the dimension of m_h is not identical with that of the coefficient of subgrade reaction. Equations 3 and 4 apply only to cohesionless sand. For clay, the usual assumption is that

$$\frac{p}{\rho} = k_h\ (\text{gm cm}^{-3}) \qquad [5]$$

The ratio between the horizontal unit pressure p and the corresponding horizontal displacement ρ represents the *coefficient of horizontal pile or soil reaction.* It may either increase with depth (eq. 4) or it may be independent of depth (eq. 5).

The discussions contained in the following articles are based on equations 1 to 5. When reading these articles the reader should always be mindful of the crude approximations which are involved in these equations. (See last paragraphs of Article 126.)

125. Subgrade reaction on the base of rigid footings. The computation of the subgrade reaction on footings is always based on equation 124(1)

$$\frac{p}{\rho} = k_s = \text{constant} \qquad [1]$$

To illustrate the procedure we determine the distribution of the subgrade reaction over the base of a perfectly rigid rectangular footing

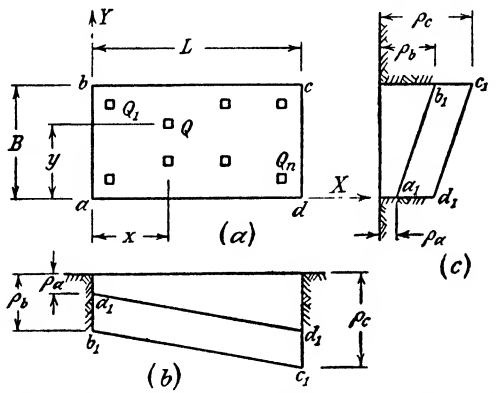

FIG. 106. (*a*) Rigid, rectangular slab acted upon by column loads Q_1 to Q_n; (*b*) and (*c*) distribution of subgrade reaction on base of the slab shown in (*a*).

(Fig. 106) acted upon by a system of column loads Q_1 to Q_n. The equilibrium of the footing requires that the sum of the column loads be equal to the total subgrade reaction, or

$$\sum_1^n Q = \int_0^L \int_0^B p \, dx \, dy \qquad [2]$$

It also requires that the point of application of the subgrade reaction be located on the line of action of the resultant loads. This condition is satisfied if

$$\sum_1^n Qx = \int_0^L \int_0^B px \, dx \, dy \quad \text{and} \quad \sum_1^n Qy = \int_0^L \int_0^B py \, dx \, dy \qquad [3]$$

In order to solve these equations we must express the subgrade reaction p as a function of the co-ordinates x and y. Since the footing is perfectly rigid its base remains plane while it settles. Figures 106*b* and 106*c* show two side elevations of the base of the footing after the settlement has occurred. If ρ_a, ρ_b, and ρ_c represent the vertical displacement of the three corners a, b, and c respectively with reference to the original surface of the ground, the settlement at a point with the co-ordinates x and y is

$$\rho = \rho_a + (\rho_c - \rho_b)\frac{x}{L} + (\rho_b - \rho_a)\frac{y}{B}$$

Substituting in this equation $\rho = p/k_s$ (eq. 1), we obtain

$$p = p_a + (p_c - p_b)\frac{x}{L} + (p_b - p_a)\frac{y}{B} \qquad [4]$$

wherein p_a, p_b, and p_c represent the soil reactions at the corners a, b, and c respectively. By means of this equation, equations 2 and 3 can be evaluated. Thus we get

$$\sum_1^n Q = \int_0^B dy \int_0^L p\,dx = BL\,\frac{p_a + p_c}{2} \qquad [5]$$

$$\sum_1^n Qx = \int_0^B dy \int_0^L px\,dx = \frac{BL^2}{2}\left(\tfrac{1}{2}p_a + \tfrac{2}{3}p_c - \tfrac{1}{6}p_b\right) \qquad [6]$$

and

$$\sum_1^n Qy = \int_0^L dx \int_0^B py\,dy = \frac{B^2L}{2}\left(\tfrac{1}{3}p_a + \tfrac{1}{2}p_c + \tfrac{1}{6}p_b\right) \qquad [7]$$

These three equations determine the three unknown quantities, p_a, p_b, and p_c in equation 4. If the line of action of the resultant of the loads passes through the center of the base of the footings the subgrade reaction is uniform,

$$p = \frac{\Sigma Q}{BL} = \text{constant}$$

Under certain soil conditions this conclusion is reasonably correct. In other instances the real distribution of the soil reactions is not even approximately uniform (see Art. 139). The source of the contradictions between existing theories and reality resides in the fact that equation 1 involves crude approximations.

126. Subgrade reactions on the base of elastic footings. Since elastic supports deflect in an upward direction between the points of load

application, the subgrade reactions are greatest beneath the loads and smallest in the intermediate areas. Owing to this influence of the deflection on the distribution of the subgrade reactions the bending moments in elastic footings may be considerably smaller than those computed on the assumption that the footings are perfectly rigid. The methods of computing the bending moments in elastic beams and

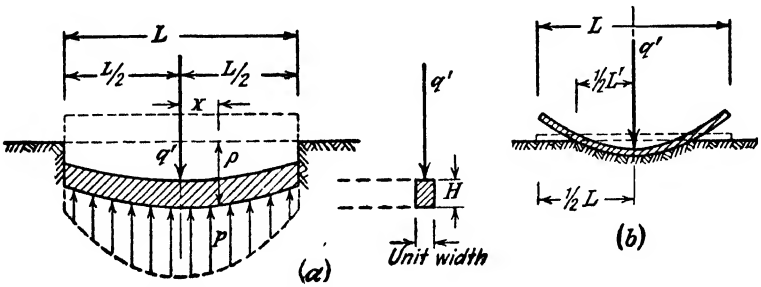

FIG. 107. (*a*) Distribution of subgrade reaction over base of elastic beam on elastic base, which is acted upon by line load q' per unit of width; (*b*) ends of very flexible loaded beam rising above surface.

footings on an elastic subgrade are described in several textbooks on applied mechanics (see, for instance, Timoshenko 1941). Therefore the following paragraphs merely contain a summary of the general principles involved.

Figure 107*a* represents a longitudinal section through an elastic beam with a length L and a constant rectangular cross section, resting on the horizontal surface of an elastic subgrade. The beam with a width B and a height H carries a load q' *per unit of width* which acts on the beam on a line equidistant from the two ends of the beam. The settlement is determined by equation 124(1)

$$\frac{p}{\rho} = k_s = \text{constant} \qquad [1]$$

Under the influence of the load the footing bends and assumes the position indicated in the figure. Let

E = the modulus of elasticity of the beam,

$I = \dfrac{BH^3}{12}$, the moment of inertia of the section through the beam,

S = the vertical shearing force at a distance x from the midpoint of the beam per unit of width,

p = the subgrade reaction at distance x from the midpoint of the beam (pressure per unit of area),

ρ = the settlement of the base of the beam at a distance x from the midpoint, and

ϵ = the base of natural logarithms.

The rate at which the shearing force changes with the distance x from the center of the beam is

$$-\frac{dS}{dx} = p = \rho k_s \qquad [2]$$

According to the theory of bending of beams the vertical displacement ρ of the beam with reference to its original position is determined by the equation

$$-\frac{dS}{dx} = \rho k_s = -EI\frac{d^4\rho}{dx^4} \qquad [3]$$

A solution of this equation is

$$\rho = C_1 \cosh\psi \cos\psi + C_2 \sinh\psi \sin\psi + C_3 \cosh\psi \sin\psi + C_4 \sinh\psi \cos\psi \qquad [4a]$$

wherein

$$\psi = x\sqrt[4]{\frac{k_s B}{4EI}} \qquad [4b]$$

is a pure number and C_1 to C_4 are the constants of integration. The corresponding bending moment per unit of width is

$$M = \frac{EI}{B}\frac{d^2\rho}{dx^2} \qquad [5]$$

The constants of integration C_1 to C_4 (eq. 4a) must be determined in such a way that the continuity and the boundary conditions are satisfied. These conditions are the following. At half the length of the beam, $x = 0$, the tangent to the elastic line is horizontal and the shearing force per unit of width is $q'/2$. At the two ends of the beam both the bending moment M and the shearing force S are equal to zero. These conditions can be expressed by the equations

$$\frac{d\rho}{dx} = 0 \qquad \text{at } x = 0 \qquad [6a]$$

$$S = \frac{EI}{B}\frac{d^3\rho}{dx^3} = \frac{q'}{2} \qquad \text{at } x = 0 \qquad [6b]$$

$$M = \frac{EI}{B}\frac{d^2\rho}{dx^2} = 0 \qquad \text{at } x = \frac{L}{2} \qquad [6c]$$

and

$$S = \frac{EI}{B}\frac{d^3\rho}{dx^3} = 0 \qquad \text{at } x = \frac{L}{2} \qquad [6d]$$

By combining equation 4*a* with these conditions one obtains for the subgrade reaction at a distance x from the midpoint of the length of the beam

$$p = \rho k_s = \frac{q'\psi_1}{2L}\frac{1}{\sinh\psi_1 + \sin\psi_1}\left\{\sin\psi\sinh(\psi_1 - \psi) - \sinh\psi\sin(\psi_1 - \psi) + 2\left[\cosh\psi\cos\frac{\psi_1}{2}\cos\left(\frac{\psi_1}{2} - \psi\right) + \cos\psi\cosh\frac{\psi_1}{2}\cosh\left(\frac{\psi_1}{2} - \psi\right)\right]\right\} \qquad [7]$$

and for the bending moment M at the same distance per unit of width

$$M = \frac{q'L}{4\psi_1}(\cosh\psi\cos\psi + \sinh\psi\sin\psi - \sinh\psi\cos\psi - \cosh\psi\sin\psi - D\cosh\psi\cos\psi + A\sinh\psi\sin\psi) \qquad [8]$$

wherein

$$\psi = x\sqrt[4]{\frac{k_sB}{4EI}}, \qquad \psi_1 = L\sqrt[4]{\frac{k_sB}{4EI}},$$

$$A = \frac{2 + \cos\psi_1 - \sin\psi_1 + \epsilon^{-\psi_1}}{\sinh\psi_1 + \sin\psi_1} \text{ and } D = \frac{\cos\psi_1 + \sin\psi_1 - \epsilon^{-\psi_1}}{\sinh\psi_1 + \sin\psi_1}$$

Both the subgrade reaction p and the bending moment M are greatest beneath the load, at $x = 0$ and $\psi = 0$. At that point they assume the values

$$p_{max} = \rho_{max}k_s = \frac{q'\psi_1}{2L}(1 + A) \qquad [9]$$

and

$$M_{max} = \frac{q'L}{4\psi_1}(1 - D) \qquad [10]$$

For a perfectly rigid beam the corresponding values are

$$p'_{max} = \frac{q'}{L} \quad \text{and} \quad M'_{max} = \frac{q'L}{8}$$

At the two ends of the elastic beam the subgrade reaction is equal to

$$p_1 = \rho_1 k_s = \frac{2}{L} q' \psi_1 \frac{\cosh \frac{\psi_1}{2} \cos \frac{\psi_1}{2}}{\sinh \psi_1 + \sin \psi_1} \qquad [11]$$

If the beam is long and slender, the value p_1 (eq. 11) becomes negative. Since there can be no tensile stresses along the surface of contact between the beam and the surface of the subgrade, the ends of the beam rise above the surface beyond a certain distance $L'/2$ from the load, as shown in Figure 107*b*. Within this distance the subgrade reactions decrease from a maximum beneath the load to zero at a distance $L'/2$ from the load.

The problem of computing the bending moments in elastically supported beams and slabs has attracted the attention of mathematically minded engineers for many decades. Therefore a great number of different problems of this type have already been solved. Originally the theory was worked out for the purpose of computing the bending moments in railroad ties supported by ballast (Zimmermann 1888). It was used for this purpose by the American Society of Civil Engineers' "Committee to report on stresses in railroad tracks" (Talbot 1918).

In 1911 the author applied the theory for the first time to the design of a foundation consisting of a grillage of heavy reinforced concrete beams. In later years the theory was also applied to the design of locks made of reinforced concrete (Freund 1917, 1924) and to the computation of the bending moments in hard road surfaces acted upon by concentrated loads (Westergaard 1926). Figures 108*a* to 108*d* show elastic beams and simple frames which transmit vertical loads onto masses of soil. The loading conditions illustrated by Figures 108*e* to 108*j* are frequently met in connection with the design of locks. The walls of a lock are practically rigid ($I = \infty$) whereas the floor construction is relatively flexible (see Figs. 108*g* and 108*h*). The symbol M in Figures 108*h* and 108*j* indicates a couple. The equations for computing the bending moments in structures acted upon by the forces shown in Figure 108 and by various other systems of forces have been assembled by Hayashi (1921) in a book which also contains several solutions based on the assumption that the coefficient of subgrade reaction is variable. Freund (1927) has also solved some of the problems on the assumption that the coefficient of subgrade reaction (eq. 124(1)) decreases with increasing intensity of the pressure p.

In connection with the practical application of the existing theories and solutions, the principal difficulty is to estimate properly the value of the coefficient of subgrade reaction k_s (eq. 124(1)). Since k_s depends on many factors other than the nature of the soil it cannot be determined directly by laboratory or by small-scale field tests. The laws of similitude which govern the influence of the size of the loaded area on the value of k_s are complex and imperfectly known. Therefore the extrapolation from test results is essentially a matter of judgment. The preceding statements also apply to all the other coefficients listed

in Article 124. A survey of the factors which determine the value k_s under field conditions has been published elsewhere (Terzaghi 1932). Fortunately the influence of an important error in estimating the coeffi-

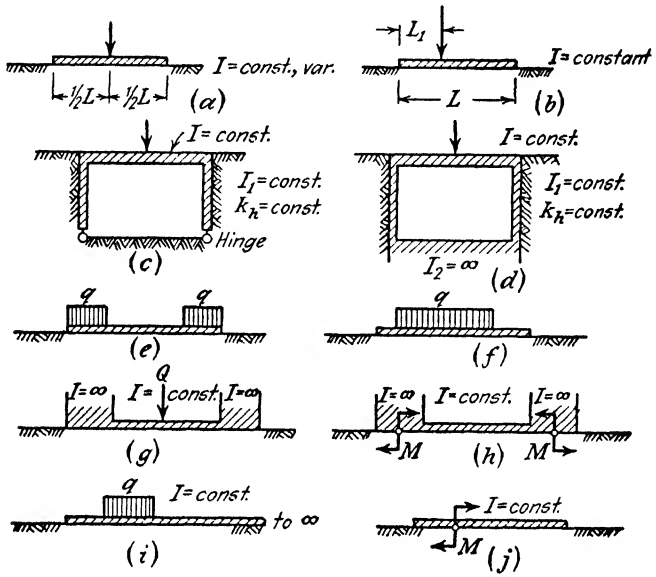

FIG. 108. Some types of elastically supported, load-bearing structures; equations for computing the subgrade reaction, side reactions, and bending moments for these structures have been published.

cient of subgrade reaction on the results of the computations is relatively unimportant, because equation 8, which determines the bending moments, contains only the fourth root of this coefficient.

127. Free, rigid bulkheads and the foundation of cable towers for transmission lines. A bulkhead is free if it owes its stability solely to the lateral resistance of the earth adjoining its buried part. The bulkhead may be acted upon by horizontal forces applied to the upper edge of the bulkhead or by the lateral earth pressure of a backfill.

Figure 109*a* is a section through a free bulkhead designed to resist a horizontal force q' per unit of length of the upper edge of the bulkhead. The soil adjoining the buried part of the bulkhead consists of sand, and the horizontal soil reaction is assumed to be determined by equation 124(4),

$$\frac{p}{\rho} = m_h z \qquad [1]$$

In this equation p represents the difference between the pressures which act at the depth z per unit of area on the two sides of the bulkhead.

The application of the force q' to the upper edge of the bulkhead produces a displacement by rotation about a point O located between the surface and the lower edge of the bulkhead. Displacements in the

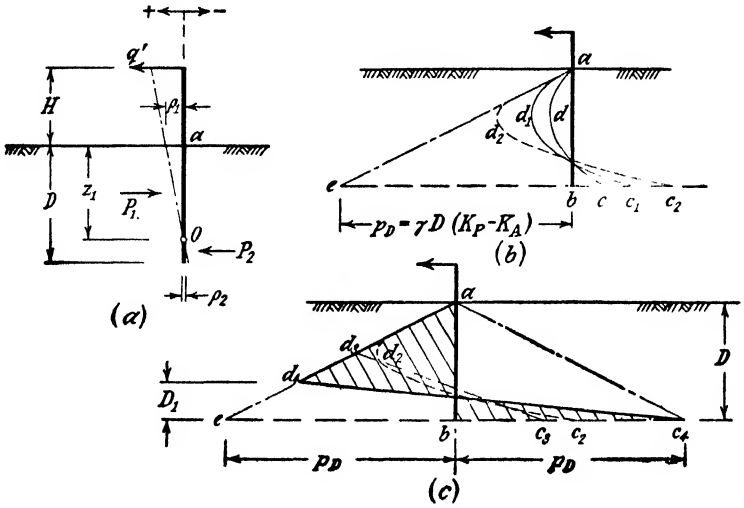

FIG. 109. (*a*) Vertical section through rigid bulkhead in sand acted upon by horizontal force q' per unit of length; distribution of resultant horizontal pressure on buried part of bulkhead (*b*) if adjoining sand is in an elastic state and (*c*) if it is in a plastic state of equilibrium.

direction of the force q' are positive and those in the opposite direction negative. At a depth z below the surface the displacement is

$$\rho = \rho_1 - (\rho_1 - \rho_2)\frac{z}{D}$$

wherein ρ_1 and ρ_2 represent the lateral displacement at the surface and at a depth D respectively. Substituting in this equation $\rho = p/m_h z$ (eq. 1) we obtain for the horizontal soil reaction at depth z the value

$$p = m_h\left[\rho_1 z - (\rho_1 - \rho_2)\frac{z^2}{D}\right] \qquad [2]$$

The unknown values ρ_1 and ρ_2 are determined by the conditions for the equilibrium of the bulkhead. These conditions require that the total horizontal soil reaction per unit of length of the bulkhead should be equal to q' and that the moments about any point (for instance point a at the surface shown in Fig. 109*a*) should be equal to zero. Hence

$$q' = \int_0^D p\,dz = m_h D^2\left(\tfrac{1}{6}\rho_1 + \tfrac{1}{3}\rho_2\right) \qquad [3a]$$

and $$q'H = \int_0^D pz\,dz = m_h D^3 \left(\tfrac{1}{12}\rho_1 + \tfrac{1}{4}\rho_2\right) \qquad [3b]$$

Solving these equations and substituting the values of ρ_1 and ρ_2 thus obtained in equation 2 we get

$$p = \frac{6q'z}{D^3}\left[3D + 4H - 2\frac{z}{D}(2D + 3H)\right] \qquad [4]$$

In Figure 109*b* the soil reactions p are represented by the horizontal distance between the parabola *adc* and the vertical line *ab*. As the force q' increases, the slope of the parabola at point *a* becomes flatter and the value of p increases. The greatest value which p can assume at any depth z is equal to

$$p_{z\,\max} = \gamma z\,(K_P - K_A) \qquad [5]$$

wherein K_P and K_A represent the coefficient of passive and active earth pressure respectively. (See Chapter XI.) At a depth D this pressure is equal to

$$p_D = \gamma D\,(K_P - K_A) \qquad [6]$$

If the soil adjoining the bulkhead rises the bulkhead also rises, because the weight of the bulkhead is small and the relative displacement between the sand and the bulkhead remains practically equal to zero. Therefore the values K_P and K_A should be computed on the assumption that the coefficient of wall friction is equal to zero. They are equal to

$$K_P = \tan^2\left(45° + \frac{\phi}{2}\right) \qquad 15(4)$$

and

$$K_A = \tan^2\left(45° - \frac{\phi}{2}\right) \qquad 15(2)$$

wherein ϕ is the angle of internal friction of the sand.

Since the soil reaction p cannot exceed the value $p_{z\,\max}$ (eq. 5), the sand starts to flow as soon as the slope of the pressure parabola at point *a* (Fig. 109*b*) becomes equal to the slope of the straight line *ae* whose abscissas represent the values $p_{z\,\max}$. This condition is satisfied if

$$\left[\frac{dp}{dz}\right]_{z=0} = \frac{6q'}{D^3}(3D + 4H) = \gamma\,(K_P - K_A)$$

or

$$q' = \tfrac{1}{6}\gamma D^3 \frac{K_P - K_A}{3D + 4H} \qquad [7]$$

However, after the flow has started, equation 1 loses its validity and the pressure line assumes more and more the shape of a broken line as indicated by the dashed curve ad_2c_2 in Figures 109*b* and 109*c*. In this stage of the process we can replace the lower part of the curve with sufficient accuracy by a straight line d_3c_3 (Fig. 109*c*). As the force q' further increases, point d_3 moves downward along ae and point c_3 moves toward the right. The lateral pressure which the sand can sustain on the right side of point b is appreciably higher than p_D (eq. 6), because at b the pressure acts on the sand only over a narrow belt. Yet it is usually assumed that the bulkhead fails as soon as the soil reaction at point b becomes equal to p_D. On this assumption the conditions for equilibrium at the instant of failure are

$$q'_{max} = \tfrac{1}{2}p_D D - \tfrac{1}{2}\,2p_D D_1 = p_D(\tfrac{1}{2}D - D_1) \qquad [8a]$$

and

$$q'_{max}\,(H + D) = \tfrac{1}{2}p_D\,D\,\frac{D}{3} - \tfrac{1}{2}\,2p_D D_1\,\frac{D_1}{3} = p_D(\tfrac{1}{6}D^2 - \tfrac{1}{3}D_1^2) \qquad [8b]$$

wherein H is the lever arm of q' about point a.

Eliminating D_1 from these equations we obtain the value of the greatest pull q'_{max} which the bulkhead can sustain. These equations can also be used to determine the minimum depth D to which the bulkhead ought to be driven at given values of q'_{max} and H. If a factor of safety G_s is required, we replace the value p_D in equations 8 by p_D/G_s. This method of computation has also been used in the design of free bulkheads (bulkheads without anchorage) which are acted upon by the active earth pressure of a backfill adjoining the upper part of the bulkhead (Krey 1936).

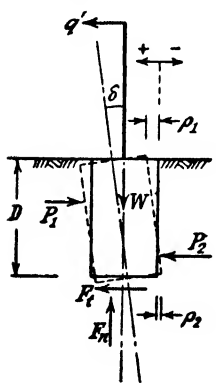

FIG. 110. Forces which act on the foundation for the mast of a transmission line.

Figure 110 is a section through the foundation of the cable tower of a transmission line. The foundation is acted upon by the weight W of the system and by the overturning moment produced by the one-sided pull of a cable, q' per unit of width measured at right angles to the section. The tilting movement of the foundation is resisted by the two components F_n and F_t of the reaction on the base and by the lateral resistance of the earth, P_1 and P_2 respectively. The forces P_1 and P_2 are determined by the same factors as the forces P_1 and P_2 in Figure 109*a*. Therefore the preceding analysis can be applied without any essential modification to the computation

of the forces P_1 and P_2 in Figure 110. Since the length of the foundation block perpendicular to the plane of tilting is finite, the tilting movement and the lateral compression of the earth adjoining the block are also resisted by friction along two planes which pass through the sides of the block parallel to the plane of tilting. By neglecting the stabilizing effect of this frictional resistance one commits an error on the safe side.

If it is required that the angular deflection of the center line of the tower should not exceed a specified amount δ it is necessary to estimate the value of the constant m_h in equation 1 by means of field tests. From Figure 110 we obtain for the angular deflection the value

$$\tan \delta = \frac{1}{D} (\rho_1 - \rho_2) \qquad [9]$$

The horizontal pull q' required to produce this deflection can be computed by combining equation 9 with equations 3. The error is on the safe side. A better approximation can be obtained if the resisting moment produced by the forces F_t and F_n in Figure 110 is taken into consideration (Sulzberger 1927).

128. Free, flexible bulkheads and piles subject to lateral loads. If a free bulkhead is flexible, it deflects and bends under the influence of a lateral force, as shown in Figure 111. Unless this bending is negligible, it invalidates the equations derived in the preceding article. The intensity and the distribution of the horizontal soil reactions over the face of flexible bulkheads can be computed by means of the method described in Article 126. The relation between the lateral deflection ρ of the bulkhead from its original position, at a depth z, is determined by equation 126(3)

$$-\frac{dS}{dz} = p = -EI \frac{d^4\rho}{dz^4} \qquad [1]$$

Assuming that the coefficient of lateral soil reaction, p/ρ, can be described adequately by some function of the depth z,

$$\frac{p}{\rho} = f(z)$$

we obtain

$$\rho f(z) = -EI \frac{d^4\rho}{dz^4} \qquad [2]$$

This equation has been solved for

$$f(z) = \frac{p}{\rho} = k_h = \text{const.} \qquad 124(5)$$

and

$$f(z) = \frac{p}{\rho} = m_h z \qquad 124(4)$$

by Rifaat (1935). The values which he calculated on the assumption that $f(z) = m_h z$ agreed very well with his measurements on a free steel bulkhead whose lower part was buried in clean sand.

If the yield of a bulkhead induces arching in the backfill, such as the yield of a flexible anchored bulkhead (see Article 78) no method of computation involving a coefficient of horizontal soil reaction can be used because arching invalidates the results.

If a bulkhead is driven to a very great depth, the curve into which the center line of the sheet piles deflects assumes the sinusoidal shape indicated in Figure 111*b*. The maximum deflection associated with the successive waves decreases with depth somewhat as the amplitude of damped vibrations decreases with time. The deflection curve has been computed by Miche (1930, equations quoted by Rifaat 1935) on the assumption that H (Fig. 111*b*) is equal to zero and that the coefficient of horizontal soil reaction is given by equation 124(4).

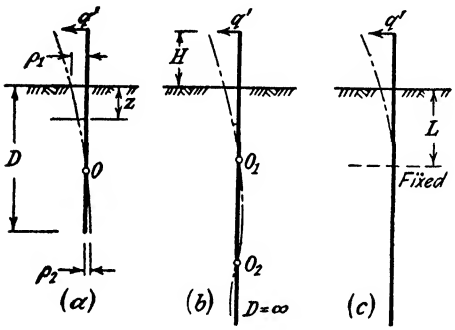

FIG. 111. (*a*) Real shape of short pile and (*b*) real shape of long pile acted upon by horizontal force; (*c*) shape of pile assumed for purpose of computation of bending moments in the pile.

The same general method of computation can also be used to compute the lateral deflection and the bending stresses in long, individual piles which are acted upon by a horizontal force at or above the surface of the ground. The problem has been solved by Titze (1932) on the assumption that the relation between the horizontal soil reaction p and the depth is determined by an equation

$$p = \rho \alpha_h z^n \qquad [3]$$

wherein α_h and n are empirical coefficients. For sand the investigator assumed $n = 1$ and for clays $n > 1$. As a limiting case, valid for ideal clays, he assumed $p/\rho = k_h$ = constant. Yet in every case the final equations are so involved that they are hardly suitable for practical application. Therefore it is preferable to simplify the problem by the further assumption that the lower part of the pile is fixed as in-

dicated in Figure 111c. The vertical distance L between the surface of the ground and the lower end of the deflecting part of the pile can be computed on the basis of the condition that the total work of deformation of the system should be a minimum. The method has been applied to the computation of the bending moments in wooden piles whose upper ends are embedded in a rigid concrete mat (Cummings 1937). The piles are surrounded by sand and the ratio between the horizontal unit pressure and the corresponding horizontal displacement increases in simple proportion to depth, as expressed by the equation

$$\frac{p}{\rho} = m_h \text{ (gm cm}^{-4}) \, z \qquad 124(4)$$

The final equations are remarkably simple. The depth L below which the pile can be considered to be fixed is

$$L = \sqrt[5]{\frac{216\,EI}{d\,m_h}} \qquad [4]$$

wherein E is the modulus of elasticity of the pile material, I the moment of inertia, and d the diameter of the pile. According to this equation the length L is independent of the intensity of the horizontal force Q which acts on the head of the pile. It would be easy to use the same method of computation on the assumption that the coefficient of horizontal soil reaction is a constant. The method could also be applied to the computation of the deflection of piles whose upper ends are free.

129. Stability of foundation piles against buckling under axial loads. If a load acts on a long, slender pile driven through soft soil to bearing on a hard stratum, there is at least a theoretical possibility of a failure of the pile due to buckling. The current methods of computing the critical load (Forssell 1926, Granholm 1929, Cummings 1938) are based on the assumption that the coefficient of horizontal pile reaction is a constant,

$$\frac{p}{\rho} = k_h \text{ (gm cm}^{-3}) \qquad 124(5)$$

The analysis leads to the conclusion that the pile would buckle into a sinusoidal curve with several waves, as shown in Figure 112. The following is a brief abstract of Cummings' article on this subject. Let

D = the depth of that part of a point-bearing pile which is embedded in soft soil,
d = the diameter of the pile,
E = the modulus of elasticity of the pile material, and
I = the moment of inertia of every section through the pile.

The pile is assumed to be hinged both at the surface and at the base of the soft layer. The number m of half waves of the sinusoidal curve into which the pile tends to buckle is determined by the equation

$$m^2 (m + 1)^2 = \frac{d\, k_h\, D^4}{\pi^4 EI} \qquad [1]$$

If this equation leads to fractional values of m it is necessary to use the next highest whole number. The value m increases with the coefficient of horizontal soil reaction, k_h. The critical buckling load is

$$Q_b = \frac{\pi^2 EI}{D^2} (2m^2 + 2m + 1) \qquad [2]$$

The factor outside the parenthesis represents the critical buckling load for the free-standing column with hinged ends. The numerical examples contained in Cummings' article demonstrate that the critical

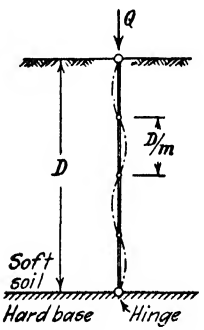

FIG. 112. Deformation of point-bearing pile embedded in soft clay under influence of heavy, vertical load.

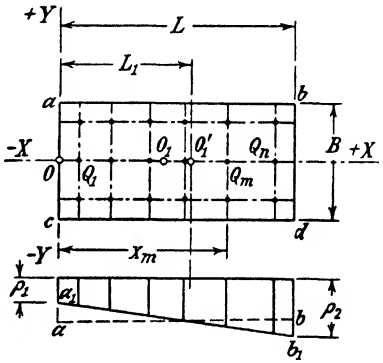

FIG. 113. Upper diagram: loaded rigid concrete slab resting on piles; lower diagram: tilting of slab due to shifting of the center of the load from O_1 to O_1'.

load Q_b exceeds the crushing strength of the pile unless the soil is excessively soft. The theory has been confirmed by experiments in the laboratory. On account of the high value of the critical load there are no records of piles which have failed in the field by buckling beneath the surface of the ground.

130. Distribution of vertical load on piles supporting rigid structures. Figure 113 represents a rigid, rectangular raft foundation supported by piles arranged in parallel rows. The rows parallel to the X axis are equally spaced and symmetrical with respect to this axis. In the other direction, the spacing of the rows is arbitrary. The total load on the

foundation is equal to Q_T for each row parallel to the X axis. We shift the point of application of the load from point O_1 on the X axis to point O_1' at a distance L_1 from the left boundary of the raft without changing the load. The displacement of the load reduces the pressure on the piles on the left and increases the pressure on those located on the right side of the foundation. The problem is to determine the pressure on the piles after the load was moved.

The displacement of the load causes the base of the raft to tilt from its original position ab into the position a_1b_1. The settlements at a_1 and b_1 are equal to ρ_1 and ρ_2 respectively. The settlement of a pile at a distance x_m from the Y axis is

$$\rho = \rho_1 + \frac{\rho_2 - \rho_1}{L} x_m \qquad [1]$$

The equilibrium of the foundation requires that the sum of the pile reactions Q_1 to Q_n should be equal to the total load Q_T and the moments of the pile reactions with reference to the Y axis should be equal to $Q_T L_1$. Hence

$$Q_T = \sum_1^n Q_m \qquad [2a]$$

and

$$Q_T L_1 = \sum_1^n Q_m x_m \qquad [2b]$$

wherein n is the number of the piles in one row parallel to the X axis. In order to solve this equation we must make some assumption regarding the relation between the settlement and the pile reaction. The customary assumption is that

$$\frac{Q_m}{\rho} = k_p \text{ (gm cm}^{-1}\text{)} = \text{constant} \qquad [3]$$

where k_p is the coefficient of vertical pile reaction (eq. 124(2)). By combining equation 3 with the preceding ones we can compute the load on the piles. The accuracy of the results depends on the errors associated with equation 3. Since the load on some piles of the group was increased and that on others was reduced, the coefficient of pile reaction k_p is not even approximately the same for all the piles. Therefore the errors involved in the computation can be very important.

131. Pile foundations for quay walls. Pile foundations for quay walls differ from pile foundations for buildings in that the direction of the resultant R of the forces which act on the quay wall foundation is inclined. In order to provide for adequate stability, quay walls are

often made to rest on one set of vertical and two sets of inclined piles which are battered in opposite directions, as shown in Figure 114*a*. The oldest and simplest method of calculating the pile loads is known as Culmann's method, described by Lohmeyer (Brennecke-Lohmeyer, 1930). We replace each group of piles by an imaginary pile located in the centerline of the group. These imaginary piles A, B, and C are shown in Figure 114*b*. The piles A and B are acted upon by axial pres-

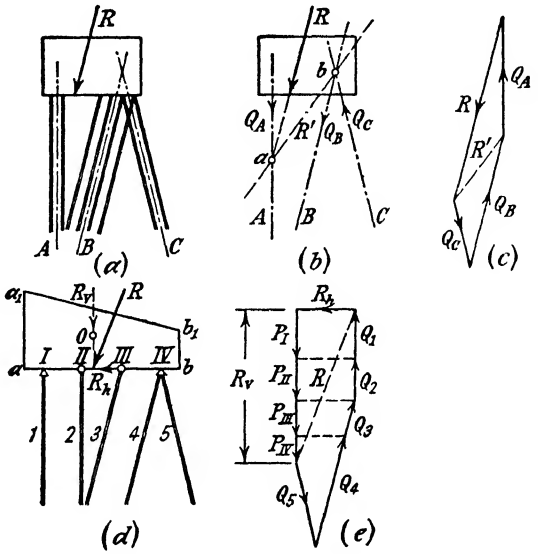

FIG. 114. (*a*) to (*c*) Culmann's method; (*d*) and (*e*) trapezoid method for computing load on piles supporting a quay wall.

sures Q_A and Q_B and the pile C by an axial pull Q_C. The resultant R' of the forces Q_B and Q_C must pass through both the point of intersection b between the lines B and C and the point of intersection a between the line A and the line of action of the external force R. Therefore the three forces Q_A, Q_B, and Q_C can be determined by means of the polygon of forces represented in Figure 114*c*. If Q is the load assigned to each real pile, the required number of piles in each group per unit of length of the wall is

$$n_A = \frac{Q_A}{Q}, \quad n_B = \frac{Q_B}{Q}, \quad \text{and} \quad n_C = \frac{Q_C}{Q} \qquad [1]$$

In each group one half of the required piles are placed on one side and the other half on the other side of the line which represents the imaginary pile.

In the layout shown in Figure 114*d* the piles are arranged in five

rows, numbered 1 to 5. The heads of the piles of rows 4 and 5 are located on the same straight line, indicated in the figure by point *IV*. For the computation of the pressure on the piles of such a foundation a method has been developed which is known as the trapezoid method (described in Brennecke-Lohmeyer, 1930). We substitute for the vertical component R_v of the resultant R a continuous load represented by a trapezoid abb_1a_1 whose area is equal to the vertical component R_v of the force R and whose center of gravity is located on the line of action of R_v. This continuous load satisfies the conditions for equilibrium in a vertical direction. Then we compute the vertical pressure P_I to P_{IV} on each of the four rows of pile heads *I* to *IV* on the assumption that the base *ab* of the trapezoidal load consists of individual sections *a II*, *II III*, and *III b* which rest on the heads of the piles, as indicated in Figure 114*d*. These sections are assumed to be hinged at *II* and *III*.

The pressures thus obtained represent the vertical force which acts on each of the four rows of pile heads per unit of length of the wall. The horizontal component R_h of the force R is exclusively carried by the battered piles labeled 3 to 5. The total pressure on the battered piles is determined by the polygon of forces shown in Figure 114*e*. The number of piles in each row per unit of length of the wall is equal to the force obtained by means of the polygon of forces divided by the load Q which is assigned to the individual piles.

The replacement of the vertical component R_v by the trapezoidal load abb_1a_1 (Fig. 114*d*) is somewhat arbitrary because any other assumption would serve the same purpose, provided the chosen pressure area is equal to R_v and its center of gravity is located on the line representing R_v. In order to eliminate the arbitrary elements in the special case of a quay wall foundation on point-bearing piles, Westergaard (1917) introduced into the analysis the condition that the displacement of the pile heads should be compatible with the rigidity of the supported structure. In its present, highly elaborate form the procedure is known as Nökkentved's method. It is based on the assumption that both the supported structure and the support of the points of the piles are perfectly rigid, that the construction material of the piles strictly obeys Hooke's law, and that the resistance against lateral deformation of the soil adjoining the piles can be neglected. In other words it is assumed that the quay wall represents a rigid body supported by perfectly elastic columns which rest on a rigid base. The existence of the soil which surrounds the piles and the deformation of the soil which supports the points of the piles are disregarded. If these assumptions are really justified it is possible to compute the pressure on the piles by means of the methods which are used in the theory of statically indeterminate structures. The statically indeterminate quantities must satisfy the condition that neither the relative position of the heads of the piles nor that of the points of the piles should change while the system is being deformed. If the piles are fixed at one or at both ends the solution of the problem must also satisfy the condition that the relative position of the tangents to the centerlines of the piles at the fixed ends remains unchanged (Nökkentved 1928).

On account of the great number of statically indeterminate quantities the computation of the pile reactions is rather involved. Therefore many efforts have been made to simplify the procedure as far as the nature of the problem permits. P. Hedde (1929) adapted the method of influence lines to the solution of the problem and A. Labutin (1933) worked out a graphical procedure. A summary of the present status of the technique of solving the problem has been published in English (Vetter 1939). It is rather difficult to imagine field conditions under which the fundamental assumptions of the theory are at least approximately satisfied. Even if the piles are driven through liquid mud to rock the results of the computations may be very inaccurate because the theory disregards the deformations at the contact between the points of the piles and the rock. These deformations invalidate the assumption that the axial deformation of the piles increases in direct proportion to the length of the piles. Therefore the practical value of the theory is doubtful.

Chapter XVII

THEORY OF SEMI-INFINITE ELASTIC SOLIDS

132. Elastic and plastic equilibrium. If the factor of safety of a mass of soil with respect to failure by plastic flow (see Section B) exceeds a value of about 3 the state of stress in the soil is likely to be more or less similar to the state of stress computed on the assumption that the soil is perfectly elastic. Hence the state of stress in a mass of soil under the influence of moderate stresses can be estimated by means of the theory of elasticity. The importance of the error associated with the results of the computation depends chiefly on the extent to which the real stress-strain relations depart from Hooke's law. This departure increases rapidly as the state of plastic equilibrium is approached. If the departure can be expected to be unimportant one can use the theory of elasticity as described in this chapter. If it is likely to be important one has to use the theory of plasticity in accordance with the procedures described in Chapters V to XI.

The following examples may illustrate this statement. Experience has shown that the earth pressure of sand on the timbering of cuts is approximately equal to the active earth pressure. This empirical fact indicates that the sand adjoining the cut is close to a state of plastic equilibrium regardless of the value of the factor of safety of the struts with respect to crushing. The existence of a state of stress close to the state of plastic equilibrium strictly excludes the application of the theory of elasticity to the computation of the stresses whereas the errors associated with the application of the theory of plasticity to such a state of stress are tolerable. For this reason, all the investigations pertaining to earth pressure are based on the theory of plasticity. The stresses in the soil in earth dams or behind the slopes of open cuts are also usually well beyond the range of approximate validity of Hooke's law. Therefore we are justified in solving problems dealing with slopes on the basis of the theory of plasticity, as described in Chapter IX. On the other hand the theory of elasticity has been successfully used for computing the intensity and the distribution of the vertical pressure on beds of clay which are located beneath strata of sand at some depth below the base of raft foundations, because the soil located beyond a certain depth is far from a state of plastic equilibrium.

133. Fundamental assumptions. In accordance with the nomenclature used in this book the term *stress* will be used exclusively for a force per unit of area. Compressive stresses are positive and tensile stresses negative. The term *strain* indicates change of length per unit of length in a given direction. A positive strain indicates shortening or con-

traction and a negative strain elongation. Every theory dealing with stresses is based on the assumption that the material subject to stress is either isotropic and homogeneous or else that the departure from these ideal conditions can be described by simple equations. In connection with elastic behavior, the term *isotropy* denotes identical elastic properties throughout the solid and in every direction through any point of it, and the term *homogeneity* involves identical elastic properties at every point of the solid in identical directions. Hence a homogeneous material is by no means necessarily isotropic. The term *aelotropy* indicates non-isotropy, regardless of the type of deviation from isotropy. If the elastic constants of an *aelotropic* material are associated with three orthogonal planes of symmetry the material is called *orthotropic*. When dealing with orthotropic materials it is usually assumed that one of these planes is horizontal and that the elastic properties with reference to the two vertical planes are identical.

Most of the theories contained in the following articles are based on the assumption that the soil is both isotropic and homogeneous. Departures from these assumptions will always be specifically mentioned. The theories are also based, with very few exceptions, on the assumption that the soil strictly follows Hooke's law, which states that the ratio between a linear stress, σ, and the corresponding linear strain, ϵ, is a constant,

$$\frac{\sigma}{\epsilon} = E \text{ (gm cm}^{-2}\text{)} \qquad [1]$$

called the *modulus of elasticity* or *Young's modulus*. The strain produced by a positive linear stress can be investigated experimentally by means of a simple compression test illustrated by Figure 115*a*. The load Q is applied to the upper surface of the specimen by means of a steel disc. Both the top surface and the base of the specimen are lubricated. Plotting in a diagram (Fig. 115*b*) the vertical strain ϵ against the stress σ, we obtain for a perfectly elastic material a straight line, OE.

The positive vertical strain produced by a vertical pressure is associated with a negative horizontal strain, $\epsilon_l = \Delta d/d$. The absolute value of the ratio between the strains ϵ_l and ϵ,

$$\mu = \frac{\epsilon_l}{\epsilon} = \frac{\epsilon_l}{\sigma} E \qquad [2]$$

is called *Poisson's ratio*, and the reciprocal $1/\mu$ is *Poisson's number*. For perfectly elastic materials the value μ is a constant. If both equations 1 and 2 are valid the strain produced by a composite state of stress is equal to the sum of the strains produced by each one of the

stresses individually. This relation is known as the *law of superposition.* Since every composite state of stress at a given point can be resolved into three principal stresses σ_I, σ_{II}, and σ_{III}, intersecting each other at right angles (see Art. 7), the strain in a given direction is equal to the sum of the strains produced by each of the principal stresses individually in this direction.

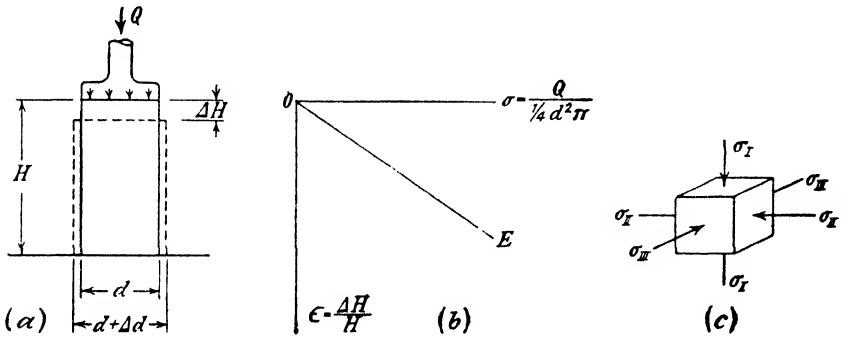

FIG. 115. (*a*) Unconfined compression test on cylindrical specimen of perfectly elastic material; (*b*) test result; (*c*) orientation of principal stresses in three-dimensional state of stress.

Figure 115*c* shows a prismatic element with a volume V whose sides are acted upon by principal stresses σ_I, σ_{II}, and σ_{III}. If these stresses are equal,

$$\sigma_I = \sigma_{II} = \sigma_{III} = \sigma_w$$

the strain in the direction of each of these stresses is

$$\frac{\sigma_w}{E} - 2\mu \frac{\sigma_w}{E} = \frac{\sigma_w}{E}(1 - 2\mu)$$

Hence the application of the all-round pressure σ_w changes the volume of the element by

$$\frac{\Delta V}{V} = 3\frac{\sigma_w}{E}(1 - 2\mu)$$

per unit volume. For $\mu = 0.5$ the volume change $\Delta V/V$ is equal to zero. Therefore elastic solids for which $\mu = 0.5$ are incompressible.

For dense soils and solid granular materials such as concrete or sandstone Poisson's ratio increases from small values of the order of magnitude of 0.2 at low stress to more than 0.5 at very high stresses. In other words materials of this category contract under small load, but they expand when the state of failure is approached. Yet, in all the theories involving the elastic properties of soils, Poisson's ratio is

assumed to be a constant. Therefore the results are valid only if the stresses are low compared to those required to produce a failure.

If the three principal stresses σ_I, σ_{II}, σ_{III} are different, the volume change $\Delta V/V$ per unit of volume is equal to the sum of the volume change produced by each one of these stresses individually. An individual principal stress, for instance σ_I, reduces the unit volume by

$$\frac{\Delta V_1}{V} = \frac{\sigma_I}{E} - 2\mu \frac{\sigma_I}{E} = \frac{\sigma_I}{E}(1 - 2\mu) \qquad [3]$$

Hence the volume change produced by the simultaneous application of three different principal stresses is

$$\frac{\Delta V}{V} = \frac{1 - 2\mu}{E}(\sigma_I + \sigma_{II} + \sigma_{III}) \qquad [4]$$

For a given value of $\Delta V/V$, equation 4 is the equation of a plane which intersects the three axes at equal distances from the origin O, as shown in Figure 116*a*. For different values of $\Delta V/V$, equation 4 represents a family of parallel planes. The distance between the origin O and the intersection of these planes with the three axes increases in simple proportion to the sum of the three principal stresses. Every set of stresses represented by one of the points of such a plane produces the same volume change as a linear stress equal to the distance between the origin O and the points at which the plane intersects any one of the three axes.

If $\sigma_{II} = \sigma_{III}$ the state of stress has circular symmetry about the σ_I-axis. σ_I is the axial and $\sigma_{II} = \sigma_{III}$ is the radial stress. The change of volume per unit of volume produced by such a system of stresses is

$$\frac{\Delta V}{V} = \frac{1 - 2\mu}{E}(\sigma_I + 2\sigma_{III}) \qquad [5]$$

Figure 116*a* shows that a radial stress with the intensity $\frac{1}{2}\sigma_I$ produces the same volume change as an axial stress with the intensity σ_I. Since all the points representing the volume change due to stresses having circular symmetry are located on a plane through the σ_I-axis, bisecting the angle between the two other axes, we can represent the volume change due to such a change in stress in a plane diagram (Fig. 116*b*). This diagram is obtained by rotating the plane Oa_1b_1 (Fig. 116*a*) into the plane of the paper (Rendulic 1937). In this plane, values of σ_I are represented on the vertical axis, and values of $\sigma_{III}\sqrt{2}$ on the horizontal axis. If the stresses are changed from those represented by the coordinates of any point on any one line parallel to a_1b_1 (Fig. 116*b*) to those represented by any other point on the same line, the corresponding

volume change is equal to zero. For geometrical reasons every point on a line $O\sigma_w$ at right angles to a_1b_1 represents a state of stress $\sigma_I = \sigma_{II} = \sigma_{III} = \sigma_w$.

Another graphical method of representing the volume change due to a state of stress having circular symmetry is shown in Figure 116c (Casagrande 1936). In this diagram the abscissas are equal to the stress difference $\sigma_I - \sigma_{III}$ and the ordinates are equal to the correspond-

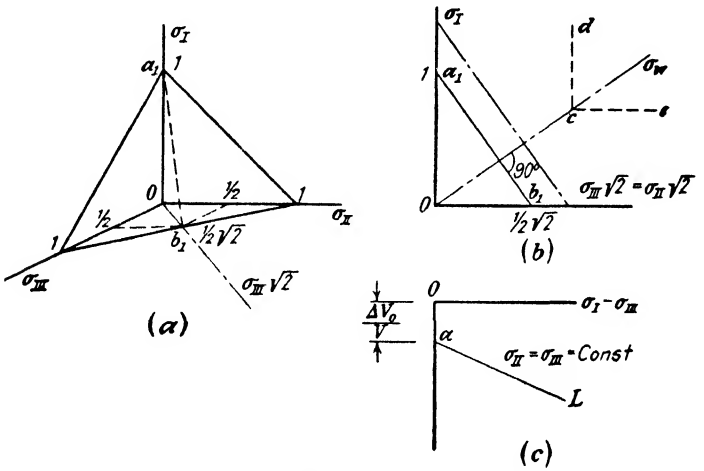

FIG. 116. (*a*) Diagram representing relation between principal stresses and unit volume change for perfectly elastic material; (*b*) and (*c*) simplified methods of representing the same relation if two principal stresses are equal.

ing volume change at a constant value of σ_{III}. By increasing all the principal stresses from an initial value of zero to $\sigma_{I0} = \sigma_{II} = \sigma_{III}$ the volume decrease per unit of volume is

$$\frac{\Delta V_0}{V} = \frac{1 - 2\mu}{E} \cdot 3\sigma_{I0} \qquad [6]$$

Subsequent increase of σ_I at a constant value $\sigma_{II} = \sigma_{III}$ increases the unit volume change from $\Delta V_0/V$ to

$$\frac{\Delta V}{V} = \frac{\Delta V_0}{V} + (1 - 2\mu)\frac{\sigma_I - \sigma_{III}}{E}$$

This relation is shown in Figure 116c by a straight line L which intersects the vertical axis at a distance $\Delta V_0/V$ below the origin. In Figure 116*b* an increase of the axial stress σ_I at a constant value σ_{III} of the radial stress is represented by a vertical line *cd*. The horizontal line *ce* represents a process involving an increase of $\sigma_{II} = \sigma_{III}$ at a constant value σ_I. In

triaxial compression tests (see Art. 6) either one of these changes of stress can be produced.

If the results of triaxial compression tests on real soils are plotted in diagrams similar to Figures 116*b* and 116*c*, we can recognize at a glance the extent to which the properties of the soil deviate from those of an ideal elastic material.

134. State of stress in a laterally confined elastic prism acted upon by its own weight. If we construct a prism *abcd* (Fig. 117) with a unit weight γ on a perfectly frictionless base the pressure due to the weight of the material causes not only a vertical compression but also a lateral expansion. If the prism had no weight it would assume the shape indicated by the rectangle *abdc*. At a depth z below the top of the prism the normal stress on a horizontal section is

$$\sigma = \gamma z$$

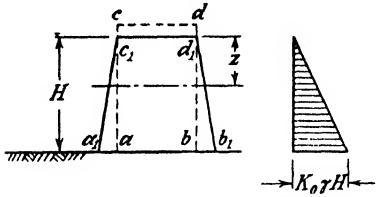

FIG. 117. Deformation of prism of elastic material due to its own weight; right-hand diagram represents horizontal pressure on smooth, confining vertical walls.

From equation 133(2) we obtain for the corresponding lateral expansion per unit of width of the prism

$$\epsilon_l = \mu \frac{\sigma}{E} = \frac{\mu\gamma}{E} z \qquad [1]$$

It increases in direct proportion to the depth z as indicated in Figure 117 by the lines c_1a_1 and d_1b_1.

If the prism is laterally confined between perfectly smooth, vertical walls or within a layer of identical material on a rough base no lateral expansion can occur. Therefore at any depth z every vertical side of the prism will be acted upon by a horizontal pressure σ_{III} per unit of area whose intensity suffices to reduce the lateral expansion of the prism at depth z to zero. These pressures produce in every horizontal direction a strain

$$\epsilon' = \frac{\sigma_{III}}{E} - \mu\frac{\sigma_{III}}{E} = \frac{\sigma_{III}}{E}(1 - \mu)$$

Substituting $\epsilon' = \epsilon_l$ (eq. 1), we obtain

$$\sigma_{III} = \gamma z \frac{\mu}{1 - \mu} = \gamma z K_0 \qquad [2]$$

wherein

$$K_0 = \frac{\mu}{1 - \mu} \qquad [3]$$

corresponds to the coefficient of earth pressure at rest (eq. 10(1)) in the theory of earth pressure. For practically incompressible materials the value of μ is 0.5 and the corresponding value of K_0 is unity.

135. Stresses and displacements due to a point load on a semi-infinite solid with a horizontal surface. If an external force acts on a very small area of the surface of a solid or on the walls of a little cavity in the interior of the solid it is called a *point load,* and the area which is acted upon by the force is called the *point of application* of the load. It represents the center of the perturbation in the state of stress, caused by the load. The vertical component of an inclined point load acting on the horizontal surface of a semi-infinite solid produces a state of stress which has circular symmetry about a vertical line through the point of application. The state of stress due to the horizontal component is symmetrical with reference to a vertical plane through the line of action of the horizontal component.

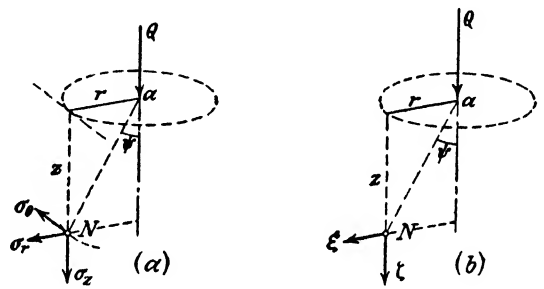

FIG. 118. (*a*) Stresses at point N and (*b*) displacements of point N in interior of semi-infinite solid acted upon by point load Q.

The simplest and by far the most important state of stress ensues if a vertical point load acts on the horizontal surface of a semi-infinite solid (Fig. 118*a*). Let

Q = the load,

r = the horizontal radial distance between an arbitrary point N below the surface and a vertical axis through the point a of application of Q,

ψ = the angle between the vector aN and the vertical axis through the point of application,

z = the vertical co-ordinate of point N, measured from the surface downward,

σ_z, σ_r, σ_θ = the vertical stress, the horizontal radial stress and the horizontal circumferential stress; all normal stresses,

τ_{rz} = shearing stress in the directions of r and z, and

μ = Poisson's ratio for the solid.

On account of the circular symmetry of the state of stress about the vertical axis through a the shearing stresses in vertical, radial planes are equal to zero. The intensity of the other stresses has been computed by means of a stress function which strictly satisfies the boundary conditions (Boussinesq 1885). The stresses are

$$\sigma_z = \frac{3Q}{2\pi z^2} \cos^5 \psi \qquad [1a]$$

$$\sigma_r = \frac{Q}{2\pi z^2} \left[3 \cos \psi^3 \sin^2 \psi - (1 - 2\mu) \frac{\cos^2 \psi}{1 + \cos \psi} \right] \qquad [1b]$$

$$\sigma_\theta = -(1 - 2\mu) \frac{Q}{2\pi z^2} \left[\cos^3 \psi - \frac{\cos^2 \psi}{1 + \cos \psi} \right] \qquad [1c]$$

$$\tau_{rz} = \frac{3Q}{2\pi z^2} \cos^4 \psi \sin \psi \qquad [1d]$$

These equations are known as *Boussinesq's equations*. The circumferential stress σ_θ is negative for every value of $\mu < 0.5$. It should be noted that the vertical stress σ_z is the only normal stress which is independent of Poisson's ratio μ. In this and in all the following articles it is assumed that the unit weight of the elastic material is zero. Therefore the computations furnish only the stresses produced by the surface loads. In order to get the total stresses in an elastic material with unit weight γ one has to combine the stresses due to the loads with those produced by the weight of the supporting material. These stresses are

$$\sigma_z = z\gamma \qquad [2a]$$

$$\sigma_r = \sigma_\theta = K_0 z\gamma \qquad [2b]$$

and

$$\tau_{rz} = 0 \qquad [2c]$$

wherein K_0 is the coefficient of earth pressure at rest for the lateral earth pressure in the semi-infinite solid.

If one computes by means of equations 1 the principal stresses produced by the point load Q one finds that the direction of the largest principal stress at any point intersects the horizontal surface of the mass in the immediate vicinity of the point of application a (Fig. 118a) of the load and that the two other principal stresses σ_{II} and σ_{III} are very small. If $\mu = 0.5$ one obtains $\sigma_{II} = \sigma_{III} = 0$. The direction of the largest principal stress σ_I passes through point a and the intensity

of this stress is

$$^{\sigma}I = \frac{3}{2}\frac{Q}{\pi z^2}\cos^3\psi \qquad [3]$$

This means that for $\mu = 0.5$ the load Q produces a unidirectional state of stress.

The equations for the stresses due to a horizontal point load acting at a point of the horizontal surface have been derived by Cerruti (1882, quoted by Love, 1934). They are not as simple as equations 1. Still more cumbersome are the equations which represent the stresses due to a vertical and a horizontal force acting at a point beneath the horizontal surface (Mindlin 1936). In order to use these equations for solving practical problems it would be necessary to simplify them at the expense of accuracy.

With increasing depth below the surface the state of stress represented by Mindlin's equations approaches that which is produced by a force acting at a point in the interior of an infinite solid. The corresponding stress equations have been derived by Kelvin (about 1850). Introducing the special value $\mu = 0.5$ (Poisson's ratio for incompressible elastic solids) into his equations one finds that the stresses produced by the point load Q applied at a given point within an infinite solid are equal to one half of the stresses acting at the same point in a semi-infinite solid whose plane surface passes through the point of application of Q at a right angle to the direction of Q. Hence one obtains these stresses by dividing the stresses determined by equations 1 by two, provided $\mu = 0.5$.

If the stresses in a semi-infinite elastic solid are known, the corresponding deformations can be computed by means of the fundamental equations of the theory of elasticity. From a practical point of view, the most interesting displacements are those produced by a vertical point load Q applied to the horizontal surface of a semi-infinite solid. They have been computed by Boussinesq (1885). Since the state of stress produced by such a point load is symmetrical about the line of action of the load, the displacement of a point N (Fig. 118*b*) is determined by two components of the displacement, for instance

ζ = the vertical displacement of the point N, positive in a downward direction,

ξ = the horizontal, radial displacement, positive in an outward direction.

The displacements ζ and ξ are determined by the equations

$$\zeta = \frac{Q}{2\pi r}\frac{1+\mu}{E}\left[2\,(1-\mu) + \cos^2\psi\right]\sin\psi \qquad [4a]$$

and

$$\xi = \frac{Q}{2\pi r}\frac{1+\mu}{E}\left[-(1-2\mu) + \cos\psi + \cos^2\psi\right]\sin\psi\tan\frac{\psi}{2} \qquad [4b]$$

At the surface $\psi = 90°$, $\cos\psi = 0$, $\sin\psi = 1$, and $\tan\psi/2 = 1$. With these values we obtain for the displacement of a point on the surface at a distance r from the load

$$\zeta_0 = \frac{Q}{\pi r}\frac{1-\mu^2}{E} \qquad [5a]$$

$$\xi_0 = -\frac{Q}{2\pi r}\frac{1-\mu-2\mu^2}{E} \qquad [5b]$$

136. Stresses due to a flexible area load covering a part of the horizontal surface. The term *flexible* indicates that no stiff structure such as a footing is inserted between the load and the surface of the semi-infinite solid. The load q per unit of the loaded part A of the surface of the solid can be divided into an infinite number of discrete point loads $q\,dA$. Since the material is assumed to be perfectly elastic the stress produced by the total load is equal to the sum of the stresses produced by the point loads $q\,dA$. Therefore the resultant state of stress can be determined by integration.

A load q' per unit of the length of a straight line of infinite extension on the surface of the solid produces a state of plane strain. The stresses at an arbitrary point N of every plane section at a right angle to the line, represented in Figure 119*a* by point a, are

$$\sigma_z = \frac{2}{\pi}\frac{q'}{z}\cos^4\psi \qquad [1a]$$

$$\sigma_x = \frac{2}{\pi}\frac{q'}{z}\cos^2\psi\sin^2\psi \qquad [1b]$$

and

$$\tau_{xz} = \frac{2}{\pi}\frac{q'}{z}\cos^3\psi\sin\psi \qquad [1c]$$

It should be noted that these equations do not contain Poisson's ratio. By integration one obtains the following values for the stresses due to a load q per unit of area on a strip of infinite length and a constant width $2B$ (Fig. 119*b*):

$$\sigma_z = \frac{q}{\pi}\Big[\sin\psi\cos\psi + \psi\Big]_{\psi_1}^{\psi_2} \qquad [2a]$$

$$\sigma_x = \frac{q}{\pi}\Big[-\sin\psi\cos\psi + \psi\Big]_{\psi_1}^{\psi_2} \qquad [2b]$$

and

$$\tau_{xz} = \frac{q}{\pi}\left[\sin^2\psi\right]_{\psi_1}^{\psi_2} \qquad [2c]$$

On the basis of equations 7(1) and 7(2) one gets for the corresponding principal stresses the values

$$\sigma_I = \frac{q}{\pi}(\psi_0 + \sin\psi_0) \qquad [3a]$$

and

$$\sigma_{III} = \frac{q}{\pi}(\psi_0 - \sin\psi_0) \qquad [3b]$$

wherein $\psi_0 = \psi_2 - \psi_1$ (see Fig. 119b). According to these equations the principal stresses for a given value q depend solely on the value ψ_0.

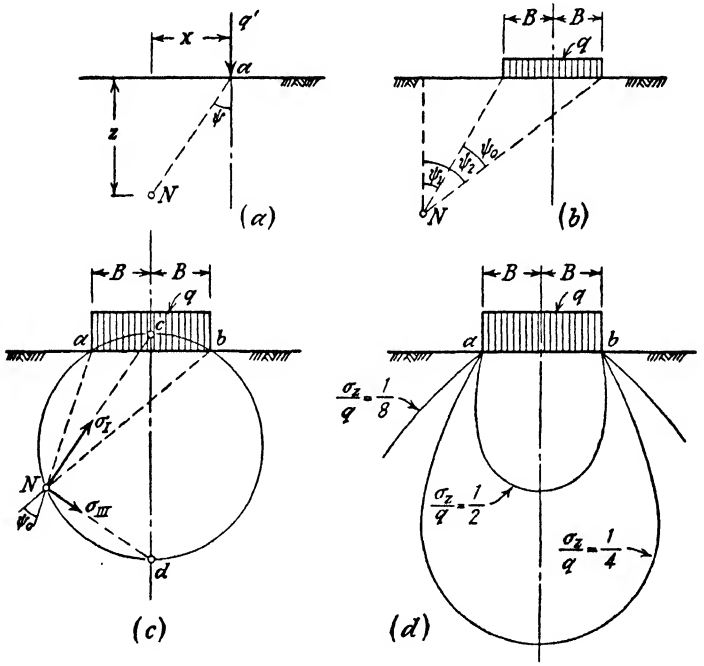

FIG. 119. (*a*) Line load; (*b*) strip load acting on surface of semi-infinite solid; (*c*) orientation of principal stresses at N due to strip load; (*d*) curves of equal ratio between vertical pressure and unit load on strip with infinite length (pressure bulbs).

Hence for every point on a circle through a, b, and N (Fig. 119c) the principal stresses have the same intensity. By means of a simple computation it can also be shown that the directions of the two prin-

cipal stresses in every point on the circle *abN* (Fig. 119*c*) pass through the points *c* and *d* respectively. These two points are located at the intersection between the circle and the plane of symmetry of the loaded strip. Furthermore by means of equation 2*a* it can be shown that all the points with equal vertical normal stress σ_z are located on curves (Fig. 119*d*) which resemble sections through the boundaries between the individual layers of a bulb. Therefore the space located beneath the loaded area is commonly called the *bulb of pressure*. From this explanation of the meaning of the term it is obvious that no definite dimensions can be assigned to the bulb of pressure beneath a given loaded area, unless one specifies that the vertical normal stress at the boundary of the bulb should correspond to a certain fraction, for instance ½ or ¼, of the unit load *q*.

The computation of the stresses due to a uniformly distributed load on a rectangular or a circular area are rather involved, and the results of the computation cannot be represented by a simple set of equations. However, the problem has been solved and the results have been compiled in tables which make it possible to determine the stresses in any point by means of a simple process of interpolation (Love 1928). The vertical normal stress at a depth *z* below the center of a circular area with a radius *R* which carries a unit load *q* is

$$\sigma_z = q\left\{1 - \left[\frac{1}{1 + (R/z)^2}\right]^{\frac{3}{2}}\right\} \qquad [4]$$

In many practical cases it is sufficient to know the intensity and the distribution of the normal stresses over horizontal sections through the loaded solid. In order to get this information with a minimum amount of labor it is desirable to express the equations for the normal stress in terms of dimensionless ratios. In this form an equation can be solved once and for all for different values of the dimensionless ratios. For instance by dividing both sides of equation 135(1*a*) by Q/z^2 we obtain

$$\sigma_z \frac{z^2}{Q} = \frac{3}{2\pi}\cos^5\psi = \frac{3}{2\pi}\left[\frac{1}{1 + (r/z)^2}\right]^{\frac{5}{2}} = f(r/z) = I_\sigma \qquad [5]$$

I_σ is a pure number. It is called an *influence value*, because it determines the influence of a vertical point load at point *a* (Fig. 118*a*) on the vertical normal stress σ_z at point *N*. It depends only on the value of the ratio r/z. The numerical values of I_σ (eq. 5) for different values of

r/z are given in Table I of the Appendix. From equation 5 we get

$$\sigma_z = I_\sigma \frac{Q}{z^2} \qquad [6]$$

The vertical normal stress σ_z at point N (Fig. 119a) of a semi-infinite solid acted upon by a line load q' per unit of length (eq. 1a) is given by

$$\sigma_z = \frac{q'}{z}\frac{2}{\pi}\cos^4\psi = \frac{q'}{z}\frac{2}{\pi}\left[\frac{1}{1+(x/z)^2}\right]^2 = \frac{q'}{z}I_\sigma \qquad [7a]$$

wherein

$$I_\sigma = \frac{2}{\pi}\cos^4\psi = \frac{2}{\pi}\left[\frac{1}{1+(x/z)^2}\right]^2 \qquad [7b]$$

is the influence value for the line load. This equation is so simple that no tables are required for determining the values of I_σ.

Figure 120a represents a rectangular area which carries a uniformly distributed load q per unit of area. Point N is located at a depth z below an arbitrary point N' of this area. In order to determine the vertical normal stress σ_z at point N we divide the total area by two lines through point N' into four rectangular sections, marked I to IV. Each of these areas contributes one share, $\Delta\sigma_z$, to the total vertical normal stress σ_z produced at point N by the load. Using Boussinesq's equation 135(1a) as a starting point one obtains by integration (Newmark 1935)

$$I_\sigma = \frac{\Delta\sigma}{q} = \frac{1}{4\pi}\left[\frac{2mn\,(m^2+n^2+1)^{\frac{1}{2}}}{m^2+n^2+m^2n^2+1}\cdot\frac{m^2+n^2+2}{m^2+n^2+1}\right.$$
$$\left. + \tan^{-1}\frac{2mn\,(m^2+n^2+1)^{\frac{1}{2}}}{m^2+n^2-m^2n^2+1}\right] \qquad [8]$$

wherein

$$m = \frac{B}{z} \quad \text{and} \quad n = \frac{L}{z}$$

are pure numbers. The value I_σ is dimensionless and represents the influence of a surcharge covering a rectangular area on the vertical normal stress at a point located at a depth z below one of its corners. Plotting in a diagram (Fig. 120b) the values of $I_\sigma = \Delta\sigma/q$ on the horizontal axis and the values $1/m = z/B$ on the vertical axis we obtain for different values of $L/B = n/m$ the curves shown in the figure (Steinbrenner 1934).

Table II and plate 1 in the Appendix contain the influence values I_σ (eq. 8), for different values of m and n. The Appendix also con-

tains the influence values for a point load (Table I) and for a circular surcharge (Table III). In order to compute the vertical normal stress σ_z at point N in Figure 120*a* one computes the ratios m and n

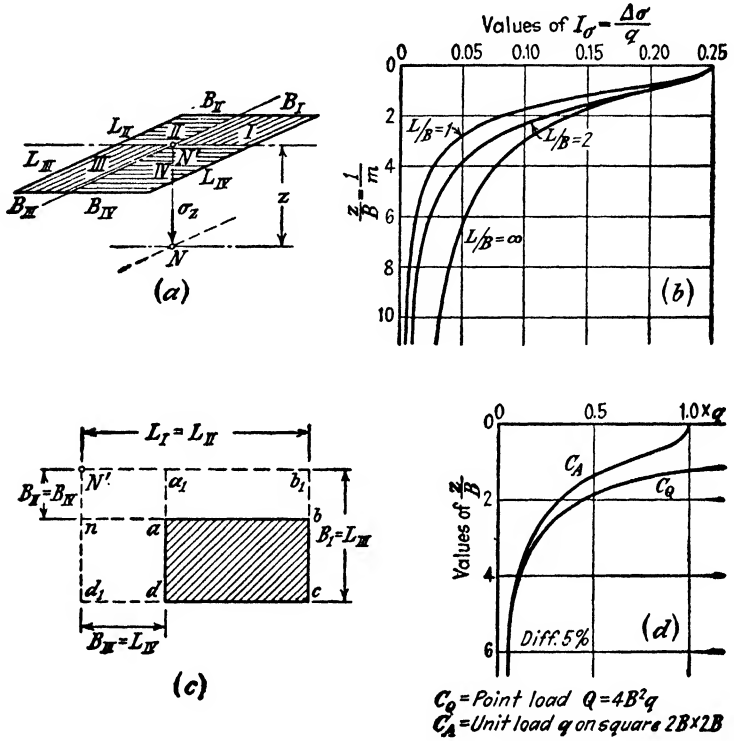

FIG. 120. (*a*) Uniformly loaded rectangular area on surface of semi-infinite solid; (*b*) influence values for vertical normal stress at point N due to load on either one of the four areas I to IV in (*a*); (*c*) diagram illustrating method of computing influence values, if N' is located outside of loaded area; (*d*) diagram illustrating the influence of replacement of uniformly distributed load on square area by an equivalent point load at the center of the area on the vertical unit pressure along vertical line through center of the loaded area. (*After Steinbrenner 1934.*)

for each one of the areas marked I to IV respectively and determines the corresponding influence values $I_{\sigma I}$ to $I_{\sigma IV}$ by means of the graph or the table. The total normal stress at point N is

$$\sigma_z = q\,(I_{\sigma I} + I_{\sigma II} + I_{\sigma III} + I_{\sigma IV}) \qquad [9]$$

If point N' is located outside the loaded area we construct a rectangle $N'b_1cd$ (Fig. 120c) whose sides are oriented as shown in the

figure. From the figure it can be seen that

$$\text{area } abcd = N'b_1cd_1 - N'nbb_1 - N'a_1dd_1 + N'a_1an \qquad [10]$$

The vertical normal stress σ_z at point N located at a depth z below point N' due to a surcharge q per unit of the area $abcd$ is equal to the algebraic sum of the normal stresses produced by loading each one of the areas listed on the right-hand side of the preceding equation with q per unit of area. Hence, after we have determined the influence values $I_{\sigma I}$ to $I_{\sigma IV}$, for the areas indicated on the right-hand side of equation 10, for instance, by means of Table II in the Appendix, we obtain for the vertical normal stress σ_z

$$\sigma_z = q\,(I_{\sigma I} - I_{\sigma II} - I_{\sigma III} + I_{\sigma IV}) \qquad [11]$$

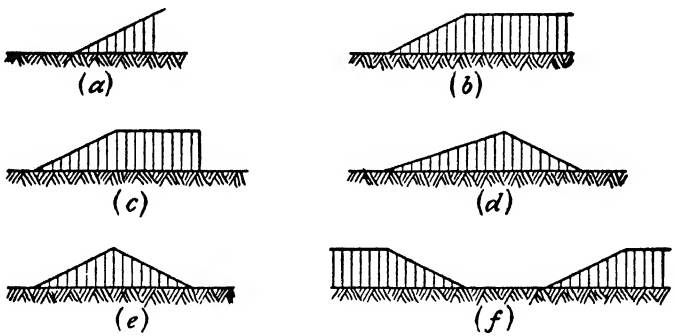

FIG. 121. Some types of flexible loads on surface of semi-infinite solid; equations for computing vertical pressure produced by these loads have been published.

The method described in the preceding paragraphs is only one of several methods which have been worked out for the purpose of determining the normal stresses on horizontal sections beneath finite loads. (See Burmister 1938, and discussion of his paper by Newmark, Krynine, and others.)

In Figure 120*d* the abscissas of the curve C_A represent the vertical normal stress at different depths z below the center of a square area $2B$ by $2B$ which carries a surcharge q per unit of area or a total surcharge $4B^2q$. The abscissas of the curve C_Q represent the corresponding stresses due to a concentrated load $Q = 4B^2q$ acting at the center of the square area. The figure shows that the difference between the two curves becomes very small for values of z/B in excess of six. Hence in a computation of the normal stresses on a horizontal section at a depth z below a continuous load on a finite area it is admissible to replace this load by point loads spaced not in excess of $z/3$. The stresses produced

at a given point of the section by the point loads can be computed by means of tables of influence values for point loads.

Figures 121*a* to 121*f* represent different surcharges resembling fills with inclined slopes. Perpendicular to the plane of the paper the surcharges extend to infinity. The equations which determine the normal stresses due to the weight of these surcharges on horizontal sections, together with references to the original publications, have been compiled by Gray (1936). Tables and charts have been prepared by Jürgenson (1934). The results of recent investigations were published by Holl (1941).

137. Settlement of the surface of a semi-infinite solid due to a flexible, vertical load on a finite area. Assuming that the solid is perfectly elastic, the law of superposition of stress and strain is valid. Hence the settlement due to a load on a finite area can be computed by integration as was done in Article 136 for the purpose of determining the stresses produced by such a load. To illustrate the procedure we compute the vertical displacement of point N', located within the rectangular area shown in Figure 120*a*. The area carries a uniformly distributed surcharge q per unit of area. The vertical displacement $d\zeta_0$ of point N' due to a surcharge $dQ = q\,dx\,dy$ acting at an arbitrary distance r from point N' is determined by equation 135(5*a*). By integrating over a rectangular area with a width B and a length L one gets for the settlement $\Delta\rho$ of the corners of the loaded area the equation

$$\Delta\rho = qB\frac{1-\mu^2}{E}\frac{1}{\pi}\left[l\log\frac{1+\sqrt{l^2+1}}{l} + \log\left(l+\sqrt{l^2+1}\right)\right] \qquad [1a]$$

wherein

$$l = \frac{L}{B} \qquad [1b]$$

is a pure number (Schleicher 1926). Substituting

$$I_\rho = \frac{1}{\pi}\left[l\log\frac{1+\sqrt{l^2+1}}{l} + \log\left(l+\sqrt{l^2+1}\right)\right] \qquad [2a]$$

one gets

$$\Delta\rho = qB\frac{1-\mu^2}{E}I_\rho \qquad [2b]$$

The value I_ρ is also a pure number. It determines the influence of a uniform surcharge covering a rectangular area on the settlement of the corners of this area and represents an analogue to the influence value I_σ (eq. 136(8)). Figure 122*a* shows the relation between I_ρ and the

ratio l between the length and the width of the loaded area. For $l = \infty$ we obtain $I_\rho = \infty$, which shows that the settlement of a uniformly loaded strip on the surface of a semi-infinite solid is equal to infinity for any finite value of the load and the width of the strip.

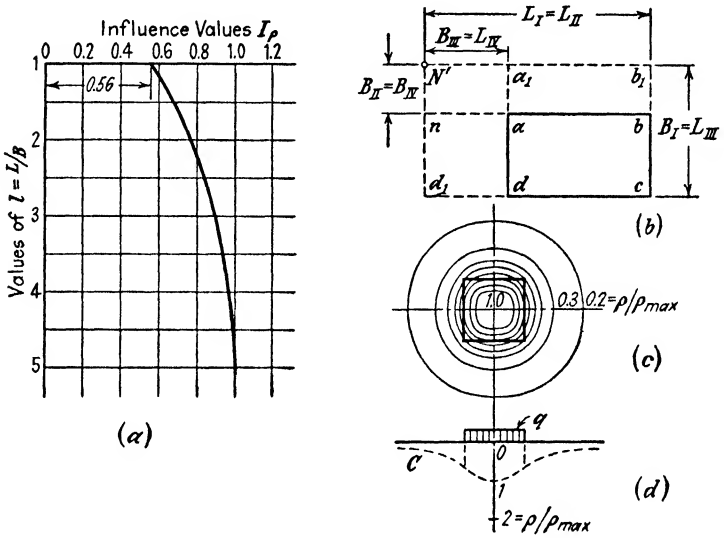

FIG. 122. (*a*) Influence values for computing settlement of a corner of a loaded rectangular area $L \times B$ on surface of semi-infinite solid; if $L/B = \infty$, $I_\rho = \infty$; (*b*) diagram illustrating method of determining settlement of point located outside of loaded area; (*c*) curves of equal settlement for square loaded area; (*d*) settlement profile.

In order to determine the settlement of point N' (Fig. 120*a*) we compute the values of l for each one of the rectangles I to IV. From the diagram (Fig. 122*a*) we obtain the corresponding values of I_ρ. They are represented by the values $I_{\rho I}$ to $I_{\rho IV}$. The total settlement of point N' is

$$\rho = q \frac{1 - \mu^2}{E} (B_I I_{\rho I} + B_{II} I_{\rho II} + B_{III} I_{\rho III} + B_{IV} I_{\rho IV}) \qquad [3]$$

If point N' is located outside the loaded area we construct a rectangle $N'b_1cd_1$ (Fig. 122*b*) whose sides are oriented as shown in the figure. From the figure we obtain

$$\text{area } abcd = N'b_1cd_1 - N'a_1dd_1 - N'b_1bn + N'a_1an$$

The areas indicated on the right-hand side of this equation have the corner N' in common. The influence values $I_{\rho I}$ to $I_{\rho IV}$ for the settlement of these areas can be obtained from Figure 122*a*.

The settlement of point N' (Fig. 122*c*) due to a load q per unit of the area *abcd* is equal to the algebraic sum of the settlements produced by loading each one of these areas with q per unit of area. Hence, after we have determined the influence values $I_{\rho I}$ to $I_{\rho IV}$ for each one of these areas, we obtain for the settlement ρ of point N'

$$\rho = q\frac{1-\mu^2}{E}(I_{\rho I}B_I - I_{\rho II}B_{II} - I_{\rho III}B_{III} + I_{\rho IV}B_{IV}) \qquad [4]$$

The results of the computation of the settlement for different points within and outside a loaded area can be represented by *curves of equal settlement*, like those shown in Figure 122*c* for a square loaded area. Sections through the loaded area, such as that shown in Figure 122*d*, are called *settlement profiles*. The settlement produced by a uniformly distributed load acting on part of the surface of a semi-infinite elastic solid has always the character of a bowl-shaped depression. In other words, the central part of the loaded area settles more than the peripheral parts.

138. Transition from state of elastic to that of plastic equilibrium beneath flexible loads. As soon as the stresses due to an increasing load satisfy the stress conditions for failure at one point the loaded material fails at that point and a further increase of the load causes the failure to spread until the bearing capacity of the material is exceeded. In relatively rigid solids, such as concrete, very stiff clays, or cemented sand, the failure eliminates the cohesion at the point of failure and the propagation of the failure produced by an increase of the load is associated with progressive injury to the loaded material. Therefore the load required to establish the stress conditions for failure at one point of the loaded material is almost equal to the greatest load which the footing can carry.

In perfectly plastic materials the transition from the state of elastic equilibrium to that of incipient failure also spreads from local centers, but the transition is not associated with a loss of strength. Therefore the critical load is considerably greater than the load required to produce incipient failure at some point of the loaded material. During the transition from incipient to ultimate failure an increase of the load produces merely an increase of the size of the zone of plastic equilibrium.

Before the flow begins in a material combining ideal elasticity and ideal plasticity, the stresses due to the load increase in simple proportion to the load and the orientation of the principal stresses remains unchanged. After the flow has started this rule loses its validity and the orientation of the principal stresses also changes. A very convenient method of visualizing this change consists in plotting the trajectories

of stresses. (See any textbook on applied mechanics, for instance Timoshenko 1940.) The trajectories can be obtained by determining for a considerable number of points the direction of the principal stresses and by tracing two sets of curves which are at every point tangent to the direction of the principal stresses. Since the principal stresses intersect at right angles, the two sets of trajectories also intersect at right angles, as do the two sets of curves in a flow net. Figures 123*a* and

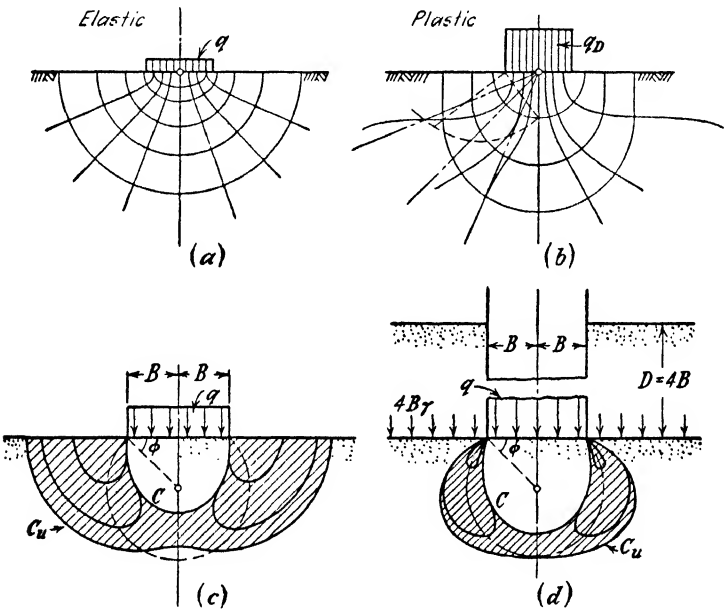

FIG. 123. (*a*) Trajectories in semi-infinite solid beneath flexible strip load, if loaded material is in elastic state; (*b*) trajectories at instant of failure in solid by general shear; (*c*) spread of plastic state in sand due to increase of strip load on surface; (*d*) as before, if strip load acts beneath level of surface. (*After O. K. Fröhlich 1934a.*)

123*b* represent the trajectories for the state of elastic and of plastic equilibrium respectively in an ideal solid beneath a flexible, loaded strip of infinite length.

For states intermediate between elastic and plastic equilibrium the location of the outer boundary of the zone of plastic flow can be estimated by combining the equations which represent the stresses due to the surcharge and to the dead weight of the loaded solid with those expressing the stress conditions for flow failure. In every section through the loaded material, the boundary is located at the points where the sum of the stresses due to the surcharge and the dead weight satisfy

the conditions for flow failure. The following example illustrates the procedure. The stresses due to a uniform surcharge on a flexible strip with infinite length are determined by equations 136(2). The equations for the stresses due to the weight of the loaded solid, γ per unit of volume, are

$$\sigma_z = \gamma z, \quad \sigma_x = K_0 \gamma z \quad \text{and} \quad \tau_{xz} = 0$$

wherein K_0 is the coefficient of earth pressure at rest (eq. 10(1)). Combining these equations with equations 136(2) and 7(1) and 7(2) one can compute the principal stresses σ_I and σ_{III}. The stress conditions for flow failure are determined by equation 7(6),

$$\frac{\sigma_I + \sigma_{III}}{2} \sin \phi = \frac{\sigma_I - \sigma_{III}}{2} - c \cos \phi$$

wherein ϕ is the angle of shearing resistance and c the cohesion. Introducing into this computation the simplifying assumptions $c = 0$ and $K_0 = 1$ (ideal sand, hydrostatic distribution of the stresses due to the weight of the sand) Fröhlich (1934*a*) obtained for the boundaries of the zone of plastic flow in different stages intermediate between the state of elastic and plastic equilibrium the lines indicated in Figures 123*c* and 123*d*. In Figure 123*c* the surface of the sand on both sides of the loaded strip carries no surcharge. The width of the zone of plastic flow is greatest at the surface. In Figure 123*d* the surface adjoining the strip carries a uniformly distributed surcharge γD per unit of area due to the weight of a layer of sand with a depth D. At the level of the loaded strip the width of the zones of plastic flow is equal to zero and it assumes a maximum at some depth below the strip. In both cases (Figs. 123*c* and 123*d*) an increase of the load causes the deepest points of the zones of plastic flow to advance on a circle through the rims of the load. The center of the circle is at a depth $B \tan \phi$ below the center of the load as shown in the figures. Finally the two zones of plastic flow merge into one, which is separated from the loaded area by a zone of elastic equilibrium. In the figures the section through the lower boundary of this zone is indicated by the curve C_u. As this final stage of transition from elastic equilibrium to plastic equilibrium is approached, the equations of Boussinesq lose their validity completely and the remainder of the process is described by the theory of plasticity.

Fröhlich's computations are based on the assumption that the transition from elastic to plastic behavior occurs abruptly. In reality, at every point of every soil the process of elastic deformation passes imperceptibly into plastic flow. The theory also disregards the conditions for equilibrium within the zone of plastic deformation. Therefore it leads to the erroneous conclusion that the depth of the zone of plastic

flow is capable of increasing indefinitely. According to Chapter VIII the depth of the zone of plastic flow cannot possibly exceed a certain critical value which depends on the width of the loaded area and on the coefficient of internal friction. However, up to the stage when the zones of plastic flow merge beneath the center of the loaded area, as indicated by the curves C_u in Figure 126, the theory appears to be fairly reliable. If the load covers a long strip, the load required, according to Fröhlich's theory, to produce the merger of the plastic zones is approximately equal to the lower limit of the ultimate bearing capacity, determined by the dashed curves in Figure 38c. (See Art. 46.)

If the angle of internal friction ϕ of a plastic material with a cohesion c is equal to zero, the factor $\sin \phi$ in equation 7(6) is also equal to zero and the stress conditions for failure are determined by the equation

$$\sigma_I - \sigma_{III} = 2c$$

As soon as the unit load on a flexible strip with infinite length becomes equal to πc this condition is satisfied at every point of a semicircle whose center is located at the midpoint of ab in Figure 119c. Hence if $\phi = 0$ the propagation of the plastic state starts simultaneously at every point of a cylindrical section through the edges of the loaded area. According to equation 46(9f) the bearing capacity of the material is

$$q_c = 5.14c = (\pi + 2)c$$

Hence the bearing capacity exceeds the load πc required to establish the nucleus of a zone of plastic equilibrium by 39 per cent.

139. Distribution of contact pressure over the base of footings. The term *contact pressure* indicates the normal stress at the surface of contact between a footing and the supporting earth. In Article 137 it was shown that a surcharge uniformly distributed over a finite part of the horizontal surface of a semi-infinite elastic solid always produces a bowl-shaped settlement of the loaded area, similar to the settlement illustrated by Figures 122c and 122d. In order to produce at least a fairly uniform settlement the unit load on a circular area must be very much greater at the rim than at the center. In Figure 124a the surcharge increases from zero at the center in direct proportion to the square of the distance from the center. Nevertheless the center settles almost as much as the rim, as indicated by a dotted line below the base of the load (Boussinesq 1885). Hence if a perfectly uniform settlement is enforced by the absolute rigidity of a footing, the contact pressure must increase from the center of the base of the footing toward the rim, provided the supporting material is perfectly elastic. For an elastic footing the distribution of the contact pressure depends on the elastic properties of the supporting medium, on the flexural rigidity of the footing, and on the distribution of the loads on the footing.

The computation of the contact pressure on the base of both rigid and elastic footings represents a problem in advanced theory of elasticity. The following paragraphs contain a summary of the most important results. The simplest problem is the computation of the contact pressure on the base of a rigid circular footing (Fig. 124*b*) with a radius R which carries a centric load

$$Q = \pi R^2 q$$

The value q is equal to the total load Q divided by the area πR^2 of the base of the footing. If the surface of contact between the footing and the

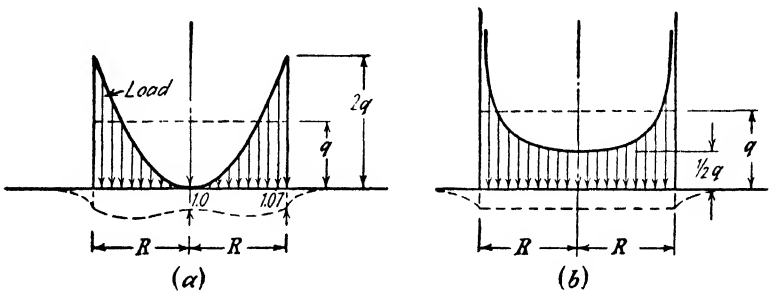

FIG. 124. (*a*) Flexible load on circular area required to produce almost uniform settlement; (*b*) contact pressure on base of rigid, circular footing. (*After Boussinesq 1885.*)

supporting elastic medium remains plane (rigid footing) and the shearing stresses at the surface of contact are equal to zero (perfectly frictionless base), the contact pressure increases from $q/2$ at the center to infinity at the rim, as shown in the figure (Boussinesq 1885). The character of the pressure distribution can be visualized in the following manner. If we spread the entire load on the footing uniformly over the surface of a hemisphere whose equator is identical with the rim of the base of the footing, the contact pressure is identical with the vertical projection of the hemispherical load onto the base of the footing. Since the area of the surface of the hemisphere is equal to twice the area of the base of the footing, the load per unit of area of the hemisphere is equal to $\frac{1}{2}q$. Hence the unit pressure at the center of the footing is also equal to $\frac{1}{2}q$. The calculated settlement of the footing is about 7.3 per cent smaller than the calculated average settlement produced by a uniformly distributed flexible surcharge of equal intensity q acting on the area covered by the base of the footing (Schleicher 1926).

Figure 125*a* represents the distribution of the pressure on the base of an elastic, circular footing with a radius R and a thickness H acted upon by a load q per unit of area (Borowicka 1936). The stiffer the footing the less uniform is the distribution

of the contact pressure over the base of the footing. The final equations contain a factor

$$K_r = \frac{1}{6}\frac{1-\mu_S^2}{1-\mu_P^2}\frac{E_P}{E_S}\left(\frac{H}{R}\right)^3 \qquad [1]$$

wherein μ_P and μ_S represent Poisson's ratio for the footing and the subgrade respectively and E_P and E_S the corresponding values of Young's modulus. This factor can be considered a measure for the relative stiffness of the footings. A value $K_r = 0$ indicates perfect flexibility. For values of K_r ranging between 0 and about 0.1 the contact pressure is smallest at some distance intermediate between the center and

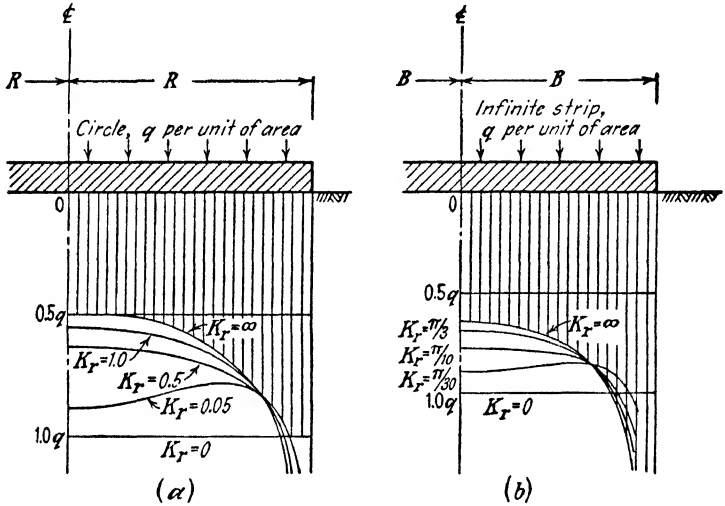

FIG. 125. (*a*) Contact pressure on base of uniformly loaded, circular plate with different degrees of flexural rigidity; (*b*) as before, for load applied on a strip. (*After Borowicka 1936 and 1938.*)

the edge of the footing, as indicated in the figure for $K_r = 0.05$. With increasing stiffness the pressure distribution approaches that shown in Figure 124*b* for a rigid footing. Habel (1937) computed the contact pressure for circular, elastic footings supporting a load which acts on the central part of the upper surface of the footing. Figure 125*b* illustrates the influence of the flexural rigidity of a uniformly loaded elastic slab, with a constant width $2B$, a thickness H, and an infinite length, on the distribution of the soil reactions over its base (Borowicka 1938). The value K_r is given by equation 1. The value $K_r = 0$ indicates perfect flexibility of the slab and $K_r = \infty$ means a perfectly rigid slab.

Biot (1937) worked out a rigorous solution of the problem of computing the contact pressure on the base of an elastic beam of infinite length, resting on the horizontal surface of a semi-infinite solid. This solution made it possible to compute the value of the coefficient of subgrade reaction which must be introduced into the elementary theory of beams on an elastic subgrade (Art. 126) in order to establish a reasonable agreement with the results obtained by means of the rigorous theory. The investigation led to the conclusion that the ratio between the average unit load and the corresponding average settlement is a complicated function not only of the

modulus of elasticity of the subgrade and of the width of the beam but also of the flexural rigidity of the beam. Hence no definite value can be assigned to the coefficient of subgrade reaction for a given subgrade.

Finally Habel (1938) derived approximate equations for the contact pressure on the base of elastic beams which transmit an arbitrary system of loads onto the surface of a semi-infinite solid.

In all the investigations cited in this article it has been assumed that the shearing stresses at the base of the footing are equal to zero. In reality this condition is never satisfied. An attempt to investigate the influence of the shearing stresses on the state of stress in the loaded material was made by Fröhlich (1934*a*) on the basis of equations derived by Boussinesq (1885). Fröhlich concluded that friction forces directed radially inward may be expected to produce an increase of the normal stresses on horizontal sections beneath the loaded area. With increasing depth this influence decreases. At depths in excess of about twice the width of the loaded area it is negligible. An investigation of the distribution of the shearing stresses over the base of foundations was made by Vogt (1925). The effect of the shearing stresses at the base of footings on the distribution of the contact pressure has not yet been analyzed.

140. Change in the distribution of the contact pressure due to an increase of the load. The increase of the load on a footing causes progressive transition of the loaded material from the state of elastic to that of plastic equilibrium. This transition influences not only the intensity and the distribution of the stresses in the loaded material, as described in Article 138, but it also changes the distribution of the contact pressure on the base of the footing. The theories of contact pressures described in the preceding article led to the conclusion that the contact pressure at the edge of a rigid footing is equal to infinity for every finite value of the load. Since there is no material which can sustain such a state of stress the plastic flow begins as soon as load is applied. As the load increases, the zone of plastic flow spreads, as indicated in Figures 123*c* and 123*d*, and the difference between the real and the calculated distribution of the contact pressure becomes more and more conspicuous. As soon as the two zones of plastic flow shown in Figures 123*c* and 123*d* merge into one, the distribution of the contact pressure approaches the distribution which prevails after the load has become equal to the bearing capacity of the loaded material. This distribution has been discussed in Article 48.

The effect of the transition of the loaded material from the elastic to the plastic state on the distribution of the pressure on the base of a rigid footing is illustrated by Figures 126*a*, 126*b*, and 126*c*. These

figures show the contact pressure on the base of perfectly rigid slabs with a width $2B$ and an infinite length resting on the surface of homogeneous soil deposits with great depth. In each figure, the load on the footing is assumed to increase from a small value to a value equal to the bearing capacity of the footing. It is further assumed that the base of the footings is perfectly smooth. The ordinates of the curves C_1 represent the contact pressure produced by loads which are too small to establish a state of plastic equilibrium beyond the immediate vicinity

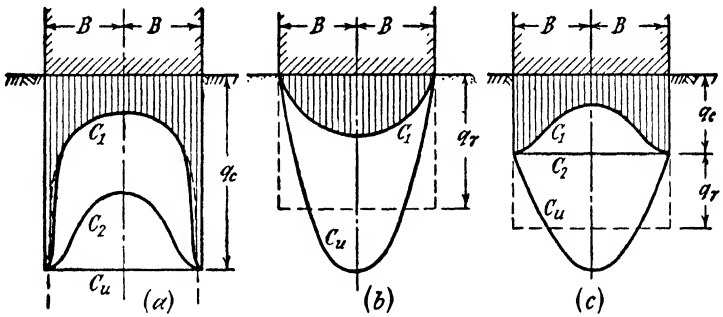

FIG. 126. Influence of cohesion c and angle of internal friction ϕ of semi-infinite solid and of intensity of unit load on distribution of contact pressure on base of rigid, continuous footing with frictionless base. (*a*) $\phi = 0$; (*b*) $c = 0$; (*c*) c and ϕ greater than 0.

of the rims of the footings. Those of the curves C_u represent the contact pressure for the instant when the load on the footing becomes equal to the ultimate bearing capacity of the footing. The curves C_2 represent the contact pressure for an intermediate state of loading. In each figure and for each stage, the total load per unit of length of the strip is equal to the area between the base of the footing and the corresponding curve. In Figure 126*a* the footing rests on an ideal material without internal friction which passes with increasing load from an ideal elastic into an ideal plastic state. In Figure 126*b* the footing is assumed to rest on ideal sand and in Figure 132*c* on a sand-clay mixture. The contact pressures represented by the curves C_u have been discussed and computed in Article 48.

The dashed line in Figure 126*a* shows the distribution of the contact pressure on the assumption that Hooke's law is valid throughout the loaded material. It is identical with the curve labeled $K_r = \infty$ in Figure 125*b*. At the edges of the strip the theoretical value of the contact pressure is equal to infinity. As a consequence the plastic flow starts along the edges as soon as load is applied, as explained at the beginning of this article. On account of the plastic flow the contact

pressure along the edges assumes the highest value compatible with the stress conditions for plastic flow and retains this value during the subsequent process of loading. The distribution of the contact pressure under a small load is shown by the plain curve C_1. As the load increases the pressure beneath the central part of the slab increases (curve C_2), and finally the distribution of the pressure becomes uniform, as indicated by the horizontal line C_u whose ordinate q_c represents the bearing capacity. The value q_c is equal to $5.14c$ (eq. 46(9*f*)) wherein c is the cohesion of the material. If the base of the footing is rough, the ultimate unit pressure at the edge is somewhat greater than the ultimate unit pressure at the center, as shown in Figure 39*a*, and the average value of the corresponding contact pressure is equal to $5.7c$ (eq. 46(7*c*)).

Figure 126*b* represents the contact pressure beneath a slab resting on the surface of a deposit of cohesionless sand. At the surface, at the rim of the base of the slab, even a very small stress exceeds the stress conditions for failure. Hence at the rim the contact pressure can never become greater than zero (see Art. 16). As the load increases the contact pressure on the central part of the base increases, and at the instant of failure the distribution of the contact pressure is roughly parabolic as indicated by the curve C_u. In that stage the average contact pressure q_γ is equal to the bearing capacity factor N_γ (eq. 45(4*b*)) times the unit weight γ of the sand times one half of the width of the footing.

If the bearing capacity of the soil is due to internal friction as well as to cohesion, the successive stages are as indicated by the curves C_1, C_2, and C_u (Fig. 126*c*), which corresponds to Figure 39*c*. A similar distribution of the contact pressure should be expected if the base of a rigid footing is located at a considerable depth below the surface of a layer of dense sand.

According to the methods of computation based on the assumption that the coefficient of subgrade reaction is constant (Chapter XVI), the contact pressure on the base of a rigid footing should always be perfectly uniform provided the resultant of the load passes through the center of gravity of the base. Figure 126 illustrates the type and importance of the errors which are likely to be associated with this radically simplifying assumption.

141. Stresses due to a vertical load on the horizontal surface of orthotropic and of nonhomogeneous semi-infinite solids. The theories discussed above are based on the assumption that the semi-infinite solid is both isotropic and homogeneous with respect to its elastic properties. In nature this condition seldom exists. The most common deviations from the ideal state of elastic isotropy and homogeneity are stratification

or lamination, characteristic of practically all sedimentary deposits and a rapid decrease of compressibility with depth, which is typical of sandy soils.

In stratified soils, consisting of a succession of highly compressible and feebly compressible layers, the strain produced by an effective all-around pressure, $\sigma_I = \sigma_{II} = \sigma_{III}$, is very much smaller in directions parallel to the bedding planes than at right angles to these planes. This is an analogue to the fact that the average coefficient of permeability of every stratified mass of soil is greater parallel to the planes of stratification than at right angles to these planes (see Art. 89). In the theory of elasticity the ideal substitute for a thin-bedded mass of soil is a semi-infinite, homogeneous but orthotropic elastic solid whose modulus of elasticity has the same value E_h in every horizontal direction and a smaller value E_v in a vertical direction. Wolf (1935) assumed that the ratio E_h/E_v is equal to an empirical constant n, or

$$\frac{E_h}{E_v} = n \qquad [1]$$

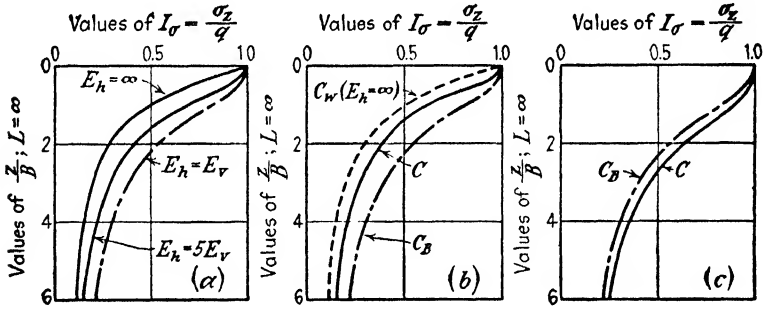

FIG. 127. Relation between depth and vertical unit pressure beneath center line of flexible strip load (*a*) if modulus of elasticity in horizontal direction is greater than in vertical direction; (*b*) if solid is reinforced in horizontal direction by unstretchable, flexible layers, and (*c*) if modulus of elasticity increases with depth. Dash-dotted curves correspond to isotropic and homogeneous, semi-infinite solid.

On this assumption he computed the stresses produced by a point load and by a flexible strip load of infinite length having a width $2B$. (See also Holl 1941.) In Figure 127*a* the abscissas represent the influence values $I_\sigma = \sigma_z/q$ for the influence of the load, q, per unit of area of the strip, on the vertical normal stress σ_z at depth z beneath the center line of the strip, for different values of the ratio E_h/E_v. The ordinates represent the ratio z/B between the depth and one half of the width of the strip. The diagram shows that the stress decreases for high values

of the ratio $n = E_h/E_v$ much more rapidly with depth than it does for low values. For $E_h = E_v$ the curve is identical with the curve obtained by means of Boussinesq's equations.

Another possible method of investigating the influence of lamination on the distribution of the stresses due to a surcharge consists in assuming that the semi-infinite solid is reinforced by horizontal, perfectly flexible membranes, which prevent completely any deformation in a horizontal direction without interfering with deformations in a vertical sense. This assumption has been made by Westergaard (1938). For the vertical normal stress at a point N, produced by a vertical point load Q applied at point a (Fig. 118a) he obtained the equation

$$\sigma_z = \frac{Q}{z^2}\frac{C}{2\pi}\left[\frac{1}{C^2 + (r/z)^2}\right]^{\frac{3}{2}} \qquad [2]$$

In this equation r is the horizontal distance of the point N from the line of action of the load Q, z is the vertical distance between the point and the surface, C is a constant whose value is given by the equation

$$C = \sqrt{\frac{1 - 2\mu}{2(1 - \mu)}} \qquad [3]$$

and μ is Poisson's ratio for the material located between the membranes. If $\mu = 0$, C becomes equal to $C_0 = 1/\sqrt{2}$.

The Boussinesq value for the stress σ_z is

$$\sigma_z = \frac{Q}{z^2}\cdot\frac{3}{2\pi}\left[\frac{1}{1 + (r/z)^2}\right]^{\frac{5}{2}} \qquad 136(5)$$

Curve C in Figure 127b represents the influence values $I_\sigma = \sigma_z/q$ for the vertical normal stresses σ_z beneath the center line of a uniform strip load with a width $2B$, plotted against the depth ratio z/B. It is located between the curve C_B, which represents the influence values according to Boussinesq, and the curve C_W, which represents Wolf's solution for $n = \infty$ or $E_h = \infty$. Fadum (1941) has computed the influence values for the Westergaard solution on the assumption that $\mu = 0$ or $C = C_0 = 1/\sqrt{2}$. (See eq. 3.) His tables include the influence values for point load, line load, and uniformly distributed loads on circular and rectangular areas.

A second deviation of the elastic properties of soils from those of Boussinesq's ideal elastic solid consists of a decrease of the compressibility of the soil with increasing depth below the surface of the soil stratum. It is due to the fact that the law of superposition does not

hold for soils. This deviation is typically developed in cohesionless sand. It can easily be demonstrated by laboratory experiments.

If we apply a load on a sample of a perfectly elastic material, acted upon by an initial all-round pressure, we find that the vertical strain produced by the load is independent of the initial pressure. On the other hand, if we repeat the same test on a sand sample we find that the strain due to the load decreases with increasing intensity of the all-round pressure. In a sand stratum the sand is under the influence of an all-round pressure due to the weight of the sand. The intensity of this pressure increases with the depth below the surface. Hence, the strain produced by a given change of the stress in the sand decreases with increasing depth below the surface. In order to take this property of sands into account without losing the simplicity resulting from assuming the validity of the law of superposition, we proceed in the following manner. We assume that the sand strictly obeys Hooke's law but we also assume that the modulus of elasticity of the sand increases with depth according to a definite law. In other words we assume that the sand is perfectly elastic and isotropic in every horizontal direction but elastically nonhomogeneous in a vertical direction.

In order to estimate the stresses in such materials Griffith (1929) and Fröhlich (1934*a*) proposed a semi-empirical modification of Boussinesq's theory of incompressible elastic solids (Poisson's ratio $\mu = 0.5$). If $\mu = 0.5$ the stresses produced by a vertical point load Q at any point N (Fig. 118*a*) of a semi-infinite, homogeneous solid represent the components of a linear, principal stress σ_I, whose intensity is determined by Boussinesq's equation 135(3)

$$\sigma_I = \frac{3\,Q}{2\pi z^2}\cos^3\psi$$

By replacing the exponent of the factor $\cos^3\psi$ in this equation by an arbitrary exponent ν one also changes the distribution of the stresses in the solid. At the same time one must satisfy the condition that the total pressure on every horizontal section through the solid must be equal to the point load Q. The equation which satisfies this condition is

$$\sigma_I = \frac{\nu\,Q}{2\pi z^2}\cos^\nu\psi \qquad [4]$$

The value ν will be called the *concentration index* because it determines the intensity of the pressure on horizontal sections beneath a given point load Q. It must be selected in such a way as to comply with the type of deviation of the deposit from the homogeneous state. The normal stresses at point N (Fig. 118*a*) in a vertical, radial, and circum-

ferential direction (σ_z, σ_r, and σ_θ) and the shearing stresses are determined by the equations

$$\sigma_z = \frac{\nu\, Q}{2\pi z^2} \cos^{\nu+2} \psi \qquad [5a]$$

$$\sigma_r = \frac{\nu\, Q}{2\pi z^2} \cos^{\nu} \psi \sin^2 \psi \qquad [5b]$$

$$\sigma_\theta = 0 \qquad [5c]$$

$$\tau_{rz} = \frac{\nu\, Q}{2\pi z^2} \cos^{\nu+1} \psi \sin \psi \qquad [5d]$$

On the basis of certain simplifying assumptions regarding the elastic properties of sands, Fröhlich arrived at the conclusion that the concentration index for sands should be approximately equal to $\nu = 4$. The corresponding values $I_\sigma = \sigma_z/q$ for the influence of a strip load on the vertical normal stresses σ_z beneath the center line of the strip are represented by the curve C in Figure 127c. The position of this curve with reference to the Boussinesq curve C_B indicates that the elastic properties of the sand tend to increase the concentration of the normal stresses beneath the center line of the loaded strip.

In a general way this theoretical conclusion is in accordance with the results of the measurement of the normal stresses at the base of layers of sand which are acted upon by local surcharges. However, the major part of the observed deviation of the measured stresses from the stresses computed by means of equation 135(1a) is due to the rigidity of the base which supported both the layer of sand and the pressure cells in the experiments. This rigidity alone produces a very appreciable deviation of the pressure distribution from that computed by means of equation 135(1a). (See Art. 149.) This fact was ignored by many investigators. Hence several of the proposed methods of eliminating the discrepancies between theory and observation are based on an inadequate interpretation of the test results (Strohschneider 1912, Kögler and Scheidig, 1927) and their use should be discontinued.

142. Influence of size of loaded area on settlement. If the load is applied on the surface of a semi-infinite, elastic and isotropic mass, the settlement of any point of the surface can be computed by means of equation 135(5a) or, if the loaded area is rectangular or square, by means of equation 137(3) and the data contained in Figure 122a. The following examples illustrate the results of such computations.

The settlement of the center of a uniform surcharge on a square area, $2B$ by $2B$, on the surface of a semi-infinite solid is

$$\rho_0 = 2.24\, qB \frac{1 - \mu^2}{E}$$

wherein E is Young's modulus and μ is Poisson's ratio. The settlement of the corners is

$$\rho_c = \tfrac{1}{2}\rho_0$$

and the average settlement

$$\rho_a = 0.848\,\rho_0 = 1.90\,\frac{q}{E}\,(1 - \mu^2)B = B \times \text{const.} \qquad [1]$$

The settlement of the center of a circular area with a radius R is

$$\rho_0 = 2\,qR\,\frac{1 - \mu^2}{E} \qquad [2]$$

The edge settles through a distance

$$\rho_r = \frac{2}{\pi}\,\rho_0 \qquad [3]$$

and the average settlement is

$$\rho_a = 0.85\,\rho_0 = 1.7\,\frac{q}{E}\,(1 - \mu^2)R = R \times \text{const.} \qquad [4]$$

(Schleicher 1926). Equations 1 and 4 show that the average settlement produced by a given load q per unit of square and of circular areas on the surface of semi-infinite solids increases in direct proportion to the width of these areas.

These and similar computations lead to the following conclusion. For a given load q and a given ratio l between the length and the width of the loaded area, both the settlement at the center of the area and the average settlement increase in simple proportion to the width of the loaded area. The settlement of a circular area increases in direct proportion to the radius. However, the validity of this conclusion is limited by the conditions that the loaded material is elastically isotropic and homogeneous and that it obeys Hooke's law. The following deviations from these conditions will be considered: (*a*) The compressibility of the material decreases with increasing depth below the surface; (*b*) the loaded material does not obey Hooke's law, and (*c*) the strain increases with time at constant state of stress.

In practice we are never able to obtain more than an approximate knowledge of the elastic properties of a natural soil deposit. For this reason a rigorous analysis of the influence of aforementioned deviations of the elastic properties of soils from those assumed by Boussinesq on the settlement is only of theoretical interest. The information which is needed for practical purposes can be obtained on the basis of radically simplifying assumptions.

In order to get a general conception of the influence of a decrease of the compressibility of a soil with increasing depth below the surface we assume that the ratio M between the normal stress on a horizontal section at a depth z below the loaded area and the corresponding vertical strain at that depth is a function solely of z. We replace the real distribution of the normal stresses on the horizontal section by a similar one which can be expressed by a simpler equation. Finally we confine

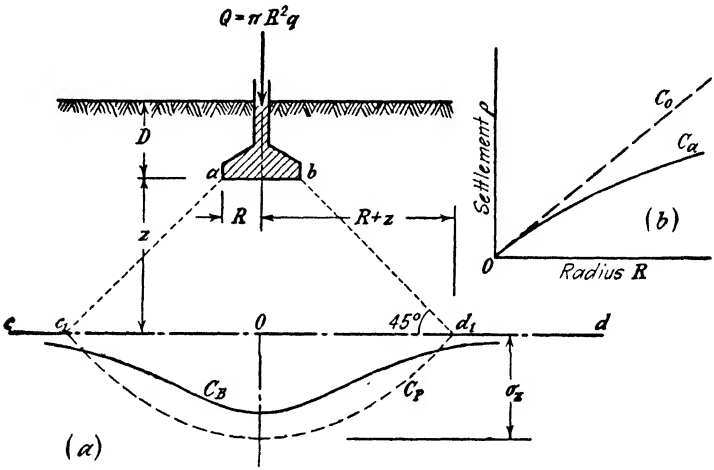

FIG. 128. (*a*) Distribution of vertical pressure on horizontal section beneath loaded circular footing resting on a soil whose compressibility decreases with depth; (*b*) relation between radius of footing and settlement (unbroken curve) computed on the assumption that the depth of soil stratum is infinite.

our investigation to the settlement of a circular footing with a radius R and assume that the distribution of the contact pressure on the base of the footing is represented by a paraboloid.

Figure 128*a* is a section through the footing. The curve C_B shows the distribution of the normal stresses on the horizontal section *cd* according to Boussinesq. In order to simplify the computation we replace this pressure distribution by another one in which the normal unit pressure on the section is given by the ordinates of a paraboloid. In Figure 128*a* this paraboloid is represented by the parabola C_P. The points of intersection c_1 and d_1 between the parabola and the line *cd* are assumed to be located on straight lines ac_1 and bd_1, respectively, which pass through the outer edges of the footing at angles of 45° to the horizontal. If σ_z is the vertical unit pressure on *cd* beneath the center of the footing, the total pressure represented by the paraboloid is $\frac{1}{2}\pi(R+z)^2\sigma_z$. Since this pressure must be equal to the load $Q = \pi R^2 q$

on the footing we can write

$$\pi R^2 q = \frac{\pi}{2}(R + z)^2 \sigma_z$$

or

$$\sigma_z = 2q \frac{R^2}{(R + z)^2}$$

This value is somewhat greater than the value computed by means of Boussinesq's equations. The vertical strain at depth z beneath the center of the footing is

$$\frac{\sigma_z}{M} = \frac{2q}{M} \frac{R^2}{(R + z)^2}$$

wherein M is the ratio between the vertical unit pressure and the corresponding vertical strain. The simplest assumption one can make regarding the relation between M and the depth z is a straight line relation

$$M = M_0 + az \qquad [5]$$

In this equation M_0 (gm cm^{-2}) and a (gm cm^{-3}) are empirical constants whose values express in a general way the degree of elastic homogeneity. For an elastically homogeneous material a is equal to zero and $M = M_0$. On the other hand, for a material whose compressibility decreases with increasing depth both M_0 and a are greater than zero.

On the basis of equation 5 we obtain for the settlement of the footing

$$\rho = \int_0^\infty \frac{2q}{M_0 + az} \frac{R^2}{(R + z)^2} dz = 2qR \frac{M_0 - Ra\left(1 + \log \frac{M_0}{Ra}\right)}{(M_0 - Ra)^2} \qquad [6]$$

If the loaded material is perfectly elastic, a is equal to zero and

$$\rho = 2qR \frac{1}{M_0}$$

The exact value of ρ for $a = 0$ (perfectly homogeneous material) is given by the equation

$$\rho = 2qR \frac{1 - \mu^2}{E} \qquad 142(2)$$

For $M_0 = E/(1 - \mu^2)$ these two equations become identical. The relation between the radius R of the footing and the settlement ρ for $a = 0$ is shown by the straight line OC_0 (Fig. 128*b*). When dealing with soils we must always assume that a is greater than zero, whereupon we

obtain for the relation between R and ρ a curve similar to OC_a. The greater the value a at a given value of M_0 the more rapidly does the slope of the curve decrease with increasing values of R.

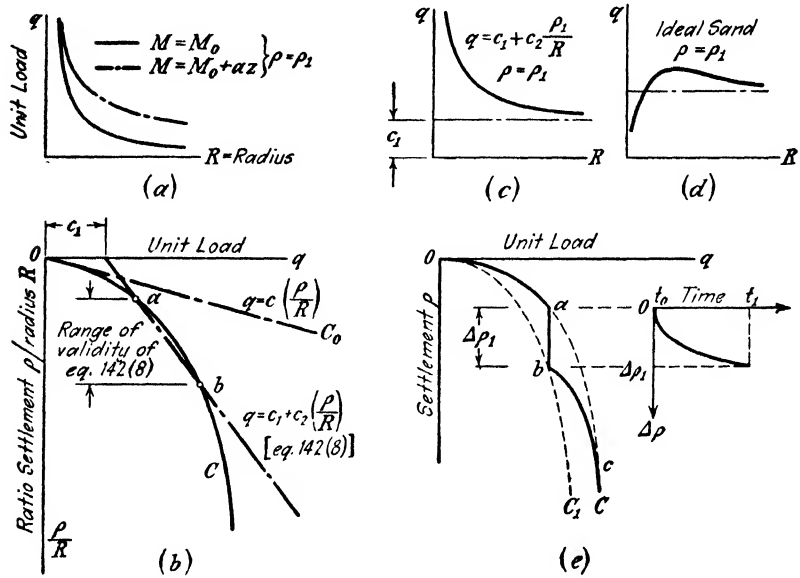

FIG. 129. Unit load on circular area required to produce a given settlement ρ_1, if load rests (*a*) on ideal, perfectly elastic base, (*c*) on clay and (*d*) on sand; (*b*) empirical relation between settlement and unit load, if load is applied at a constant rate; (*c*) same as (*b*), with one intermission in process of loading.

Equation 6 also determines the relation between the radius of the loaded area and the unit load q required to produce a given settlement ρ_1. Substituting $\rho = \rho_1$ in equation 6 and solving for q we obtain

$$q = \rho_1 \cdot \frac{1}{2R} \cdot \frac{(M_0 - Ra)^2}{M_0 - Ra\left(1 + \log \frac{M_0}{Ra}\right)} \qquad [7]$$

If $a = 0$, equation 7 becomes

$$qR = \tfrac{1}{2}\rho_1 M_0 = \text{constant}$$

which is the equation of a hyperbola, represented by the plain curve in Figure 129*a*. If $a > 0$, the curve which represents the relation between R and q for a given value of M_0 approaches the horizontal asymptote less rapidly than the curve for $a = 0$ as shown by the dash-dotted curve.

In the preceding computations it has been assumed that the ratio between the vertical unit pressure and the corresponding vertical strain

is independent of the unit pressure. Therefore the calculated settlement ρ (eq. 6) increases at a given value of R in direct proportion to the unit load q, as shown by the straight line OC_0 in Figure 129*b*. However, if we investigate this relation by means of a loading test on a real soil, we always find that the ratio between the settlement and the unit load increases with increasing load, as indicated in Figure 129*b* by the settlement curve OC. Only the uppermost part of this curve is approximately straight. This observation indicates that equations 6 and 7 are valid only for very low loads. The increase of the rate of settlement under higher loads is due to the fact that soils do not obey Hooke's law. In order to make a rough estimate of the influence of this fact on the relation between the radius of a loaded circular area and the settlement at a given unit load, we replace the middle part of the curve OC in Figure 129*b* by a straight line with the equation

$$q = c_1 + c_2\left(\frac{\rho}{R}\right) \qquad [8]$$

valid for the range indicated in the figure. If we further assume that the load rests on a thick stratum of soft clay which is fairly homogeneous with respect to its elastic properties, the values of c_1 and c_2 are independent of the radius R. On these assumptions we obtain for the load q required to produce a given average settlement ρ_1 the equation

$$q = c_1 + c_2\left(\frac{\rho_1}{R}\right) \qquad [9]$$

This equation is represented by a hyperbolic curve (Fig. 129*c*) which has a horizontal asymptote with the equation $q = c_1$. It can also be written in the form

$$q = c_1 + \frac{c_2\rho_1}{2}\frac{2R\pi}{R^2\pi} = c_1 + m_s\frac{P_r}{A} \qquad [10]$$

wherein P_r is the length of the perimeter of the loaded area A and c_1 (gm cm^{-2}) and m_s (gm cm^{-1}) are empirical constants which can be determined by loading tests on circular areas with different radii. Housel (1929) has shown experimentally that equation 10 is also valid, within the range of conditions covered by the tests, for square and rectangular loaded areas underlain by clay. The total load required to produce the settlement ρ_1 is

$$Q = Aq = Ac_1 + m_sP_r \qquad [11]$$

The value m_s (gm cm^{-1}) is called the *perimeter shear*. The conditions for the validity of the equation have been stated above.

The term *perimeter shear* could convey the erroneous impression that the symbol m_s represents a shearing resistance per unit of length of the perimeter. Therefore it should be emphasized that there is no material to which one could assign a shearing resistance per unit of length. In order to visualize the physical significance of m_s we apply equation 11 to a perfectly elastic, isotropic and homogeneous material and compare the result with the rigorous equation for the load which is required to produce a given settlement. For such a material, c_1 in Figure 129*b* and in equation 11 is equal to zero, whence

$$Q = m_s P_r$$

For a square area $2B$ by $2B$ which carries a unit load q, the total load is $Q = 4B^2q$ and the perimeter is $P_r = 8B$. Introducing these values into the preceding equation and solving for q we get

$$q = m_s \frac{8B}{4B^2} = 2m_s \frac{1}{B} \qquad [12]$$

The value q represents the unit load required to produce a settlement ρ_1. The relation between unit load and the average settlement of the loaded area is determined by the equation 142(1)

$$\rho = 1.9q \frac{1 - \mu^2}{E} B$$

The unit load q required to produce a settlement ρ_1 is

$$q = \rho_1 \frac{E}{1.9(1 - \mu^2)} \frac{1}{B}$$

Combining this equation with equation 12 we get for perfectly elastic solids

$$m_s = \frac{\rho_1 E}{3.8(1 - \mu^2)} \qquad [13]$$

This equation demonstrates that the perimeter shear m_s represents by no means a specific shearing resistance which has its seat at the perimeter of the loaded area. The value m_s has no physical significance other than that of an empirical coefficient with the dimension gm cm^{-1}. The presence of the quantity c_1 on the right-hand side of equation 10 is due to the imperfect elasticity of the loaded material, as shown in Figure 129*b*. It disappears if the loaded material is perfectly elastic, whereupon $Q = m_s P_r$. It should also be mentioned that the application of a load on a limited area of the horizontal surface of a semi-infinite elastic solid causes every point of the surface to move down. An increase of the load increases the settlement of the surface which surrounds the loaded area. On the other hand, if we apply the load on the surface of a semi-infinite, imperfectly elastic solid such as clay, the material rises beyond the boundaries of the loaded area as soon as the load approaches the value given by the abscissa of point *b* (Fig. 129*b*). This is the edge action referred to in Article 46 and illustrated by Figures 37*a* and 37*b*.

For a perfectly cohesionless sand, the settlement due to a load on an area of a given size also increases much more rapidly than the load, as indicated by the curve *C* in Figure 129*b*. At the same time the values c_1 and c_2 in equation 9 are not even approximately independent of the

radius R. This extreme case has been theoretically investigated by Aichhorn (1931). The results of the investigation are shown in Figure 129*d*. For a certain radius R_1 the load per unit of area required to produce a given settlement ρ_1 is a maximum. This conclusion has been confirmed repeatedly by experiment.

The influence of time on the settlement is illustrated by Figure 129*e*. This figure shows the relation between unit load and settlement obtained by means of a loading test on a mass of soil. If the unit load has been increased at a constant rate, the line which connects the points representing the results of the observations is a smooth curve *OacC*. On the other hand, if the load has been kept constant for several hours or days, from time t_0 to t_1, the intermission appears in the diagram as a vertical line *ab*, regardless of the nature of the loaded soil. The relation between time and settlement at constant load is shown to the right of the line *ab*. If the process of loading is continued after time t_1 at the original rate of loading, the load-settlement curve gradually approaches the curve *OacC*, which represents the settlement associated with the uninterrupted loading process. The relative importance of the time effect shown by the vertical line *ab* and its physical causes are different for different soils. In a test on sand or a sandy soil, the time effect is chiefly due to a lag in the adjustment of the sand grains to a change in the state of stress. In connection with clays it is chiefly due to a temporary disturbance of the state of hydrostatic equilibrium of the water contained in the voids of the clay, as described in Chapter XIII. In either case the final result is the same as if the elastic constants of the loaded material were a function of the rate at which the load is applied.

Finally, in all the theories presented in the preceding articles it has been assumed that the compressible material which supports the load extends to an infinite depth. In nature every compressible soil stratum rests at a finite depth on a relatively incompressible base. The distance between the loaded area and this base represents one more variable factor. The influence of this factor on the settlement will be discussed in Article 150. It is illustrated by Figure 138.

The preceding review of our present knowledge of the relation between the settlement and the size of the loaded area demonstrated that this relation is rather complicated. On account of the great number of variable factors involved, it cannot be expressed by a simple rule of general validity. For the same reason the usefulness of small-scale loading tests is limited. The extrapolation from the results of such tests to the settlement of loads on large areas can be very misleading. In no case should such an extrapolation be attempted without careful consideration of all the factors which are likely to influence the difference

between the settlement of the small area and that of the large one. Foremost among these factors are the variations of the elastic properties of the soil with depth. In the past this factor has very often been disregarded.

143. Stresses in a semi-infinite solid due to loads transmitted by skin friction on piles. Figure 130*a* shows a cross section through a row of sheet piles, which is acted upon by a load q' per unit of length of its upper edge and Figure 130*b* is a vertical section through a loaded foundation pile. The piles are assumed to be embedded in a homogeneous mass of soil. Since the point resistance of the piles is very small practically the entire load is transferred onto the soil by shearing stresses acting at the surface of contact between the sides of the piles and the soil.

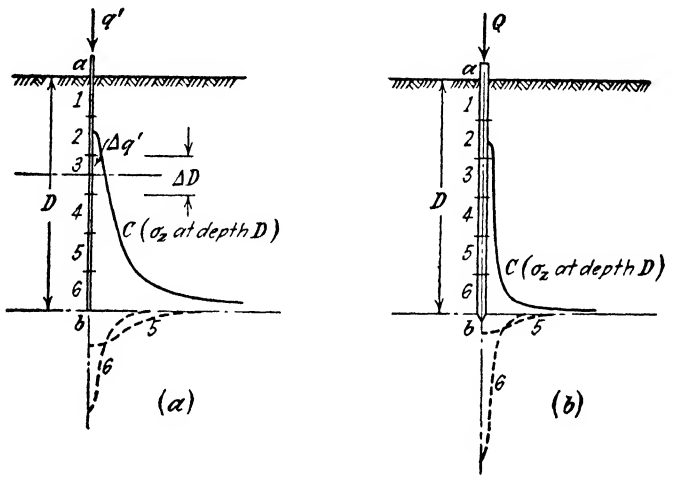

FIG. 130. Approximate distribution of vertical pressure on horizontal section (*a*) through lower edge of loaded row of sheet piles and (*b*) through point of a loaded pile.

The resistance to shear may be due either to adhesion or to friction or to both. In accordance with prevalent usage the shearing resistance along the surface of contact will be designated as skin friction regardless of its real physical causes. The following analysis applies to piles in clay.

In order to compute the state of stress produced by a loaded pile in the adjoining material one must know the distribution of the shearing stresses over the skin of the pile. The state of stress on the skin of loaded piles in clay can be expected to be at least fairly similar to that on the skin of piles which are embedded in and adhere to a perfectly elastic matrix.

From model tests with loaded rigid walls embedded in gelatine we

know that the shearing stresses are practically uniformly distributed over the sides of the wall from the surface downward to a depth a short distance above the lower rim of the wall. Immediately above the lower rim the shearing stresses increase and at the lower rim they exceed the strength of the bond between the sheet piles and the adjoining material. However, for practical purposes, this local departure from a uniform stress distribution can be disregarded. Therefore we are justified in assuming that the shearing stress τ along the surface of the embedded part of loaded sheet piles is equal to the total load q' per unit of length of the row of sheet piles divided by the total area of contact between the sheet piles and the soil per unit of length, or

$$\tau = \frac{q'}{2D}$$

An estimate of the intensity and the distribution of the normal stresses over a horizontal section through the lower edge b of the sheet piles at depth D can be made in the following manner. We divide the sheet piles into horizontal strips with a height ΔD. Each side of each strip transmits onto the soil a load $\Delta q'/2 = \tau \Delta D$ per unit of length of the strip. In order to estimate the normal stresses on a horizontal plane section at depth D, we first determine, by means of Boussinesq's theory, the normal stresses which would be produced by each of the load fractions $\Delta q'$ if the surface of the embedding material were located at mid-height of the corresponding strip and the load fraction represented a line load acting on this imaginary surface. For strip 3 the imaginary surface is indicated in Figure 130*a* by a dash-dotted line. The force $\Delta q'$ represents a vertical load, per unit of length of the line of intersection between the imaginary surface and the sheet piles. The normal stresses produced by this line load on the horizontal section through the lower edge of the sheet piles can be computed rapidly by means of equation 136(1*a*). The result is shown beneath the horizontal line through b, for the strips marked 5 and 6. The normal stress at any point of the horizontal plane through b is equal to the sum of the stresses produced at that point by the load fractions $\Delta q'$. It is represented by the ordinates of the curve C in Figure 130*a* for one side of the horizontal section.

A similar method can be used for estimating the normal stresses on a horizontal section through the point b of a single pile (Fig. 130*b*). The distribution of the shearing stresses over the sides of such a pile was also found by experiment to be practically uniform. In order to obtain an approximate solution of the problem we divide the pile into several sections. Then we replace the shearing force which acts on each of these

sections by a point load and compute the stresses produced by this load on the assumption that the horizontal surface of the semi-infinite mass passes through the midpoint of the section. This can be done by means of Table I in the Appendix (influence table for point load). The curves marked *5* and *6* represent the results of the computation for the sections *5* and *6*. The ordinates of the curve *C* are equal to the sum of the ordinates of the curves obtained for the individual sections. The error is on the safe side because the presence of material above the midpoint of each section relieves the stresses produced by the point load in the material below the midpoint. In order to reduce the theoretical error one can compute the stresses on the horizontal section through *b* by means of Mindlin's equations (see Art. 135). However, the error due to assuming perfectly elastic behavior of the material surrounding the pile is likely to be far greater than the error associated with the simplified method of computation.

It should be emphasized that either method of computation can be applied only to the computation of the stresses in the vicinity of single piles, because these methods are based on the assumption that the pile is surrounded by a homogeneous material. The material which surrounds a pile in the interior of a pile group consists of an elastic matrix reinforced by relatively rigid piles. As a matter of fact, the experimental investigation of the state of stress in a group of piles embedded in gelatine has shown that the distribution of the shearing stresses over the sides of a pile in the interior of the group has no resemblance to that for an individual pile (Terzaghi 1935).

Experimental data concerning the distribution of the shearing stresses on the sides of loaded sheet piles or piles in sand are not yet available. The results of theoretical investigations concerning this distribution cannot be trusted unless they are adequately confirmed by experiments.

144. Stress distribution in semi-infinite, elastic wedges. A semi-infinite wedge is a body whose boundaries consist of two intersecting planes, as shown in Figure 131*a*. The wedge is acted upon by the force of gravity in the direction of *OA* at an angle α to the line *OB*, which bisects the angle between the boundaries of the wedge. If one side of the wedge, for instance *OC* in Figure 131*a*, is very steep and is acted upon by an external pressure $q_0 r_0$ whose intensity increases in direct proportion to the distance r_0 from the apex *O* of the wedge, the wedge represents a simplified section through a concrete gravity dam whose steep side sustains the pressure exerted by the water in the reservoir. Therefore the problem of computing the stresses in such a wedge received early attention. The first rigorous solution of the problem was published by Lévy (1898). It is based on the assumption that the wedge is semi-infinite. On account of this assumption the solution does not apply to the immediate vicinity of the base of a dam, but it can be

expected to furnish relatively accurate values for the rest of the structure, provided the material is perfectly elastic. Lévy proved that the distribution of the normal stresses on a plane section due to the weight of the wedge alone or combined with a hydrostatic pressure on one side of the wedge can always be represented by a straight line, provided the wedge strictly obeys Hooke's law.

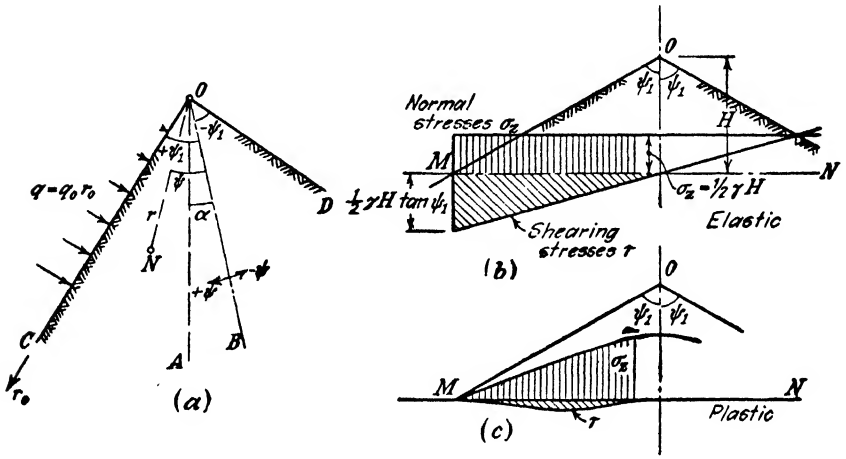

FIG. 131. (*a*) Vertical section through infinite wedge whose left-hand face is acted upon by a fluid pressure; (*b*) distribution of normal and shearing stresses on horizontal section through symmetrical wedge due to the weight of the wedge, if the material is perfectly elastic; (*c*) as before, if the wedge consists of ideal sand in state of plastic equilibrium.

Fillunger (1912) solved the same problem by a different method and arrived at the same conclusion. The following equations represent Fillunger's solution. Let

σ_r, σ_θ = the normal stresses (positive in compression) at point N in the direction of the vector r, and at right angles to it, respectively,

τ = the shearing stress on planes having normal stresses σ_r and σ_θ,

ψ = the angle between the vector r and the line which bisects the angle $2\psi_1$ between the sides of the wedge; ψ is positive for a clockwise deviation from the bisecting line OB and

γ = the unit weight of the wedge.

The stresses due to the weight of the wedge are

$$\sigma_r = r\gamma[(a + \cos\alpha)\cos\psi + (b + \sin\alpha)\sin\psi - c\cos 3\psi - d\sin 3\psi] \qquad [1a]$$

$$\sigma_\theta = r\gamma[(3a + \cos\alpha)\cos\psi + (3b + \sin\alpha)\sin\psi + c\cos 3\psi + d\sin 3\psi] \qquad [1b]$$

and

$$\tau = r\gamma(a\sin\psi - b\cos\psi + c\sin 3\psi - d\cos 3\psi) \qquad [1c]$$

wherein

$$a = -\frac{\cos\alpha\sin 3\psi_1}{2(\sin\psi_1 + \sin 3\psi_1)}, \qquad b = \frac{\sin\alpha\cos 3\psi_1}{2(\cos\psi_1 - \cos 3\psi_1)}$$

$$c = \frac{\cos\alpha}{8\cos^2\psi_1} \qquad \text{and} \qquad d = -\frac{\sin\alpha}{8\sin^2\psi_1}$$

The stresses due to the external pressure are

$$\sigma_r = rq_0\,(a\cos\psi + b\sin\psi - c\cos 3\psi - d\sin 3\psi) \qquad [2a]$$

$$\sigma_\theta = rq_0\,(3a\cos\psi + 3b\sin\psi + c\cos 3\psi + d\sin 3\psi) \qquad [2b]$$

and

$$\tau = rq_0\,(a\sin\psi - b\cos\psi + c\sin 3\psi - d\cos 3\psi) \qquad [2c]$$

wherein

$$a = \frac{\sin 3\psi_1}{16\sin\psi_1\cos^3\psi_1}, \qquad b = -\frac{\cos 3\psi_1}{16\cos\psi_1\sin^3\psi_1}$$

$$c = -\frac{1}{16\cos^3\psi_1} \qquad \text{and} \qquad d = \frac{1}{16\sin^3\psi_1}$$

Evaluation of the preceding equations shows that the distribution of both the normal and the shearing stresses on plane sections parallel to the crest of the wedge is governed by a straight line law. If $q_0 = 0$ and $\alpha = 0$ (symmetrical wedge) the normal stress at every point of a horizontal section at a depth z below the crest of the wedge is equal to $\gamma z/2$ and the shearing stresses increase in simple proportion to the distance from the center line of the section.

Figure 131*b* shows the distribution of the normal stresses σ_z and of the shearing stresses τ over a horizontal section *MN* through one half of a wedge which is symmetrical with reference to a vertical plane through its crest and is acted upon only by its weight. Figure 131*c* represents the distribution of the corresponding stresses over the horizontal base of a sand embankment in a state of plastic equilibrium, whose cross section is identical with that of the wedge *OMN* in Figure 131*b*. These stresses have been discussed in Article 65. There is no doubt that the stresses in every earth embankment are far more similar to those shown in

Figure 131c than to those computed by means of equations 1 and 2 regardless of the value of the factor of safety of the slopes with respect to sliding. As a matter of fact, it is inconceivable that the normal stress on the base of an earth embankment should be uniform. Hence the solution represented by equations 1 and 2 corresponds to a limiting case which is never even approached in practice, except on plane sections through masonry gravity dams.

As a supplement to equations 1 and 2 Fillunger's publication contains the equations for the stresses in a semi-infinite wedge acted upon by an external pressure which is uniformly distributed over one of its sides. A mathematical method of computing the stresses in a semi-infinite wedge with arbitrary boundary forces has been worked out by Brahtz (1933).

145. Stress distribution in the vicinity of shafts and tunnels in semi-infinite elastic solids with a horizontal surface. Figure 132*a* is a section through a cylindrical shaft in an elastic, semi-infinite solid with a unit weight γ. Let

z = vertical co-ordinate, measured downward from the horizontal surface,

r = horizontal, radial distance from the Z-axis which is identical with the centerline of the shaft,

r_0 = radius of the shaft,

σ_z, σ_r, σ_θ = vertical stress, horizontal radial stress and horizontal circumferential stress, respectively; all are normal stresses,

τ_{rz} = shearing stress in the direction of r and z.

Before the excavation of the shaft the stresses at any point at a depth z are

$$\sigma_z' = \gamma z, \qquad \sigma_r = \sigma_\theta' = K_0 \gamma z, \quad \text{and} \quad \tau_{rz}' = 0 \qquad [1]$$

wherein K_0 is the coefficient of earth pressure at rest (eq. 10(1)). Since the shearing stresses on cylindrical sections are equal to zero, one can replace the material located within the boundaries of the future shaft by a liquid with a unit weight $K_0\gamma$ without changing the state of stress in the surrounding material. The stresses which act at any point in the material surrounding the shaft can be resolved into two parts. One part is due to the weight of the material and the other is due to the pressure exerted by the heavy liquid. The sum of these two stress components is equal to the initial stresses given by equation 1, and the stresses produced by the liquid alone can easily be computed. After a shaft has been excavated, the shearing stresses along the walls of the

shaft are equal to zero and the radial normal stresses are also equal to zero. Therefore the effect of excavating the shaft on the stresses in the surrounding material is identical with the effect of pumping the heavy liquid out of a cylindrical hole whose dimensions are identical with those of the shaft. (Biot 1935c).

By adapting Lamé's formulas for the state of stress in thick-walled cylinders subject to internal pressure (Lamé 1852, see Timoshenko 1941) to the computation of the stresses produced by the heavy liquid at a depth z below the surface and at a distance r from the centerline of the shaft, one obtains

$$\sigma_z'' = 0 \qquad [2a]$$

$$\sigma_r'' = K_0 \gamma z \frac{r_0^2}{r^2} \qquad [2b]$$

$$\sigma_\theta'' = -K_0 \gamma z \frac{r_0^2}{r^2} \qquad [2c]$$

$$\tau_{rz}'' = 0 \qquad [2d]$$

After excavation of the shaft, the stresses at any point in the solid adjoining the shaft are equal to the difference between the initial stresses (eqs. 1) and those given in equations 2. Therefore they are equal to

$$\sigma_z = \sigma_z' - \sigma_z'' = \gamma z \qquad [3a]$$

$$\sigma_r = \sigma_r' - \sigma_r'' = K_0 \gamma z \left(1 - \frac{r_0^2}{r^2}\right) \qquad [3b]$$

$$\sigma_\theta = \sigma_\theta' - \sigma_\theta'' = K_0 \gamma z \left(1 + \frac{r_0^2}{r^2}\right) \qquad [3c]$$

and

$$\tau_{rz} = 0 \qquad [3d]$$

Westergaard (1940) has derived the same equations by means of the stress function. At the walls of the shaft ($r = r_0$) the radial stress is equal to zero and the circumferential stress is equal to twice the initial value of the horizontal stress. The vertical stress σ_z (eq. 3a) is equal to the stress σ_z which acted on a horizontal section at depth z prior to the excavation of the shaft. The distribution of the stresses represented by equations 3 over horizontal sections is shown in Figure 132a. If the soil surrounding the shaft is in a state of plastic equilibrium the distribution of the stresses on horizontal sections is similar to that shown in Figure 132b (see Articles 73 and 74).

In all soils, including the stiffest varieties, the stress distribution is

similar to that shown in Figure 132*b*, because in the vicinity of the walls of a shaft the high circumferential stresses σ_θ determined by equation 3c are likely to be greater than the compressive strength of the soil. As a consequence these stresses produce a plastic flow of the soil adjoining the walls of the shaft which continues until a state of plastic equilibrium or of failure is reached. Hence the stress distribution shown in Figure 132*a* corresponds to a limiting case which does not exist in reality except in the vicinity of shafts in hard and sound rock.

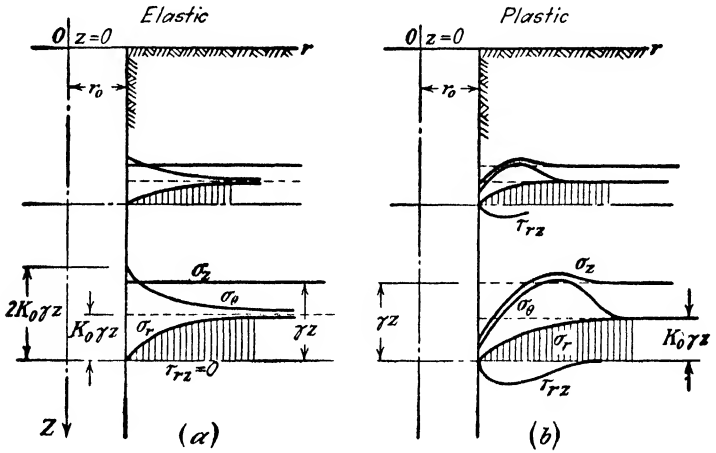

FIG. 132. State of stress along horizontal sections through material surrounding a cylindrical hole (*a*) if material is perfectly elastic and (*b*) if it consists of cohesive sand which is strong enough to stand up without lateral support.

The reasoning which led to equations 3 can also be used for the purpose of visualizing the effect of a tunnel on the state of stress in a semi-infinite elastic solid. To simplify the investigation we assume that the tunnel is cylindrical and that the value K_0 in equations 1 is equal to unity, in other words, that there is a hydrostatic state of stress in the solid prior to the excavation of the tunnel. Let

D = the vertical distance between the centerline of the tunnel and the horizontal surface,

r_0 = the radius of the tunnel,

γ = unit weight of the solid, and

σ_r, σ_θ = radial stress and circumferential stress at an arbitrary radial distance r from the centerline of the tunnel, both normal stresses.

In accordance with the assumption that $K_0 = 1$ the initial stress at

any point of the walls of the tunnel, at depth z below the surface, is determined by the simple equations

$$\sigma_r' = \sigma_\theta' = \gamma z \qquad [4]$$

By excavating the tunnel we reduce the radial stress at every point of the walls of the tunnel from its initial value γz to zero. Therefore the state of stress at every point of the solid after excavation is equal to the difference between the initial stress and the stresses produced at that point by a radial pressure γz on the walls of the tunnel. Such a pressure can be produced by filling the tunnel with a liquid with a unit weight γ in such a manner that the liquid would rise in a piezometric tube to the level of the horizontal surface of the solid. In order to visualize the state of stress produced by the liquid pressure we investigate this state independently of the stresses produced by the weight of the material surrounding the tunnel. This can be accomplished by assuming that the tunnel filled with the liquid is located in a weightless material.

If the depth D (Fig. 133a) is great compared with the diameter $2r_0$ of the tunnel, the liquid pressure is approximately equal to γD per unit of area at every point of the walls of the tunnel and the surface of the ground is located beyond the range of influence of the liquid pressure on the stress in the adjoining material. Therefore the stresses can be computed by means of Lamé's equations for the stresses in tubes with very thick walls, equations 2. By substituting the values $K_0 = 1$ and $s = D$ in these equations, we obtain

$$\sigma_r'' = \gamma D \frac{r_0^2}{r^2} \quad \text{and} \quad \sigma_\theta'' = -\gamma D \frac{r_0^2}{r^2} \qquad [5]$$

In the paragraphs dealing with shafts it was shown that the stresses in the material after excavation are equal to the difference between the initial stresses and the stresses produced by the heavy liquid. Since we assumed that K_0 equals 1 and that the radius r_0 of the tunnel is very small compared to the depth D, the initial stresses at the walls of the tunnel (stresses prior to excavation) are approximately equal to

$$\sigma_r' = \sigma_\theta' = D\gamma$$

The stresses produced by the heavy liquid are determined by equation 5. Therefore the stresses after the excavation of the tunnel are

$$\sigma_r = \sigma_r' - \sigma_r'' = D\gamma\left(1 - \frac{r_0^2}{r^2}\right) \qquad [6a]$$

and

$$\sigma_\theta = \sigma_\theta' - \sigma_\theta'' = D\gamma\left(1 + \frac{r_0^2}{r^2}\right) \qquad [6b]$$

The corresponding distribution of the stresses is shown in Figure 133*a*. On the left-hand side of the plane of symmetry of the tunnel the liquid pressure γD has been plotted from the walls of the tunnel in a radial direction toward the center of the tunnel. Since it was assumed that K_0 equals unity, the liquid pressure γD is equal to both the circumferential and the radial stress along the walls prior to the excavation of the tunnel. On the right-hand side the circumferential stresses $\sigma_{\theta 0}$ for $r = r_0$ are shown in a similar manner. The ordinates of the curves located above a horizontal line through the center of the tunnel section represent the radial and circumferential stresses σ_r and σ_θ respectively, which act along a horizontal section through the centerline of the tunnel.

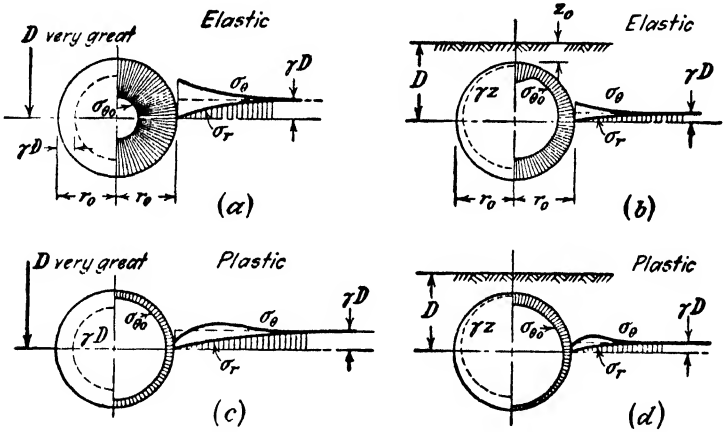

FIG. 133. State of stress along horizontal section through center line of horizontal cylindrical holes through perfectly elastic material (*a*) at great depth below surface and (*b*) at shallow depth. Left-hand side of each diagram represents state of stress before hole was made. If holes are located in cohesive sand strong enough to stand without support, state of stress is as shown in (*c*) and (*d*).

If the tunnel is located close to the surface, as shown in Figure 133*b*, the hydrostatic analogue retains its validity, but equations 2 cannot be used, because the distribution of the hydrostatic pressure exerted by the liquid on the walls of the tunnel is not even approximately uniform. The pressure increases rapidly from the roof toward the bottom. Furthermore the material surrounding the hole cannot be considered as representing a tube with a very thick wall, because above the roof the wall is very thin. On account of the weakness of the roof the horizontal components of the liquid pressure, which tend to force the sides of the tunnel apart, produce tensile stresses of great intensity at the roof. If the thickness of the roof were great compared with the diameter of the

tunnel the circumferential tensile stress at the roof would be approximately equal to the liquid pressure γz_0. A reduction of the thickness of the roof to its real value z_0 has little effect on the total tensile force on a vertical section through the roof. Yet it reduces the area which is acted upon by the tensile force. Hence if the roof is very thin the tension per unit of area of the section must be considerably greater than γz_0. With increasing distance of a wall point from the highest point of the roof the vertical distance of this point from the surface increases. Therefore with increasing distance from the roof point the value of the circumferential tensile stress approaches the value of the liquid pressure and at the bottom it may even be smaller than the liquid pressure, because the stretching of the roof is likely to relieve the tension at the bottom. These conditions determine the distribution of the tensile stresses due to the liquid pressure over the walls of the tunnel. The stresses after excavation of the tunnel are equal to the difference between the circumferential stresses prior to excavation and those produced by the liquid pressure. These stresses are represented by the radial width of the shaded area on the right-hand side of Figure 133*b*. The circumferential and radial stresses along a horizontal section through the centerline are equal to the ordinates of the plain curves σ_θ and σ_r respectively.

If the stresses in the vicinity of the tunnel exceed the yield point of the soil, the preceding analysis cannot be applied. The stresses corresponding to a state of plastic equilibrium are shown for a deep tunnel in Figure 133*c* and for a tunnel at a shallow depth in Figure 133*d*. The radial distance between the dotted line and the wall of the tunnel on the left-hand side of each profile represents the state of stress prior to the construction of the tunnel.

The problem of computing the stresses in the vicinity of a cylindrical tunnel corresponding to the elastic state of equilibrium has been solved rigorously by Mindlin (1939). He made the following assumptions regarding the value of the coefficient of earth pressure at rest K_0 contained in equations 1:

$$(a)\quad K_0 = 1$$

$$(b)\quad K_0 = \frac{\mu}{1-\mu} \qquad \text{(see eq. 134(3))}$$

and

$$(c)\quad K_0 = 0$$

The symbol μ represents Poisson's ratio. However, the final equations are so involved that they cannot be applied to practical problems until they have been condensed into tables or graphs similar to those which are used in connection with the equations of Boussinesq. Here again it should be emphasized that the results can be applied only to hard rock tunnels on the assumption that the rock has not been injured by the blasting operations. The principal field for the practical application

of the theory is the computation of the stresses in the concrete at the walls of conduits or inspection galleries in large concrete dams. In the vicinity of tunnels through soil we must expect the stress conditions illustrated by Figures 133*c* and 133*d*.

An attempt to investigate the state of stress in the vicinity of tunnels through a material which does not obey Hooke's law has been made by Schmid (1926). The final equations are also very cumbersome. However, graphs and tables facilitate to a certain extent their interpretation.

Chapter XVIII

THEORY OF ELASTIC LAYERS AND ELASTIC WEDGES ON A RIGID BASE

146. Problems defined. The preceding chapter dealt with the stresses and the settlement due to loads on the horizontal surface of semi-infinite masses. It also dealt with the stresses in semi-infinite wedges. In nature every layer of soil and every wedge-shaped body of soil rests at a finite depth on a relatively rigid base. In the following articles the influence of the rigidity of the base of elastic masses on the state of stress and on settlement will be investigated. The investigations also include the influence of stratification on the state of stress produced by surcharges.

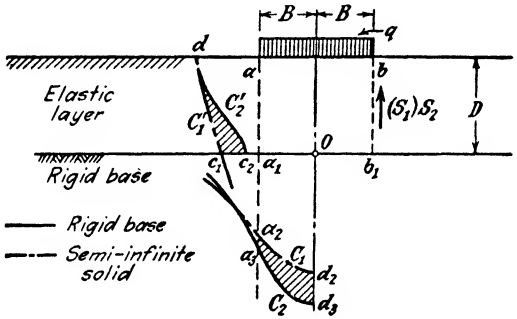

FIG. 134. Intensity and distribution of normal stresses on rigid base of elastic layer beneath flexible strip load and of shearing stresses on vertical sections through edges of loaded strip.

147. Influence of a rigid lower boundary on the stresses produced by surface loads. Curve C_1 in Figure 134 represents the distribution of the normal stresses on a horizontal section at depth D through a semi-finite elastic mass whose surface is acted upon between a and b by a load uniformly distributed over a strip with a width $2B$. The shearing stresses on a vertical section through a are represented by the horizontal distance between aa_1 and the dash-dotted curve C_1'. The total shearing force S_1 on aa_1 is given by the area aa_1c_1d. The area $a_1a_2d_2O$ represents

one half of the total normal pressure P_1 on the base a_1b_1 of the prismatic block aa_1b_1b per unit length of the block. The equilibrium of the block requires that the sum of the total normal pressure P_1 on the base of the block, and the shearing forces $2S_1$ on aa_1 and bb_1 should be equal to the total load Q on ab or

$$Q = 2Bq = P_1 + 2S_1 \qquad [1]$$

If the layer rests at depth D on the surface of a perfectly rigid layer the shearing stresses in the lowest part of the vertical sections aa_1 and bb_1 are very small compared with those at the same depth in the semi-infinite solid, because the rigid support prevents free angular distortion of the material located immediately above the base. If there is neither adhesion nor friction between the elastic layer and its base, the shearing stresses at a_1 and b_1 are equal to zero. The plain curve C_2' represents the distribution of the shearing stresses over aa_1 on the assumption that the elastic layer adheres to its base. Yet, for the reasons stated before, the lower part of the curve C_2' is much closer to aa_1 than the lower part of C_1', and the shearing force S_2 represented by the area aa_1c_2d is smaller than the shearing force S_1 represented by the area aa_1c_1d. The sum of $2S_2$ and the vertical reaction P_2 on the base a_1b_1 of the block must be equal to Q. Hence P_2 must be greater than P_1 in equation 1. At the same time the total normal pressure on every horizontal section must always be equal to Q. A pressure distribution which satisfies this condition together with the condition $P_2 > P_1$ is represented in Figure 134*a* by the plain curve C_2. Its maximum ordinate is greater than that of the curve C_1 and its slopes are steeper. The shaded area $a_2a_3d_3d_2$ is equal to the shaded area dc_1c_2.

148. Pressure on the rigid base of an elastic layer due to point and line loads. In order to compute the intensity and the distribution of the pressure on the rigid base of an elastic layer acted upon by a load covering a finite area one needs equations similar to Boussinesq's equations 135(1*a*) and 136(1*a*). These equations can be derived on two different assumptions. Either it is assumed that there is neither friction nor adhesion between the elastic layer and its base (frictionless base) or else perfect adhesion between the layer and the base is assumed (adhesive base). The problem of computing the pressure due to line loads has been solved for elastic layers on a frictionless base by Melan (1919) and on an adhesive base by Marguerre (1931). The equations for the pressures produced by a point load on a layer with a frictionless base have been derived by Melan (1919) and for a layer on an adhesive base by Biot (1935*a*) and Passer (1935). Biot's solution for a point load on an elastic layer with an adhesive base may serve as an example

of the results thus obtained. Let

Q = the point load,
D = the thickness of the elastic layer,
r = the horizontal radial distance between an arbitrary point N on the adhesive and rigid base of the layer and the line of action of the load Q,
μ = Poisson's ratio of the elastic layer, and
p_D = normal unit pressure on the base at point N.

If $\mu = 0.5$ the unit pressure p_D is determined by the equation

$$p_D = \frac{Q}{D^2}\frac{3}{2\pi}\left\{\frac{2}{\left[1+\left(\frac{r}{D}\right)^2\right]^{\frac{5}{2}}} - \frac{0.25}{\left[1+\left(\frac{r}{2_D}\right)^2\right]^{\frac{5}{2}}}\right.$$

$$\left. - 0.039\,\frac{1-3\left(\frac{r}{4D}\right)^2+\frac{3}{8}\left(\frac{r}{4D}\right)^4}{\left[1+\left(\frac{r}{4D}\right)^2\right]^{\frac{9}{2}}} - 0.154\,\frac{1-5\left(\frac{r}{3D}\right)^2+\frac{15}{8}\left(\frac{r}{3D}\right)^4}{\left[1+\left(\frac{r}{3D}\right)^2\right]^{\frac{11}{2}}}\right\} \quad [1]$$

If point N were located in a semi-infinite solid the vertical normal stress σ_z at point N, which corresponds to the unit contact pressure p_D, could be computed by substituting the values

$$z = D \quad \text{and} \quad \cos\psi = \frac{D}{\sqrt{D^2+r^2}}$$

into Boussinesq's equation 135(1a). Thus we get

$$\sigma_z = \frac{Q}{D^2}\frac{3}{2\pi}\left[\frac{1}{1+(r/D)^2}\right]^{\frac{5}{2}}$$

This example shows that the equations representing the pressure on a rigid base are by no means as simple as the equations of Boussinesq. The results of the investigations regarding the pressure on a rigid base beneath a point load are shown in Figure 135a. In this figure the curve C_B represents the distribution of the normal stresses over a horizontal section at depth D through a semi-infinite mass, acted upon by a vertical point load Q. It has been computed by means of Boussinesq's equation 135(1a). Curve C_0 represents the corresponding distribution on the assumption that the plane separating the elastic layer from the rigid base is perfectly frictionless. If there is perfect adhesion between the elastic layer and the rigid base the pressure distribution is as shown by the curve C_a. The greatest ordinate of the curve C_0

exceeds the greatest ordinate of C_B by about 71 per cent. Perfect adhesion between the layer and its base (curve C_a) reduces this value to about 56 per cent.

Figure 135*b* shows the normal stresses on a horizontal plane at depth D due to a vertical load q' per unit of length of a straight line at right angles to the plane of the drawing. C_B represents the Boussinesq solution for a semi-infinite solid (eq. 136(1*a*)), C_0 the solution for a perfectly frictionless rigid base, and C_a the solution for an elastic layer which adheres to its base. The greatest normal stress on the frictionless rigid base exceeds the Boussinesq value by about 44 per cent. Perfect adhesion between the layer and its base reduces this value to about 28 per cent (curve C_a).

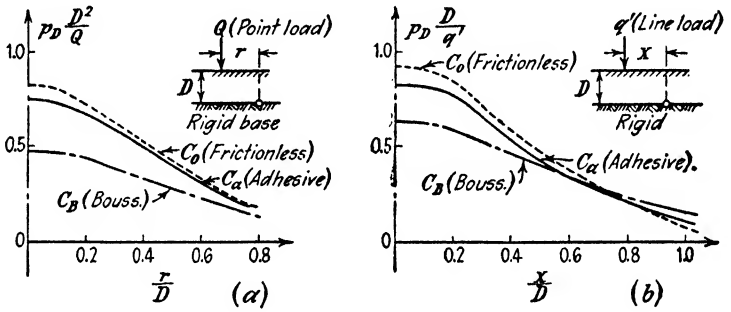

FIG. 135. Distribution of normal pressure on rigid base of elastic layer acted upon (*a*) by point load and (*b*) by line load. (*Sources of data given in text.*)

By evaluating the equations represented by the curves in Figures 135*a* and 135*b*, Biot (1935*a*) found that the maximum ordinates of these curves, corresponding to points immediately under the load, are as follows:

	Point Load	*Line Load*
Section through semi-infinite mass (curves C_B)	$3/2\pi = 0.477$	$2/\pi = 0.637$
Rigid base with adhesive surface (curves C_a)	$1.557 \times 3/2\pi$	$1.281 \times 2/\pi$
Rigid base with frictionless surface (curves C_0)	$1.711 \times 3/2\pi$	$1.441 \times 2/\pi$

Biot (1935*a*) also computed the distribution of the normal stresses produced by point and line loads on a horizontal, perfectly flexible membrane embedded at some depth below the horizontal surface of a semi-infinite solid. At the surfaces of contact between the solid and the membrane the lateral displacements are assumed equal to zero. He found that the normal stress on the membrane vertically beneath the load is about 5 per cent lower than the corresponding stress at the same depth on a horizontal section through a semi-infinite solid.

149. Elastic layer acted upon by a flexible load on a finite area. If the load is uniformly distributed over a finite area on the surface of an elastic layer the rigorous computation of the intensity and the distribution of the vertical unit pressure on the base of the layer is rather cumbersome. Cummings (1941) computed the pressure by means of equation 148(1), represented by the curve C_a in Figure 135*a*, on the following assumptions: the load q per unit of area acts on a circular area with a radius R; Poisson's ratio of the elastic layer is 0.5; the base of the elastic layer is rigid and the elastic layer, with a thickness D, adheres perfectly to the rigid base. On these assumptions he obtained for the vertical unit pressure p_D on the rigid base beneath the center of the loaded area the equation

$$p_D = q\left\{1 - \frac{2}{\left[1+\left(\frac{R}{D}\right)^2\right]^{\frac{3}{2}}} + \frac{1}{\left[1+\left(\frac{R}{2D}\right)^2\right]^{\frac{3}{2}}} + \frac{0.234\left(\frac{R}{4D}\right)^4 - 0.935\left(\frac{R}{4D}\right)^2}{\left[1+\left(\frac{R}{4D}\right)^2\right]^{\frac{7}{2}}} + \frac{1.555\left(\frac{R}{3D}\right)^4 - 2.08\left(\frac{R}{3D}\right)^2}{\left[1+\left(\frac{R}{3D}\right)^2\right]^{\frac{9}{2}}}\right\} \qquad [1]$$

The equation for the vertical unit pressure at other points of the rigid base would be still more complicated. In order to obtain simpler though less exact equations for the pressure we take advantage of the following fact. The shape of the plain curves shown in Figures 135*a* and *b* is similar to that of curves which represent the distribution of the normal stresses on horizontal sections through semi-infinite masses which are acted upon by the same loads. In order to compute the vertical pressure at depth D below the surface of a semi-infinite mass acted upon by a point or a line load we must replace the value z in Boussinesq's equations, 135(1*a*) and 136(1*a*) respectively, by D. By means of this procedure the curves C_B in Figures 135*a* and 135*b* were obtained. If we substitute for the value D an appropriately selected fictitious value D' which is smaller than D the Boussinesq curves become almost identical with the curves representing the real distribution of the pressure on a rigid base at depth D. The same procedure can also be used to estimate the pressure on a rigid base beneath an elastic layer if the load is distributed over part of the surface of the elastic layer (Terzaghi 1932). If the load which produces the pressure p_D (eq. 1) acts on the surface of a semi-infinite mass, the vertical normal stress σ_z

at depth D beneath the center of the loaded area is equal to

$$\sigma_z = q\left\{1 - \left[\frac{1}{1 + (R/D)^2}\right]^{\frac{3}{2}}\right\} \qquad 136(4)$$

The normal stress σ_z is smaller than p_D (eq. 1). However, if we replace the value D in this equation by

$$D' = 0.75D \qquad [2]$$

the value σ_z becomes practically identical with the value p_D (eq. 1). Hence we can write

$$p_D = q\left\{1 - \left[\frac{1}{1 + (R/0.75D)^2}\right]^{\frac{3}{2}}\right\} \qquad [3]$$

In Figure 136*a* the abscissas of the plain curve represent the exact values of p_D, determined by equation 1, and those of the dashed curve the values computed by means of the simplified equation 3. The two curves are almost identical. The distribution of the vertical pressure over the rigid base of an elastic layer with a depth D is also very similar to that over a horizontal section at depth $0.75D$ below the surface of a semi-infinite mass which is acted upon by the same load. These statements are valid regardless of the shape of the area covered by the load. Hence the pressure on the rigid base of an elastic layer with a depth D is approximately identical with the pressure on a horizontal section at a depth $D' = 0.75D$ through a semi-infinite solid whose surface carries the same load.

The normal stress at point N (Fig. 120*a*) in a semi-infinite solid beneath a loaded rectangular area is determined by equation 136(9). The influence values I_σ which appear in this equation are given by equation 136(8). They are a function solely of $m = B/z$ and of $n = L/z$. In order to obtain an approximate value for the unit pressure p_D at an arbitrary point N on the rigid base of an elastic layer with a depth D one must replace the values of m and n in equation 136(8) by

$$m' = \frac{B}{0.75D} \quad \text{and} \quad n' = \frac{L}{0.75D} \qquad [4]$$

The corresponding influence values can be obtained by means of Table II in the Appendix.

Figures 136*b* and 136*c* show the distribution of the pressure produced by a load on a strip of infinite length on a rigid base at a depth D below the surface of an elastic layer. In Figure 136*b* the depth D is equal to 0.84 and in Figure 136*c* it is equal to 0.5 times the width $2B$ of the strip. In each figure the ordinates of the dash-dotted curve represent the

ratio σ_z/q between the normal stresses σ_z and the unit load q for a horizontal section at depth D through a semi-infinite mass and those of the plain lines represent the ratio p_D/q between the unit pressure p_D on a rigid base at tha depth and the unit load q. A comparison of the data

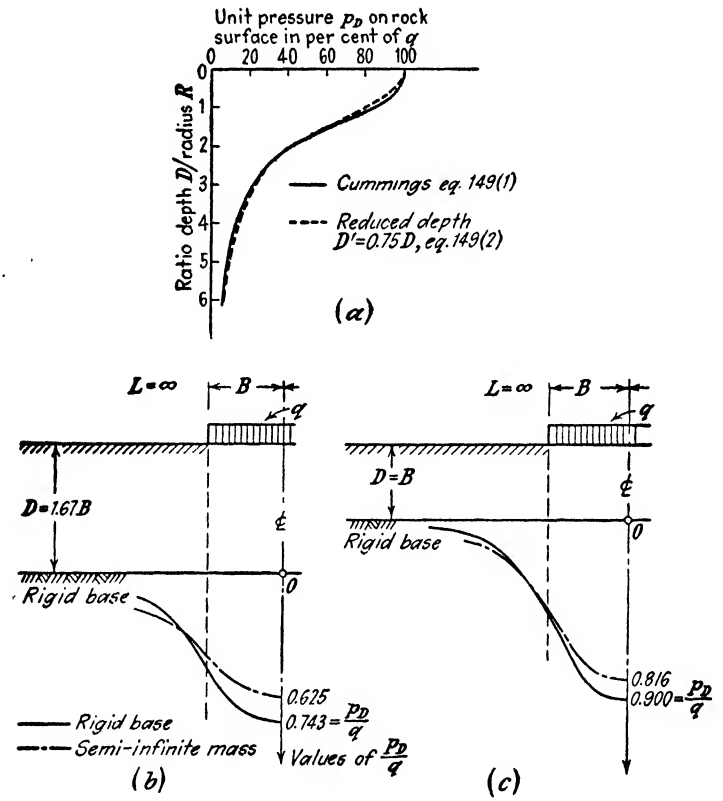

FIG. 136. (*a*) Influence of depth ratio on unit pressure on rigid base of elastic layer beneath center of a circular loaded area; (*b*) and (*c*) distribution of pressure on rigid base of elastic layer acted upon by flexible strip load, for two different depth ratios. The distribution of the pressure on a horizontal section through a semi-infinite mass at the level assigned to the rigid base is indicated by dash-dotted curves.

shown in Figures 136*b* and 136*c* indicates that the influence of the ridigity of the base on the maximum value of the unit pressure p_D is different for different depth ratios D/B. Combining equations 2 and 136(2*a*) it can be shown that the influence is greatest if the depth D is roughly equal to five times the width of the loaded strip. For very small and very large values of D/B the influence is negligible.

The equations given in this article apply only to the stresses at the base of the elastic layer and in its immediate vicinity, because according to St. Venant's principle the influence of the rigidity of the base on the state of stress in an elastic layer decreases rather rapidly with increasing elevation above the base. In the upper half of the layer the state of stress is practically identical with that in an elastic, semi-infinite deposit which is acted upon by the same load. Therefore the equations contained in this article cannot be used for computing the settlement of a loaded area on the surface of such a layer.

150. Approximate method of computing the settlement due to loads on the surface of elastic layers. The problem of computing rigorously the settlement of loads covering a finite part of the surface of elastic layers on a rigid base has not yet been solved. However, Steinbrenner (1934) worked out an approximate solution which is accurate enough for every practical purpose. He computed the settlement $\Delta\rho$ of the corners of a uniformly loaded rectangular area on the horizontal surface of a semi-infinite mass. Then he computed the vertical displacement $\Delta\rho'$ of the points located at a depth D below these corners and assumed that the settlement $\Delta\rho_D$ of the corners of the loaded area on the surface of an elastic layer with the thickness D is equal to the difference $\Delta\rho - \Delta\rho'$, or

$$\Delta\rho_D = \Delta\rho - \Delta\rho' \qquad [1]$$

Let
L = the length of a rectangular area,
B = the width of the area,
$l = L/B$ = the length factor,
D = the depth of the elastic layer,
$d = D/B$ = the depth factor,
q = the unit load,
E = the modulus of elasticity of the layer, and
μ = Poisson's ratio.

The vertical displacement $\Delta\rho$ of the corner of the rectangular area is given by equations 137(1). The vertical displacement ζ of a point in the interior of the semi-infinite mass due to a point load acting on the surface is determined by equation 135(4*a*), and the vertical displacement $\Delta\rho'$ of a point at a depth D below one of the corners of the rectangular area can be computed by a simple integration. By means of this procedure one obtains

$$\Delta\rho_D = \Delta\rho - \Delta\rho' = q\frac{B}{E}\left[(1-\mu^2)F_1 + (1-\mu-2\mu^2)F_2\right] = q\frac{B}{E}I_\rho \qquad [2a]$$

wherein

$$F_1 = \frac{l}{\pi}\left[l \log \frac{(1+\sqrt{l^2+1})\sqrt{l^2+d^2}}{l(1+\sqrt{l^2+d^2+1})} + \log \frac{(l+\sqrt{l^2+1})\sqrt{1+d^2}}{l+\sqrt{l^2+d^2+1}} \right] \quad [2b]$$

and

$$F_2 = \frac{d}{2\pi} \tan^{-1} \frac{l}{d\sqrt{l^2+d^2+1}} \quad [2c]$$

The value

$$I_\rho = (1-\mu^2)F_1 + (1-\mu-2\mu^2)F_2 \quad [3]$$

is a pure number. It determines approximately the influence of a rectangular surcharge which rests on the surface of an elastic layer with a thickness D on the settlement of the corners of the area. Figure 137*a* represents the relation between the depth factor $d = D/B$ and the values F_1 and F_2 in equation 3 for different values of the length factor $l = L/B$. If Poisson's ratio $\mu = 0$ the influence value I_ρ (eq. 3) is equal to

$$I_\rho = F_1 + F_2 \quad \text{for} \quad \mu = 0 \quad [4]$$

If $\mu = 0.5$ the second term on the right-hand side of equation 3 is equal to zero and the influence value is

$$I_\rho = 0.75F_1 \quad \text{for} \quad \mu = 0.5 \quad [5]$$

For intermediate values of μ the value I_ρ can be computed by means of equation 3 and the data contained in Figure 137*a*.

In order to compute the settlement of a point N located within the rectangular area shown in Figure 137*b* we compute for each one of the four areas I to IV the values l and d and determine the corresponding influence values $I_{\rho I}$ to $I_{\rho IV}$ by means of equation 3 and the data shown in Figure 137*a*. The settlement of point N is

$$\rho = \frac{q}{E}(I_{\rho I}B_I + I_{\rho II}B_{II} + I_{\rho III}B_{III} + I_{\rho IV}B_{IV}) \quad [6]$$

If point N is located outside the loaded area the settlement of the point can be computed by means of the process of algebraic summation described in Article 137 and illustrated by Figure 122*b*.

Figures 138*a* to 138*c* illustrate the influence of the depth ratio $d = D/R$ and of Poisson's ratio on the settlement of a flexible load on a circular area with a diameter $2R$. If the depth ratio is smaller than about $\frac{1}{2}$ and Poisson's ratio close to one half, the settlement

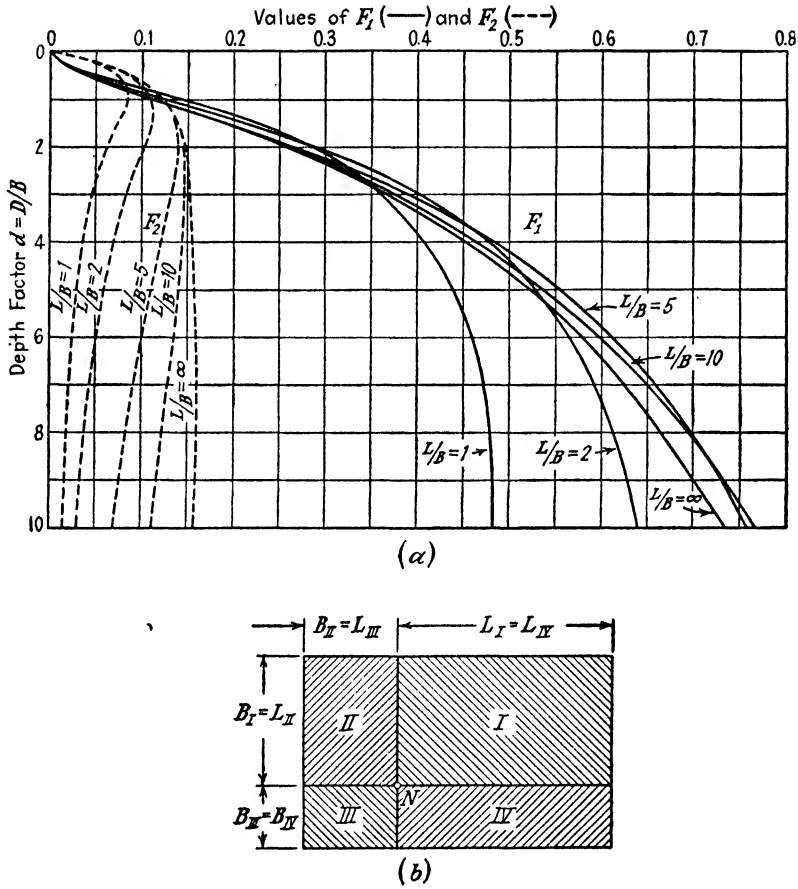

FIG. 137. Settlement due to load on surface of elastic layer. (*a*) Graph for estimating settlement of a corner of a loaded rectangular area on surface of elastic layer with rigid base; (*b*) diagram illustrating method of estimating settlement of point located within loaded area. (*After Steinbrenner 1934.*)

is greatest at a distance of about $2R/3$ from the center of the area, as indicated in Figure 138*c*. This conclusion has been confirmed by field observations (Terzaghi 1935). Figure 138*c* also shows that the free surface of a thin elastic layer rises in the vicinity of the loaded area, provided Poisson's ratio is close to 0.5.

In Figure 138*d* the abscissas represent the ratio between the given thickness D_1 of an elastic layer and one half of the variable width $2B$ of a square area on the surface of the layer which carries a given unit load q_1 per unit of area. By means of equation 6 we obtain for the

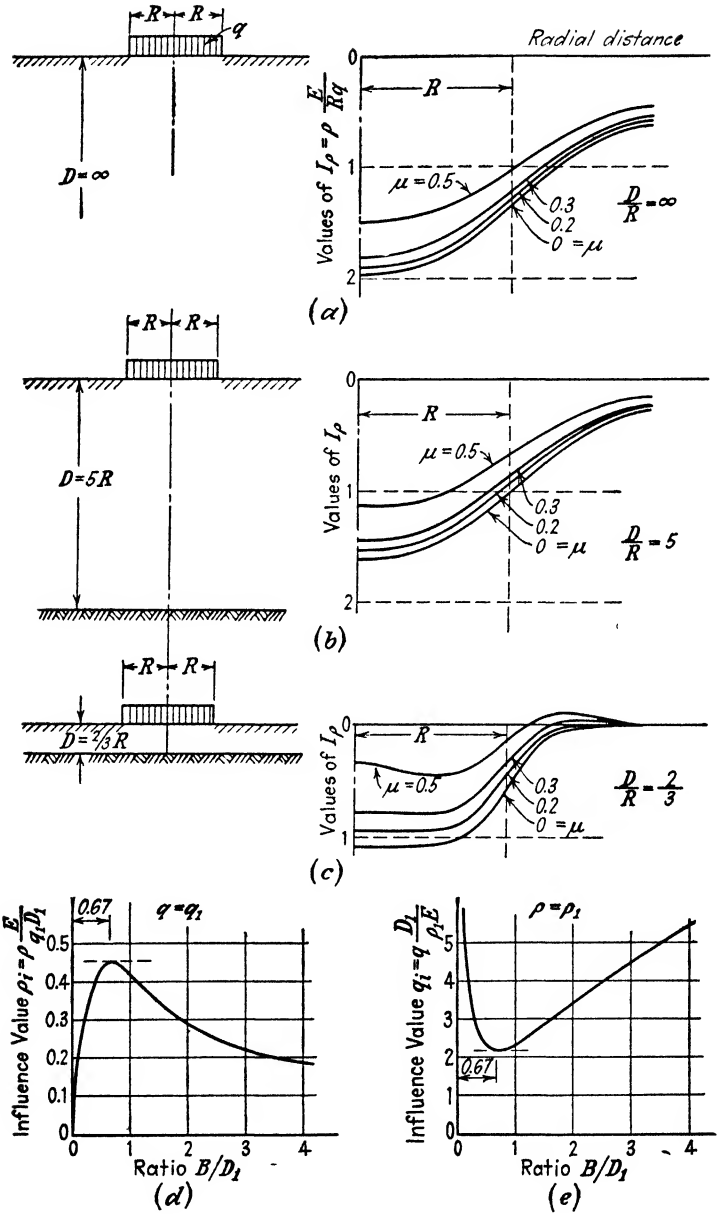

FIG. 138. (*a*) to (*c*) Settlement of flexible load on circular area on surface of elastic layer for three different depth ratios; (*d*) influence of size of a square loaded area on the surface of an elastic layer on the settlement of the center point of the area at a given unit load, and (*e*) influence of the same factor on the unit load required to produce a given settlement of the center point.

settlement of the center of the loaded area

$$\rho = 4 \frac{q}{E} BI_\rho$$

wherein I_ρ is the influence value (eqs. 2 and 3) for square areas. For such areas the value l in equation 2 is equal to unity. Hence at a given value μ of Poisson's ratio the value I_ρ depends only on the depth factor $d = D/B$. In order to investigate the influence of the width $2B$ of the loaded area on the settlement ρ at a given depth D_1 of the elastic layer we write

$$\rho = 4 \frac{q}{E} \frac{B}{D_1} D_1 I_\rho = q \frac{D_1}{E} \left(4 \frac{B}{D_1} I_\rho \right) = q \frac{D_1}{E} \rho_i \qquad [7]$$

whence

$$\rho_i = \rho \frac{E}{qD_1} \qquad [8]$$

At a given value μ the influence value ρ_i depends only on the ratio B/D_1. Assuming $\mu = 0.5$ (incompressible elastic layer) we get for ρ_i corresponding to different values of B/D_1 the values given by the ordinates of the curve in Figure 138*d*.

Figure 138*d* shows that the settlement is greatest if the width $2B$ of the loaded area is roughly equal to 1.3 times the thickness D_1 of the layer. Figure 138*e* illustrates the influence of the width $2B$ of the loaded area on the unit load which must be applied on the square area in order to produce a given settlement ρ_1 of the centerpoint of the area. If we assign to ρ in equation 8 a constant value ρ_1, we get

$$q = \rho_1 \frac{E}{D_1} \left(\frac{1}{\rho_i} \right) = \rho_1 \frac{E}{D_1} q_i$$

wherein

$$q_i = \frac{1}{\rho_i} = q \frac{D_1}{\rho_1 E}$$

The values q_i are given by the ordinates of the curve shown in Figure 138*e*. The value $q_{i\,\min}$ is equal to $1/\rho_{i\,\max} = 1/0.45 = 2.2$.

151. Distribution of the vertical pressure on a bed of clay between sand layers. Important settlements have frequently occurred on account of the gradual consolidation of beds of clay enclosed between strata of sand. On account of the low permeability of the clay the compression of the clay occurs very slowly as explained in Chapter XIII.

Between two beds of sand a layer of clay is laterally almost completely confined unless the layer is very thick. Therefore the fundamental assumptions specified in Article 98 are valid and the rate of consolidation can be computed by means of the method described in Article 102.

In order to illustrate the influence of a process of gradual consolidation of a bed of clay on the distribution of the stresses we investigate the state of stress beneath a loaded strip with a width $2B$, shown in Figure 139. The load acts on the surface of a bed of sand, which rests at a depth D on a horizontal layer of clay with a thickness $2H$. We assume that the theory of Boussinesq would be valid for the sand, if it did not contain a layer of clay.

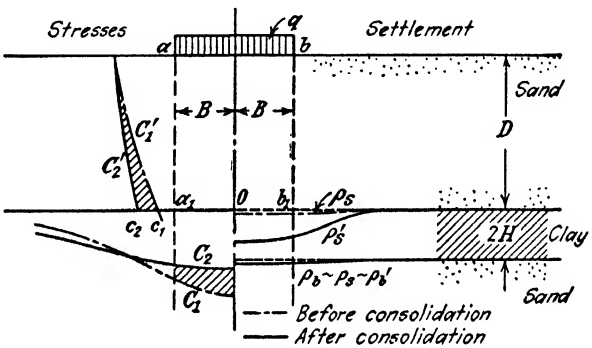

FIG. 139. Effect of gradual consolidation of bed of clay between two sand strata on the stresses produced by a flexible strip load in the loaded soil and on the settlement.

The normal stresses on a horizontal section at a depth D beneath a loaded strip on the surface of a homogeneous semi-infinite solid are determined by equation 136(2a) and the shearing stresses on vertical sections through the rims of the loaded strip can be computed by means of equation 136(2c). In Figure 139 the normal stresses on a horizontal section at a depth D are represented by the vertical distance between this section and the dash-dotted curve C_1 and the shearing stresses on the vertical section aa_1 by the horizontal distance between this section and the dash-dotted curve C_1'.

Owing to the low rate of consolidation of clay, a bed of clay acts at the outset of the process of consolidation like a flexible but practically incompressible layer, and the distribution of the stresses in this stage is nearly the same as though the elastic properties of the clay were identical with those of the sand. In this initial state the deflections of both the top and bottom surfaces of the bed of clay, ρ_s and ρ_b respec-

tively, are almost identical; they are as indicated in Figure 139 on the right-hand side of the diagram.

As the process of consolidation proceeds the top surface of the clay settles more than its base and in the final state of consolidation the difference between the settlement of the two surfaces may be very important. The influence of the excessive settlement of the upper surface on the shearing stresses on vertical sections through the rim of the surcharge is opposite to that of a rigid base. It increases the shearing stresses in the vicinity of a_1 and b_1 so that the distribution of the shearing stresses is such as indicated by the curve C_2' in Figure 139. An increase of the shearing forces on the two vertical sides of the block abb_1a_1 involves a decrease of the normal pressure on its base. Hence if we compute the normal pressure on the clay by means of Table II in the Appendix, which is based on Boussinesq's equations, the error is on the safe side. On the other hand the error due to ignoring the influence of the lack of elastic homogeneity of the sand strata on the distribution of the pressure (see Art. 141 and Fig. 127*c*) is on the unsafe side and partly compensates the error mentioned before.

The settlement due to the compression of the sand strata is usually neglected. In accordance with this procedure the settlement ρ of the surface at any point is equal to the decrease of the thickness of the clay bed vertically below the point. After consolidation is complete this decrease is equal to

$$\rho = \rho_s' - \rho_b' = 2pHm_v$$

wherein p is the normal stress on a horizontal section at mid-height of the bed of clay, computed by means of the graph in Figure 120*b*, $2H$ is the thickness of the bed, and m_v is the coefficient of volume compression (eq. 98(5)); the symbols ρ_s' and ρ_b' represent the settlement of the two surfaces of the clay stratum.

152. Elastic wedge on a rigid base. Article 144 contains the equations for the stresses in elastic wedges derived on the assumption that the sides of the wedges extend to infinity. These stresses are associated with a troughlike deformation of every horizontal section through the wedge. Hence if a wedge rests at a finite depth below its crest on a rigid, horizontal base the distribution of the stresses on the base must be different from that on a horizontal section through a semi-infinite wedge. On the basis of the reasoning illustrated by Figure 134 we should expect that the rigidity of the base increases the normal stresses on the central part of the rigid base at the expense of the stresses along the rims. This conclusion is in accordance with the results of a mathematical investigation made by Wolf (1914) on the basis of the assump-

tion that the wedge adheres to its base. In order to satisfy the condition that the deformation of the base of the wedge should be equal to zero, Wolf replaced the stress function F in equation 17(5) by a series of polynomials and selected the coefficients in the polynomials in such a manner that the boundary condition at the base is at least approxi-

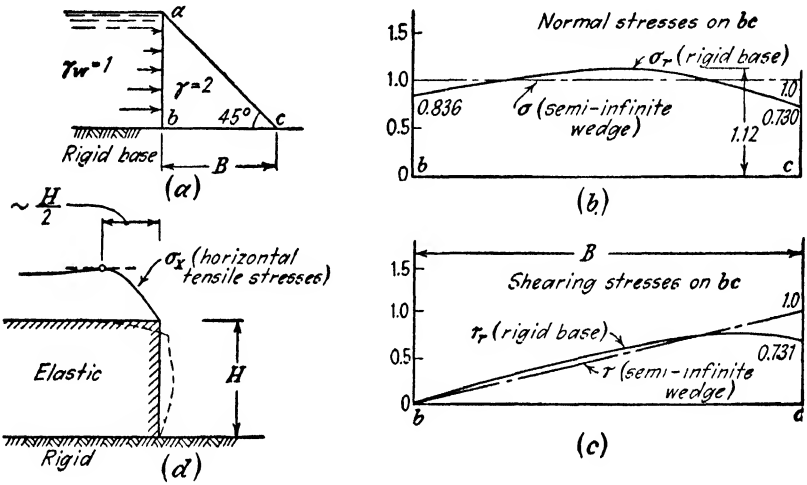

FIG. 140. (*a*) Section through elastic wedge on a rigid base, acted upon by water pressure; (*b*) distribution of normal stresses and (*c*) of shearing stresses along base of wedge (*a* to *c after Wolf 1914*); (*d*) tensile stresses along upper horizontal surface of elastic layer with vertical lateral boundary.

mately satisfied. Figure 140*a* is a section through the wedge which he investigated. The vertical side of the wedge is acted upon by the hydrostatic pressure of a liquid whose unit weight is equal to one half of the unit weight of the construction material of the wedge, and the inclined side of the wedge rises at 45° to the horizontal. On these simple assumptions the distribution of the normal stresses on the base, computed by means of equations 144(1) and 144(2) for the semi-infinite wedge, should be perfectly uniform as indicated in Figure 139*b* by a horizontal dash-dotted line. The rigidity of the base changes the distribution, as shown by the plain curve. Figure 140*c* shows the influence of the rigidity of the base on the distribution of the shearing stresses on the base. The figures demonstrate that the effect of the rigidity of the base on the stress distribution at the base is negligible compared to the difference between the distribution of stresses in a state of elastic equilibrium and that in a state of plastic equilibrium, illustrated by Figures 131*b* and 131*c* respectively. For sections at a higher level it is insignificant, because with increasing elevation above the base the

stress distribution rapidly approaches that for a semi-infinite wedge. Further contributions to the mathematical theory of elastic wedges have been made by Brahtz (1933). The equations which he presents may apply to concrete dams on a rock foundation but there is no evidence to indicate that the theoretical state of stress which he postulates has any resemblance to that in an earth dam or in a fill.

Figure 140*d* is a section through a semi-infinite wedge with one horizontal and one vertical surface. If we replace the lower part of the wedge, beneath a depth H, by rigid material, the state of stress in the wedge becomes identical with that in an elastic layer with a vertical face and a thickness H, supported by and adhering to a rigid base. The dashed line indicates the deformation of the layer due to its weight. Along its upper horizontal surface the layer is in a state of tension.

From the results of strain measurements on a small gelatine model the author concludes that the distribution of the tensile stresses along the horizontal surface is approximately as indicated by the stress area between the original surface and the plain curve marked σ_x (Fig. 140*d*). At a distance of about $H/2$ from the upper rim of the vertical face the tensile stresses are a maximum. A failure of the bank starts with the formation of a tension crack at a distance of about $H/2$ from the rim of the bank. Once the failure has started it proceeds by shear from the bottom of the crack to the foot of the bank along a curved surface of failure.

153. Experimental stress determination based on the laws of similitude and on mathematical analogues. Rigid boundaries complicate the determination of the stresses produced in elastic material by mass forces such as the force of gravity or the pore-water pressure, and mathematical solutions are not yet available for many problems of practical importance such as that illustrated by Figure 140*d*. In such cases, the required information can be obtained from small-scale model tests. The interpretation of the results of such tests is based on the laws of similitude. These laws are determined by the general equations which represent the quantities under investigation. For instance, the equations of flow nets or the equations representing the distribution of the stresses due to a surcharge on the surface of an elastic solid can always be presented in such a form that the coefficients on one side of the equation are pure numbers. Therefore the quantity on the other side of the equation is independent of the scale of the model.

If the unknown stresses are due only to gravity or to pore-water pressures, the law of similitude is very simple, because such stresses increase in direct proportion to the linear dimensions of the body. But the experimental difficulties are very considerable because the

stresses produced by these forces on small-scale models are extremely small. When investigating states of stress produced by gravity, Bucky (1931) eliminated this difficulty by mounting his models on a centrifuge. Thus he was able to increase the intensity of the mass force and the stresses due to this force to any desired value. By means of this method he attempted to determine the safe width of mine workings at different depth below the surface (Bucky 1934).

Another method of overcoming the experimental difficulties is the employment of mathematical analogues. Many of the differential equations used in hydraulics and in applied mechanics are identical with differential equations expressing fundamental relations in other fields, such as flow of heat or diffusion. The existence of such an identity establishes a *mathematical analogue.* One mathematical analogue has been described in Article 100, and many others are known (Timoshenko 1934). If the boundary conditions for a specific problem in one realm of physics are selected in such a way as to correspond to those in another, as explained in Article 100, the solutions of the differential equation for both problems are numerically identical.

One of the best-known mathematical analogues is the soap film analogue for the state of stress due to torsion (Prandtl 1903, see Southwell 1936). On account of this analogue the deflection of a uniformly stretched soap film is identical with the stress function in the differential equation for torsion, provided the following conditions are satisfied. The area covered by the soap film must be similar to the section through the bar under torsion, and the film must be acted upon by a uniform pressure which can, for instance, be produced by a one-sided air pressure. Once the stress function is known the stresses can be determined by graphic integration or some other process. It is relatively simple to measure the deflection of the film, but it is impossible to measure the stresses in the bar. A membrane analogue has been used by Brahtz (1936) to determine the pore-water pressure at the impermeable base of permeable storage dams.

Hence the existence of mathematical analogues permits a simple experimental solution of many difficult theoretical problems. The practical value of the results depends on the importance of the difference between the properties of the soil used in construction and the ideal material to which the analogue applies. In soil mechanics the difference is usually so important that the field for the practical application of the analogue method is rather limited.

154. Photoelastic method of stress determination. The photoelastic method is based on Brewster's law which states that stress causes every optically isotropic material to become doubly refracting. When passing through a sheet of transparent material under stress, a ray of polarized light is resolved into two rays, one of which is polarized in a plane at right angles to one of the principal stresses, σ_I, and the other

one at right angles to the other principal stress, σ_{II}. The phase difference between the two rays increases in direct proportion to the difference $\sigma_I - \sigma_{II}$ between the two principal stresses. By measuring the position of the planes of polarization of the two rays and their phase difference one obtains all the data required to trace the trajectories of the stresses and to compute the difference between the principal stresses for every point of the photoelastic model. The data required to compute the sum of the principal stresses can be obtained by measuring the change of the thickness of the model due to the application of the stresses, by a soap film test based on a mathematical analogue discovered by Den Hartog, or by other independent methods (Southwell 1936). Quite recently Brahtz and Soerens (1939) described a procedure for the direct determination of individual principal stresses.

The model is made of glass, celluloid, bakelite, phenolite or some other transparent material. It is mounted at right angles to the path of a beam of polarized light and subjected to a system of forces in accordance with the problem under consideration. In most test arrangements the plane of polarization of the ray which enters the model remains stationary while the model can be rotated around an axis parallel to the beam of light and shifted in two directions at right angles to each other and to the beam of light (Coker and Filon, 1931). The trajectories of stresses can be determined graphically.

The technique described in the preceding paragraphs can be used only for the investigation of plane states of stress. However, quite recently successful efforts have been made to apply the photoelastic method to the investigation of triaxial states of stress (Hiltscher 1938).

The photoelastic method is extensively used by the U. S. Bureau of Reclamation for determining stresses in concrete structures. The limitations of the method in connection with problems of soil mechanics are identical with those of the theory of elasticity in general. (See Article 132.)

Chapter XIX

VIBRATION PROBLEMS

155. Introduction. If an elastic or elastically supported structure, such as a water tower or a tall building, is temporarily forced out of its normal position by an impact or by the sudden application and removal of a force, the elastic forces in the supporting earth and in the members of the structure are no longer in equilibrium with the external forces and vibrations ensue. The disturbance of the static equilibrium can be produced by earthquakes, explosions, operating machinery, traffic, pile-driving operations, and many other agents. The amount of disturbance of the equilibrium produced by a single impulse can be expressed either by the intensity of the force which causes the disturbance or by the distance to which the force removes the center of gravity of the structure from its equilibrium position. The force is called the *disturbing force,* and the displacement produced by the force is the *initial displacement.*

If the elastic support of a rigid system is of such a nature that the system can only vibrate parallel to a given straight line or in a plane about a fixed axis the system is said to have only one degree of freedom. Otherwise it has two or more degrees of freedom. The *degree of freedom* is equal to the number of quantities or coordinates which are required to define the displacement of the body. In the most general case the movement of a rigid system can be resolved into three translatory and three rotational components. Each one of these components can be defined by a single value. Therefore a rigid system can have no more than six degrees of freedom. Since the relative position of the particles of such a system does not change, the system is called a *single mass system.* On the other hand if a system consists of several relatively rigid bodies which are connected with each other by relatively flexible members one has to deal with a *multiple-mass system.*

The vibrations caused by a single impulse are called *free vibrations.* The time between two successive arrivals of any one particle in its extreme position in a given direction is the *natural period* of the vibration for this direction. An elastically supported rigid system with a single degree of freedom has only one natural period. If a system has several degrees of freedom the natural frequency of the components of its free vibrations can be different.

In contrast to the free vibrations produced by a single impulse, the vibrations produced by a periodic impulse with an arbitrary period are called *forced* vibrations. A periodic impulse can be produced by operating machinery, street traffic, pile-driving operations, and many other causes. If the origin of the periodic impulse is distant from the structure, the impulse reaches the base of the structure through the subgrade. Within the subgrade the impulse travels like a sound wave. As time goes on, the distance between the seat of the impulse and the outer boundary of the zone which vibrates under the influence of the impulse increases. This outer boundary is the *wave front.* The velocity with which the wave front advances represents the *velocity of wave propagation.* Since it depends to a large extent or entirely on the elastic properties of the subgrade, it is possible to utilize vibration methods for the purpose of ascertaining certain elastic properties of the subgrade without sampling and testing.

The major part of this chapter deals with the influence of the mechanical properties of the soil on the vibrations of superimposed structures and the influence of the vibrations on the settlement of the structures. To demonstrate these influences it suffices to consider the rectilinear vibrations of single-mass systems with one degree of freedom. The theory of the effect of the vibrations on the structures themselves is beyond the scope of this book.

In order to grasp the fundamental principles of the subject it is sufficient to know the theory of undamped free and forced rectilinear vibrations. In order to be able to understand the publications dealing with the effect of vibrations on structures and their foundations the reader also needs a knowledge of the damping effect. The methods of designing engine foundations involve in addition the theory of vibrations about a fixed axis of rotation. The theory of undamped vibrations appears in the following articles in large print, the theory of damped vibrations in small print and for the theory of vibrations about a fixed axis the reader is referred to general textbooks, such as Timoshenko (1937).

This chapter also deals with the exploration of soil conditions in the field by means of vibrators, with the principles of seismic soil exploration, and with the mechanical effects of earthquakes.

The contents of the entire chapter are limited to an elementary exposition of the fundamental principles of the subject. However, special attention will be called to the controversial character of the assumptions on which the theories of vibrations in soils are based. Many of the publications in this field, particularly those which deal with engine foundations and with soil exploration by means of vibrators, fail to mention the appalling approximations involved in the computations. Hence an unprepared reader may be led to overestimate the reliability of the results.

156. Free harmonic vibrations. Figure 141*a* shows a prismatic block with a weight W supported by a bed of identical, uniformly spaced, and perfectly elastic springs. This arrangement corresponds to the mental picture on which the concept of subgrade reaction (Art. 124) is based. If a centric vertical load Q is applied to the block,

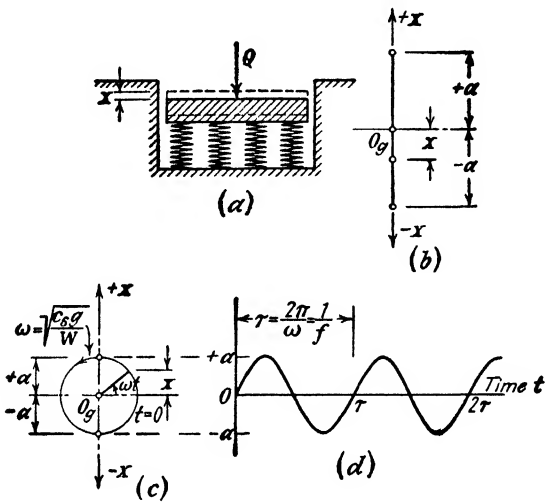

FIG. 141. (*a*) Piston on spring support for demonstrating free vibrations; (*b* to *d*) three different graphic representations of vibrations of piston.

the block descends through a distance x. The load q per unit of the area A of the base of the block is $q = Q/A$. Since the springs are perfectly elastic, the ratio

$$\frac{q}{x} = k_s \text{ (gm cm}^{-3}\text{)} \qquad [1]$$

is a constant. This equation is essentially identical with equation 124(1). The value k_s represents the coefficient of subgrade reaction for a block or a footing supported by a spring bed. The ratio

$$\frac{Q}{x} = c_s \text{ (gm cm}^{-1}\text{)} = Ak_s \qquad [2]$$

is called the *spring constant* of the support of the block. The spring constant represents the total load required to move the block in the direction of the force exerted by the load through a distance 1.

Application and subsequent sudden removal of a vertical load Q_1 on the block shown in Figure 141*a* causes the block to vibrate, whereby its center of gravity moves up and down on a vertical line through its original position.

The following computation of the vibratory movement of the block is based on the assumptions that the block is rigid, the mass of the springs is negligible compared with that of the block, and the movement of the block is resisted by no friction forces whatsoever.

At a time t after the load Q_1 was removed the center of gravity of the block is at a distance x (Fig. 141*b*) from its original position O_g. The velocity of every particle of the block is equal to dx/dt and the acceleration equal to d^2x/dt^2. Newton's second law of motion states that the product of the mass of a body into the acceleration is equal to the force which acts on the body in the direction of the acceleration. This condition can be expressed by the equation

$$\frac{W}{g}\frac{d^2x}{dt^2} + Q = 0 \qquad [3]$$

wherein g is the acceleration due to gravity and Q is the force required to maintain the center of gravity of the block at a vertical distance x from its original position O_g. When written in this form the condition constitutes what is known as D'Alembert's principle of rectilinear motion. From equation 2 we obtain

$$Q = c_s x$$

whence

$$\frac{W}{g}\frac{d^2x}{dt^2} + c_s x = 0 \qquad [4]$$

The solution of this equation is

$$x = C_1 \sin\left(t\sqrt{\frac{c_s g}{W}}\right) + C_2 \cos\left(t\sqrt{\frac{c_s g}{W}}\right)$$

wherein C_1 and C_2 represent the constants of integration. Counting the time from the instant when the center of gravity of the block passes through its equilibrium position for the first time and the displacement x positive in an upward direction, the solution must satisfy the condition $x = 0$ if $t = 0$, which requires $C_2 = 0$ and

$$x = C_1 \sin\left(t\sqrt{\frac{c_s g}{W}}\right)$$

Until the instant when the disturbing force Q_1 ceases to act on the block the displacement of the center of gravity is

$$x = -\frac{Q_1}{c_s} = -a \qquad [5]$$

This condition is not satisfied unless $C_1 = a$. Therefore

$$x = a \sin\left(t\sqrt{\frac{c_s g}{W}}\right) \qquad [6]$$

The term $\sqrt{c_s g/W}$ has the dimension $\sec^{-1}$ or that of an angular velocity

$$\omega = \sqrt{\frac{c_s g}{W}} \qquad [7]$$

which is equal to the ratio between the velocity of the movement of a point along a circle and the radius of the circle. The angular velocity ω represented by equation 7 is a constant and is called the *natural circular frequency* of the vibration produced by the impulse. Substituting ω in equation 6 we obtain

$$x = a \sin \omega t \qquad [8]$$

This relation can be represented by means of a vector with a length a, which rotates with a constant angular velocity ω around the equilibrium position of the center of gravity of the block, as shown in Figure 141*c*. At any time t the distance x (eq. 8) is equal to the vertical distance between the moving end of the rotating vector and the horizontal diameter of the circular path of this end. Vibrations which satisfy equation 8 are called *harmonic vibrations.*

Another method of representing equation 8 graphically is illustrated by Figure 141*d*. It consists in plotting the distances x against time. The curve thus obtained is a simple sine curve.

The time τ required for the vector in Fig. 141*c* to move through a complete circle is equal to the time interval which corresponds to a complete wave in Figure 141*d*. It is determined by the equation

$$\tau\omega = 2\pi$$

or

$$\tau = \frac{2\pi}{\omega} \qquad [9]$$

The value τ is called the *period* of the vibration. The number of cycles per unit of time,

$$f = \frac{1}{\tau} = \frac{\omega}{2\pi} = \frac{1}{2\pi}\sqrt{\frac{c_s g}{W}} \qquad [10]$$

is the *frequency* of the vibration.

The preceding equations were obtained on the assumption that the vibratory movement of the block is resisted by no friction force whatsoever. In reality this

condition is never strictly satisfied. As a consequence the amplitude of the vibrations gradually decreases and finally becomes equal to zero. This process is known as *damping*. If a rigid system rests on the soil the damping is chiefly due to the viscous resistance of the soil to rapid deformation. Our knowledge of this resistance is still inadequate. For the time being it is generally assumed that the damping force is equal to the rate of deformation of the soil times a constant c_d. This constant has no relation to the other elastic constants of the soil. If a footing rests on the soil the rate of deformation of the soil at a time t is related to the velocity dx/dt with which the base of the footing moves at the time t. Therefore it is assumed that the damping force is

$$P_d = c_d \text{ (gm cm}^{-1} \text{ sec)} \frac{dx}{dt} \qquad [11]$$

The spring bed shown in Figure 141*a* represents an imaginary substitute for the earth support of a footing. In order to introduce a damping force into the system which is independent of the elastic properties of the spring bed one can connect the

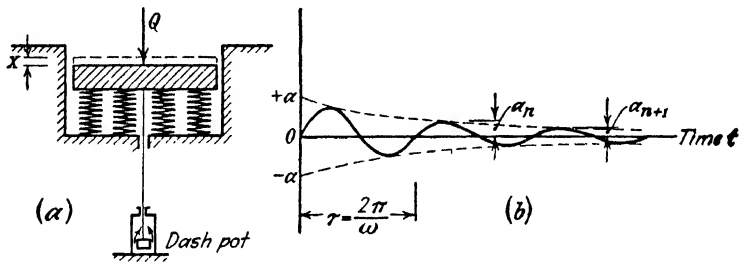

FIG. 142. (*a*) Spring-supported piston connected with dash pot for demonstrating damped free vibrations; (*b*) graphic representation of movement of piston.

block with a small piston surrounded by a viscous liquid which is contained in a stationary vessel, as shown in Figure 142*a*. Such vessels are known as *dash pots*. The damping force P_d exerted by the viscous liquid is approximately determined by equation 11. D'Alembert's principle requires that

$$\frac{W}{g}\frac{d^2x}{dt^2} + c_d\frac{dx}{dt} + c_s x = 0 \qquad [12]$$

The constant c_d has the dimension gm cm^{-1} sec and the dimension of the spring constant c_s is gm cm^{-1}. In order to establish uniformity in the dimensions of the coefficients it is customary to express the value c_s in terms of the circular frequency ω, equation 7, and to replace c_d by the term

$$c_d = 2\lambda\frac{W}{g} \qquad [13]$$

wherein the coefficient λ also has the dimension of a circular frequency, which is sec^{-1}. The coefficient λ is known as the *damping factor*. From equation 7 we get

$$c_s = \omega^2\frac{W}{g}$$

Replacing the values of c_d and c_s in equation 12 by those given above we obtain

$$\frac{d^2x}{dt^2} + 2\lambda \frac{dx}{dt} + \omega^2 x = 0 \qquad [14]$$

By solving this equation it has been found that the effect of the damping force on the vibrations depends on the value $\sqrt{\lambda^2 - \omega^2}$. (See for instance Timoshenko 1937.) If this value is real (high values of the damping force) the initial displacement does not produce any vibration at all. Instead of vibrating, the block slowly returns to its equilibrium position at a decreasing rate and reaches this position at time infinity. This is known as the *overdamped condition*. On the other hand, if $\sqrt{\lambda^2 - \omega^2}$ is imaginary (low values of the damping force) the sudden removal of the disturbing force causes the block to vibrate, but the period τ_d of the vibrations is slightly smaller than the natural period τ of the block. This is the normal case. Since the difference between the period τ_d of the vibration and the natural period τ of the block is very small, it will be disregarded and we assume $\tau_d = \tau$.

Figure 142*b* represents the relation between time and displacement for the normal case. If a_n and a_{n+1} are the amplitudes for any two successive oscillations the ratio a_n/a_{n+1} is a constant

$$\frac{a_n}{a_{n+1}} = \epsilon^{\tau\lambda}$$

or

$$\log a_n - \log a_{n+1} = \tau\lambda \qquad [15]$$

This value is called the *logarithmic decrement*. It expresses the intensity of the damping effect. The values a_n, a_{n-1}, and τ are obtained by direct measurement of the amplitude of the free vibrations of the block. Hence the value λ can be computed by means of the simple equation

$$\lambda \ (\text{sec}^{-1}) = \frac{1}{\tau} \log \frac{a_n}{a_{n+1}} \qquad [16]$$

157. Forced harmonic vibrations. The vibrations of a system are said to be forced if the impulse which causes the vibrations is repeated periodically. Pulsating storm winds and the vibrations of the base of a building due to pile-driving operations are examples of such periodic impulses. In order to explain the essential characteristics of forced vibrations we assume that the elastically supported block with a weight W, shown in Figure 143*a*, is acted upon in a vertical direction by a periodic impulse whose intensity is determined by the equation

$$Q = Q_1 \sin \omega_1 t \qquad [1]$$

If x denotes the vertical displacement of the block at time t, D'Alembert's principle requires that

$$\frac{W}{g} \frac{d^2x}{dt^2} + c_s x = Q_1 \sin \omega_1 t$$

wherein c_s is the spring constant of the elastic support. By means of

equation 156(2) one obtains for the vertical displacement a_1 produced by Q_1 the value

$$a_1 = \frac{Q_1}{c_s} \qquad [2]$$

whence

$$Q_1 = a_1 c_s$$

and

$$\frac{W}{g}\frac{d^2x}{dt^2} + xc_s = a_1 c_s \sin \omega_1 t \qquad [3]$$

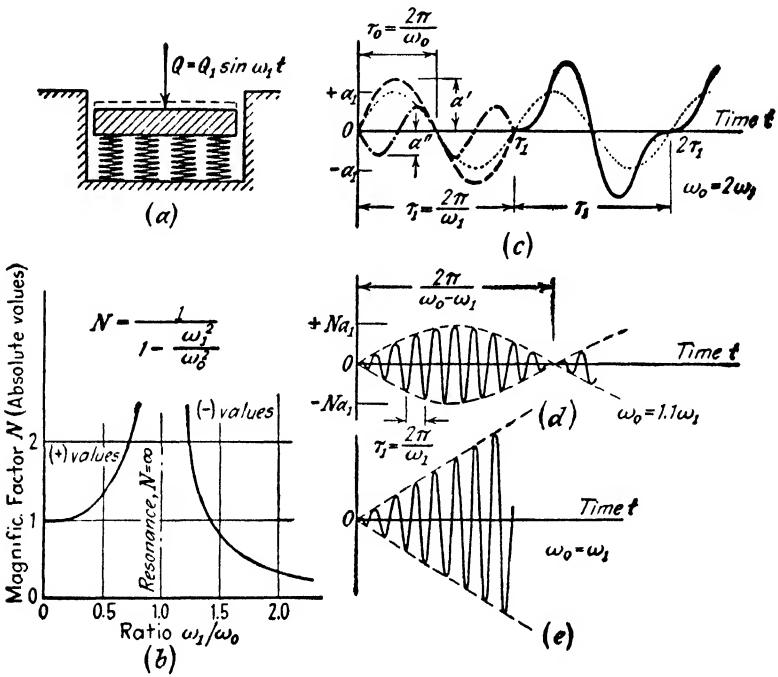

FIG. 143. (*a*) Piston on spring support with natural circular frequency ω_0 acted upon by periodic impulse to demonstrate undamped, forced vibrations; (*b*) relation between circular frequency ratio ω_1/ω_0 and magnification factor; (*c* to *d*) graphic representation of forced vibrations for three different values of circular frequency ratio.

Expressing the value c_s by means of equation 156(7) in terms of the natural circular frequency ω_0 of the block we get

$$\frac{d^2x}{dt^2} + \omega_0^2 x = a_1 \omega_0^2 \sin \omega_1 t \qquad [4]$$

The solution of this equation is

$$x = \frac{a_1}{1 - \omega_1^2/\omega_0^2}\left(\sin \omega_1 t - \frac{\omega_1}{\omega_0} \sin \omega_0 t\right) \qquad [5]$$

Equation 5 demonstrates that the vibration of the block can be resolved into two parts. The first one

$$x' = \frac{a_1}{1 - \omega_1^2/\omega_0^2} \sin \omega_1 t \qquad [6a]$$

is a forced vibration with a circular frequency ω_1 and an amplitude

$$a' = \frac{a_1}{1 - \omega_1^2/\omega_0^2} = Na_1 \qquad [6b]$$

wherein

$$N = \frac{1}{1 - \omega_1^2/\omega_0^2} \qquad [6c]$$

is called the *magnification factor*. Plotting the value N against the ratio ω_1/ω_0 we obtain the curve shown in Figure 143*b*. For $\omega_1/\omega_0 = 1$ its ordinate is equal to infinity. This is the *resonance condition* for the undamped forced vibration. The second part

$$x'' = \frac{a_1}{1 - \omega_1^2/\omega_0^2} \frac{\omega_1}{\omega_0} \sin \omega_0 t = a_1 N \frac{\omega_1}{\omega_0} \sin \omega_0 t \qquad [7a]$$

is a free vibration with a circular frequency ω_0 and an amplitude

$$a'' = a_1 N \frac{\omega_1}{\omega_0} \qquad [7b]$$

In order to illustrate the character of the resulting vibration the curves shown in Figure 143*c* have been plotted. They represent the vibrations of a spring-supported block whose natural circular frequency ω_0 is equal to twice the circular frequency of the impulse. The period of the impulse is $\tau_1 = 2\pi/\omega_1$. In the diagram the thin dotted line represents the vibration which the pulsating disturbing force Q would produce if it acted statically. On account of the dynamic action of this force the real vibration of the block is different. The heavy dashed curves shown within a distance τ_1 from the origin represent the two components of the real vibration and the plain curve located beyond a distance τ_1 represents the total real vibration.

An investigation of the influence of the ratio ω_1/ω_0 on the amplitude of the resulting vibrations by means of equation 5 leads to the following conclusions. When the frequency ω_1 of the impulse approaches the

natural frequency ω_0 of the system the vibration assumes the character of a vibration with a circular frequency ω_1 and a variable amplitude as shown in Figure 143*d*. This phenomenon is called *beating*. For $\omega_1 = \omega_0$ the period of the beats become equal to infinity. As a consequence the amplitude increases in simple proportion to time, as shown in Figure 143*e*, and approaches the value infinity. This figure illustrates the *phenomenon of resonance*. The resonance is due to the fact that each new impulse reaches the block exactly at the time when the block is in an extreme position. Thus the effect of the successive impulses is additive.

Equation 5 also discloses the following relation. If the ratio ω_1/ω_0 is very small, i.e., if the natural frequency of the system is very high compared with the frequency of the impulse, the magnification factor is equal to unity and the vibration of the system is identical with that of the impulse. On the other hand, for very high values of ω_1/ω_0 the magnification factor is almost equal to zero and the impulse produces a vibration with the circular frequency ω_0 and a very small amplitude, $a_1\omega_0/\omega_1$.

Furthermore, if the ratio ω_1/ω_0 is smaller than unity the magnification factor N (eq. 6*c*) is positive and if ω_1/ω_0 is greater than unity it is negative. This abrupt change of sign at $\omega_1/\omega_0 = 1$ has the following physical significance. If ω_1/ω_0 is less than unity the impulse and the forced vibration represented by equations 6 are synchronous. If ω_1/ω_0 is greater than unity, the impulse precedes the forced vibration by half a period. This time lag of the forced vibration is called a *phase difference*.

Since each of the two components of the resultant vibration is a simple harmonic vibration, each can be represented by the vertical component of the movement of the free end of a rotating vector (Figure 141*c*). If the two components of a vibration are not synchronous the rotating vectors which correspond to the components must form an angle, called the *phase angle*. A phase difference of half a period requires a phase angle π. Since the phase difference between the two components of an undamped, forced vibration is either equal to zero ($\omega_1/\omega_0 < 1$) or equal to half a period ($\omega_1/\omega_0 > 1$), an increase of the value ω_1/ω_0 beyond unity involves an abrupt increase of the phase angle from zero to π. For damped forced vibrations the phase angle increases gradually from zero to π. (See below.)

The greatest vertical pressure exerted by the periodic impulse on the spring bed is equal to

$$P'_a = a_{\max} c_s$$

wherein $a_{\max}$ is the greatest amplitude of the forced vibrations. Figure

143*c* shows that a_{max} cannot be greater than $a' + a''$, whence

$$P_a' \gtreqless P_a = (a' + a'')c_s$$

The value P_a represents an upper limiting value for P_a'. In the following computations it will be assumed that $P_a' = P_a$. The values of a' and a'' are given by equations 6*b* and 7*b* respectively. Substituting these values in the preceding equation one obtains

$$P_a = \pm N a_1 \left(1 + \frac{\omega_1}{\omega_0}\right) c_s$$

Since $a_1 = Q_1/c_s$ (eq. 2) one can write

$$P_a = \pm Q_1 N \left(1 + \frac{\omega_1}{\omega_0}\right) = \pm Q_1 \frac{1}{1 - \omega_1/\omega_0} \qquad [8]$$

wherein N is the magnification factor (eq. 6*c*) and ω_1/ω_0 is the ratio between the circular frequency of the impulse and the natural frequency of the block. The force P_a represents the greatest value of the pressure exerted by the impulse on the spring bed. Hence the total vertical pressure on the spring bed varies between the limits

$$W + P_a \quad \text{and} \quad W - P_a$$

Equation 8 shows that these limiting values depend not only on the magnitude of the disturbing force Q_1 but also on the ratio ω_1/ω_0.

If the block is connected with a dash pot, as shown in Fig. 142*a*, it is acted upon not only by the disturbing force Q (eq. 1), by the inertia force $\frac{W}{g}\frac{d^2x}{dt^2}$, and the reaction xc_s of the spring bed but also by the damping force

$$P_d = c_d \frac{dx}{dt} \qquad 156(11)$$

Since

$$c_d = 2\lambda \frac{W}{g} \qquad 156(13)$$

one can write

$$P_d = 2\lambda \frac{W}{g} \frac{dx}{dt}$$

wherein λ (sec $^{-1}$) denotes the damping factor. The force P_d must be added to the forces represented on the left-hand side of equation 3. Thus one obtains

$$\frac{W}{g}\frac{d^2x}{dt^2} + 2\lambda \frac{W}{g}\frac{dx}{dt} + xc_s = a_1 c_s \sin \omega_1 t$$

Expressing the value c_s by means of equation 156(7) in terms of the natural circular frequency ω_0 of the block we get

$$\frac{d^2x}{dt^2} + 2\lambda \frac{dx}{dt} + \omega_0^2 x = a_1 \omega_0^2 \sin \omega_1 t \qquad [9]$$

Like the vibration represented by equation 4, the vibration determined by the preceding differential equation consists of two parts, one free and one forced vibration. However, if damping takes place, the free vibration is rapidly obliterated by the damping force. Therefore it is customary to disregard the free vibration and to identify the total with the forced component

$$x = a_1 \frac{1}{\sqrt{\left[1 - \left(\frac{\omega_1}{\omega_0}\right)^2\right]^2 + \left(\frac{2\lambda}{\omega_0}\right)^2 \left(\frac{\omega_1}{\omega_0}\right)^2}} \sin\left[\omega_1 t - \arctan \frac{2\omega_1\lambda}{\omega_0^2 - \omega_1^2}\right] \qquad [10]$$

Introducing the symbols

$$N_1 = \frac{1}{\sqrt{\left[1 - \left(\frac{\omega_1}{\omega_0}\right)^2\right]^2 + \left(\frac{2\lambda}{\omega_0}\right)^2 \left(\frac{\omega_1}{\omega_0}\right)^2}} \qquad [11a]$$

and

$$\alpha = \arctan \frac{2\omega_1\lambda}{\omega_0^2 - \omega_1^2} \qquad [11b]$$

we obtain

$$x = a_1 N_1 \sin(\omega_1 t - \alpha) \qquad [11c]$$

This is the equation of a harmonic vibration whose frequency is equal to the frequency of the impulse. The value N_1 represents the magnification factor. The forced vibration lags behind the impulse, and the importance of the lag is determined by the phase angle α (eq. 11*b*). The amplitude of the forced vibration is

$$a = a_1 N_1 = \frac{a_1}{\sqrt{\left[1 - \left(\frac{\omega_1}{\omega_0}\right)^2\right]^2 + \left(\frac{2\lambda}{\omega_0}\right)^2 \left(\frac{\omega_1}{\omega_0}\right)^2}} \qquad [12]$$

Hence the greatest pressure exerted by the impulse on the spring bed is

$$P_a = c_s a = c_s a_1 N_1 = Q_1 N_1 \qquad [13]$$

wherein N_1 represents the magnification factor for damped, forced vibrations (eq. 11*a*).

The amplitude a (eq. 12) is a maximum for

$$\omega_1 = \omega_{1\,res} = \omega_0 \sqrt{1 - \tfrac{1}{2}\left(\frac{2\lambda}{\omega_0}\right)^2}$$

This is the condition for resonance. Introducing this value into equation 12 we obtain for the amplitude at resonance

$$a_{max} = a_1 \frac{1}{\frac{2\lambda}{\omega_0}\sqrt{1 - \frac{1}{4}\left(\frac{2\lambda}{\omega_0}\right)^2}}$$

Plotting the value N_1 (eq. 11*a*) against the ratio ω_1/ω_0 we obtain a curve similar to those shown in Figure 144*a* for values of $2\lambda/\omega_0 = 0.2$ and 0.5 respectively. The

figure shows that the value of ω_1/ω_0 for resonance is close to unity. Therefore it is customary to simplify the resonance condition by assuming that the circular frequency for resonance, $\omega_{1\,res}$, is equal to ω_0 or

$$\omega_{1\,res} = \omega_0 \qquad [14]$$

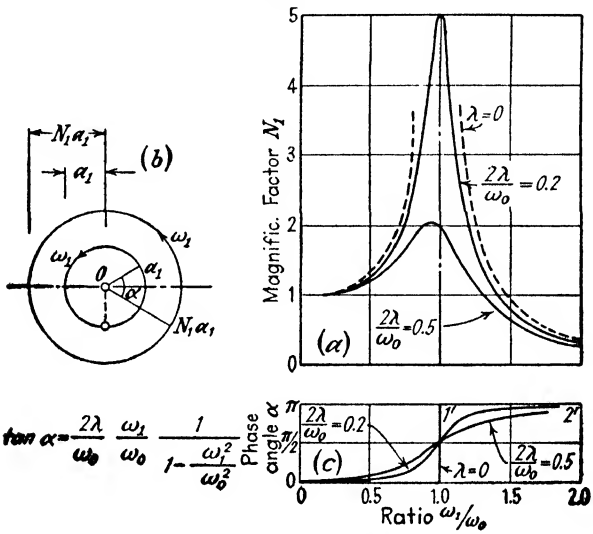

FIG. 144. Damped, forced vibration of spring-supported piston with natural circular frequency ω_0. (*a*) Magnification factor and (*c*) phase angle for three different values of damping factor λ, both plotted against circular frequency ratio ω_1/ω_0; (*b*) representation of vibration of piston by means of a rotating vector labeled N_1a_1.

The amplitude a_{max} is determined with sufficient accuracy by the equation

$$a_{max} = a_1 \frac{\omega_0}{2\lambda} \qquad [15]$$

At any time t the periodic disturbing force Q (eq. 1) is equal to

$$Q = Q_1 \sin \omega_1 t = a_1 c_s \sin \omega_1 t$$

If the spring bed were acted upon by no other force the vertical displacement at time t would be

$$y = \frac{Q}{c_s} = a_1 \sin \omega_1 t$$

The real displacements of the block are given by equation 11*c*,

$$x = a_1 N_1 \sin (\omega_1 t - \alpha)$$

These displacements are identical with the vertical component of the displacements of the moving ends of two vectors with a length a_1 and a_1N_1 respectively which rotate with a circular frequency ω_1, as indicated in Figure 144*b*. The angle between the two vectors is equal to the phase angle α. At any time t the distances

y and x are equal to the vertical distance between a horizontal axis through the center of rotation and the moving end of the vectors a_1 and $N_1 a_1$ respectively. Plotting the phase angle α (eq. 11*b*) against the values of ω_1/ω_0 we obtain a curve similar to those shown in Figure 144*c* for values of $2\lambda/\omega_0 = 0.2$ and 0.5 respectively. For $\lambda = 0$ (undamped vibration) we obtain the vertical line labeled $\lambda = 0$ instead of a curve. This line expresses the abrupt increase of the phase angle at $\omega_0/\omega_1 = 1$ from zero to π, associated with undamped, forced vibrations.

158. Coefficient of dynamic subgrade reaction. In Article 156 it was demonstrated that the spring constant c_s and the coefficient of subgrade reaction k_s of the spring bed shown in Figure 141*a* are connected by the simple relation

$$c_s = Ak_s$$

or

$$k_s = \frac{c_s}{A} \qquad [1]$$

wherein A is the area of the base of the block. According to the theory of subgrade reaction (Chapter XVI) the spring bed shown in Figure 141*a* represents the mechanical equivalent of a real earth support. In reality the analogy is very incomplete because the value k_s for a uniform spring bed is independent of the size of the loaded area, whereas the value k_s for an earth support depends on the size of the loaded area and on several other factors which are independent of the elastic properties of the soil (see Art. 124).

However, at the time when the theory originated it was generally believed that k_s (eq. 1) was a constant not only for a given spring bed but also for a given soil and that the settlement of a foundation could be determined if k_s was known. Therefore the simple theoretical relation expressed by equation 1 suggested the idea of determining the value of the coefficient of subgrade reaction k_s of a given soil by means of a vibration test. This can, for instance, be done by placing a thick steel disk on the surface of the soil, subjecting the disk to a pulsating force with a variable frequency, and measuring the amplitude of the forced vibrations produced by the impulse. The disk and the source of the impulse together constitute a *vibrator*. According to Article 157 the amplitude of the vibrator is greatest if the frequency f of the impulse is equal to the natural frequency f_0 of the vibrator. From equation 156(10) we obtain

$$f_0 = \frac{\omega_0}{2\pi} = \frac{1}{2\pi}\sqrt{\frac{c_s g}{W}} \qquad [2]$$

whence

$$c_s = 4\pi^2 f_0^2 \frac{W}{g}$$

and

$$k_s = \frac{c_s}{A} = \frac{4\pi^2}{A} f_0^2 \frac{W}{g}$$

wherein A is the area of the base of the vibrator and W the weight of the vibrating system.

The weight W in equation 3 is equal to the sum of the known weight W_1 of the vibrator and the unknown weight W_s of the body of soil which participates in the vibrations of the system. Hence we can write

$$k_s = \frac{4\pi^2}{A} f_0^2 \frac{W_1 + W_s}{g} \qquad [3]$$

The experimental method of estimating the unknown weight W_s will be described below.

Equation 3 is based on the tacit assumption that the weight W_s of the vibrating soil constitutes part of the weight of the rigid vibrator and that the seat of the forces of elastic restitution has no weight. In reality the system operates rather like a rigid mass with a weight W_1 (weight of the vibrator) supported by springs with a weight W_s. In order to get a more accurate conception of the interaction between the vibrator and the supporting soil it is necessary to take into consideration the mass forces which act on the soil located beneath the base of the vibrator. This has been accomplished by E. Reissner (1936) on the simplifying assumption that the vibrator rests on the horizontal surface of a semi-infinite elastic-isotropic mass. However, no attempt has yet been made to apply the results of this analysis to the practice of vibrator investigations.

In spite of the inconsistencies in the theoretical concepts on which the interpretation of the test results was based the investigation of soils by means of vibrators brought out various facts of considerable practical importance. The following is a summary of the results which have been obtained to date.

The natural frequency of a vibrator with a given weight and a given base area is directly related to the elastic properties of the subgrade. The more compact and less compressible is the subgrade the greater is the spring constant. Therefore vibrators can be and have been successfully used to determine the relative degree of compaction of artificial fills consisting of sandy soil. For similar reasons there is a definite relation between the natural frequency of the vibrator and what is considered on the basis of general construction experience the allowable bearing value for sandy subgrades. The following data abstracted from Lorenz (1934) illustrate this relationship.

TYPE OF SOIL	FREQUENCY f IN SEC^{-1}	ALLOWABLE BEARING VALUE IN TONS/SQ. FT.
Loose fill	19.1	1.0
Dense artificial cinder fill	21.3	1.5
Fairly dense medium sand	24.1	3.0
Very dense mixed-grained sand	26.7	4.5
Dense pea gravel	28.1	4.5
Limestone	30	—
Hard sandstone	34	—

The natural frequencies given in the table are those obtained by means of a vibrator with a weight of 6000 pounds whose base covers an area of about 11 square feet. The results of seismic observations suggest that every mass of soil with fairly well defined boundaries has a natural frequency of its own. However, this frequency is not identical with the natural frequency obtained by a vibrator test on the surface of such a mass (Ramspeck 1938).

In connection with the table it should be emphasized that both the frequencies and the allowable bearing values apply only to the general characteristics of the subgrade and not to a definite settlement, because the settlement of an area which carries a given unit load depends on several factors other than the mechanical properties of the subgrade (see Art. 142).

It has been found that the values of k_s obtained by means of equation 3 are consistently considerably larger than those obtained by means of static loading tests on the same area. For this reason the ratio between unit load and settlement determined by means of a vibrator test will be designated by another symbol

$$d_s = \frac{c_s}{A} \qquad [4]$$

The value d_s is called the *coefficient of dynamic subgrade reaction.* It represents the dynamic equivalent of the coefficient of subgrade reaction k_s (eq. 124(1)). When applied to the computation of the settlement $\Delta\rho$ produced by a change Δp of the vertical pressure, equation 124(1) is valid only for positive values of Δp, because the settlement ρ in this equation includes both the reversible and the permanent settlement. On the other hand equation 4 is valid for both increase and decrease of the pressure.

Information regarding the influence of different variables, such as the size of the loaded area on the value of the coefficient of dynamic subgrade reaction d_s, is still rather incomplete. Lorenz (1934) states that the influence of the size of the loaded area on the value of d_s for sand is insignificant. On the other hand, according to Figure 10 in Seismos (no date), which represents the results of field tests on dense, loamy pea gravel, an increase of the loaded area from 0.25 to 1.00 square meter was

associated with an increase of d_s from 15 to 23 kg cm^{-3} at a unit load of 0.6 kg cm^{-2} and from 27 to 34 kg cm^{-3} at 1.5 kg per square centimeter. These figures also imply that d_s increased with increasing values of the unit load whereas the coefficient of static subgrade reaction k_s usually decreases with increasing unit load. According to Figure 5 in Lorenz (1934) the value of d_s for sand also decreases with increasing unit load.

If the frequency of the impulses imparted to a soil by a vibrator increases, the settlement of the base of the vibrator begins to increase rapidly as soon as the frequency f_1 becomes greater than about one half or two thirds of the natural frequency f_0 of the soil-vibrator system. As the frequency approaches the value f_0 the settlement of the base of the vibrator becomes many times greater than the settlement corresponding to the static equivalent of the inertia pressure involved. The range of frequencies within which the impulse produces excessive settlement will be referred to as the *critical range*. The critical range seems to include the frequencies between about $0.5 f_0$ and $1.5 f_0$ and to be fairly independent of the size of the vibrator. Hence if the frequency of the vibrations of a foundation on sand are within the critical range for the frequency of a vibrator operating on the same sand, excessive settlement should be anticipated. The knowledge of the relation between frequency and settlement became a vital factor in the design of the foundation for rapidly revolving machines on sand strata. It was also instrumental in the development of heavy machinery for artificially compacting sandy fills.

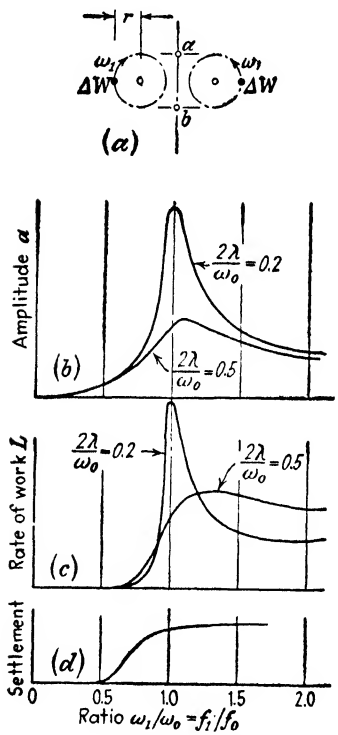

FIG. 145. (*a*) Diagram illustrating principle of Degebo vibrator; (*b* to *d*) illustrate the influence of the frequency ratio on amplitude, rate of work, and settlement.

Most of the aforementioned investigations have been carried out since 1930 by the Degebo (Deutsche Gesellschaft für Bodenmechanik). The same institution has worked out the theory of the procedure (Degebo 1933). The reports on the test results are not easily accessible, and very little has been published in English. The following review of the theory and practice of the procedure is entirely based on the publications of the Degebo.

The vibrator developed by the Degebo produces periodic impulses by means of two equal weights ΔW which rotate about parallel axes in opposite directions in such a manner that the common center of gravity of the two weights moves up and down on a vertical line between the extreme positions a and b, as shown in Figure 145a. The number of revolutions, f_1 per unit of time, of the weights can be varied between wide limits. According to equations 156(10) the circular frequency of the periodic impulse produced by the weights is

$$\omega_1 = 2\pi f_1 \qquad [5]$$

and the period is

$$\tau = \frac{1}{f_1} = \frac{2\pi}{\omega_1} \qquad [6]$$

Each of the rotating weights is acted upon by a centrifugal force

$$\tfrac{1}{2}Q_1 = \frac{\Delta W}{g}\omega_1^2 r$$

wherein g is the acceleration of gravity and r the eccentricity. At a given number of revolutions the force Q_1 can be varied by changing the eccentricity r of the rotating weights. Since the two weights rotate synchronously in opposite directions, the horizontal components of the centrifugal forces cancel each other and the vertical ones represent a periodic disturbing force with the intensity

$$Q = Q_1 \sin \omega_1 t = \frac{2\Delta W}{g} r\omega_1^2 \sin \omega_1 t = C\omega_1^2 \sin \omega_1 t \qquad [7a]$$

wherein

$$C = \frac{2\Delta W}{g} r \qquad [7b]$$

is a constant which depends only on the design of the vibrator and on the eccentricity r. The rotating weights are mounted on a heavy base plate covering an area A. The total weight of the base plate and of the machinery supported by the plate is W_1. The pulsating force Q (eq. 7a) produces a forced, damped vibration in a vertical direction not only of the vibrator but also of the soil located immediately below the vibrator. According to definition the spring constant c_s in the differential equation of the process, 157(9), is equal to the force required to produce a reversible displacement equal to unity of the center of gravity of the vibrating system in the direction of the vibration. The load per unit of area required to produce a reversible settlement equal to unity of the surface of the subgrade is equal to the coefficient of dynamic subgrade reaction d_s. Therefore the spring constant for a vibrator with a base plate covering an area A is

$$c_s = d_s A$$

provided we tolerate the assumption that the vertical displacement of the center of gravity of the vibrating system is identical with the displacement of the base of the vibrator. The weight W of the vibrating mass is equal to the sum of the weight W_1 of the vibrator and the weight W_s of the body of soil which participates in the movement of the vibrator. Substituting into equation 156(7)

$$c_s = d_s A, \quad W = W_1 + W_s$$

and solving for ω_0 we obtain for the natural circular frequency of the

system the value

$$\omega_0 = \sqrt{\frac{d_s A g}{W_1 + W_s}} \qquad [8]$$

On account of the damping properties of the subgrade the impulse $Q_1 \sin \omega_1 t = C\omega_1^2 \sin \omega_1 t$ (eq. 7a) produces forced vibrations with viscous damping. The reversible part of the settlement produced by a static load $Q_1 = C\omega_1^2$ is

$$a_1 = \frac{C\omega_1^2}{c_s} \qquad [9]$$

This value represents the displacement which the maximum disturbing force Q_1 would produce statically. Substituting the value given by equation 9 for a_1 in equation 157(12), we obtain for the amplitude a of the resulting forced vibration at a given circular frequency ω_1 of the impulse

$$a = \frac{C\omega_1^2}{c_s} N_1 \qquad [10]$$

wherein N_1 is the magnification factor (eq. 157(11a)). The observer records the frequency

$$f_1 = \frac{\omega_1}{2\pi}$$

Expressing ω_1 in equation 10 in terms of the frequency f_1 we get

$$a = \frac{4\pi^2 C N_1}{c_s} f_1^2$$

Plotting the values of a against the value of the ratio $f_1/f_0 = \omega_1/\omega_0$ we obtain a curve similar to those shown in Figure 145b for two different values of the ratio $2\lambda/\omega_0$ (see Art. 157). The resonance condition is approximately satisfied if $f_1/f_0 = \omega_1/\omega_0 = 1$ (see eq. 157(14)).

Another record which is kept by the observer is the work per unit of time required to operate the vibrator. This work consists of two parts. One part is used up in overcoming the friction in the bearings and other resistances within the mechanism. It has been found that this part increases approximately in direct proportion to the square of the frequency. The second part is consumed by the viscous resistance of the soil against periodic deformation. The damping force is determined by equation 156(11)

$$P_d = c_d \frac{dx}{dt}$$

At any time t the distance between the center of gravity of the vibrating system and its equilibrium position is equal to

$$x = a_1 N_1 \sin (\omega_1 t - \alpha) \qquad 157(11c)$$

its velocity is

$$\frac{dx}{dt} = a_1 N_1 \omega_1 \cos (\omega_1 t - \alpha)$$

and the damping force is

$$P_d = c_d \frac{dx}{dt} = c_d\, a_1 N_1 \omega_1 \cos(\omega_1 t - \alpha)$$

The work performed in overcoming the damping force during one complete cycle with the period $\tau = 1/f_1$ is

$$L_\tau = \int_0^\tau P_d \frac{dx}{dt}\, dt = c_d\, a_1^2 N_1^2 \omega_1 \pi$$

and the work per unit of time is

$$L = f_1 L_\tau = \pi c_d\, a_1^2 N_1^2 \omega_1 f_1$$

Substituting in this equation

$$\omega_1 = 2\pi f_1 \qquad \text{(eq. 5)}$$

and

$$a_1 = \frac{C\omega_1^2}{c_s} = \frac{4\pi^2 f_1^2 C}{c_s} \qquad \text{(eq. 9)}$$

we obtain

$$L = 32\pi^6 C^2 N_1^2 \frac{c_d}{c_s^2} f_1^6 \qquad [11]$$

The value C is determined by equation 7*b* and the value N_1 by equation 157(11*a*). According to equation 156(13) the value c_d is equal to $2\lambda W/g$, wherein λ is the damping factor and W the weight of the vibrating system.

Plotting the rate of work L against the ratio f_1/f_0 we obtain a curve similar to those shown in Figure 145*c* for two different values of $2\lambda/\omega_0$. With increasing values of $2\lambda/\omega_0$ the peak of the amplitude curve in Figure 143*b* moves toward the right and the peak of the work curve becomes lower and flatter.

A third characteristic curve which can be obtained by means of the vibrator observations is the phase angle curve. The phase angle curves are similar to those shown in Figure 144*c* for values of $\lambda > 0$. Since the equation for the phase angle (eq. 157(11*b*)) contains the damping factor λ, the shape of the phase angle curve is to a certain extent indicative of the damping properties of the soil on which the vibrator operates.

When performing a vibrator test the experimenter plots the amplitudes, the rate of work, and the phase angle against the frequency f_1 of the vibrator. He also measures the total settlement of the base of the vibrator at different frequencies.

Since the natural frequency f_0 of the vibrator is approximately equal to the frequency f_1 at resonance which is equal to the abscissa of the peak of the frequency-amplitude curve one can compute d_s by substituting $f_0 = f_{1\,\text{res}}$ in equation 3, provided the weight W of the vibrating system is known. This weight is equal to the sum of the weight W_1 of the vibrator and the weight W_s of the body of soil which participates in the vibrations of the system. In order to estimate the weight W_s the observer increases the weight of the vibrator by means of a surcharge and repeats the test, whereupon the natural circular frequency of the system decreases from ω_0 to ω_0'. Assuming for the sake of simplicity that the increase of the weight of the vibrator has no effect on the weight W_s he obtains a second equation which makes it possible to compute W_s.

On the basis of the results of such an operation, involving the increase of the

weight of a vibrator from 1.8 to 3.3 tons, it was found that the weight W_s was equal to 12.5 tons (Lorenz 1934). The base of the vibrator covered an area of 3 square feet. Another set of tests mentioned toward the end of the same paper indicated that W_s was equal to not more than 1 ton. The weight of the vibrator was increased from 2.0 to 2.7 tons. The area covered by the base of the vibrator was apparently equal to 11 square feet. The soil conditions are not specified. These results seem to indicate that the weight W_s is likely to vary between wide limits. Since the method of computing the weight W_s is rather unreliable the results of the investigations can only be used for estimating the extreme values between which W_s may range. By means of these values one computes an upper and lower limit for the value d_s of the coefficient of dynamic subgrade reaction. These values represent the statistical average for the upper and lower limit of the value d_s of the soil located within the seat of the forces of elastic restitution. Considering that the weight W_s of the soil which participates in the vibrations of a vibrator with a base up to 11 square feet in area does not exceed about 15 tons the depth of this seat is hardly greater than about 7 feet and it may be considerably less. The elastic properties of the strata located at a greater depth have no influence on the test result unless the strata are abnormally loose or almost liquid. In order to get information on the elastic properties of stratified deposits with an appreciable depth it is necessary to combine the vibrator method with seismographic observations as described in Article 163. In no case can the results of vibrator tests be used as a basis for computing settlement due to consolidation, because there is no relation between the soil properties revealed by the vibrator tests and the coefficient of compressibility a_{vc} (eq. 98(1)). At the very best the observations can disclose the existence of compressible beds of clay beneath the site, before any borings are made.

The value of the damping factor λ can be computed by combining equation 11 with equation 156(13). A value of λ in excess of about 3 or 4 sec^{-1} combined with an important settlement of the base of the vibrator is considered an indication of high compressibility and sensitivity to vibrations (Lorenz 1934).

The Degebo vibrators are constructed in such a way that the periodic impulse can be applied either in a vertical or in a horizontal direction. The data obtained while subjecting the vibrator to a horizontal periodic impulse have been used for determining the coefficient of dynamic subgrade shear reaction d_T. This coefficient represents the force per unit of area of the base of the vibrator required to produce a reversible horizontal displacement of this area through a distance equal to unity (Lorenz 1934). This coefficient together with the coefficient d_s is used in connection with the computation of the natural frequency of engine foundations, described in Article 160.

159. Natural frequency of a water tower. On account of the possibility of resonance effects, the effect of periodic impulses, such as those produced by heavy street traffic or by earthquakes, on structures and their foundations depends to a large extent on the ratio between the frequency of the impulse and the natural frequency of the structures. In order to illustrate the influence of the elastic properties of the subgrade on the natural frequency of superimposed structures we investigate the vibrations of the water tower shown in Figure 146 under the influence of a single impulse. The tower rests on four footings and the impulse acts on the tank in a horizontal direction in one of the planes of symmetry of the tower.

The greatest part of the mass of the tower is concentrated in the tank. The possibility of a relative displacement between the center of gravity of the water and that of the container complicates the problem very considerably (Ruge 1938). However, for practical purposes, according to Williams (1937), one can consider the tower a single mass system provided one assigns to the water only about three quarters of its real weight. Therefore we neglect the mobility of the water contained in the tank; we also neglect the weight of the framework which supports the tank and assume that the effective weight W of the tank (weight of the container plus three quarters of the weight of the water) is concentrated in the center of gravity O_g of the tank.

The natural frequency of the tower with respect to the vibrations produced by the impulse depends on the elastic properties of the soil beneath the footings and on those of the framework which supports the tank. One extreme possibility is that the displacements due to the elastic deformation of the soil are negligible compared to those due to the elastic deformation of the framework. In this case the tower acts like a mass point attached to the upper end of a flexible vertical rod whose lower end is fixed. The vibrations of a tower with such characteristics have been investigated by Williams (1937). The second extreme possibility is that the tower is a rigid structure resting on an elastic subgrade. Since we are exclusively interested in the interaction between subgrade and structure only the second possibility will be considered.

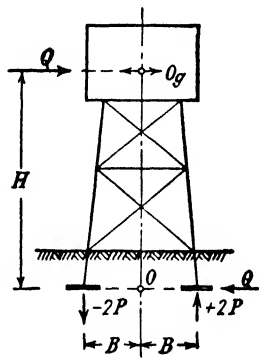

FIG. 146. Vertical section through rigid water tower on perfectly elastic foundation.

If one assumes that the center O of the base of the tower maintains its position the tower represents a single mass system with one degree of freedom. The system can only vibrate parallel to the plane of the drawing by oscillating around a horizontal axis through O (Fig. 146). It is further assumed that the coefficient of dynamic subgrade reaction d_s has been determined by means of a vibrator test. The impulse produces an overturning moment M about the axis of rotation through O. This moment increases the total pressure on the two footings on the right-hand side of O by $2P$ and reduces that on the two others by the same amount. Equilibrium requires that

$$M = 4PB$$

or

$$P = \frac{M}{4B}$$

If A is the area of the base of one footing the pressure P produces a vertical displacement of the footings of

$$\pm\rho = \pm\frac{P}{A}\frac{1}{d_s} = \pm\frac{M}{4AB}\frac{1}{d_s}$$

It is associated with an angular displacement of the tower through an angle

$$\delta = \frac{\rho}{B} = \frac{M}{4AB^2}\frac{1}{d_s}$$

about the axis of rotation through O. Since the tower is rigid and the axis is stationary the vertical axis OO_g of the tower swings through the same angle and the center of gravity O_g of the tower moves through a distance

$$x = \delta H = \frac{MH}{4AB^2}\frac{1}{d_s}$$

On account of the small value of δ the displacement x is almost horizontal and rectilinear. For an estimate one can assume that every particle of the tank moves through the same horizontal distance, δH. This assumption reduces the problem to one involving linear vibrations. In order to determine the corresponding spring constant c_s we make

$$M = QH$$

or

$$Q = \frac{M}{H}$$

wherein Q is a horizontal force which passes through the center of gravity O_g of the tank. The moment produced by Q about the axis of rotation through O is equal to the impulse moment M. Since we assumed that every particle of the tank moves simultaneously through the same horizontal distance x the spring constant c_s is equal to the force required to move the tank through a horizontal distance 1 (see Art. 156 and eq. 156(2)), whence

$$c_s = \frac{Q}{x} = 4A\frac{B^2}{H^2}d_s$$

Introducing this value into equation 156(7) one obtains for the natural circular frequency

$$\omega_0 = \frac{2B}{H}\sqrt{\frac{A}{W}g\,d_s}$$

The natural frequency (eq. 156(10)) is

$$f_0 = \frac{\omega_0}{2\pi} = \frac{B}{\pi H}\sqrt{\frac{A}{W} g\, d_s}$$

The static pressure per unit of area of the base of the footings is

$$q = \frac{W}{4A}$$

whence

$$f_0 = \frac{\sqrt{g}}{2\pi}\frac{B}{H}\sqrt{\frac{d_s}{q}} \qquad [1]$$

From this equation one can draw the following conclusions regarding the natural frequency of a rigid tower representing a single mass system with one degree of freedom. The softer the supporting soil the lower is the frequency f_0. In order to increase the frequency of a tower with a given height one must increase the width of the base of the tower or reduce the unit pressure on the base of the footings.

If the frequency of a periodic impulse on the tower resting on a mass of sand is within the critical range for the sand the impulse is likely to increase the permanent settlement of the tower regardless of the natural frequency of the tower. If it is also close to the natural frequency of the tower, resonance occurs which is likely to produce severe supplementary stresses in the members of the supporting framework.

It is common practice to judge the effect of periodic impulses such as earthquake shocks on structures without considering the influence of the natural frequency of the structure on the amplitude of the vibrations. Such a procedure is justified only if the frequency of the impulse is very much greater or smaller than the natural frequency of the structure (see Art. 164). Otherwise the results can be very misleading.

160. Natural frequency of engine foundations. Every engine is a source of a periodic impulse. The frequency f_1 of the impulse is equal to the number of complete cycles or revolutions of the engine. If the frequency of the impulse is equal to the natural frequency of the foundation, resonance occurs. As a consequence the base of the engine vibrates excessively. The vibrations are transmitted to the soil and are likely to cause damage to neighboring buildings. In order to eliminate the danger of resonance and of its harmful effects the foundation for an engine should be designed in such a way that its natural frequency is much smaller or much greater than the frequency of the impulse. When choosing the factor of safety with respect to resonance it is necessary to consider the degree of accuracy with which the natural frequency of

the foundation can be computed. This degree is very different for different types of foundation.

If the foundation of an engine consists of a massive block or of a cellular structure with massive walls, the natural frequency can be computed on the assumption that the foundation represents a single mass system on an elastic support. In order to obtain a uniform distribution of the static pressure on the supporting soil the base of the foundation is laid out in such a way that the center of gravity of the stationary masses is located on a vertical line through the center of gravity of the base. Furthermore engines are usually installed in such a manner that their plane of symmetry coincides with the plane of symmetry of the foundation. If the impulse acts on such a system in a vertical line through the center of gravity of the base, the vibrations occur only in a vertical direction similar to those of the block shown in Figure 141*a* and the system has only one natural frequency f_0. The value f_0 is determined by the equation

$$f_0 = \frac{1}{2\pi}\sqrt{\frac{c_s g}{W}} \qquad 156(10)$$

wherein W is the weight of the vibrating system and c_s is the spring constant. If the foundation rests on the soil, the weight W is equal to the sum of the weight W_1 of the loads which rest on the soil (weight of the engine and of the foundation) and the weight W_s of the body of soil which participates in the vibrations of the foundation, whence

$$f_0 = \frac{1}{2\pi}\sqrt{\frac{c_s g}{W_1 + W_s}} \qquad [1]$$

In order to avoid the condition of resonance the foundation should be so designed that f_0 is smaller or greater than the frequency of the impulse. The greater the difference between these two frequencies the smaller is the magnification factor N (eq. 157(6*c*)) which determines the amplitude of the forced vibrations of the foundation. If f_1 is greater than f_0 or

$$\frac{f_1}{f_0} = \frac{\omega_1}{\omega_0} > 1$$

the magnification factor N approaches the value zero with increasing values of $f_1/f_0 = \omega_1/\omega_0$, as shown in Figure 143*b*. On the other hand, if f_1 is smaller than f_0 the magnification factor approaches with decreasing values of the ratio $f_1/f_0 = \omega_1/\omega_0$ the value unity. Hence if possible the foundation is so designed that its natural frequency f_0 is smaller than f_1.

The only disadvantage of the condition $f_0 < f_1$ is that the starting and the stopping of the engine temporarily establishes resonance. However, the resonance occurs at a low frequency of the impulse and it has a very short duration. Experience has shown that this temporary resonance is harmless.

If $f_0 < f_1$ the weight W_s of the soil reduces the value f_0 and the danger of resonance. Therefore, if $f_0 < f_1$ one usually disregards the weight W_s and writes

$$f_0 = \frac{1}{2\pi}\sqrt{\frac{c_s g}{W_1}}$$

In this equation W_1 represents the weight of the foundation and of the stationary parts of the engine. Substituting $c_s = A d_s$ (eq. 158(4)), one gets

$$f_0 = \frac{\sqrt{g}}{2\pi}\sqrt{\frac{A}{W_1} d_s} \qquad [2]$$

wherein A is the area of the base of the foundation and d_s is the coefficient of dynamic subgrade reaction. The total pressure on the foundation is equal to the sum of the static weight W_1 and of the inertia force $\pm P_a$. If the damping force is negligible the value of P_a is given by equation 157(8). Otherwise it is determined by equation 157(13). The total pressure on the base of the foundation varies periodically between $W_1 + P_a$ and $W_1 - P_a$. Since the influence of a pulsating load on the settlement is greater than that of a constant load it is customary to design the foundation on the assumption that the greatest total pressure on the subgrade is equal to

$$Q = W_1 + 3P_a$$

The greatest unit pressure is

$$q = \frac{Q}{A} = \frac{W_1 + 3P_a}{A}$$

per unit of area (Rausch 1936). This load should not exceed the allowable bearing value q_a for the soil, whence

$$A = \frac{W_1 + 3P_a}{q_a}$$

Introducing this value into equation 2 we obtain

$$f_0 = \frac{\sqrt{g}}{2\pi}\sqrt{\frac{W_1 + 3P_a}{W_1}\frac{d_s}{q_a}} \qquad [3]$$

In centimeter-gram-second units g is equal to 981 cm sec^{-2} and

$$f_0 \text{ (sec}^{-1}) = 5\sqrt{\frac{W_1 + 3P_a}{W_1}}\sqrt{\frac{d_s}{q_a}}$$

For sand the ratio $\frac{d_s}{q_a}$ (cm^{-1}) ranges between about 2 for loose sand and about 3 for dense sand. The corresponding range for f_0 is

$$f_0 \text{ (sec}^{-1}) = (7 \text{ to } 9)\frac{W_1 + 3P_a}{W_1}$$

or

$$f_0 \text{ (min}^{-1}) = (420 \text{ to } 540)\frac{W_1 + 3P_a}{W_1}$$

These equations show that the condition $f_1/f_0 > 1$ can only be satisfied if the frequency of the impulse is very high. If it is medium or low one may try to design the foundation in such a way that its natural frequency f_0 is considerably higher than f_1. If this attempt is not successful it is necessary to insert between the engine and the base of the foundation either an elastic layer, for instance made out of cork, or else a spring support. If the elastic support of the foundation is merely due to the elasticity of the supporting soil, the natural frequency f_0 is given by equation 1, which contains the weight W_s of the body of soil participating in the vibrations of the system. By neglecting W_s in the design of a system whose natural frequency f_0 should be higher than f_1 one overestimates the safety with respect to resonance. Hence if $f_0 > f_1$ the weight W_s must be taken into consideration. The uncertainties involved in estimating W_s should be compensated by an ample margin of safety.

The preceding analysis merely served as an elementary introduction into the principles of the design of engine foundations. It is based on the assumption that the aggregate acts like a single mass system with one degree of freedom. In practice the conditions of impulse and support are always such that the aggregate acts like a system with as many as six degrees of freedom which involve up to six different values for the natural frequency (see Art. 155). Each one of these frequencies should satisfy the condition that it is lower or higher than the frequency of the impulse. The equations for computing the frequencies are available (see for instance Rausch 1936). All these equations contain the spring constants of the elastic supports. In order to find out whether resonance can be avoided without artificial means, such as spring supports, one

needs to know the coefficient of subgrade reaction for both vertical and horizontal loads.

According to Article 158 the value of the coefficient of subgrade reaction depends on several factors other than the nature of the subgrade. In order to determine this coefficient one should use a vibrator which permits variation of the test conditions, such as the unit pressure on the base of the vibrator and the intensity of the impulse. The value corresponding to the full-sized foundation is obtained by extrapolation (Seismos, no date). On account of the uncertainties involved in this process the results should be given in the form of a range of values.

If the frequency of the impulse exerted by an engine founded on a stratum of sand is within the critical range for the sand, even very gentle vibrations are likely to cause important settlement of both the foundation of the engine and of adjacent structures. Everything else being equal, the settlement increases rapidly with decreasing density of the sand. In order to avoid excessive settlement on loose or medium sand one should not only provide an ample margin of safety with respect to resonance but one should also increase the density of the sand by means of piles.

At present one of the most important motors is the steam turbine. In the early days of steam turbine construction little attention was paid to the effect of the inevitable unbalance of the rotating parts until the owners complained about foundation defects. At that time the influence of the natural frequency of the foundations on the mechanical effect of the disturbing force was not yet appreciated. Therefore the manufacturers tried to remedy the situation by steadily increasing the requirements concerning the solidity and the mass of the foundations, which led to very clumsy and uneconomical constructions. Rational methods of design were not developed until the natural frequency of the foundations received the attention which it deserved.

The following abstract from German standard specifications for the foundation of steam turbines illustrates the importance which is attributed to the natural frequency of the foundation. If the natural frequencies of the foundation have not been computed or if the difference between the number of revolutions n of the turbine and one of the frequencies is smaller than $\pm$ 30 per cent of n the designer is required to assume that the members of the support of the turbine are acted upon by a centrifugal force Q_1 equal to 20 times the weight of the rotating parts. For differences between 30 and 50 per cent the centrifugal force can be assumed to be equal to 10 times the weight of the rotating parts, and for differences in excess of 50 per cent equal to 5 times this weight (Ehlers 1934).

Steam turbines are supported either by rigid or by elastic structures such as heavy slabs resting on relatively flexible columns, as shown in Figure 147. The foundations of the rigid type can be designed by means

of the method whose principles were explained in the first part of this article.

The design of the elastic type of foundation (Fig. 147) is usually based on the assumption that the earth support is rigid and that the seat of the periodic deformations produced by the disturbing agent resides

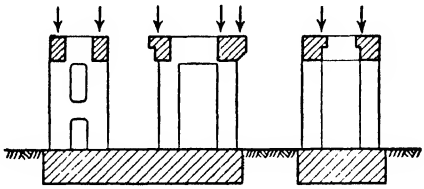

FIG. 147. Simplified vertical sections through table-support for turbo-generator.

exclusively in the columns which transfer the weight of the aggregate onto the base plate. Foundations of this type represent the equivalent of foundations on a spring support, and the elastic properties of the soil have no bearing on the design.

161. Waves and wave transmission. The vibrations which have been discussed in the preceding articles occur in closed systems. If an elastically supported system is rigid, all the points of the system pass simultaneously through the equilibrium position, provided it has only one degree of freedom. However, in addition to vibrating in itself, the system represents the center of a vibratory disturbance which proceeds like a sound wave from the center into the subgrade in every radial direction. It imparts to the subgrade the capacity of producing forced vibrations in structures resting on the subgrade at a considerable distance from the center of the disturbance. The event which starts the disturbance is the impulse. The duration of the impulse may be very short, as is that of the impulse produced by an explosion or an earthquake. In this case the intensity of the waves produced by the impulse dies out on account of viscous damping. On the other hand a periodic impulse, such as that produced by operating machines, pile-driving operations, or street traffic, maintain a permanent state of vibration.

The general characteristics of the waves have been discussed in Article 155. A line which intersects all the consecutive wave fronts at right angles is called a *line of wave propagation*. A particle a on such a line (Fig. 148a) starts to vibrate at the instant when the wave front passes through the particle. At the time when the particle a has completed its first cycle with a period τ the wave front has arrived at a distance

$$l = \tau v \qquad [1]$$

from particle a. The length l is called the *wave length* and v is the velocity of wave propagation.

The type of vibration produced by an impulse and the velocity v of wave propagation depend essentially on the elastic properties of the medium through which the wave travels and on the location of the surfaces of discontinuity with reference to the center of the impulse. The theories dealing with these relations are based on the fundamental equations of the theory of elasticity and involve the most advanced methods of higher mathematics. The following paragraphs contain a brief summary of those results which have a direct bearing on foundation problems.

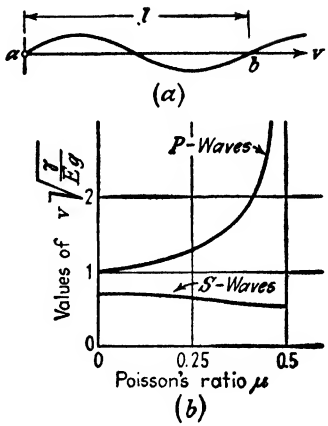

FIG. 148. (*a*) Diagram illustrating wave propagation; (*b*) relation between Poisson's ratio μ of vibrating medium and velocity of propagation of compression (P) and shear waves (S).

An impulse originating at a point located in the interior of a homogeneous, infinite elastic solid can produce only two types of waves, known as *compression, push,* or P waves and *transverse, shear,* or S waves. A compression wave is one in which the particles vibrate in the direction of wave propagation, like the particles in the path of a sound wave. The velocity of these waves is

$$v = \sqrt{\frac{Eg(1-\mu)}{\gamma(1-\mu-2\mu^2)}} \qquad [2]$$

wherein E = Young's modulus,
μ = Poisson's ratio,
γ = unit weight of the solid, and
g = acceleration of gravity.

In a transverse or S wave the particles vibrate in a plane at right angles to the direction of wave propagation and the waves travel with a velocity

$$v_s = \sqrt{\frac{Eg}{2\gamma(1+\mu)}} = \sqrt{\frac{Gg}{\gamma}} \qquad [3]$$

wherein G is the modulus of shear. Figure 148*b* shows the influence of Poisson's ratio on the velocities v and v_s. The velocity of S waves is always smaller than that of P waves and for $\mu = 0.5$ the value v becomes

equal to infinity while the value v_s of the S waves is finite and equal to

$$v_s = \sqrt{\frac{Eg}{3\gamma}}$$

In a semi-infinite or stratified solid, an impulse can also produce several other types of waves. Since these other types of waves travel along and parallel to the surface of semi-infinite solids or to the surfaces of discontinuity in stratified deposits they are called *surface waves.* The displacements produced by these waves decrease with the distance from the surface. The best-known types of surface waves are the *Rayleigh* and the *Love* waves. In a Rayleigh wave the particles vibrate in elliptical orbits in planes parallel to the direction of wave propagation and at right angles to the surface. The Love waves are special types of shear waves. Along the surface of a semi-infinite solid all the surface waves travel with a velocity slightly smaller than that of the shear waves (eq. 3). In relatively thin elastic layers the velocity of certain types of surface waves, including the Love waves, is a function of both the wave length and the thickness of the layer.

The theory of surface waves has been developed on the basis of the assumption that the vibrating medium is perfectly elastic. It can be found in any text book on theoretical seismology, for instance Macelwane (1936). A mathematical investigation of the relation between the amplitude of Rayleigh waves in elastic layers with a finite thickness and the distance from the surface of the layer has been published by Marguerre (1933). On account of the simplifying assumptions on which the theory of surface waves is based and of the complex character of these waves the interpretation of the results of field observations concerning surface waves is always somewhat uncertain.

At the boundary between two media with different elastic properties a wave may be reflected back into the medium through which it came or it may be refracted, i.e., it may change its direction when entering the second medium. If a particle receives two impulses, for instance one by a direct wave and a second one by a reflected wave, the resulting motion is equal to the geometric sum of the motions which would be produced by each one of the impulses individually. If the two impulses are equal and opposite, the particle remains in a state of rest. These are *interference phenomena.*

The laws which govern the aforementioned phenomena are similar to the laws of reflection, refraction, and interference in optics. A mathematical study of the application of these laws to the problems of seismic soil investigations has been published by Ramspeck (Degebo 1936).

162. Longitudinal impact on piles. One of the simplest phenomena of wave propagation occurs in a pile after it has been struck by a falling hammer. The impact of the hammer on the head of the pile produces in the pile a compression wave which travels through the pile toward the point, where it is reflected back into the pile. Since the older theories of dynamic pile-driving resistance, described in Article 52, failed to take this phenomenon into consideration they furnished misleading information concerning the influence of the weight of the pile on the effect of the pile-driving operations.

The theories of longitudinal impact on piles are based on the differential equation of longitudinal vibrations in bars which in turn is based on the following assumptions. The pile is perfectly elastic, every cross section through the pile remains plane during the process of vibration, and the particles of the pile vibrate only in a longitudinal direction, i.e., parallel to the axis of the pile. The lateral deformation of the pile is disregarded. In other words it is assumed that Poisson's ratio μ is equal to zero. Let

ρ = the longitudinal displacement of any cross section of the pile during the vibration, at a depth z below the head of the pile and at a time t,
ζ = the compressive strain or the compression of the pile per unit of length, at depth z and time t,
A = the area of the cross section of the pile,
L = the length of the pile,
P = the total pressure which acts on the cross section of the pile at depth z and time t.
$\sigma = P/A$, the compressive stress on this cross section,
E = Young's modulus of the pile material, and
γ = its unit weight.

The compressive strain ζ is equal to

$$\zeta = \frac{\partial \rho}{\partial z}$$

Since

$$\zeta = \frac{\sigma}{E} = \frac{P}{AE}$$

we can write

$$P = AE\frac{\partial \rho}{\partial z}$$

The total pressure on a cross section at depth $z + dz$ is

$$P + dP = AE\left(\frac{\partial \rho}{\partial z} + \frac{\partial^2 \rho}{\partial z^2}\, dz\right)$$

By D'Alembert's principle the resultant of the static forces which act on the slice of the pile must equal the inertia force (mass of the slice times its acceleration). The mass of the slice is

$$\frac{\gamma A}{g}\, dz$$

and the inertia force is

$$\frac{\gamma A}{g}\, dz \cdot \frac{\partial^2 \rho}{\partial t^2}$$

The resultant of the static forces is

$$P + dP - P = AE\,\frac{\partial^2 \rho}{\partial z^2}\, dz$$

Therefore D'Alembert's principle requires that

$$AE\,\frac{\partial^2 \rho}{\partial z^2} = \frac{\gamma A}{g}\,\frac{\partial^2 \rho}{\partial t^2}$$

or

$$\frac{\partial^2 \rho}{\partial t^2} = \frac{Eg}{\gamma}\,\frac{\partial^2 \rho}{\partial z^2} \qquad [1]$$

This is the differential equation of the longitudinal vibrations in a pile regardless of whether the end bearing of the pile is rigid or elastic. Since the theory disregards the lateral deformations of the pile the velocity v of the propagation of the wave through the pile is obtained by substituting $\mu = 0$ in equation 161(2). Thus we get

$$v = \sqrt{\frac{Eg}{\gamma}} \qquad [2]$$

Hence equation 1 can be replaced by

$$\frac{\partial^2 \rho}{\partial t^2} = v^2\,\frac{\partial^2 \rho}{\partial z^2} \qquad [3]$$

wherein v is the velocity of propagation of the impact wave through the pile.

If the upper end of a rigidly supported pile with a weight W_P and a length L is struck by a hammer with a weight W_H, falling with a velocity v_H, the solution of equation 3 furnishes for the greatest compressive

stress σ_{max} produced by the impact on the base of the pile the value

$$\sigma_{max} = 2E \frac{v_H}{v} (1 + \epsilon^{-2W_P/W_H}) \qquad [4]$$

provided W_P/W_H is smaller than 5 (Boussinesq 1885). The value ϵ is the base of the natural logarithms.

In contrast to the assumptions on which this equation is based, the support of the point of a pile is never perfectly rigid and the head of the pile is protected against direct impact by a pile cap or cushion. In order to adapt the theory to pile-driving problems, the British Building Research Board solved equation 3 on the basis of the modified assumptions that the lower end of the pile rests on a perfectly elastic support and that the head of the pile is protected by a perfectly elastic cushion (Glanville et al., 1938). The final equations are very complicated, but they can be replaced by simple equations which give fairly satisfactory values. One of these is

$$\sigma_{max} = E \frac{v_H}{v} \sqrt{\frac{W_H}{W_P(1 + E/T_c L)}} \qquad [5]$$

wherein T_c is a constant with the dimension gm cm^{-3} whose value depends on the elastic properties of the pile cushion (Cummings 1940). In order to decide whether or not equation 5 applies to a given case the ratio

$$N = \frac{W_P}{3W_H(1 + E/T_c L)} \qquad [6]$$

is computed. If the ratio N is smaller than about 0.1 or 0.15 equation 5 gives fairly accurate results. Otherwise it would be necessary to use the unabridged equations.

If the upper ends of two piles with identical dimensions but with different Young's modulus, E and E', and different unit weights, γ and γ' respectively, are struck by the same hammer with the same velocity the ratio between the maximum compressive stress produced by the impact on the lower end of the piles depends on the rigidity of the support of the lower end and on the type of protection of the upper end. For rigid support of the lower end and unprotected upper ends we obtain from equations 2 and 4

$$\frac{\sigma_{max}}{\sigma'_{max}} = \sqrt{\frac{E\gamma}{E'\gamma'}} \cdot \frac{1 + \epsilon^{-2W_P/W_H}}{1 + \epsilon^{-2W'_P/W_H}} \qquad [7]$$

wherein W_P and W'_P represents the weights of the piles. For elastic point support and impact on cushions with the same stiffness constant for both cushions we obtain from equations 2 and 5

$$\frac{\sigma_{max}}{\sigma'_{max}} = \sqrt{\frac{E\gamma W'_P(1 + E'/T_cL)}{E'\gamma' W_P(1 + E/T_cL)}} \qquad [8]$$

In a discussion of the practical implications of equations 4 and 5 Cummings (1940) presented the following numerical example. One reinforced concrete and one wooden pile with equal dimensions are driven with a drop hammer with a weight of $W_H = 5000$ pounds through soft strata of fill and silt to bearing in a hard stratum of sand and gravel. The velocity of the hammer at the instant of impact is equal to $v_H = 14$ feet per second. The heads of the piles are protected by identical cushions with a stiffness constant $T_c = 10{,}000$ pounds per cubic inch. The data regarding the piles are as follows:

	CONCRETE PILE	WOODEN PILE
Length L	25′	25′
Cross-sectional area A	12″ × 12″	12″ × 12″
Weight W_P	3750 lbs.	1000 lbs.
Unit weight γ	150 lbs./cu. ft.	40 lbs./cu. ft.
Young's modulus E	3,000,000 lbs./sq. in.	1,200,000 lbs./sq. in.
$v = \sqrt{\frac{Eg}{\gamma}}$	9610 ft./sec.	11,800 ft./sec.

Calculation by means of equation 4 shows that the greatest force $A\sigma_{max}$ produced by the impact on the piles with rigidly supported ends and with unprotected heads is 1,540,000 pounds for the concrete pile and 685,000 pounds for the wooden pile. Computing the value $A\sigma_{max}$ by means of equation 5, which takes the cushion and the elastic point support into consideration, we obtain for the concrete pile 514,000 pounds and for the wooden pile 389,000 pounds. The real pressures will very likely be still lower because the theory on which equation 5 is based disregards the skin friction and the existence of a damping force in the pile. Nevertheless, the results of the computation justify the conclusion that the greatest pressure produced by a given impact is greater at the point of the concrete pile than at the point of the wooden pile. The approximate validity of the theory on which this conclusion is based has been demonstrated by large-scale tests (Glanville et al., 1938). As a consequence of the difference between the maximum pressure at the points of the two piles discussed before, the concrete piles should penetrate deeper into the firm stratum than the wooden pile and its static bearing capacity after the pile has been driven to refusal should be higher. Yet, according to all those pile formulas which take only the weight of the pile into consideration (see Art. 52) the bearing capacity of the wooden pile should be higher than that of the concrete pile provided both piles have been driven to refusal. This is an example of one of the many erroneous conclusions to which the pile formulas may lead. The reasons for the deficiencies of these formulas have been discussed in Article 52.

163. Soil exploration by means of explosives and vibrators. Equations 161(2) and 161(3) show that the velocity of wave propagation depends on Young's modulus and on Poisson's ratio. Strata with very

different elastic constants are usually separated by fairly sharp boundaries likely to give rise to well-defined reflection and refraction phenomena. Therefore it is theoretically possible to obtain information on the elastic properties and on the thickness of the strata located beneath the surface of the earth by recording the vibrations produced by an impulse on the surface at different distances from the focus of the disturbance. Such methods have been used for many years and if the geological conditions are favorable, the results are very satisfactory. The impulse is produced either by an artificial explosion or by a vibrator. In both methods the vibrations are recorded simultaneously at different distances from the focus of the disturbance by means of portable seismographs. Therefore the methods are also called *methods of scismic soil exploration.*

In the explosion methods the impulse is produced by exploding a blasting cap or a small charge of dynamite. An impulse of this type produces chiefly compression waves. In a saturated soil the velocity of compression waves is much higher than in the same soil in a moist state. Therefore the upper boundary of the zone of capillary saturation represents a prominent surface of discontinuity with respect to the velocity of propagation of the explosion waves. The seismographs are located on straight lines through the point of explosion. They record both the instant of the explosion and the subsequent vibrations. In exploration to great depth, for instance in salt dome exploration, the interpretation of the seismographic records is based either on the time between the explosion and the arrival of the first energetic impulse or on the time which elapses before the waves with a lower velocity arrive. Within a certain distance, whose magnitude depends on the thickness of the unconsolidated stratum, the first impulse registered by the seismograph is produced by a wave which travels along a fairly straight line from the site of the explosion to the receiver. Beyond this distance the first energetic impulse is produced by the refracted waves which travel along the path of least resistance at depth. The later ones are due to direct and to reflected waves which travel within the media of high resistance. Therefore the two methods are known as *refraction* and *reflection method* respectively (see for instance Leet 1938 or Heiland 1940).

In soil exploration for engineering purposes only the refraction method is used, and its application is limited to the determination of the total depth of unconsolidated deposits resting on a rock surface and of loose, unconsolidated strata overlying dense ones. The velocity of compression waves in rock is at least ten times as great as in the unconsolidated material. Therefore the boundary between the two materials gives rise to very conspicuous refraction phenomena (Shepard 1935).

The principle of the method is illustrated by Figure 149. Let

v_1 = the velocity of wave propagation in the unconsolidated material,
v_2 = the corresponding velocity in the bedrock,
t_1 = the time at which the first energetic impulse reaches the detector I at a short distance L_1 from the site of the explosion,
t_2 = the corresponding time for the detector II, and
D = the depth of the rock surface below the ground surface.

Since v_2 is very much greater than v_1 the first waves which reach detector II at a considerable distance L_2 from the site of the explosion are the refracted waves which travel chiefly immediately below the

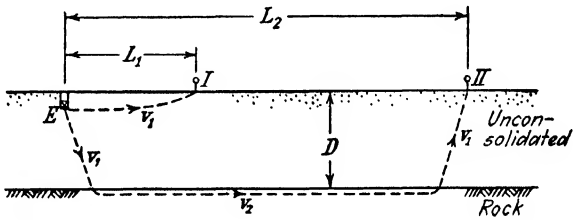

FIG. 149. Diagram illustrating principle of refraction method for seismic soil exploration.

rock surface, as indicated in the figure. On the other hand, detector I located fairly close to the site of the explosion receives the first impulse through a direct wave. For the sake of simplicity it is usually assumed that the wave travels from the surface of the ground to the bedrock and back again at right angles to the surface of the bedrock and that both surfaces are parallel. On this assumption we obtain for detector I the equation

$$t_1 = \frac{L_1}{v_1} \quad \text{or} \quad v_1 = \frac{L_1}{t_1}$$

and for detector II

$$t_2 = \frac{2D}{v_1} + \frac{L_2}{v_2} \quad \text{or} \quad D = \left(t_2 - \frac{L_2}{v_2}\right)\frac{v_1}{2}$$

Thus we have two equations with three unknown quantities, D, v_1, and v_2. In order to get a third equation we install a third detector at a distance L_3 from the site of the explosion (not shown in the figure) and record the time t_3 at which this detector registers the first strong impulse.

If the surface of the rock is not parallel to the surface of the ground or if we want to determine the bottom of a buried valley the explosion is repeated at different points E_1, E_2, etc., of the surface and seismo-

graphic observations are made along different straight lines through the site of each explosion. One of the principal errors involved in this procedure is due to the assumption that the velocity of wave propagation immediately below the surface between E and I is identical with the velocity in a vertical downward direction across the ground-water level and the beds of stratification. Yet, under favorable geological conditions the method has been found to give satisfactory results (Shepard 1935).

On account of the relation shown in Figure 148*b* the influence of variations of μ on the velocity v of P waves is likely to efface the corresponding influence of variations of other, much more important soil constants, such as the modulus of elasticity. As a rule the value μ is not known. Hence the explosion method does not permit the determination of the modulus of elasticity of the strata through which the explosion waves travel. Furthermore, since the explosion produces a single impulse there is no possibility of determining the thickness of individual soil strata by means of observing interference phenomena on the surface of the ground.

In order to increase the amount of information to be derived from seismographic records the Degebo in Berlin in conjunction with the Geophysical Institute of the University of Göttingen adopted the vibrator described in Article 158 as a source of wave impulses. The waves produced by the vibrator are chiefly shear waves in the category of surface waves. A differentiation of this wave complex into well-defined types such as Rayleigh or Love waves has only been accomplished in a general way. The ground water has no influence on the velocity of shear waves. On the other hand along the boundaries of relatively thin strata the velocity of certain types of surface waves is a function of the frequency of the impulse and of the thickness of the stratum. However, if the frequency exceeds a certain value, the velocity of these waves is independent of the frequency and becomes equal to that of the other surface waves, which is only slightly smaller than the velocity v_s (eq. 161(3)) of shear waves. Hence the measured velocities of wave transmission are a measure of the elastic properties of the medium through which the wave travels, provided the frequency of the impulse has been so chosen that the velocity of all the waves is independent of the frequency.

Since the vibrator produces a periodic impulse, the determination of the velocity of the waves is not as simple as it is in the method of refraction shooting described before. Nevertheless the problem of measuring this velocity has been successfully solved.

In order to determine the boundary between two different uncon-

solidated strata, the amplitude is measured at different points on straight lines through the center of the vibrator. A consistent decrease of the amplitude with increasing distance from the vibrator, as shown in Figure 150*a*, indicates a homogeneous stratum of great depth. On the other hand, if the subsoil is stratified, the surface waves interfere with the reflected waves and produce a phenomenon comparable to Newton's rings in optics. As a result of this interference the amplitude

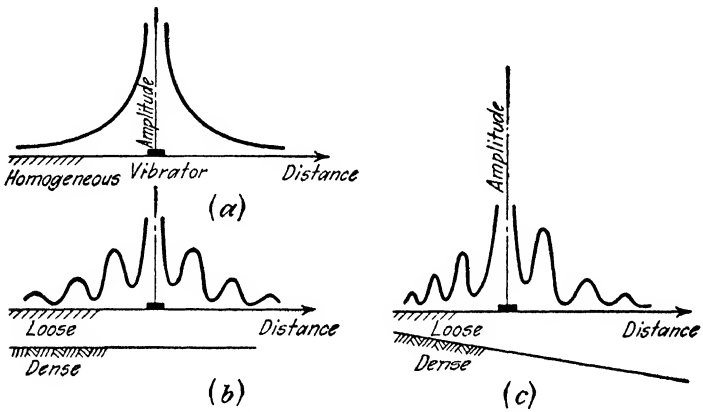

FIG. 150. Diagram illustrating effect of stratification on amplitude of waves emanating from an operating vibrator.

becomes a periodic function of the distance from the vibrator. If the thickness of the stratum is everywhere the same, the amplitude diagram is symmetrical with reference to a vertical line through the center of the vibrator, as shown in Figure 150*b*, and the peaks of the curve are equally spaced. If the thickness of the layer increases in one direction the distance between the peaks increases in the same direction as shown in 150*c*. In any event the thickness of the layer can be computed from the spacing of the peaks. The theory on which the interpretation of the vibration records is based is well established (Degebo 1936). The theory also makes it possible to compute from the records the velocity of wave propagation in deeper layers. The principle of this method is somewhat similar to that of the refraction method illustrated by Figure 149. The results of the computation are represented by *travel-time curves*, in which the distance covered by the wave is plotted against time.

In order to investigate the subsoil over large areas, the vibrator is operated in succession at the points of intersection between the two sets of lines in a gridiron and the observations are made along the lines which constitute the gridiron. The upper layers are investigated by means

of high-frequency and the deeper layers by means of low-frequency impulses.

Since the vibrator produces only shear waves the measured velocities do not permit the computation of Young's modulus (see eq. 161(3)). However, by combining the vibrator method with the measurement of the velocity of compression waves produced by artificial explosions, the investigators obtained two independent sets of data which made it possible to compute both the values E and μ by means of the equations 161(2) and 161(3).

164. Earthquake waves. The mechanics of earthquakes are essentially identical with those of the vibrations produced by artificial impulses in connection with seismic prospecting (Art. 163).

An earthquake may be caused by a sudden slip along fault planes at a moderate depth below the surface (tectonic earthquake), by explosions or other events associated with volcanic activities (volcanic earthquake), or by processes of an unknown nature at great depth below the zone in which rocks behave as solids (plutonic earthquakes). The zone in which the earthquake originates is called the *focus* and the point or line on the earth's surface located above the focus is the *epicenter*. In the vicinity of the epicenter the seismographic instruments usually register in succession the arrival of P, S, and various surface waves. The surface waves always include Rayleigh waves, Love waves, and several other types. At a greater distance from the epicenter the records are still more complex on account of various reflection and refraction phenomena. In every case the earthquake represents a periodic impulse which transfers every object supported by the earth into a state of forced vibrations. Since the intensity of forced vibrations depends chiefly on the ratio between the natural frequency of the object and the frequency of the impulse, the latter represents a factor of vital importance. Unfortunately the records of earthquake vibrations are so complex that they leave a wide margin for interpretation. The vibrations are in every respect similar to those produced by quarry blasts. Figure 151 represents a record obtained during and after such a blast (Leet 1939).

The charge consisted of 19,000 pounds of 40 per cent Red Cross extra gelatine dynamite. It was placed in mine pockets in a short tunnel behind the 190-foot face of a quarry in a trap rock sill in the Connecticut Valley. The seismograph was located on the surface of an alluvial fill in a valley at a distance of 1800 feet from the seat of the impulse, 125 feet below the level of the quarry floor. The record shows the transverse, the vertical, and the longitudinal components of the displacements and covers a period of 5.9 seconds. The recorded waves have the characteristics of surface waves. The dashed line indicates a wave with a period of about 0.3 second which is

masked by waves with shorter periods. Toward the end of the period of observation the vertical and the longitudinal displacements become imperceptible while the transverse displacements continue.

In connection with engineering problems, the most important components are the horizontal ones, designated in Figure 151 as transverse and longitudinal components, because they represent the cause of tilting and bending in structures. For this reason the vertical component is customarily disregarded. The intensity of the earthquakes is usually expressed by the ratio n_g between the greatest acceleration

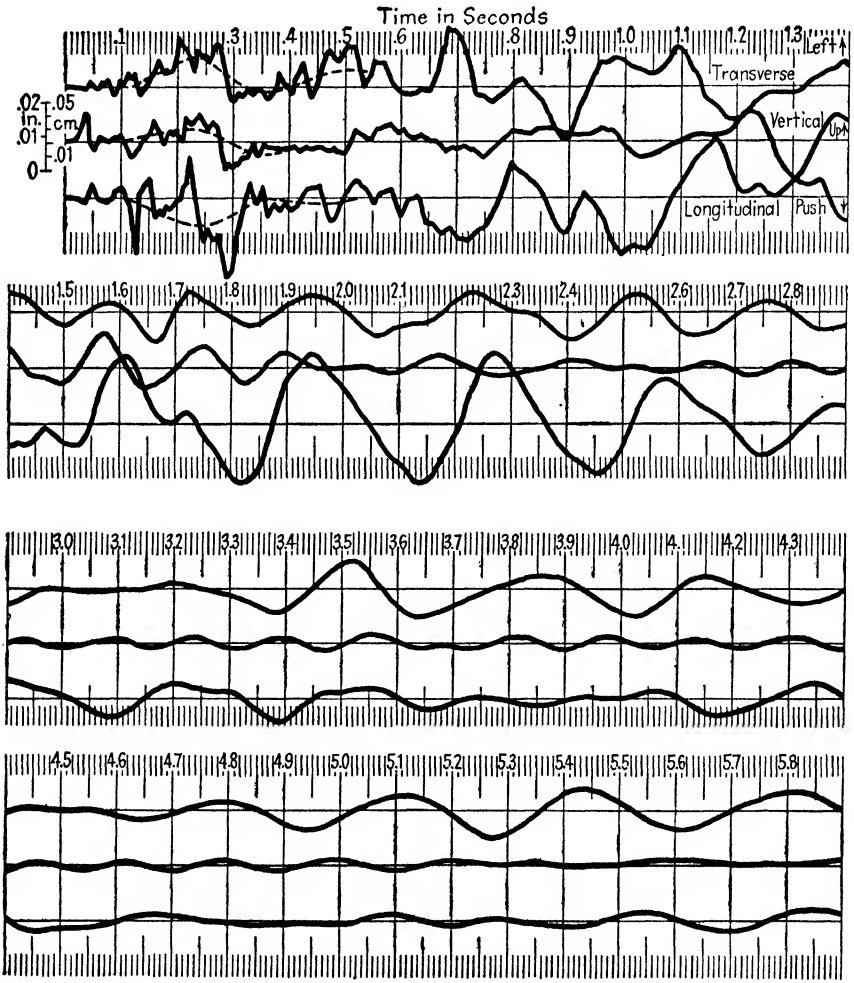

FIG. 151. Seismic record of vibrations at surface of alluvial fill due to quarry blast. (*After Leet 1939.*)

produced by the earthquake in a horizontal direction and the acceleration g produced by the force of gravity. In order to estimate the value n_g one replaces the seismographic record of the horizontal vibrations by a similar, simplified record representing a free harmonic vibration such as that shown in Figure 141*d*, with an amplitude a and a circular frequency ω_1. By differentiation of equation 156(8) one obtains for the greatest acceleration of the particles $d^2x/dt^2 = n_g\, g$ the value

$$n_g\, g = \left(\frac{d^2x}{dt^2}\right)_{\max} = a\omega_1^2$$

or

$$n_g = \frac{a}{g}\omega_1^2 = \frac{4\pi^2 a}{g\tau^2} \qquad [1]$$

If the natural frequency f_0 of a structure is very high compared with the frequency of the impulse produced by the earthquake, the ratio $f_1/f_0 = \omega_1/\omega_0$ is close to zero. As a consequence the amplitude of the vibrating structure is practically equal to that of the earthquake waves, as shown in Figures 143*b* and 144*a*. This condition is satisfied by most low buildings and ordinary retaining walls. Such structures can be designed on the assumption that they are permanently acted upon by a mass force equal to the resultant between the vertical force of gravity g and a horizontal force $n_g g$. The mechanical effect of this mass force on high buildings is somewhat similar to that of a wind pressure, and the stresses in the members of the structure can be computed accordingly (Fleming 1930). However, the results of such computations can be very misleading unless the natural frequency of both the entire building and its individual constituents, such as walls and columns, is beyond the range of the frequency of the earthquake waves. In order to compute the earth pressure which acts during an earthquake with an intensity n_g on a retaining wall (Fig. 152*a*) we tilt the wall and the backfill through an angle $\tan^{-1} n_g$, as shown in Figure 152*b*, and increase the unit weight of both the earth and the wall by multiplying it by $\sqrt{1 + n_g^2}$. The balance of the investigation is identical with that described in Chapter VI.

Figure 152*c* represents a section through a concrete gravity dam. An earthquake moves both the dam and the base of the reservoir in rapid succession through a distance a to the right and to the left. The water tends to remain where it is because the shearing stresses along the bottom of the reservoir are negligible. Therefore the mechanical effect of the earthquake on the system dam-water is the same as if the dam were rapidly advanced through a distance a toward a stationary

body of water. Westergaard (1933*a*) has shown that the resistance p of the water against rapid displacement, per unit of area of the vertical face of the dam at a depth z below the water level, increases approximately in direct proportion to the square root of the depth below the surface. It can be computed from the approximate equation

$$p = Cn_g\sqrt{Hz} \qquad [2]$$

wherein C is a function of the ratio between the depth H of the reservoir and the period τ of the earthquake shock. For a given period τ the value

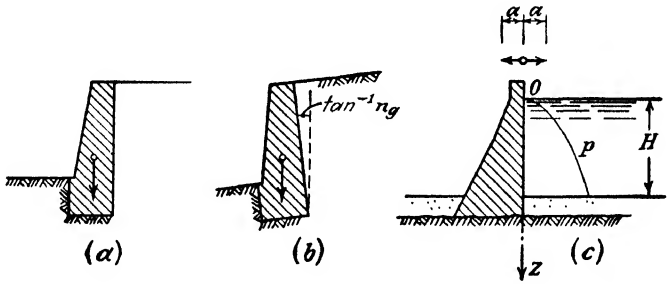

FIG. 152. (*a*) Section through retaining wall; (*b*) imaginary angular displacement of wall and back fill which would have approximately the same effect on stability of wall as an earthquake with intensity $n_g g$; (*c*) dynamic water pressure p on face of concrete gravity dam during earthquake.

n_g depends on the amplitude a (see eq. 1). In Figure 144*c*, equation 2 is represented by the parabola labeled p. For a period $\tau = 4/3$ seconds and for different values of H Westergaard obtained

H = 0–310 ft	310–540 ft	540–680 ft
C = 0.026	0.027	0.028 tons/cu ft

The stresses produced by the force p (eq. 2) must be added to the stresses produced by the earthquake acceleration which acts on the dam itself. Westergaard also presented a rigorous solution of the problem.

If the natural frequency of a structure is considerably outside the range of frequency of earthquake vibrations, the errors associated with the method of computation illustrated by Figure 152*b* are on the safe side because the method is based on the assumption that the structure is permanently under the influence of the horizontal body force $n_g g$. In reality this body force acts only during a brief period. Every harmful effect of the force $n_o g$ involves a displacement against resisting forces. Such a displacement represents work whose performance requires time. We assumed in contrast to reality that the force acts

forever. Therefore the results of the computation inform us on the greatest amount of destruction which can be wrought by an earthquake of given intensity n_0 provided the natural frequency of the structure is very different from that of the earthquake waves. On the other hand, if the natural frequency of the structure or of parts of the structure approach that of the earthquake vibrations, resonance phenomena are likely to intensify the effect of the periodic impulse to such a degree that the sign of the error associated with the method illustrated by Figure 152*b* is reversed. Such a condition can be anticipated for tall buildings or very high smoke stacks and requires that the method illustrated by Figure 152*b* be replaced by another which takes the natural frequency of the structure into consideration. A simple method of this type, applicable to framed structures, has been described by Westergaard (1933*c*) and another for tall smoke stacks by Briske (1927). The theoretical investigations in this field have been supplemented repeatedly by laboratory investigations involving measurement of the stresses in small-scale models mounted on shaking tables (see for instance Williams 1937, Ruge 1938).

In connection with any investigation involving resonance phenomena produced by earthquakes the investigator faces the delicate problem of selecting an appropriate value for the frequency of the earthquake vibrations. The earthquake shock produces simultaneous vibrations with very different frequencies similar to those produced by a quarry blast (see Fig. 151). Therefore the damage to two different structures subject to the same earthquake shock may be due to two entirely different components of the same vibration. The one factor in common to the destructive impulse on the two structures is the amount of kinetic energy which is supplied by the earthquake to the foundations per unit of time and per unit of volume of the subgrade. Hence, if resonance phenomena must be considered it would appear logical to express the intensity of the earthquake in terms not of maximum acceleration but by the intensity of the flow of energy (Mendenhall 1888). Another method has recently been suggested by Westergaard (1933*b*). Substituting a simple harmonic vibration with the amplitude a and the circular frequency ω for the real earthquake vibrations we obtain for the distance x of a particle from its equilibrium position at a time t from equation 156(8)

$$x = a \sin \omega t$$

for its velocity

$$v = \frac{dx}{dt} = a\omega \cos \omega t$$

and for its acceleration

$$\frac{d^2x}{dt^2} = -a\omega^2 \sin \omega t$$

The corresponding maximum values are

$$v_{max} = a\omega \quad \text{and} \quad \left(\frac{d^2x}{dt^2}\right)_{max} = n_g g = a\omega^2$$

Combining these two equations we obtain

$$v_{max} = \frac{n_g g}{\omega} = \frac{n_g g}{2\pi} \tau$$

wherein τ is the period of the vibration. The kinetic energy E_k which is supplied to the subgrade of a structure per unit of time and per unit of volume, while the velocity is greatest, is

$$E_k(\text{gm cm}^{-2}) = \frac{1}{2} \frac{\gamma}{g} v_{max}^2 = n_g^2 \tau^2 \frac{\gamma g}{8\pi^2} \qquad [3]$$

The value E_k has the dimension of a force per unit of area and represents the proposed substitute for the measure n_g.

Another complication associated with the estimate of the period of earthquakes is due to the well-known influence of the character of the uppermost strata on the value n_g which is considered a measure of the intensity of earthquakes. On rock outcrops the value n_g is always very much smaller than on the surface of loose, alluvial fills. An alluvial fill which occupies a depression in the surface of the rock represents an elastic unit with well-defined boundaries, having a natural frequency of its own. Therefore the high values of n_g for loose surface deposits may represent the result of a resonance phenomenon which occurs in the soil before the earthquake waves reach the foundations of the structures. One can visualize this process in the following manner. If the rock extends to the very surface of the earth the greatest part of the kinetic energy which flows toward the surface is reflected and flows back again into the rock. On the other hand, if the rock is covered with a bed of sediments the energy is absorbed by the sediments, a process comparable to the accumulation of kinetic energy in a pendulum acted upon by a periodic impulse whose frequency is equal to the natural frequency of the pendulum. This process intensifies the effect of the earthquake on structures whose foundations are supported by the sediments. In the derivation of equation 3, this possibility was not taken into consideration.

In the present state of our knowledge the influence of the geologic conditions on the character and the intensity of the impulse produced by a given earthquake can only be investigated by field observations. Even the most refined theoretical methods of evaluating the stresses in a building due to earthquakes (for instance Biot 1942) can be used only if the impulse which acts on the building is known in advance.

APPENDIX

INFLUENCE VALUES FOR VERTICAL STRESSES IN A SEMI-INFINITE ELASTIC SOLID DUE TO SURFACE LOADS

1. Point load. The vertical normal stress σ_z at a point located at a depth z below the surface of the solid at a horizontal distance r from the point of application of a point load Q (Fig. 118*a*) is given by the equation

$$\sigma_z = \frac{Q}{z^2} I_\sigma$$

wherein

$$I_\sigma = \frac{3}{2\pi}\left[\frac{1}{1 + (r/z)^2}\right]^{\frac{5}{2}} \qquad 136(5)$$

The following table contains the values of I_σ for different values of r/z.

TABLE I[1]

r/z	I_σ	r/z	I_σ	r/z	I_σ	r/z	I_σ
0.00	0.4775	0.40	0.3294	0.80	0.1386	1.20	0.0513
1	0.4773	1	0.3238	1	0.1353	1	0.0501
2	0.4770	2	0.3181	2	0.1320	2	0.0489
3	0.4764	3	0.3124	3	0.1288	3	0.0477
4	0.4756	4	0.3068	4	0.1257	4	0.0466
5	0.4745	5	0.3011	5	0.1226	5	0.0454
6	0.4732	6	0.2955	6	0.1196	6	0.0443
7	0.4717	7	0.2899	7	0.1166	7	0.0433
8	0.4699	8	0.2843	8	0.1138	8	0.0422
9	0.4679	9	0.2788	9	0.1110	9	0.0412
0.10	0.4657	0.50	0.2733	0.90	0.1083	1.30	0.0402
1	0.4633	1	0.2679	1	0.1057	1	0.0393
2	0.4607	2	0.2625	2	0.1031	2	0.0384
3	0.4579	3	0.2571	3	0.1005	3	0.0374
4	0.4548	4	0.2518	4	0.0981	4	0.0365
5	0.4516	5	0.2466	5	0.0956	5	0.0357
6	0.4482	6	0.2414	6	0.0933	6	0.0348
7	0.4446	7	0.2363	7	0.0910	7	0.0340
8	0.4409	8	0.2313	8	0.0887	8	0.0332
9	0.4370	9	0.2263	9	0.0865	9	0.0324
0.20	0.4329	0.60	0.2214	1.00	0.0844	1.40	0.0317
1	0.4286	1	0.2165	1	0.0823	1	0.0309
2	0.4242	2	0.2117	2	0.0803	2	0.0302
3	0.4197	3	0.2070	3	0.0783	3	0.0295
4	0.4151	4	0.2024	4	0.0764	4	0.0288
5	0.4103	5	0.1978	5	0.0744	5	0.0282
6	0.4054	6	0.1934	6	0.0727	6	0.0275
7	0.4004	7	0.1889	7	0.0709	7	0.0269
8	0.3954	8	0.1846	8	0.0691	8	0.0263
9	0.3902	9	0.1804	9	0.0674	9	0.0257
0.30	0.3849	0.70	0.1762	1.10	0.0658	1.50	0.0251
1	0.3796	1	0.1721	1	0.0641	1	0.0245
2	0.3742	2	0.1681	2	0.0626	2	0.0240
3	0.3687	3	0.1641	3	0.0610	3	0.0234
4	0.3632	4	0.1603	4	0.0595	4	0.0229
5	0.3577	5	0.1565	5	0.0581	5	0.0224
6	0.3521	6	0.1527	6	0.0567	6	0.0219
7	0.3465	7	0.1491	7	0.0553	7	0.0214
8	0.3408	8	0.1455	8	0.0539	8	0.0209
9	0.3351	9	0.1420	9	0.0526	9	0.0204

[1] G. Gilboy (1933), Influence Tables for Solution of Boussinesq Equation. In "Earth and Foundations," Progress Report of Special Committee, *Proc. Am. Soc. C.E.*, Vol. 59, p. 781.

TABLE I—*continued*

r/z	I_σ	r/z	I_σ	r/z	I_σ	r/z	I_σ
1.60	0.0200	2.00	0.0085	2.40	0.0040	2.80	0.0021
1	0.0195	1	0.0084	1	0.0040	1	0.0020
2	0.0191	2	0.0082	2	0.0039	2	0.0020
3	0.0187	3	0.0081	3	0.0038	3	0.0020
4	0.0183	4	0.0079	4	0.0038	4	0.0019
5	0.0179	5	0.0078	5	0.0037	5	0.0019
6	0.0175	6	0.0076	6	0.0036	6	0.0019
7	0.0171	7	0.0075	7	0.0036	7	0.0019
8	0.0167	8	0.0073	8	0.0035	8	0.0018
9	0.0163	9	0.0072	9	0.0034	9	0.0018
1.70	0.0160	2.10	0.0070	2.50	0.0034	2.90	0.0018
1	0.0157	1	0.0069	1	0.0033	1	0.0017
2	0.0153	2	0.0068	2	0.0033	2	0.0017
3	0.0150	3	0.0066	3	0.0032	3	0.0017
4	0.0147	4	0.0065	4	0.0032	4	0.0017
5	0.0144	5	0.0064	5	0.0031	5	0.0016
6	0.0141	6	0.0063	6	0.0031	6	0.0016
7	0.0138	7	0.0062	7	0.0030	7	0.0016
8	0.0135	8	0.0060	8	0.0030	8	0.0016
9	0.0132	9	0.0059	9	0.0029	9	0.0015
1.80	0.0129	2.20	0.0058	2.60	0.0029	3.00	0.0015
1	0.0126	1	0.0057	1	0.0028	1	0.0015
2	0.0124	2	0.0056	2	0.0028	2	0.0015
3	0.0121	3	0.0055	3	0.0027	3	0.0014
4	0.0119	4	0.0054	4	0.0027	4	0.0014
5	0.0116	5	0.0053	5	0.0026	5	0.0014
6	0.0114	6	0.0052	6	0.0026	6	0.0014
7	0.0112	7	0.0051	7	0.0025	7	0.0014
8	0.0109	8	0.0050	8	0.0025	8	0.0013
9	0.0107	9	0.0049	9	0.0025	9	0.0013
1.90	0.0105	2.30	0.0048	2.70	0.0024	3.10	0.0013
1	0.0103	1	0.0047	1	0.0024	1	0.0013
2	0.0101	2	0.0047	2	0.0023	2	0.0013
3	0.0099	3	0.0046	3	0.0023	3	0.0012
4	0.0097	4	0.0045	4	0.0023	4	0.0012
5	0.0095	5	0.0044	5	0.0022	5	0.0012
6	0.0093	6	0.0043	6	0.0022	6	0.0012
7	0.0091	7	0.0043	7	0.0022	7	0.0012
8	0.0089	8	0.0042	8	0.0021	8	0.0012
9	0.0087	9	0.0041	9	0.0021	9	0.0011

TABLE I — *continued*

r/z	I_σ	r/z	I_σ	r/z	I_σ
3.20	0.0011	3.40	0.0009	3.75	
1	0.0011	1	0.0008	to	0.0005
2	0.0011	2	0.0008	3.90	
3	0.0011	3	0.0008		
4	0.0011	4	0.0008	3.91	
5	0.0011	5	0.0008	to	0.0004
6	0.0010	6	0.0008	4.12	
7	0.0010	7	0.0008		
8	0.0010	8	0.0008	4.13	
9	0.0010	9	0.0008	to	0.0003
				4.43	
3.30	0.0010	3.50		4.44	
1	0.0009	to	0.0007	to	0.0002
2	0.0009	3.61		4.90	
3	0.0009				
4	0.0009	3.62		4.91	
5	0.0009	to	0.0006	to	0.0001
6	0.0009	3.74		6.15	
7	0.0009				
8	0.0009				
9	0.0009				

2. Uniformly distributed load on a rectangular area. If B is the width and L the length of a rectangular area, which carries a load q per unit of area the vertical normal stress at a point N (Fig. 120*a*) at a depth z below one of the corners of the area is equal to

$$\Delta\sigma_z = qI_\sigma$$

The influence value I_σ is determined by the equation

$$I_\sigma = \frac{1}{4\pi}\left[\frac{2mn\sqrt{m^2+n^2+1}}{m^2+n^2+m^2n^2+1}\cdot\frac{m^2+n^2+2}{m^2+n^2+1} + \tan^{-1}\frac{2mn\sqrt{m^2+n^2+1}}{m^2+n^2+1-m^2n^2}\right] \qquad 136(8)$$

wherein

$$m = \frac{B}{z} \quad \text{and} \quad n = \frac{L}{z}$$

The values of I_σ for given values of m and n can be determined from the graph on Plate 1, which has been prepared by R. E. Fadum. They are also contained in the following table.

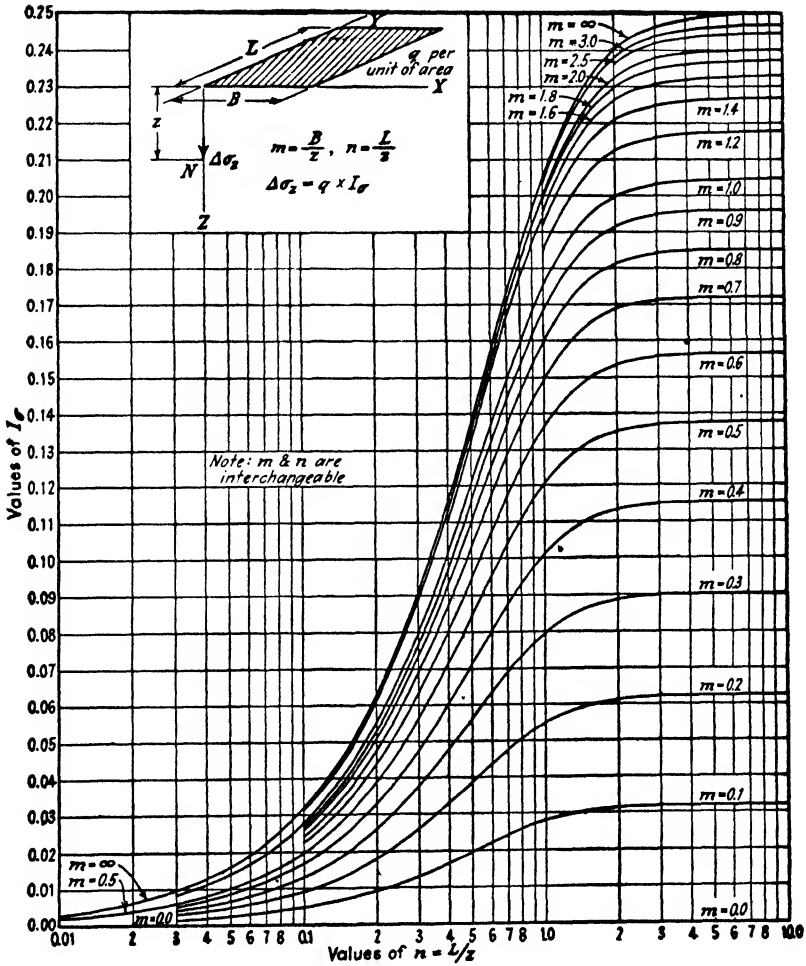

PLATE 1. Graph for determining influence value for vertical normal stress $\Delta\sigma_z$ at point N located beneath one corner of a uniformly loaded rectangular area.

TABLE II[1]

m	n											
	0.1	0.2	0.3	0.4	0.5	0.6	0.7	0.8	0.9	1.0	1.2	1.4
0.1	0.00470	0.00917	0.01323	0.01678	0.01978	0.02223	0.02420	0.02576	0.02698	0.02794	0.02926	0.03007
0.2	0.00917	0.01790	0.02585	0.03280	0.03866	0.04348	0.04735	0.05042	0.05283	0.05471	0.05733	0.05894
0.3	0.01323	0.02585	0.03735	0.04742	0.05593	0.06294	0.06858	0.07308	0.07661	0.07938	0.08323	0.08561
0.4	0.01678	0.03280	0.04742	0.06024	0.07111	0.08009	0.08734	0.09314	0.09770	0.10129	0.10631	0.10941
0.5	0.01978	0.03866	0.05593	0.07111	0.08403	0.09473	0.10340	0.11035	0.11584	0.12018	0.12626	0.13003
0.6	0.02223	0.04348	0.06294	0.08009	0.09473	0.10688	0.11679	0.12474	0.13105	0.13605	0.14309	0.14749
0.7	0.02420	0.04735	0.06858	0.08734	0.10340	0.11679	0.12772	0.13653	0.14356	0.14914	0.15703	0.16199
0.8	0.02576	0.05042	0.07308	0.09314	0.11035	0.12474	0.13653	0.14607	0.15371	0.15978	0.16843	0.17389
0.9	0.02698	0.05283	0.07661	0.09770	0.11584	0.13105	0.14356	0.15371	0.16185	0.16835	0.17766	0.18357
1.0	0.02794	0.05471	0.07938	0.10129	0.12018	0.13605	0.14914	0.15978	0.16835	0.17522	0.18508	0.19139
1.2	0.02926	0.05733	0.08323	0.10631	0.12626	0.14309	0.15703	0.16843	0.17766	0.18508	0.19584	0.20278
1.4	0.03007	0.05894	0.08561	0.10941	0.13003	0.14749	0.16199	0.17389	0.18357	0.19139	0.20278	0.21020
1.6	0.03058	0.05994	0.08709	0.11135	0.13241	0.15028	0.16515	0.17739	0.18737	0.19546	0.20731	0.21510
1.8	0.03090	0.06058	0.08804	0.11260	0.13395	0.15207	0.16720	0.17967	0.18986	0.19814	0.21032	0.21836
2.0	0.03111	0.06100	0.08867	0.11342	0.13496	0.15326	0.16856	0.18119	0.19152	0.19994	0.21235	0.22058
2.5	0.03138	0.06155	0.08948	0.11450	0.13628	0.15483	0.17036	0.18321	0.19375	0.20236	0.21512	0.22364
3.0	0.03150	0.06178	0.08982	0.11495	0.13684	0.15550	0.17113	0.18407	0.19470	0.20341	0.21633	0.22499
4.0	0.03158	0.06194	0.09007	0.11527	0.13724	0.15598	0.17168	0.18469	0.19540	0.20417	0.21722	0.22600
5.0	0.03160	0.06199	0.09014	0.11537	0.13737	0.15612	0.17185	0.18488	0.19561	0.20440	0.21749	0.22632
6.0	0.03161	0.06201	0.09017	0.11541	0.13741	0.15617	0.17191	0.18496	0.19569	0.20449	0.21760	0.22644
8.0	0.03162	0.06202	0.09018	0.11543	0.13744	0.15621	0.17195	0.18500	0.19574	0.20455	0.21767	0.22652
10.0	0.03162	0.06202	0.09019	0.11544	0.13745	0.15622	0.17196	0.18502	0.19576	0.20457	0.21769	0.22654
∞	0.03162	0.06202	0.09019	0.11544	0.13745	0.15623	0.17197	0.18502	0.19577	0.20458	0.21770	0.22656

[1] N. M. Newmark (1935), Simplified Computation of Vertical Pressures in Elastic Foundations: Circ. 24, Eng. Exper. Sta., University of Illinois.

TABLE II — *Continued*

m	n										
	1.6	1.8	2.0	2.5	3.0	4.0	5.0	6.0	8.0	10.0	∞
0.1	0.03058	0.03090	0.03111	0.03138	0.03150	0.03158	0.03160	0.03161	0.03162	0.03162	0.03162
0.2	0.05994	0.06058	0.06100	0.06155	0.06178	0.06194	0.06199	0.06201	0.06202	0.06202	0.06202
0.3	0.08709	0.08804	0.08867	0.08948	0.08982	0.09007	0.09014	0.09017	0.09018	0.09019	0.09019
0.4	0.11135	0.11260	0.11342	0.11450	0.11495	0.11527	0.11537	0.11541	0.11543	0.11544	0.11544
0.5	0.13241	0.13395	0.13496	0.13628	0.13684	0.13724	0.13737	0.13741	0.13744	0.13745	0.13745
0.6	0.15028	0.15207	0.15326	0.15483	0.15550	0.15598	0.15612	0.15617	0.15621	0.15622	0.15623
0.7	0.16515	0.16720	0.16856	0.17036	0.17113	0.17168	0.17185	0.17191	0.17195	0.17196	0.17197
0.8	0.17739	0.17967	0.18119	0.18321	0.18407	0.18469	0.18488	0.18496	0.18500	0.18502	0.18502
0.9	0.18737	0.18986	0.19152	0.19375	0.19470	0.19540	0.19561	0.19569	0.19574	0.19576	0.19577
1.0	0.19546	0.19814	0.19994	0.20236	0.20341	0.20417	0.20440	0.20449	0.20455	0.20457	0.20458
1.2	0.20731	0.21032	0.21235	0.21512	0.21633	0.21722	0.21749	0.21760	0.21767	0.21769	0.21770
1.4	0.21510	0.21836	0.22058	0.22364	0.22499	0.22600	0.22632	0.22644	0.22652	0.22654	0.22656
1.6	0.22025	0.22372	0.22610	0.22940	0.23088	0.23200	0.23236	0.23249	0.23258	0.23261	0.23263
1.8	0.22372	0.22736	0.22986	0.23334	0.23495	0.23617	0.23656	0.23671	0.23681	0.23684	0.23686
2.0	0.22610	0.22986	0.23247	0.23614	0.23782	0.23912	0.23954	0.23970	0.23981	0.23985	0.23987
2.5	0.22940	0.23334	0.23614	0.24010	0.24196	0.24344	0.24392	0.24412	0.24425	0.24429	0.24432
3.0	0.23088	0.23495	0.23782	0.24196	0.24394	0.24554	0.24608	0.24630	0.24646	0.24650	0.24654
4.0	0.23200	0.23617	0.23912	0.24344	0.24554	0.24729	0.24791	0.24817	0.24836	0.24842	0.24846
5.0	0.23236	0.23656	0.23954	0.24392	0.24608	0.24791	0.24857	0.24885	0.24907	0.24914	0.24919
6.0	0.23249	0.23671	0.23970	0.24412	0.24630	0.24817	0.24885	0.24916	0.24939	0.24946	0.24952
8.0	0.23258	0.23681	0.23981	0.24425	0.24646	0.24836	0.24907	0.24939	0.24964	0.24973	0.24980
10.0	0.23261	0.23684	0.23985	0.24429	0.24650	0.24842	0.24914	0.24946	0.24973	0.24981	0.24989
∞	0.23263	0.23686	0.23987	0.24432	0.24654	0.24846	0.24919	0.24952	0.24980	0.24989	0.25000

3. Vertical normal stress beneath the center of a uniformly loaded circular area. The vertical normal stress at depth z beneath the center of a circular area with a radius R carrying a load q per unit of area is

$$\sigma_z = qI_\sigma$$

wherein

$$I_\sigma = 1 - \left[\frac{1}{1 + (R/z)^2}\right]^{\frac{3}{2}} \qquad 136(4)$$

The following table contains the values of I_σ for different values of R/z.

TABLE III[1]

R/z	I_σ	R/z	I_σ	R/z	I_σ	R/z	I_σ
0.00	0.00000	0.40	0.19959	0.80	0.52386	1.20	0.73763
1	0.00015	1	0.20790	1	0.53079	1	0.74147
2	0.00060	2	0.21627	2	0.53763	2	0.74525
3	0.00135	3	0.22469	3	0.54439	3	0.74896
4	0.00240	4	0.23315	4	0.55106	4	0.75262
5	0.00374	5	0.24165	5	0.55766	5	0.75622
6	0.00538	6	0.25017	6	0.56416	6	0.75976
7	0.00731	7	0.25872	7	0.57058	7	0.76324
8	0.00952	8	0.26729	8	0.57692	8	0.76666
9	0.01203	9	0.27587	9	0.58317	9	0.77003
0.10	0.01481	0.50	0.28446	0.90	0.58934	1.30	0.77334
1	0.01788	1	0.29304	1	0.59542	1	0.77660
2	0.02122	2	0.30162	2	0.60142	2	0.77981
3	0.02483	3	0.31019	3	0.60734	3	0.78296
4	0.02870	4	0.31875	4	0.61317	4	0.78606
5	0.03283	5	0.32728	5	0.61892	5	0.78911
6	0.03721	6	0.33579	6	0.62459	6	0.79211
7	0.04184	7	0.34427	7	0.63018	7	0.79507
8	0.04670	8	0.35272	8	0.63568	8	0.79797
9	0.05181	9	0.36112	9	0.64110	9	0.80083
0.20	0.05713	0.60	0.36949	1.00	0.64645	1.40	0.80364
1	0.06268	1	0.37781	1	0.65171	1	0.80640
2	0.06844	2	0.38609	2	0.65690	2	0.80912
3	0.07441	3	0.39431	3	0.66200	3	0.81179
4	0.08057	4	0.40247	4	0.66703	4	0.81442
5	0.08692	5	0.41058	5	0.67198	5	0.81701
6	0.09346	6	0.41863	6	0.67686	6	0.81955
7	0.10017	7	0.42662	7	0.68166	7	0.82206
8	0.10704	8	0.43454	8	0.68639	8	0.82452
9	0.11408	9	0.44240	9	0.69104	9	0.82694
0.30	0.12126	0.70	0.45018	1.10	0.69562	1.50	0.82932
1	0.12859	1	0.45789	1	0.70013	1	0.83167
2	0.13605	2	0.46553	2	0.70457	2	0.83397
3	0.14363	3	0.47310	3	0.70894	3	0.83624
4	0.15133	4	0.48059	4	0.71324	4	0.83847
5	0.15915	5	0.48800	5	0.71747	5	0.84067
6	0.16706	6	0.49533	6	0.72163	6	0.84283
7	0.17507	7	0.50259	7	0.72573	7	0.84495
8	0.18317	8	0.50976	8	0.72976	8	0.84704
9	0.19134	9	0.51685	9	0.73373	9	0.84910

[1] Computed by R. E. Fadum and checked by J. Levings.

TABLE III — *continued*

R/z	I_σ	R/z	I_σ	R/z	I_σ	R/z	I_σ
1.60	0.85112	1.90	0.89897	2.90	0.96536	8.00	0.99809
1	0.85312	1	0.90021	.95	0.96691		
2	0.85507	2	0.90143			9.00	0.99865
3	0.85700	3	0.90263	3.00	0.96838		
4	0.85890	4	0.90382	.10	0.97106	10.00	0.99901
5	0.86077	5	0.90498	.20	0.97346		
6	0.86260	6	0.90613	.30	0.97561	12.00	0.99943
7	0.86441	7	0.90726	.40	0.97753		
8	0.86619	8	0.90838	.50	0.97927	14.00	0.99964
9	0.86794	9	0.90948	.60	0.98083		
				.70	0.98224	16.00	0.99976
1.70	0.86966	2.00	0.91056	.80	0.98352		
1	0.87136	.02	0.91267	.90	0.98468	18.00	0.99983
2	0.87302	.04	0.91472				
3	0.87467	.06	0.91672	4.00	0.98573	20.00	0.99988
4	0.87628	.08	0.91865	.20	0.98757		
5	0.87787	.10	0.92053	.40	0.98911	25.00	0.99994
6	0.87944	.15	0.92499	.60	0.99041		
7	0.88098	.20	0.92914	.80	0.99152	30.00	0.99996
8	0.88250	.25	0.93301				
9	0.88399	.30	0.93661			40.00	0.99998
		.35	0.93997	5.00	0.99246		
1.80	0.88546	.40	0.94310	.20	0.99327	50.00	0.99999
1	0.88691	.45	0.94603	.40	0.99396		
2	0.88833	.50	0.94877	.60	0.99457	100.00	1.00000
3	0.88974	.55	0.95134	.80	0.99510		
4	0.89112	.60	0.95374			∞	1.00000
5	0.89248	.65	0.95599	6.00	0.99556		
6	0.89382	.70	0.95810	.50	0.99648		
7	0.89514	.75	0.96009				
8	0.89643	.80	0.96195	7.00	0.99717		
9	0.89771	.85	0.96371	.50	0.99769		

REFERENCES

AICHHORN, W. (1931), *Über die Zusammendrückung des Bodens infolge örtlicher Belastung*, Diss. Bergak. Freiberg; see also *Geologie u. Bauwesen*, Vol. 4 (1932), pp. 2–46.

AIRY, G. B. (1862), On the Strains in the Interior of Beams, *Brit. Assoc. Advancement Sci. Rept. Meeting* 1862 (no volume number), pp. 82–86.

BAVER, L. D. (1940), *Soil Physics*, New York, John Wiley & Sons, Inc.

BIERBAUMER, A. (1913), *Die Dimensionierung des Tunnelmauerwerkes*, Leipzig, W. Engelmann.

BIOT, M. A. (1935*a*), Effect of Certain Discontinuities on the Pressure Distribution in a Loaded Soil, *Physics*, Vol. 6, pp. 367–375.

—— (1935*b*), Le Problème de la Consolidation des Matières Argilleuses sous une Charge, *Ann. soc. sci. Bruxelles*, Sér. B, Vol. 55, pp. 110–113.

—— (1935*c*), Distributed Gravity and Temperature Loading in Two-Dimensional Elasticity Replaced by Boundary Pressures and Dislocations, *J. Applied Mechanics*, Vol. 57 of *Trans. Am. Soc. Mech. Engrs.*, pp. A41–A42.

—— (1937), Bending of an Infinite Beam on an Elastic Foundation, *J. Applied Mechanics*, Vol. 59 of *Trans. Am. Soc. Mech. Engrs.*, pp. A1–A7.

—— (1941*a*), General Theory of Three-Dimensional Consolidation, *J. Applied Physics*, Vol. 12, pp. 155–164.

—— (1941*b*), Consolidation under a Rectangular Load Distribution, *J. Applied Physics*, Vol. 12, pp. 426–430.

—— (1942), Analytical and Experimental Methods in Engineering Seismology, *Proc. Am. Soc. Civil Engrs.*, January 1942, pp. 49–69.

BIOT, M. A., and CLINGAN, F. M. (1941), Consolidation Settlement of a Soil with an Impervious Top Surface, *J. Applied Physics*, Vol. 12, pp. 578–581.

—— (1942), Bending Settlement of a Slab Resting on a Consolidating Foundation, *J. Applied Physics*, Vol. 13, pp. 35–40.

BLUM, H. (1930), *Einspannungsverhältnisse bei Bohlwerken*, Diss. tech. Hochschule Braunschweig, 1930.

BOROWICKA, H. (1936), Influence of Rigidity of a Circular Foundation Slab on the Distribution of Pressures over the Contact Surface, *Proc. Intern. Conf. Soil Mechanics*, Cambridge, Mass., Vol. 2, pp. 144–149.

—— (1938), The Distribution of Pressure under a Uniformly Loaded Elastic Strip Resting on Elastic-Isotropic Ground, *Second Cong. Intern. Assoc. Bridge and Structural Eng.*, Final Report, VIII 3, Berlin.

BOUSSINESQ, J. (1885), *Application des Potentiels à l'Étude de l'Équilibre et du Mouvement des Solides Élastiques*, Paris, Gauthier-Villard.

BRAHTZ, J. H. A. (1933), Stress Distribution in Wedges with Arbitrary Boundary Forces, *Physics*, Vol. 4, pp. 56–65.

BRAHTZ, J. H. A. (1936), Rational Design of Earth Dams (*Pt. II of* Proposed Methods of Calculating the Stability of Earth Dams, by D. R. May and J. H. A. Brahtz), *Proc. Second Cong. Large Dams*, Washington, D.C., Vol. 4, pp. 543–577.

—— (1939), *Notes on Analytic Soil Mechanics*, U. S. Bureau of Reclamation, Denver, Colo.

BRAHTZ, J. H. A., and SOERENS, J. (1939), Direct Optical Measurement of Individual Principal Stresses, *J. Applied Physics*, Vol. 10, pp. 242–247.

BRENNECKE, L., and LOHMEYER, E. (1930), *Der Grundbau*, Vol. 2, 4th ed., p. 549, Berlin, 1930, W. Ernst und Sohn.

BRISKE, R. (1927), Die Erdbebensicherheit von Bauwerken, *Die Bautechnik*, Vol. 5, pp. 425–430, 453–457, 547–555.

BUCKY, P. B. (1931), Use of Models for the Study of Mining Problems, *Am. Inst. Mining Met. Engr. Tech. Pub.* 425, *Class A, Mining Methods*, No. 44.

—— (1934), Application of Principles of Similitude to Design of Mine Workings, *Trans. Am. Inst. Mining Met. Engrs.*, Vol. 109, pp. 25–42.

BURMISTER, D. M. (1938), Graphical Distribution of Vertical Pressure Beneath Foundations, *Trans. Am. Soc. Civil Engrs.*, Vol. 103, pp. 303–313.

CAIN, W. (1916), *Earth Pressure, Retaining Walls and Bins*, New York, John Wiley & Sons, Inc.

CAQUOT, A. (1934), *Équilibre des Massifs à Frottement Interne*, Paris, Gauthier-Villard.

CARRILLO, N. (1942*a*), Differential Equation of a Sliding Surface in an Ideal Saturated Plastic Soil, *J. Math. Physics*, Vol. 21, pp. 6–9.

—— (1942*b*), Simple Two and Three Dimensional Cases in the Theory of Consolidation of Soils, *J. Math. Physics*, Vol. 21, pp. 1–5.

—— (1942*c*), *Investigations on Stability of Slopes and Foundations*, Doctor's thesis, Graduate School of Engineering, Harvard University.

CASAGRANDE, A. (1936), Characteristics of Cohesionless Soils Affecting the Stability of Slopes and Earth Fills, *J. Boston Soc. Civil Engrs.*, Vol. 23, pp. 13–32.

—— (1937), Seepage Through Dams, *J. New England Water Works Assoc.*, Vol. 51, pp. 131–172.

CLOVER, R. E., and CORNWELL, F. E. (1941), Stability of Granular Materials, *Proc. Am. Soc. Civil Engrs.*, Vol. 67, pp. 1639–1656.

COKER, E. G., and FILON, L. N. G. (1931), *Photo-Elasticity*, Cambridge (England), University Press.

COULOMB, C. A. (1776), Essai sur une Application des Règles des Maximis et Minimis à quelques Problèmes de Statique Relatifs à l'Architecture, *Mém. acad. roy. prés. divers savants*, Vol. 7, Paris.

CROSS, HARDY (1932), Analysis of Continuous Frames by Distributing Fixed-End Moments, *Trans. Am. Soc. Civil Engrs.*, Vol. 96, pp. 1–10.

CULMANN, C. (1866), *Graphische Statik*, Zürich.

CUMMINGS, A. E. (1937), Discussion, *Trans. Am. Soc. Civil Engrs.*, Vol. 102, pp. 255–264.

CUMMINGS, A. E. (1938), The Stability of Foundation Piles against Buckling under Axial Load, *Proc. Highway Res. Board*, 18th Ann. Meeting, Part II, Dec. 1938, pp. 112–119.

—— (1940), Dynamic Pile Driving Formulas, *J. Boston Soc. Civil Engrs.*, Vol. 27, pp. 6–27.

—— (1941), Foundation Stresses in an Elastic Solid with a Rigid Underlying Boundary, *Civil Eng.*, Vol. 11, pp. 666–667.

DARCY, H. (1856), Les Fontaines Publiques de la Ville de Dijon, Dijon.

DE SAINT VENANT, M. (1871), Formules des Augmentations, *J. Math.*, Vol. 16, pp. 275–307.

DEGEBO (Deutsche Forschungsgesellschaft für Bodenmechanik) (1933), *Veröffentl.*, Heft 1, Berlin.

—— (Deutsche Forschungsgesellschaft für Bodenmechanik) (1936), *Veröffentl.* Heft 4, Berlin.

DÖRR, H. (1922), *Die Tragfähigkeit der Pfähle*, Berlin, W. Ernst und Sohn.

EHLERS, G. (1934), Dampfturbinenfundamente und damit zusammenhängende Fragen des Eisenbetonbaues, *Der Bauingenieur*, Vol. 15, pp. 295–198, 312–314.

ENGESSER, F. (1880), Geometrische Erddrucktheorie, *Z. Bauwesen*, Vol. 30, p. 189.

—— (1882), Über den Erddruck gegen innere Stützwände, *Deut. Bauzeitg*, Vol. 16, pp. 91–93.

FADUM, R. E. (1941), *Influence Values for Vertical Stresses in a Semi-Infinite Solid Due to Surface Loads.* (Mimeographed copies at Graduate School of Engineering, Harvard University.)

FELLENIUS, W. (1927), *Erdstatische Berechnungen*, Berlin, W. Ernst u. Sohn. (Revised edition 1939.)

FILLUNGER, P. (1912), Drei wichtige ebene Spannungszustände des keilförmigen Körpers, *Z. Math. Physik*, Vol. 60, pp. 275–285.

FLEMING, R. (1930), *Wind Stresses in Buildings*, New York, John Wiley & Sons, Inc.

FORCHHEIMER, PHILIPP (1917), Zur Grundwasserbewegung nach isothermischen Kurvenscharen, *Sitzber. kais. Akad. Wiss. Wien, Abt. IIa*, Vol. 126, pp. 409–440.

FORSSELL, C. (1926), Knäcksäkerhet hos Pålar och Pålgrupper, Uppsats N.° 10, Festskrift, *Kungl. Väg-och Vattenbyggnadskåren (Stockholm)*, 1851–1926.

FREUND, A. (1917), Theorie der gleichmässig elastisch gestützten Körper, *Beton u. Eisen*, Vol. 16, pp. 144–147, 165–167.

—— (1924), Beitrag zur Berechnung der biegsamen Gründungssohlen, *Z. Bauwesen*, Vol. 74 (Ingenieurbauteil), pp. 109–115.

—— (1927), Erweiterte Theorie für die Berechnung von Schleusenböden und ähnlichen Gründungskörpern, *Z. Bauwesen*, Vol. 77 (Ingenieurbauteil), pp. 73–88, 108–120.

FRÖHLICH, O. K. (1934*a*), *Druckverteilung im Baugrunde*, Berlin, J. Springer.

—— (1934*b*), Elementare Druckverteilung und Verschiebungen im Elastisch-

Isotropen Vollraum, *Der Bauingenieur*, Vol. 15, pp. 298–301; correction on p. 414.

FRONTARD, M. (1922), Cycloides de Glissement des Terres, *Compt. rend. hebdom. Acad. sci., Paris*, Vol. 174, pp. 526–528.

GARDNER, W. (1936), The Role of the Capillary Potential in the Dynamics of Soil Moisture, *J. Agri. Research*, Vol. 53, pp. 57–60.

GILBOY, G. (1934), Mechanics of Hydraulic Fill Dams, *J. Boston Soc. Civil Engrs.*, Vol. 21, pp. 185–205.

GLANVILLE, W. H., GRIME, G., FOX, E. N. *2d*, and DAVIES, W. W. (1938), An Investigation of the Stresses in Reinforced Concrete Piles During Driving, *Dept. Sci. Ind. Research, Building Research Station (Great Britain), Tech. Paper* 20.

GOLDER, H. Q. (1942), The Ultimate Bearing Pressure of Rectangular Footings, *J. Inst. Civil Engrs.*, Vol. 18, Paper 5274, pp. 161–174.

GRANHOLM, H. (1929), On the Elastic Stability of Piles Surrounded by a Supporting Medium, *Ingeniörs Vetenskaps Akad. Hand.* 89, Svenska Bokhandelscentralen, Stockholm.

GRAY, H. (1936), Stress Distribution in Elastic Solids, *Proc. Intern. Conf. Soil Mechanics*, Vol. 2, Cambridge, Mass., pp. 157–168.

GRIFFITH, J. H. (1929), The Pressures under Substructures, *Eng. Contr.*, Vol. 1, pp. 113–119.

HABEL, A. (1937), Die auf dem elastisch-isotropen Halbraum aufruhende zentral-symmetrisch belastete elastische Kreisplatte, *Der Bauingenieur*, Vol. 18, pp. 188–193.

—— (1938), Näherungsberechnung des auf dem elastisch-isotropen Halbraum aufliegenden elastischen Balkens, *Der Bauingenieur*, Vol. 19, pp. 76–80.

HAYASHI, K. (1921), *Theorie des Trägers auf elastischer Unterlage*, Berlin, J. Springer.

HEDDE, P. (1929), Einflusslinien zur statischen Untersuchung der Grundbauwerke, *Der Bauingenieur*, Vol. 10, pp. 1–6.

HEILAND, C. A. (1940), *Geophysical Exploration*, New York, Prentice Hall, Inc.

HEINRICH, G. (1938), Wissenschaftliche Grundlagen der Theorie der Setzung von Tonschichten, *Wasserkraft u. Wasserwirtsch.*, Vol. 33, pp. 5–11.

HILEY, A. (1930), Pile Driving Calculations, *Structural Eng.*, London, Vol. 8, pp. 246–259, 278–288.

HILTSCHER, R. (1938), Polarisations Untersuchung des räumlichen Spannungszustandes im Konvergenten Licht, *Forsch. Gebiete Ingenieurw.*, Vol. 9, pp. 91–103.

HOLL, D. L. (1941), Plane-Strain Distribution of Stress in Elastic Media, *Iowa Eng. Exp. Sta., Iowa State College, Bull.* 148.

HOUSEL, W. S. (1929), A Practical Method for the Selection of Foundations Based on Fundamental Research in Soil Mechanics, *Univ. Michigan, Ann Arbor, Dept. Eng. Research, Eng. Research Bull.* 13.

JÁKY, J. (1936), Stability of Earth Slopes, *Proc. Intern. Conf. Soil Mechanics*, Cambridge, Mass., Vol. 2, pp. 125–129.

JÁKY, J. (1938), Die klassische Erddrucktheorie mit besonderer Rücksicht auf die Stützwandbewegung, *Abhandl. Intern. Verein. Brückenbau u. Hochbau (Trans. Intern. Assoc. Bridge and Structural Eng.)*, Vol. 5, pp. 187–220.

JANSSEN, H. A. (1895), Versuche über Getreidedruck in Silozellen, *Z. Ver. deut. Ing.*, Vol. 39, p. 1045.

JÜRGENSON, L. (1934), The Application of Theories of Elasticity and Plasticity to Foundation Problems, *J. Boston Soc. Civil Engrs.*, Vol. 21, pp. 206–241.

KÁRMÁN, TH. V. (1926), Über elastische Grenzzustände, *Proc. Second Congr. Applied Mechanics*, Zürich.

KOENEN, M. (1896), Berechnung des Seiten- und Bodendrucks in Silozellen, *Centrbl. Bauverwaltung*, Vol. 16, pp. 446–447.

KÖGLER, F., and SCHEIDIG, A. (1927), Druckverteilung im Baugrunde, *Die Bautechnik*, Vol. 5 (1927), 6 (1928), 7 (1929).

KÖTTER, F. (1888), Über das Problem der Erddruckbestimmung, *Verhandl. Physik. Ges. Berlin*, Vol. 7, pp. 1–8.

—— (1892), Die Entwicklung der Lehre vom Erddruck, *Jahresber. deut. Math. Ver.*, Vol. 2 (1891–1892), pp. 75–150.

—— (1899), Der Bodendruck von Sand in vertikalen zylindrischen Gefässen, *J. Math.*, Vol. 120, pp. 189–241.

KOZENY, J. (1933), Theorie und Berechnung der Brunnen, *Wasserkr. u. Wasserwirtsch*, Vol. 28.

KREY, H. (1936), *Erddruck, Erdwiderstand und Tragfähigkeit des Baugrundes*, 5th ed., Berlin, W. Ernst u. Sohn, (1st ed., 1912).

LABUTIN, A. (1933), *Die graphische Berechnung von Pfahlrosten für Quaimauern*, Riga, Abh. d. lettländ. Univ., Ingenieurabt, Reihe 1, 7.

LEET, L. DON (1938), *Practical Seismology and Seismic Prospecting*, New York, D. Appleton-Century Co., Inc.

—— (1939), Ground Vibrations near Dynamite Blasts, *Bull. Seismol. Soc. Am.*, Vol. 29, pp. 487–496.

LÉVY, M. (1898), Sur la Légitimité de la Règle Dite du Trapèze dans l'étude de la Résistance des Barrages en Maçonnerie, *Compt. rend. hebdom. Acad. sci. Paris*, Vol. 126, pp. 1235–1240.

LOHMEYER, E. (1930), Die Berechnung verankerter Bohlwerke, *Bautechnik*, Vol. 8, pp. 60–65.

LORENZ, H. (1934), Neue Ergebnisse der dynamischen Baugrundforschung, *Z. Ver. deut. Ing.*, Vol. 78, pp. 379–385.

LOVE, A. E. H. (1928), The Stress Produced in a Semi-Infinite Solid by Pressure on Part of the Boundary, *Phil. Trans. Roy. Soc., London*, Series A., Vol. 228, pp. 377–420.

—— (1934). *A Treatise on the Mathematical Theory of Elasticity*, 4th ed., Cambridge (England), Univ. Press.

MACELWANE, J. B. (1936), Introduction to Theoretical Seismology, Part 1, *Geodynamics*, New York, John Wiley & Sons, Inc.

MALCOLM, CH. M. (1909), *A Textbook on Graphic Statics*, New York, Myron C. Clark Publishing Co.

MARGUERRE, K. (1931), Druckverteilung durch eine elastische Schichte auf starrer, rauher Unterlage, *Ing. Archiv*, Vol. 2, pp. 108–117.

—— (1933), Spannungsverteilung und Wellenausbreitung in der dicken Platte, *Ing. Archiv*, Vol. 4.

MELAN, E. (1919), Die Druckverteilung durch eine elastische Schicht, *Beton u. Eisen*, Vol. 18, pp. 83–85.

MENDENHALL, T. E. (1888), On the Intensity of Earthquakes with Approximate Calculations of the Energy Involved, *Proc. Am. Assoc. Adv. Sci.*, Vol. 37, pp. 190–195.

MICHE, R. (1930), Investigation of Piles Subject to Horizontal Forces, Application to Quay Walls, *J. School of Engin., Giza*, No. 4.

MINDLIN, R. D. (1936), Forces at a Point in the Interior of a Semi-Infinite Solid, *Physics*, Vol. 7, pp. 195–202.

—— (1939), Stress Distribution Around a Tunnel, *Trans. Am. Soc. Civil Engrs.*, Vol. 104, pp. 1714–1718.

MOHR, O. (1871), Beiträge zur Theorie des Erddruckes, *Z. Arch. u. Ing. Ver. Hannover*, Vol. 17 (1871), p. 344, and Vol. 18 (1872), pp. 67, 245.

—— (1928), *Abhandlungen aus dem Gebiete der technischen Mechanik*, 3d ed., revised by K. Bayer and H. Spangenberg, Berlin, W. Ernst u. Sohn.

MUSKAT, M. (1937), *The Flow of Homogeneous Fluids through Porous Media*, New York, McGraw-Hill Book Company, Inc.

NADAI, A. (1931), *Plasticity*, New York, McGraw-Hill.

NEWMARK, N. M. (1935), Simplified Computation of Vertical Pressures in Elastic Foundations, *Univ. Illinois Eng. Exper. Sta. Circular* 24.

NEWTON, J. (1726), *Philosophiae Naturalis Principia Mathematica*, 3d ed., Scholium to Corollary VI.

NÖKKENTVED, Ć. (1928), *Berechnung von Pfahlrosten*, Berlin, W. Ernst u. Sohn.

OHDE, J. (1938), Zur Theorie des Erddruckes unter besonderer Berücksichtigung der Erddruck Verteilung, *Die Bautechnik*, Vol. 16, pp. 150–159, 176–180, 241–245, 331–335, 480–487, 570–571, 753–761.

PASSER, W. (1935), Druckverteilung durch eine elastische Schichte, *Sitzber. Akad. Wiss. Wien, Abt. IIa*, Vol. 144, pp. 267–275.

PONCELET, V. (1840), Mém. sur la Stabilité des Revêtements et de leur Fondations, *Mém. de L'Officier du génie*, Vol. 13.

PRANDTL, L. (1920), Über die Härte plastischer Körper, *Nachr. kgl. Ges. Wiss. Göttingen, Math. phys. Klasse.*

RAMSPECK, A. (1938), Die Anwendung dynamischer Baugrunduntersuchungen, *Die Bautechnik*, Vol. 16, pp. 85–86.

RANKINE, W. J. M. (1857), On the Stability of Loose Earth, *Phil. Trans. Roy. Soc. London*, Vol. 147.

RAUSCH, E. (1936), Maschinenfundamente und andere dynamische Bauaufgaben, Berlin, *Z. Ver. deut. Ing.* Verlag, 1 vol. (Vols. 2 and 3 not yet published in fall 1939).

REBHANN, G. (1871), *Theorie des Erddruckes und der Futtermauern;* Wien.

REDTENBACHER, F. (1859), *Prinzipien der Mechanik und des Maschinenbaues.*

REISSNER, E. (1936), Stationäre, axialsymmetrische durch eine schüttelnde Masse erregte Schwingungen eines homogenen elastischen Halbraumes, *Ing. Archiv*, Vol. 7, pp. 381–396.

REISSNER, H. (1909), Theorie des Erddrucks, *Encyklopädie math. Wiss.*, Vol. 4 (2, II, Heft 3), Leipzig, G. B. Teubner.

—— (1924), Zum Erddruckproblem, *Proc.* 1st *Intern. Congr. Applied Mechanics*, Delft (Holland).

RENDULIC, L. (1935*a*), Der hydrodynamische Spannungsausgleich in zentral entwässerten Tonzylindern, *Wasserwirtsch. u. Technik*, Vol. 2, pp. 250–253, 269–273.

—— (1935*b*), Ein Beitrag zur Bestimmung der Gleitsicherheit, *Der Bauingenieur*, Vol. 16, pp. 230–233.

—— (1936), Porenziffer und Porenwasserdruck in Tonen, *Der Bauingenieur*, Vol. 17, pp. 559–564.

—— (1937), Ein Grundgesetz der Tonmechanik und sein experimenteller Beweis, *Der Bauingenieur*, Vol. 18, pp. 459–467, see also *Proc. Intern. Conf. Soil Mechanics*, Cambridge, Mass., 1936, Vol. 3, pp. 48–51.

—— (1938), Der Erddruck im Strassenbau und Brückenbau, *Forschungsarb. Strassenwesen*, Bd. 10, Volk u. Reich Verlag, Berlin.

RÉSAL, JEAN (1910), *La Poussée des Terres, Deuxième Partie: Théorie des Terres Cohérantes*, Paris, Béranger.

RIFAAT, T. (1935), Die Spundwand als Erddruckproblem, *Mitt. Inst. Baustatik, Zürich.*

RIMSTAD, I. A. (1937), Unpublished report.

RUGE, A. C. (1938), Earthquake Resistance of Elevated Water-Tanks, *Trans. Am. Soc. Civil Engrs.*, Vol. 103, pp. 889–938.

SAMSIOE, A. F. (1931), Einfluss von Rohrbrunnen auf die Bewegung des Grundwassers, *Z. angew. Math. u. Mech.*, Vol. 11, pp. 124–135.

SCHLEICHER, F. (1926), Zur Theorie des Baugrundes, *Der Bauingenieur*, Vol. 7, pp. 931–935, 949–952.

SCHMID, H. (1926), *Statische Probleme des Tunnel- und Druckstollenbaues*, Berlin, J. Springer. (English transl. by C. Voetsch, U. S. Bur. Reclamation, Tech. Memo. 262, 1931.)

SCHOENWELLER, G. (1929), Calcul des Murs de Quai, *Proc. World Eng. Cong. Tokio*, Paper 416, Vol. 11, pp. 309–318.

SEISMOS, HANNOVER, *Dynamische Baugrund-Untersuchungen für den Industriebau* (Prospectus).

SHEPARD, E. R. (1935), Subsurface Exploration by Earth Resistivity and Seismic Methods, *Public Roads*, Vol. 16, pp. 57–67, 74.

SKEMPTON, A. W. (1942), An Investigation of the Bearing Capacity of a Soft Clay Soil, *J. Inst. Civil Engrs.*, Vol. 18, Paper No. 1305, pp. 307–321.

SOUTHWELL, R. V. (1936), *An Introduction to the Theory of Elasticity*, London, Oxford University Press.

—— (1940), *Relaxation Methods in Engineering Science*, Oxford (England), Clarendon Press.

STEINBRENNER, W. (1934), Tafeln zur Setzungsberechnung, *Die Strasse*, Vol. 1,

pp. 121–124; see also *Proc. Intern. Conf. Soil Mechanics*, Cambridge, Mass., 1936, Vol. 2, pp. 142–143.

STEINBRENNER, W. (1937), Der zeitliche Verlauf einer Grundwasserabsenkung, *Wasserwirtsch. u. Technik*, Vol. 4, pp. 27–33.

STERN, O. (1908), *Das Problem der Pfahlbelastung*, Berlin, W. Ernst u. Sohn.

STROHSCHNEIDER, O. (1912), Elastische Druckverteilung und Drucküberschreitung in Schüttungen, *Sitzber. kais. Akad. Wiss. Wien, Abt. IIa*, Vol. 121, pp. 299–336.

SULZBERGER, G. (1927), Die Fundamente der Freileitungstragwerke und ihre Berechnung, *Bull. Schweiz. Electrotech. Verein.*

SYFFERT, O. (1929), *Erddrucktafeln*, Berlin, J. Springer.

TALBOT, A. N. (1918), Progress Report of the Special Committee to Report on Stresses in Railroad Track, *Trans. Am. Soc. Civil Engrs.*, Vol. 82, pp. 1191–1383.

TAYLOR, D. W. (1937), Stability of Earth Slopes, *Boston Soc. Civil Engrs.*, Vol. 24, pp. 197–246.

TERZAGHI, K. (1919), Die Erddruckerscheinungen, *Österr. Wochenschr. öffentl. Baudienst*, Jg. 1919, Heft 17–19.

—— (1922), Der Grundbruch an Stauwerken und seine Verhütung, Forchheimer-Nummer der *Wasserkraft*, p. 445.

—— (1923), Die Berechnung der Durchlässigkeitsziffer des Tones aus dem Verlauf der hydrodynamischen Spannungserscheinungen, *Sitzber. Akad. Wiss. Wien, Abt. IIa*, Vol. 132.

—— (1925), *Erdbaumechanik*, Vienna, F. Deuticke.

—— (1932), Bodenpressung und Bettungsziffer, *Österr. Bauzeitung*, Heft 25, June 18, 1932.

—— (1934), Large Retaining-Wall Tests. I. Pressure of Dry Sand, *Eng. News-Record*, Vol. 112, pp. 136–140.

—— (1935), The Actual Factor of Safety in Foundations, *Structural Eng.* (London), Vol. 13, pp. 126–160.

—— (1936*a*), Critical Height and Factor of Safety of Slopes against Sliding, *Proc. Intern. Conf. Soil Mechanics*, Cambridge, Mass., Vol. 1, pp. 156–161.

—— (1936*b*), A Fundamental Fallacy in Earth Pressure Computations, *J. Boston Soc. Civil Engrs.*, Vol. 23, pp. 71–88.

—— (1936*c*), Distribution of the Lateral Pressure of Sand on the Timbering of Cuts, *Proc. Intern. Conf. Soil Mechanics*, Cambridge, Mass., Vol. 1, pp. 211–215.

—— (1936*d*), Effect of the Type of Drainage of Retaining Walls on the Earth Pressure, *Proc. Intern. Conf. Soil Mechanics*, Cambridge, Mass., Vol. 1, pp. 215–218.

—— (1936*e*), Stress Distribution in Dry and in Saturated Sand above a Yielding Trap-Door, *Proc. Intern. Conf. Soil Mechanics*, Cambridge, Mass., Vol. 1, pp. 307–311.

—— (1941), General Wedge Theory of Earth Pressure, *Trans. Am. Soc. Civil Engrs.*, Vol. 106, pp. 68–97.

TERZAGHI, K. (1942*a*), Linerplate tunnels on the Chicago [Ill.] Subway, *Proc. Am. Soc. Civil Engrs.*, June 1942, pp. 862–899.

—— (1942*b*), Soil Moisture and capillary phenomena in soils, Ch. IXA in Vol. IX of *Physics of the Earth*, New York, McGraw-Hill.

TERZAGHI, K., and FRÖHLICH, O. K. (1936), *Theorie der Setzung von Tonschichten*, Vienna, F. Deuticke. (French transl. by M. Adler, Théorie des Tassements des Couches Argileuses, Paris (1939), Dunod.)

THEIS, C. V. (1940), The Source of Water Derived from Wells, *Civil Eng.*, Vol. 10, pp. 277–280.

TIMOSHENKO, S. P. (1934), *Theory of Elasticity*, New York, McGraw-Hill.

—— (1937), *Vibration Problems in Engineering*, D. Van Nostrand. 2d ed., New York.

—— (1940), *Strength of Materials*, Part 1, 2d ed., New York, D. Van Nostrand.

—— (1941), *Strength of Materials*, Part 2, 2d ed., New York, D. Van Nostrand.

TITZE, E. (1932), *Widerstand des Pfahles gegen wagrechte Kräfte*, Dissertation. (Tech. Hochschule Wien 1932.)

VETTER, C. P. (1939), Design of Pile Foundations, *Trans. Am. Soc. Civil Engrs.*, Vol. 104, pp. 758–778.

VOGT, F. (1925), Über die Berechnung der Fundamentdeformation, *Avhandl. kgl. Norske Videnskaps-Akad. Oslo, I., Mat.-Naturv. Klasse*, No. 2, Oslo.

VÖLLMY, A. (1937), Eingebettete Rohre, *Mitt. Inst. Baustatik, Eidgen. Tech. Hochschule, Zürich, Mitt.* No. 9.

WEBER, HERMANN (1928), *Die Reichweite von Grundwasserabsenkungen mittels Rohrbrunnen*, Berlin, J. Springer.

WESTERGAARD, H. M. (1917), The Resistance of a Group of Piles, *J. Western Soc. Engrs.*, Vol. 22, pp. 704–713.

—— (1926), Stresses in Concrete Pavements Computed by Theoretical Analysis, *Public Roads*, Vol. 7, pp. 25–35.

—— (1933*a*), Water Pressures on Dams During Earthquakes, *Trans. Am. Soc. Civil Engrs.*, Vol. 98, pp. 418–433.

—— (1933*b*), Measuring Earthquake Intensity in Pounds per Square Foot, *Eng. News-Record*, Vol. 110, p. 504.

—— (1933*c*), Earthquake-Shock Transmission in Tall Buildings, *Eng. News-Record*, Vol. 111, pp. 654–656.

—— (1933*d*), Stresses at a Crack, Size of the Crack, and the Bending of Reinforced Concrete, *J. Am. Concrete Inst., Proc.*, Vol. 30, pp. 93–102.

—— (1938), A Problem of Elasticity Suggested by a Problem in Soil Mechanics: Soft Material Reinforced by Numerous Strong Horizontal Sheets, *Contrib. Mechanics of Solids*, Stephen Timoshenko 60th Anniversary Volume, New York, The Macmillan Co.

—— (1939), Bearing Pressures and Cracks, *J. Applied Mechanics*, Vol. 61 of *Trans. Am. Soc. Mech. Engrs.*, pp. A49–A53.

—— (1940), Plastic State of Stress around a Deep Well, *J. Boston Soc. Civil Engrs.*, Vol. 27, pp. 1–5.

WIEGHARDT, K. (1922), Über den Balken auf nachgiebiger Unterlage, *Z. angew. Math. u. Mech.*, Vol. 2, p. 165.

WILLIAMS, H. A. (1937), Dynamic Distortions in Structures Subjected to Sudden Earth Shock, *Trans. Am. Soc. Civil Engrs.*, Vol. 102, pp. 838–850.

WILSON, B. D., and RICHARDS, S. J. (1938), Capillary Conductivity of Peat Soils at Different Capillary Tensions, *J. Am. Soc. Agronomy*, Vol. 30, pp. 583–588.

WOLF, K. (1914), Zur Integration der Gleichung $\Delta\Delta F$ durch Polynome im Falle des Staumauerproblems, *Sitzber. kais. Akad. Wiss., Wien, Abt. IIa*, Vol. 123, pp. 281–311.

—— (1935), Ausbreitung der Kraft in der Halbebene und im Halbraum bei anisotropem Material, *Z. angew. Math. u. Mech.*, Vol. 15, pp. 249–254.

ZIMMERMANN, H. (1888), *Die Berechnung des Eisenbahn Oberbaues*, Berlin, W. Ernst u. Sohn.

AUTHOR INDEX

SUBJECT INDEX

D

G

H

I